

CTU REPORTS

Proceedings of

WORKSHOP 2007

Part A

Czech Technical University in Prague

SPECIAL ISSUE

February 2007
Volume 11

These are the Proceedings of the Thirteenth Annual university-wide seminar WORKSHOP 2007 which took place at the Czech Technical University in Prague from 19th to 23rd February, 2007.

The aim of the seminar is to present and discuss the latest results obtained by researchers especially at the Czech Technical University in Prague and at collaborating institutions.

The organizing committee has selected a total of 349 contributions divided into 15 different areas of interest:

• Part A:

- mathematics
- physics
- informatics and automation engineering
- electrical engineering and instrumentation
- materials engineering

• Part B:

- mechanics and thermodynamics
- mechanical engineering
- production systems, technology and technological processes automatisation
- energetics and power engineering
- nuclear engineering
- chemistry
- biomedical engineering
- civil engineering
- architecture, town planning, geodesy and cartography
- transportation, logistics, economy and management

Organizing committee:

Chairman: Bohuslav Říha

Members (in alphabetical order):
Karel Andrejsek, Tomáš Brandejský, Radek Holý, Jiří Houkal, Libor Husník, Michaela Ibehejová, Vladimír Jirka, Květa Lejčková, Petr Musil, Milan Němec, Ladislav Prskavec, Markéta Růžičková, Bohuslav Říha, Ida Skopalová, Pavel Smrčka, Jaroslav Zeman

Prague, February 2007

ISBN 978-80-01-03667-9

This book was prepared from the input files supplied by the authors. No additional English style corrections of the included articles were made by the compositor.

Published by the Czech Technical University in Prague. Printed by CTU Publishing House.

CONTENTS

1. MATHEMATICS

Qualitative properties of some mathematical models of uid mechanics 16
M. Beneš

The two-step method calibration of digtal camera utilising non-linear transformation 18
B. Koska,V. Obr

Implementation of many-valued sequential systems 20
M. Petrík

Enhancement of Technical Applications in the Subject Mathematics for Aeronautical Branches at the Faculty of Transportation Sciences, CTU 22
M. Hykšová

2. PHYSICS

Study of Thin Metallic Sputtered Layers 26
P. Buchar

Diagnostics of Radiation and Nuclear Processes in High-parameter Plasma 28
P. Adámek, L. Drška

Coherently Pumped Broadly Tunable Cr:ZnSe laser 30
P. Koranda, H. Jelínková, J. Šulc

Atmospheric turbulence in uence on the precision of laser rangefinders 32
L. Král, I. Procházka, K. Hamal

Mode locked Nd:YVO4 laser with intracavity synchronously pumped optical parametric oscillator for laser sensor and gyroscope 34
A. Zavadilová, V. Kubeček, J. Diels

Relativistic Hypernuclei Decay Based on Dalitz Diagrams 36
V. Sopko, O. Majlingová

Evaluating the Thermal Performance of Repairs Made on the CERN ATLAS Pixel Detector 38
V. Vacek, M. Galuška, M. Doubrava

RF Plasma Modification of Polyester Fabrics in Multi-Layer Arrangement 40
J. Píchal

The sensitivity of negative dispersion induced by introducing the curvature into the Index Guiding Photonic Crystal Fiber for deviation of geometrical parameters 42
M. Lucki, L. Boháč

Hydration of Portland Cement Paste 44
P. Tichá, P. Demo, P. Semerák

Theoretical Analysis of Properties of Optical Systems 46
A. Mikš, J. Novák, P. Novák

Modern Methods of Surface Topography and Defectoscopy 48
A. Mikš, J. Novák, P. Novák

Microwave Phase Interferometry for Nondestructive Testing 50
A. Mikš, J. Novák, P. Novák

CTU Prague Contribution to the Project AIRFLY in 2005 and 2006 52
V. Vacek, M. Doubrava

Non-Thermal Plasma Ecological Applications 54
S. Pekárek, M. Pospíšil, C. Leys

Time-resolved Energy Neutron Spectra in D-D Fusion Reactions 56
P. Kubeš, D. Klír, J. Kravárik, K. Řezáč

Study of Fusion Neutrons at PF-1000 in Frame ICDMP 58
P. Kubeš, D. Klír, J. Kravárik, K. Řezáč

Computer modeling of solid state crystallographic texture 60
L. Kalvoda, A. Grishin

Powder Neutron Diffraction Study of Crystal, Magnetic and Transport Properties of Layered Cobalt Oxides 62
S. Vratislav, M. Dlouhá, A. Chichev

Decomposition of Volatile Organic Compounds by Plasma Enhanced Photocatalyst 64
S. Pekárek, C. Leys

On the Road to Shorter Wavelength X-ray Z-pinch Laser Using Wire Explosion in Shock Wave Focus in Water 66
M. Martínková, M. Kálal, K. Koláček

Low-energy Nuclear Excitation by Laser-produced Plasma 68
J. Kuba, C. Granja Bustamante, L. Drška, J. Jakůbek, V. Linhart, S. Pospíšil, J. Uher, Z. Vykydal, M. Šiňor

The In uence of Dielectric Barrier Discharge on Polyester Fabric Wettability 70
J. Klenko

Generation of Neutrons from D-D Fusion Reactions at CTU 72
P. Kubeš, D. Klír, J. Kravárik, K. Řezáč

Measurement of Double Beta Decay of Mo100 and Cd116 with the NEMO 3 Detector 74
L. Vála,J. Jerie

Experimental Studies Leading to Enhanced de-NOx Processes in Non-Equilibrium Atmospheric Pressure Discharges 76
S. Pekárek

Verification of function and application of radial scanning system for studying DC glow discharge 78
Š. Němcová, J. Čáp, J. Zicha, A. Kaňka, V. Hrachová

Structure Analysis of Faujasite Zeolitic Catalysts Chemisorbed by Methyl Groups 80
S. Vratislav, M. Dlouhá

Numerical Simulation of Dark Photovoltaic Solitons with Beam Propagation Method 82
M. Bodnár

Position Sensitive Spectroscopy of Fission Fragments 84
C. Granja Bustamante, J. Jakůbek, S. Pospíšil, Z. Vykydal

Microwave Plasma Modification of PE Powder 86
L. Aubrecht

Luminescence Spectroscopy of BaxSr1-xTiO3 Thin Films 88
Z. Potůček, Z. Bryknar

3. INFORMATICS AND AUTOMATION ENGINEERING

Coordinate Systems Transformation and Its Implementation in Web Application Based on Java Server Pages Technology 92
J. Ježek

GRASS GIS Metadata Management Analysis 94
M. Landa

Support for Coordinate Systems Operations in GIS and Developing Map Servers 96
R. Sklenička

Design of Mobile Ad Hoc Networks in Domains with High Level of Communication Inaccessibility 98
P. Benda

Reconfiguration in Competitive Multi-Agent Environments 100
J. Bíba

Re ection and Cognition in Multi-Agent Systems with Constrained Computational Resources 102
L. Foltýn

Advanced stream routing protocol for non-stable environment 104
P. Jisl

Analysis and synthesis of behavior of intelligent agents in context of selected parts from artificial life domain 106
K. Kohout

Intelligent device for insomnia. 108
P. Kolman, K. Malý

Inference Support for Semantic Annotations in Description Logics 110
P. Křemen

Coordination of mobile robot group for unknown environment mapping 112
M. Saska, T. Krajník, L. Přeučil

Metaheuristics Based on Occams Razor Principle in Search Algorithms 114
J. Suchý

Automatic Object Modelling and Tracking 116
K. Zimmermann, T. Svoboda, J. Matas

Semantic annotation of medical records 118
M. Žáková

Ventilation control in highway tunnels 120
L. Ferkl

Recursive Subspace Identification Algorithm Incorporating Prior Information 122
P. Trnka, V. Havlena

Hardware Support for Exact Computer Arithmetic based on Continued Fractions 124
T. Brabec, R. Lórencz

Formalization of UML Profile for Safety Critical Systems 126
M. Komárek

Syntax-Driven Find/Replace for Java 128
M. Píše

The Time Complexity Reduction of Design-for-Test Sequential Circuits Testing 130
M. Šťáva, O. Novák

Parallel Pattern Matching 132
J. Šupol

Statistical analysis of subjective tests of audio-coding systems 134
M. Herrera Martinez

Electroacoustic transducers with direct D/A conversion. 136
P. Valoušek

Optical measurement of cosmic objects with laser time tags 138
I. Procházka, K. Hamal, M. Němec

Method of construction scheme of object database to using in data mining. 140
M. Jeřábek, J. Krčál, L. Krčálová

Innovation of the Subject Signal Processors - Digital Signal Processing 142
M. Vlček

Simulation of Behavior in ALife Domain 144
K. Kohout, P. Nahodil, A. Elmahalawy

Flexible Booting Strategy for FPGA-based Systems 146
M. Šimek

Automated Creation of Students' Accounts in the Moodle System Using Data of the KOS Information System 148
P. Soukup, P. Žofka

Application of Artificial Life in Robot Navigation 150
P. Nahodil,V. Svatoš

Laboratory Station for Video Signal Processing 152
J. Volf

Methodical handbook for creating multimedia courses 154
M. Fejtová, P. Novák

User Modelling in Adaptive Systems 156
I. Jelínek, M. Balík

The Constrained Longest Common Subsequence Problem for Generalized Strings 158
M. Voráček

Evaluation of 3SQM algorithm performance on fixed point DSP 160
Z. Bečvář, P. Slepička

Innovation of subject 162
P. Bezpalec

Intelligent web technologies 164
I. Jelínek

Improvements of the Subject Digital Signal Processing in Telecommunication 166
B. Šimák

Hotel Yield Management Matlab Toolbox 168
T. Vítek

Inovations in The Laboratory of Control Engineering 170
K. Hyniová

Innovation of Data Networks 172
L. Konopka,P. Hampl

Lab Station with Communication Processors 174
V. Doleček

Innovation of the Subject Implementation of DSP Algorithms in Telecommunication 176
P. Slepička, P. Zahradník

Innovation of the Course 178
T. Vaněk

Innovation of the subject Artificial Inteligence I. 180
L. Nováková, O. Štěpánková

Evolutionary Numerical Optimization 182
J. Zeman, M. Lepš, A. Kučerová

Subjective Image Quality Evaluation and Enhancement 184
M. Klíma

Hybrid Approach to HDR Tone Mapping 186
M. Čadík

Matlab-Aimsun Toolbox 188
P. Dohnal

On Relation between Parallel Reduction and Leader Election Problem in Distributed Systems and Networks 190
M. Nehéz

Usability Testing and Development of Car Simulator - City Rider 192
I. Malý, D. Tichý

Hybrid Real-Time Software Architecture with Low System Overhead and Table Driven FSAs 194
J. Zděnek

Cache Misses Prediction by Means of Data Mining Methods 196
I. Šimeček, P. Kordík

A New Format for the Sparse Matrix-vector Multiplication 198
I. Šimeček

An Adaptive Solver for Fluid Dynamics on the GPU 200
I. Šimeček, O. Šťava

A New Approach for Accelerating the Sparse Matrix-vector Multiplication 202
I. Šimeček

Prototype Implementation of the Execution Engine VPU 204
L. Kalvoda, S. Vratislav, M. Dlouhá, M. Dráb

Automatic Integration of Ontologies 206
I. Jelínek,R. Jun

Using of Hyperspectral Satellite Data for Environment Monitoring in the Czech Republic 208
K. Pavelka, J. Svatušková

Updated Virtual Control Laboratory 210
M. Hofreiter, P. Trnka, M. Kopecký

4. ELECTRICAL ENGINEERING AND INSTRUMENTATION

Device for synthetysing optical holograms 214
J. Svoboda, P. Fiala

Active Control of Sound Radiation from Vibrating Bodies Using Piezoelectric Actuators 216
V. Jandák, O. Jiříček

Providing of third generation mobile services via High Altitude Platforms 218
J. Holiš

Measurement of small enclosure shielding efficiency 220
T. Kořínek

A Scalar Microwave Interferometric Measurement System
for Nondestructive Testing 222
J. Zela, K. Hoffmann, P. Hudec

Satellite Navigation Applications in Indoor Environment 224
P. Puričer

EGNOS Signal Monitoring Station 226
J. Špaček, P. Kovář

Noise Removing from an Image Data based on Bayesian Statistics 228
J. Švihlík

Modelling of the system for dynamic ADC parameters measurement 230
P. Česák

Dual-mixer time-difference multiplier 232
A. Kuna, J. Roztočil

The Methods of random signals generation with given distribution of amplitudes 234
J. Neškudla, J. Vedral

Flight data measurement system for small airplanes 236
P. Pačes

Digital signal generation used for dynamic testing of broad-band ADCs 238
P. Suchánek

Methods of synthesis the gauging devices with CMOS image sensor
for dedicated applications 240
J. Třeštík,J. Fischer

Implementation of New Practice Exercises into the Digital Signal Processing
in Telecommunications 242
Z. Bečvář

Compact Control Circuit of the InGaAs Photon Counter 244
J. Kodet, I. Procházka, K. Hamal

Planar Lightwave Hybrid Integration Circuits 246
V. Prajzler, V. Jeřábek, Z. Burian, J. Armas Arciniega

Innovation of Courses on Design of Integrated Electronic Systems 248
P. Hazdra

Wavefront Aberrations in the Ultra Wide-Field Camera and Shift
Variant Image Data Processing 250
M. Řeřábek

Optical Characterisation of MOVPE Grown Engineered InAs/GaAs Quantum Dot Structures 252
P. Hazdra

Low-Temperature Radiation Enhanced Diffusion of Palladium and Platinum in Silicon 254
P. Hazdra, J. Vobecký

Verification of Laser Scanning Systems Quality 256
B. Koska, T. Křemen, J. Pospíšil

Laboratory Models for Student of the Subject Automation Control 258
P. Jakoubek, P. Trnka

5. MATERIALS ENGINEERING

Experimental Method for Monitoring of Salt Transport Induced by External Electric Field 262
L. Fiala

Dependence of Ductility of FRC on Strength of Fibers 264
G. Djimaldé, J. Vodička

Study of engineering and technological properties of the carbon/carbon composite and it is surfaces modification 266
Z. Tolde, V. Starý

Development of fiber optic sensor of alkali ions in water 268
L. Kalvoda, R. Klepáček

The Comparision of Testing Methods Dealing with Open Porosity Determination of Hydrophobic Mortars 270
M. Ibehejová, L. Balík, J. Kolísko

Modeling of microstructure of cement paste using image analysis 272
K. Forstová, J. Němeček

Properties of Alkali Activated Aluminosilicate Materials with Different Aggregates 274
R. Černý, L. Zuda

High-Temperature Properties of Alkali Activated Aluminosilicates 276
R. Černý,L. Zuda

Mechanical Properties of High Strength Steel Sheets 278
R. Mušálek, P. Haušild, J. Bensch, J. Siegl

Detection of Gaseous Ammonia Using Evanescent Optical Sensor 280
L. Kalvoda, J. Aubrecht

Alkali Activated Slag as Cement Replacement in High-Temperature Applications 282
R. Černý, J. Toman

Properties of Concrete Damaged by Salt Action 284
R. Černý, M. Pavlíková, E. Mňahončáková

Properties of Lightweight Carbon Fiber Reinforced Cement Composite 286
R. Černý, P. Tesárek, E. Mňahončáková, P. Konvalinka

Plastics welding – welding parameters optimalisation
through the use of statistical software 288
J. Beránek

Corrosion and Fatigue Degradation of Stainless High Alloyed
Steels and Nickel Alloys 290
K. Dalíková, J. Kunz,V. Číhal

Metakaolin - Active Micro-filer for High Performance Concrete 292
P. Konvalinka, J. Kolář, K. Kolář

Coupled Water and Salt Transport with Crystalization: Calibration
of the Computational Model 294
R. Černý, J. Maděra, J. Kelnar

Modeling of hardening, softening and critical state of fine grained soils 296
T. Janda

Properties of Fiber Reinforced Cement Composites during
High-Temperature Exposure 298
R. Černý, P. Tesárek, E. Mňahončáková, P. Konvalinka

Carbon Layers Doped with Erbium or Erbium and Ytterbium Ion 300
V. Prajzler, Z. Burian

Polymer Optical Planar Waveguides Doped by Erbium Ions 302
V. Prajzler, V. Jeřábek, M. Myslík, O. Hlaváč

Gallium Nitride Layers Doped by Er3+ or Er3+ and Yb3+ by Ion Implantation 304
V. Prajzler, Z. Burian

Fracture Toughness Testing of Iron Aluminides Based Intermetallic Alloys 306
M. Karlík, P. Haušild, A. Kubošová, J. Prahl

Comparison of Several Computational Models of Coupled Heat
and Moisture Transport 308
R. Černý, J. Maděra

The In uence of Salt Ionic Concentration on Electro-osmotic Flow 310
L. Balík

Computer Analysis of Heat Conduction in Concrete 312
P. Konvalinka, T. Doležel, P. Rybár

Modeling and Analysis of Prestressed Lightweight Aggregate Concrete
Beams – Time Dependent Deformations 314
O. Bacarreza Nogales

Modeling of deformation processes in Fe-3%Si single crystals 316
M. Karlík, J. Prahl, C. Rey, P. Haghi-Ashtiani, M. Clavel

Heat Feedback System for Curing Concrete Specimens under Prescribed Temperature History 318
A. Kohoutková, P. Štemberk, N. Pokorná

Properties of Silicate Protecting Layers of Concrete Structures 320
R. Černý, M. Pavlíková

Moisture and Salt Transport and Storage Parameters of Materials Used in Historical Buildings 322
R. Černý, Z. Pavlík, M. Pavlíková, R. Pernicová

Numerical Modelling of Timber Reinforced with Carbon 324
P. Konvalinka, L. Hluší

Physical Aspects of the Transition Behaviour of Ferritic Steels 326
M. Karlík, P. Haušild, B. Strnadel, M. Kytka

Monitoring of Salt Imbibition Using TDR and Electrical Conductivity Method 328
M. Pavlíková

Optical Properties of Thin Nanodiamond Films 330
Z. Potůček, Z. Bryknar

Study of Transition Metal Oxides: the Mixed-Valent Cobaltite Perovskites 332
A. Chichev

Homogenization Techniques for TDR Calibration 334
R. Černý, L. Fiala, Z. Pavlík

Properties of Biological Agricultural Materials Measured by Methods Common in Building Physics 336
R. Černý, Z. Pavlík, M. Pavlíková

Degradation of Structure and Fatigue Properties of Structural CrMo Steels ČSN 15313 and P91 338
M. Svobodová, J. Kunz

Computational Design of the Properties of Water Vapor Retarders for Interior Thermal Insulations 340
R. Černý, J. Maděra, M. Jerman

Methods for Assessment of Utility Properties of Modified Calcium Sulfate Hemihydrates 342
R. Černý, P. Tesárek, P. Konvalinka

X-ray stress analysis of oxide layers formed on Zr alloys specimens with Zro2 coating 344
G. Gosmanová, I. Kraus

Effect of Alloying on the Microstructure of Aluminium Sheets Prepared by Accumulative Roll Bonding Process 346
M. Karlík, P. Homola

Deformation Induced Martensitic Transformation in Austenitic Stainless Steel 348
M. Karlík, P. Haušild, K. Kolařík

Usage of Binarized Image in Evaluation of Plastics and Composites 350
M. Černý, H. Harcová

Moisture Absorption of Carbon/ Epoxy Composites..... 352
M. Černý, D. Čuprová

Micro-mechanisms of Fracture in 15Ch2MFA Steel..... 354
Š. Válek, P. Haušild, M. Kytka

Fracture behaviour of Fe3Al based alloys with Cr and Zr addition 356
M. Karlík, P. Haušild, A. Kubošová, J. Prahl

Local Conditions at the Growing Fatigue Crack in CCT Specimens
of Different Thicknesses 358
A. Materna, O. Šimek, V. Oliva

Quantitative Texture Analysis by the Orientation-Distribution
Function (ODF) on the KSN-2 Diffractometer..... 360
L. Kalvoda, A. Grishin, S. Vratislav, M. Dlouhá

Effect of Austenitizing Parameters on Structural Characteristics
of Steels Type HSLACS. 362
J. Cejp, K. Macek

Welding of Commercially Pure Titanium..... 364
J. Cejp, Z. Kinter, J. Prajer

Laser Surface Treatment of 2024 – T3 Aluminium Alloy..... 366
J. Cejp, I. Pavlásková

Section 1

MATHEMATICS

Qualitative Properties of Some Mathematical Models of Fluid Mechanics

Michal Beneš

benes@mat.fsv.cvut.cz

katedra matematiky, stavební fakulta ČVUT v Praze, Thákurova 7, 166 29 Praha 6

In [1] we consider the mixed boundary value problem for the steady Navier-Stokes equations. Let Ω be a two-dimensional domain with corner points on boundary where the boundary conditions change their type. We suppose that Ω is a bounded domain, $\Omega \subset \boldsymbol{C}^{0,1}$. Further, we suppose that $\Omega = \Gamma_1 \cup \Gamma_2$ and Γ_2 are cosed, $\mathrm{meas}\Omega = \Gamma_1 \cap \Gamma_2 = 0$ and $\mathrm{meas}\Gamma_2 > 0$. We consider the steady Navier-Stokes problem with mixed boundary conditions

$$-\Delta \mathbf{u} + (\mathbf{u}.\nabla)\mathbf{u} + \nabla P = \mathbf{g} \quad \text{in } \Omega \tag{1}$$

$$\nabla \,.\, \mathbf{u} = 0 \quad \text{in } \Omega \tag{2}$$

$$\mathbf{u} = 0 \quad \text{on } \Gamma_1 \tag{3}$$

$$-P\mathbf{n} + \mathbf{u}'_n = 0 \quad \text{on } \Gamma_2 \tag{4}$$

Solution of this problem is a couple ($\mathbf{u}$, p), where $\mathbf{u}$ is a velocity and p is the pressure. The existence and local regularity of the weak solution of this problem is known. Our goal is to prove some regularity results near corner points, where the boundary conditions change. We get the regularity results in Slobodeckii and weighted Sobolev spaces. Using the well known imbeddings theorem between the weighted and classical Sobolev spaces we prove regularity of the weak solution in Slobodeckii spaces.

We also deal with the problem, in which (2)-(4) hold and in (1) the convective term "$(\mathbf{u}.\nabla)\mathbf{u}$" is not included. This problem is called the steady Stokes problem with the mixed boundary conditions. The Dirichlet boundary condition (3) expresses a non-slip behaviour of the fluid on fixed walls of the channel. The condition (4) expresses "do nothing" boundary condition. Essential problems are:

- How does the smoothness of the weak solution $(\mathbf{u}, P) \in [\boldsymbol{W}^{1,2}(\Omega)]^2 \times \boldsymbol{L}^2(\Omega)$ depends on the size of the angle at the corner in polygonal domain, i.e., how regular is the weak solution?
- How depends the convergence rate of numerical methods on the regularity of the weak solution $(\mathbf{u}, P)$?

Using regularity results for the weak solution $(\mathbf{u}, P)$ in corresponding weighted Sobolev spaces we prove the error estimate for the finite element approximations of velocity $\mathbf{u}_h$ and pressure P_h, i.e.

$$\| \mathbf{u} - \mathbf{u}_h \|^2_{[\boldsymbol{W}^{1,2}(\Omega)]^2} + \| P - P_h \|^2_{\boldsymbol{L}^2(\Omega)} = \boldsymbol{O}(h^{1-\delta}) \tag{5}$$

for certain sufficiently small δ, h is parameter of discretization by means of the finite element method.

In [2], a stationary Stokes problem equipped with mixed boundary conditions in polygonal domain have been analyzed. The regularity results, which are presented, are important for an error analysis of numerical methods, i.e., the regularity of the weak solution has a great influence over the rates of convergence for finite element methods. The main result is the proof of error estimate for finite element approximation of the weak solution in polygonal domain.

Now we consider the non-steady Navier-Stokes equations with homogeneous mixed boundary conditions. Let $T \in (0,\infty]$, $Q = \Omega \times (0,T)$. The formulation of our problem is as follows:

$$\mathbf{u}' - \Delta\mathbf{u} + (\mathbf{u}.\nabla)\mathbf{u} + \nabla P = \mathbf{g} \quad \text{in } Q \tag{6}$$

$$\nabla \cdot \mathbf{u} = 0 \quad \text{in } Q \tag{7}$$

$$\mathbf{u} = 0 \quad \text{on } \Gamma_1 \times (0,T) \tag{8}$$

$$-P\mathbf{n} + \mathbf{u}'_n = 0 \quad \text{on } \Gamma_2 \times (0,T) \tag{9}$$

$$\mathbf{u}(0) = \boldsymbol{\gamma} \quad \text{in } \Omega \tag{10}$$

$$\boldsymbol{\gamma} = 0 \quad \text{on } \Gamma_1. \tag{11}$$

We consider that the functions $\mathbf{g}$, $\boldsymbol{\gamma}$ are smooth enough.
In [3] we prove the existence and uniqueness of this problem on some time interval $(0, T^*)$ for sufficiently small T^*, $0 < T^* < T$.

References:

[1] BENEŠ, M.: *The qualitative properties of the Stokes and Navier-Stokes system for the mixed boundary problem in a nonsmooth domain.* Accepted in journal Mathematics and Computers in Simulation. 2006.

[2] BENEŠ, M.: *Regularity and FEM Error Estimates of Viscous Incompressible Stokes Flow in Polygonal Domains near Corners.* 5. matematický workshop s mezinárodní účastí - sborník, FAST VUT v Brně, 2006, pp. č. 23-24.

[3] BENEŠ, M. – KUČERA, P.: *Non-steady Navier-Stokes Equations with Homogeneous Mixed Boundary Conditions and Arbitrary Large Initial Condition.*. Fifth International Conference on Applied Mathematics – ICAM5, North University of Baia Mare, Romania, 2006, submited to Carpathian J. Math.

This research has been supported by CTU0600111.

The two-step method calibration of digital camera utilizing non-linear transformation

B. Koska, V. Obr*

bronislav.koska@fsv.cvut.cz

Department of Special Geodesy, *Department of Advanced Geodesy,
Faculty of Civil Engineering, Czech Technical University in Prague,
Technická 2, 166 27 Prague 6, Czech Republic

Resolution of digital cameras is growing up approximately one hundred percent a year in the last few years. That's why the number of its application is also rapidly increasing. On the other hand there isn't any radical technological improvement in the field of objective development. Therefore mathematical modeling of objective flaws is necessary in precise applications. There are presented suitability tests of plane transformations for digital camera objective distortion correction in the paper.

The precise plane calibration field was created at first. The number of control (identical) points is 300 and the field size is about 100x70 centimeters. The shape of control points is black annular ring with the outer radius four millimeters and the inner radius one millimeter. The shape is suitable for reading by planimeter and also for reading from digital images (it is aimed at the annular ring or the inner circle depending on image resolution). The calibration field was measured two times with double reading by planimeter made by Altec Corporation. The accuracy of one measuring is determined from two measuring differences and the standard deviation in both coordinates is approximately 0.04 millimeter (the standard deviation of average value is about 0.03 millimeter).

Then a few pictures were made by cameras Canon EOS D350 (reflex camera, eight mega-pixels) and Canon PowerShot S200 (compact camera, two mega-pixels, f5.4-10.8). There were used the high quality objective Canon EF 50 (f1.8) with fixed focal length and Tamron AF SP 28-75 (f2.8) with variable focal length. The chosen objectives suitably represent different quality categories.

Image coordinates of identical points were two times read by the software "odecitacv2" which was made by Ing. M. Štroner, Ph.D. This software enables a sub pixel selection of points by a method of RGB filter. After clicking into a pixel fulfilling the set filter, all neighboring pixels fulfilling the RGB filter are automatically selected and their average is calculated. The standard deviation of read coordinates was determined from multiple points reading. It is in the interval from 0.05 to 0.2 pixels depending on the used image.

The library Alltran [1] was used for assessing of transformation suitability. Alltran is a library of classes and function for computation of transformation key and for transformation of coordinates. It was suggested especially for transformations based on the least square method. All included transformations are in close relation with the branch of geodesy and photogrammetry. The library is written in C++ language under the condition of General Public Licence GNU. The simple console program Alltran_console was created for using the library and another one Alltran_test for testing of the suitability of used transformations.

The modified program Alltran_test was used for testing. The program uses set percent of randomly chosen points for transformation key computation (identical points) and left points (testing points) are transformed using the key and are compared by computing standard deviation of coordinates in global coordinate system (image system). The file vector_field.txt is also generated. The file contains read and transformed image coordinates of testing points. The vector field is graphically showed by program in Matlab (the scale for vector is ten). We used

fifty percent (about one hundred identical points) and suitability percentage for getting 20 identical points for each image. These numbers are in accordance with numbers of control points of plane and spatial calibration fields used in practice.

The following transformations were used for testing (the transformation names in the library Alltran are placed in parenthesis): collinear (dlt_2d, also called projective, etalon with full distortion), collinear with polynomials for radial distortion removing (dlt_2d_rd), collinear with polynomials for radial distortion removing with the ideal center (dlt_2d_rd2), collinear and thin plate splines [2] (dlt_2d_plus_tps_2d), dlt_2d_rd2 and thin plate splines (dlt_2d_rd2_plus_tps_2d), collinear and polynomials for radial distortion removing (dlt_2d_plus_rd), collinear and polynomials for radial distortion removing with the ideal center (dlt_2d_plus_rd2), collinear and plane quadratic (dlt_2d_plus_quadratic_2d), collinear and plane cubic (dlt_2d_plus_cubic_2d), collinear and plane quartic (dlt_2d_plus_quartic_2d).

The main criterion for assessing of transformation suitability is standard deviation of testing point coordinates and visual checking of nonsystematic influence in vector field. Thin plate splines transformation gives the best results for large number of identical points (about one hundred), but cubic and quartic transformations give only little bit worse results. The best result for approximately twenty identical points has the transformation titled above dlt_2d_rd2_plus_tps_2d, but similar results have also dlt_2d_rd, dlt_2d_rd2 and cubic transformation.

The test results of transformation for removing of digital camera objective distortion are presented in the paper. The significant influences of different objective quality and different point numbers were considered. Cubic transformation seems to be the most universal solution and it is useful under all tested conditions.

The presented results are directly applicable in methods of one-image photogrammetry and indirectly for distortion solving in the others photogrammetric methods.

References:

[1] B. KOSKA: *Project Alltran* [cit. 2.1.2007] http://k154.fsv.cvut.cz/~koska/projects/alltran/alltran.htm

[2] OBR, V.: Thin-Plate Splines transformation as a power tool for elimination geometric deformation of DTP scanners, Physical and material engineering 2005. Praha, 2005, p. 163-165.

This research has been supported by CTU grant No. CTU0604411.

Implementation of Many-Valued Sequential Systems

Milan Petrík

petrikm@cmp.felk.cvut.cz

Center for Machine Perception, Department of Cybernetics
Faculty of Electrical Engineering, Czech Technical University
Technická 2, 166 27 Prague 6, Czech Republic

The importance of memory circuits in the hardware design is crucial considering that they enable implementation of sequential logical circuits, i.e. logical circuits where the output value depends also on the previous values of the input. Furthermore, they allow to build registers, to synchronize combinational logical circuits, etc.

Therefore if we want to design many-valued hardware at least as strong as the classical two-valued one, we will need a way of implementing a many-valued memory circuit. A *memory circuit* is a logical circuit able to remember a logical value and to hold it on its output for a defined period of time regardless of its input. It usually has two types of input, D and T, and an output Q. Input T determines whether the memory circuit is *open* (the value of input D is "passed" to output Q) or it is *closed* (the old value of output Q is kept regardless of input D). Input T usually has the form of a periodic rectangular signal (called the *clock signal*).

Two groups of memory circuits are distinguished: *Level-controlled* and *edge-controlled*. Level-controlled memory circuits are open or closed depending on the value of input T while edge-controlled memory circuits are open when input T changes its value from one defined value to another defined value, otherwise they are closed.

As it has been mentioned above memory circuits are used to synchronize combinational logical circuits. This means that singular parts of combinational logical circuits are separated by memory circuits; inputs T of the memory circuits are synchronized by a periodic rectangular clock signal oscillating between 0 and 1. The output value given by the combinational circuits is then stored to the memory circuits where it is hold until the start of the next cycle. This way of constructing logical circuits assures that the signal

is spread through combinational logical circuits uniformly and it prevents various hazards.

For this purpose edge-controlled memory circuits show to be a better solution. Comparing to level-controlled memory circuits the duration of the open state is much shorter than the duration of the closed state. Since during the open state the input of a memory circuit must remain constant it can be seen that the synchronization by edge-controlled memory circuits allows a higher frequency of the clock signal; this makes the whole logical circuit faster.

Fuzzy memory circuits have been already studied in a number of papers; e.g. the memory circuits studied by Ozawa, Hirota, and Koczy or the sequential systems studied by Pedrycz and Hirota or other approaches.

In this paper we bring a different solution based on a generalization of the R-S memory circuits known from the two-valued logical circuits. We show a way of implementing memory circuits in the model of many-valued logical circuits which is based on a generalization of the R-S memory circuit known from the classical logical circuits. We present the standard fuzzy Sheffer operation defined as $\underset{S}{\wedge}(x, y) = 1 - \min(x, y)$, which shows as suitable for the generalized R-S memory circuits. With this operation the many-valued R-S memory circuit has similar properties as the classical one allowing to store a fuzzy logical value, i.e. a value from the real interval $[0, 1]$. This memory circuit moreover allows to build more complex memory circuits as a level-controlled many-valued memory circuit and an edge-controlled many-valued memory circuit. Yet the operation of standard fuzzy Sheffer operation is not the only possible; we discuss the general many-valued R-S memory circuit and we find the set of all possible operations which can be used. We also discuss the problem of a feedback in many-valued logical circuits and we show that a many-valued memory circuit cannot generaly store any value from the real interval $[0, 1]$. The set of the values which can be stored in such a circuit must be a discrete subset from the interval $[0, 1]$.

This research has been supported by CTU grant No. CTU0608513.

Enhancement of Technical Applications in the Subject Mathematics for Aeronautical Branches at the Faculty of Transportation Sciences, CTU

Magdalena Hykšová

hyksova@fd.cvut.cz

Department of Applied Mathematics, Faculty of Transportation Sciences,

Czech Technical University, Na Florenci 25, 110 00 Prague 1, Czech Republic

The aim of this contribution is to report on the results of the project *Enhancement of Technical Applications in the Subject Mathematical Analysis for the Branches Professional Pilot and Technology of the Aircraft Maintenance at the Faculty of Transportation Sciences of the CTU*, supported by the Universities Development Fund of the Czech Republic.

In the connection with the establishment of the structure studies at the Faculty of Transportation Sciences of the Czech Technical University in Prague, two new study branches were successively founded: *Professional Pilot* and *Technology of the Aircraft Maintenance*. To meet the requirements for technical knowledge and skills, the teaching of mathematical subjects was substantially reduced. In comparison with other study branches, two mathematical subjects are missing there: *Algebra and Graph Theory* in the first semester and *Differential and Difference Equations* in the third semester. At the beginning the students of the aeronautical branches visited the courses *Mathematical Analysis I, II* together with the students of all other programs; their mathematical education was therefore somewhat inconsistent, calling for an innovation.

To provide consistent mathematical grounds even in this reduced form and to cover the knowledge necessary in other subjects, two separate subjects oriented to mathematical analysis were formed, namely *Mathematics for Aeronautical Branches I, II*, designated solely for students of the branches *Professional Pilot* and *Technology of the Aircraft Maintenance*. It was necessary to conceive the subjects in such a way that they form a consistent whole with some parts taught usually in the first two semesters of mathematical analysis replaced by the fundamental knowledge of algebra and the theory of differential equations. Moreover, technical applications of a theoretic subject matter were enhanced. The project reflected the increasing need to motivate students to study mathematics and to show them that mathematics is exceptionally important, useful, interesting and closely related to many other domains that they meet during their further studies.

For both subjects study materials based on the mentioned innovation were created, namely Internet pages, interactive study text and the collection of solved and unsolved problems and exercises, stressing practical applications in transportation engineering and other technical and economic domains. The text corresponds to the modified content of the course, incorporating the necessary parts of algebra and the theory of differential equations into the usual areas of introductory mathematical analysis. All materials were prepared with the program LATeX and transformed into the format PDF whose display is independent of a specific browser (unlike many other formats). Together with a detailed list of available

Czech and foreign literature, requirements for an examination and other information and interesting links, the materials are available at the following Internet addresses:

http://euler.fd.cvut.cz/predmety/ml1 and *http://euler.fd.cvut.cz/predmety/ml2*

The materials for both subjects have already been used in praxis and they have proved useful.

In the first semester the students are acquainted with the foundations of linear algebra and one-variable calculus, that is, with both linear and calculus-based models. From the methodological point of view, an outstanding source of application examples in the field of algebra is represented by the book [4] by Alan Tucker that is remarkable also for the way of exposition. Inspired by this approach, the part of the created text dealing with algebra proceeds in a similar way: the basic concepts of linear algebra (vectors, matrices and operations with them, inverse matrices, determinants, vector spaces, systems of linear equations) are always first introduced intuitively, with the help of their practical interpretation that is familiar to everyone, and only then in the usual abstract way. This part seems to be a favourite with the students, since it is possible to use simple and illustrative models to demonstrate the motivation of the fundamental concepts and their close relation to practical problems.

Also all parts devoted to mathematical analysis try to prepare the students for technical applications that will come in their further study. Theoretic exposition is interlaced with understandable utilization of theoretic concepts and methods. The usual applications of calculus in physics and economy (including optimization problems leading to searching extremes of functions of one or more variables) are supplemented with the use of calculus in such domains as for example traffic flow modeling and simple routing problems. For the area of differential equations, a remarkable source of inspiration for preparing the course is represented by the book [3] by George F. Simmons that combines a highly rigorous exposition with the applications in the fields of physics, chemistry, biology, engineering, economics and other fields of applied sciences.

Any study material is useless without an interest and effort of students and it cannot substitute their hard work. Nevertheless, it can help them to find the way to the world of mathematics and to discover at least a small part of its potential.

References:

[1] HYKŠOVÁ, M.: *Matematika v praxi, In: Kombinované studium na VŠCRHL, 1. semestr,* VŠCRHL, 2003, 37 pp. [textbook on CD-ROM].

[2] HYKŠOVÁ, M.: *Modul Matematika - dle Jar-66.* Cerm, 2003, 114 pp. [textbook].

[3] SIMMONS, G. F.: *Differential Equations with Applications and Historical Notes* McGraw-Hill, 1991, 629 pp.

[4] TUCKER, A.: *Linear Algebra. An Introduction to the Theory and Use of Vectors and Matrices,* Macmillan, 1993, 440 pp.

This research has been supported by the Universities Development Fund of the Czech Republic, grant FRV 744/2006.

Section 2

PHYSICS

Study of Thin Metallic Sputtered Layers

P. Buchar

bucharp@fel.cvut.cz

Department of Electromagnetic Field, Faculty of Electrical Engineering,
Czech Technical University, Technická 2, 166 27 Prague 6, Czech Republic

For their special properties, thin metallic layers have been investigated in many laboratories all over the world. They can be applied, e.g., in the field of so-called active packaging or electromagnetic shielding. For correct application, their impedance, or resulting reflection coefficient and other scattering parameters, must be known.

Within the frame of this work, electrical properties of sputtered metallic layers were investigated. The main feature of sputtered layers is that they are inhomogeneous for short sputtering times – layers consist of disconnected metallic islands. Modelling of their electrical properties was based on this fact. Metallic islands are replaced by metallic spheres that are well described analytically. Spheres are distributed on an aperture. The sputtering process itself is simulated by decreasing the distance between spheres or by increasing their number.

The set of spheres is illuminated by a plane electromagnetic wave. The interaction of the wave with spheres may be described in several ways.

The first way is taken from [1]. The spheres are described by their polarizability, for which an analytical formula exists. Electrical dipole moment induced in the spheres by the incident wave and resulting electrical field is calculated and, subsequently, equivalent impedance of the layer is derived in analytic form.

The second way was derived within the frame of this work. It describes spheres by their mutual capacities. The value of the capacity is calculated on the basis of a known analytical formula and the value of the equivalent impedance is calculated from this.

The third way is modelling of the structure by software simulator CST Microwave Studio, which provides directly scattering parameters.

For long sputtering times spheres merge to form a continuous block. Then, the equivalent impedance of the layer may be easily obtained from an analytical formula. It is equal to the square resistance of the layer given by layer conductivity and layer thickness. The equivalent impedance of the layer or its scattering parameters can be also obtained numerically using the CST Microwave Studio software.

When modelling thin layers, the fact that effective conductivity of such layers is lower than conductivity of gold material must be taken into account. This fact has been proved in, e.g., [2] and is caused by microscopic behaviour of electrons in layers. The thinner the layer is the lower the conductivity is. For layers having several nanometres or tens of nanometres in thickness, the conductivity is reduced by several times.

Several models were introduced to describe the reduction in conductivity by analytical formulas. However, experiments showed [3] that the conductivity of real sputtered layer is even lower than that predicted by models. This is caused by the fact that the sputtered layer is porous, while models expect homogeneous flat layers. Thus, the experimentally measured conductivity has been used in our models.

Reflection coefficient of the layer as a function of sputtering time was calculated. Gold layer illuminated by a plane wave of frequency of 10 GHz was assumed. Results show that for short sputtering times the reflection coefficient is low and the equivalent impedance has capacitive character. This corresponds to the state when the layer consists of disconnected spheres. At a certain sputtering time, the reflection coefficient quickly arises. This corresponds to the first

mutual touch of spheres and the creation of the first conducting path. For long sputtering times, the reflection coefficient slowly grows to unity, as the layer becomes more and more homogeneous and thicker. The equivalent impedance of the layer is purely resistive.

The reflection coefficient of the layer calculated by all models has been compared with measured reflection coefficient. A relatively good accord has been found. The advantage of analytical models is that the result is computed quickly by analytical formulas; its disadvantage is that they assume only regular distribution of spheres and cannot assume random distribution. The advantage of numerical model in CST Microwave Studio is its versatility; its disadvantage is comparatively long computation time and computer memory exigency.

MIM (metal-insulator-metal) structures have been also widely investigated. According to, e.g. [4], several interesting electrical phenomena, such as negative differential difference or electroluminescence, occur in MIM structures, where insulator has several tens or hundreds of nanometres in thickness. The aim of this work was to prepare such structures, and to measure and assess VA characteristics.

Within the frame of this work, metal layers with thickness of approx. 50 nm were prepared by sputtering. Insulator layer of approx. 200 nm was made from polystyrene by spin coating.

VA characteristics were measured under low pressure. According to available equipment, used pressure was in the order of 10^2 Pa, and 10^0 Pa. For small voltages current was very small – in the order of 10^{-12} – 10^{-9} A. At a certain voltage a quick increase in current to approx. 10^{-8} A occurred. This phenomenon is called electroforming and occurred at approx. 80 V under the pressure of 10^2 Pa and at approx. 20 V under the pressure of 10^0 Pa. Significant current fluctuations occurred during electroforming.

According to literature, this phenomenon should be followed by decreasing current with increasing voltage, i.e., so-called negative differential resistance should occur. However, during measurement within the frame of this work, this phenomenon was found only in two cases and was not repeatable.

Further research is necessary in this field. According to literature, searched phenomena should be significant under even lower pressures that have been so far available for this work.

References:

[1] TRETYAKOV, S.: *Analytical Modeling in Applied Electromagnetics* ARTEC HOUSE INC., 2000.

[2] HANSEN, R. C. – PAWLEWICZ, W. T.: *Effective Conductivity and Microwave Reflectivity of Thin Metallic Films* IEEE Transaction on Microwave Theory and Techniques, vol. 82, 1982, pp. 2064–2066.

[3] ŠVORČÍK , V. – ZEHENTNER, J. – RYBKA, V., – SLEPIČKA, P. – HNATOWITZ, V.: *Characterization of thin Au layers on PET: discontinuous to continuous, homogenous layer* Applied Physics A 75 2002 pp. 541–544.

[4] DEARNALEY, G. – STONEHAM, A. M.: *Electrical phenomena in amorphous oxide films* Reports on Progress in Physics, Volume 33, Issue 3, 1970 pp. 1129–1191.

This research has been supported by CTU grant No. CTU0606413.

Diagnostics of Radiation and Nuclear Processes in High-parameter Plasma

P. Adámek, L. Drška

adamek@kfe.fjfi.cvut.cz

Czech Technical University, FNSPE, Prague, Czech Republic

Studies of matter with high density of energy involve, as a crucial diagnostic technique, analysis of x-ray spectra emitted by hot dense plasma. Spectral line intensities, shapes and shifts reveal important information about the physical parameters and the phenomena related to the creation and evolution of hot dense plasmas as well as the information about the potential existence or non-existence of the laser-induced nuclear excitation processes.

Decomposition of measured emission spectra into individual spectral lines represents an example of a global optimization problem, which usually cannot be efficiently solved by traditional optimization techniques. The well-known algorithms incorporated into most of the standard spectral analysis packages (based e.g. on Levenberg-Marquardt or downhill-simplex methods) can be successfully used for simple spectra with well-separated peaks and low noise levels. The analysis of complex noisy spectra containing overlapping peaks requires an application of robust optimization methods. Improved optimization tools often benefit from the genetic algorithm (GA) approach. The GAs solve global optimization problems by examining typically hundreds or thousands of trial solutions encoded into data structures called genomes. The algorithm starts with a set of randomly generated genomes defining the first-generation population. The selective exploration of the search space is performed by applying genetic operators to the solutions - randomly combining and perturbing them and choosing the better ones according to the survival-of-the-fittest philosophy. The principle of working with a large number of solutions at once constitutes the main difference between evolutionary methods and most of the other global optimization methods. However, the way of encoding the physical problem into genomes as well as the actual methods of crossover, mutation and selection depend on the problem itself. Although there are general concepts of applying the GA to any optimization task, the GAs tailored to the specific problem generally show significantly better performance in terms of stability and convergence.

This contribution presents a new version of genetic-algorithm-based code GASPED [1] [2] developed for the analysis of x-ray line spectra emitted by hot dense plasmas. The problem-dependent modification of standard genetic algorithm concepts allows efficient decomposition of spectroscopic data with utilization of complex models of spectra and various information supplied by atomic codes. Compared to a common GA, our algorithm includes several new genetic operators designed to move through the search space more effectively, a problem-dependent genome structure (consisting of a variable number of spectral lines and a background component), and several techniques preventing premature convergence, which is a common problem of GA and other evolutionary optimization methods. The advantage of the algorithm is the ability to work with additional constraints imposed on particular sought parameters. Several lines can also be grouped together by introducing additional common parameters (e.g., the group shifts of the parent transitions and their satellites).

In the papers [3] [4], GASPED was applied to the decomposition of precise K-shell spatially-resolved time-integrated spectra emitted from highly stripped Al ions immersed in

dense, constrained-flow plasma. The spectra were resolved into particular pseudo-Voigt components and a background component by using anticipatory theoretical knowledge of the satellite structure simulated by the multilevel collisional-radiative atomic code. Assuming the aggregate plasma-induced shifts of the parent lines and their satellites, it was found that the trends in the line shifts of the resonance and intercombination line observed as a function of the variable plasma parameters qualitatively follow the predictions of the quantum mechanical impact theory.

The algorithm was also used in the search for low-lying nuclear transitions in hot dense laser-produced plasmas [4]. The spectra of highly ionized Ta were decomposed by combining the GASPED code with results of atomic calculations. Utilizing the results of decomposition performed with two models of Ta spectra (both including and excluding the nuclear transition line), the upper limits for observation of the controversial radiative decay of Ta nuclei at 6.238 eV were estimated.

In both above mentioned applications of the code, the data included a large number of overlapping peaks and a severe noise with a relatively low signal-to-noise ratio (e.g. the mutual line shifts estimated from the K-shell spectra are very sensitive to the robustness of decomposition technique). In terms of spectral decomposition as an optimization problem, this constitutes a multidimensional objective function with many local optima, making the problem of decomposition extremely difficult. In most cases, however, GASPED was able to find a very good solution in a relatively short time (typically minutes on a common workstation PC). Repeated runs of the code with the same input data revealed a good stability of the method.

We have shown that a problem-dependent genetic algorithm can significantly contribute to the advanced analysis of complex emission spectra. The code was successfully used to decompose x-ray spectra emitted by plasma produced by laser-irradiated Al and Ta targets. Compared to traditional decomposition techniques, the problem-dependent approach allowed us to work with complex models of spectra including numerous constraints, leading to more precise and physically interpretable results.

References:

[1] P. ADÁMEK: *Application of Genetic Algorithms to Analysis of High-Parameter Plasma* Diploma Thesis, CTU-FNSPE, 2004.

[2] P. ADAMEK, L. DRŠKA, O. RENNER: *Evolutionary Methods in HED Matter Diagnostics.* In: 26th Workshop on Physics of High Energy Density in Matter, Hirschegg, January 29 - February 3, 2006. http://vega.fjfi.cvut.cz/docs/hirschegg26p/.

[3] O. RENNER, P. ADAMEK, P. ANGELO, E. DALIMIER, E. FÖRSTER, E. KROUSKY, F. B. ROSMEJ, R. SCHOTT: *Spectral line decomposition and frequency shifts in Al He-α group emission from laser-produced plasma.* Journal of Quantitative Spectroscopy & Radiative Transfer 99, 2006 523–536.

[4] P. ADAMEK, O. RENNER, L. DRŠKA, F. B. ROSMEJ, J.-F. WYART: *Genetic algorithms in spectroscopic diagnostics of hot dense plasmas.* Laser and Particle Beams 24, 2006, 511–518.

This research has been supported by CTU grant No. CTU11-86111 and by the Grant Agency of the Czech Republic under contract No. 202/06/0697.

Coherently Pumped Broadly Tunable Cr:ZnSe laser

P. Koranda*, H. Jelínková*, J. Šulc*, M. E. Doroshenko, V. K. Komar*****

koranda@troja.fjfi.cvut.cz

*Department of Physical Electronics, Faculty of Nuclear Sciences and Physical Engineering, Czech Technical University, Břehová 7, 115 19 Prague 1, Czech Republic

**Laser Materials and Technology Research Center, General Physics Institute, Vavilov Str. 38, 119991 Moscow, Russia

***Institute for Single Crystals, 60 Lenin Ave., Kharkov, Ukraine

Solid-state compact room-temperature operating laser radiation sources emitting broadly continuously tunable laser radiation are desired in many applications such as spectroscopy, ranging, remote-sensing, medical diagnosis and treatment, and also for pumping of nonlinear (OPO) and other laser materials.

The Cr:ZnSe is a promising laser active material from the group of transition metal ion-doped II-VI semiconductor compounds. From the spectroscopic evaluation the absorption spectrum was detected to be from 1500 up to 2050 nm and the emission spectrum from 2100 up to 2900 nm.

Up to now the Cr:ZnSe active material samples investigated by other groups was produced entirely by the diffusion-doped technique [1,2,3]. The dimensions of these crystals are limited to few millimeters and the concentration of Cr^{2+} active ions in the ZnSe matrix is not homogenous in the whole sample.

From the above mentioned disadvantages we have investigated the Cr.ZnSe crystals produced by the Bridgman technique which enables to produce larger samples (up to several centimeters) with the homogenous concentration profile of the Cr^{2+} active ions inside the crystal. The investigated crystals was produced in the Institute for Single Crystals, Ukraine. The aim of this study was to demonstrate the laser operation in Cr:ZnSe laser crystals produced by Bridgman technique, to measure the laser output characteristics in pulsed and continuous-wave regime, and to perform the laser emission wavelength tuning.

During our study we have investigated Cr:ZnSe crystals with dimensions 10x10x6 mm and the Cr^{2+} concentration $1x10^{19}$ cm^{-3}. For the purpose of coherent longitudinal pumping of the investigated Cr:ZnSe crystals we have constructed and optimized pulsed flashlamp-pumped Er:YAP laser (emitting wavelength 1658 nm) and diode-pumped Tm:YAP laser (emitting wavelength 1970 nm, operating in pulsed as well as in continuous-wave regime). The emitting laser radiation of both mentioned lasers is effectively absorbed in the Cr:ZnSe.

In the first step we have constructed the fundamental Cr.ZnSe laser coherently longitudinally pumped with the Er:YAP laser radiation. The maximal Er:YAP pulse energy used for pumping was 200 mJ, the maximal pulse duration was 200 μs FWHM, the repetition rate was set to be 1 Hz. The Er:YAP laser radiation was focused by the CaF2 lens (f = 100 mm) inside the Cr:ZnSe crystal. The optical resonator of the Cr:ZnSe laser consisted of the two plane dielectric mirrors (1 - high reflective mirror for laser radiation and high transparent mirror for the pump radiation, 2 – high reflective for pump radiation and R ~ 60% for wavelength 2100-2600 nm). The maximal output pulse energy of the Cr:ZnSe laser was 14 mJ for the absorbed energy 23 mJ (slope-efficiency was 61%). To perform the laser emitting wavelength tuning the dispersive prism was inserted and adjusted inside the optical

resonator. The continuous laser emitting wavelength tuning was demonstrated in the range from 2160 nm to 2600 nm with the drop of the maximal output pulse energy to 6 mJ.

In the following step we have constructed and optimized Cr:ZnSe laser coherently longitudinally pumped with the diode-pumped Tm:YAP laser. The maximal Tm:YAP laser output pulse energy was 45 mJ (for pulse duration 10 ms and repetition rate 10 Hz) and the maximal output power was 2.9 W in the continuous-wave regime. The laser emission wavelength was measured to be 1970 nm.

The Tm:YAP laser radiation was focused inside the Cr:ZnSe laser crystal by the CaF_2 lens (f = 55 mm). The optical resonator of the Cr:ZnSe laser was formed by the flat dielectric mirror (highly transparent for the pump Tm:YAP laser radiation and highly reflective for wavelength from 2100 nm to 2900 nm) and the concave dielectric output coupler (R ~ 96% for radiation wavelength from 2100 nm to 2600 nm, r = 150 mm). The resonator length was 34 mm.

In case of pulse regime the maximal output energy was 3.2 mJ for the absorbed energy 5.3 mJ (slope-efficiency was 60%, pulse duration 10 ms, repetition-rate 10 Hz).

In case of continuous regime the maximal output power was 200 mW for the absorbed power 300 mW (the slope-efficiency was 67%).

The spectrum of the output Cr:ZnSe laser radiation covered the interval from 2120 nm to 2380 nm.

The dependency of maximal Cr:ZnSe laser output energy and laser threshold in relation to the reflectivity of the used output coupler was measured. Therefore, the Findlay-Clay analysis was carried out and as a result the round-trip intracavity loss value of the Cr:ZnSe optical resonator was estimated to be 1.72%.

In this study we have demonstrated the laser operation in Cr:ZnSe laser crystals produced by Bridgman technique. We have measured the output characteristics of the Cr:ZnSe lasers pumped either with Er:YAP laser (in pulsed regime) or with Tm:YAP laser (in pulsed and continuous-wave regime). We have performed the continuous Cr:ZnSe laser emission wavelength tuning in the broad range from 2160 nm to 2600 nm.

References:

[1] DELOACH, L.D. – PAGE, R.H.: *Chromium-Doped Zinc Chalcogenide laser* Journal of Quantum Electronics, 1996, pp. 885.

[2] SOROKINA, I. T. – VODOPYANOV, K. L.: *Solid-State Mid Infrared Laser Sources* Springer-Verlag , 2003 .

[3] DEMIRBAS, U. – SENNAROGLU, A.: *Continuous-Wave Fiber-Pumped Cr2+:ZnSe Laser* Proceedings of SPIE, 2006, 0A-1.

This research has been supported by CTU0611214.

Atmospheric Turbulence Influence on the Precision of Laser Rangefinders

L. Král, I. Procházka, K. Hamal

krall@troja.fjfi.cvut.cz

Faculty of Nuclear Sciences and Physical Engineering, Czech Technical University,
Břehová 7, 115 19 Prague 1, Czech Republic

Laser ranging is a well-established technique of non-contact measurement of a distance between an observer and a target by measuring the time of flight of a laser pulse, which is emitted towards the target and then reflected back to the observer. However, the accuracy of such measurement depends on precise knowledge of the light speed along the beam path, which usually leads through the Earth's atmosphere. Reliable models of air refractive index temperature and pressure dependence are available for this purpose [1]; however, there is also a random fluctuation of the air refractive index, which is completely unpredictable: *the optical turbulence*. This refractive atmospheric turbulence originates in turbulent mixing of air of different temperatures, resulting in rapidly varying random fluctuations from the average air refractive index.

The initial motivation of our research was to determine all the individual contributors to the satellite laser ranging (SLR) error budget. SLR is routinely used for determining the distances of Earth-orbiting satellites placed at orbits up to 20 000 kilometers high. Among the applications of the SLR data, gathered by a worldwide network of stations, are geodesy and geodynamics, remote sensing, navigation systems, as well as fundamental research like tests of the General Theory of Relativity. The SLR accuracy is being constantly improved: currently, the best stations achieve single shot precision of 3 mm RMS and accuracy of 1 cm RMS. We are especially interested in further improvement of the SLR precision, which requires an analysis of all the random error sources such as detector timing uncertainty, laser pulse width, etc. The worst known contributor was the atmospheric turbulence – the refractive index fluctuations introduce unpredictable random errors to the measured range, because they influence the optical path length of the beam, and cannot be corrected.

We tried to find or develop a model of the turbulence-induced ranging errors magnitude as a function of the turbulence strength along the beam path. Our first attempt was to use a commercial version of the GLAD code for numerical modeling of this problem. GLAD (General Laser Analysis and Design) is an extensive computer program for modeling of diffractive propagation of light through various optical devices and media. The electromagnetic field in GLAD is described by its two-dimensional transversal distribution (amplitude and phase arrays).

We developed a GLAD model of the laser beam propagation through the turbulent atmosphere, consisting of several alternating steps of random wavefront aberration and diffractive propagation. However, the developed model predicted extremely small turbulence-induced errors (of the order of micrometers), which did not correspond to our preliminary estimates. According to recent findings, the reason is that GLAD internally uses a model of the turbulence-induced aberrations that is not suitable for this particular task. Therefore, we tried to find another suitable model.

Another approach has been introduced by Gardner [2], who derived equations describing this problem analytically on the basis of geometrical optics. With application of up-to-date standard models of turbulence strength height profile, we used the Gardner's model to predict the turbulence-induced SLR jitter: the results were of the order of 0.1–1 mm RMS for common observing conditions, which looked quite realistically.

It was necessary to obtain an experimental proof of these theoretical predictions. We took advantage of a long-term cooperation with the satellite laser station in Graz, Austria, which is among the most precise SLR stations in the world, and performed a series of experiments with high precision, high repetition rate laser ranging, using a ground-based targets as well as low-orbit satellites. We developed a special algorithm for analysis of the acquired data to reveal the tiny turbulence-induced fluctuations that are mixed together with the instrumental noise. The amplitude of the turbulence-induced jitter was within the range predicted by the Gardner's model, i.e. up to one millimeter RMS.

To obtain a direct evidence of applicability of the Gardner's model, we needed to correlate the measured turbulence-induced ranging jitter with the instantaneous turbulence strength. The turbulence strength is proportional to a quantity named astronomical seeing that can be measured by optical telescopes equipped with fast CCD cameras. We tried several techniques of the seeing measurement: differential image motion monitoring (DIMM) [3], scintillometry, etc. Finally, we purchased a special camera for seeing monitoring, developed our custom software package, and used it together with a small telescope as a "portable seeing monitor", which underwent extensive testing at the Vyškov astronomical observatory.

Finally, the seeing measurement allowed us to determine the instantaneous turbulence strength along the laser rangefinder beam path, and to compare it with the observed turbulence-induced ranging jitter. The resulting dependence is in good agreement with the Gardner's equations, both for the horizontal paths and the slant paths to space [4]. Hence, we obtained a proven model that enables us to estimate the turbulence contribution to the laser ranging error budget under various observing conditions.

References:

[1] KILLINGER, D. K. – CHURNSIDE, J.H. – ROTHMAN, L. S.: *Atmospheric optics. In Handbook of Optics.* McGraw-Hill 1995, vol. 1, chapt. 44.

[2] GARDNER, C. S.: *Effects of random path fluctuations on the accuracy of laser ranging systems.* Applied Optics 15, 1976, pp. 2539–2545.

[3] SARAZIN, M. – RODDIER, F.: *The ESO differential image motion monitor.* Astronomy&Astrophysics 227, 1990, pp. 294–300.

[4] KRÁL, L. – PROCHÁZKA, I. – HAMAL, K: *Random fluctuations of optical signal path delay in the atmosphere.* Optics in Atmospheric Propagation and Adaptive Systems IX: Proceedings of SPIE vol. 6364, 2006.

This research has been supported by grant CTU0611414 of the Czech Technical University.

Mode-locked Nd:YVO4 Laser with Intracavity Synchronously Pumped Optical Parametric Oscillator for Laser Sensor and Gyroscope

A. Zavadilová*, V. Kubeček*, J-C Diels**

zavadilo@troja.fjfi.cvut.cz

*Fakulta jaderná a fyzikálně inženýrská, Břehová 7, 115 19 Praha 1

**University of New Mexico, Department of Physics and Astronomy and Center for High Technology Materials, 800 Yale Blvd. NE, 87131 Albuquerque, NM, USA

The topic of this report is a mode-locked laser that generates two interwoven frequency combs. A mode-locked laser can be turned into an ultrasensitive phase interferometer, if two pulses are made to circulate simultaneously in the cavity, with no phase coupling between their carrier frequencies. In the time domain, this corresponds to a laser cavity in which two pulses circulate, meeting at each round trip at the same location. Any differential path length experienced by the two pulses results in a difference in carrier frequency between the two pulse trains [1]. This frequency difference can be measured as a beat note, by making the pulse trains interfere on a detector. This conversion of phase differential into frequency can be exploited for sensing applications like inertial sensing (rotation and acceleration), magnetic field measurements, and nonlinear index (with an accuracy of 10^{-21} cm^2/W). The accuracy of the measurement is limited by the bandwidth of the beat note, which has been shown to be of the order of 1 Hz (hence considerably narrower than the bandwidth as the individual modes of the laser), bandwidth that can be reduced through active cavity stabilization techniques.

The main technical challenge is to design a laser configuration ensuring identical repetition rate for the two pulses, and two crossing points (of these pulses) in air or vacuum, to prevent any coupling that would eliminate the beat note, through mutual injection locking of one circulating pulse into the other. In our laser system two pulses are created in the signal cavity, at each passage of the pump pulse through the OPO crystal. The repetition rate of the pulses in the signal cavity is determined only by the pump cavity length. The location of the pulse crossing points can be set by the location of the OPO crystal in the pump cavity to be remote from any scattering optical element. Finally, the fact that the crystal shares the pump and signal cavity, ensures that the two circulating signal pulses share the same spatial mode of the OPO cavity. The OPO crystal introduces coupling between the pump and signal cavities, that can result in complex dynamics. For applications such as accelerometer, displacements or index of refraction variations a linear cavity as is preferred. The set up can be modiffed into a (signal) ring cavity for gyro applications.

The first task was to develop the stable mode-locked pumping laser. We compared two different mode-locking methods - mirror with solid state saturable absorber, and nonlinear mirror with generation of second harmonic frequency from the point of view of best stability of the cw mode-locked regime against Q-switched operation, and long term stability. Because of its better performance, a $Nd:YVO_4$ laser mode-locked with semiconductor saturable absorber as OPO pump source [2] was selected. The active medium of the pump laser is a 5 mm long AR coated $Nd:YVO_4$ crystal (Nd doping 0.5 %), placed in a water-cooled copper heat sink. The crystal is end pumped by a 20 W 808 nm laser diode (LIMO

type HLU 20F400-808) coupled with an optical fiber of 400 μm diameter and a numerical aperture of 0.22. The optical length of both resonators (pump Nd:YVO_4 laser and OPO) is the same corresponding to the pulse repetition rate around 132 MHz. Both resonators are nearly symmetrical with respect to the position of the PPLN crystal.

In our case a periodically poled magnesium doped lithium niobate crystal (MgO:PPLN) was chosen as nonlinear medium for OPO. The advantages of using MgO doped $LiNbO_3$ over undoped, are better performance, poling quality and stability, a higher damage threshold, and less sensitivity to photorefractive damage. The crystal (20 mm long), contains single grating with period of 30.3 μm that corresponds to OPO signal wavelength of 1526 nm for 1064 nm pump at room temperature. To avoid back reflections from the crystal end faces, they were cut under Brewster angle of 64.5° Tunability of the OPO radiation was achieved by inserting the PPLN crystal in a heated copper holder, capable of maintaining a stable crystal temperature in the range of 25 to 50°C.

The threshold pump power of the Nd:YVO_4 laser, including all intracavity elements, is as low as 2 W. Stable continuous mode-locked operation is observed at pump powers exceeding 8 W. All measurements are performed at an operating point corresponding to the laser diode output power of 10 W. The intracavity power is estimated to be 5 W, from the measured 10 mW output power through the curved folding mirror which has a reflectivity of 99.8 %. The pulse duration was 15 ps (FWHM). It is possible, however, after careful alignment, to achieve stable operation of the OPO without readjustment for several hours. In the output OPO spectrum, the wavelengths of the second harmonic of the pump (532 nm), the signal wave (765 nm) and sum frequency of pump and signal waves (628 nm) are emitted simultaneously.

The temporal profiles of the OPO and pump radiation are very sensitive to the length of OPO resonator. By careful alignment it was possible to obtain continuously mode-locked operation. Blocking the OPO resonator resulted in transition of pump laser into the Q-switched mode-locked regime. This transition is expected, since the operation of the OPO drains power from the pump pulse, acting as passive negative feedback to prevent Q-switching.

We demonstrated mode-locked operation of a synchronously pumped optical parametric oscillator based on a periodically poled $LiNbO_3$ crystal pumped inside the resonator of a diode pumped Nd:YVO_4 laser. This linear OPO resonator was also successfully modified to ring configuration necessary for sensor of rotation.

References:

[1] DIELS, J.-C. – JONES, J. – ARISSIAN, L..: *Femtosecond Optical Frequency Comb: Principle, Operation and Applications* Applications to sensors of extreme sensitivity, Springer, 2005, pp. 333-335.

[2] ZAVADILOVÁ, A. – KUBEČEK, V.: *Passively mode-locked operation of diode pumped Nd:YVO4 laser using either second harmonic nonlinear mirror or semiconductor saturable absorber* SPIE, 2006, pp. 61801.

This research has been supported by CTU grant No. CTU0611614.

Relativistic Hypernuclei Decay Based on Dalitz Diagrams

Olga Majlingova* and Vit Sopko†

*Czech Technical University, Karlovo nam.13, 12000 Praha 2,Czech Rep.
†Czech Technical University, Technicka 4, 160000 Praha 6, Czech Rep.

Abstract. Reliable model for three and four particle decays is still open problem in subnuclear physics. In several laboratories, such as JINR Dubna (Russia), KEK (Japan), COSY (Germany), INFN Frascati (Italy, Collaboration FINUDA), T.Jefferson National Laboratory, USA, experiments for study Λ hypernuclei are underway or upcoming. This contribution is devoted to kinematic analysis of weak decay of Λ hypernuclei produced on nuclei beams in Nuclotron experiments in Joint Institute for Nuclear research.

Keywords: hypernuclei, three-particl decay
PACS: 21.80-a

INTRODUCTION

The study of the ΛN interaction is folded into the field of the many bodies hadronic problem; many theoretical models have been developed in this context, but they can be selected and optimized only by taking into account a lot of experimental data. However, hypernuclear physics allows the study of the baryon-baryon interaction at normal nuclear densities, since an effective ΛN potential can be extracted from hypernuclear spectra [1].

Λ HYPERON AND Λ HYPERNUCLEI.

The properties of the free Λ hyperon decay are well known. It decays mostly in non-leptonic mode [2]:

$\Lambda \longrightarrow \pi^- + p + 38$ MeV$(63.9 \pm 0.5)\%$ and $\Lambda \longrightarrow \pi^0 + n + 41$ MeV$(35.8 \pm 0.5)\%$

If the Λ hyperon decays in a nucleus the decay properties are changed considerably. The two principal weak decay mechanisms inside a hypernucleus are [3]: the mesonic decay and the non-mesonic decay. Mesonic decay process occurs when the bound Λ decays inside the nuclear medium following the weak channels of the Λ_{free} hyperon. A standard way to describe this mechanism is $\Lambda \longrightarrow N + \pi$. Non mesonic process is induced by nucleons. This decay is possible only inside a hypernucleus.

The dominant mechanism of hypernuclear decay of heavy hypernuclei $(Z > 2)$ is not the pionic mode, favoured by free Λ hyperon, but a far more complex $\Lambda + N \longrightarrow N + N$ process. The 176 MeV energy release in this process corresponds to final state nucleon momentum of the order of 400 MeV/c. The total decay width of a hypernucleus is defined in terms of its mesonic and non mesonic decay modes. $\tau^{-1} = \Gamma_{tot} = \Gamma_m + \Gamma_{nm}$; where $\Gamma_m = \Gamma^{\pi^-} + \Gamma^{\pi^0}$, $\Gamma_{nm} = \Gamma^p + \Gamma^n$ [3].

In JINR (Dubna, Russia) there are upcomming experiments on hydrogen hypernuclei. The start point of these experiments is to restore the tradition of experiments on hydrogen. First experiments use 2 particle decay modes as it was for ${}^{3}_{\Lambda}$H and ${}^{4}_{\Lambda}$H several years ago. The uniqueness of Dubna's experiments is that the hypernuclei are recognized by their decay. In such way the experiment for ${}^{6}_{\Lambda}$H hypernuclei identification is prepared [4].

Hydrogen hypernuclei decay

π^- Decay Channels of Hyper Hydrogen Isotopes

	${}^{3}_{\Lambda}$**H**:	${}^{4}_{\Lambda}$**H**:	${}^{5}_{\Lambda}$**H**:	${}^{6}_{\Lambda}$**H**:	${}^{7}_{\Lambda}$**H**:	${}^{8}_{\Lambda}$**H**:
π^-+1	**^{3}He**	**^{4}He**		**^{6}He**		**^{8}He**
π^-+2	**d p**	^{3}He n **t p** **d d**	^{4}He n **t d**	**t t**	^{6}He n	

The table of hydrogen hypernuclei's decay shows us that most of these are identifiable by 2-particle decay. ^{A}He daughter nuclei are recognized and kinematics of 2-particle decay is described by well known precise mathematical formulas. For decay of particle with mass m_0 into particle $m_1 + m_2$ we have :
In CMS:

$$E_1^* = \frac{m_0^2 + m_1^2 - m_2^2}{2m_0}, \quad E_2^* = \frac{m_0^2 - m_1^2 + m_2^2}{2m_0},$$

$$p_1^* = p_2^* = \frac{[(m_0^2 + m_1^2 - m_2^2)^2 - 4m_0^2 m_1^2]^{1/2}}{2m_0}$$

In LS:

$$E_1 = \frac{m_0 E_1^* E_0^* \pm p_0 cos\theta_1 R_1^2}{E_0^2 - p_0^2 cos^2\theta_1}, \quad R_1^4 = m_0^2 p_0^{*2} - m_1^2 p_0^2 sin\theta_1,$$

$$p_1 = \frac{m_0 E_1^* p_0 \pm E_0 R_1^2}{E_0^2 - p_0^2 cos^2\theta_1}$$

Using these techniques, binding energy for hyperon, B_Λ, in hypernuclus ${}^{6}_{\Lambda}$H can be estimated [**?**].

The next part of the table consists of 3-particle decays. There are two kinds of them: decays where all particles are charged (e.g. deuteron, triton, proton) and may be well detected, and, decay with neutron - at present hardly detectable. For example, ${}^{5}_{\Lambda}$H cannot be observed through 2-particle decay technique. The problem in 3-particle

Evaluating the Thermal Performance of Repairs Made on the CERN ATLAS Pixel Detector

M. Galuska, V. Vacek, M. Doubrava

Michal.Galuska@fs.cvut.cz

Department of Physics, Faculty of Mechanical Engineering,
Czech Technical University in Prague, Technická 4, 166 07 Praha 6, Czech Republic

The Pixel barrel detector, a component of the ATLAS Inner Detector being installed on the CERN Large Hadron Collider, is composed of 112 structures called staves, which act simultaneously as the detector support and as the evaporator of an integrated evaporative cooling system that uses a fluorocarbon refrigerant. A significant number of these staves have been found to suffer from galvanic corrosion and the integrated refrigerant tubes have ceased to be leak-tight, allowing the fluorocarbon refrigerant to escape. The galvanic corrosion was caused by the combining presence of aluminum (construction material of the refrigerant tubes), nickel (present in brazed connection joints) and water, introduced during production tests that were not followed by a proper drying procedure. Because the staves have already been mounted with expensive detector electronics, repair measures have been investigated from the point of view of thermal performance and resulting detector electronics' temperatures and from the point of view of influence on refrigerant flow through the circuit.

The project approaches the problem theoretically, determining which repair approaches could be feasible, and concentrates on these in further experimental measurements. The repairs influence the cooling performance in two ways: first, changes in hydraulic diameters of the cooling tubes integrated in the evaporator structures change (worsen) pressure drops along the evaporator, increasing evaporation temperature in comparison to undamaged original structures. Secondly, the repairs introduce additional thermal interfaces between detector electronics and the evaporating refrigerant, worsening heat transfer and causing increase in the detector electronics' temperature.

The pressure conditions in the evaporator structures are theoretically predicted using three semi-empirical correlations frequently used in cooling systems – according to Lockhart-Martinelli, according to Grönnerud and according to Pierre. The analyses are made for various operating conditions that influence the vapor quality change inside the evaporator. From the predicted pressure drops, the evaporation pressure and therefore evaporation temperature can be estimated along the evaporator structure.

The thermal interface between the detector electronics and the evaporating refrigerant is examined using two thermal models. To demonstrate a simple engineering approach, a one-dimensional model using analogy with electrical circuits is constructed. The second model uses a computational finite element method using the ANSYS® software. Both types of models are constructed for each repair measure being studied, as well as for the original evaporator design to provide comparison. The models provide a prediction of the temperature of the detector electronics in relation to the evaporation temperature of the refrigerant.

Based on the results of the theoretical predictions for the various evaporator constructions, several combinations of repair measures were dismissed as unsuitable for operation in the detector, because the detector electronics would operate at too high temperatures. The combinations that according to the theoretical predictions should be suitable were examined experimentally.

To verify the predicted behavior of the evaporators, a laboratory cooling circuit was designed to work with one branch of the circuit and cool one Pixel barrel evaporator structure.

Another purpose of the circuit was to test final design prototypes of other circuit components, such as the in-circuit sub-cooling heat exchanger and connecting tubes, and to test all the components together. Furthermore test runs on the circuit simultaneously served for studying and testing capillaries, which are used as throttling elements, and to dimension them to give the required refrigerant mass flow [2].

To provide as accurate results as possible, the laboratory circuit had to simulate the full scale ATLAS Pixel and SCT cooling system as best as possible, which meant it had to be able to provide the same pressures, mass-lows, simulate the same temperatures, and with the same refrigerant. It was therefore based on an older system that has been previously used to test prototypes and perform design verifications of early Pixel and SCT components and modified to bring the circuit closer to the final full-scale system and provide more control over the refrigerant conditions to simulate various effects of the ATLAS detector environment. It was also mounted with an electronic data acquisition (DAQ) system to measure refrigerant conditions around the circuit, the temperature of detector electronics and to provide data for further detailed analyses.

The DAQ system employed during these measurements is the Mobile DAQ system developed at the DAQ systems laboratory of the Applied Physics Department of the Czech Technical University. Its development and use during these measurements was driven by the fact that it is composed of CERN standard components – on technology that is being developed for the general measurement needs of ATLAS and other LHC experiments. The CERN standard DAQ system is based on the industrial-standard CAN network, which it utilizes for communication and data transfer, on commercially available CAN controllers and CAN communication software (the OPC Server), on a commercially available graphical object-oriented programming environment (PVSS II by ETM), and on a measurement card being custom co-developed by CERN – the ELMB, or Embedded Local Monitor Board.

The experimental measurements mostly confirmed the theoretical predictions about the performance of various evaporator structures, differing in the repair measures employed. Recommendations have been made on the use of the repair measures in the construction of the Pixel barrel detector and on further steps to be taken. For the evaporator structures that could be used on the detector, reference capillaries which provide an adequate mass flow have been created and tested. All work has been completed in a shorter time period than expected and the results obtained contributed significantly to an overall reduction of repair costs.

References:

[1] VACEK V., ET AL.: *Perfluorocarbons and their use in cooling systems for semiconductor particle detectors,* in Fluid Phase Equilibria, 174th edition, Elsevier, 2000, pp. 191–201.

[2] VACEK V., VINŠ V.: *A study of the flow through capillary tube tuned up for the cooling circuit with fluoroinert refrigerants,* proceeding from17th EUROPEAN CONFERENCE ON THERMOPHYSICAL PROPERTIES, Bratislava, 2005, pp. 17-32.

[3] BAYER C., ET AL.: *Development of Fluorocarbon Evaporative Cooling Recirculators and Controls for The ATLAS Inner Silicon Tracker,* in IEEE Nuclear Science Symposium and Medical Imaging Conference: NSS-MIC 2000, Lyon, 15 - 20 Oct., 2000, pp. 10.

[4] VACEK V., VINŠ V., DOUBRAVA M., GALUŠKA M.: *DAQ and DCS sensors database, Capillary studies and Thermophysical property Database for the C.S. applications at SR Bldg.,* CERN Pixel Mechanics Meeting, February 2003, pp. 12.

RF Plasma Modification of Polyester Fabrics in Multi-Layer Arrangement

J. Pichal

pichal@fel.cvut.cz

Department of Physics, Faculty of Electrical Engineering, Czech Technical University, Technicka 2, 166 27 Prague 6, Czech Republic

The modification of textiles means a change of structure, which leads to the improvement of fibers qualitative parameters. Due to ecological demands and cost-effectiveness requirements there is tendency for removal of classical treatment technologies (chemical modification) and their substitution by plasma technologies.

The major advantage of the plasma modification represents its environmental characteristics in contradistinction to those of chemical processes [1-3]. Plasma modification and penetration through multi-layer of fabrics is not widely used in the textile industry at present, but there is permanent effort to incorporate this method among other general technologies.

Results presented in this paper are connected with the influence of plasma pressure, modification time and ion bombardment on the penetration of plasma particles in treated multi-layer of textiles. The penetration of radicals is expressed in this paper through the change of hydrophilicity.

RF plasma generator consisted of a large–volume reactor equipped with a planar RF electrode [3]. Plasma reactor contained vacuum chamber made from aluminum alloy. The rotary flat copper electrode placed in the middle of the chamber was supplied by radio-frequency generator operating at 13.56 MHz with maximum power 300 W. Chamber was filled with air under pressure of 10 – 300 Pa. Modification time was chosen 60 – 600 s. For all experiments described in this paper the specimens made from the polyester fabric with the trade name Tesil 12 were used. During penetration effect studies a multi-layer of 6 PES fabric pieces was inserted into low pressure RF discharge.

In first series of experiments the textile substrate was placed on the insulated vertically adjustable substrate holder. The distance between substrates and electrode was 20 mm. This distance was chosen so that substrate was placed into the region with the highest plasma density. In the second series of experiments the substrate was placed directly on the RF capacitively coupled and shielded electrode, so that additional ion bombardment of the substrate took place.

Our experiments proved that the pressure rise is directly proportional to that of radicals´ penetration. However, our tests failed to achieve hydrophilicity values matching for all layers in the modified substrate. We can assume that further increase of pressure might lead in better penetration of radicals into the fabric.

In unmodified sample three types of C bonds had been found: C-H and C-C (aliphatic and aromatic) with bond energy 284.8 eV, C-O (methylene carbon) (286.5 ± 0.1) eV with single bond to oxygen and O-C=O (ester carbon) (287.7 ± 0.1) eV. Two different oxygen atoms were observed, C=O (531.3 ± 0.1) eV and C-O (532.8 ± 0.1) eV. These corresponded to bounded oxygen [4]. After modification increase of C-O bonds had been observed. This change could be attributed to the substitution of hydrogen atoms on the benzene ring by hydroxyl groups.

The highest modification effect was achieved within the range (70 – 100) Pa, when all layers seemed to be approximately equally influenced. On the other hand further pressure increase led to

reduction of effectiveness. Modification effectiveness achieved at pressure of 300 Pa was comparable with that obtained at pressure 10 Pa. Comparison both of the modification effectiveness for substrate positioning directly on the electrode and of the modification effectiveness for substrate positioning in 20 mm distance showed distinct difference of effectiveness values. The bulk arrangement makes sure that rising pressure is directly proportional to penetration intensity up to 300 Pa (the maximum value tested). However, this value is not high enough for active particles sufficient penetration into the last layer. The difference in modification effect caused by these two types of arrangements confirms the fact that the influence of ion bombardment is important, as assumed before.

If the substrate was put directly on the electrode, then the diffusing mechanism of ions was combined with ion bombardment. When the substrate was put 20 mm above from the electrode, it was exposed only to ions and radicals. Whole process was accompanied with deceleration of particles and reduction of ion bombardment in the electrode area; hence the substrate was impacted by particles with smaller kinetic energy. Modification effectiveness rose only in limited pressure range. The pressure range to the optimal modification of fabric substrate seemed to be (70 – 100) Pa. Results of this experiment indicate that ion bombardment part in the substrate characteristics alteration is very important.

The subject of the other part of measurement was oxygen radicals´ penetration ability. The results did not confirm the assumption. Chemical changes of fibers tested by XPS analysis did confirm increased existence of C-O bonds in comparison with unmodified substrate. This was caused by substitution of hydroxyl groups for hydrogen on benzene nuclei. Within the time period of 60 – 600 s that we used for testing we could see that modification of all layers in the fabric was comparable at the maximum time used which was 600 s.

We showed that active particles of the oxygen plasma penetrated into textile structure and improved its wettability considerably. The permanency of the hydrophilicity improvement induced by plasma modification strongly depended on the substrate positioning and plasma pressure.

References:

[1] FERRERO, F. ET ALL.: *Wettability Measurements on Plasma Treated Synthetic Fabrics by Capillary Rise Method* Polymer testing, 2003, pp. 571-578 .

[2] OKUNO, T. ET ALL.: *Effect of Crystallinity of PET and Nylon 66 Fibres on Plasma Etching and Dyebility Characteristics* Textile Res. Journal, 1992, pp. 474-480.

[3] VATUNA, T., ET ALL.: *Plasma Modification of the PES by Oxygen and Nitrogen Plasma* 5th Int. Conf. "TEXSCI 2003", Liberec, 2003, pp. 120-123.

[4] RICCARDI, C. ET ALL.: *Surface modification of poly(ethylene terephthalate) fibers induced by radio frequency air plasma treatment* Appl. Surf. Sci., 2003 pp. 386-397

The sensitivity of negative dispersion induced by introducing the curvature into the Index Guiding Photonic Crystal Fiber for deviation of geometrical parameters

M. Łucki, L. Boháč

luckim1@fel.cvut.cz

Department of Telecommunication Engineering, Faculty of Electrical Engineering, Czech Technical University, Technická 2, 166 27 Prague 6, Czech Republic

This work is a modeling paper which purports to show that a negative dispersion may be generated in a microstructured fiber by introducing a curvature into the fiber. Negative dispersion might be used in telecommunication for pulse distortion compensation. To extend the length of optical line without the necessity of signal recovery, the compensation of positive dispersion should be done. Negative dispersion could be achieved by different methods [1-2]. The relevancy of this subject is in proposing a novel method and in the study of the sensibility of the dispersion with respect to the bent radius. The goal is to find proper curvature to ensure negative dispersion in the third telecommunication window. It is possible to reach thousands of ps/nm/km of negative dispersion.

The simulation tool used in the calculations of the dispersion curves is developed by Lumerical Solution using a full vector FDTD method. By using this algorithm, constant of propagation as a function of the wavelength can be evaluated. Then the effective index corresponding to the selected mode can be obtained as a quotient of constant of propagation and a free space wave vector. Having this, dispersion could be calculated. To apply this algorithm, the mechanism of bending should be studied first and then a fiber should be designed. As I noticed, curvature characterized by bent radius of thousands of microns causes in modal solution strong confinement, deformation of a fundamental mode and spillover effect at the wavelength for which it is highly dispersive, start bent radius was set to 66000 microns. Then, for assumed normalized hole diameter and bent radius we plot the dispersion wavelength dependency over wide range of waves to find the peak of negative dispersion. Greater curvature or greater hole diameter could shift the peak on negative dispersion towards shorter waves. It is possible to adjust hole diameter to receive the peak of negative dispersion at 1550nm. Shifting the peak through the wavelength is accompanied by changing the peak minimum value. The influence of changing the bent radius is mainly in the wavelength at which negative dispersion occurs. Hole diameter deviations affects mainly the value of dispersion and exhibits only weak impact on the wavelength corresponding to the peak. We ought to search the proper bent radius for which there is negative dispersion at 1550nm and then search proper normalized hole diameter which is working as a scaling factor for dispersion value at certain wavelength (as it weakly influences the value of lambda). Negative dispersion accompanies side mode causing loss of about 1dB/cm. No side mode at 1550nm means that there is no negative dispersion at this wavelength (it would occur at some other λ or maybe hole diameter and bent radius are not matched). I obtained the biggest peak for combination of normalized hole diameter 0.50453 and curvature represented by bent radius equal to 69080 microns at 1.5599μm. Negative dispersion was -185420 ps/nm/km and the bandwidth in which it occurs (peak's bandwidth) was 0.07nm. The possible highest value of negative dispersion -71994 ps/nm/km at 1.550μm was possible for bent radius 69909 microns and normalized hole diameter 0.50453.

During the fabrication process, the value of normalized hole diameter or bent radius could have some deviations from the values of the theoretical design predictions. Holes could be made with different radius (if the air pressure while drawing process is not proper) or elliptic (we investigate here only deviation of radius for circular holes). The prediction of chromatic dispersion of the fiber with the deviations of bent radius and normalized hole diameter is presented. A reference configuration is chosen as the pitch Λ= 23.2μm, normalized hole diameter d/Λ=0.504530 for investigation of bent radius deviation; bent radius R=66116μm for the investigation of hole diameter deviation. As the deviation could have different impact for different reference configuration (as suggested in [3]), investigation of hole diameter deviation was repeated for various ranges of parameters' value. The dispersion peak exhibits small shift towards shorter wavelength and its value demonstrates little variation when increasing the hole diameter, while the dispersion peak is being shifted towards longer wavelength, its value demonstrates a remarkable variation when decreasing the hole diameter. A certain negative tolerance of the hole diameter is preferred (smaller holes). (Peak value decreased about 74% for certain negative deviation while 90% for analogical positive one). Value of the wavelength at which negative dispersion occurs is sharply sensitive for bent radius. The bandwidth of the peak is more or less constant and is very narrow: 0.07nm. Small imprecision of bent radius results with loosing the negative dispersion because local extreme will be shifted in wavelengths. Dispersion peak absolute value decreases much slower for negative bent radius deviation and after, half-attenuated peak is kept over wide range of bent radius (and corresponding range of waves), greater deviation of bent radius shifts the peak of dispersion in wavelength without further affection peak's value. Then, if minimal negative dispersion was -188000ps/nm/km, the negative dispersion of about -50000 ps/nm/km is kept over wide wavelength range at assumed hole diameter.

Important question is about the value at required wavelength. If there is a requirement to fabricate the fiber that would work at 1.55μm it is worth nothing to say that dispersion decreases by couple of picoseconds if the extreme is no longer at 1.55μm. Decrease of 20000 ps/nm/km at 1.55μm corresponds to 5μm deviation in bent radius. The sensitivity is less sharp for greater deviation. The input power is of a Gaussian shape; the outer power of a bent fiber may be also Gaussian (if it is not highly dispersive at 1.55μm) or asymmetrical is concentrated in the core but is not a Gaussian shape and accompanied by side mode. This could be the problem to match the Numerical Aperture of a fiber of which dispersion we will compensate. We found negative dispersion the most sensitive to the bent radius (wavelength at which negative peak occurs) and hole diameter (peak value, peak amplitude scaling factor).

References:

[1] SAKAMAKI, K. – NAKAO, M.: *oliton Induced Supercontinuum Generation in Photonic Crystal Fiber* IEEE Journal of Selected Topics in Quantum Electronics vol.10, 2004, No.5.

[2] ZSIGRI, B. – LAEGSGAARD, J. – BJARKLEV, A.: *A novel photonic crystal fibre design for dispersion compensation* J. Opt. A: Pure Appl. Opt. 6, 2004, pp. 717–720.

[3] YANG, S. – ZHANG, Y. – PENG, X. – LU, Y. – XIE, S.: *Theoretical study and experimental fabrication of high negative dispersion photonic crystal fiber with large area mode field,* Optics Express 3015, vol.14, 2006, No. 7.

HYDRATION OF PORTLAND CEMENT PASTE

P.Tichá*,, P.Demo*,**, P.Semerák***

petra.ticha@fsv.cvut.cz

*Department of Physics, Faculty of Civil Engineering, Czech Technical University, Thákurova 7, 166 29 Praha 6, Czech Republic
**Institute of Physics, Academy of Sciences of the Czech Republic, Cukrovarnická 10, 162 53 Praha 6, Czech Republic

During hydration and hardening, the concrete is gaining mechanical strength, resistibility and chemical stability, while physical and chemical reactions are in progress. Workability of concrete belongs to the crucial parameters. Knowledge of the rate of reaction between cementing materials and water (hydration) is important to determine setting time and hardening. An electrical measurement technique was used to measure the electrical resistivity of cement paste at various temperatures. The different hydration periods were identified from the electrical resistivity curve, where inflex points mark the beginning and the end of a certain period.

The process of hydration begins with the addition of water. In the very beginning liquid and cement grains are present, shortly after addition of water the so-called chemical stage is in process. Ions from portland cement are released into the solution and the coating gel appears around the grains. Next stage is the so-called induction period, the value of pH is increasing steadily and the concentration of calcium ions together with CSH gel on the surface of grains is responsible for decrease in the solubility of phases of portland cement. The formation of ettringit is developed and the hardening of cement is initiated. Finally the fibrils of hydrated calcium silicate grow into a cluster (for details, see, e.g. [3]).

The beginning of macroscopic growth (and, thus, termination of incubation period) can be characterized by dramatical change in the time-dependency of electrical resistance because of appearing of the massive clusters with very low mobilities. This process is accompanied by increasing release of the latent heat Q_L.

Duration of incubation period, τ_N, can be estimated using following path. Due to chemically based process of salvation of the cementitious material in water, various types of charge carriers (monomers Ca^{2+}, OH^-, etc.) are released and free to move within the system. Due to chemical reaction and physical processes occurring within hardening cementitious paste, a number density of ions changes with time logically followed also by the change of electric properties of the system. In particular, temporal dependency of electrical resistance (resp. conductivity) may be closely related to τ_N. For this purpose, we have measured electrical resistance of hardening cement paste.

Formation of clusters in material is a consequence of fluctuations. If the classical Boltzmann theory from statistical physics is applied on the process of cluster formation, it can be found out that the probability of appearing of a cluster consisting of n-building units can be expressed as follows:

$$\Pr(n) \approx \exp\left[-\frac{\Delta G(n)}{kT}\right], \qquad (1)$$

where k is Boltzmann constant, T is the temperature, and the ΔG is the change of Gibbs potential given by

$$\Delta G = -n \cdot \ln \mathscr{S} + \gamma \cdot \sigma \cdot n^{2/3}, \qquad (2)$$

where n is number of monomers in the newly-forming cluster, $\mathscr{S}$ is given supersaturation of the system (water+cement), σ represents surface energy between cluster and its environment and γ expresses geometrical shape of the cluster. ΔG reaches maximum at the moment when the newly forming clusters have the critical size n_C. When the clusters consists of n particles and n is less than n_C, then dissolution takes place, otherwise, the cluster tends to grow.

Following formula for the critical size of cluster can be derived from extremum condition for ΔG:

$$n_c = \left[\frac{2\gamma\sigma(T)}{3\ln \mathscr{S}} \right]^3 , \qquad (3)$$

Crucial quantity entering above relationship, dividing the unstable (undercritical) and stable (supercritical, growing) regimes of evolution via n_C is temperature dependent surface energy $\sigma(T)$ between solid cluster and original liquid phase. Dependency of n_C versus temperature can be derived from formula for the critical size of cluster. Since σ decreases with increasing temperature, taking in to account eq. (3), it can be assumed for given supersaturation that n_c decreases as function of T.

The newly-forming cluster becomes stable and growable when overcross the so-called nucleation barrier ΔG_C that can be determined from relationships (2), resp. (3) to be:

$$\Delta G_C = \frac{4\gamma^3}{27(\ln \mathscr{S})^2}\sigma^3(T) , \qquad (4)$$

Consequently, with increasing temperature T the nucleation barrier decreases. Thus, the boltzmannian probability (1) defining, in fact, a boundary separating unstable and growable states strongly depends on temperature dependent surface energy of cluster.

$$\Pr(n) \approx \exp\left[-\frac{const.\,\sigma^3(T)}{kT} \right]. \qquad (5)$$

In other words, the higher temperature T, the higher probability of formation of a new, growable cluster [4].

Summarizing, in terms of temporal behavior of electrical resistance the rate of evolution of a very first stage of solidification (i.e., nucleation) within cementitious materials can be indirectly estimated. The crucial role is played by surface energy of newly-forming cluster which modulates the height of nucleation barrier and separates the unstable and growable regimes of system.

References:

[1] ČSN 72 7031: *Měření součinitele difúze vodní páry stavebních materiálů metodou bez teplotního spádu.* ÚNM Praha, 1974, pp. 1-7.

[2] H.F.W.TAYLOR: *Cement Chemistry.* Thomas Telford London, 1997.

[3] P. DEMO, Z. KOŽÍŠEK: *RThermochimica Acta 280/281,* 1996, 101-126.

[4] P. DEMO, Z. KOŽÍŠEK: *Philosophical Magazine B70,* 1994 49-57.

This work was support by the Ministry of Education of the Czech Republic under project No. CEZ MSM 6840770003. One of us, A.S., also gratefully acknowledges the support of the Grant Agency of the Czech Republic, Project No. 101/05/2214.

Theoretical Analysis of Properties of Optical Systems

A. Mikš, J. Novák, P. Novák

miks@fsv.cvut.cz

Department of Physics, Faculty of Civil Engineering, Czech Technical University,
Thákurova 7, 166 29 Prague 6, Czech Republic

The imaging quality is a very important characteristic of optical system and it depends on many factors. A primary source of decreasing of the imaging quality is the wave character of light that causes the diffraction of light. As a result of this phenomenon the image of a point object is not a point but some diffraction pattern (point spread function) that is characterized by the distribution of energy in dependence on the wavelength of light. Another factor that causes decrease in quality of imaging is the wave aberration of the optical system.

Aberrations can be caused by many reasons of the physical, material and technological origin. Some aberrations of optical system are also dependent on the wavelength of light. Such aberrations are called chromatic aberrations of optical system. Our work deals with the influence of the wavelength of light on values of wave aberration coefficients. A theoretical analysis of chromatic aberration and one of possible approaches to the expression of the dependence of aberration coefficients on the wavelength was performed [1]. The method for calculation of chromatic aberration coefficients was shown for the case of the imaging of axial point by the rotationally symmetrical optical system. Derived formulas enable calculation of chromatic aberration coefficients up to the fifth order. Furthermore, the calculation of the Strehl definition using chromatic aberration coefficients was carried out. These relations are accurate enough for most optical systems in practice.

Another basic characteristic of imaging properties of optical systems is a point-spread function (PSF). This characteristic is closely related with the problem of the resolving power and optical transfer function of an optical system. In optical books, the PSF is given only for the cases of optical systems with very small value of numerical aperture. These relations are accurate enough for a wide range of optical systems that one can meet in practice, because many of these optical systems (telescopes, camera lenses, etc.) have a small value of numerical aperture. But this relation is not accurate enough for optical systems with large value of numerical aperture. A typical representative of optical systems with large numerical aperture is a microscope objective. In our work, we dealt with the problem of calculation of the point-spread function of an optical system with finite value of numerical aperture using the scalar wave theory [2]. We performed theoretical analysis of the problem and we had shown the effect of the properties of optical system (numerical aperture value, transverse magnification, aberrations) on the PSF. Furthermore the analytical expression for calculation of the PSF for the case of diffraction limited optical system with circular exit pupil was derived. This formula is a generalization of the classic relation and it holds also for systems with a large numerical aperture. The calculation of the amplitude of wave field of diffraction limited optical system having numerical aperture of finite value, constant amplitude transmission and imaging with transverse magnification, can be done using derived formula. From derived equations it can be seen that the point-spread function of an optical system depends on the transverse magnification and the value of numerical aperture of the optical system.

The imaging quality of optical systems also depends on the value of the wave aberration of given optical system. Therefore during the design process of optical systems, it is desirable to obtain residual aberrations of designed optical systems as small as possible. By analysis of the dependence of aberrations on numerical aperture and field of view, it is

possible to find such values of the numerical aperture and field of view, where the residual aberration is zero. Such values of the numerical aperture and field of view are called correction zones. By detailed analysis of primary aberrations (spherical aberration and coma) of optical systems, we can see that the imaging quality depends on values of correction zones. Values of correction zones are dependent on the criterion that is used for evaluation of the quality of optical systems. In our work, we performed a theoretical analysis of this problem and we derived general formulas for the coefficients of wave aberration in dependence on the values of correction zones [3]. These formulas were derived for primary aberrations of optical systems (spherical aberration, coma, field curvature and distortion) of the third and the fifth order.

Finally, there was done an analysis of optimal values of correction zones and optimal position of the centre of reference sphere using derived equations. The analysis and calculation of optimal values of correction zones and the optimal position of the reference sphere was performed for two types of the evaluation criterion (criterion for the quality of designed optical system). In the first case, we required the maximal value of wave aberration to be minimized and in the second case we required the root mean square of the wave aberration to be minimized (i.e. maximization of the Strehl definition). The wave aberration was expressed using polynomials orthogonal over the area of the exit pupil of optical system. In our work a set of polynomials orthogonal on unit circle was described [4] (for the circular shape of exit pupil). This set of polynomials is closely related to Zernike, Legendre and Jacobi polynomials. Using derived relations and orthogonal polynomials, optimal values of correction zones for both types of evaluation criterion were calculated.

References:

[1] MIKŠ, A. – NOVÁK, J. – NOVÁK, P.: *Chromatic aberration coefficients* XVth Czech-Polish-Slovak Optical Conference.(Book of Abstracts), Agentura Action M, 2006, pp. 83–84.

[2] MIKŠ, A. – NOVÁK, J. – NOVÁK, P.: *Analýza vlivu numerické apertury a zvětšení na hodnotu rozptylové funkce bodu* Technical Computing Prague 2005: [CD-ROM]. Praha: VŠCHT, 2005 .

[3] MIKŠ, A. – NOVÁK, J. – NOVÁK, P.: *Calculation of point-spread function for optical systems with finite value of numerical aperture* Optik - International Journal for Light and Electron Optics, (in press) .

[4] MIKŠ, A. – NOVÁK, J. *Aplikace ortogonálních polynomů v teorii optického zobrazení* Jemná mechanika a optika , roč. 51, č. 3, 2006, pp. 71–75.

This research has been supported by MŠMT grant No. MSM6840770022.

Modern Methods of Surface Topography and Defectoscopy

A. Mikš, J. Novák, P. Novák

miks@fsv.cvut.cz

Department of Physics, Faculty of Civil Engineering, Czech Technical University,
Thákurova 7, 166 29 Prague 6, Czech Republic

The problems of topography of surfaces are very important in various parts of science and engineering. Several approaches exist for surface shape measurement. The measurement methods can be divided into two distinct categories, contact and non-contact techniques. Contact techniques use mainly linear sensors for measurement, e.g. dial indicators based either on a mechanical principle (sprockets and geared transmission) or on the principle of sensing mechanical probe movement using measurements of electromagnetic induction (inductive sensors), capacitance (capacitive sensors), resistance (resistive sensors), and using contact optical sensing systems. Main disadvantage of contact methods is the possibility of damaging the investigated surface with the mechanical sensor. The accuracy of measurement with contact sensors is mainly within the range 0.1 – 1 μm. On the other hand, non-contact methods are mainly based on the principle of optical non-contact sensing systems or measurements of the change of capacitance. Interferometric methods are most frequently used for very accurate measurements of surface topography. With these methods, one can obtain the accuracy up to 0.1Å. Further methods that can be used for topography of surfaces are, for example, atomic force microscopy (AFM) and scanning tunneling microscope (STM). The accuracy that can be reached with these methods is within the range of nanometers. However, such measurement systems are very expensive, can be applied only to special specimens, and their dynamic range is limited.

The aim of our work was to propose and analyze several modern non-contact methods for surface topography measurements that are relatively simple and cost effective. First method that we focused on is based on chromatic sensor [1]. This method uses special optical systems (hyperchromats) with a linear dependence of longitudinal chromatic aberration on the wavelength of light. General equations for calculation of parameters of such optical systems were derived. Examples were shown for calculation of hyperchromatic doublets and triplets with the linear dependence of longitudinal chromatic aberration on the wavelength. On the basis of the performed analysis, optical systems can be designed that permit to perform measurements of topography of surfaces. We analysed and designed individual components and proposed an optical system for measurements of topography of surfaces using hyperchromats. Further research will be devoted to designing, fabrication, and application of chosen hyperchromatic doublets and triplets for topography measurements.

Another method for testing shape of general optical surfaces (i.e. flat, spherical or aspherical surfaces) that was proposed and analyzed is based on the correlation analysis and mathematical optimization techniques [2]. It is a relatively simple evaluation method that enables to speed up the process of optical surfaces testing. The deviation of the tested surface from its nominal shape is characterized by the correlation coefficient between the tested wave field and reference wave field that corresponds to the nominal shape of surface. By maximization of the correlation coefficient, one can obtain information about the deviation of the tested optical surface from its nominal shape, i.e. it is possible to evaluate whether the tested optical surface fulfils the tolerance requirements. The proposed method can be used for testing of flat, spherical or aspherical optical surfaces in optical industry.

The next method for shape measurement of optical surfaces that we focused on is based on the Shack-Hartmann wave-front sensor. We designed, fabricated and tested wave-

front sensor that is based on the principle of the Shack-Hartmann method [3]. This method uses the microlens array and the CCD sensor for wave-front evaluation. The sensor estimates the wave-front local slopes (wave-front gradient) at points located in a regular grid given by the dimensions and distance of microlenses. The tested wavefront is spatially sampled by the lenslet array and impinges on the CCD sensor that is located in the focal plane of the microlens array. From the detected intensity distribution, one can calculate the values of wave-front gradient. The wavefront-shape can be numerically reconstructed from the values of the spot displacements using various mathematical procedures, e.g. by integration or by approximation using polynomials. The wave-front reflected from the object under test carries the information about the topography of measured surface. Various evaluation algorithms were tested on examples of real and computer simulated wavefronts. These algorithms were compared with respect to their robustness, accuracy, number and position of grid points. The most suitable methods were chosen for implementation into the evaluation software for the wave-front sensor. Wave-front analysis software was optimized with respect to given parameters of the system (detector resolution, focal length of microlens array, source of light) and the system was implemented for industrial testing of optical systems and elements.

Finally, we proposed and analyzed method for detecting defects of optical materials such as optical glass or plastics [4]. The quality of optical materials can affect the imaging quality of completed optical systems thus is important to be able to detect the defects in optical materials. For many applications, it is important to know if some kind of defect is present and what is its frequency. Main defects in optical materials are striae, gas bubbles, inclusions and scratches. We proposed a method that enables to highlight selected groups of defects with different colors. The tested sample is positioned at the front focal plane of a lens and it is illuminated by collimated beam (plane wave). In the rear focal plane, the Fourier spectra of the tested sample is located. By inserting special colored filters in the spectral plane one can increase contrast and perform color discrimination of different types of defects. The enhanced image is obtained using another lens with same parameters placed in a way that the spectral plane is located at the front focal plane of the lens. Nowadays, it is possible to realize computer generated adaptive filtering using transmissive spatial light modulators based on LCD technology.

References:

[1] MIKŠ, A. – NOVÁK, J. – NOVÁK, P.: *Využití hyperchromátů pro měření topografie ploch* Defektoskopia 2006. Leopoldov: VM-print, 2006, pp. 70–76.

[2] NOVÁK, P. – NOVÁK, J.: *Analysis of Correlation Method for Testing and Adjusting Optical Surfaces* Physical and Material Engineering 2005. Czech Technical University in Prague, 2005, pp. 156–158.

[3] NOVÁK, J. – MIKŠ, A. – NOVÁK, P.: *Application of Shack-Hartmann wave-front sensor for testing optical systems* XVth Czech-Polish-Slovak Optical Conference.(Book of Abstracts), Agentura Action M, 2006, pp. 42–43.

[4] MIKŠ, A. – NOVÁK, J. – NOVÁK, P.: *Metoda pro barevnou diskriminaci defektů* Defektoskopia 2006. Leopoldov: VM-print, 2006, pp. 77–83.

This research has been supported by MŠMT grant No. MSM6840770022.

Microwave Phase Interferometry for Nondestructive Testing

A.Mikš, J.Novák, P.Novák

miks@fsv.cvut.cz

Department of Physics, Faculty of Civil Engineering, Czech Technical University,
Thákurova 7, 166 29 Prague 6, Czech Republic

Nowadays, various measurement methods are used for non-destructive analysis of physical and geometrical properties of structural materials in mechanical and civil engineering (e.g. measurement of shape, roughness, deformation, elastic properties, material defects, etc.) [1]. These techniques are based on interaction of acoustic or electromagnetic waves with investigated objects. There exists a wide spectrum of electromagnetic waves for application in non-destructive testing.

Microwave measurement techniques can be also used for measurements of structural materials successfully. Compared to optical methods, their main advantage is the possibility to investigate the properties of opaque materials, i.e. most of structural materials. Compared to optical frequencies, the bandpass of microwave frequencies enables to carry out technically the larger variability of applications. Measurements can be not only scalar, but also directly vectorial, and can be carried out in a wide and successively tunable bandpass with microwaves. It enables to apply various types of correction methods, which significantly improve the measurement accuracy. One can also obtain information about spatial orientation of vectors of the electromagnetic field. Therefore, it can be expected that microwave frequency bandpass offers a considerable area for further development and application of measurement methods, originally developed for optical frequencies. It concerns especially phase-shifting interferometry [1,2], which is used in optical metrology over thirty years.

The aim of our research project was to develop a mathematical model of the microwave phase interferometer for evaluation of the wavefront shape of the investigated microwave wave fields, propose suitable mathematical algoritms for measurement data evaluation, design the laboratory model of the microwave interferometer, and carry out subsidiary experiments for verification our measurement and evaluation methods. Regarding to used wavelengths, the research and the experimental verification of the method is not simple, because measuring instruments needed are not commonly accessible and some of them were proposed, designed and constructed.

For a practical application of various measurement methods in optics or microwave engineering, an important task is determination of the wave-front shape (or phase of wave field). Several different methods exist for microwaves and various measuring instruments are available for vectorial and scalar measurements of microwave field. However, those methods are relatively time consuming and can be hardly used for measurements of dynamic effects. The research project was focused on a quite new method for evaluation of microwave fields. Our work deals with suitable methods for wave-front shape evaluation in microwave range. The evaluation is carried out by measurement and analysis of the interference field that originates from interference of the reference microwave field with the investigated (object) wave field. The phase of investigated microwave field can be then determined directly or using scalar measurements from values of squared amplitude of the electric field intensity using appropriate phase evaluation techniques [3,4]. The advantage of the proposed method is the fact that the method is based only on scalar measurements of microwave field.

In the theoretical part of the project, we firstly considered the transfer of the phase-shifting interferometry into the microwave area along with investigating the possibility of improving the mentioned technique with respect to the availability of tunable frequencies, vectorial correction measurement methods, and other technical possibilities in microwave frequency bandpass. The analysis of the phase of microwave interference field was carried out using the array microwave detector (analogy to array detectors in optics). It was proposed an array microwave vector and scalar detector that can perform field measurements in a relatively short time. In case of scalar measurements, the phase change of the microwave field can be determined from values of the intensity of electromagnetic field using special evaluation techniques that are well adopted for interferometric methods in optics. Introducing the controlled change of the phase of investigated wave field, we obtain interference signals as the output from every point of the array detector. By analysis of interference signals with suitable phase evaluation techniques, one can obtain the phase values at every point of the investigated wave field. The analysis of algorithms for phase microwave interferometry was performed and suitable phase evaluation algorithms were proposed. The novel concept of the vector microwave phase interferometer was also proposed and realized. The measuring device enables fast vector measurements of amplitude and phase distribution of interference field. The realized system was experimentally tested. It is prepared further extension to higher frequencies in microwave region.

Advantages of microwaves over light can lead to proposal of novel measurement techniques for nondestructive testing [3,4]. The wavelength of microwaves is approximately thousand times longer than the wavelength of light and one can carry out nondestructive measurements in the range that is impossible with light. The microwave array detector then enables to obtain the values of phase simultaneously at every point of the detector. Various physical properties of investigated materials can be determined from the phase values. Microwave phase interferometry enables measurements of large surface displacements and visualization of material defects in optically non-transparent materials. Both scalar and vectorial measurements are possible. The proposed methods can be used for design and application of new microwave measurement systems for evaluation of physical properties of structural materials in civil and mechanical engineering. Taking into account physical properties of microwaves, one can obtain new diagnostic method for non-destructive testing that make possible to perform static and dynamic measurements, which is either impossible or difficult with current methods in the microwave frequency band.

References:

[1] NOVÁK, J. - MIKŠ, A.: *Modern Optoelectronic Methods for Non-Contact Deformation Measurement in Industry.* Journal of Optics A: Pure and Applied Optics, 2002, vol. 4, no. 6, pp.413-420.

[2] NOVÁK, J.: *Five-step phase-shifting algorithms with unknown values of phase shift.* Optik, 2003, Vol. 114, No. 2, pp. 63-68.

[3] MIKŠ, A. - NOVÁK, J. - NOVÁK, P.: *Určování defektu stavebních materiálů pomocí fázové mikrovlnné interferometrie.* Defektoskopie 2004, ČNDT, Brno, 2004, pp.145-150.

[4] MIKŠ, A. - NOVÁK, J.: *Phase-Shifting Microwave Interferometry for Nondestructive Testing* Proceedings of SPIE Vol. 6158 . Washington: SPIE, 2006, pp. 154-158.

This research has been supported by GA ČR grant No. GA 102/04/0898.

CTU Prague Contribution to the Project AIRFLY in 2005 and 2006

V. Vacek, M. Doubrava,

vaclav.vacek@fs.cvut.cz

Department of Physics, Faculty of Mechanical Engineering, Czech Technical University, Technická 4, 166 07 Prague 6, Czech Republic

This note describes shortly contribution of the Department of Applied Physics at the Faculty of Mechanical Engineering of the CTU in Prague to the AIRFLY experimental program over the past two years.

The origin of very high-energy cosmic rays is still a great question in high-energy physics. The Pierre Auger observatory [1], nowadays built in Argentina, is destined to solve this question as well as the project HIRES or Telescope Array for instance. The observatory consists of several fluorescence telescopes and an array of surface water detectors. The task for fluorescence detectors is to detect the feeble fluorescence light emitted by nitrogen molecules excited by collision with cosmic rays of very high energy in high-level atmosphere (at altitude up to 20 km). This process is also accompanied by the Cherenkov emission, which has its characteristic forward anisotropy. The spectrum of the fluorescence light falls within 300 – 400 nm range. The knowledge of the fluorescence emission efficiency is the relevant contribution to the absolute energy calibration which is essential for the Pierre Auger experiment and others concerning with the task of high energy cosmic rays with the aid of fluorescence detectors.

In the past, there were two experiments AGASA and HIRES having dealt with the fluorescence and Cherenkov yield measurement. Unfortunately the results of both differ a lot; the divergence makes 15 – 20 %. The AIRFLY experimental program [2] is the measurement of the fluorescence and Cherenkov yields as a function of particle energy in wide energy interval from 50 to 800 MeV with the precision better than 5 %. The project has been realized at the Beam Test Facility (BTF) of the Laboratori Nazionali di Frascati near to Roma, where high-energy particles, particularly electrons or positrons, are generated by linear accelerator (LINAC). The other tests have taken its place in Argonne National Laboratory, situated in the suburb of Chicago, Illinois, USA.

The aim of our work was to propose a suitable design of chamber with controlled atmosphere. Final design should serve for simulations of Earth` s atmosphere in different altitudes and its dimensions should suite into laboratory possibilities. From it follows the requirements for the final design: inside temperature, air pressure and air humidity must be controlled and maintained at desired levels, chamber must be leak-tight, easily mounted to the accelerator outlet and must enable us finally to connect some measuring devices to its body (photo-multipliers, pressure and temperature probes etc.). It is obvious that the chamber has to cope with temperature changes ranging from –50 ˚C up to +30 ˚C and maintain to keep the inner pressure from almost perfect vacuum (about 20 mbar) up to atmospheric pressure (1013 mbar). Once these two properties are selected, they should stay relatively constant.

The first prototype was designed at our Department of Applied Physics and

successfully tested at Frascati in 2005 [3]. Liquid nitrogen was used to cool down of the inner volume of the chamber. Nitrogen flowed through 2 heat exchangers that were coiled inside the chamber-box. There were several minor problems that led to second and improved design.

VAKUUM Praha – a specialist in vacuum equipment production, manufactured the second chamber. The cooling system for this second prototype is very different. The cooling performance is achieved by the submerging the whole chamber into well-insulated bow filled with the dry-ice (melting temperature -79 °C). Temperature control is provided via the heating tape attached to chamber body. Chamber was tested during the May in our laboratory and also in a workshop of Institute of Physics of the Academy of Sciences. We were able to stabilize the temperature down up to -40 °C. Further improvement is expected once the final insulation will be used around the box housing both dry-ice and chambers itself. The second round of cooling performance tests was done during the September 2006, just before the planned measurements in Argonne National Laboratory. The results of these tests were quite satisfactory.

Our second task was to propose and design protective environment for the attached electronics around chamber body (photomultipliers, etc.). The reason for that is obvious. Condensation and further freezing of this condensate may damage or even destroy the electronics. We have finally chosen simple flushing of dry air around the equipment, placing the electronics in plastic tubes that were firmly attached to chamber. This protective accessory was made-up in workshops during the summer 2006.

The last part of our contribution was to design and prepare the mobile DAQ system suitable for chamber parameters monitoring, like the humidity, temperature and the inner pressure. The system is required to deal with several resistance and voltage signals. The whole system consists of 3 main parts: computer with PVSS software (preferably on laptop), USB CAN-BUS card and ELMB unit. Standard ELMB unit is capable to read 3 types of resistance temperature sensors (8x Pt 100, 16x Pt 1000, 16x NTC). The last fourth slots were dedicated for 16 voltage signals, so the configuration fully satisfies the desired reading needs for chamber operation. We have used PVSS software for that. It is object-oriented tool for system control. The PVSS project also offers simple export of data into commonly used Microsoft Excel.

References:

[1] THE AUGER COLLABORATION: *Pierre Auger Project - Design Report,* FNAL, 2001-2003

[2] PRIVITERA, P.: *Status and Prospects of the AIRFLY experiment,* AirLight 03, 2003, pp. 11-14.

[3] V. VACEK, M. DOUBRAVA, L. NOŽKA, M. HRABOVSKÝ *Chamber with controlled atmosphere for the project AIRFLY,* Fine Mechanics and Optics Vol.51, 2/2006, pp. 51-54.

[4] L. NOŽKA, P. SCHOVÁNEK, M. PALATKA, M. HRABOVSKÝ, J. ŘIDKÝ, V. VACEK ET.AL.: *Czech contribution to the project AIRFLY,* Fine Mechanics and Optics Vol.50, 1/2005, pp. 11-13.

This research has been supported by GAČR grant No. GA 101/01/

Non-Thermal Plasma Ecological Applications

S. Pekárek*, M. Pospíšil , C. Leys**

pekarek@feld.cvut.cz

*CTU, Faculty of Electrical Engineering, Department of Physics
Technická 2, 166 27 Prague 6, Czech Republic
Institute of Chemical Technology, Faculty of Environmental Technology, Department of Petroleum Technology and Petrochemistry, Technická 3, 166 28 Prague 6, Czech Republic
**Ghent University, Faculty of Engineering, Department of Applied Physics
Rozier 44, B-9000 Ghent, Belgium

Non-thermal plasmas offer good perspectives for the removal of low concentrations of pollutants in air at high flow rates. In this area, research is driven by the ever more stringent European legislation on emissions and by the limitations of conventional technologies such as thermal incineration, catalytic oxidation and adsorption. Since in a non-thermal plasma most of the input electrical energy goes into the production of energetic electrons rather than into gas heating, the energy cost for cleaning diluted VOC laden air streams is drastically lower than in thermal incineration. The decomposition mechanism in non-thermal plasmas is based on radical production through electron-molecule collisions and is therefore non-selective, allowing for treatment of mixed waste streams. The low temperature operation reduces the risk for toxic byproduct formation when destroying chlorinated compounds. In spite of the apparent advantages, non-thermal plasma technology has not yet been deployed on an industrial scale. The generation and stable operation of non-thermal plasmas at atmospheric pressure indeed remains a challenging problem for modern plasma science and technology. Other roadblocks towards industrial implementation are the poor scalability of many lab-scale prototypes and the lack of knowledge on the plasma-chemical kinetics that govern volatile organic compounds (VOC) decomposition and by-product formation.

Based on the common research interest in the field of non-thermal plasmas and their applications in environmental technology, scientific contacts between Department of Physics of the Faculty of Electrical Engineering of CTU and the Research Unit Plasma Technology at the University of Ghent, Belgium, were first established in 1998. In 1999 a NATO Collaborative Linkage Grant, involving additional partners from Russia, Italy and Slovakia, was applied for. Although the application was not supported, the progress and results of the parallel research efforts on gas cleaning by means of non-thermal plasmas continued to be discussed during occasional mutual visits and international scientific conferences. In 2003 the Flemish and Czech promoters received a teachers mobility grant in the frame of a Socrates/Erasmus agreement between the Faculty of Engineering of University of Ghent and the Faculty of Electrical Engineering of Czech Technical University. The purpose was to give lectures at the partner university in the field of plasma physics and plasma technology. However the main attention was paid to the scientific collaboration in the field of the research of the non-thermal plasma produced by the corona discharge. To optimise plasma source based on the corona discharge stabilized by the gas flow CTU and UGhent obtained a grant within a program of bilateral Czech Flemish collaboration. To analyze the end products of decomposition and to utilize the know how concerning the chemistry of studied VOCs the Institute of Chemical Technology in Prague became also the member of the team.

Corona discharge is however relatively low power electrical discharge, which changes into spark when the discharge voltage is exceeded. One of the ways, which can be used to enhance the discharge power and to maintain the discharge stability [1] is to use a flowing medium (air or a mixture of air with volatile organic compounds) delivered to the discharge volume.

The application of the gas flow for the needle to plate corona discharge stabilization is performed both at CTU in Prague and at the UGhent. However the implementation of this method at each of these universities is different. At CTU the flow of air is delivered to the discharge parallel with the discharge axis through the needle electrode and at UGhent perpendicularly to the discharge axis through the solid needle. Each of these methods has its advantages and drawbacks.

The objective of the project is to develop an optimised plasma source for the decomposition of pollutants, using the expertise and know-how of participating laboratories. To arrive at this aim, the specific research tasks are:

- Study of the physical principles underlying the differences and similarities between the non-thermal plasma sources that are under development at UGhent and at CTU.
- Plasma-chemical case studies for selected VOCs in order to map the main reaction channels leading to VOC decomposition and by-product formation in both plasma sources.
- Optimization of both non-thermal plasma reactors in terms of energy cost.
- Study of the combination of non-thermal plasma with a catalyst with the aim to decrease decomposition energy cost. From a wide range of catalysts the photo catalyst TiO_2 appears more efficient.

The results obtained in the field of non-thermal plasma application for decomposition of pollutants in air streams are summarized in [2-3].

It can be expected that non-thermal plasma technologies will be the core parts of a future integrated plasma-based system for the treatment of wastes and hazardous substances. However, further basic research is still required to bring the technologies to a level that allows industrial application.

References:

[1] PEKÁREK, S. – LEYS C., NEIRYNCK D., KHUN J. *Two Hollow Needles to Mesh Electrical Discharge with TiO2 Catalyst for VOC Decomposition* Proceedings of 17th Int. Symposium on Plasma Chemistry, CD-ROM, Toronto 2005, pp.11–15.

[2] PEKÁREK, S. – POSPÍŠIL M., KRÝSA J. *Non Thermal Plasma and TiO2 Assisted n-heptane Decomposition* Plasma Processes and Polymers 2006 pp.308-315.

[3] NEIRYNCK D. – KHUN J.: *Electrical Discharges in Flowing Medium* Proceedings of 4th Int. Workshop and School: Towards Fusion Energy-Plasma Physics, Diagnostics, Apppůlication, Kudowa Zdroj, Poland 2004 pp.677-684.

This work has been supported by the Czech-Flemish scientific cooperation research program under contract No. 1-2006-2007.

Time-resolved Energy Neutron Spectra in D-D Fusion Reactions

K. Řezáč, D. Klír, P. Kubeš, J. Kravárik

rezack@fel.cvut.cz

Department of Physics, Faculty of Electrical Engineering, Czech Technical University, Technická 2, 166 27 Prague 6, Czech Republic

The neutron diagnostic is very important for analyzing fusion plasma. By using the diagnostic methods we can identify many parameters of fusion plasma. The neutron spectroscopy diagnostic is a well-established diagnostic for short-lived plasma such as plasma foci and Z-pinches. The energy spectrum of neutrons produced in fusion plasmas provides information on the production mechanisms of the emitted neutrons and the energy distributions of the reacting ions.

The aim of this work is reconstruct time-resolved energy spectra of neutrons which are emitted in intense bursts. A typical example is the neutron emission from hot dense magnetized plasma in fusion D-D reaction on plasma focus or Z-pinches devices.

From a theoretical point of view, reconstruction of time-resolved energy neutron spectra with limited data is a highly underdetermined ill-posed problem. There are several theoretical approaches for the development of algorithms. One of these methods is Analog Monte-Carlo technique. The basic reconstruction algorithm consists of two steps. First, without any prior knowledge, generate of events, by uniform random generation, in the plane (t, E) at the "source position" (0 m). Then the algorithm tests if the even is detectable on all detectors. If test is passed the event is accepted and the corresponding element in reconstruction matrix accordant with plane (t, E) is increased by one unit and the corresponding bins in every detector are decreased by a unit. The first step of reconstruction process stops when a lot of events are not passed the test. Second step, the reconstruction follows like algorithm described at the first step. The difference is in generating of events. The events are not generating by uniform random generation but they are now governed by probability function, which have been reconstructed in the first step. The second step is iterated in order to obtain a maximum reconstruction efficiency factor. Detailed description of this method is in [1-3].

The basic formulation of the problem as well as test results indicates that the method could give better results when detectors in the opposite direction are also included. If we want to employ both directions of neutron detection, we must know the relation between the neutrons which are emitted in one direction and the opposite direction. The improvement includes the transformation of the neutron energies and anisotropy in neutron yield. The transformation of the neutron energies is based on the kinematics of the binary fusion system and it is applied specifically to the D-D fusion reaction. For the present, anisotropy in neutron yield wasn't included. The reason is discrepancy between mentioned facts in theory and measurements on plasma focus device.

This method was used in the processing of data from experiments in the PF-1000 facility. The experiments were performed with electrical energy of (600 ÷ 650) kJ, voltage of 27 kV, and current maximum of 2 MA. Neutron diagnostic contained chain of six detectors. The detectors were situated downstream (at distances of 7.00 m, 16.34 m and 58.34 m) and

upstream (at distances of –7.00 m, –17.01 m, and –58.21 m). The results of the application of the modified Analog Monte Carlo reconstruction method are shown in [1, 4].

Future prospects are modification of this method for data processing from S 300 facility and another improvement of the reconstruction method, where we will include anisotropy of target deuterons. Either, I suppose clearing discrepancy between mentioned facts about theory of anisotropy in neutron yield and measurements on plasma focus device. Then the neutron emission intensity will be included into relation between the emitting neutrons in one and in opposite direction. Further, I suppose application of another reconstructed method (Genetic algorithm), which provides better results than Monte Carlo method.

References:

[1] K. REZAC, D. KLIR, P. KUBES, J. KRAVARIK, M. STRANSKY: *Monte Carlo Simulations for Reconstruction of Neutron Time-Resolving Energy Distribution in D-D Fusion Reactions,* Czechoslovak Journal of Physics 56 Suppl. B, 2006, pp. 357–363.

[2] I. TISEANU, G. DECKER, W. KIES: *A Monte-Carlo technique for the reconstruction of time dependent spectra of short-pulse neutron sources,* Nuclear Instruments and Methods in Physics Research A 373, 1996, pp. 73–80.

[3] K. REZAC: *Time-resolved Energy Neutron Spectra in Fusion Reactions,* FEL ČVUT in Prague (study report), 2006.

[4] P. KUBES, J. KRAVARIK, D. KLIR, K. REZAC, ET AL.: *Correlation of Radiation with Electron and Neutron Signals Taken in a Plasma Focus Device,* NIEEE Transactions on Plasma Science 34, 2006, pp. 2349–2355.

This research has been supported by the research program No. 1P04LA235 "Research in Frame of the International Center for Dense Magnetized Plasmas", No. 1P05ME761 "Study of Imploding Loads at the S-300", "Research Center of Laser Plasma" LC528 of the Ministry of Education, Youth and Sport of the Czech Republic and the GACR grant No. 202-03-H162 "Advanced study in Physics and Chemistry of the Plasma".

Study of Fusion Neutrons at PF-1000 in Frame ICDMP

P. Kubeš*, D. Klír*, J. Kravárik*, K. Řezáč*, I. Ivanova-Stanik, L. Karpinski**, M. Paduch**, M. Scholz****

kubes@fel.cvut.cz

*ČVUT FEL Praha, Technická 2, 166 27 Praha 6
**IPPLM, Hery 23, 00-908 Warsaw, Poland

The reason why the plasma focus (PF) discharges are studied is the high efficiency of the x-ray generation, the acceleration of high-energy electrons and ions and (if one uses deuterium as a filling gas) the neutron production. A plasma-focus device is very convenient equipment for study of D-D reactions [1, 2].

In this paper we give an overview of the studies performed at the Institute of Plasma Physics and Laser Microfusion in frame of collaboration of International Centre on Dense Magnetized Plasmas during 2006.

The measurements were realized within the PF-1000 facility at electrical energy of 600-650 kJ, voltage of 30-33 kV, and the maximum current of 1.5-1.8 MA. The length of both electrodes was 600 mm. The outer cathode (400 mm in diameter) consisted of 8 parallel stainless-steel rods distributed symmetrically. The inner copper anode was made in a tubular form and it was embraced (at its base) with an alumina insulator of 230 mm in diameter. The filling pressure of deuterium was 3 torr. The total neutron yield was $10^{10} – 10^{11}$ per shot. The Ne102a scintillator covered with 10-μm-thick Al-foil detected x-rays in the range above 4 keV. Fast electrons of energies in range 50-400 keV were registered with three Cerenkov detectors (made of rutil crystals and shielded with 20-μm Al) located downstream (along the current sheath movement), upstream (behind of the hole of 5-cm-diameter in the top of the anode, in opposite direction to the current sheath movement) as well as side-on. 10 scintillation probes Ne102 with photomultipliers were used to perform the detailed time-resolved measurements of the hard x-ray (3 - 5 cm of steal or of lead was used as a filter) and the neutron emission. They were situated downstream (at distances of 7.0 m and 16.3 m, 58 m, 84 m) and upstream (at distances of 7.0 m, 16.3 m, 30.3 m, 58 m and 84 m). For neutron yield measurement indium and silver-activation counters were applied.

The profile of the detected neutron pulse is influenced by two factors: the time of neutron emission and the velocity of the neutrons. The influence of the emission time registered signals is strong near the source, whereas the influence of the velocity distributions of the neutrons is strong at large distances from the source. To estimate the influence of both mentioned factors, we used set-ups of nine detectors arranged in axial direction.

The influence of the scattered neutrons from the floor and the walls might substantially influence only the second part of the signal, i.e. the tail. We can see a partly confirmation of this statement in the decrease of the upstream signals, when the neutrons of the beam-target origin have the lowest energy. This decrease is very sharp in the first part (when the influence of the scattered neutrons can be neglected), and in the later part (the tail) which might contain scattered neutrons.

For a more exact determination of the time evolution of neutron spectra, a Monte Carlo simulation was used. With these calculations we can estimate the time of production and energy distribution of 90 % of the neutrons.

The results of this research on the temporal- and energy-distribution of neutrons and temporal correlations of radiation, fast electrons, high-speed camera frames and neutrons, as

produced in the deuterium current sheath and the plasma focus within the PF-1000 facility, can be summarized as follows:

The hard X-rays and fusion neutrons are usually emitted in two pulses. The first pulse correlates with the dip of the current derivative (i.e. the current peculiarity), and with the minimum diameter of the pinch column, observed in visible radiation frames. The second neutron pulse is usually emitted 120 to 200 ns later, simultaneously with intense hard X-rays, and it dominates the neutron production. In this pulse the number of fusion-produced neutrons is 3 to 10 times higher than that emitted in the first pulse.

The fast electrons are emitted mainly at the beginning of the first neutron pulse, usually in both axial directions, firstly in downstream and later on in upstream direction.

A temporal evolution of neutron energies (emitted downstream) in the pulse is manifested with the dominating initial high energies of neutrons 2.7 to 3.2 MeV, and with a part of neutrons with energies of 2.2 to 2.4 MeV at the final part of the neutron pulses.

In the high-speed images in visible wavelength, one can see the correlation of the first neutron pulse with the axial motion of the radiating plasma, and with the forming and existence of a spherical structure at the bottom of the dilating current sheath. The maximum of the second neutron pulse is observed during the explosion of the second pinch. We have not found any evidence of the movement of the plasma in the downstream direction during this phase. We have recorded only a structure at the bottom of the dilated current sheath at the final phase of the neutron pulse, similar to that formed after the first pinch.

The major part of the fast deuterons producing neutrons has velocities in downstream direction. A small part of fast deuterons producing the final part of neutrons has velocities in opposite upstream direction. The origin of fast neutrons emitted in downstream direction seems to be of a beam-target mechanism. A small part of neutrons with final energies of 2.2 to 2.4 MeV, emitted downstream at the final part of the neutron pulse, can either be of thermonuclear or more probably of beam-target origin from fast deuterons moving in upstream direction.

In future studies we will concentrate to the experimental and simulation studies of the possibility of the heating of the dense structures with the ion beam, accelerated during the pinch phases of the discharge.

References:

[1] SOTO L.: *New Trends and Future Perspectives on Plasma Focus Research,* Plasma Physics and Controlled Fusion,vol. 47, 2005, pp. A361-A381.

[2] KUBES P., KRAVARIK J., KLIR D., REZAC K., SCHOLZ M., PADUCH M., TOMASZEWSKI K., IVANOVA-STANIK I., BIENKOWSKA B., KARPINSKI L., SADOWSKI M.J., SCHMIDT H.: *Correlation of Radiation with Electron and Neutron Signals Taken in a Plasma-Focus Device,* IEEE Transactions on Plasma Science Vol. 34, Issue 5, Part 3, 2006, pp. 2349-2355.

This research has been supported by grants 1P04LA235, 1P05ME761, LC 528, GD 202/03/H2162.

Computer modeling of solid state crystallographic texture

A. Grishin*, L. Kalvoda

grishin@fjfi.cvut.cz

*Department of Solid State Engineering, Faculty of Nuclear Science and Physical Engineering
Czech Technical University, Trojanova 13, 120 00 Prague 2, Czech Republic

Crystallographic preferred orientation, or texture, is a non-random distribution of the crystallites in a polycrystalline material as a consequence of nature of the crystallites or the manufacturing process. For that reason texture contains detailed information about the production history of a work piece. On the other hand, texture has a strong effect on properties so that it contains easily accessible information on the interrelation between processing parameters and material performance. In many alloying systems the interrelationship between microstructure and properties contains the key information for establishing the strategies of material development. Texture is an essential part of the microstructure and can play a dominant role when the anisotropy of single crystals is large and crucial. Enhanced formability in steel and aluminum sheet products used in stamping of automotive panels follow from control of texture through control of the production processes. Quantitative texture analysis provides the essential feedback for tuning the thermo-mechanical history on the basis of detailed insight into controlling mechanisms, thereby leading to desired properties in the finished product. Economic savings through control of texture can be significant: due to the large production volume of sheet material, such as aluminum can body stock, great savings can be achieved through the reduction of scrap caused by earing.

The presented work was focused on simulation of the general relationship: deformation - crystalline structure – polycrystalline texture – material properties. In the following, the applied techniques and approaches are briefly summarized.

Modulation and simulation of the grain growth and recrystallization were made with the help Material Studio (MS, Accelrys, USA) software, which used Monte Carlo method to simulate microstructural evolution where equilibrium occurs on a local basis at best (e.g. at triple junctions). In general, the system is far from equilibrium and we attempt to study the kinetics of the processes that lead to equilibrium as a function of time e.g. grain growth or recrystallization. Powder diffraction patterns are calculated for a large number of trial structures and compared to the experimental powder pattern. The trial structures are generated using a Monte Carlo/simulated annealing algorithm or a Monte Carlo/parallel tempering algorithm.

Both approaches are designed to locate the global minimum of the weighted R-factor, R_{wp}, which is a measure of the similarity between the experimental powder data and the simulated powder patterns. Lattice symmetry is explicitly taken into account. The atoms in the asymmetric unit are gathered together into motion groups. Each motion group is described by three translational and three rotational degrees of freedom, as well as a certain number of torsional parameters.

Typically, each molecular fragment in the asymmetric unit corresponds to a motion group. Apart from the torsional degrees of freedom, the conformation of each motion group has to be determined prior to structure solution using potential energy calculations or structural information from related crystal structures. In the Monte Carlo search, only the translational, rotational and torsional degrees of freedom of the motion groups are considered. Structure solution has to be attempted separately for all relevant space groups.

The growth rate of the crystal face is assumed to be proportional to its attachment energy; that is, faces with the lowest attachment energies are the slowest growing and, therefore, have the most morphological importance.

Simulated trial structures taken during the growing process were processed with MS Reflex Plus, MS Amorphous Cell, MS Morphology and MS Discover modules for diffraction pattern simulation and comparison with the experimental data.

Finally, the result of the structure solution step was further improved by Rietveld refinement and ODF (Orientation Distribution Function) with pole figures for different times obtained. The MAUD (Material Analysis Using Diffraction) program was used for that.

Even with the high resolution of neutron diffraction, deconvolution of diffraction spectra by profile analysis remains a major obstacle for texture analysis of materials with complex diffraction spectra. Conventionally peaks *hkl* have been fitted with Gauss functions to obtain integrated intensities. From such deconvoluted pole figures the 3-D OD can be determined. However, rather than extracting information from single diffraction peaks, it would be more efficient to use the whole diffraction spectrum and extract texture information in a similar way as crystallographers extract structural information from a powder pattern with the Rietveld technique. The Rietveld refinement proposes weights for each peak to improve the fit, these are then used for the OD calculation with the discrete WIMV (Williams-Imhof-Matthies-Vinel) algorithm that refines the weights based on texture correlations. The iterative procedure converges very rapidly and provides quantitative information about texture, crystal structure, elastic strains, and microstructural parameters (such as grain size). A powder diffraction pattern from a specimen exhibiting preferred orientation will display intensity values that differ systematically from those of a specimen with random orientation. Comparison of modeled and experimental diffraction patterns showed good convergence.

The upper described complex model was employed for two classes of geological materials, calcium carbonates and meta-gabros. The results will be published in a forthcoming paper.

References:

[1] KOCKS,U.F., TOME C.N., WENK H.-R.: *Texture and Anisotropy. Preffered Orientations in Polycrystals and their Effect on Materials properties,* Cambridge University Press, 2005.

[2] SIEPMANN J.I., FRENKEL D.: *Configurational bias Monte Carlo,Molecular Physics, 75,* Taylor & Francis, 1992, pp. 59-70.

[3] MATTHIES, S. & VINEL, G. W.: *On the reproduction of the orientation distribution function of texturized samples,* Phys. Status Solidi B, 1982, pp. 111–120.

[4] MATTHIES S., LUTEROTTI L., WENK H.-R.: *Advances in Texture Analysis from Diffraction Spectra,* J. Appl. Cryst.,30, 1997, pp. 31–42.

This research has been supported by FRVŠ grant No. 33-06005.

Powder Neutron Diffraction Study of Crystal, Magnetic and Transport Properties of Layered Cobalt Oxides

M. Dlouhá, S. Vratislav, A. Chichev, Z. Jirák*

dlouha@troja.fjfi.cvut.cz

CTU, Faculty of Nuclear Physics and Physical Engineering
Břehová 7, 115 19 Praha 1
*Institute of Physics CAS
Cukrovarnická 10, 162 53 Prague 6

Transition metal oxides with 3d electrons exhibit unusual magnetic and transport properties due to the subtle balance between the crystal-field-splitting Δ_{CF} , on-site Coulomb repulsion expressed by Hubbard parameter U and the energy of charge transfer between transition metal and oxygen $\Delta_{TM\text{-}O}$. Moreover, Co^{3+} ion in octahedral coordination could exists in three spin states, the non-magnetic low spin state, that in the limit of fully localized electrons in strong crystal field corresponds to filled t_{2g} levels and empty e_g states (LS, $t_{2g6}e_{g0}$, S = 0), and two states that can give rise to the magnetism corresponding either to the intermediate spin (IS, $t_{2g5}e_{g1}$, S = 1) or to the high spin state (HS, $t_{2g4}e_{g2}$, S = 0).

Presently studied system can be structurally classified as a member of the Ruddlesden-Popper series $(AO)(ABO_3)_n$. Ruddlesden-Popper phases are formed by *n*-layer slabs of perovskite ABO_3, which are separated by rock-salt layer AO. For the magnetic and transport properties, it is especially important that the presence of the AO layer disturbs the 3-dimensional periodicity of the perovskite structure. The end members $La_{2-x}Sr_xCoO_4$ and $La_{1-x}Sr_xCoO_3$ ($n = \infty$) represent thus closely related systems with quasi-2D and 3D character, respectively.

The purpose of the present work is to investigate the $La_{2-x}Sr_xCoO_4$ system in the whole accessible region of $Co^{3+/4+}$ valence, using the X-ray and neutron diffraction, measurements of magnetization, electric and thermal conductivity, and thermopower. The study will try to show how the quasi 2D character of the samples modifies the properties, as compared to their 3D counterparts with a similar extent of hole doping.

The ceramic samples of $La_{2-x}Sr_xCoO_4$ ($0.9 \le x \le 1.5$) were prepared by a sol-gel method. The starting compounds La_2O_3, $SrCO_3$ of the actual contents of the cationic components determined by chemical analysis, were separately dissolved in nitric acid, mixed together with citric acid and ethylene glycol in the ratio of (2-*x*[La]+*x*[Sr]+[Co]) / 1.5[citric acid] / 2.25[ethylene glycol] and pH was adjusted to 9 by addition of NH_4OH. Further steps included evaporation of water at 80 – 90°C, drying at 160°C and calcination at 400°C (4 h) in air. The resulting powder was ground and pressed into pellets and annealed at 1000 °C for 100 h in an oxygen atmosphere. By X-ray diffraction analyses (Bruker D8, CuKα, SOL-X energy dispersive detector), the single n=1 Ruddlesden-Popper phase was observed in the studied system except for sample x=1.5 where traces of unknown impurity were detected. More detailed investigation of physical properties was, therefore, performed up to the limit x=1.4.

The electrical resistivity, magnetic susceptibility data and magnetization curves were measured using the SQUID (T < 300 K) or torque (T >300 K) magnetometers at the Institute symmetry were determined at room temperature by X-ray powder analyses using the FULLPROF program. The neutron diffraction has been performed on a selected sample x=1.4

on the diffractometer KSN-2 at room temperature using an improved resolution and neutron wavelength λ=1.363 A. The study was completed down to low temperatures, both at normal pressure and up to 4.3 GPa, on the high pressure facility DN12 at pulsed reactor IBR-2. The experimental data were analysed with the Rietveld method using the MRIA and FULLPROF programs. Neutron diffraction study of $La_{0.6}Sr_{1.4}CoO_4$ taken at room temperature was carry out on the diffractometer KSN-2. The spectra at 16 K do not show any new line that could be ascribed to an antiferromagnetic order. Absence of ferromagnetic contribution at the diffraction peak (004) reveals that the magnetic moments of cobalt ions are oriented along the c axis of the I4/mmm structure, i.e. perpendicular to the layers. Their calculated magnitudes amount to 0.7 μ_B per Co, which is in agreement with the above mentioned magnetization data. These finding confirm that ferromagnetically ordered regions really exist in the paramagnetic matrix and are not just field-induced in $La_{0.6}Sr_{1.4}CoO_4$.

It is generally accepted that the magnetism and transport in mixed valent perovskites are predetermined by the extent of carrier doping and by the bandwidth. Lowering of the dimensionality brings about an anisotropic reduction of the bandwidth, modifying physical properties.

The physical properties of $La_{2-x}Sr_xCoO_4$ perovskite cobalt oxides have been measured and analyzed. Investigated cobaltites have the tetragonal crystal symmetry (space group I4/mmm). The lattice constant a decreases with increase of strontium concentration and c has maximum at x=1.2. All samples exhibit an insulating behaviour which doesn't change with x. With the increasing strontium concentration spin-state transition HS to IS and appearing of FM order (T_c =150K) are to be observed. Thus the physical properties of $La_{2-x}Sr_xCoO_4$ perovskite cobalt oxides obtained in the present paper concur with recently described [see 1, 2, 3]. However in works [4] was revealed that influence of a high pressure leads to significant change of magnetic and transport properties cobalt oxides $La_{1-x}Sr_xCoO_3$. Most likely similar changes can occur in the investigated samples $La_{1-x}Sr_xCoO_4$. Thus high-pressure study planned for near future.

The neutron diffraction study evidences a presence of the long range ferromagnetic order in $La_{0.6}Sr_{1.4}CoO_4$ at low temperatures. The relatively low magnitudes of cobalt moments 0.7 - 0.8 μ_B suggest that the magnetic state is in fact non-uniform. It consists of ferromagnetic regions aligned by strong Co^{3+}- O - Co^{4+} double exchange interactions, which coexist with paramagnetic or spin-glass regions.

References:

[1] Y. MORTOMO, K.HIGASHI, K. MATSUDA, A. NAKAMURA : *Phys. Rev.* B 55 1997, 14725.

[2] Y.FURUKAWA, S. WADA, Y.YAMADA .: *Canted Structures in the Mn3+ /Mn4+ Perovskites by Neutron Diffraction,* J.Phys Soc. Japan. (1993) 1127.

[3] M. DLOUHÁ, S. VRATISLAV, Z. JIRÁK : Condens Matter 12(2000), 7425-7432.

[4] R.LENGSDORF, S. AIT-TAHA, S. RSAXENA, M. ELLERBY, D. KHOMSKII, H.MICKLOTZ, T. LORENZ : Phys. Rev., B 69, 12(2004).

This research has been supported by GA CAS No. IAA100100611, MSM 6840770021

Decomposition of Volatile Organic Compounds by Plasma Enhanced Photocatalyst

S. Pekárek

pekarek@feld.cvut.cz

CTU, Faculty of Electrical Engineering, Department of Physics
Technická 2, 166 27 Prague 6

For decomposition of pollutants such as toluene $C_6H_5CH_3$, trichlorethane $C_2H_3Cl_3$, *n*-Heptane $CH_3(CH_2)_5CH_3$ etc. in air streams the non-thermal plasma technologies based on electrical discharges are intensively studied. Electrical discharges tested for these purposes are mainly corona discharge and dielectric barrier discharge in a confined space. The corona discharge reactors involve different electrode configurations, the most frequently wire-to-cylinder, corona torch, pin-to-plate and a multi-pin-to-plate electrode configuration.

Corona discharge is however relatively low power electrical discharge, which changes into spark when the discharge voltage is exceeded. To increase the discharge current-voltage range, that is to increase power delivered to the discharge without the discharge transition into spark, following approaches are used:

- Application of a pulse voltage.
- Usage of resistive electrode and electrode with a shaped surface.
- Application of a gas flow with respect to the active electrode.
- Application of the ultrasound waves.

In our laboratory we use discharge stabilization by the gas flow or by the application of the gas flow together with ultrasound waves [1].

Recently, it has been shown that a combination of non-thermal plasma with a catalyst leads to very promising results for the decomposition of atmospheric pollutants at relatively low energy cost. There were many catalysts tested for this purpose. Among them were TiO_2**,** ZnO, V_2O_5, SnO_2, WO_3, CdS, ZnS etc. Of all these, the photocatalyst TiO_2 appears more efficient. Titanium dioxide TiO_2 is an n-type semiconductor, biologically and chemically inert existing in rutile and anatase phase. For VOC decomposition the anatase TiO_2 is predominantly used, because it has a higher O_2 adsorbing capacity than rutile TiO_2.

We studied hollow needle to mesh discharge enhanced by the flow of the mixture of air with VOC through the needle electrode with three different versions of the mesh electrode. The first version involves simple stainless steel mesh, the second version deals with the stainless steel mesh coated with a layer of TiO_2 and the third version involves a stainless steel mesh with a layer of TiO_2 globules. As a representative of VOC for decomposition studies we chose *n*-Heptane $CH_3(CH_2)_5CH_3$ because it is not only a part of organic solvents but also a part of automotive and aviation fuels. It also represents a wide group of saturated hydrocarbons with single bounds**.**

From the study of discharge operational regimes we found that the hollow needle to mesh discharge stabilized with the flow of the mixture of air with VOC through the needle electrode

can operate with currents exceeding corona currents in stable regimes without the discharge transition into spark [2]. The values of current, which were achieved, allow the usage of the discharge for VOC decomposition.

From the decomposition experiments several conclusions can be taken [3,4]. First of all in each investigated cases (that is uncoated mesh, mesh with a TiO_2 coating and mesh with TiO_2 globules) the *n*-Heptane decomposition efficiency increases with increased energy density. Maximum decomposition efficiency 50.4 % was obtained for the discharge with TiO_2 globules for energy density 350 kJ/m^3 and for relative humidity of the mixture 27 %.
The second conclusion is that for particular energy density the decomposition efficiency is the smallest for the discharge with an uncoated mesh and the highest for the discharge with TiO_2 globules. This result of *n*-Heptane decomposition in the presence of TiO_2 can be explained by the combined effect of processes associated with discharge physics, processes associated with the presence of photocatalyst TiO_2 in the discharge volume and finally by the adsorption. In case of TiO_2 globules the photocatalysts area exposed to the UV radiation emitted from the discharge as well as the surface area of the photocatalyst is greater than for the case of TiO_2 coated mesh, therefore the decomposition efficiency is higher.
The end products of decomposition experiments were analysed using the gas chromatography. The experimental results reveal that there were no traces of partially oxidated organic structures (e.g. formaldehyde) and no cracking volatile products (e.g. ethylene or propylene) found at the exhaust gas. On the other hand there were traces of carbon monoxide and carbon dioxide. Pulsed corona discharge in a mixture of air with some VOC produces a large amount of nanometer size aerosols. However in our case that is for a DC discharge with a TiO_2 photocatalyst by simple visual observation no aerosols were found. From the experiments we can also conclude that no change of the surface of TiO_2 globules induced by non-thermal plasma has been observed.

We showed that combination of the non-thermal plasma with photocatalyst leads to promising results for the decomposition of atmospheric pollutants at relatively low energy cost.

References:

[1] PEKÁREK, S. – BÁLEK, R.: *Ultrasound and Airflow Induced Thermal Instability Suppression of DC Corona Discharge: Experimental Study* Plasma Sources Science and Technology 2006, pp.52–58.

[2] PEKÁREK, S. – BÁLEK, R.: *Effect of Ultrasound Waves on Electrical Characteristics of Hollow Needle to Plate Discharge in Air or Mixture of Air with VOCs* Czechoslovak Journal of Physics, Suppl. B 2006 pp.982-989.

[3] PEKÁREK, S. – KHUN, J.: *Non Thermal Plasma Enhanced PtRhPd/Al2O3 Honeycomb Catalyst for n-Heptane Decomposition* Proceedings of XVIth Int. Conf. on Gas Discharges and their Applications, CD-ROM, Xi´an, Čína 2006 pp.489-492.

[4] PEKÁREK, S. – POSPÍŠIL, M.: *Non Thermal Plasma and TiO2 Assisted n-Heptane Decomposition* Plasma Processes & Polymers, 2006 pp.308-315.

This research has been supported by GA ČR grant No. 202/04/0728.

On the Road to Shorter Wavelength X-ray Z-pinch Laser Using Wire Explosion in Shock Wave Focus in Water

M. Martínková, K. Koláček *, M. Kálal

martinkovam1@km1.fjfi.cvut.cz

Department of Physical Electronics, Faculty of Nuclear Sciences and Physical Engineering, Czech Technical University in Prague, Břehová 7, 115 19 Prague 1, Czech Republic

*Institute of Plasma Physics, AS CR, Za Slovankou 3, 182 00 Prague 8, Czech Republic

During the last two years a new approach to generators of X-ray radiation with high degree of coherence has been pursued both experimentally as well as by simple analytic modeling at the Department of Pulse Plasma Systems of the Institute of Plasma Physics, AS CR. The main innovation consists in the use of an exploding wire in water creating a conducting channel surrounded by the water wall, which stabilizes a shape of the channel. Subsequent electric discharge causes the so called Z-pinch effect (the electric current generates magnetic field which compresses the plasma as the current increases). An additional converging cylindrical shock wave in water simultaneously pushes the plasma density to even higher values.

In order to perform these novel experiments, the apparatus CAPEX-U (CAPillary EXperiment Upgraded – used earlier for high voltage Z-pinch discharge in argon prefilled capillaries to produce plasma radiating at the wavelength ~ 46 nm) [1] has been converted into a joint apparatus: CAPEX-U combined with a new sophisticated SHOW (SHOck Wave) device [2] (designed especially for these experiments) to replace the classical capillary. Wavelengths generated by this joint apparatus were expected to be lower than 40 nm.

The main purpose of the SHOW device is to produce focused cylindrical shock wave in water. The device consists of a capacitor bank, a spark gap, and a cylindrical experimental chamber of dimensions ∅40x20 cm filled by a conducting water. The capacitance of the bank is 18 μF/50 kV. The shock wave is initiated by a pulsed multi-streamer high voltage discharge generated at the inner surface of the cylindrical stainless steel wall covered by porous ceramics (that serves as a grounded electrode). A co-axial metallic mesh, placed at the diameter of 30 cm, serves as a high-voltage electrode, which is transparent for the shock wave [3].

To successfully perform its important role (i.e. additional compression of the Z-pinch plasma) the generated shock wave needs to arrive to the axis of symmetry (where the wire was initially placed) just in the moment of wire explosion. Estimated pressure of the shock wave at its focus (radius ~ 1 mm) is supposed to reach ~ 1GPa using the charging voltage of 45 kV.

It is presumed that similarly to the Z-pinch stabilization effect by the wall proximity in solid capillaries, the same role can be played by the liquid wall (with its pressure further enhanced by the shock wave) in the case of exploding wire plasma. Moreover, reduction of instabilities growth rate in the imploding plasma is also expected.

The pressure of the shock wave in its focus has been measured by off-axis shadowgraphy, as well as by piezoelectric and fibre-optic sensors. A simple analytical estimation of the achieved pressure was also performed and compared to the experimentally observed values [4].

References:

[1] KOLACEK, K. - SCHMIDT, J. - PRUKNER, V. - STRAUS, J. - BOHACEK, V. - FROLOV, O. - VRBA, P.: *Fast Capillary Discharge – Environment for Amplified Spontaneous Emission in Soft X-ray Region*, 2nd European Pulsed Power Symposium, EPPS 2004, DESY, Hamburg, Germany, September 20-23, 2004, p. 19-23.

[2] PRUKNER, V. – KOLACEK, K. - SCHMIDT, J. - STRAUS, J. - FROLOV, O. - MARTINKOVA, M.: *Apparatus for converging cylindrical shock wave in water generated by pulsed multi-streamer discharge at one cylindrical electrode*, International Conference PLASMA, and the 3rd German-Polish Conference on Plasma Diagnostics for Fusion and Applications, 2005.

[3] KOLACEK, K. - SCHMIDT, J. - PRUKNER, V. - FROLOV, O. - STRAUS, J. - BOHACEK, V. - MARTINKOVA, M.: *Pulsed High-Current Experiments At IPP ASCI CR Prague*, 6th International Conference On Dense Z-Pinches, Oxford, UK, 25-28 JULY, 2005.

[4] MARTÍNKOVÁ, M.: *Characteristics Measurement of Convergent Cylindrical Shock Wave in Water*, Diploma Thesis (in Czech), FNSPE CTU in Prague, 2006.

This research has been supported by the grants GACR 202/03/0711 and 202/06/1324.

Low-energy Nuclear Excitation by Laser-produced Plasma

C. Granja*, J. Jakůbek*, V. Linhart*, S. Pospíšil*, T. Slavíček*, J. Uher*, Z. Vykydal*
J. Kuba, M. Šiňor**, L. Drška****
O. Renner*, L. Juha***, J. Krása***, E. Krouský***, M. Pfeiffer*****
J. Ulschmied***

carlos.granja@utef.cvut.cz

*Institute of Experimental and Applied Physics, Czech Technical University, Horská 3a/22, 128 00 Prague 2, Czech Republic

**Faculty of Nuclear Sciences and Physical Engineering, Czech Technical University, Břehová 7, 115 19 Prague 1, Czech Republic

***Institute of Physics, AS CR, Na Slovance 2, 182 21 Prague 8, Czech Republic

Nuclear excitation induced by laser-produced plasma radiation is well demonstrated at ultra-short and ultra-intense lasers [1]. Such large-scale systems generate power well over 10^{18}Wcm^{-2} and plasma radiation with energy spectrum well above 100 keV. Such hard X-rays induce nuclear reactions at non-negligible rates. However, regarding the excitation of atomic nuclei with *low-energy* photons, experiments have yielded inconclusive evidence which require confirmation and unequivocal demonstration. Similarly, the interaction of nuclear *isomers* with laser-produced plasma radiation (perspective for studies of stimulated energy release) has been demonstrated namely using high-energy radiation. These experiments are carried out also at synchrotron sources, or even with a dental X-ray unit (which is however considered unrealistic namely by the low power of such source; more precise experiment using a more intense source yielded negative results).

The radiation spectrum of laser-produced plasma depends on the laser-matter interactions, the specific laser pulse characteristics and the particular target material used. The medium-size high-power laser system Prague Asterix Laser System PALS facility (see http://www.pals.cas.cz) operates with a fundamental laser wavelength 1.315 μm, pulse duration 250 ps, plasma pulse power energy of order several hundreds of J and subrelativistic intensity of order 10^{16} Wcm^{-2}.

Plasma-nuclear interactions in hot, dense laser plasmas can result in nuclear-photonic and nuclear-electronic excitations. A number of interactions can occur such as direct photoexcitation, nuclear excitation by electronic transition (NEET), nuclear excitation by electron capture, X-ray electron-nuclear transition, excitation upon collective atomic shell transition and inelastic electron scattering [2]. Under the PALS plasma and selected target (^{181}Ta) conditions, direct photoexcitation and NEET are considered [3] as preferred mechanism for eventual low-energy nuclear excitation.

This work [4] investigates the possibility of induced low-energy excitation of atomic nuclei by plasma radiation of medium-size high power laser systems such as PALS. The main aim is to test operation of active detectors for plasma radiation diagnosis as well as to study processes and new methods between nuclear and plasma-laser physics. The application of various active detector systems intents to increase the sensitivity and selectivity of detection of rare events (photons) in a high background medium. As part of this effort, a detailed survey of possible targets suitable has been performed [3] from which ^{181}Ta is proposed and

confirmed as suitable experimental candidate for experiments of nuclear excitation by laser-produced plasma at PALS.

The experiments carried out at PALS use [4] a massive Ta target onto which a single laser beam (150-180 J, 1.315 μm, 0.25 ns) was focused to a diameter of 80 μm yielding an intensity of $1.2x10^{16}Wcm^{-2}$. Using a ^{181}Ta target at a laser shot intensity of $7x10^{16}Wcm^{-2}$ and focal spot 80 μm in diameter, at a distance of about 10 μm the plasma electron temperature is approximately 1 keV, the electron plasma density is of order $10^{20}cm^3$, the number of ions is about 10^{13}, the ion charge distribution is up to 40, and plasma volume of about $3x10^{-6}cm^{-3}$ [3]. In frame of these experiments on this target [4], feasibility tests are carried out of operation of various experimental arrays including active detection systems in the extreme conditions (detection of weak signal in high electromagnetic and radiation background). The radiation detector systems used are of both types passive or active detection systems and may be classified in two groups according to their purpose: *Monitoring*: Dosimeters (TLD detectors and X-ray streak camera; *Spectroscopic*: Time-integrated X-ray spectroscopy (bent--crystal + film), Scintillator detectors (inorganic and plastic scintillators), PIN photodiodes, Semiconductor position--sensitive pixel detectors (Medipix2).

Currently, this work [4] aims at estimating upper limits for observation of this phenomenon as well as to examine the feasibility of experiments directed to nuclear studies at laser intensities producing subrelativistic plasmas. Results can have also significance for studies of triggered nuclear decay (stimulated energy release) [1] and gamma--ray lasers.

References:

[1] K.W.D. LEDINGHAM, P. MCKENNA, R.P. SINGHAI: *Applications for nuclear phenomena generated by ultra-intense lasers,* Science 300 (2003) 1107

[2] M. R. HARSTON, J. F. CHEMIN: *Mechanisms of nuclear excitation in plasmas,* Phys. Rev. C 59 (1999) 2462

[3] C. GRANJA, J. KUBA, A. HAIDUK, O. RENNER: *Survey of nuclei for low-energy nuclear excitation in laser-produced plasma,* Nuclear Physics A (2007) in print

[4] C. GRANJA, J. JAKUBEK, V. LINHART, S. POSPISIL, T. SLAVICEK, J. UHER, Z. VYKYDAL, J. KUBA, M. SINOR, L. DRSKA, O. RENNER, L. JUHA, J. KRASA, E. KROUSKY, M. PFEIFER, J. ULLSCHMIED: *Search for low-energy nuclear transitions in laser-produced plasma,* Czech. J. Phys. 56 (2006) pp. 478--484

This work was funded by the Grant Agency of the Czech Republic under Grant No. 202/06/0697 and in part by the Research Program No. 6840770029 Fundamental experiments in Physics of the Microworld of the Ministry of Education, Youth and Sports of the Czech Republic. Work with the Medipix2 detector is done in frame of the CERN Medipix Collaboration. The authors appreciate the support given by the staff of PALS.

The Influence of Dielectric Barrier Discharge on Polyester Fabric Wettability

Y. Klenko

klenkj1@fel.cvut.cz

Department of Physics, Faculty of Electrical Engineering, Czech Technical University, Technická 2, 166 27 Prague 6, Czech Republic

Plasma treatment of textile fabrics is being investigated as an alternative to wet chemical fabric treatment and pretreatment processes, which lead to altering fabric mechanical properties and are environmentally hazardous. Operation at the atmospheric pressure plasma in comparison with low-pressure plasma treatment have some significant advantages so as low cost of the work equipment and simplicity of the process condition. The transfer of research results connected with atmospheric pressure plasma into the technological field occurred already some years ago. But is necessary to go on very thorough laboratory study of influence of various types of atmospheric plasma on textile fibers modification [1-3]. First of all the influence of plasma characteristics (e.g. exposure time and discharge power) must be explored.

Plasma consists of many excited particles (e.g. electrons, radicals, ions, photons etc.). During plasma treatment the uppermost atomic layers of material surface are modified and the bulk characteristics remain unaffected. This treatment of textiles may result in desirable surface modification (surface etching, surface activation, cross-linking, chain scission, decrystallization, and oxidation). Plasma-chemical conversion of the atmospheric air produces chemically active particles able to modify textile surface molecules via chemical reactions after striking on the surface. The radicals generated inside the plasma region must be given the opportunity to move to the reaction place at the textile fiber surface [4]. Thereby the path of radicals between the points of their generation and subsequent reaction is limited on one hand by the distance between single fibers, and on the other hand by the gas density, i.e. by the mean free path of the gas particles. Assuming radicals react or recombine after several impacts with gas particles and at surface sites on fibers there is a relationship between penetration depth of the plasma effect inside the textile structure and process pressure as well as the textile structure itself.

This contribution is focused on a study of treatment of polyester fabric by an atmospheric dielectric barrier discharge (DBD). For all the experiment the polyester fabric (TIS/05/F04/hot 9858) was used as the test specimen. Before insertion into the plasma reactor fabric specimens had to be cleaned. The cleaning consisted of following steps: washing, rinsing, chemical cleaning, drying. Thereafter the PES samples were placed into the DBD reactor - open cylindrical vessel (diameter 15 cm, height 15 cm) containing two plane iron electrodes, both with diameter 45 mm and thickness 10 mm. The glass barrier was created with the (83x83) mm, 2 mm thick glass table stuck to one of the electrodes. Discharge was fed by the HV transformer connected to an electrical power network 220 V/50 Hz. The DBD input voltage varied between $(18.0 \div 18.5) \times 10^3$ V and discharge current $(1.1 \div 1.9) \times 10^{-3}$ A. All experiments were performed in stationary air under atmospheric pressure (745÷753) torr and room temperature (20÷23)°C. The sample treatment times were 60 s, 150 s, 240 s and 360 s. The experiments have been done in flowing air, flow rate of 0.075 m^3/s. Continual pumping provided stable air composition during the treatment. The wettability was evaluated by means of the drop test. Water solution of potassium dichromate (5×10^{-3} g/µl) was used as a test liquid for better visualization. The 20 µl of the solution was dropped on the textile sample and after start of every experiment the feathering spot size was recorded with a camera. Monitoring was performed in 5 seconds intervals within the first 30 seconds after drop

incidence on the fabrics and in 10 seconds intervals afterwards. The total observation time was 200 seconds. The area of the spot in the 60th second after the drop release was used as the standard for the evaluation.

The results of the experiment with modification time 60 s were compared with the experiments without pumping and with unmodified samples. The wettability measurements were taken immediately after the treatment and then in the 3rd, 7th, 13th, 17th and 20th day.

The positive influence of the plasma treatment was observed on all samples exposed to modification. Evidently, the modification effect for both regimes and various treatment times was identical when measured on the same day immediately after the DBD treatment. The first differences between samples from various modification regimes and treatment times occurred on the 3rd day after modification. The modification effect of the samples with "150-seconds" or "60-seconds treatment time" modified in the "with pumping" regime had reduced to 50% on the 3rd day after modification. On the 7th day after modification the feathering area of these samples was similar to unmodified samples.

The time dependence of the fabric feathering area for the samples with "240-seconds treatment time" decreased similarly as in the case of samples after 3 days and practically by the same way as for the samples after 7th day. The feathering area gradually decreased and on the 13rd day after plasma modification became alike to the unmodified state.

The 60 s ("without pumping" regime) and 360 s samples behaved approximately equally: from 3rd to 17th day feathering area kept near the stable value (600 mm^2).

References:

[1] PICHAL, J., KOLLER, J., AUBRECHT, L., VATUNA, T., SPATENKA, P., WIENER, J.: *Application of atmospheric corona discharge for PES fabric modification,* Czech. J. Phys., Vol. 54, 2004, pp. 828–834.

[2] KLENKO, Y., PICHAL, J., AUBRECHT, L.: *Application of dielectric barrier discharge for treatment of polyster fabric,* Czech. J. Phys., Vol. 56, 2006, pp. 837–842.

[3] HOCKER, H.: *Plasma treatment of textile fibers,* Pure Appl.Chem., Vol. 74, No. 3, 2002, pp.423–427.

[4] POLL, H.U., SCHLADITZ, U., SCHREITER, S.: *Penetration of plasma effects into textile structures,* Surface and Coatings Technology, 142-144, 2001, pp. 489–493.

This research has been supported by the GACR grant No. 202-03-H162 "Advanced study in Physics and Chemistry of the Plasma".

Generation of Neutrons from D-D Fusion Reactions at CTU

D. Klír, P. Kubeš, J. Kravárik, K. Řezáč

klird1@fel.cvut.cz

Department of Physics, Faculty of Electrical Engineering, Czech Technical University, Technická 2, 166 27 Prague 6, Czech Republic

Z-pinches are nowadays the most intensive laboratory sources of soft X-rays, and this is also the main reason why they are studied. The application of Z-pinches as neutron sources has been somewhat problematic from the beginning of Z-pinch research primarily because of serious doubts in issues of crucial importance. The fundamental questions that have been studied were the origin of neutrons and the scaling of neutron yield with the current. In order to solve these questions and to achieve a higher neutron yield, various types of Z-pinch configurations and deuterium loads (compressional Z-pinch, plasma focus, gas embedded Z-pinch, fibre/wire Z-pinch, X-pinch, vacuum spark, imploding gas-puff or wire-array Z-pinch, etc.) have been tried from that time on.

In retrospect it is evident that fundamental experimental results were made already in the 1950s. As examples we can mention the impressive number of neutrons despite a low current, the crucial influence of MHD instabilities, neutron emission anisotropy, etc. In subsequent years, these results were repeated in most of experiments however diverse experimental configurations were. The situation did not change even after the development of modern pulsed power generators. Even though the thermonuclear component could be significant in recent > 10 MA experiments at Sandia National Laboratories, neutron yields cannot be enlarged above 10^{15} unless higher-current devices are built up and/or deuterium-tritium mixture is used. If we look away from the usage of Z-pinches as ICF drivers, Z-pinches are not favourable for fusion energy. However, they still remain effective pulsed sources of neutrons that could find some applications.

As regards our experiments at small Z-pinch Z-150 in Prague, the primary purpose was related to plasma diagnostics. On the one hand, it is not easy to interpret neutron measurements. But on the other hand, neutron diagnostics could provide invaluable data since it gives insight into the most energetic processes taking place in Z-pinches. For this reason, we added “deuterated tracers" in our carbon fibre Z-pinch at the Czech Technical University.

The generator used to drive our experiment consisted of one capacitor with the capacitance of 3 μF. In the case of a 20 kV charging voltage, the current was peaking at 80 kA with a quarter period of 850 ns. The Z-pinch was formed from carbon fibres of 15 μm diameter and of 9 mm length. We also added deuterated polyethelene fibre of 100 μm diameter and 2-3 mm length near the anode. The Z-pinch dynamics was similar to the one when a carbon fibre was used without the deuterated fibre [1]. It was found out that after the breakdown a low density coronal plasma was formed while the fibre diameter remained almost unchanged. This low density corona (ion density of about 10^{16} cm^{-3}) was carrying almost all the current of the order of 10 kA. When the current had built up, i.e. after about 150 ns, the implosion of the corona onto the central fibre occurred. The implosion velocity approached the value of $2x10^5$ ms^{-1}. When the imploded corona had reached the fibre, the dip in dI/dt, voltage peak up to 10 kV, and XUV pulse of a 10÷30 ns width were observed. XUV radiation was emitted from several bright spots which corresponded to the interaction of m=0 instability necks with the dense core. The electron temperature and density were approximately 80 eV and 10^{19} cm^{-3},

respectively. Although the presence of a fibre did not significantly suppress MHD instabilities, they were not disruptive.

After the fibre ablation, i.e. after 500 ns, material evaporated from electrodes started to play a dominant role. The observed plasma column seemed to be MHD unstable and when m=0 instabilities had developed; neutron emission was detected. As regards neutron yield, it was shot-to-shot dependent; however the peak reached the value of 10^3 to 10^4. As regards the energy of neutrons, the time-of-flight detector (Bicron BCF-12 scintillator and Hamamatsu H1949-1 photomultiplier) registered around 2.45 MeV neutrons. Such energy corresponds to D-D fusion reactions. Since the time-of-flight detector was placed in the vicinity of the Z-pinch (at about 25 cm), it was easy to prove that neutrons were emitted at the time of soft X-ray emission and hard X-ray emission from the bright spots near the anode. At that time, the plasma voltage also approached the peak value of 30 kV.

On the basis of our experimental results we would like to stress that high energy processes (such as generation of fusion neutrons) could be studied at the small 500 J Z-pinch and it could provide invaluable information about neutron emission.

References:

[1] KLÍR, D., KUBEŠ, P., KRAVÁRIK, J.: *Imploding Z-Pinch Plasmas Formed from a Carbon Fiber* IEEE Trans. Plasma Sci. 34 (2006) pp. 2303-2311.

This research has been supported by the research programs MSMT No. 1P04LA235, No. 1P05ME761, No. LC528 and by GACR grant No. 202-03-H162.

Measurement of Double Beta Decay of ^{100}Mo and ^{116}Cd with the NEMO 3 Detector

L. Vála, J. Jerie

ladislav.vala@utef.cvut.cz

Institute of Experimental and Applied Physics
Czech Technical University in Prague
Horská 3a/22, 128 00 Praha 6 - Albertov

Interest in neutrinoless double beta decay has significantly increased in the last few years after the evidence of neutrino oscillations has been observed in atmospheric and solar neutrino experiments (SuperKamiokande, SNO, and KamLAND). Neutrinoless double beta decay ($0\nu\beta\beta$), a process violating lepton number by two units, is the best experimental test for Majorana character of neutrinos. This kind of decay, involving a new physics beyond the Standard Model, constrains also the type of mass spectrum hierarchy (quasi-degenerate, normal, inverse) and the absolute mass of the neutrinos.

The currently running NEMO 3 detector is devoted to the search for $0\nu\beta\beta$ decay of ^{100}Mo and ^{82}Se and to the accurate measurement of two-neutrino double beta decay ($2\nu\beta\beta$) of several other isotopes by means of the direct detection of the two electrons emitted in double beta decay. NEMO 3 is installed in the Fréjus Underground Laboratory (4800 m water equivalent) in France. The experiment combines two detection techniques: a tracking wire chamber and a calorimeter, made of 1940 plastic scintillators coupled to very low radioactivity PMTs, for simultaneous particle detection and energy measurements. The experimental set-up is cylindrical in design and is divided into twenty equal sectors. Seventeen sectors accommodate almost 10 kg of different, highly enriched (95% – 99%) $\beta\beta$ isotopes: ^{100}Mo (6914 g), ^{82}Se (932 g), ^{116}Cd (405 g), ^{130}Te (454 g), ^{150}Nd (34 g), ^{96}Zr (9 g), and ^{48}Ca (7 g). Remaining three sectors are used for external background measurement and are equipped with pure copper and natural tellurium. The detector is able to identify electrons, positrons, α-particles, and photons and allows us to study different $\beta\beta$ decay modes. Detailed description of the detector and more information about the NEMO 3 experiment and its performances are given in Ref. [1].

The NEMO 3 detector has been routinely taking data since February 2003. Data corresponding to the first running period (Phase I) from February 2003 to September 2004 contain additional background from radon ($A(Rn) \cong 900$ mBq) which is due to radon diffusion into the wire chamber through tiny air leaks. This level of radon background did not allow us to reach the designed sensitivity for the $0\nu\beta\beta$ decay search. Nevertheless, the radon level inside NEMO 3 has been decreased by a factor of ten after the installation of a tent around the detector, which is supplied with radon-free air from a radon trapping facility. The latter consists of two tanks filled with 1 ton of charcoal cooled down to -50 °C through which the air is flushed. Radon from the air is trapped in the charcoal where it decays before getting to the output of the factory. Remaining low radon activity inside NEMO 3 during Phase II of data acquisition (from October 2004 up to now) is due to detector component degassing.

In order to study $\beta\beta$ decay, two-electron events are selected from data. A candidate for $\beta\beta$ decay has to satisfy, for instance, the following conditions: an event has to contain two tracks coming from the same vertex in the source foils, the curvature of each track has to correspond to a negative charge, both tracks have to be associated to fired scintillators, and the time-of-flight has to satisfy the hypothesis of two electrons emitted simultaneously from the same

vertex. Afterwards, a set of conditions on particle energy, which was optimised with Monte-Carlo simulations with respect to the studied isotope and decay mode, is applied on data.

Thanks to relatively high quantity of ^{100}Mo (7 kg) installed in NEMO 3, the 2νββ decay of ^{100}Mo to the ground state (g.s.) of ^{100}Ru is measured with high statistics and accuracy. In this case the observed signal-to-background ratio is S/B = 40. The obtained half-life for Phase I data, corresponding to efficient running time of 389 days, is $T_{1/2} = [7.11 \pm 0.02(stat.) \pm 0.54(syst.)] \times 10^{18}$ y (see Ref. [2] for more details). The $T_{1/2}$ value is in agreement with previous measurements but it has higher precision. Moreover, the shape of single electron energy spectrum is in favour of the Single State Dominance model [3].

As regards the 0νββ decay of ^{100}Mo, the two-electron events are looked for in the energy window for the summed energy of the electrons between 2.8 and 3.2 MeV. There are 14 events observed in this window for combined Phase I and Phase II data (693 days) while, according to Monte-Carlo simulations based on background measurement, 13.4 events are expected from background. The resulting half-life limit at 90% C.L. is then $T_{1/2} > 5.8 \times 10^{23}$ y. The ββ decay of ^{100}Mo to the excited 0_1^+ state of ^{100}Ru has been also studied by our group. In this decay, the emission of two electrons is followed by two γ-rays of 590 and 540 keV respectively which are registered by the NEMO 3 calorimeter. The half-life for the 2νββ decay mode obtained for Phase I data is $T_{1/2} = [5.7^{+1.3}_{-0.9}(stat.) \pm 0.7(syst.)] \times 10^{20}$ y (S/B = 3) [4]. This result is in a good agreement with values measured previously in spectroscopic experiments using HPGe detectors. No evidence for the 0νββ decay to the excited 0_1^+ state has been found. Then the resulting half-life limit for this process is $T_{1/2} > 8.9 \times 10^{22}$ y at 90% C.L. [4] which is at present the best experimentally obtained limit. The preliminary results from the Phase II data with reduced level of radon background confirm these $T_{1/2}$ values.

Another isotope, which ββ decay is studied by author, is ^{116}Cd. This isotope is mounted in only one of the NEMO 3 sectors. In consequence of much lower mass of ^{116}Cd (405 g) than that of ^{100}Mo (6914 g), there is also a great difference in number of two-electron events observed in data. In addition, the importance of internal background due to contamination of source foils is more important than for ^{100}Mo whereas that of external background, except contribution from radon inside the wire chamber, is less crucial. Nevertheless the S/B ratio is quite high and is equal to 7.6. The preliminary half-life value for the 2νββ decay of ^{116}Cd is $T_{1/2} = [2.8 \pm 0.1(stat.) \pm 0.3(syst.)] \times 10^{19}$ y.

The NEMO 3 detector is still taking data in the Fréjus Underground Laboratory and the analysis of Phase II data is in progress. It will produce improved results with higher sensitivity for neutrinoless double beta decay and also more accurate half-life values for two-neutrino double beta decay of isotopes present in lower quantities inside NEMO 3.

References:

[1] R. ARNOLD, C. AUGIER, A.M. BAKALYAROV *et al.* (NEMO Collaboration): *Technical design and performances of the NEMO3 detector,* Nucl. Instr. and Meth. in Phys. Res. A **536**, 2005, pp. 79 – 122.

[2] R. ARNOLD, C. AUGIER, J. BAKER *et al.* (NEMO Collaboration): *First Results of the Search for Neutrinoless Double Beta Decay with the NEMO3 detector,* Phys. Rev. Lett. **95**, 2005, 182302.

[3] F. ŠIMKOVIC, P. DOMIN, S.V. SEMENOV: *The Single State Dominance Hypothesis and the Two-Neutrino Double Beta Decay of ^{100}Mo,* J. Phys. G **27**, 2001, p. 2233 – 2240.

[4] R. ARNOLD, C. AUGIER, J. BAKER *et al.* (NEMO Collaboration): *Measurement of double beta decay of ^{100}Mo to excited states in the NEMO 3 experiment,* Nuclear Physics A **781**, 2007, pp. 209 – 226.

This research has been supported by GAČR grant No. 202/05/P293.

Experimental Studies Leading to Enhanced de-NOx Processes in Non-Equilibrium Atmospheric Pressure Discharges

S. Pekárek

pekarek@feld.cvut.cz

CTU, Faculty of Electrical Engineering, Department of Physics
Technická 2, 166 27 Prague 6

Nitrogen oxides formed in combustion processes are toxic and cause serious health problems. An efficient tool for their decomposition is a non-thermal plasma produced by different types of electrical discharges. For the study of NO decomposition we used hollow needle to plate DC corona discharge enhanced by the flow of N_2-NO mixture through the needle electrode. There are several important advantages of this type of discharge enhancement; namely the application of the flow rate through the needle:

- protects the needle from overheating,
- shifts the mean streamers repetition frequency towards higher values therefore the discharge is better stabilized, and
- all the mixture supplied into the needle electrode passes through the discharge region and therefore is affected by plasma chemical processes.

The corona discharge exhibits strong dependence on the polarity of the coronating electrode. This dependence is caused by the different mechanism of electron multiplication. If the coronating electrode is the cathode then avalanche multiplication takes place. The secondary process is the emission from the cathode, and possibly, photoionization in the bulk of the gas. On the other hand, if the coronating electrode is the anode then the remote large cathode does not participate in multiplication of electrons on account of the weak field in its vicinity. The reproduction of electrons is ensured by secondary processes in the gas around the electrode. Different mechanisms of electron multiplication for different polarities of the coronating electrode are reflected by different discharge regimes.
With the aim to clarify the effect of polarity on NO decomposition we investigated the NO decomposition as a function of energy density and different initial NO concentrations in the N_2-NO mixture for both polarities of the needle electrode [1]. We found that for each of investigated flow rates and initial NO concentrations the discharge with the needle biased positively requires for the same NO decomposition smaller energy density than the discharge with the needle biased negatively. Another conclusion is that NO decomposition depends on energy density for all investigated initial NO concentrations and for all investigated mixture flow rates through the discharge. Finally NO removal efficiency depends on initial NO concentration; complete NO removal is obtained for lower initial NO concentrations with lower energy density.
To find stable operational discharge regimes we also explored various combinations of the mixture mass flow through the needle electrode and discharge voltage. We found that depending on the energy density the discharge exists in two different modes [2]. For low energy density dissipated between electrodes, the discharge resembles a diffuse weekly luminous cone bridging completely the gap. This is a regime, which corresponds to the glow corona. With increasing discharge energy density, the continuous cone is superimposed with

pulsed luminous filamentary streamers. As a rule a streamer regime is a regime with intermittent transitions between glow and streamers. The occurrence of streamers is associated with current pulsations and pulsations of light emitted by the discharge. We found that mean repetition frequency of current pulses related to the occurrence of streamers ranges from ~ 0.1 to 5 kHz [3].

In order to evaluate the efficiency of NO removal processes we calculated the dependence of the NO removal energy cost of as a function of energy density:

$$Energy\ \cos t = \frac{Energy\ density}{Change\ in\ NO\ concentration} \times 253 \quad [\text{eV/molecule, kJ/m}^3\text{, ppm}],$$

where constant 253 is a conversion factor at 20° C and at pressure 1.01×10^5 Pa.

The NO removal energy cost for energy densities exceeding 2 kJ/m^3 converges to about 100 eV/molecule independently of the initial NO concentration [4]. The spread of energy cost values for lower energy densities is very likely a consequence of large uncertainty associated with energy density evaluation in the discharge regime with the DC current being superimposed with streamer current pulses. In addition, energy density is a complex parameter describing both the effect of DC gas energization (discharge voltage) as well as the effect of flow rate (residence time) on NO removal.

The values of NO removal energy cost presented in the literature vary in a wide range depending on the type of the discharge used as well as on the particular energy densities. Thus for example the NO removal energy cost around 240 eV/molecule for a pulsed corona discharge was obtained. The difference between NO removal energy cost 100 eV/molecule obtained in our experiments and the NO removal energy cost presented by other authors can be explained by the contribution of short streamer pulses typical for positive point to plate corona, making thus better conditions for NOx removal than for the pulsed corona discharge.

References:

[1] PEKÁREK, S. – ŠIMEK, M. – KHUN, J.: *De-NOx Efficiency of Positive/Negative DC Corona Discharge: a Comparative Study* Proceedings of the XVI International Conference on Gas Discharges and their Applications, Xi´an, Čína, 2006, pp. 533-536.

[2] KHUN, J. – ŠIMEK, M. – PEKÁREK, S. – SCHMIDT, J.: *Dynamic Characteristics of Positive Hollow Needle to Plate Atmospheric Pressure Discharge* Czechoslovak Journal of Physics, Suppl. B, 2006, pp. B 830-836.

[3] ŠIMEK, M. – SCHMIDT, J.– PEKÁREK, S. – KHUN, J.: *Optical and Electrical Characteristics of Hollow Needle to Plate Atmospheric Pressure Discharge in Nitrogen* Bulletin of the American Physical Society, 2006, pp. 27.

[4] PEKÁREK, S. – ŠIMEK, M. – SCHMIDT, J. – KHUN, J.: *De-NOx Efficiency of Gas Flow Enhanced DC Positive Corona Discharge* Submitted to Plasma Processes & Polymers, 2006.

This research has been supported by GA AV grant No. IAA1043403.

Verification of function and application of radial scanning system for studying DC glow discharge

J. Čáp, Š. Němcová, J. Zicha, A. Kaňka*, V. Hrachová*

jiri.cap@fs.cvut.cz

Department of Instrumentation and Control Engineering, Division of Precision Mechanics and Optics, Faculty of Mechanical Engineering, Czech Technical University in Prague, Technická 4, 166 07 Prague 6, Czech Republic

* Charles University in Prague, Faculty of Mathematics and Physics, Department of Surface and Plasma Science, V Holešovičkách 2, 180 00 Prague 8, Czech Republic

Introduction

The excited particles can play very important role in low-temperature discharge plasma. The behavior of these species may be determined by means of the spectroscopic methods on the basis either of emission or of absorption spectroscopy. Considering cylindrically symmetric plasma, it is rather necessary to take into account the radially decreasing character of the emitted radiation in the direction axis – wall. In some cases the line intensity, especially near the wall, can decrease under the threshold of detectability. To solve this problem, we proposed an original experimental set-up: the radial scanner.

Function principle and construction of radial scanner

Two conic mirrors – a negative and a positive one - are the most important parts of the scanner. Assuming the positive column of the glow discharge to be cylindrically symmetric, this system selects (from all rays emitted by positive column) the rays parallel to the optical axis. These rays form a hollow cylinder, whose base is a circular zone concentric with the axis of discharge tube. Both optical surfaces of the mirrors are coated with aluminium and with protective layer of MgF_2. With the thickness of the testing cylinder about equal to 10% of the internal diameter of discharge tube D, the same spectrum has to be obtained, compared to the case when the testing bundle has the form of the cylinder with the diameter of 0.1D. Intensity is increased by the factor of 80r/D, where r is the mean radius of the wall of the testing cylinder. The rays are optically processed by the achromatic objective and collected into focus. The axis of symmetry of both mirrors and the optical axes of the successive optical elements must coincide. The position of the negative conic mirror is continuously controlled by 6 plastic screws and by 3 springs. Close to the focus of the objective entering rays, which are very slightly deviated from the optical axis, form a large circular spot in the focus plane. Its area is limited by the field stop whose optimum diameter was determined by the method of ray tracing.

The basic element of the construction is the achromatic objective with concentrically cemented conic mirror placed in an aluminium cylinder. The negative conic mirror moves along optical axis to alter the radius of the testing bundle. Measuring of this axial movement is enabled by dial gauge Mitutoyo with accuracy of 0.01mm.

To ensure correct function, scanning system must fulfill these requirements: ensuring the alignment of the mirrors and merging their common axis with the optical axes of the next optical elements; the precision control of the parameters of the conic mirrors; the alignment control of the achromatic objective with the positive conic mirror; positioning the field stop

into the focus of the achromatic objective; adjusting the initial zero position of the scanning system. The construction of the scanner has been verified in series of measurements. The measuring accuracy of the position of the conic mirrors has been improved.

Function verification by method of ray tracing

The source of radiation used for verification of function by the method of ray tracing is considered to be a cylinder radiating uniformly inside its volume. This source, corresponding to the central part of the discharge tube, is divided into segments radially and angularly. The number of these elements is variable. Each of them emits radiant flux proportional to its volume. This segment is replaced by a point source placed in its center, which emits radiant flux corresponding to the entire segment. This source is assumed to be omnidirectional uniformly radiating to all directions with constant radiance. The entrance pupil of the optical system is divided into segments analogously to the source. Directions of rays reaching the optical system are defined by merging all point sources originated from the segmentation of cylindrical source and all points of segments of the entrance pupil. These rays are traced through the optical system. Rays falling on the apex of the conic mirror are not taken into account. Radiant flux, which represents rays, is found from the solid angle determined by surface of the corresponding segment of the entrance pupil and distance between the entrance pupil and the point source from which the ray arises. We can calculate the solid angle for one segment from entrance pupil segment area and its distance. The radiating flux from source segment into solid angle is given as part of total flux. We used 10^7 rays for calculation. The source of radiation was divided into 128 segments radially and into 16 segments angularly. The entrance pupil was divided into 256 segments radially and 19 segments angularly. Raytracing is processed at programming environment Visual Basic for Application. We arrived at the conclusion by method of ray tracing that the system is very sensitive to oblique rays especially near the zero position (outer conic mirror is near the apex of the inner mirror). For this reason it is necessary to limit undesirable rays by field stop at the entrance of the detecting system to achieve correct function of the scanning system.

Experimental set-up for analysis of radial profiles

As an example of application of the scanner and for the comparison of published radial profiles, the positive column of DC glow discharge was investigated. Radial profiles of emission spectra were analyzed in spectral range (580-750) nm for pressures (1-6) Torr under such conditions, when the positive column was homogeneous. Lines detected correspond to transitions between various quantum states of neutral neon atom. Considering the investigated set of lines, two persistent lines 585.3 nm and 640.2 nm were recorded.

References:

[1] VALIGNAT, S. – LEVEAU, J.- DEIGAT, F.: J. Physique 40 C7, 1979, 7.

[2] PANTEL, R. - RICARD, A. - MOISAN, M.: Beitr. Plasmaphys. 23, 1983, 561.

[3] ZICHA, J. - HRACHOVÁ, V. - KAŇKA, A. - NĚMCOVÁ, Š.: *in Proc. 41th Int. Scientific Colloqium,* Technische Universitat Ilmenau, Germany, 1996, 405.

[4] HRACHOVÁ, V. - KAŇKA, A.: Acta Phys. Slov. 41, 1991, 293.

This work is a part of the research plan MSM 0021620834, that is financed by the Ministry of Education of the Czech Republic.

Structure Analysis of Faujasite Zeolitic Catalysts Chemisorbed by Methyl Groups

S. Vratislav, M. Dlouhá, V. Bosáček*,

vratisla@troja.fjfi.cvut.cz

CTU, Faculty of Nuclear Sciences and Physical Engineering, Dept. of Solid State Engineering
Břehová 7, 115 19 Praha 1
*CAS, J. Heyrovský Institute of Physical Chemistry
Dolejškova 4, 182 23 Praha 8

Microporous materials like faujasite zeolitic catalysts have common and diverse applications in a wide variety of industrial processes that use catalysis or molecular separation. Nature of acid or basic sites and the distribution of sodium cations and chemisorbed methyl groups in the zeolitic lattice belong to the most important problems of surface chemistry. There is a great deal of fundamental interest in understanding how zeolites function at the atomic or molecular level. This knowledge will provide the means to design novel catalyst materials. Zeolites exhibit regular structure which can be easily modified. The building block of zeolites is SiO_4 and AlO_4 –tetrahedra, which can be assembled to form a wide variety of crystal structure with pores and channels of varying dimensions. These are important candidates for different types of catalysts and many laboratories try therefore to „tailor“ zeolitic catalysts of the requested properties.

Chemical composition of investigated dehydrated zeolites NaX and NaY was $Na_{80.0}Ca_{1.2}[(AlO_2)_{82.4}(SiO_2)_{109.6}]$ and $Na_{48.9}Ca_{1.6}[(AlO_2)_{52.1}(SiO_2)_{139.9}]$, respectively. Sample of NaLSX was a sodium form of faujasite structure with ratio of Si/Al = 1. Neutron powder diffraction patterns were collected at temperature of 298 and 7 K on the KSN-2 diffractometer, which is placed at the LVR-15 research reactor in Řež near Prague. This device - was equipped with close circuit liquid helium cryostat - type CP-62-ST/5 (Cryophysics SA). The wavelength of 0.1362 nm was used and the resolution $\delta d/d=0.00075$ was achieved (d is the interplanar spacing). The complete structural parameters were determined by Rietveld analysis of powder neutron diffraction data using the GSAS package and a Fourier difference density maps. The NMR results altogether confirm the results from diffraction methods.

The aim of our studies was to investigate the regular distribution of cations and the location of chemisorbed species CH_3^+ in the lattice and to elucidate the role and participation of various lattice oxygen types in chemisorptions of methyl cations in NaX, NaY and NaLSX zeolites.

Our results obtained by powder neutron diffraction and ^{13}C MAS NMR were summarized in this way:

- The crystal structure parameters of NaY, NaX and NaLSX (Si/Al ratio of 1) zeolites (initial dehydrated samples) are in agreement with results refined in the Fd3 space group by Olson [1]. Structural parameters of NaLSX were refined in both recently discussed space groups [2], as in Fd3 space group as in Fddd (orthorhombic) group but without significant difference. Cations are distributed over six possible sites as proposed by Olson [1] in the frame of Fd3 space group.
- The complete structure parameters of the chemisorbed (by CH_3I ore CD_3I groups) faujasite zeolies (NaY, NaX and NaLSX) were determined [3, 4]. Changes in the distribution of

structural sodium cations in the lattice after chemisorption of methyl cations have been detected. These changes were observed not only in occupation factors but sometimes also in coordinates of Na^+ cations. Typical example was found for NaX in the cases without and with chemisorbed species where is demonstrated a splitting of the position $S_{I'}$ into two sites Na2 and Na3. These positions are separated at helium temperature but fused together at room temperature. On the other hand, cations in S_{II} positions, are represented after chemisorptions only with fully occupied Na4 site. Na4 (32e position) as well as Na5, Na6 and Na7 (96g position) take part in the reaction of CH_3I preferentially due to their easy accessibility in large α-cavities. Cations and especially extra-framework cations play an important role in determining the adsorption, separation and catalytic properties of zeolites. The positive charge of the cations produces electric fields within the zeolite pores, which can strongly influence absorptive behavior and catalytic activity.

-Chemisorbed methylium ions are located in the Y type faujasites structure at the lattice oxygen O_1 as bridging-type methoxy group characterized by the ^{13}C MAS NMR signal at 56.5 ppm. For the sodium ions, the S_I sites in the hexagonal prism and the $S_{I'}$ sites in the sodalite cage are both partially occupied with occupation factors of 0.14 and 0.57 respectively, whereas the S_{II} site in the supercage is full. An agreement factors on integrated intensities R_{wp} = 6.02% and R_p =5.11% were obtained. The space group is Fd3m with a lattice parameter a=2.4851(7) nm [3].

-Methylium ions are located in X faujasite at O4 and O1 lattice oxygen atoms only in α-supercavity. The location at two different sites corresponds well with two observed ^{13}C MAS NMR signals at 54 and 58 ppm of surface bridging methoxyls. The structural analysis [4] was treated in frame of Fd3 space group with a = 2.4895(6) nm, R_{wp} = 5.23%, R_w = 4.87% (chemisorbed NaX sample) [4]. We have determined the occupation numbers of cations and the location of CD_3 groups with the center in the position 96*g* (0.387, 0.387, 0.119). The occupation numbers of Na cations in chemisorbed NaX were decreased for $S_{I'}$ and $S_{I''}$ and increased for S_{III} in comparison with the initial NaX. S_{II} is practically fully occupied in both cases.

References:

[1] D. H. OLSON: *The crystal structure of dehydrated NaX,* Zeolites 15, 1995, pp. 439-443. ISBN 0144-2449

[2] J. PLEVERT, F. DI RENZO, F. FAJULA, G. CHIARY: *Structure of dehydrated zeolite Li-LSX by neutron diffraction: evidence for a low-temperature orthorhombic faujasite.* J. Phys. Chem. B 101, 1997, pp.10340-10346. ISBN S 1089-5647.

[3] S. VRATISLAV, M. DLOUHÁ, V. BOSÁČEK: *Location of chemisorbed methylium ions in zeolites by neutron diffraction and 13C MAS NMR.* Appl. Phys. A 75, 2002, pp.1320 - 1322. ISBN 33-9020-1698.

[4] S. VRATISLAV, M. DLOUHÁ, V. BOSÁČEK: Acta physica slovaca 56, 2006, pp. 137 - 140. ISBN0323 - 0465.

This work has been supported by the Czech Ministry of Education within the framework of the grant No. MSM6840770021.

Numerical Simulation of Dark Photovoltaic Solitons with Beam Propagation Method

M. Bodnár

bodnar@troja.fjfi.cvut.cz

Department of Physical Electronics, Faculty of Nuclear Sciences and Physical Engineering, Czech Technical University in Prague, V Holešovičkách 2, Prague 8, 180 00

The beam propagation method (BPM) is a numerical technique for simulating the propagation of optical field. BPM is powerful technique that can simulate any arbitrary refractive index profile. In this article we used this method for the solution of nonlinear Schrödinger equation (NLSE). NLSE defines the propagation of optical solitons in the nonlinear media. The simulation is focused on the propagation of optical field in iron doped crystal $LiNbO_3$. These types of nonlinear crystal allow a generation of dark photovoltaic solitons.

What is the spatial optical soliton? Spatial optical solitons is separated into two basic types: the bright solitons and the dark solitons. The bright soliton, in which a beam of light propagates without change in its transverse profile, occurs when self-focusing due to the light-induced change in the index of refraction balances diffraction. The resulting index of refraction is positive; it is proportional to the intensity of the beam. The dark soliton, in which a dark band, or notch, is superimposed on an otherwise uniform background illumination, occurs when self-defocusing due to a light -induced index change balances the diffraction of the notch. The resulting index of refraction is negative. A dark soliton may be black, in which the intensity minimum is zero, or gray, in which it is nonzero but less than the background intensity.

Photovoltaic soliton is one type of photorefractive solitons. At present, several generic types of photorefractive solitons are known: quasi-steady-state solitons, screening solitons (with external applied voltage), and photovoltaic solitons. Photovoltaic solitons are used photovoltaic current. This current is generated upon illumination the crystal.

The optical nonlinearity responsible for soliton formation is due to the transport of electronic charge dominated by the bulk photovoltaic current (for photovoltaic solitons). Electrons are photo exited from impurity centers with momentum preferentially directed along the x axis of a ferroelectric crystal (optical axis), and are then trapped in different impurity centers. The resulting space-charge distribution gives rise to an index gradient through the electro-optic effect. This index gradient is responsible for the self-guiding needed to generate photovoltaic solitons. These solitons do not necessitate application of an external electrical field.

Spatial photorefractive solitons have attracted much interest in the past two decades. Their potential applications are in waveguides, directional coupling, electro-optical switching, and frequency conversion. Soliton-induced waveguides are key elements in the development of reconfigurable optical switches and dynamic interconnects. In particular, spatial photorefractive solitons have the advantage to be generated from low-power sources. Moreover, their photo-induced waveguides can be temporarily stored, erased or rewritten or can even be permanently fixed.

The beam propagation method is a numerical simulation of the field in a guide, not an approximate solution to the exact wave equation. The BPM can help us determine the mode profile in a unusual waveguide, and can determine the dynamic behavior of a mode as the index profile changes along z.

BPM works by decomposing a spatial mode into a superposition of plane waves, each traveling in a slightly different direction. After advancing each wave certain distances through the dielectric structure of interest, the plane waves are added back together to reconstruct the spatial mode. This process requires the use of Fourier transforms to convert from the spatial mode into the superposition of plane waves, and back again.

To understand the philosophy behind the BPM, it is useful to write Schrödinger equation

$$\frac{\partial E(x,z)}{\partial z} = \left(\frac{i}{2k} \frac{\partial^2}{\partial x^2} \right) E(x,z) + \left(i \frac{k}{n} \Delta n \right) E(x,z)$$

formally in the form

$$\frac{\partial E}{\partial z} = \left(\hat{D} + \hat{N} \right) E ,$$

where $\hat{D}$ is a differential operator that accounts for divergence and absorption in linear medium and $\hat{N}$ is a nonlinear operator that governs the effect of crystal nonlinearities. *E(x,z)* is the intensity of optical field, *i* is the complex number, *k* is the wave number, *n* is the refractive index number (crystal before illumination), and Δn is the value of refractive index changes (after illumination). The refractive index change represents all nonlinearities in the crystal. Operators $\hat{D}$, and $\hat{N}$ are given by

$$\hat{D} = \frac{i}{2k} \frac{\partial^2}{\partial x^2} , \qquad \hat{N} = i \frac{k}{n} \Delta n .$$

In general, dispersion and nonlinearity act together along the length of the crystal. The BPM obtains an approximate solution by assuming that in propagating the optical field over a small distance *h,* the dispersive and nonlinear effects can be pretended to act independently. More specifically, propagation from z to *z* + *h* is carried out in two steps. In the first step, the nonlinearity acts alone, and $\hat{D} = 0$. In the second step, dispersion acts alone, and $\hat{N} = 0$.

The numerical method was programmed in Matlab, and was designed a GUI (graphical user interface) for better simulations. Our obtained data are consisted with our experimental measurements. This program is able to simulate all types of dark solitons in photovoltaic crystal. The program has different types of input variables: the profile of the input beam, the input phase of the beam, the input power, the electro-optic coefficient, the photovoltaic coefficient, and the dimensions of the crystal. In this article, the BPM was programmed in one dimensional case. The BPM has very good accuracy and it is faster than finite-difference methods.

References:

[1] BODNÁR, M. – HŘÍBEK, P.: *Photovoltaic effect and generation of dark photovoltaic solitons in Fe : LiNbO3* Proc. SPIE Vol. 5949, 2005, pp. č.106–116.

[2] BODNÁR, M.: *Simulace tmavých fotovoltaických solitonů pomocí BPM* Technical Computing Prague, 2006, pp. č. 21.

[3] AGRAWAL, G. J.: *Nonlinear Fiber Optics (Third Edition)* Academic Press, USA 2001

[4] POLLOCK C.R..: *Fundamentals of Optoelectronics* Irwin, USA 1995

This research has been supported by MSM6840770022.

Position Sensitive Spectroscopy of Fission Fragments

C. Granja*, Z. Vykydal*, J. Jakůbek*, S. Pospíšil*
Y. Kopatch, S.A. Telezhnikov****

carlos.granja@utef.cvut.cz

*Institute of Experimental and Applied Physics, Czech Technical University, Horská 3a/22, 128 00 Prague 2, Czech Republic

**Joint Instittute for Nuclear Research JINR, 141 980 Dubna, Moscow Region, Russia

The hybrid semiconductor Medipix2 detector (see http://www.cern.ch/medipix and http://www.utef.cvut.cz/medipix) has found wide application in real-time imaging using X-rays, electrons, alpha particles and neutrons [1]. Medipix2 consists of a silicon semiconductor *sensor chip* bump-bonded to a *readout chip*. The sensor chip is equipped with a single common back-side electrode and a front-side matrix of electrodes 256x256 square pixels with pitch of 55 μm. Each of the 64 k elements of the matrix (pixel) is connected to its respective preamplifier, double discriminator and digital counter integrated on the readout chip. On-line operation and visualization is made possible by the newly developed USB-based readout interface [2]. Operation and monitoring of the system is driven by a software package Pixelman [3] running under MS-Windows. Data stream acquisition and storage proceed on-line at overall rate of about 5 frames per second. This compact and portable radiation camera operates as an active nuclear emulsion [1] also for heavy charged particles in the MeV range for which Medipix2 provides 100 % detection efficiency, energy discrimination, noiseless digital integration (single-quantum counting), wide (unlimited) and linear dynamic range.

Study of nuclear fission demands fast response and precise position and energy sensitive spectroscopy. Investigations include systematics and variations in fragment-mass and kinetic-energy distributions of spontaneous fission as well as measurements of rare fission processes such as ternary and quaternary fission which require precise coincidence spectroscopy in terms of energy resolution and angular correlation.

In this work [4] we examine the response of Medipix2 to spontaneous fission products of ^{252}Cf which are heavy-mass charged particles in the 40-120 MeV range. Measurements were made in vacuum using a thin source containing low activity of ^{252}Cf. Clusters of pixels formed upon impact of single particles were analyzed with the aim to obtain information about position and energy. Complementary information on the energy of the individual particles is provided by the amplitude of back-side pulse [2]. Using a linear calibration, the kinetic-energy distribution of fission fragments was extracted. The fission products were detected with two Medipix2 detectors (each fabricated with a 700 μm thick silicon sensor) opposite placed from the source. Both Medipix2/USB cameras operating either independently or also in coincidence mode.

Heavy charged particles produce upon impact on the Medipix2 sensor matrix a collection of pixels so-called *clusters* [1] of several pixels. The area of a cluster (i.e., number of pixels involved) is determined by the ionizing power and kinetic energy of the hitting particle. The cluster area and perimeter (sum of contour pixels) were determined for every event [4]. Heavy-mass fragments are identified namely by their characteristic cluster shape i.e. by their area, perimeter and roundness. A special equalization of pixel region matrix was

done for each detector and measurement which accounts for non-uniforme gain of different regions of the detector sensor surface.

Fission fragments were identified by evaluation of cluster pattern characteristics [4]. A number of filters were successively applied according to cluster area, perimeter, shape (roundness, elongation), and ratio among the above. Careful evaluation of values and range for these quantities were set for each measurement due to particular detector and preamplifier settings. From the distribution of cluster area of fission fragments is obtained the distribution of kinetic energy of the fission fragments. In addition to the characteristic cluster area size of fission fragments, the signal taken from the back-side contact of the sensor chip contains spectroscopic information and can be used for trigger generation or energy amplitude measurement by a 12-bit ADC. The correlation of back-side pulse height to cluster area size of the heavy-mass fission fragments can provide complementary information and confirmation of identification. Using merely a two-point linear calibration, the energy distribution of fragments is fairly well reproduced. The energy resolution attained is in the range 3-5 MeV which could be improved by a factor of 100 by back-side pulse spectroscopy.

The results obtained demonstrate the capability of the Medipix2 device for position-sensitive and spectroscopy measurements of fission fragments and heavy ions in the 40-120 MeV range [4]. The combined Medipix2/USB camera serves as a portable digital on-line nuclear emulsion operating at room temperature and in vacuum with position-sensitive and spectrometric capability for single-quantum counting and tracking of both light- and heavy-charged particles.

References:

[1] J. JAKŮBEK: *Data processing and image reconstruction methods for pixel detectors,* Nuclear Instruments and Methods in Physics Research A (2007) in print

[2] Z. VYKYDAL, J. JAKŮBEK, S. POSPÍŠIL: *USB interface for Medipix2 enabling energy and position detection of heavy-charged particles,* Nuclear Instruments and Methods in Physics Research A 563 (2006) 112

[3] T. HOLY, J. JAKŮBEK, S. POSPÍŠIL, ET AL: *Data acquisition and processing software package for Medipix2,* Nuclear Instruments and Methods in Physics Research A 563 (2006) 254

[4] C. GRANJA, Z. VYKYDAL, J. JAKŮBEK, S. POSPÍŠIL, Y. KOPATCH, S.A. TELEZHNIKOV: *Position-sensitive spectroscopy of 252Cf fission fragments,* submitted to Nuclear Instruments and Methods in Physics Research A (2006) under review

This work has been carried out in frame of the CERN Medipix Collaboration and has been supported in part by the Research Grant Collaboration of Czech Republic with CERN No. 1P04LA211,by the Fundamental Research Center Project LC06041, by Grant MSMT No. 05-61308 and the Research Program 210000018 of the Ministry of Education, Youth and Sports of the Czech Republic and by Grant 01-05005 of the Committee for Cooperation with JINR Dubna. The authors appreciate the provision of the target by the JINR Dubna.

Microwave Plasma Modification of PE Powder

L. Aubrecht

aubrecht@fel.cvut.cz

Department of Physics, Faculty of Electrical Engineering, Czech Technical University, Technická 2, 166 27 Prague 6, Czech Republic

The difficulty of the powder treatment was related to the three-dimensional character of the powder and a large area to be treated. Ideal uniform stirring was a necessary condition for homogeneous modification of polymer powder. For a reasonably long time each powder particle had also to be in contact with plasma [1-3].

Used set-up consisted of vacuum process chamber made from stainless steel cylinder with inner diameter of 50 cm equipped on the upper and lower side with a standard ISO K 250 flanch. Inside the reactor a stainless-steel blender with a horizontal propeller stirrer was placed. The stirrer axis was brought out from the reactor through a vacuum trough-out placed at the reactor's bottom. A sealing lip prevented penetration of the powder into the bearing. An electrical engine placed outside the reactor drove the propeller via a vacuum throughout and a vertical movable shaft. This construction enabled distance variation between the blender and the plasma source. Approximately one revolution per second was typically used in most experiments.

For measurements of penetration a glass cylinder was placed inside the reactor. Bottom of the cylinder was adaptable and its position was adjusted by a fine threat screw. The cylinder was filled up to the top with the powder under modification. After modification a shift of the bottom upwards enabled to stirr the powder layer of definite thickness.

The high-density polyethylene powder Borealis CB 9155-01 used as the test medium was characterized with particle average diameter 250 μm, powder density 0.95 kgm^{-3} and the mass specific surface area of 0.033 m^2g^{-1}. All experiments were performed in stationary oxygen under pressure 70 – 100 Pa and room temperature. Treatment time was (60 – 600) s.

The adhesion of the powder was determined by measurement of the strength forces demanded for displacement of the polyethylene-metal joint performed in homemade specimen. For comparison the adhesion between the stainless steel and special PE copolymers were determined, too. The degree of the modification was normalized to the suction of the unmodified powder. For all measurements the Fraunhofer Institute measuring unit HBM MVD 2555 was used.

In experiments there were used polished stainless steel and aluminium substrates. Maximum reached tensile strength value of the unmodified powder was 0.15 MPa, but most acquired values were under the measurement method sensitivity limit (0.05 Mpa). Values achieved for modified polyethylene powder varied mostly between 6 and 7 MPa, but in some cases exceeded 11 Mpa, which was the tensile strength of the bulk material. For comparison the adhesion strength of commercially produced PE-copolymers fabricated for metal coatings Flamulit F-HTC 214 produced by DuPont and Microthene RL MR SP010 produced by Equistar Chemicals LP were analysed, too. The adhesion grade of the plasma-modified conventional polymer is higher than those reached for Flamulit, unfortunately our Borealis values are also lower than that of Microthene adhesion, but we have to keep in mind that Microthene polymer has been specially designed as an adhesion layer to steel substrate.

Determined adhesion forces exceeded even limits necessary for the probe rupture from the holder.

Modified polyethylene powder Borealis CB 9155-01 in MW discharge in oxygen under pressure of 100 Pa led to distinctive increase of powder adhesion to the metal substrate. Adhesion improvement for powder on steel substrate was approximately tenfold, for powder on aluminium substrate was approximately fivefold. The same values were found also for modification in air.

For perspective industrial application of the MW plasma modification the process effectivity is of the highest importance. Estimation might be based on comparison of adhesion and wettability. Adhesion and wettability tests in air and in oxygen plasma had shown about 20 % improvement in case of modification in air than for modification in oxygen. This outcome is very important from the economical point of view due to minimum costs of the air supply.

a) Study demonstrated a novel method of MW plasma treatment of powder particles at low pressures.

b) Obtained results confirmed MW plasma modification efficiency to change surface properties of a polyethylene powder and increase its wettability.

c) Modified powder exhibits very good adhesion to steel, aluminium and probably other metal surfaces, too.

d) Presented method is widely adaptable.

Although the research has to be continued, powder stirring inside the reactor improved modification effect homogeneity and facilitated modification of larger powder batches.

References:

[1] ARPAGAUS, C. - VON ROHR, P.R. - ROSSI, A.: *Short-Time Plasma Surface Modification of HDPE Powder in a Plasma Downer Reactor – Process, Wettability Improvement and Ageing Effects,* Applied Surface Science, 2005, pp. 1581-1595

[2] AREFI-KHONSARI, F. - TATOULIAN, M. - BRETAGNOL, F. - BOULOUSSA, O. - RONDELEZ, F.: *Processing of Polymers by Plasma Technologies,* Surface & Coatings Technology, 2005, pp. 14-20.

[3] PICHAL, J. - KOLLER, J. - AUBRECHT, L. - VATUNA, T. - SPATENKA, P. - WIENER, J.: *Application of Atmospheric Corona Discharge for PES Fabric Modification,* Czech. J. Phys., 2004, pp. 828-834.

This research has been supported by project of Ministry of Education, Youths and Sports of the Czech Republic MSMT NANOPIN 1M0577.

Luminescence Spectroscopy of $Ba_xSr_{1-x}TiO_3$ Thin Films

Z. Potůček, Z. Bryknar

potucek@troja.fjfi.cvut.cz

Czech Technical University in Prague, Faculty of Nuclear Sciences and Physical Engineering, Department of Solid State Engineering, Trojanova 13, 120 00 Praha 2

$Ba_xSr_{1-x}TiO_3$ (BST) is a typical perovskite solid solution. The temperature T_c of the cubic-tetragonal ferroelectric phase transition is a linear function of x in the case of ceramic and bulk single crystal samples with x values from 0.2 to 1.0, where three ferroelectric phases exist [1]. For $x < 0.2$ the transition temperature is proportional to $(x - x_c)^{1/2}$, where $x_c = 0.035$. For $x < x_c$ glasslike behavior is observed. The experimental observation of ferroelectric phase transitions in BST thin films is more difficult because of the presence of tensile residual stress. For example, this stress induces a ferroelectric phase transition near 125 K in $SrTiO_3$ thin films that appears almost simultaneously with the structural antiferrodistortive phase transition [2]. Understanding differences between bulk and thin film behavior is very important because of the great potential of BST thin films for device applications, such as tunable microwave devices or random access memories.

Photoluminescence (PL) of the octahedral coordinated Cr^{3+} ions has a characteristic sharp zero-phonon line (ZPL) corresponding to $^2E \rightarrow {}^4A_2$ emission transition that is very sensitive to the changes of Cr^{3+} ion environment. Since PL allows to detect low concentrations of defects and chromium seems to be unavoidable impurity in $SrTiO_3$, PL of BST thin films deposited by a hollow cathode plasma jet system was systematically studied within wide temperature (12 – 300 K) and spectral (350 – 850 nm) regions for the first time [3].

The BST thin films with thickness between 200 - 700 nm were prepared on Pt surface of multi-layer $Si/SiO_2/TiO_2/Pt$ substrate that were heated to 360 – 800 K in the course of deposition. In order to deposit BST thin films with $0 < x < 1$ the first part of the nozzle was made of nominally pure or slightly Cr doped $SrTiO_3$ ceramic and the second part from $BaTiO_3$ crystal. The morphology of BST films and grain size distribution were investigated with AFM. The grain sizes were found from ~ 50 to 250 nm. The chemical composition of deposited films was measured by electron microprobe providing information on average composition over the whole depth profile of the analyzed films. X-ray diffraction patterns obtained from Bragg-Brentano geometry revealed BST microcrystalline perovskite phase. Its typical diffraction lines shift with increasing Ba content between corresponding characteristic lines of $SrTiO_3$ and $BaTiO_3$.

PL emission spectra of investigated BST thin films with $0 \leq x \leq 1$ revealed broad emission band peaking in the vicinity of 2.1 eV and rather pronounced lines centered at 12 K in the spectral region 1.570 – 1.600 eV (789.8 – 774.9 nm) in dependence on increasing Ba content. These lines were accompanied by a wide structured emission extending behind 1.48 eV. Intensity of both emissions was strongly sample-dependent but no clear correlations with deposition conditions of BST thin films were found. Broadband emission in the visible spectral region is a characteristic property of practically all self-activated ABO_3 perovskites but its origin has not been satisfactorily cleared up so far. The pronounced lines in the near infrared spectral region that appeared at BST thin films deposited from both nominally pure and Cr doped $SrTiO_3$ nozzles but only for $x \leq 0.84$ were attributed to the zero-phonon transitions $^2E \rightarrow {}^4A_2$ of octahedral coordinated Cr^{3+} ions in Ti sites of BST and corresponding structured emission to electron-phonon vibronic sidebands.

The observed shift of Cr^{3+} ZPL to higher energies with increasing Ba content is in accordance with behavior of PL of Cr^{3+} ions in the pure $SrTiO_3$ and $BaTiO_3$ [4]. However, the influences of BST thin film characteristics, such as grain size, thickness, and morphology, on fine changes of the Cr^{3+} ZPL position was not possible to distinguish because of their great scatter. The half-width of ZPL of Cr^{3+} ions in BST thin films is relatively very high (~ 150 cm^{-1}) in comparison with the $SrTiO_3$ crystal (~ 1 cm^{-1}). This broadening evidences, for example, strong interaction of Cr^{3+} ions with the grain interfaces and strongly disordered structure with a diffusive phase transitions, inhomogeneities, and random fields.

The most efficient excitation of Cr^{3+} PL in BST thin films occurs via interband transitions with photon energy higher than 3.3 eV. These excitation bands are probably related to charge conversion $Cr^{3+} \rightarrow Cr^{4+}$ and/or Cr^{2+} with a creation of free electrons and/or holes. In the course of recombination of electrons (holes) produced in the conduction (valence) band the population of the radiative ^2E level occurs followed by observed emission.

The temperature dependences of integral intensity of PL of Cr^{3+} ions excited at 4.00 eV (310 nm) are fitted well at $T \geq 165$ K by the curve $I(T) = I_0/(1 + a \exp(-E_q/kT))$ that describes temperature dependence of PL intensity in the simple model of temperature quenching with activation energy E_q. The fitted parameters I_0, a, and E_q are temperature-independent. The activation energy of PL quenching $E_q \sim 215$ meV was found almost independent on x. This indicates that at temperatures $T \geq 165$ K the intra ion d-d transitions in Cr^{3+} ions are not significantly influenced by the neighborhood of CrO_6 complexes. At temperatures lower than 165 K the situation is more complicated and the observed dependence of integral intensity of PL of Cr^{3+} ions on the Ba content in BST thin film is probably related to the appearance of phase transitions.

The first results of PL study of BST thin films carried out on nominally pure and slightly Cr doped samples deposited by the hollow cathode plasma jet system proved that Cr^{3+} ions can be used as a spectroscopic probe of the BST lattice behavior. A study of behavior of the characteristic ZPL of octahedral coordinated Cr^{3+} ions in BST thin films can give additional information on structural transformations.

References:

[1] LEMANOV, V. V. – SMIRNOVA, E. P. – SYRNIKOV, P. P. – TARAKANOV, E. A.: *Phase transitions and glasslike behavior in $Sr_{1-x}Ba_xTiO_3$* Phys. Rev. B 54, 1996, pp. 3151–3157.

[2] OSTAPCHUK, T. – PETZELT, J. – ŽELEZNÝ, V. – PASHKIN, A. – POKORNÝ, J. – DRBOHLAV, I. – KUŽEL, R. – RAFAJA, D. – GORSHUNOV, B. P. – DRESSEL, M. – OHLY, CH. – HOFFMANN-EIFERT, S. – WASER, R.: *Origin of soft-mode stiffening and reduced dielectric response in $SrTiO_3$ thin films* Phys. Rev. B 66, 2002, pp. 235406-1–235406-11.

[3] BRYKNAR, Z. – POTŮČEK, Z. – HUBIČKA, Z. – OLEJNÍČEK, J.: *Luminescence Properties of $Ba_xSr_{1-x}TiO_3$ Thin Films Deposited by RF Hollow Cathode Plasma Jet System* Ferroelectrics 335, 2006, pp. 95–102.

[4] EDEN, S. – KAPPHAN, S. – HESSE, H. – TREPAKOV, V. – VIKHNIN, V. – GREGORA, I. – JASTRABÍK, L. – SEGLINS, J.: *Observations of the absorption, infra-red emission, and excitation spectra of Cr in $BaTiO_3$* J. Phys.: Condens. Matter 10, 1998, pp. 10775–10786.

This research has been supported by MŠMT grant No. MSM 6840770021.

Section 3

INFORMATICS
&
AUTOMATION ENGINEERING

Coordinate system transformations and its implementation in web application using Java server Pages technology

J. Ježek

jan.jezek@fsv.cvut.cz

*Department of Mapping and Cartography, Faculty of Civil Engineering, Czech Technical University, Thákurova 7, 166 29 Praha 6, Czech Republic

One of the frequently required operations in GIS (geographic information system) is to convert coordinates derived in one geographic coordinate system to the values expressed in another. Almost all geodata which are available in Czech Republic are referenced in coordinate system called S-JTSK. On other hand there are a lot of users using WGS-84 to work with their data. Project Coordinate system transformations and its implementation in web application using Java server Pages technology has been focused on development of the web based application that allows users to convert their data between one coordinate reference and another and to cover almost all coordinate systems that are used all around the world. This paper deals with the problem from the developer's point of view. The theoretical background of coordinate transformation has been already discussed. See [3] for details.

The brain of the developed application is GeoTools referencing package. GeoTools is an open source (LGPL) Java code library which provides standards compliant methods for the manipulation of geospatial data. It consists of variety of modules where the referencing module was the most important for proposed work. Referencing module provides implementations for general positioning, coordinate reference systems (CRS), and coordinate transformations. Coordinates can have any number of dimensions. So this implementation can handle 2D and 3D coordinates, as well as 4D, 5D, etc.

Before using this module we have to add the implementation of projection that is used in Czech Republic (Krovak projection), that was missing in this library. After communication with module maintainer (Martin Desruisseaux) we have added this projection and it became part of the GeoTools 2.3. which has been released in late December 2006. The advantage during these phases of the project was the fact that the author is a member of GeoTools community and has already the commit access to the code repository. As a side effect of this new implementation, two more GIS open source projects that are built upon GeoTools (uDig and Geoserver) can also operate with Czech data located in S-JTSK/Krovak coordinate system (see fixed bug report at http://jira.codehaus.org/browse/UDIG-623). GIS product uDig is developed by Refractions Research (http://udig.refractions.net/) so we have discussed the problem with them either. The implementation has been made with respect to OGC (open geospatial consortium) specifications. For more implementation details see the javodoc documentation at http://javadoc.geotools.fr/2.3/.

Architecture of web applications is based on Model, View, Controller design patterns and is just the kind of user interface for GeoTools functionality. From the technical point of view the application is 100% pure Java implementation using the jsp and servlet technology for handling user request and generating appropriate response. Calculation as such takes place in referencing jar archive.

The user can define the source and target coordinate systems by variety of different ways. Most common way of definitional of coordinate reference system is EPSG codes. EPSG

(European Petroleum Survey Group) is the authority that maintains and publishes a dataset of parameters for coordinate reference system and coordinate transformation description. This database is located on the server and is accessed through one of the GeoTools plug-ins. For example when the user wants to transform data from Czech coordinate system to WGS-84 they can put the 2065 EPSG code as the source and 4326 code as target. More information about EPSG code see [1].

After specifying the EPSG code the wkt (well known text) definition of selected Coordinate system is displayed. The OpenGIS Consortium "Simple Features for SQL" specification defines the well-known text representation to exchange geometry data in ASCII format. This representation is also referenced by the ISO "SQL/MM Part: 3 Spatial" standard. See "Spatial functions that convert geometries to and from data exchange formats" for information on functions which accept and produce WKT data. The user can eventually edit this wkt representation so he can setup or edit things like projection parameters or parameters of the transformation very easily. After that they can simply upload the ASCII file containing the coordinates and they receive a download link to get the file with transformed data.

One of very important question concerning the geography system transformations is the accuracy. Accuracy of any transformation is determined by the transformation method and by parameters that are used. For example - by default transformation from Czech system S-JTSK to WGS-84 has accuracy approximately 1 meter (we are using global key for Bursa Wolf transformation method from EPSG database). When we want precise transformation just for small locality we have to calculated our own transformation parameters and set it up through wkt definition. This fact is caused by local deformations of the Czech system. In the future work we are going to implement one of the precise methods which deal with this problem.

Described project has two consequences. It brings the functionality of coordinate system transformations implemented in GeoTools library into simple web application so the users can transform their data without installing anything (just Internet browser is required). The users can easily transform coordinates located in almost all coordinate systems used all around the world. Another thing which requires attention (and which was not the aim of this project originally) is the improvement of GeoTools as such. This improvement is a side effect of this project and brings the Krovak projection into few other GIS products that are built upon GeoTools. Developed web application can be accessed through http://gist.fsv.cvut.cz address.

References:

[1] GEOTOOLS HOME PAGE: *http://docs.codehaus.org/display/GEOTOOLS/Home*

[2] OGP SURVEYING & POSITIONING COMMITTEE HOME PAGE: *http://www.epsg.org/*

[3] SKLENIČKA, R., JEŽEK, J. *Transformace souřadnicových systémů ve vybraných GIS produktech* Geodetický a kartografický obzor (GaKo) č. 6-7/05, s. 129-132 2005, ISSN 0016-7096

This work was funded by the Czech Ministry of Education within the framework of the programs INGO (Grant LA055) and National Research Centers (Grant LN00A100). The authors appreciate very much the support given by the staff of PALS.

GRASS GIS Metadata Management Analysis

M. Landa

martin.landa@fsv.cvut.cz

Department of Mapping and Cartography, Faculty of Civil Engineering, Czech Technical University, Thákurova 7, 166 29 Prague 6, Czech Republic

Introduction to Geospatial Metadata

General conception of "metadata" has been studied in several scientific papers since the 1970s. The origin of the word came from the Greek and can be translated as "data about data". The ISO 211 Technical Committee defines metadata as a structured data describing content, its quality and other (geo)data properties.
Metadata is an essential addition for particular and accurate identification, verification and interpretation of data. Metadata for spatial-oriented data follows the same basic principals as metadata for non-spatial data. On the other hand metadata for spatial data has unique characteristics whose formulation (i.e. description and structure) is still under development. This kind of metadata is oriented rather on spatial data description and should be organized using specialized metainformation systems.

Geodata documentation can be different depending on the regional or national nature of the geospatial infrastructure. Moreover the documentation is very often mutually incompatible. This fact justifies the effort of creating an international standard for metadata description – *ISO 19115, Geographic Information – Metadata*.
Beginning of the standardization process in this field dates back to the 1990s. Internationally used standards for metadata in geoinformatics are mainly U.S. standard *FGDC Content Standard for Digital Geospatial Metadata*, European *CEN ENv 12657, Geographic Information – Data description – Metadata* (its development has been stopped) and finally the *ISO 19115, Geographic Information – Metadata*. There is strong tendency to integrate the FGDC and ISO standards.
One of the prominent initiatives in information technology (IT) field is *The Dublic Core Metadata Initiative* (DCMI). DCMI is an open organisation engaged in the development of interoperable online metadata standards. DCMI defines the Dublin Core Metadata Element Set (DC) which is a vocabulary of fifteen properties for use in resource description (the ISO standard 15836). All metadata standards should follow the DC instructions.

Sophisticated metadata management is going to be an essential feature of all GIS applications. Most of the commercial GIS products reflect this need and support in a given level the ISO standard 19115.

GRASS GIS and Metadata Management

Capabilities of the world's leading Free Software GIS – GRASS – in metadata handling are strongly delimited and moreover not unified. In the result, GRASS GIS is not able to compete in this field (in contrast with e.g. raster data processing) with comparable applications.
Metadata management in GRASS GIS is relatively poor, considerably out-of-date, and not extensible. Metadata form, user interface and especially API (Application Programming Interface) is different depending on the data type (raster, vector map layers). The core libraries

(GIS, raster and vector library) have been created and maintained in different stages of the GRASS development.

Metadata can be an integral part of the data (often without any significant organisation) or stored as a separate unit. Metadata management which is the specific part of the system has more flexible structure. The next stage is an independent metainformation system separated from the data management system. In any case metadata management should be a fundamental part of any Geographic Information System (GIS) and not an extension of functionality.

Metadata can be stored in various formats, which are very often XML-based. XML as a language is highly worth considering metainformation model requirements. Data structure is strictly defined; XML documents can be validated against DTD (Document Type Definition) or XSD (XML Schema Definition). XML is an open and widely used industrial platform independent standard orientated to data publication and distribution. XML documents can be kept as flat files in file system or stored in database management system (DBMS). There are various implementations available based on the relational, object-oriented and native XML DBMS.

GRASS metadata can be represented as a tree structure; the root of the structure is “GRASS location”. A GRASS location is defined by its coordinate system, map projection and geographical boundaries. Each GRASS location can have many mapsets. Metadata of the GRASS data layer contains metadata elements of mapset and location metadata set.

Conclusion

The ISO standard 19115 is going to be widely used. In this connection we can also mention harmonization effort with U.S. standard FGDC-CSDGM or the INSPIRE project in Europe. Although software support of the ISO standards in this field is not so great after all.

Currently GRASS GIS includes very limited metadata management system (no support of any standard). New design and subsequent implementation of metainformation management GRASS subsystem should reflect the prevailing trends, natively support the international ISO standard 19115 including ISO 19139 implementation and other ISO standards.

References:

[1] LANDA M.: *GRASS GIS Metadata Management Analysis* In GIS Ostrava 2007 Proceedings. VŠB - Technical University of Ostrava, 2007 .

[2] LANDA M.: *GRASS GIS: Importing and processing of cadastral data in Czech cadastral exchange data format* In GIS Ostrava 2006 Proceedings. VŠB - Technical University of Ostrava, 2006, ISBN 1213-239X.

This research has been supported by CTU0604711.

Support for Coordinate Systems Operations in GIS and Developing Map Servers

R. Sklenička

radek.sklenicka@fsv.cvut.cz

Department of Mapping and Cartography, Faculty of Civil Engineering, Czech Technical University, Thákurova 7, 16629 Prague 6, Czech Republic

Distributed Geographic Information Systems

Geographic Information System (GIS) development has been highly influenced by the progress of Information Technology. The first GIS project was established in Canada, almost fourty years ago, and a mainframe GIS technology was used at that time. Since, desktop GIS was evolved, and currently distributed GIS, based on web services is supposed to be the future model of GIS. While the traditional desktop GIS relies on a GUI for users to interact with GIS programs, the distributed GIS relies on the World Wide Web (shortly Web) and its add-ons to provide interactivity between the user and the distributed GIS programs. Distributed GIS takes advantage of the Internet as a huge distributed system where GIS tools and the GIS data reside in different servers or computers on the Internet and users can access those data and applications on demand from anywhere across the Internet or wireless networks. Distributed GIS are not limited to any kind of operating system or platform, and are cross-platform accessible.

Open Geospatial Consortium

There is a need to set up standards and specifications to achieve full integration of heterogenous geospatial data and geoprocessing resources. There is also the need of standards to address common means to access, describe, advertise and discover these resources. One of the main organizations, developing specifications for geo-spatial data and applications, is well known Open Geospatial Consortium (OGC), the international, non-profit, voluntary consensus standards organization [1].

OGC Web Coordinate Transformation Service

Coordinate transformation of geospatial data is one of the most common operation used in GIS [2] and enables to process together the data that are referenced in various coordinate reference systems. The main goal of the research is the development of the web service for coordinate transformations of spatial data. This web service is based on the OGC specification WCTS (Web Coordinate Transformation Service) [1]. This standardized web service is designed to be a suitable component for spatial data coordinate transformations within the distributed GIS.

WCTS is being implemented in Python programming language [3]. There is an effort to implicate the Open Source OGR/OSR modules, OGR module enables some data format access (e.g. shapefile, GML 2, …) and OSR module enables coordinate transformations. The effort here in the development of the transformation service is to take advantage of OGR/OSR, but also built own transformation library to extend potential of the service with the support for another coordinate transformations. Small library for coordinate systems operation is designed, and is called CRS (Coordinate Reference System). Documentation and source code can be found on the server gist.fsv.cvut.cz.

Mapservers

Traditional server applications called mapservers have been used for storing and providing geo-spatial data through the Web, and have been widely expanded all over the world within recent several years. Geospatial data has been provided in the traditional client-server way, but now more web map services is being appeared. Mapserver applications are designed to be web-services-standards oriented. Most of these applications are based on OGC specifications WMS (Web Map Service), WFS (Web Feature Service), WCS (Web Coverage Service), SLD (Styled Layer Descriptor). This effort enables to plug-in map servers into the distributed GIS.

Within this research, some sample mapserver applications have been developed. Open Source sotware UMN MapServer as the mapserver engine has been used, and the free available spatial data set has been applied. Although we were limited by the amount of available data, for the purpose of sample testing applications this free data set was quite sufficiet. Sample mapserver applications are developed by means of Python/Mapscript and PHP/Mapscript. Spatial data are stored in file system and we also test storing data in a spatial database by means of PostGIS, which is the spatial extention on the database management system PostgreSQL. One of the objective is to demonstrate the powerfull Open Source geospatial software and provide documentation and source codes of the designed applications, which can be found on the server gist.fsv.cvut.cz.

Future work

As for the future work, implementation of a WSDL/SOAP interface into the WCTS service is proposed. This would make the service implementable in a remote service chain, for example with the use of Business Process Execution Language (BPEL).

References:

[1] SKLENIČKA, R.: *Interoperabilita v GIS podle specifikací OGC.* Geoinformatics FCE CTU 2006, 2006, pp. 170–175. ISSN 1802-2669.

[2] SKLENIČKA, R. – JEŽEK, J: *Transformace souřadnicových systémů ve vybraných GIS produktech.* Geodetický a kartografický obzor (GaKo), 2005, č.6-7/05, pp. 129–132. ISSN 0016-7096

[3] SKLENIČKA, R.: *Programovací jazyk Python v geoinformatice.* In GEOS conference of the 1st International Trade Fair of Geodesy, Cartography, Navigation and Geoinformatics, Prague, 16-18 March, 2006

This research has been supported by CTU grant No. CTU0604811.

Design of Mobile Ad Hoc Networks in Domains with High Level of Communication Inaccessibility

P. Benda

bendap1@labe.felk.cvut.cz

Department of Cybernetics, Faculty of Electrical Engineering, Czech Technical University, Technická 2, 166 27 Prague 6, Czech Republic

A mobile ad hoc network (MANET) is comprehended as a self-configuring communication network where each node can chaotically move in space. Network topology is rapidly changing in such types of networks. Support for communication through transitively accessible MANET is provided by a mobile routing protocol. This type of networks is suitable in emergency situations like disasters and battlefield operations for their quick deployment and minimal configuration time.

Nowadays, a lot of mobile routing protocols are used in mobile ad hoc networks in practice. However, all the protocols fail if a network topology consists of several mutually inaccessible components. In such a case, it is necessary to introduce artificial intelligence to the behavior of mobile routers to solve the problem of inaccessibility. Moreover, by using this artificial intelligence for mobility control we are able to increase capacity of existing mobile ad hoc networks. So, the mobile network can be viewed as a multi-agent system (MAS) and therefore it is natural to adopt the terminology and knowledge from that field. Let each mobile intelligent router be represented by a software agent that can control position of its physical device – a machine where the agent is loaded. A group of these agents forms a multi-agent system.

In our research we use A-globe [1] multi-agent platform that is suitable for real-world simulations including both static and mobile units (e.g. logistics, ad-hoc networking simulation), where the core platform is extended by a set of services provided by a Master GIS (Geographical Information System) container hosting various environment simulator (ES) agents. The system simulates geographical position and time dynamics of each unit. Simulation scenario is defined by a set of actors represented by agents residing in the agent containers. All agent containers are connected together to one system by the GIS services. Beside the simulation of dynamics the ES agents can also control communication accessibility among all agent containers. The GIS service applies accessibility restrictions in the message transport layer of the agent container.

Research of mobility control in ad hoc networks is a relatively new research area. The fundamental work "Towards Mobility as a Network Control Primitive" [1] appeared in 2004. Its authors presented a distributed asynchronous algorithm for optimizing positions of relays. This algorithm assumes that a routing protocol is used in that network that is able to find single path between the data source node and data destination node. The next assumption of the algorithm makes is a common goal of relay agents, i.e. building the network infrastructure. Moreover, the algorithm supposes that routers can move freely in space without barriers.

In our research we designed a centralized algorithm for optimal motion control for reaching connectivity of agents. The algorithm permits existence of barriers in the space and also solves the collision avoidance problem. The algorithm is based on the A* algorithm and is able to reduce the size of expanded state space in the most practical cases as it doesn't explicitly expand all possible combinations of concurrent move of all agents. On the other

side, the algorithm is usable for small instances of the problem. To solve larger instances, we must use a suboptimal approach. Each agent (mobile intelligent router) has local information about the world in which it lives. This information is incomplete and an agent can reason only about this local information. We proposed to use framework of Markov Decision Processes for local decision making in the agent. In the local knowledge of the agent we isolated a set of goals (places where the agent wants to go independently on communication intentions) and a set of planned communication meetings with other agents. We equipped the agent with adaptation mechanism for agent state probability. We evaluate each agent state by an economic profit and we generate agent's behavioral strategy using the value iteration method.

We excepted from our decentralized algorithm suboptimal behavior because an agent maximizes only his own profit and not summarized profit of all agents. However, we achieved much less effective behavior than we expected. It seems that we need to make another state model of the agent state space or to use different approach based on domain dependent social knowledge.

Social knowledge of an agent contains information for efficient operation in a multi-agent system. Using social knowledge leads to long-term reduction of communication traffic in multi-agent systems. Agents can also reason about social knowledge of others and optimize its actions. Social knowledge can be also used for reasoning about short-term inaccessibility as in the stand-in [2] agent case. For longer-term inaccessibility reasoning, social knowledge must represent future course of intentions, resource allocation or negotiation preferences. Social knowledge of an agent is stored in a special knowledge structure – in an acquaintance model. Two basic types of acquaintance models were presented: tri-base acquaintance model and [4] and twin-base acquaintance model.

Future research will be focused on using social knowledge for agent's decision making. This approach should lead to more efficient operations in multi-agent systems with high level of communication inaccessibility.

References:

[1] D. ŠIŠLÁK, M. PĚCHOUČEK, M. ROLLO, M. REHÁK, J. TOŽIČKA: *Simulating agent's mobility and inaccessibility with A-globe multi-agent system.* In Multiagent System Technologies, 2004, pp. 258-272.

[2] D. GOLDENBERG, J. LIN, A. S. MORSE, B. ROSEN, Y. R. YANG: *Towards Mobility as a Network Control Primitive,* In Proceedings of the Fifth ACM International Symposium on Mobile Ad Hoc Networking and Computing, 2004, pp. 166-174.

[3] M. REHÁK, M. PĚCHOUČEK, J. TOŽIČKA, D. ŠIŠLÁK: *M. REHÁK, M. PĚCHOUČEK, J. TOŽIČKA, D. ŠIŠLÁK:* In Proceedings of Engineering Societies in the Agents World, 2004, pp. 277-291.

[4] M. PĚCHOUČEK, V. MAŘÍK, O. ŠTĚPÁNKOVÁ: *Role of acquaintance models in agent-based production planning systems,* In Proceedings of the Cooperative Infromation Agents IV, 2000, pp. 179-190.

This research has been supported by CTU grant No. CTU0607413.

Reconfiguration in Competitive Multi-agent Environments

J. Bíba

biba@labe.felk.cvut.cz

Gerstner Laboratory, Department of Cybernetics, Faculty of Electrical Engineering, Czech Technical University, Technická 2, 166 27 Prague 6, Czech Republic

Flexibility is one of the most crucial properties demanded from information, manufacturing, logistics, and other solutions deployed into industry, because it enables companies to keep up with rapid changes on contemporary globalized market. Reconfiguration in multi-agent systems introduces a means for implementation of system flexibility. Even though the flexibility is considered to be one of the most beneficial multi-agent systems properties, a reconfiguration itself was deeply studied only rarely. Moreover, only collaborative (cooperative) multi-agent environments have been considered. Unfortunately, such approaches are not fully applicable in competitive environments and the role of a reconfiguration also differs. As self-interested agents must be motivated to behave responsibly, the reconfiguration to take place must be also beneficial for the parties involved. A possible decommitment is an issue to be included into a commitment concept. The reconfiguration then may facilitate a more profitable resolution of unexpected events (e.g. a better third-party contract offer, a resource failure) than a decommitment - a decommitment in a competitive environment is often bound with a payment of a penalty. Thus, a reconfiguration may also introduce a means for a reduction of the penalty.

Although there are some domain-dependent application implementations of a reconfiguration in multi-agent systems - e.g. (Coudert et al., 2003; Inohira et al., 2003; Brennan et al., 2001), the first deep study of a reconfiguration and its formalization was published merely recently by Dunin-Keplicz in (Dunin-Keplicz and Verbrugge, 2003). The multi-agent environment has been assumed being collaborative. Thus, if a failure occurred, then all the agents involved in achieving their common goal made their best for establishing a recovery in order to complete their task successfully (a reconfiguration occurred). This behaviour has been given by their persistent collective intention set to achieve their common goal in accordance to a definition of a joint persistent goal (Levesque et al., 1990). However, in competitive environments the collective intention does not need to be kept unconditionally by all the agents – any agent may decommit from the actual contract (e.g. on account of a more profitable third-party contract offer). A decommitment as a concept was not considered in the above-mentioned research, while according to ('T Hoen and La Poutre, 2003) it may become a means for an optimization of agents' individual profits. While an implementation of a reconfiguration in collaborative environments was facilitated by the agents' primary motivation (i.e. maximization of their social welfare), in competitive environments it is even more difficult. In collaborative environment, the decommitment or replanning is driven by the common goal. It is obvious that both partners of the 'contract' have the same motivation to keep it or change it. In competitive environment the agents need to be motivated not only to agree on a contract and to keep their commitments, but also to perform reconfiguration if it is necessary. A self-interested agent will be rather reluctant to take on further obligations if it had not been rewarded or if it had even entailed its profit loss. One of the motivations at hand is to use the reconfiguration as an alternative to a decommitment if keeping of the actual contract did not contribute to maximization of the agent's individual utility (e.g. a more profitable offer appeared). For example, the agent may find subcontracting being reimbursable from the

reward promised by its contractor and to take advantage both from the actual and the new contracts without decommitting. Of course, the reasoning about decommitment might have started also on account of unexpected events occurring, e.g. resources failure, unexpected delay that might threaten meeting of the contract deadline, etc. Thus, a reconfiguration may appear to be useful for optimization of resources load and also profit maximization by means of optimizing eventual or necessary decommitments. In collaborative environment reconfiguration is usually driven by individual tasks (it is invoked top-down by decomposition means) rather then by intentions of the contracted agents. In competitive environments reconfiguration can be naturally driven by means of utility gained or prevented from loss.

A contract is reconfigurable if there exists an alternative way of its implementation (a reconfiguration alternative) which is acceptable for all the involved parties (including the customer), it is technically feasible and it is more advantageous than breaching of the contract. Otherwise, the contract may be either implemented according to the formerly agreed way or breached. Thus, the reconfigurability heavily depends on the agreed contract conditions. Agents in competitive environments are rather reluctant to share information as it may result in private information leakage – agents share not more than inevitably necessary. Therefore, the setting of contract conditions is a non-trivial issue. One of the ways to deal with information inaccessibility in competitive environments is a use of acquaintance models. We proposed an iterative approximate acquaintance model consisting of three modules: (i) profitability module, (ii) reputations module and (iii) commitments-resources module [2]. The information stored and updated in the acquaintance model enables setting and adaptation of contract conditions with respect to rapid changes occurring in the competitive environment. As task decomposition is closely coupled with contracting as well as reconfiguring of existing contracts, we proposed an iterative-query based approach to efficient task decomposition [3]. The contracting and reconfiguring negotiations among the agents are controlled by means of interaction protocols. We proposed an interaction protocol for contracting and reconfiguration in competitive multi-agent environments – Competitive Contract Net Protocol [4].

Reconfiguration in competitive environment cannot rely on centralized knowledge, because the assumptions on information accessibility cannot be received. The basic distributed approach we proposed may bypass these difficulties by means of using iterative approximate acquaintance model, suitable negotiation protocol and efficient task decomposition. Though, contracting and reconfiguration are still open issues and require further extensive research.

References:

[1] BÍBA, J. - VOKŘÍNEK, J.: *Agent Contracting and Reconfiguration in Competitive Environments,* Austrian Society for Cybernetics Studies, 2006, pp. 527-532.

[2] BÍBA, J. - VOKŘÍNEK, J.: *Multi-agent Contracting and Reconfiguration in Competitive Environments using Acquaintance Models,* ČVUT, 2006, [CD-ROM].

[3] PĚCHOUČEK, M. - LERCH, O. - BÍBA, J.: *Iterative Query Based Approach to Efficient Task Decomposition and Resource Allocation,* Springer, 2006, pp. 259-271.

[4] VOKŘÍNEK, J. - BÍBA, J. - HODÍK, J. - VYBÍHAL, J. - PĚCHOUČEK, M.: *Competitive Contract Net Protocol,* Springer-Verlag, accepted for publication in 2007, pp. 656–668.

This research has been supported by CTU grant No. CTU0607413.

Reflection and Cognition in Multi-Agent Systems with Constrained Computational Resources

L. Foltýn

lfoltyn@labe.felk.cvut.cz

Department of Cybernetics, Faculty of Electrical Engineering, Czech Technical University, Karlovo náměstí 13, 121 35 Praha 2, Czech Republic

Contemporary computational systems are implemented in a way that they have only limited adaptive capabilities. Typical approach to the computational systems design including distributed multi-agent systems is to implement a very complex and entangled decision-making code which is able to react to all possible changes in the environment including dynamics of such changes. Even a small change in environment settings often results in laborious redesign of the reasoning code. The greatest disadvantages of this approach is that the reasoning code must be created during design phase prior to the deployment phase and that only small portion of the complex code is used for particular environment state. The later disadvantage becomes a key restriction in systems which have to deal with constrained computational resources.

In our project aim to create agent architecture which would be able to adapt to the limited computational resources and changes in the environment by means of runtime code alteration, to share and incorporate previously unknown code and to keep this architecture as lightweight as possible including a simple code development and deployment.

The ability of a computational entity to reason about its computational state and computational code is referred to as **reflection** and is a cornerstone of our Reflective-Cognitive (RC) agent architecture [1]. In the software engineering we distinguish between two types of reflection: *structural* and *behavioral* [2]. By using the structural reflection the system structure can be dynamically modified, while the computational (behavioral) reflection modifies the system semantics (behavior). The reflection in multi-agent system could be also viewed from another perspective. If we take the degree of interaction with other agents as a criterion, we can consider three types of the reflection in multi-agent systems. (i) ***individual reflection*** is a revision of agent's isolated behavior. Individual reflection is an operation that works with agent's awareness of its own knowledge, resources, and computational capacity. (ii) ***Mutual reflection*** is a revision of agent's interaction with another agent. This kind of revision is based on agent's knowledge about other agents, trust and reputation, knowledge about the others' available resources, opponents' (or collaborators') long-term motivations and intentions. This knowledge is referred to as social knowledge. (iii) ***Collective reflection*** is a revision of agents' collective behavior as a result from their complex interaction. Unlike in the case of the mutual reflection, in the collective reflection the agents update not only their own social knowledge bases and reasoning processes but they also make attempts to indirectly revise other agents' social knowledge and reasoning.

Our RC agent architecture is composed of two layers. Lower layer, called **reasoning layer**, contains all agent's algorithms and thus ensures agent's functionality and upper layer, called **reflective layer**, manages the adaptation and optimization. This separation of responsibility tackles the complexity and dynamics of the environment without increasing the complexity of the business logic within the reasoning layer – if a need arises, the reflective layer re-programs the reasoning to better react to the new situation, eliminating the need to predict and represent all possible environment states at design time. In order to do so, it takes into account agent's

computational status, resources and efficiency and based on this automatically changes the operation of the running program.

For easier code description and manipulation, functional pieces of agent's algorithms are encapsulated into **components** which follows so called component approach [3]. Components accompanied by meta-description are then during the reflective process chained into algorithms which are "tuned" to the current state of the scenario and these algorithms are deployed in agent's reasoning layer. The component approach enables easy code exchange among agents which is crucial feature for the collective reflection.

In our implementation we don't restrict ourself to forming agent's algorithms from pre-prepared components only. Using methods from Inductive Logic Programming, we are able to create brand new code for certain components based on agent's observations. Component code creation along with implemented methods for collective reflection are described in [4].

In our experiments, [1] and [4] we have tested on logistics scenario that RC architecture is able to cope with changes in computational resources, changes in agents' society, new component creation and new component deployment. For these reasons we believe that reflective approach to agent design is a promising way for future distributed pervasive systems.

In our future work, we would like to reuse presented reflective concepts in scenario with even more constrained computational resources such as sensor networks or computer network protection.

References:

[1] FOLTÝN, L. - TOŽIČKA, J. - ROLLO, M. - PĚCHOUČEK, M. - JISL, P. *Reflective-cognitive architecture: From abstract concept to self-adapting agent* IEEE Comp. Soc., 2006.

[2] ORTIN, F.- CUEVA, J.M. *Non-restrictive computational reflection* Comput. Stand. Interfaces 25(3) 2003, pp. 241–251.

[3] WIEDERHOLD, G. - WEGNER, P. - CERI, S. *Toward megaprogramming* Commun. ACM 35(11), 1992, pp. 89–99.

[4] TOŽIČKA, J. - JAKOB, M. - PĚCHOUČEK, M. *In Klusch, M., Rovatsos, M., eds.: Cooperative Information Agent VII. LNAI* Springer-Verlag, Heidelbergl, 2006.

This research has been supported by CTU grant No. CTU0607713.

Advanced stream routing protocol for non-stable environment

P. Jisl

jisl@labe.felk.cvut.cz

Department of Cybernetics, Faculty of Electrical Engineering, Czech Technical University, Technická 2, 166 27 Prague 6, Czech Republic

Traditionally, the control systems are build with a central unit, which collects information from all controlled units and on the basis of these information acts as a task coordinator. This approach may encounter problems in cases, where the communication accessibility between central unit and controlled units cannot be guaranteed.

There are mainly two problems in systems the with central unit in environments with limited communication accessibility. The first problem is the limited communication range, because the controlled units may easily get out from central unit's communication range. The second problem is a malfunction of the central unit. As the controlled units are not equipped with their own planning capabilities, they fail to operate efficiently and coordinate their own actions. In these cases we can successfully use multi-agent systems with autonomous and self-interested units, where each of the units can take a role of task coordinator. Units in multi-agent systems can communicate and negotiate in a peer-to-peer manner when fulfilling their tasks.

This work is targeted to the problem of streaming large data feeds, like streams from camera or audio data, in the wireless ad-hoc networks. This is one of the most challenging problems, because in static networks, this problem is simplified by using a central unit, which has complete information about positions of all the units (nodes) in the given environment. Therefore, it can simply plan a transmission over these nodes, taking into account the constrains given by the environment.

In mobile networks the nodes are not static – they can move in the environment – and the problem consists in the dealing with their possible inaccessibility and their movement in the environment. In presence there is a lot of different approaches solving the routing of streams in mobile networks. The most used protocols are Ad-hoc On-demand Distance Vector (AODV), Dynamic Source Routing protocol, Optimized Link State Routing protocol and their modifications.

The ad-hoc routing protocols are usually categorized as (i) proactive (table-driven) and (ii) reactive (source-initiated or demand driven). (i) The proactive protocols maintain consistent, up-to-date routing information from each node to every other nodes in the network. Each node maintains one or more tables to store routing information and they respond to changes in a network topology by propagating updates through network in order to maintain a consistent network view. (ii) The reactive protocols in contrast to the proactive protocols create routes only when there is a need for sending data from a source to a destination node. The source node initiates a processes of discovering the network, which is finished, when the desired route is found or all possible route permutations have been examined. Once the route is established, it is maintained by a maintenance procedure until either the destination node is inaccessible along every path from the source or the route is no longer needed.

In our research we proposed the implementation of the Middle-agents [3] in integrated FlexFeed/A-globe architecture [1,4] for distributed coordination of resource allocation for routing streams of large amounts of data. The A-globe is lightweight multi-agent platform with environmental simulation and mobility support. The FlexFeed framework [2] provides the mechanisms to configure and task network resources in order to deploy the allocation

schemes determined by the coordination components. This framework relies on mobile software agents to transparently enable capabilities in network nodes for data processing and distribution between multiple (possibly disparate) applications.

At this moment, FlexFeed provides only centralized approach to coordination of data stream delivery. In A-globe simulation scenarios the partially and fully decentralized coordinations were implemented.

Fully decentralized approach for coordination [1] in the integrated FlexFeed/A-globe architecture was implemented using the Middle agent architecture. It was chosen because it is fully distributed and it appears to provide all necessary mechanisms for implementation of streaming large data feeds. It is also multi-agent approach which provides system robustness, flexibility, encapsulation and interoperability which are required in real-world applications.

The Middle agents were primary designed for matchmaking and negotiation. The extension, described in [3,4], was designed to migrate autonomously within the network and to clone and destroy its copies. These agents are also without any social knowledge, because are used for building a message passing and routing system. The key issue for efficient operation of middle agents is their proper location in network. The distributed mechanism uses only locally accessible information, which is obtained by means of monitoring neighborhood by identifying the currently visible neighbors and other middle agents.

The middle agents as message routing system were implemented into integrated FlexFeed/A-globe architecture. The changes in NOMADS (FlexFeed underlaying multi-agent architecture) and FlexFeed core were applied. The middle agent's implementation was divided into middle agent Core and platform-dependent implementation of underlaying infrastructure. For easy implementation, the interfaces for middle agent required infrastructure were implemented. Platform-dependent part of middle agent provides infrastructure for middle agent creation and clonning, message propagation and solving the visibility of containers and environments. A set of experiments was carried out in order to study the middle agent behavior in non-stable environment. We measured the evolution of the number of middle agents at three levels of inaccessibility dynamics.

The future work will involve the fully distributed system for routing large data streams. We will implement also techniques for securing the required QoS for stream delivery and policy framework for secure delivery of streams. We will also create social knowledge module for storing state information about the routes, neighbors and also about network.

References:

[1] BENDA, P. – JISL, P. – PĚCHOUČEK, M. – SURI, N. – CARVALHO, M.: *A Distributed Standin Agent based Algorithm for Opportunistic Resource Allocation* Applie d Computing 2006, New York: ACM, 2006, vol. 1, pp. 119 – 125.

[2] CARVALHO, M. – BREEDY, M. R.: *Supporting flexible data feeds in dynamic sensor grids throught mobile agents* MA 02: Proceedings of the 6th International Conference on Mobile Agents, Springer-Verlag, 2002, pp. 171 – 185.

[3] REHÁK, M. – PĚCHOUČEK, M. – TOŽIČKA, J. – ŠIŠLÁK, D.: *Using Standin Agents in Partially Accessible Multi-agent Environment* In Proceedings of Engineering Societies in the Agents World V, Toulouse, LNAI 3451, Springer-Verlag, 2005, pp. 277 – 291.

[4] BENDA, P. – JISL, P.: *A distributed stand-in agent based algorithm for opportunistic resource allocation* In Automation Systems, I*PROMS, 2006 (in preparation).

This research has been supported by CTU grant No. CTU0608013.

Analysis and synthesis of behavior of intelligent agents in context of selected parts from artificial life domain

Karel Kohout

kohoutk@fel.cvut.cz

Department of Cybernetics, Faculty of Electrical Engineering, Czech Technical University, Technická 2, 166 27 Prague 6, Czech Republic

This paper presents our approach to design, simulation and visualization of selected ALife agents. This topic has been addressed in our research group for almost six years. In last two years there is a growing interest on the field of anticipatory behavior. The existing simulation environment called WAL (World of Artificial Life) which was designed for the purpose of simulation of various ALife phenomena in our research group [1], [2], [3], was modified and is being currently modified to be able to aid us in the research, simulation and testing of anticipatory agent architecture.

Since the beginning of this decade there has been an increasing interest in the field of research of algorithms realizing anticipation. We try to show that under anticipation we understand much more that prediction or estimation of the future states. Anticipation takes the information from prediction and estimation as an input and performs reasoning, learning and planning tasks based on these inputs. Because proving of functionality of designed architecture could be time and money consuming we decided to evaluate the architecture in computer simulation. Anticipation occurs in all spheres of life. Sometimes we humans are aware of anticipation, as when we plan. Often, we are not aware of it, as when processes embedded in our body and mind take place before we realize their finality. In tennis, for example, the return of a professional serve can be successful only through anticipatory mechanisms. A conscious reaction takes too long to process.

In artificial intelligence, anticipation is the concept of an agent making decisions based on predictions, expectations, or beliefs about the future states. It is widely recognized that anticipation is a vital component of complex natural cognitive systems. The opposite for anticipation behavior is reactive behavior. Let me demonstrate the fundamental difference by simple example: Elementary forms of artificial intelligence can be constructed using a decision base of simple if-then-else rules. An example of such system would be an agent following the rule: IF *it rains outside THEN take the umbrella ELSE leave the umbrella home*. A system such as the one defined above is inherently reactive because the decision making is based on the current state of the environment with no regard on the future. On the other hand an agent employing anticipation would try to predict the future state of the environment (weather in this case) and make use of the predictions in the decision making: *IF the sky is cloudy AND the air pressure is low THEN it will probably rain soon so take the umbrella with you ELSE leave the umbrella home*. The key component to anticipation is the existence of an inner model of the environment of the anticipatory system (sometimes including the system itself). Robert Rosen defined an anticipatory system as follows: “A system containing a predictive model of itself and/or its environment, which allows it to change state at an instant in accord with the model's predictions pertaining to a latter instant” [4].

Basically there are four types of anticipation which can occur. Animate with *implicit anticipation* does not perform any prediction about its future states which can influence its future decisions. Sensory inputs (possibly combined with information about its inner state)

are directly mapped to actuators of an agent. Implicit anticipation is hard coded in the animat's behavior control program. In nature all life forms have the information for implicit anticipation hard coded, even those behaving on strict reactive basis. Evolution is implicit anticipation mechanism which prints the information into genes. In case the agent takes into account the prediction of reward (either positive or negative) for action it is going to execute, we can speak about animate with *reward anticipation*. The benefit from each of action is quantified and therefore it is possible to compare them based on anticipated reward. *Anticipation of sensory data* acquired through sensors does not affect the behavior of animate directly but through the sensory data processing subsystem. Prediction of future states and therefore prediction of future stimuli influences the sensory data in the near future. For an animate in order to be able of such prediction we need at least partial model of the environment. The expected states can be processed and dealt with much faster than the unexpected and unpredictable ones. For example, if an animate anticipates to be attacked, it is more careful and ready to execute the appropriate action when it is actually attacked. One of the most interesting types of anticipation is *explicit prediction of future states*. These prediction influences directly the decision making process. Same as above, the prediction model is needed in order to perform this kind of anticipation.

The car and vehicle industry is one of the possible fields of applications. Anticipation of action of others based on the behavior patterns learned in the past combined with the estimate of the other driver's trajectories and behavior can help in collision avoidance and accident prevention. So far the estimation of the next development of prices of stocks is done by human experts. Anticipatory systems can be used in this field to recognize the hidden links between cause and effect (which means that the development of price of one commodity can influence the price development of another commodity etc.). The protection of human lives and property is very large area where anticipation can help. The forecast of earthquakes, volcanic activity or hurricanes can help to protect lives.

We are convinced that anticipation is an interesting topic that still needs to be explored. Incorporation of results of research in the field of anticipation into a decision making system of agent is our main focus now. Currently we are working on design of agent architecture with anticipation. There have been already some proposals of agent architectures based on various approaches. One of them used decision trees for knowledge capture and generalization. Second used Markov chains and reinforced learning.

References:

[1] KOHOUT, K.: *The Simulation of Animates Behavior and its Visualization* Diploma Thesis at the Czech Technical University in Prague, FEE, Dept. of Cybernetics, supervised by Nahodil, 2004, 84 pages.

[2] NAHODIL, P. - SLAVÍK, P. - KADLEČEK, D. - ŘEHOŘ, D.: *Dynamic Analysis of Agents Behaviour - Combining ALife Visualization and AI - revised, selected and invited papers* In Lecture notes in Computer Science. Volume 3071/2004, 2004. Heidelberg: Springer Verlag, 2004, p. 346 - 359. ISSN 0302-9743.

[3] KADLEČEK, D., NAHODIL, P. *New Hybrid Architecture in Artificial Life Simulation* In Lecture Notes in Artificial Intelligence No. 2159, Berlin: Springer Verlag, 2001, pp. 143-146. ISBN 3-540-42567-5

[4] ROSEN, R.: *Anticipatory Systems - Philosophical, Mathematical and Methodological Foundations,* Pergamon Press, 1985, ISBN 0-08-031158-X.

This research has been supported by internal CTU grant number 10-86081/13133/06.

Intelligent device for insomnia

P. Kolman, K. Malý

kolmanp@fel.cvut.cz

Department of Cybernetics, Karlovo nam.13 121 35 Praha 2
Faculty of Electrical Engineering, Technicka 2, 166 27 Praha 6
Czech Technical University in Prague, Czech Republic

The aim of this work is a development of a controlled device, which induces and supports quality sleep. The project is based on rich experience of many people with AVS, which allows them to reach quality sleep. Approximately fourth percent of population suffers from insomnia. For instance, in the USA 43% of population suffers from insomnia and estimated cost are 60-80 billions dollars per year. Common treatment is based on drugs. Two adaptive control systems will be incorporated. One is feedback in the real time. The second adaptive control system is influenced by discussions with doctors. Brain frequencies vary widely among each other, however in the span of life time of on individual person the frequencies remain stable. Sometimes it is even possible to trace genetic bond between two individuals. Due to predictable frequencies for an individual, we decided to individual adaptive control. The set up of the device can be done in cooperation with a doctor. The doctor could adjust particular parts of the sleep program using specially developed program for visual stimulation. By stimulation development is meant development of frequency stimulation in brain in time. The stimulation development describes how to set frequency in time and set of other parameters.

A device for biological quantity measurement was successfully tested. Its most important advantage is availability for immediate experiments without dependence on specialized laboratories. Some hypothesis can be supported or disproved. The verified hypothesis can be further examined in specialized sleep laboratories, which are busy scheduled. For instance, the sleep laboratories in the Czech Republic are booked 6 months ahead. Currently a new version of the device is being developed. The tests on this device were successful. For comparison were used medical devices available in our bio-laboratory. We successfully tested longitudinal measurements of EKG, temperature and skin conductance.

Another device developed independently of this grant was an AVS device, which is lighter than other AVS devices available on the market.

The device is integrated into light glasses. Technologies used are the newest available. It is necessary to mention variability and adjustability of programs. Another advantage is possibility to download personal programs as those set by a doctor. Due to above stated reasons I picked this device. Moreover, by device, which is currently being patented, the user would be able to influence visual stimulation.

Among unfulfilled aims belongs modification of measurement device for measuring of biological data, especially EEG. This device was postponed due to technical complications. For measurements necessary for the experiments was used medical EEG brainscope.

In process of patenting is currently the device the most suitable for detection of sleep. Due to patenting were also postponed experiments on selected subjects suffering from insomnia. Further are planned experiments in sleep laboratory in Bohnice, Prague, Czech Republic.

Control unite used in this program was successfully tested for use in cooperation with our stimulation device. The control unite uses robust algorithm, which is being patented and allows cheap evaluation of used stimulation program.

Based on already conducted experiments, AVS stimulation seems to be a good tool for enhancement of sleep. On of the positive impacts of this work is turning of attention of doctors to this device as a tool for sleep disorders. The devices developed and used are using the newest technologies and it is expected to be used in other experiments outside of faculty of cybernetics CTU.

References:

[1] P. KOLMAN: *Audio-visual stimulation treatment for insomnia,* VIII. czech and III. czech-slovak congress of sleep association, 2006, pp. 68-68.

[2] P. KOLMAN: *Intelligent device for insomnia treatment,* Preparation thesis on CTU in Prague, faculty of Electical Enginering, Department of Cybernetics, 2006, pp.12-30.

[3] K. MALY: *Modern technology in BMI application,* Diploma thesis on CTU in Prague, faculty of Electical Enginering, Department of Cybernetics, 2007, pp. 2-64.

This research has been supported by CTU grant No. CTU0608213.

Inference Support for Semantic Annotations in Description Logics

P. Křemen

kremen@labe.felk.cvut.cz

Department of Cybernetics, Faculty of Electrical Engineering, Czech Technical University, Technická 2, 166 27 Prague 6, Czech Republic

Efficient searching in large document repositories, and especially semantic web searching, needs semantic annotations that are both expressive enough to capture knowledge precisely, and weak enough to enable efficient reasoning. Lack of usable automatic procedures for creating such annotations drives the research in algorithms and methods for semi-automatic knowledge base building.

Creating annotation knowledge bases without intelligent support of the annotation tool is very time consuming, in case of large knowledge bases even empirically intractable. To make the annotation process more efficient, several aspects influence the design of intelligent annotation systems: 1) Users of annotation tools will be non-experts in knowledge representation and/or semantic web. Therefore, it is necessary to separate logic background of the underlying knowledge management system from user interface. 2) To reduce the number of generated annotations, it is useful to provide expressive modeling constructs, like n-ary relations. 3) Automated inducing of new annotations or annotation patterns could significantly accelerate the annotation process. 4) Efficient consistency checking and error explanations support helps in detecting and repairing of modeling errors.

In this work we will contribute to the last point – error detection and explanation. Current state of the art in the languages for semantic web is represented by description logics based languages of the OWL family. This family consists of 3 language versions with increasing expressiveness – Lite, DL, Full. The Lite and the DL versions represent decidable subsets of first order logics, thus providing sound and complete reasoning services. During the last two years, several reasoning services for knowledge base consistency checking, concept satisfiability testing, error explanations and error repairing appeared in [3] and [4]. In these works two approaches to error explanations are introduced – black-box and white-box. Black-box methods use an existing reasoner for given logic language and perform a many satisfiability/consistency tests to find explanations for given modeling error (either unsatisfiable concepts, or inconsistencies in the knowledge base). These methods are universal, as they can be used with any existing reasoner. Glass-box methods integrate the explanation support directly into the reasoning algorithm, thus decreasing the number of required satisfiability/consistency test, but increasing the complexity of a single algorithm run and disallowing its reuse in other algorithm types.

In this work we propose two novel incremental approaches to error explanations that were inspired by [2] and [3]. Incremental methods lie somewhere between black-box and white-box methods. Contrary to the black-box techniques, they require the reasoner to make its inner state accessible, but there is no interference with internals of the reasoner, like in glass-box methods. For our purposes, we use tableau-based algorithm that represent current state of the art technique for basic inference services in description logic languages. An

intermediate state of such an algorithm is represented by a set of completion graphs, partially expanded by a set of predefined inference rules, together with used axioms. Each of these graphs represents a set of candidate models that need to be explored until a clash occurs, or a clash-free completion is found. As the discussed tableau algorithms have high worst-case complexity, we need to avoid as many satisfiability/consistency tests as possible.

Our first approach extends the incremental algorithm presented in [2]. This algorithm assumes that the intermediate incremental state depends on the order, in which axioms are tested. An incremental state of a tableau algorithm, on the contrary, shall depend just on the set of used axioms. We use this feature to avoid useless satisfiability/consistency testing by caching intermediate tableau algorithm states. Our second proposal, an incremental version of the Reiter's algorithm-based black-box technique introduced in [3], replaces several full satisfiability/consistency tests with their less expensive incremental versions.

We have compared the original algorithms, to their refined versions. Results show, that in both cases we gain significant improvements in algorithm performance. Generally the refined algorithms save a significant amount of full tests – approximately 10-40% and they are half to three times faster than the original versions. Comparing our proposals to each other, their performance ratio highly depends on the structure of the knowledge base and explanation axiom set. The first (fully incremental) method performs better for large knowledge bases with many equivalence axioms, and vice versa.

For the purpose of testing and comparing, we have implemented a tableau reasoner in Java. It is able to cope with OWL-DL without nominals (i.e. its reasoning capabilities are equivalent to the SHIN(D) description logic). To cooperate with DL-compliant systems, like Protégé, the DIG 1.0 interface was implemented. By now only concept satisfiability explanation service is available. Additionally, we have integrated the explanation service based on the incremental algorithm to the new version of the DNA system prototype [1], thus providing the user with information of unsatisfiable classes in the ontology. In future work, we would like to check feasibility of the proposed incremental approaches to explain annotation errors and to support knowledge base debugging.

References:

[1] P.KŘEMEN: *Using Conceptual Graphs for Narrative Authoring* Diploma thesis, Czech Technical University in Prague, 2005 .

[2] M. G. DE LA BANDA, P.J.STUCKEY, J.WAZNY: *Finding All Minimal Unsatisfiable Subsets* ACM, Proceedings of PPDP'03, 2003 .

[3] A. KALYANPUR, B. PARSIA, B. C. GRAU, E. SIRIN: *Axiom Pinpointing: Finding (Precise) Justifications for Arbitrary Entailments in SHOIN (OWL-DL)* UMIACS, 2006 .

[4] S. SCHLOBACH, Z. HUANG, R. CORNET, F. HARMELEN: *Debugging Inconsistent Terminologies,* Kluwer 2006 .

This work has been supported by CTU grant No. CTU0608313.

Coordination of mobile robot group for unknown environment mapping

M.Saska, T.Krajník, L.Přeučil

saska@labe.felk.cvut.cz

Department of Cybernetics, Faculty of Electrical Engineering, Czech Technical University, Technická 2, 166 27 Prague 6, Czech Republic

Exploration of unknown environment is a fundamental task in mobile robotics. Exploration itself is typically solved by a combination of *Simultaneous Localization and Mapping* (SLAM), *Detection and Tracking of Dynamic Objects* (DATMO), recognition of potentially unexplored regions, path and motion planning algorithms. Cooperative exploration is performed by several independently acting homogenous or heterogenous robotic agents. Since that, the exploration problem is further enriched by intelligent distribution of elementary tasks to individual robots. Indoor simultaneous localization and mapping is usually based on planar laser rangefinders and iterative closest point algorithm. Outdoor mapping utilizes stereo vision and extraction on SIFT features. In both these cases, robot adds newly sensed points or point-like features to the current environment model, and uses the current sensory measurement and actual model to localize itself within the environment. Representation of dynamic objects usually employs switched motion models. Models of both static and dynamic are further processed to enable execution of standard path planning algorithms and extraction of so called frontiers. These are potential outskirts of unexplored areas. Once recognized, the most suitable one is selected and robotic agent is headed towards its position. In the cooperative case, extracted frontiers are assigned to individual robots or robot groups as a result of agent technology-based negotiation process. The speed of exploration process as well limits imposed on individual robots by demands on computational power is considered only in rare cases. The lack of speed seriously limits the ability to perform exploration in potentially dangerous crowded urban areas.

This contribution describes robotic system for cooperative outdoor exploration. In our case, we use outdoor robotic platforms P3AT communicating over a wireless network each equipped with sweeping laser rangefinder, monocular camera, GPS and compass. Information obtained via global positioning system, compass and odometry are fused by kalman methods to provide position estimation to support global localization. Downward inclined laser rangefinder is used for reliable detection of dynamic obstacles and recognition of traversable terrain. The information about texture of traversable terrain and obstacles is then transferred to the vision system and a local map is created. This local map in form of occupancy grid is utilized for fast collision avoidance algorithms. As the robot moves, local maps are compiled to create a global one, where frontier regions can be detected and distributed among individual robots. Laser rangefinder can be swept to obtain above-ground 3D data. Information from laser rangefinder and calibrated camera is fused to obtain colored three-dimensional environment model. When performing outdoor experiments, the major challenge was to ensure real-time response to newly obtained environment data and to moving pedestrians. Research on current collision avoidance algorithms proved those be computational too expensive or not sufficiently reliable.

Robot path planning and obstacle avoidance problems play an important role in mobile robotics. However, standard algorithms assume that a working environment is static or

slowly changing. Moreover, time to compute and traverse the planned path is usually not crucial and therefore not considered.

Description of a novel algorithm *Elliptic Net* that is focused especially to deal with this issue can be found in [1]. The main idea of the algorithm lies in covering major part of the surrounding environment by a set of nodes and to construct a graph where adjacent nodes are interconnected by edges. Weights of these edges are then computed according to their lengths and distance to obstacles. The ratio of influence of these criterions allows choosing whether a generated path should be safe (i.e. far from obstacles) or short. The biggest disadvantage of the above mentioned approach is that only partly smooth planned path can be generated.

Algorithm described in [2] corrects this deficiency. The output of both obstacle avoidance algorithms forms a sequence of strategic points to be passed through in order to avoid obstacles. Furthermore, trajectory generator of the second method produces feasible and smooth reference path from this point set. The robot is then driven along this pre-planned collision free path using a classic state space controller. As the position of the strategic points cannot be changed, the smooth solution found by the trajectory generator is suboptimal.

In paper [3], we present the last path planning algorithm that was utilized for experiments of 3D mapping. This method uses a path description by a string of cubic splines. This enables finding smooth and globally optimal solution. Such path can be easily traversed because it's natural to a nonholonomic robot. Furthermore, it is possible to ensure smooth derivative in points of connection of particular splines. Although this feature is not necessary for holonomic robots that were used in our task, unsmooth planned trajectory would force the robot to stop at the points, where splines connect, creating inefficient delays. In the third approach, the path planning is computed by optimization of spline parameters. An evolutionary technique called *Particle Swarm Optimization* (PSO) was used hereunder due to its relatively fast convergence and global search character.

The implemented version of our system was experimentally tested on P3AT mobile robotic platform by several runs inside of the university buildings, as well as outdoor at the university campus, crowded parks and other areas abundant with both pedestrians and vehicles. A partial environment model of Charles square and university offices was created.

References:

[1] SASKA, M. – PREUCIL, L. – KULICH., M.: *Elliptic Net – A Path Planning Algorithm for Dynamic Environments.* Institute for Systems and Technologies of Information, Control and Communication, 2006, 372-377.

[2] SASKA, M. – KULICH, M. – KLACNAR, G. – FAIGL, J.: *Transformed Net – Collision Avoidance Algorithm for Robotic Soccer.* Vienna: ARGESIM, 2006, ISBN 3-901608-30-3.

[3] SASKA, M. – MACAS, M. – PREUCIL, L. – LHOTSKA, L.: *Robot Path Planning using Particle Swarm Optimization of Ferguson Splines.* Piscataway: IEEE, 2006, ISBN 1-4244-0681-1.

[4] KRAJNÍK, T. – FAIGL, J. – SASKA, M. – ŠTEPÁN, P., – KULICH, M.: *Reasoning and planning for robotsoccer.* Düsseldorf: VDI Wissensforum IWB GmbH, 2006, ISBN 3-18-091956-6.

This research has been supported by CTU grant No. CTU0608613.

Metaheuristics Based on Occam's Razor Principle in Search Algorithms

J. Suchý

suchyj1@fel.cvut.cz

Gerstner Laboratory, Department of Cybernetics,
Faculty of Electrical Engineering, Czech Technical University,

Karlovo nám. 13, 121 35 Prague 2, Czech Republic

A large number of problems can be formulated as search tasks or as sequences of search tasks. The solution of such a problem is provided by an algorithm which locates the object of interest in short time, while utilizing a reasonable amount of memory. It is known that there is no universal algorithm that can solve well (i.e. quickly) an arbitrary search problem. Individual search algorithms that work well in different domains differ mainly in what prior knowledge of the solution space they employ to speed-up the search.

This work presents an experimental approach to the problem of automated construction of new or modification of existing search algorithms when a sequence of similar problems is encountered. It tries to show it can be in some cases fruitful to sacrifice some of the processing time to the modification of the solving algorithm, rather than using directly the original one.

In the field of artificial intelligence research one often faces a problem (usually deliberately) devised so that it cannot be solved with an off-the-shelf search algorithm because it would take an excessively large amount of time or memory. The solution is to come up with a faster algorithm, which is seen as intelligent because its behavior is nontrivial and it solves a "difficult" task. However, at this point it is disputable whether the intelligence should be thought as artificial, because all the sophistication embedded in the algorithm is all “human made”. Sometimes these thoughts result in effort to produce an improved algorithm with as little human intervention as possible. But is it possible (and desirable) to construct such an algorithm automatically “from scratch”? Care must be taken when formulating the goal: It could seem that output of this effort could be – at best – a search meta-algorithm which constructs search algorithms that are aimed at arbitrarily diverse set of tasks. Thus clearly impossible goal as claimed in the previous paragraph. In order not to fall into this trap one can:

- Constrain the set of possible search tasks, so that all tasks fall in a common “domain”.
- Recognize the strategy as an ever-changing, ever-growing system that evolves as new problems from the domain are solved, rather than consider it to be a single fixed meta-algorithm.

In the view outlined in the second point it makes sense to accept human knowledge as a rightful part of the system and regard as a sign of intelligence the ability of the system to preserve and reuse the external knowledge once insered. This can be formulated in terms of information conservation and data compression.

Besides the general ideas described above, the presented system has the following key features:

- Reuse of old (similar) task specifications and their corresponding solutions as a source for possible improvement of the solver: Past solutions (programs) are used to regulate the generation of new solutions if the new task is similar to the past tasks.

- Transformation of the gathered information into a compressed form that allows for simple estimation of its value for solving new task efficiently.

When a new task in the sequence is encountered, it's actual data representation is matched against saved statistics acquired from previous tasks. The actual program generation is then made of intruction sequences corresponding to closely matched previous task solutions. In principle the shorter is the current task description expressed in terms of previous task description, the closer the match between the two This approach has been inspired mainly by work [3].

To experimentally evaluate benefits of the approach, an program generating software system was implemented based on the Push programming language [1] designed for program evolution. Since automated program generation has long been studied in the field of evolutionary computation, it is natural to test this program generating system against techniques currently used in evolutionary program generation. Several problem domains were selected: sorting algorithms generation, solving multi-class classification problems with numerical attributes and generation of programs navigating a unit through two-dimensional mazes. A comparison was performed with two techniques currently used in evolutionary computation which are conceptually close to the two key features of this system mentioned earlier: Learning from previous problem instances by saving promising genetic material in so-called run transferrable libraries [2], and Autoconstructive evolution [1], which is a method that evolves its program generating strategy along with the evolution of the solution programs. These techniques partly correspond to this systems' key features mentioned earlier.

The results of the experiments show that the studied method for adapting the course of program generation can sometimes improve efficiency of generated programs, mainly for problem instances that are hard for conventional evolutionary techniques as genetic programming. It stands somewhere halfway between the conventional evolutionary techniques and ambitious systems such as [3], [4], some of whose interesting properties it applies to simpler scenarios. However, it is still too slow for practical applications. According to [4] this issue could be addressed by supplying proper man-crafted training problem sequences.

References:

[1] SPECTOR, L. - ROBINSON A.: *Genetic Programming and Autoconstructive Evolution with the Push Programming Language,* Genetic Programming and Evolvable Machines, 2002 pp. 7–40.

[2] KEIJZER, M., RYAN, C., CATTOLICO, M.: *Run Transferable Libraries - Learning Functional Bias in Problem Domains,* Genetic and Evolutionary Computation - GECCO, 2004 531–542.

[3] SCHMIDHUBER, J.: *Optimal Ordered Problem Solver,* Machine Learning, 54, 2004, pp. 211–254.

[4] SOLOMONOFF, R. J.: *Progress in Incremental Machine Learning* Technical report TR IDSIA-16-03 2003.

This research has been supported by CTU grant no. CTU0608713.

Automatic Object Modelling and Tracking

Karel Zimmermann, Tomáš Svoboda, Jiří Matas

zimmerk@cmp.felk.cvut.cz

CTU-FEL Department of Cybernetics, Karlovo nám. 13, Praha 2, 12135

We propose a multiview tracking method for rigid objects. Assuming that a part of the object is visible in at least two cameras, a partial 3D model is reconstructed in terms of a collection of small 3D planar patches of arbitrary topology. The 3D representation, recovered fully automatically, allows to formulate tracking as gradient minimization in pose (translation, rotation) space. As the object moves, the 3D model is incrementally updated. A virtuous circle emerges: tracking enables composition of the partial 3D model; the 3D model facilitates and robustifies the multiview tracking.

Existing multiview approaches mostly represent objects as blobs. Blob representation assumes that the appearance of an object does not significantly change when the object rotates. Global object position is sought and the methods do not attempt to recover the *orientation* of the object.

Most *model-based tracking* methods use 3D models prepared offline. An overview of such methods was recently published by Lepetit et al.[1]. Vacchetti et al.[2] propose a tracker based on matching with keyframes. The method demonstrates impressive results on out-of-plane rotation data. Still, it cannot track complete turn of the object and needs offline manual selection of keyframes, which are essential for its stability.

We propose a combined method that tracks objects in 3D and constructs a point based appearance model simultaneously. The primary interest is object tracking and detection. The model is rather simple, a set of 3D points associated with 3D orientation. Despite its simplicity, the model is rich enough for recovering orientation of the object. The tracking can follow a complete 360-degree turn of object.

The object, to be tracked and reconstructed, is encircled by several cameras, where at least two of them creates stereo (they are close each other). While stereo is used for 3D reconstruction [3] all cameras can be used for tracking. Given the model (from the reconstruction), the tracking is formulated as a gradient-based optimization in 6 dimensional (translation, rotation) space. Object is modeled as a spatial collection of oriented and colored pachtes. The model is iteratively aligned with the camera images. In the case, that the part of the object, which have not yet been reconstructed is visible, the stereo is invoked and the reconstructed part is merged to the model. In order to succeed in complex scenes with various light-sources, we also deal with different illumination.

Tracking is formulated as Newton-Raphson optimization method of the dissimilarity criterion function, which compares color differences between camera observation I and the corresponding projections $f : R^3 \rightarrow R^2$ of the model T

$$J(R,t) = \int_{\vec{x} \in X} (T(\vec{x}) - I(f(R\vec{x} + \vec{t})))^2 d\vec{x}$$

where $\vec{x} \in X$ are model points in 3D space. We analytically compute gradients of the criterion function and show that the method converges to the local minima in approximately a few iterations in the most of the cases.

The gradient computation is based on Taylor first order approximation of $I(f(\vec{Rx}+\vec{t}))$. This simplifies the criterion function above. Derivatives are compared to zero and R and t are computed. Since, Taylor approximation causes an inexact solution, we iterate the process to converge to the minima.

Only those points, which are visible in particular cameras are tracked. The visibility is estimated from surface normals. Particular contributions are weighted by the angle of the surface to the camera.

Illumination is compensated as follows: 3D points are clustered into the small planar patches, which are expected to be illuminated with the same portion of light. Uneven illumination is compensated in terms of Least Square Error. Each patch is associated with a scalar, which scale the observed intensity to minimize difference between observed and model intensities.

Reconstruction method [3] finds corresponding points in stereo pair. Since the cameras are calibrated, only per-line correspondences are searched in rectified images. These correspondences are carried out to 3D and clustered into the small patches (called fish-scales). Size and normal vector of each particular fish-scales is automatically estimated.

We proposed a fully automatic approach of multiview/monocular 3D object tracking interleaved with incremental model construction. Neither model nor initialization are needed to be known in advance. We showed that the fish-scale 3D model is accurate enough to support stable 3D tracking.

We experimentally demonstrated that the interleaved track-and-reconstruct approach successfully tracks a 360 degrees turn-around and a wide range of motions. A 3D model is delivered as a side product. We demonstrated the robustness of our method on a sequence with a thin object where the dominant plane was often tracked only from one view. Monocular tracking is also possible after the model is constructed but small accuracy is achieved in the direction orthogonal to the camera plane. The model projection to the tracking camera often looks correct, projections to other cameras reveals 3D inaccuracies. Still, monocular tracking can provide results acceptable for some applications. Using more cameras significantly increases stability and accuracy in critical poses and moves. Exact 3D pose may be necessary in many application ranging from virtual reality, human computer interfaces to visual surveillance.

References:

[1] LEPETIT, V. - FUA, P.: *Monocular Model-Based 3D Tracking of Rigid Objects,* Foundations and Trends in Computer Graphics and Vision, 2005, pp.1-89

[2] VACHETTI, L. - LEPETIT, V. - FUA, P.: *Stable Real-Time 3D Tracking Using Online and Offline Information,* IEEE Pattern Analysis and Machine Intelligence, 2004, pp.1385-1391

[3] KOSTKOVA, J. - ŠÁRA, R.: *Stratified Dense Matching for Stereopsis in Complex Scenes,* British Machine Vision Conference, 2003, pp.339-348

This research has been supported by CTU grant No. CTU0608813

Semantic Annotation of Medical Records

M. Žáková

zakovm1@fel.cvut.cz

Department of Cybernetics, Faculty of Electrical Engineering, Czech Technical University, Karlovo náměstí 13, 121 35 Prague 2, Czech Republic

Machine learning and data mining (DM) offer numerous semi-automated methods how to find characteristic patterns and gain better insight into data records stored in computer databases. It is tempting to apply these methods in medical domains to identify e.g. hidden relations among some symptoms, best predictors of certain diseases or possible interactions between medications. For such tasks patients' records collected in hospitals represent a valuable source of data. Unfortunately, DM cannot be applied directly to the medical records most often. One of the main reasons is the format of data stored in hospital archives - while its basic format is a text file written in a natural language, DM tools are ready to work with source data stored in a structured form. Therefore it is necessary to transform the data in patient's text files into a structured form by means of semantic annotation.

Patients' records are semi-structured; however a significant part of the report consists of notes made by the doctor written in natural language. The records are very heterogeneous, e.g. due to the different examinations and also due to personality of the doctor. For several hundreds of reports general text mining algorithms do not give sufficiently good results [4]. Therefore we are attempting only semi-automated annotation, where named entities are extracted automatically and offered to the user for checking and manual annotation of relations. For creating an information extraction prototype, information about medical drugs was used, since it is readily available on health portals. Information about drugs contains also similar named entities as patients' records and the language used is similar as well. The texts used are in Czech, since we are planning to use the system on patients' records in Czech.

In information extraction from text using statistical methods, named entity recognition (NER) is the first step of the process. For use in medical domain we have to solve extended NER task including also identification of names of symptoms, diseases, chemical substances etc. [1]. For the extended NER task we have defined classes of objects and developed annotation guidelines containing definition of classes, semantic description of objects belonging to each class and examples guiding annotators in some more difficult and marginal cases. Then a training set of texts was annotated manually using Open Ontology Forge [1]. The training set consisted of 20 texts, each containing information about one particular drug.

Since Czech is a highly inflective language, the training data set was preprocessed using language dependent morphological tools FMorph and HMMTagger developed at UFAL UK. Preprocessing was done using Perl scripts and it contained the following steps: section identification, subsection identification, morphology + tagging, processing of numbers and units, adding additional features, converting to tab-delimited text. Additional features included prefixes and suffixes, which are typical for some classes. The second type of additional features are terms commonly used in medicine that form a part of some named entity. We expect that this second type of features will not be necessary for larger data sets.

Finally machine learning algorithm was applied. Conditional Random Fields were used as a statistical machine learning technique for classification, because it has recently been successfully applied to named entity recognition [3]. An implementation of Conditional Random Fields, CRF++ was used for this purpose. The experiments were done on initial data set containing 20 documents. The data set was split into training and testing set with training set containing 66% of training examples.

Classification was relatively successful for *medicine type*, *chemical substance* and *disease type*. The main problem was low recall for *disease* and *treatment*. For class *treatment* this was mostly due to small number of training examples available. In case of class *disease*, the named entities were often misclassified as symptoms. In the data set used for experiments terms that can mean both disease and symptom were annotated using the context and most of the terms occurred more often as symptoms than as diseases. Therefore in future work they will be annotated consistently as either disease or symptom and not based on context. There was also some confusion between *chemical substance* and *measured quantity*. In some cases chemical substance was included in measured quantity. This could probably be solved by increasing size of the training set.

The results of pilot experiments look promising enough to continue in this effort. Based on the conducted experiments annotation guidelines for disease and symptom will be updated. To improve the accuracy of preprocessing, the dictionary used by morphological tools should be extended by adding medical terms of non-Czech origin. It is expected that adding several tens of terms to the dictionary would bring the desired effect. Also more annotators would have to be included to measure intra-annotator and inter-annotator agreement. Based on experience with pilot experiments and in cooperation with 2.LF UK a new version of annotation tool MedAT for annotation of patients' records was developed at our department [2]. Currently a first set of patients' records is being annotated to be used as training set for further experiments with extended NER.

References:

[1] K. TAKEUCHI, N. COLLIER: *Support vector machines in extended named entity recognition,* Proceedings of the 6th Conference on Natural Language Learning 2002 (CoNLL-2002), D. Roth and A. van den Bosch (eds), 2002, pp. 119-0125.

[2] M. ŽÁKOVÁ, O. ŠTĚPÁNKOVÁ, T. MAŘÍKOVÁ: *MedAT: Medical Resources Annotation Tool,* In Proceedings of the 3rd European Medical and Biological Engineering Conference EMBEC´05, 2005, [CD-ROM].

[3] B. SETTLES: *Biomedical Named Entity Recognition Using Conditional Random Fields and Rich Feature Sets,* In Proceedings of the COLING 2004 International Joint Workshop on Natural Language Processing in Biomedicine and its Applications (NLPBA). Geneva, Switzerland, 2004.

[4] J. ANTOLÍK: *Automatic Annotation of Medical Records,* In Proceedings of the Medical Informatics Europe 2005, Geneva, Volume 116, 2005, pp. 817-822.

This work was funded by the Czech Technical University grant No. CTU0608913. The author appreciates very much the support given by Dr. Nigel Collier during the internship at National Institute of Informatics, Tokyo, Japan and cooperation of Doc. MUDr. Taťána Mařík ová, CSc. from 2. LF UK.

Ventilation Control in Highway Tunnels

L. Ferkl

ferkll@control.felk.cvut.cz

Department of Control Engineering, Czech Technical University in Prague,
Technická 2, 166 27 Praha 6, Czech Republic

There are many large highway tunnels constructed all around the world. The operation of such tunnels has to meet several requirements, e.g. energy consumption optimization, minimal influence on the surrounding environment, lifetime conservation, minimal maintenance costs, portal protection from exhaust etc. As the tunnel system is typically very complex (consists of a large number of fans, sensors, several ventilation shafts etc.), a controller designed according to modern control design methods could be very efficient.

The task of the controller is to keep the exhaust limits inside the tunnel below desired limits, with low energy consumption. We have decided to neglect the fairly complicated tunnel dynamics, and to design a static controller.

First of all, we will find a static pollution level in one section M of a one-directional highway tunnel. The measured air flux Q can be split and we can write down the following equation:

$$p_M = \frac{k_M n_M s_M}{\sum_{i=1}^{M} a_i f_i + Q^*} \tag{1}$$

where p_M is the desired pollution level, k_M is an average exhaust production of one vehicle per second, n_M is the number of vehicles inside the tunnel, s_M is the position of the pollution sensor, S_{area} is the tunnel cross section area, a_i is a fan contribution coefficient, f_i is the fan power and Q^* is the air flux not caused by the fans.

In Equation (1), we want to set some fan powers f_i according to some desired pollution level p_M. But we want to control the entire tunnel, i.e. all the sections together. As there can be large amounts of interdependencies between the inputs and outputs of the tunnel system, the easiest solution is to formulate the problem of control as an optimization problem. Given Q^* and k_i, n_i, s_i there corresponds to each p a unique sum of air flux values, that is, a mapping P exists such that $\sum a_i f_i = P(p_i)$. So requiring p_i to be in some interval $[0, p_{i,max}]$ translates into requiring $\sum a_i f_i$ to be in some appropriate interval $[Q_{min}, Q_{max}]$. The latter involves our control variables f_i and hence the following linear program, which aims to achieve $p_i \in [0, p_{i,max}]$ with minimal power, is a possible solution to our problem:

$$\min_{f_i} \sum_i |f_i| : \quad f_i \in [0, 100], \quad \sum a_i f_i \in [Q_{\min}, Q_{\max}] \tag{2}$$

Note that this is a standard linear program – one of the basic optimization problems – and it can be solved by any of the wide variety of available solvers. Its advantage is flexibility, as more constrains can be imposed. E.g., we can achieve the portal protection from exhaust by introducing a further constrain in the form of $Q_{portal} < 0$.

The control itself has two stages – a design stage, wherein a tunnel is decomposed and basic data for the linear program are defined, and a control stage, which is responsible for the control itself.

The **design stage** may comprise several steps:

1. Divide the tunnel into control sections. Every control section has one entry and one exit only.

2. Assign indices to the control section, as well as principal air flow directions.
3. Determine the jet fans power coefficient and the vehicle pollution production coefficient.
4. Set the air flow circulation. In this step, it has to be decided, what are the relations between respective control sections.
5. Determine the exhaust transfer. Not all the air exits the tunnel through the portals – some air circulates inside the tunnel. The amount of circulated air has to be determined.
6. Impose the pollution limits.
7. Choose a control interval.

The **control stage** comprises the following steps:

1. Measure the variables needed for control (i.e. pollution levels, air flow and traffic). The average value (or some other statistical moment) over a control interval should be used.
2. Adaptation – adapt the jet fans constants during the daytime and vehicle pollution production coefficient at nighttime.
3. Separate the air flow into the jet fans contribution and other contributors.
4. Calculate the air flow limits satisfying the given pollution levels.
5. Write down the linear program according to Equation (2) and calculate the optimal fan powers.
6. Run the fans according to the linear program.
7. Return to 1.

Besides the general control algorithm, other supporting controllers had to be developed. They include the control of individual jet fans (implemented as PID controllers) and the ventilation center control (implemented as multi-input, multi-output proportional controller).

The above control strategy was designed as a general control algorithm for tunnels with one-way traffic and axial ventilation. It has been tested (in parts) in **Mrázovka** tunnel (Prague), **Libouchec** and **Panenská** tunnels (D8 highway Prague – Dresden). The entire algorithm will be used in **Blanka** tunnel, which is going to be built in Prague (scheduled to 2011); its length will be ca. 5.5 km and it will make a highway connection of Břevnov, Dejvice, Letná, Holešovice and Trója.

References:

[1] ROTHERY, R. W.: *Traffic Flow Theory: A State of Art Report.* FWHA, 2002 .

[2] BELLASIO, R.: *Modelling traffic air pollution in road tunnels,* Atmospheric Environment, Vol. 31, 1997, pp. 1539-1551.

[3] BOMAN, C. A. BRING, A., MALMSTRÖM, T. G.: *Simulation and measurement of road tunnel ventilation,* Tunnelling and Underground Space Technology, Vol. 12, No. 3, 1997, pp. 417-424.

[4] PIARC: *Road Tunnels: Emissions, Environment, Ventilation.* PIARC, 2004.

This research has been supported by CTU grant No. CTU0609013.

Recursive Subspace Identification Algorithm Incorporating Prior Information

P. Trnka*, V. Havlena * **

trnkap@control.felk.cvut.cz

* Department of Control Engineering, Faculty of Electrical Engineering, Czech Technical University, Technická 2, 166 27 Prague 6, Czech Republic

** Honeywell Prague Laboratory, Honeywell Intl., Pod vodárenskou věží 4, 182 08 Prague 8, Czech Republic

Subspace State Space System IDentification (4SID) methods [1] are used for the identification of state space dynamical model parameters directly from the experimental input/output data and they can be considered as an alternative to widely used Prediction Error Methods, like for example the maximum likelihood identification of ARX model or Gauss-Newton iterative ARMAX model identification. Compared to the others, 4SID methods are based on the geometric projections between the row spaces of certain matrices and a numerical linear algebra.

The modern control methods, like model predictive control, proved to be very effective in the industrial applications. However, the efficiency is often limited by a quality of the controlled system model, which is hard to obtain especially for the large systems with multiple inputs and multiple outputs (MIMO) and low quality experimental data. The recent advances in 4SID methods showed that they can be successful in the identification of such models from real world data. Their advantage is that the complexity of the identification for large MIMO systems is the same as for SISO (Single Input Single Output) systems, the algorithms are numerically robust (usually implemented by QR and SVD factorization), they have only few user parameters (in fact only the identified system order) and they incorporate an implicit model order reduction. However, there are also some drawbacks. The recursification for on-line identification is not straightforward [3] and as it was recently shown, the unified subspace algorithm also suffers causality problems [2].

Although, 4SID methods have already proven to be suitable for the industrial applications, the experimental input/output data by them self are in many cases not rich enough to give good model (e.g. weak system input excitation, low signal to noise ration). The black-box identification approach, such as in 4SID, relying only on the measured data, fails in such cases. However, in the practical applications there is often strong prior information about the identified system, which should be exploited by the identification algorithm to significantly improve the identified model quality [4]. Such information should be: an approximate knowledge of time constants, the known static gains, a low pass character etc.

The problems of recursification and prior information incorporation were addressed in our work to improve 4SID methods usability and performance on the industrial data. The main idea came from the fact, that unified subspace identification algorithm [1] can be expressed as a result of minimization of multi-step predictions errors for the state space model on the experimental data. It means that the important step in the unified subspace algorithm, the oblique projection, can be written as a quadratic norm minimization and the optimal solution leads to the oblique projection. The optimization structure clearly showed a loss of causality and over-parameterization, which was eliminated by a reduction of duplicate parameters and a

reformulation of optimization to enforce causality (important for closed-loop identification). The resulting optimization structure allowed to incorporated prior information using Linear Mean Square error (LMS) estimation and recursification. The important tool for obtaining the state space model parameters is a weighted lower-rank matrix approximation.

The resulting algorithm was successfully tested on the experimental data from the steam producing oil-boiler with a rated power of 100 MW. The problematic task is to identify a model representing the dynamic between the fuel flow, the air flow and the steam demand to the boiler steam pressure. The boiler operating conditions does not allow proper excitation of the boiler dynamics, which results in the poor experimental data. Using classical identification methods usually leads to the failure or a well experienced engineering approach is required. However, there are several prior information available, such as a relative static gain between the fuel flow and the steam demand inputs, which is known from the steady state characteristics. Taking the advantage of prior information in our algorithm leads to the good quality models.

References:

[1] P. V. OVERCHEE, B. D. MOOR: *Subspace Identification for Linear Systems: Theory-Implementation-Applications,* Kluwer Academic Publishers, 1996, pp. 272.

[2] S. J. QIN, W. LIN, AND L. LJUNG: *A novel subspace identification approach with enforced causal models,* Elsevier: Automatica, vol. 41, no. 12, 2005, pp. 2043-2053.

[3] H. OKU AND H. KIMURA: *Recureive 4SID algorithms using gradient type subspace tracking,* Automatica, vol. 38, 2002, pp. 1035-1043.

[4] S. GILLIJNS, B. D. MOOR: *Data-based Subsystem Identification for Dynamic Model Updating,* Proc. of the 45th IEEE Conference on Decision and Control (CDC), 2006 pp. 3303-3308.

This research has been supported by CTU grant No. CTU0609113.

Hardware Support for Exact Computer Arithmetic based on Continued Fractions

T. Brabec, R. Lórencz

brabect1@fel.cvut.cz

Department of Computer Science and Engineering,
Faculty of Electrical Engineering, Czech Technical University in Prague,
Karlovo náměstí 13, Praha 2, 121 35

A year ago, we introduced in [1] the field of exact arithmetic and discussed its importance for computer arithmetic. We particularly focused on an exact paradigm based on continued fractions, a recursive structure of folded fractions having a form like $a_1+1/(a_2+1/(a_3 + 1/(\ldots)))$. Although there is a complete theory of continued fractions, it suffices our purposes here to know that any real number can be represented as a continued fraction and that there are means to compute basic arithmetic operations with such fractions – further details on this topic are covered in [2]. In [1], we identified that though being theoretically interesting, practical application of continued fractions typically suffer from poor performance. However, we concluded that this issue might be potentially solved by proper hardware support.

We followed and developed this idea during the last year and it is our aim to present here the results achieved so far. We were concerned with a specific variant of continued fractions called continued logarithms [2] because of their higher potential for hardware implementation and because of little attraction this method draws among the community. We focused our research onto the following aspects – developing and validating the principles of continued logarithm arithmetic, proposing a hardware architecture utilizing these principles and finally evaluating the real potential such architecture may bring. These particular areas of our interest are briefly discussed in the rest of the paper; for more details, however, refer to [3].

The first researched area is development of continued logarithm arithmetic. We extended the original definition [2] to support the whole set of real numbers and we adapted algorithms for basic operations accordingly so that the final continued logarithm representation is capable of exact rational arithmetic. We implemented the proposed extension in Java to verify its correctness and to evaluate its fundamental properties. As expected, continued logarithms proved to be a legal exact (rational) arithmetic paradigm as shown on several benchmarks by comparing results with other exact arithmetic methods (namely regular continued fractions [2] and constructive reals [4]). For benchmarking purposes, we used simple applications (e.g. randomly generated bilinear rational functions) as well as more complex ones (e.g. matrix inversion). Especially the complex benchmarks allowed us to check the "exactness" of continued logarithms as we used some ill conditioned problems such as Hilbert matrix inversion. This effort also confirmed that even continued logarithms, though being primarily designed for binary arithmetic, face severe performance limitations.

Since addressing these performance issues was our primary motivation, we proposed and developed architecture of a hardware unit that may act as an application specific accelerator for continued logarithm arithmetic. Targeting the FPGA platforms (Field Programmable Gate Arrays), the proposed architecture exhibited promising results, especially in terms of high-speed operation and acceptable chip area utilization. For a moderately sized FPGA device (e.g. Xilinx Virtex II Pro zc2vp30), a 16×32-bit configuration of the continued logarithm unit could operate on frequency of 150 MHz and utilize equal area as a single precision floating-point unit (i.e. 15% of chip area). Specifically for this configuration, we

evaluated performance improvement the unit offers over its software equivalent. It turned out that the proposed unit has a 6.5 times better performance than a 32-bit processor running on the same frequency. As this evaluation was based on raw and rather optimistic estimations about performance of the processor-based implementation, it is likely for real results to be even better. There is, however, still a chance to further improve this performance advantage in several ways. We can use different configurations of the unit, which can leverage different speed/area trade-offs and thus better target the precision and performance requirements of a particular application. It is interesting that in sense of this configurability the architecture exhibits almost linear scalability in the amount of utilized resources. Another way to improve performance of the proposed unit is to utilize the spatial advantage of hardware and instantiate more units in parallel. Because of their loose interaction, these units may operate either separately or in a compound mode without any significant timing or area overhead.

Our last and the most recent contribution has a rather theoretical account as we proposed an extension of continued logarithms from exact rational to exact real arithmetic. Its idea is based on speculative detection and resolution of non-computable cases. We partially introduced this principle called *speculative redundancy* in [3], but its full details are yet to be published. An important aspect of this solution is its reliance on our original rational extension of continued logarithms, which means that the hardware architecture proposed previously can utilize this new approach; only a small adaptation of control mechanism is necessary. There is also a possibility for further cost/area trading off for highest performance. This would, however, require a significant redesign of the proposed architecture.

As presented above, we successfully followed our ideas envisioned in [1]. We considered a continued logarithm representation, which effectively combines advantageous properties of continued fractions with a logarithmic nature suitable for binary arithmetic. By inspecting their properties on several benchmark applications, we showed that continued logarithms are no worse than commonly preferred regular continued fractions and perfectly apply for hardware realization of continued fraction arithmetic. The proposed hardware architecture demonstrated viability of this idea and its positive effect for improving the performance such arithmetic. The evaluated 6 times advantage over an equivalent software implementation is adequate evidence and it is expected to improve with further development of our ideas.

References:

[1] BRABEC, T. – LÓRENCZ, R.: *High Precision Computing Based on Continued Fractions,* ČVUT Workshop, 2006, vol. A, pp. 220–221.

[2] GOSPER, R. W..: *Continued Fraction Arithmetic,* unpublished manuscript, 1977.

[3] BRABEC, T.: *On Exact Real Hardware with Specialization to Continued Methods,* PhD proposal, Dept. of CS&E, FEE, CTU, 2006, http://service.felk.cvut.cz/anc/brabect1

[4] BOEHM, H.-J.: *The Constructive Reals as a Java Library,* Technical Report HPL-2004-70, Internet Systems and Storage Laboratory, HP Laboratories Palo Alto, 2004.

This research has been supported by CTU0609213.

Formalization of UML Profile for Safety Critical Systems

M. Komárek

komarem@fel.cvut.cz

Department of Computer Science and Engineering, Faculty of Electrical Engineering,
Czech Technical University, Karlovo náměstí 13, 121 35 Praha 2, Czech Republic

Unified modeling language, the currently leading specification and modeling technique used in industry, still has not widely accepted formal representation that might decrease the costs of application of formal methods, which opens the door for intensive utilization of formal methods in workaday development of systems. Nevertheless, this seems to be a less serious problem in the case of critical systems where reliability is a very important property of the system and the portion of overall costs spent on demonstration of system's correctness is significant. The use of specialized formal specification languages and verification techniques can often bring satisfying results, and thus combination of various formal representations and verification techniques is useful.

For a long time the development of control systems has resisted the application of object-oriented techniques even though the character of these systems could gain from advantages of object orientation such as natural modularization of a system, component reuse, and module protection given by encapsulation. The existence of various object-based modeling languages for embedded devices, reactive and real-time systems manifests that the initial fear has been overcome and UML is able to fulfill successfully its duty in this application domain.

The primary goal of this research is not to develop another universal formal representation for UML, but rather to study possibilities of customizing UML using extensibility mechanism to define an UML profile that targets the application domain of the critical control system and to support the relevant part of this customized language with adequate formal representations. This will enable the employment of various specialized formal verification techniques in order to achieve results that will justify this approach. This process consists of finding specific procedures related to the safety critical systems development, proposing a framework of UML profile for each specific procedure, finding an adequate formalization of a crucial subset of proposed UML profiles, providing a methodology for writing specifications, extraction of formal representations from models, and specialization, customization and combination of formal verification methods. In this paper we focus on finding specific procedures related to the safety critical systems development and proposing a UML profile for the specific procedure.

The development of each safety critical system should be driven by one of the generic safety-related standards. Most of them are categorized and briefly commented in appendix B of the paper [1]. In the EU countries most specific domain standard are derived from the standard IEC 61508 (Functional safety of electrical/electronic/programmable electronic safety-related systems) [3]. Our research is based on this standard.

There are a few UML profiles based on the safety information requirements [1, 2], but none of them supports all safety related procedures in the whole range of the system life cycle. We assumed the following system life cycle stages: System definition and applications conditions, Risk analysis, System requirements, Design, Implementation, Installation, System Validation, Operation and maintenance, Performance Monitoring, Modification, Decommission and disposal.

The result of the system definition and conditions stage should be a platform independent model (PIM). This model should only consist of functional and high level architecture HW&SW information. Not all of the collaborators are completely familiar with UML at this stage of the development. Due to this using of any UML profile could lead to misunderstanding of the model and therefore we recommend using only the essential UML stereotypes.

The risk analysis consists of following processes: PIM improving, identification of hazards, identification of causes, identification of consequences, assessment of consequences and classification of causes. Based on the above mentioned processes and UML specification [4] we proposed these new UML stereotypes: <<hazard>>, <<cause>>, <<consequence>>. These UML stereotypes can be specified during the next development stages.

References:

[1] ZOUGHBI, G. - BRIAND, L. - LABICHE, Y.: *UML Profile For Developing Airworthinnes - Compliant (RTCA DO-178B) Safety - Critical Software,* http://squall.sce.carleton.ca/pubs/tech_report/TR-SCE-06-19.pdf, December 2006.

[2] OBJECT MANAGEMENT GROUP(OMG) INC.: *UML Profile for Schedulability, Performance and Time Specification,* http://www.omg.org/docs/formal/05-01-02.pdf, January 2005.

[3] INTERNACIONAL ELECTROTECHNICAL COMMISSION(IEC): *IEC 61508 - Functional safety of electrical/electronic/ programmable electronic safety-related systems,* http://www.iec.ch/, December 1998.

[4] OBJECT MANAGEMENT GROUP: *Unified Modeling Languange: Superstructure Specification, Version 2.0,* http://www.omg.org/docs/formal/05-07-04.pdf, August 2005.

This research has been supported by CTU grant No. CTU0609313.

Syntax-Driven Find/Replace for Java

M. Píše

pisem1@fel.cvut.cz

Department of Computer Science and Engineering , Faculty of Electrical Engineering, Czech Technical University, Karlovo náměstí 13, 121 35 Prague 2, Czech Republic

Contemporary integrated development environments (IDEs) are quite unpractical when it comes to source code manipulation. In case the same change (e.g. replacement of a function call by a call of a different function) needs to be performed on many different places of the source code, programmer's options are as follows:

- perform the change manually,
- use IDE's standard built-in find/replace feature or
- use some other means of source code manipulation such as IDE's built-in refactoring functionality.

Obviously, none of these options is satisfactory: manual change of the code is costly and prone to errors, IDE's built-in find/replace feature is applicable on the most simple problems only as it cannot operate on higher than lexical level, and the refactoring functionality, though capable of performing quite complex changes, can be used solely in predefined set of scenarios. More general solution, such as find/replace feature that takes into consideration the syntax of the programming language, is desirable.

Syntax-driven source code manipulation is currently studied in the program transformation field which is a subfield of the programming language theory. Out of current existing program transformation systems, the TXL source transformation language[1] is the one closest to our aim. It allows the user to specify a search pattern using formalism called native patterns. A native pattern is basically a derivation tree with some of its subtrees rolled back to nonterminals. This way, the programmer can intuitively specify they want to search for e.g. a while loop with a given condition expression regardless of the statements in its body.

Unfortunately, TXL does not support static semantics (i.e. name and type analysis). In other words, all terminals are compared by its string value; if the string value of the terminal in the source code and the terminal in the search pattern is the same, the two terminals are considered equal, otherwise they are considered distinct. In many cases, such as keyword comparison, such a simple criterion is sufficient. On the other hand, the criterion of equality of variables, methods and classes needs to be refined more precisely.

First, the reasons for the need of a better criterion are roughly the same for variables and methods: even though two variables or methods have the same name, they still might be distinct. Two variables with the same name defined in different scopes or two fields defined in different classes have nothing in common (besides the name). If the transformation tool handled them as equal to each other, it could perform a transformation whose correctness actually relies on their equality. Such a transformation would most likely be incorrect and therefore should not have been performed.

Second, because of method overloading, the determination of method equality is even more difficult. Even though the method in the source code and the method in the search pattern have the same name and are defined on the same class, they still might be distinct as the first one might have different type(s) of parameter(s) than the second one.

Third, classes should not be compared by name as one class might have more than one name. In many languages, namespace-like facility exists and the programmers are allowed to reference a class by its fully qualified or its non-qualified name.

Finally, type names should not by compared by name as modern polymorphic languages allow for any object to have more than one type. A search pattern referencing parent class should also match any suitable source code snippet containing an instance of descendant class; the instance of the descendant class is type compatible with the parent class.

Many current program transformation systems are forced to deal with these issues, however, to our knowledge none of them deals with them in a clean and extensible way. As our goal was to avoid ad-hoc solutions, our tool is based on reference attributed grammars[2].

Reference attributed grammars are an extension to traditional attributed grammars that allows attributes to be references to other nodes in the same derivation tree. As is proved in [2], reference attributed grammars can be implemented using traditional attributed grammars, the size of the traditional grammar may increase in order of magnitude though.

Our tool utilizes attributed grammars to perform name and type analysis. Each terminal that represents variable use, method call or class use references nonterminal representing the definition of the corresponding variable, method or class. Variables, method calls and classes are then compared not by name but by reference to the defining nonterminal. This way, only small modifications of program transformation algorithms used in TXL were needed: the whole find/replace tool is composed of two layers - semantics is encapsulated in the reference attributed grammar layer and the actual transformation is performed on top of it in. To ease implementation, JastAdd compiler construction system[3] is used.

References:

[1] CORDY, J. R.: *The TXL Source Transformation Language* Science of Computer Programming, Elsevier, 2006, pp. 190–210.

[2] HEDIN, G.: *Reference Attributed Grammars* Informatica 2000, pp. 301–317.

[3] HEDIN, G. – MAGNUSSON, E.: *The JastAdd system - an aspect-oriented compiler construction system* Science of Computer Programming, Elsevier, 2003, pp. 37–58.

This research has been supported by CTU grant No. CTU0609413.

The Time Complexity Reduction of Design-for-Test Sequential Circuits Testing

M. Šťáva, O. Novák

stavam1@fel.cvut.cz

Department of Computer Science and Engineering, Faculty of Electrical Engineering, Czech Technical University in Prague, Karlovo náměstí 13, 121 35 Praha 2, Czech Republic

There are two approaches used for the deterministic test generation [1, 2, 3, 4]. In the structural approach the idea is to convert the problem of deterministic test generation into a finite space search and to operate directly on the network of gates. The D-algorithm was the first structural algorithm. The branch-and-bound based algorithm PODEM was proposed later. It makes the decision points at primary inputs applying a novel heuristic, called backtrace. The backtrace determines which of primary inputs of a circuit should be set to achieve an objective. Several improved techniques, such as RAPS, FAN and others were proposed based on PODEM further to prune the search space. RAPS uses a similar backtrace procedure, called random backtrace, to that implemented in PODEM only the selection of a gate input is random. FAN makes a decision on always-justifiable internal lines and has an improved backtrace procedure, called multiple backtrace, at the attempt to satisfy several objectives simultaneously. The second approach applies Boolean satisfiability solving algorithms. A number of algorithms using fast SAT solvers were recently proposed. We have used methods similar to the heuristics mentioned above to shorten a test length of sequential circuits and to reduce the power consumption in the circuits containing a scan chain.

The most popular structured design-for-testability technique used for external testing is the scan design, which employs a scan chain, marked as SC. The SC divides a sequential circuit into several combinational parts. Thus any algorithm to generate test vectors for combinational circuits, such as PODEM or FAN, can be used. That is an advantage, because combinational ATPG algorithms are much simpler than sequential ones. It is assumed that a circuit to be made testable is synchronous and let any combinational part of a sequential circuit be called an *SQ-combinational circuit*. Further it is assumed to have a list of test vectors, marked as L. Consider a simple task: applying L to an SQ-combinational circuit, whose inputs and outputs are directly connected to the SC. Thus they make a feedback. And this is just an interesting task. Assume that the number of test vectors in L is t and the length of the SC is k. The simplest way to apply L is to perform the simple known procedure: selection of a vector p of the length k from L and its scanning into the SC during k clock cycles, loading a response during the $(k + 1)st$ clock cycle; it is repeated until L is empty and finally the last response is scanned out from the SC. The computing complexity of the procedure is also $\{t*(k+1)+k\}$ clock cycles. Due to reduce this complexity, the whole time to apply L and the power consumption etc. would lower. And that is why we have focused on its reduction. Reduction of the operational complexity rests in finding such a sequence of test vectors that a response to a being-processed vector will fulfil one of two following conditions: the response equals to the subsequent test vector (optimal case) or the subsequent test vector can be achieved from the response by scanning as few values as possible in the SC.

There are two main approaches how to achieve the test length reduction. In the first approach, values kept in the SC are considered as an input vector applied to the input signals of the SQ-combinational circuit. Responses, being obtained from the output signals of the SQ-

combinational circuit, are saved into the SC consequently. Thus, computation of the responses is provided forwards the output signals in the SQ-combinational circuit. In the second approach, values kept in the SC are considered as an input vector applied to the output signals of the SQ-combinational circuit. Responses, being obtained from the input signals of the SQ-combinational circuit, are saved into the SC consequently as well. Thus, computation of the responses is provided backwards the input signals in the SQ-combinational circuit. We have focused on this backward computation, which is similar to the operation *backtrace* and its implementation into an FPGA. It is necessary to transform an SQ-combinational circuit structure into a backward-determining one.

An SQ-combinational circuit has to be converted into a corresponding structure, called a *transformed circuit*, to perform the backtrace. The transformed circuit generates one input vector by one clock cycle for an applied output vector and all possible input vectors to an applied output vector are founded. Each generated input vector can be valid or invalid. Both input and output vector consist of three-value signals. An SQ-combinational circuit is transformed as follows. Each gate is replaced by a corresponding block LogicElement representing a backward implication table of the being-replaced gate. Each fan-out stem has to be replaced by a block Cond, which performs a matching operation by the binary intersection operator between signal values. When a non-x value of one Cond input differs from non-x values of other Cond inputs, it means that a collision has occurred.

The results of experiments were carried out for the ISCAS'85 benchmarks. The area overhead is expressed in the thousands of equivalent gates. A clock speed and an average number of clock cycles for generating the first valid input vector, marked as VIV, are presented. In order to determine the average number of clock cycles we have applied output vectors, where *m* denotes the number of outputs of a benchmark circuit, and observed the first occurrence of a valid input vector, if any, for each output one. As a target platform, we used the Xilinx FPGA of the Spartan 2E series. All circuits were synthesised by Xilinx XST 6.3i.

Each of the benchmarks was converted into a transformed circuit to use the backtrace algorithm and to perform the backward determination of input vectors. For the selected set of the benchmarks, the complexity of the area overhead is polynomial. The maximal clock speed of the transformed circuits decreases exponentially for the selected set of the benchmarks. We can assume that these results would be accepted for any combinational circuit generally. The backtracing unit can be used in various applications based on automatic test pattern generation, for example: a backtracking accelerator co-operating with a software ATPG tool, a computing unit for compacted test generation for sequential circuits with a scan-chain.

References:

[1] ABRAMOVICI, M., BREUER, M. A., FRIEDMAN, A. D.: *Digital Systems Testing and Testable Design,* IEEE Press, 1990, pp. 100-385.

[2] BUSHNELL, M. L., AGRAWAL, V. D.: *Essentials of Electronic Testing for Digital, Memory and Mixed-Signal VLSI Circuits,* Kluwer Academic Publishers, 2000, pp. 120-295.

[3] LARSSON, E.: *Introduction to Advanced System-on-Chip Test Design and Optimization: Problems, Modelling, Design, and Optimization,* Kluwer Academic Publishers, 2005.

[4] KRISHNENDU, C., VIKRAM, I., ANSHUMAN, C.: *Test Resource Partitioning for System-On-A-Chip,* Kluwer Academic Publishers, 2002.

This research has been supported by CTU grant No. CTU0609513.

Parallel Pattern Matching

J. Šupol

jan.supol@gmail.com

Department of Computer Science and Engineering, Faculty of Electrical Engineering, Czech Technical University in Prague, Karlovo nám 13., 121 35 Praha 2, Czech Republic

Pattern matching problem is a matching of all occurrences of pattern $P=p_1p_2\ldots p_m$ in text $T=t_1t_2\ldots t_n$, $n > m$. Parallel pattern matching is a problem of a faster pattern matching using many processors on a parallel machine with some well defined structure; we use PRAM machine in our algorithms.

Parallel pattern matching algorithms have been discussed since 70s, but there still some unanswered questions remain. One of them is an optimal approximate parallel pattern matching algorithm, where we allow some edit operations, such as substitutions, insertions, and deletions. Optimal algorithm is a parallel algorithm, where processor-time product is equal to the time of the sequential algorithm. We have developed two different parallel pattern matching algorithms.

The first methodology for parallel pattern matching using different metrics that preserve the length of approximate pattern is based on the suffix automata [1]. Suffix automaton is a finite automaton accepting any suffix of a given pattern. The text is split into $\lceil n / (m - 1) \rceil$ parts, which ensures each occurrence of the pattern exactly in two consecutive parts of the text. Then we find all prefixes of the pattern which end at the last position of one part and all suffixes of the pattern which begin at the first position of the consecutive part. Both prefixes and suffixes are accepted by suffix automaton, because the suffix automaton for reversed pattern accepts prefixes of that pattern. We store the lengths of the prefixes and suffixes as they are accepted in linear time. Then we compare the length of prefix u for each position $v = m - u$ in one part of the text with the length of suffix $v = m - u$ at position v in the consecutive part of the text. These interesting properties are valid just because of the usage of parts of the text of length $m - 1$ and because even the approximate pattern has the length equal to m. In the approximate pattern matching we need to ensure that the number of errors in the prefix and the number of errors in the suffix is not greater then allowed number of errors k.

Since the accepting of the prefixes and suffixes takes $\boldsymbol{O}(m)$ time and the verification phase also takes $\boldsymbol{O}(m)$ time, the algorithm takes $\boldsymbol{O}(m)$ parallel time using $\boldsymbol{O}(n / m)$ processors. Even though this algorithm is optimal, it is not sub-linear as some elder parallel pattern matching algorithms are, and it cannot handle the case when the approximate pattern does not preserve its length. On the other hand, the methodology works fine even with some new musicology distances as we show in [1], where no other parallel pattern matching algorithms were already defined.

The second algorithm uses well known bit-parallel simulation technique (preliminary version [2]). This technique simulates the run of the nondeterministic finite automaton such that each of m states corresponds to one bit in a bit-vector. We have used its recursive formula and we have rewrote it such that the new formula can be simply computed using another well know parallel prefix computation algorithm, which is one of the most basic algorithms in parallel computing.

We split the text into $\lceil n / m \rceil$ parts, and we assign a bit-vector of length $2m - 1$ to each symbol of the text. We use m bits for simulation of active states of the pattern matching automaton and the rest are for computation reasons. Then we twice apply the parallel prefix computation.

The first computation propagates non-active states (bits) into the very consecutive part, which is the only part under a direct dependency. The second parallel prefix computation computes active states as they are already influenced by the previous part and therefore now each bit-vector is freely computed in parallel independently on the bit-vectors on the other parts of the text. These parallel prefix computations need to be computed for each of k levels (allowed errors) because it parallelizes the simulation technique.

Each parallel prefix computation is optimally computed by $\boldsymbol{O}(m / \log m)$ processors in $\boldsymbol{O}(\log m)$ parallel time. There are $\boldsymbol{O}(n / m)$ parallel prefix computations at a time, one at each part of the text, and therefore we need $\boldsymbol{O}(n / \log m)$ processors to run our parallel pattern matching algorithm in $\boldsymbol{O}(k \log m)$ time. This algorithm is very fast, however, its processor-time product is equal to the time $\boldsymbol{O}(k n)$ of the bit-parallel pattern matching. Since there exist $\boldsymbol{O}(n)$ time pattern matching algorithms, our algorithms is not optimal and the optimal sub-linear parallel pattern matching algorithm remains an open question.

As a result of our work on [2] we have developed a very fast algorithm for determinisation of the non-deterministic finite pattern matching automata [3]. This algorithm is also based on bit-parallel simulation technique and it simulates the determinisation process. Since we use bit-vector of m bits simulating m states of the automaton, our determinisation algorithm is up to m times faster then usual subset construction determinisation algorithm. Moreover, we have developed direct simulation of ε-transitions in nondeterministic finite automaton.

References:

[1] ŠUPOL, J. – MELICHAR, B.: *Suffix Automata and Parallel String Matching* London Algorithmics and Stringology, 2007, 25 pages, to appear.

[2] ŠUPOL, J. – MELICHAR, B.: *2D Bitwise Memory Matrix: A Tool for Optimal Parallel Approximate Pattern Matching* In Proceedings of the Prague Stringology Conference '06. Praha, Vydavatelství ČVUT, 2006, pp. 18–28.

[3] ŠUPOL, J. – MELICHAR, B.: *A New Approach to Determinisation Using Bit-Parallelism,* Theoretical Aspects of Computing - ICTAC 2006, Heidelberg: Springer, 2006, pp. 228–241.

This research has been supported by the Ministry of Education, Youth, and Sport of the Czech Republic under research program MSM6840770014, by the Czech Science Foundation as project No. 201/06/1039, and by the Czech Technical University as project No. CTU0609613

Statistical Analysis of Subjective Tests of Audio - Coding Systems

M. Herrera

herrerm@feld.cvut.cz

Department of Radioelectronics, Faculty of Electrical Engineering, Czech Technical University, Technická 2, 166 27 Prague 6, Czech Republic

Compression systems have a remarkable importance in nowadays communication systems. They minimize the data volume of the audio file, thus reducing channel bandwidth and capacity storage costs. Nevertheless, the quality of service (QoS) is degraded because irrelevancies and redundancies of the signal are discarded. This degradation can be measurable either by subjective or objective procedures. Since available objective procedures are built on the same principles as the compression systems they do not represent a reliable tool for this evaluation. This work is then a contribution to subjective procedures of evaluation where two of them were used. These tests should fulfill basic requirements for homogeneity. None of the audio excerpt should be an extreme interesting musical excerpt in order to allow the listener to concentrate on the evaluation and not on the aesthetics of the excerpt itself. Signal sources are CD-audio files. Four musical signals, castanets, piano, choral and drums were chosen, and one speech signal from a male French person. The listener panel was conformed by 15 listeners with some experience with the problematic and/or musicians. The measurement system for the playback and headphones was maintained equal, as well as the room conditions. The system used for coding the signals to each of the compression formats was the same. The first method of evaluation was DBTS (Double-Blind-Triple-Stimulus with Hidden Reference), recommended by the ITU-R 1116-1 BS. This method belongs to the methods of successive categories. The critical excerpts were chosen, coded by four compression algorithms at five bit rates and presented to the listeners' panel in the following manner. The original excerpt is presented to the listener, followed by two versions of the same excerpt. The listener has to find which of the two versions is the original, and which the coded one, and grade the coded one in a scale of one to five. Results are processed with descriptive statistics as mean value and standard deviation. Results from DBTS show that Ogg Vorbis is the compression system which performed best already at 96 kbit/s. Inter-individual reliability is analyzed with a t-test statistics in order to evaluate listeners' performance, and state which listeners were just guessing the results. Variability of the results related to each factor (excerpt and compression system) and the interaction of both also is analyzed with a significance level of 0.95. Another remarkable result is that DBTS resulted a stricter method than SR (Simple Rating), a method used in a previous research. A training session was needed in order to introduce to the listener the effects of audio compression. The second method of evaluation used is the Method of Similar Attributes. This method is used for the investigation of similar patterns of compression noise in several excerpts. Three typical audible compression noises (artifacts) are presented to the panel: pre-echo, speech reverberation and birdies. After the panel has recognized them at the training session, evaluation starts. The task is to find similarities between the coded excerpts to the artifacts in a defined scale. The results are then processed by MDS (Multidimensional Statistics methods) in order to find a multidimensional space describing the relations between several excerpts and the artifacts produced by the compression. The multidimensional approach is sustained by

the fact that each audio excerpt can be described by a multidimensional space where a definite set of attributes constitute the basis for that space. Besides the artifact space, a second variant of Similar Attributes Method is carried on the basis of psychoacoustic attributes as sharpness, roughness and sensory pleasantness. Overall correlation between methods is also presented, and a 3-D geometric representation of the procedures is depicted in order to have a general idea of the tests. These results are, moreover a contribution to the assessment of codecs, which has been performed also by methods as constant stimuli (CM), simple rating (SR), and the pair comparisons (PC) method. The overall problematic can be described in the following patterns. Audio signals are affected by a mathematical procedure –compression-, which includes an orthogonal transform (FFT, DCT, DWT) and other mathematical models for discarding the irrelevancies and redundancies of the signal. Irrelevancies are discarded on the base of models from hearing physiology and redundancies on models from coding theory (Huffman coding). The subjective measurement procedures mentioned above come from Psychometrics, a science built upon notes from experimental psychophysics (in our case, psychoacoustics), and mathematical tools as scales, ratios, limits and dimensionality for retrieving and quantifying subjective responses. In the case where these procedures are used properly, minimizing systematic errors in such a way that there is neither influence nor distorsion of the results because of the application of a definite method, there is possible to retrieve from the experiment a mathematic expression or number which will represent the measured phenomenon, in our case, compression artifacts, with an appropriate significance level. Each method has his own results' descriptors expressed in mathematic terms: Limen identification for CM (bit-rate/compression at which artifact is sensed), Comparative judgments for PC, a number in a scale 1-5 for DBTS and SR, and the position on a multidimensional space for the method of Similar Attributes. Each of them describe and quantify the artifact phenomenon. The actual state of the work is the application of these obtained results for the realization of an objective system for evaluation. Subjective attributes of the signal are calculated based on experimental psychoacoustic formulae, followed by an RBFN (Radial Basis Function Network) which processes them. RBFN function is chosen because after training, weighting coefficients and biases levels are automatically set. The target values for training the network are the subjective values obtained by DBTS method. There is the possibility to enhance this system with target values from the the other four subjective methods.

References:

[1] M. HERRERA: *Beyond the evaluation of audio coding systems,* IV Student International Conference VRSOV, IEEE, 2006, pp. 60-63.

[2] M. HERRERA: *Evaluation of audio coding artifacts,* Proceedings of the 10th. International Student Conference on Electrical Engineering, POSTER 2006, Prague, 2006.

[3] M. HERRERA: *Summary of the subjective audio coding tests during the 2003-2005 period at the CVUT,* XI International Symposium, ISSET 2005, AES, 2005, pp. 153-159.

This work has been supported by the Grant of the National Science Foundation No. 102/05/2054 „Qualitative aspects of Audiovisual Information Processing in Multimedia Systems" and the Internal Grant CTU0609813, FIS No. 10-86098/13137.

Electroacoustic Transducers with Direct D/A Conversion

P. Valoušek

valousp@feld.cvut.cz

Department of Radioelectronics, Faculty of Electrical Engineering, Czech Technical University, Technická 2, 166 27 Prague 6, Czech Republic

A concept of a multi-bit digital loudspeaker is discussed and a single-bit digital loudspeaker design is presented. Almost all experimental realizations of a digital loudspeaker are based on the same principle of a digital to analog conversion as in case of parallel electric converters. An acoustic signal is created as a sum of partial acoustic pressures generated by a number of electro-acoustic transducers. The number of transducers always somehow corresponds to a bit depth of an input signal. For commonly used bit depths of an audio signal the number of transducers can range from tens to millions according to coding scheme of a digital loudspeaker. For direct radiating speaker the transducers are arranged in an array, where distances between single transducers and listening point are the main limiting factor for correct function of such a speaker. When these distances are greater than a fraction of one period of a sampling frequency, an unavoidable timing distortion occurs.

Finite dimensions of single transducers and their great number make manufacturing of a suitable transducer array very difficult. For the same reasons current commercial electric digital to analog converters for audio use noise shaping technique and reduced bit depth which can in extreme become a one bit system. The same idea is used in digital amplifiers. These systems use one-bit modulation PWM or PDM with an acoustic signal in a base band. A PDM signal is a sequence of pulses with the same energy and varying density according to a low frequency input signal. A PWM scheme uses different energy for each pulse and it can be expected, that these energy variations can not be precisely transformed into an acoustic pressure by electroacoustic transducer. Therefore the single-bit digital loudspeaker design uses modified PDM modulation.

A disadvantage of a one bit modulation is higher sampling frequency which slightly raises demands on frequency response of an electroacoustic transducer. It is not necessary to reproduce steep square signal, the only requirement is that energy of all pulses must be the same. Therefore the driving pulses can be shaped to reduce high frequency content. This can be done by a simple analog filtering of a driving signal right before the transducer. Because of limited frequency response of traditional electroacoustic transducers, it is necessary to dramatically reduce sampling frequency of sigma-delta modulator.

To achieve acceptable bandwidth a 7^{th} order modulator with three notches in a frequency response was designed. With modulator sampling frequency of 44.1 kHz or 48 kHz the modulator provides 2 kHz bandwidth with noise below -60 dB FS. This performance should be sufficient for experimental purposes.

A relatively low pulse frequency of the modulator running at a frequency of tens of kHz is still too high for conventional electroacoustic transducers. Responses of various transducers to a pulse driving signal were simulated with the result that dynamic or electrostatic transducers can not be used for this task because of their very low resonant frequency which distorts the pulse response. The only electroacoustic principle able to work at these high frequencies is the piezoelectric principle.

The quantization noise of the modulator running at very low sampling frequency lies in the audio band and may become irritating. This quantization noise must be filtered out by a low-pass acoustic filter after the electroacoustic transducer. This filtering would be necessary also in the case of multi-bit digital loudspeaker to remove higher order images of digital signal. Acoustic filter can be realized as combination of serial connection of an acoustic mass and an acoustic spring. Cut off frequency and values of the filter parts must be calculated according to used digital modulation and electroacoustic transducer parameters.

The fundamental parts of the single-bit digital loudspeaker were simulated and implemented in Matlab and could be used in the future for experimental realization.

References:

[1] FLANAGAN, J. L.: *Direct Digital-to-Analog Conversion of Acoustic Signals,* The Bell Systems Technical Journal, 1980, Vol. 59, No.9.

[2] BUSBRIDGE, S.C. ET AL.: *Digital loudspeaker technology: current state and future developments,* AES 112TH convention, 2002,

[3] HUANG, Y., BUSBRIDGE, S.C., GILL, D.S.: *Distortion and Directivity in a Digital Transducer Array Loudspeaker,* J. Audio. Eng. Soc., 2001, Vol.49, No.5.

[4] HUSNÍK, L.: *Audio Going Digital – Present State and History of Digital Transducers* Proceedings of X Symposium New Trends in Audio and Video, 2004, , pp47-52

This research has been supported by CTU0610313.

Optical measurement of cosmic objects with laser time tags

M. Němec, I. Procházka, K. Hamal *
G. Kirchner, F. Koidl, W. G. Voller **
Yang Fumin ***

nemecm1@troja.fjfi.cvut.cz

* Department of Physical Electronics , Faculty of Nuclear Sciences and Physical Engineering, Czech Technical University in Prague, Trojanova 13, 120 00 Praha 2, Czech Republic
** Institute for Space Research, Austrian Academy of Sciences, Lustbuehelstr. 46, A-8042 Graz, Austria
*** Shanghai Astronomical Observatory, Chinese Academy of Sciences, 80 Nandan Road, 200030 Shanghai , China

There exists a strong interest to determine the accurate trajectories of the objects orbiting the Earth. The small planets, asteroids, space debris and possible ballistic or orbiting missiles are targets of interest.

Optical tracking is a pretty standard technique to determine the orbit of space objects, space debris in particular. The sequence of angular measurements of an object position relative to catalogued stars is used to calculate the orbit [1]. Although the registration methods have changed from original visual, over photographic to the presently used a CCD sensor, the basic principle remains unchanged. The ultimate precision of the recorded angular positions is limited mainly by the atmospheric properties. The observation time slot is limited by the requirements that the object has to be illuminated by the Sun and the observation has to be carried out under local nighttime. The typical precision of the angular position reading is of the order of units of arc seconds. Considering the apparent angular speed of the objects on low Earth orbits, the exact epoch of position reading (exposure) has to be determined with (sub) millisecond accuracy, what is a non-trivial task. Calculating the final orbit, the time interval between the observations and the angular position resolution and accuracy are the key limiting factors in the resulting orbit determination. To generate orbit parameters of the space object on a Low Earth Orbit (LEO), at least four observations spanned over one to several days are needed [2-3]. To increase the orbit solution stability, the angular observations from two different locations are usually needed.

We are presenting new optical tracking techniques of space objects based on simultaneous CCD (Charge Coupled Devices) and laser measurements. In standard optical tracking techniques, the orbit of an object may be calculated from the sequence of angular CCD measurements relative to the positions of catalogued stars. The time interval between the observations and the angular position resolution and accuracy are the limiting factors in the resulting orbit determination.

Our new optical tracking techniques provide three additional options - the CCD tracking of laser illuminated object, the simultaneous CCD tracking and laser ranging, and the higher resolution of the tracked object positions obtained from the CCD exposures, in the both time and space domain, improved by the laser time-tagging.

The first two options can be performed on cooperative - corner retroreflectors equipped - satellites. High power lasers could be used in the future for even non-cooperative objects [4]. While the third option is applicable to any space object, the space debris in particular. The laser time-tags are formed by the atmospherically back-scattered photons

transmitted by the laser ranging system and are recorded simultaneously with the space objects on the CCD. The laser time emission is recorded with nanosecond precision providing multiple time-tags for each image exposure. The high accuracy and density of laser ranging data and additional time tags in the CCD image contribute to the higher solution stability of computed orbits from data based even on a single tracking location within a single pass. We have tested the combined laser and CCD tracking at the facilities of the Institute for Space Research, Graz, Austria and at the facilities of SLR (Satellite Laser Ranging) station of Chinese Academy of Sciences, Shanghai, China. Our results of the tested satellites tracking demonstrate the techniques feasibility and their higher accuracy over existing optical methods.

References:

[1] L. AARDOOM, A. GIRNIUS, G. VEIS: *Geometric methods,* Geodetic Parameters for a 1966 Smithsonian Institution Standard Earth, vol. 1, edited by C. A. Lundquist and G. Veis, Smithsonian Astrophys. Obs. Spec. Rep. No. 200, 1966, pp. 63-75.

[2] 2. S. ISOBE, T. TAJAINA: *CHOPPING TECHNIQUES TO DETECT GEOSYNCHRONOUS SPACE DEBRIS,* Proceedings of the Second European Conference on Space Debris, ES0C, Darmstadt, Germany, 17-19 March 1997, ESA SP-393, 1997, pp. 89-92.

[3] 3. T. SCHILDKNECHT, U. HUGENTOBLER, G. BEUTLER: *TECHNIQUES FOR OPTICAL OBSERVATIONS OF SPACE DEBRIS - PERFORMANCE TESTS WITH THE NEW 1 METER ZIMMERWALD TELESCOPE,* Proceedings of the Second European Conference on Space Debris, ES0C, Darmstadt, Germany, 17-19 March 1997, ESA SP-393, 1997 pp. 93-98.

[4] 4. B. GREENE, C. SMITH, Y. GAO, J. COTTER, C. MOORE, I. RITCHIE, C. BURMAN: *Advanced Techniques at the EOS Space Research Centre,* 14th International Laser Ranging Workshop, San Fernando, Spain, June 7-11, 2004, published in Boletin ROA No. 4/2004, Real Instituto Observatorion de la Armada, en San Fernando, ISSN 1131-5040, edited by J.M.Davila, 2004

This research has been supported by CTU grant No. CTU0611514 and by MŠMT grant No. ME 848. The authors would like to express their thanks to Lukas Kral from CTU in Prague, Martin Fuchs from the Stefanik observatory in Prague and Joerg Weingrill from Austrian Academy of Sciences in Graz for the technical assistance.

Method of Construction Scheme of Object Database to Using in Data Mining.

M. Jeřábek, J. Krčál, L. Krčálová

jerabekm@fd.cvut.cz

Department of Informatics and Telecommunications,
Faculty of Transportation Sciences, Czech Technical University,
Konviktská 20, 110 00 Prague 1, Czech Republic

The goal of this article is provide a result of the CTU internal grant regarding to method of construction scheme of object database to using in data mining and to available methods of data mining for object databases.

Data mining, also known as knowledge discovery in databases (KDD), is a process. The particular standard process used is the CRISP-DM (CRoss-Industry Standard Process for Data Mining). CRISP-DM demands that the life cycle of a data mining project consists of six phases [1] (the sequence of the phases is not rigid – moving back and forth between different phases is always required):

- business understanding – this initial phase focuses on understanding the project objectives and requirements from a business perspective, then converting this knowledge into a data mining problem definition and a preliminary plan designed to achieve the objectives
- data understanding – this phase starts with an initial data collection and proceeds with activities in order to get familiar with the data, to identify data quality problems, to discover first insights into the data or to detect interesting subsets to form hypotheses for hidden information
- data preparation – this phase covers all activities to construct the final dataset (data that will be fed into the modeling tool(s)) from the initial raw data. Data preparation tasks are likely to be performed multiple times and not in any prescribed order
- modeling – in this phase, various modeling techniques are selected and applied and their parameters are calibrated to optimal values
- evaluation – at this stage in the project must be built a model (or models) that appears to have high quality from a data analysis perspective. At the end of this phase, a decision on the use of the data mining results should be reached
- deployment – if the purpose of the model is to increase knowledge of the data, the knowledge gained will need to be organized and presented in a way that the customer can use it. It often involves applying "live" models within an organization's decision making processes. However, depending on the requirements, the deployment phase can be as simple as generating a report or as complex as implementing a repeatable data mining process across the enterprise

In two phases of data mining - data understanding and data preparation - when is important find and prepare the right data, very often are using databases. Best known and most widespread are relational databases. There are plenty of remarkably good applications out there that have been running on relational databases for years.

Less known and very few widespread are object-oriented databases [2, 3]. ODBMS (Object Database Management System) supports the modeling and creation of data as object. This includes some kind of support for classes of objects and the inheritance of class properties and methods by subclasses and their objects.

An applications of object-oriented database technology is available for applications which [2, 3]:

- involve the interrelationship of many parts
- must manipulate large amounts of data
- involve predictable type of data access
- have limited need for ad hoc querying

Design of object database for data mining is important in phase data preparation of data mining. To elimination problems of redundancy and non-consistency of data, it is very suitable data normalization. But in the object-world data normalization only deals data and not behavior. The process by which reorganized the structure of object schema in such a way as to increase the cohesion of classes while minimizing the coupling between them is called class normalization. It's ideal when object schema is in third object normal form (3ONF). It means all of object schema's classes are in 3ONF [4].

Disadvantage of object-oriented database is navigational nature. It's means that queries must follow predefined relationships and cannot insert new relationships on the fly. Also object-oriented databases aren't as well suited to ad hoc querying as relational database, although ad hoc queries are typically supported.

Methods of data mining suitable when are used object-oriented databases as a source of date for data mining are some few. For example traditional decision tree that are simple to understand and interpret and require little data preparation. Another useful data mining's method is nearest neighbor classification or rule induction.

It is hard to designate object-oriented database as unavailable to use for any method of data mining. Object-oriented databases are unlikely to replace relational databases for all applications in the same way that relational databases have replaced data models and that's why it is necessary to research usage of object-oriented database for data mining. For example inheritance it's very interesting feature and could be more used. Usage of inheritance in data mining is object of our next research.

References:

[1] CHAPMAN, P. – CLINTON, J. – KERBER, R. – KHABAZA, T. – REINARTZ, T. – SHEARER, C. – WIRTH, R.: *CRISP-DM 1.0 Step-by-step data mining guide* SPSS Inc, 2000 pp. 13–15

[2] HARRINGTON, J. L. : *Object-Oriented Database Design Clearly Explained* M. Kaufmann 2000

[3] GREHAM, R.: *Introduction to ODBMS* < http://www.odbms.org/ > [cit. 5. 1. 2007]

[4] AGILE DATA: *Introduction to Class Normalization* < http://www.agiledata.org/ > [cit. 5. 1. 2007]

This research has been supported by CTU grant No. CTU0612016.

Innovation of the Subject Signal Processors - Digital Signal Processing

M. Vlček

vlcek@fd.cvut.cz

Department of of Applied Mathematics, Faculty of Transportation Sciences, Czech Technical University, Na Florenci 25, 110 00 Praha, Czech Republic

This project deals with the innovation of the subject Signal Processors - Digital Signal Processing. New topic is represented by the digital signal processors Texas Instruments TMS320C6x. The newly developed low cost Multiformat Video Daughter Card card for the TMS320C6x DSP Starter Kits is introduced.

The practical training in the digital signal processing in this subject was based on the Matlab experiments in the past exclusively. In order to cope with the advances in the DSP technology, the syllabus of the subject was substantially changed. The practical training is based on the Very Long Instruction Word (VLIW) DSPs, both with the floating point (320C6711) and fix point (320C6416) arithmetic in form of commercial DSP Starter Kits (DSK) [1]. In order to make the training more efficient, the Multiformat Video Daughter Cards (MVDC) were designed and realized.

The MVDC combined with the DSK forms a cost effective, high performance video and imaging platform intended for the development of multi-format digital media applications. The TMS320CC64xx DSKs are preferred. The MVDC is compliant with the TMS320 cross-platform daughtercard specifications Rev1.0. It is interconnected to the External Memory Interface (EMIF) and Peripheral Interface through two 80-pin connectors.
The MVDC includes SD-Card, USB and PS/2 interface. The SD-Card flash memory combined with the MVDC and DSK may form an useful unit for media players or recorders. The SD interface standard is not limited to removable memory storage devices. It has been adapted to many different classes of devices, including 802.11 cards, bluetooth devices, and modems [3]. Personal computer (PC) can access the MVDC via the USB port. Designers may profit from the mouse or keyboard interface in order to control their applications via the PS/2 port. These options make the MVDC an attractive choice for video applications and for educational purposes. Features of the card are as follows :

- Video IN
  - One Multiformat Video Decoder with 10-bit ADCs (SDTV inputs)
    - One Female RCA connector for Composite Video input (CVBS)
    - One Female 4-Pin Mini DIN connector for S-Video input (Y/C)
    - One Female 6-Pin Mini DIN connector for Differential Component Video input
- Video OUT
  - One Multiformat Video Encoder with 11-bit DACs (SD and HD output)
    - One Female RCA connector for Composite Video output (CVBS)
    - One Female 4-Pin Mini DIN connector for S-Video output (Y/C)
    - One Female 6-Pin Mini DIN connector for Differential Component Video output (YUV/YPrPb)
  - One 24-bit High Speed Video RGB DAC for VGA
    - One Female 15-Pin D-SUB connector for Vesa Compatible monitor output
- Memory
  - Two 4-Mbits dualport FIFO for video frame buffer

  - One 4-Mbit Serial Configuration memory for FPGA
- External Interfaces
  - Two 80-pin connectors for C6000 EVM/DSK interface compliant to TMS320 Crossplatform daughtercard specifications V1.0
  - One 10-pin header for AS Configuration FPGA
  - One USB interface version 1.1 and 2.0 compatible
    - Supported Full Speed mode
    - Supported JTAG Configuration FPGA
    - Type B connector
  - One PS/2 interface (6-pin Mini DIN connector) for Mouse or Keyboard
  - One SD-Card Interface for removable memory storage devices or others devices
- Uses high performance, 6K usable logic elements (LEs) FPGA
- Four status LEDs, Programable Clock Source, Power Regulation (3.3V, 2.5V, 1.8V, 1.5V)

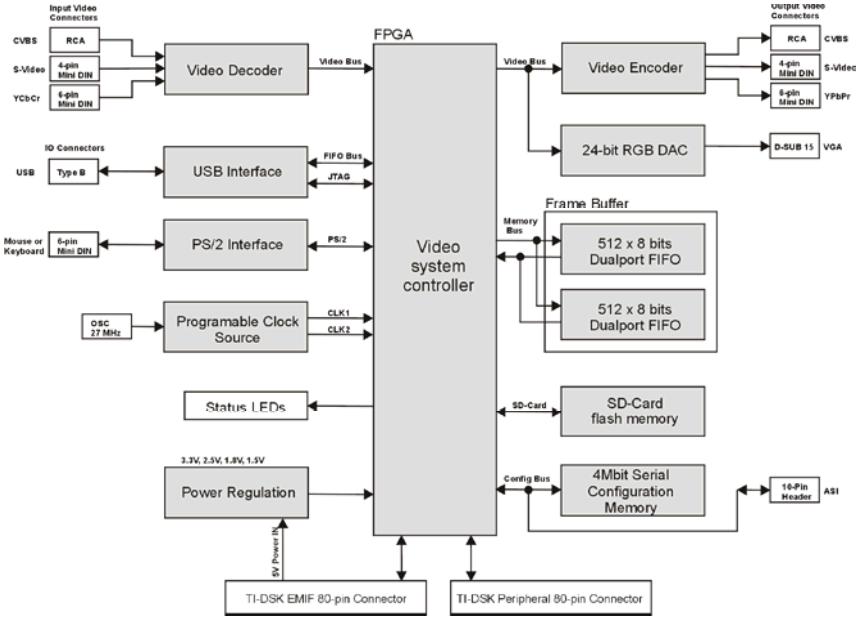


Figure 1. Simplified block diagram of the MVDC system architecture.

References:

[1] WWW.TI.COM

This work has been supported by MŠMT grant No. FRVŠ F1-2719.

Simulation of Behavior in ALife Domain

A. Elmahalawy, K. Kohout and P. Nahodil

elmahal@labe.felk.cvut.cz

CTU, Faculty of Electrical Engineering, Dept. of Cybernetics
Karlovo náměstí 13, 121 35 Praha 2

This work is aimed at simulating the behavior in Artificial Life (ALife) domain with the use of the *World of Artificial Life* (WAL) system. This simulator was developed in the research group *Mobile Robotic Group* "MRG" (leaded by P. Nahodil) in last years [1]. We made some modification in the *agent architecture*.

ALife [2] is an important part of *Artificial Intelligence* (AI), which tries to model "*the world as it is*" or "*the world as it could be*". The Mother Nature had billions of years to undertake experiments with living mass and people reached the point when they can imitate her. ALife gets the inspiration how to solve it from many other disciplines, namely biology, ethology, sociology, psychology, mathematics, physics and, of course, cybernetics.

One of the most interesting problems in ALife is the cooperation and communication of animals. Ethology – study of animal behavior in its natural environment – can provide a lot of inspiration in this respect. To the strict ethologist, behavioral studies must be undertaken in the wild; animals' responses have no meaning outside their natural setting. An animal itself is just one component of the overall system; additionally the environment in which it resides must be taken into account. Also, ethological studies show, that multi-agent societies offer significant advantages for achieving community tasks. There is a wide range of animal social structures that support agent-agent interactions.

The animal's behavior itself can be categorized into the three major classes [3]:

Reflexes are rapid, automatic involuntary responses triggered by certain environmental stimuli. A reflexive response persists only as long as the stimulus is active. Further, the responsive intensity correlates with the stimulus's strength. Reflexes are used for either simple activities or highly coordinated ones like locomotion.

Taxes are behavioral responses that orient the animal toward or away from a stimulus (attractive or aversive.) Taxes occur in response to visual, chemical, mechanical, and electromagnetic phenomena in a wide range of animals.

Fixed-action patterns are time-extended response patterns triggered by a stimulus but persisting for longer time than stimulus itself. In contrary to the reflexive behavior, the intensity and duration of the response are not governed by the stimulus' strength and duration, instead they may be motivated, and they may result from a much broader range of stimuli than those that govern a simple reflex.

We will concentrate our attention to the architecture of an agent for ALife purposes. It is called an *Architecture Lemming* [1] and it is hybrid architecture with adaptive and generalizing abilities. The *Architecture Lemming* is based on the data processing both from sensors and inner states. If we follow a *data flow*, we start in a block ***Environment***. The *Environment* supplies agent through ***Sensors*** with sensory data and through ***Inner States*** block with information about inner variables. Data are filtered by ***Mood Filter*** and passed to ***Action Selection Mechanism*** and ***Memory***. Action Selection Mechanism compiles available data and using ***Knowledge Base*** and ***Long-Term Goals*** agent makes decision

about future actions which are performed by ***Actuators***. ***History***, ***Rules Generator*** and ***New Rules Repository*** are used for generalization [1].

The drawback of this architecture is in ignoring of real values of inner state values. It was assumed that all inner state values are optimal at the beginning of the experiment. Thus, we propose a modification that adds a new block to this architecture. This new block is for testing the inner state values at the beginning of the experiment. If these values are not optimal, then we have to adjust them accordingly.

The *architecture lemming* was applied in a chimpanzee life. The chimpanzee was closed in the cage with 10 different crates lying on the floor. Each crate needed certain tool to be opened. Such a tool was always locked in another crate. The experiment had two parts; the first one was try to discover the influence of changing the chemical levels on behavior and life of the chimpanzee using the original *architecture lemming*. We had six chemicals (Water, Sugar, SexHormone, Melatonin, Adrenaline, and LifeSubstance). We changed the values of these chemicals in the beginning of the experiment and watched if there was a discrepancy in the behavior of lemming or not. This followed to the second part of our experiment, which is adding a new block that test and update the inner state value, we successful applied our modification to the architecture lemming and received much better results than before.

We can see now that the behavior of the chimpanzee is changed according to changing of the inner state values. If there is a decrease in these values with a small value, there will change the mode and behavior of lemming, as it get aggressive quickly. Decreasing these values by grater amount leads to the death of lemming.

It is important to test and adjust the chemical levels at the beginning of an experiment to avoid an unexpected behavior or the fast death of lemming. If the value of water is low at the beginning of the experiment, then the lemming goes to pure spring to drink resulting the increase of water value, similarly if the value of sugar is low then lemming goes to an apple tree to eat resulting increase of sugar value We can see that our modification of the lemming architecture is very important and allows the lemming evolve in the expected way.

We also add a new *fire behavior* to the experiment mentioned above. In this case, there are two sources of fire in our environment. If the lemming will be near to the one of them (and self discovers a possibility of harming) then it goes away from this source of danger.

Some of the last obtained results are connected with the anticipatory block adding to the described architecture. It seems to be very useful to add this block to have much better results than all the previous. The main goal of our future work is to verify this last premise.

References:

[1] FOLTÝN, L.: Realization of Intelligent Agents Architecture for Artificial Life Domain, *Diploma Thesis.* Supervised by Nahodil, P., Department of Cybernetics, Faculty of Electrical Engineering, Czech Technical University in Prague, Prague: 2005.

[2] NAHODIL, P. From Slow Machines towards Anticipators Creatures. In: *Proc of Interdisciplinary Aspects of Human-Machine Co-existence and Co-operation, IFAC Workshop „e-Golems´05“, 2005. Prague, Czech Republic.* Prague: 2005, pp. 110 -119

[3] ARKIN, R.C. Behavior Based Robotics: Intelligent Robots and Autonomous Agents. The MIT Press: Mass, 1999.

Flexible Booting Strategy for FPGA-based Systems

M. Šimek

simekm2@fel.cvut.cz

Department of Computer Science and Engineering,
Faculty of Electrical Engineering, Czech Technical University in Prague,
Karlovo náměstí 13, Praha 2, 121 35

The embedded system market has rapidly grown and systems based on FPGA have gained high credit among developers and companies. Masses of developers create operating systems with many programs but without concentrating on reliability and security at the same time. The throughput of embedded systems increase and parallel systems are the only way how to design these systems. Now it is the right time to start a project dealing with parallel systems in conjunction with their reliability. The goal of the project is to propose a full-scale embedded system with multiple heterogeneous cores (Microblaze, PowerPC) which we can sharply and effectively control booting an operating system with respect to fail safe properties of the whole system.

We focus on Xilinx FPGAs. The manufacturer provides the Microblaze soft core (VHDL, Verilog) and the PowerPC hard core (layout). We have some previous experience with designing CSoCs (Configurable Systems on Chip) for both these cores [1], [3], [4]. The designing a system with multiple cores has the biggest problem with memory controllers because ordinary development boards have only one external memory and so we have to use one memory controller for multiple cores. Connecting a memory controller and multiple cores through one internal bus isn't a suitable solution because the bus is congested. A better solution is linking a memory controller with the Microblaze via FSL (Fast Simplex Link) which eliminates congestion of the internal bus. Another FSL bus may be used for synchronization among processor cores. The PowerPC hasn't got an FSL bus that is why we connect the memory controller to PLB (Processor Local Bus) bus.

Software designers for embedded systems focus especially on operating systems. But the category of bootloaders is crucial in all the embedded systems. A bootloader is a program which initializes the embedded system and loads an operating system. We can meet a term monitor. A monitor is a program which has properties of a bootloader and provides other features, which aren't related to only starting an operating system. The monitor typically has a command line interface and can work with memory and all peripherals. Several years ago the term bootloader approximated with the term monitor and at the present time the term bootloader is mainly used. Bootloader's abilities allow comfortable and flexible work for developing standalone applications and operating systems. It is very helpful for higher level debugging via e.g.: JTAG.

There are several booting strategies for the FPGA based processor Microblaze, which are particularly depended either on properties of development board, or on implementation a system design with integrated functions of development tools. These alternatives are usually called as the first stage of a bootloader. After this first stage it is possible either to copy an operating system to the main memory and to start it or to use the second stage of a bootloader. For our aims, we concentrate on this second stage of a bootloader because it enables to make use of a simple bootloader with abilities of a monitor. The second stage of a bootloader provides us the appropriate background for implementation of a sophisticated booting strategy with a booting safety support.

We have used "Das universal bootloader U-BOOT" [2] which had originally a basic support for the Microblaze processor. U-BOOT provided access to the serial interface and the memory. We decided to use an Ethernet interface for uploading a vast bulk of data. For the Ethernet support it was necessary to implement a software control for an interrupt controller, a timer and ancillary functions of starting operating systems. At the beginning of the project, the bootloader was used only as the second stage with a standalone application as the first stage. At the end of U-BOOT porting to Microblaze, both stages were linked together. A simple booting strategy expects separated partitions of a permanent flash memory, which are accurately intended for a default kernel of an operating system. In the case of using Linux operating system it is necessary to allocate another partition for a root file system. We can also use one image which has the Linux kernel and the root file system included. The type of the root file system is dependent on the final application. We have experience with many types of embedded file systems such as ROMFS (Rom File System), CRAMFS (Compressed Read Only File system), JFFS (Journaling Flash File System) and NFS (Network File System).
For security and fail safe properties, a bootloader may support watchdog functions which protect the whole system against a deadlock. The watchdog is practically unused in a large operating system. U-BOOT provides protection of all images (an operating system image and a root file system image) by CRC (Cyclic Redundancy Check) code.
We made a proposal of reliable system update from an operating system as well as from U-BOOT. An operating system employs MTD (Memory Technology Device) and U-BOOT employs very similar system of operations. The key point is in storing a new image of the operating system and the root file system to the flash memory with checking CRC code. After system restart, bootloader checks CRC and starts new operating system. In the case of verification failure, the default operating system is used.
We have fully tested hardware designs based on Microblaze and PowerPC cores. We have developed the same booting strategy using U-BOOT for both cores. For easier configuration we have created files for automatic setting from a development tools. We can flexibly choose proper peripherals such as a timer, an Ethernet interface, a serial line and design dependent parameters.
We are concentrating on development of watchdog checking mechanism incorporated in bootloader U-BOOT for increasing reliability. We plan to extend U-BOOT for FSL support to allow low level testing of connection between two Microblaze cores or the Microblaze and memory controller. We are going to create a new testing design with multiple Microblaze cores and another one with the Microblaze and the PowerPC. Fully tested parallel design will be supported by U-BOOT. Homogenous and heterogeneous parallel system will be fully supported by bootloader with safety booting strategy and checking mechanism.

References:

[1] ŠIMEK, M.: *Embedded Operating System for Microblaze* in proceedings of POSTER 2006, 2006,

[2] DENX, W.: *U-BOOT* web page available at http://www.denx.de 2006,

[3] ŠIMEK, M. - BRABEC, T. - BEČVÁŘ, M.: *Running Linux on an FPGA-based Embedded Platform* in proceedings of CTU Workshop 2006, 2006, pp. 222 - 223.

[4] ŠIMEK, M.: *Embedded Operating Systems for Microblaze* web page available at http://www.monstr.eu, 2006.

Automated Creation of Students' Accounts in the Moodle System Using Data of the KOS Information System

P. Soukup *, P. Žofka **

soukup@fsv.cvut.cz

*Department of Mapping and Cartography, Faculty of Civil Engineering, Czech Technical University in Prague, Thákurova 7, 166 29 Prague 6, Czech Republic

**Department of Geodesy and Land Adjustment, Faculty of Civil Engineering, Czech Technical University in Prague, Thákurova 7, 166 29 Prague 6, Czech Republic

The actual teaching process may be supported by the advanced computer and information technology. The tools for management of tutorial courses (CMS – Course Management System) are a specific kind of the tutorial process support. They serve for all-round assistance in the administration of education which uses personal computers. Nowadays, a relatively great number of these systems are available for teachers. One of them is the computer program system Moodle (Modular Object-Oriented Dynamic Learning Environment) [http://moodle.org], that is developed as an Open source and therefore it is free available for all users, source codes inclusive.

Today, obviously all the universities use some computer system to registration of the students and their educational activities. The Faculty of Civil Engineering, Czech Technical University in Prague (CTU), uses for these purposes a system named KOS (the component of study). It is a relatively complex system which besides of common registration of students preserves all the classifications, the terms of examinations, the schedules of students, content of studies, etc. The system is accessible either by a basic terminal interface or by a supplemental web interface, which offers only a limited set of basic functions at present. In the KOS system, a personal user's account protected by a password is created for every student of faculty. The password is verified by a secure method at the faculty LDAP server. All students without limitation (or only registered users) have an active access to the tutorial texts and other materials that are included in courses of the Moodle system. The restriction of access for registered users only has an advantage which enables better control and transparency of educational process.

Users may register into the course either themselves or their registration must be performed by the course manager. The latter way is preferable for more extensive courses. The student's registration to the Moodle system constitutes creation of a unique user's account protected by a password. The student's account contains a basic contact data (account name, first and last name, e-mail, etc.). An automated creation of students' accounts is one of the first conditions for successful application of any CMS in education.

Currently, the accounts can be created in automated way mentioned in [1]. This method is based on a specific data file which is exported from the KOS system and contains the information about students. For security reasons, only an authorized worker of the CTU computer centre is able to export this file. Subsequent creation of accounts requires the installation of a database module in the client's computer. Below, there is shortly described the procedure of automated creation of students' accounts in the Moodle system implemented by us. The entire procedure is in a full competency of every teacher and it does not require any additional installation.

The automated creation of user's account in the Moodle system represents a basic motivation for the integration of both Moodle and KOS system. Using of the same name and preferably even the same password that are used in the KOS system is a logical requirement for creation of accounts in the Moodle system. The students registered in the Moodle system are then inserted into the relevant tutorial course. Entire procedure of students' accounts creation including the inserting of students into the courses consists of three simple related steps.

First of all, it is necessary to create a list of students who want to study a relevant subject. Every teacher of the subject is able to generate this text file from the KOS system. The original offer of format types of these files didn't contain all the data needed for successful generation of accounts in the Moodle system, so it was necessary to collect data by hand using another sources. On our requirement, the developers of the KOS system created a new output which already includes all the necessary data in one file.

The Moodle system allows the creation of the students' accounts by a mass method, when all necessary data are imported from a selected text file. The second step of automated creation of students' accounts in the Moodle system is the transformation of a file format generated by the KOS system into the format required by the Moodle system. The program in PHP language was created for this purpose. The program easily allows ordering needed data and performing the required conversion by the help of one interactive window.

The automated account creation with using of prepared text file is the third and the last step of creation of students' accounts in the Moodle system. The procedure is realized by the standard function of the Moodle system. This fact ensures the compatibility of entire procedure even for the incoming version of the Moodle system. Students' accounts and their assignment into selected tutorial courses are the result of the entire procedure.

A certain complication of the procedure described here is the fact that for security reasons it is not possible to check the passwords of created accounts by the faculty LDAP server. The passwords are therefore saved in the Moodle system and during the accounts´ creation they are activated via students´ IDs included in the data retrieved from the KOS system. Every student knows his/her ID and he/she is of course allowed to change the password after login to the system.

We successfully use the mentioned procedure in the subjects of study that we are teaching [2]. In fact, the described possibility of an automated generation of students' accounts is necessary for larger usage of the Moodle system at our faculty.

References:

[1] S. DUBEN: *Automatizace přihlašování do Moodle,* BELCOM'06 - Spolupráce univerzit při efektivní tvorbě a využívání vzdělávacích zdrojů, Editor: Karel Květoň, Czech Technical University in Prague, Proceedings ISBN 80-01-02923-9, 2006, pp. 3-8.

[2] P. SOUKUP: *Správa výukových kurzů v systému Moodle,* Geoinformatics CTU 2006, Proceedings of the workshop, Published by Faculty of Civil Engineering, Czech Technical University in Prague, ISSN 1802-2669, 2006, pp. 152-157.

Application of Artificial Life in Robot Navigation

V. Svatoš, P. Nahodil

svatosv©fel.cvut.cz

Department of Cybernetics, Faculty of Electrical Engineering, Czech Technical University, Karlovo náměstí 13, 121 35 Prague 2, Czech Republic

Communication capability allows building pure goal-oriented control system of mobile robots. There we can illustrate advantages of communication on control system based on hybrid architecture. Our designed system for navigation in a sample in-door environment [1] combines top-down commands (sub-goal assignment) with bottom-up instinctive responses. In our conception the hybrid architecture is formalized in one data-driven generative device entity for the robot. It highlights namely a reactive part of decision; when each immediate reaction still reflects actual local context. Auxiliary activities are completed by active sub-optimal response respecting the most frequent trends to come near to required state.

Mobile robotics interprets such decision in sense and action terms. Moreover, the robot rates efficient actions in two horizons: long time strategy has influence to instant control of elementary steps. Its equilibrium can be located in local extreme of superposition of adequate criterions. Some of the criterions might also implement behavioral principles: we utilize desirability as the weighted criterion actions involved in one behavior set. Moreover the desirability accepts cross reinforcements among consequents and relation-based navigation in the state space.

We put into control system the behaviors in several layers [2]. Namely a duplex communication in a generalized layer interpretation makes an efficient tool to integrate several behavior preconditions in one act – it could be done in form of b cues coming from several domains. At social domain level, global parameters determine major aims of social behavior. Then each individual robot domain accepts parameters as external consequents of goal-oriented acts. They are taken to be input cues for his decisions. Applied reactive action selection mechanism (ASM) for singular robots takes participation in the task according to actual opportunity. It includes also adequate individual robot responsibility for final task achievement. During each derivation step, the control system rates local impact in differential phenomenon (integral one for social impact respectively).

As a background of such communicative system conception one can apply also results from formal language theory [3]. Our multi-domain hybrid architecture was formalized in the eco-grammar system framework. Eco-grammatical frame concerns evolutionary rules and action ones of group behavior. Parametrical L-systems make particular elements to describe multiple movements over shared environment. Evolutionary rules induce an inner string representation from local perception. Attractive, opposite and coherent communication patterns were introduced to be basic communication channels to goal-oriented ASM. Additive parameters received from participants allow foraging robots, more balanced in the task context.
Experiments with real community of four mobile robots demonstrated key features of the hybrid architecture deployment. There were perceived many attractive cues emerging from the real robot performance. As the social feedback, they allowed next refining reaction. Especially in cases that the reaction was represented by brief sense information.

Following research activities will be focused to spread ASM to large network – on the social layer one can adapt the individual navigation rules to large traffic split decomposition. It should

be scaled to permanent event occurrence, solving a limited channel capacity well-known from telecommunication area (daily in real time routing hundreds million communication events).

References:

[1] SVATOŠ, V. - KURZVEIL, J. - NAHODIL, P.: *Imitation Principle to Navigation in Robot Group.* In: IFAC Workshop on Mobile Robot Technology. Seoul: IFAC, 2001, vol. 1, 2001, 140-145

[2] SVATOŠ, V. *Behavioural Formation Management in Robotic Soccer.* LNAI 2159. Berlin: Springer, vol. 1 2001 553-562.

[3] SVATOŠ, V. *Low-band Communication to Dynamical Role Assignment in Robotic Soccer* CTU 2002 348-349.

Laboratory Station for Video Signal Processing

J. Volf

volfj@fel.cvut.cz

Department of Telecommunication Engineering, Faculty of Electrical Engineering,
Czech Technical University in Prague, Technická 2, 166 27, Praha 6 - Dejvice

The paper deals with the innovation of the subject Digital signal processing in Telecommunications. Main goal of the innovation is the preparation of three laboratory stations for video signal processing. These stations are realized in form of DSP development kits TMDXDSK6416-TE based on TMS320C64x (Texas Instruments) with a Video Daughter Board for C6000 EVM/DSK used for video signal processing. The changes will be introduced to education starting in winter semester 2006.

Old Seminar Syllabus

- Program tools for the analysis and synthesis of discrete systems
- Matlab basics
- Integral transforms (DFT, FFT, DCT)
- Analysis and synthesis of digital IIR filters
- Analysis and synthesis of digital FIR filters
- Decimation and interpolation filters, signal resampling
- Development tools for the realization of digital systems using digital signal processors
- Instruction sets of digital signal processors
- Design and simulation of discrete systems
- Discrete system realization
- Speech compression
- Test
- Evaluation of the properties of discrete systems

New Seminar Syllabus

- Program tools for the analysis and synthesis of discrete systems Matlab basics
- Integral transforms, decimation, interpolation, resampling
- Analysis and synthesis of digital IIR and FIR filters
- DSP VLIW TMS320C6x
- Development tools for DSP, Code composer studio, DSK 320C6711
- Implementation of convolution and correlation on DSK TMS320C6711
- Implementation of echo on DSK TMS320C6711
- Implementation of FFT, DFT, DCT on DSK TMS320C6711.
- Implementation of DTMF coding and decoding on DSK TMS320C6711
- Implementation of echo canceling on DSK TMS320C6711
- Implementation of motion detection on DSK TMS320C6416
- Implementation of image filtering on DSK TMS320C6416
- Presentation of semester projects

Today a lot of communication over large distances has the need of video signal transmission. So the students should be prepared for video signal processing. Within education of telecommunication engineering at the Czech Technical University in Prague, traditionally practical training in the digital signal processing (DSP) was mainly based on Matlab experiments in the past. In order to cope with progress in DSP technology, new laboratory exercises were made for students to become familiar with new types of processors and extended equipment for video processing. Practical training is based on the Very Long Instruction Word (VLIW) DSPs with the fix point (320C6416) arithmetic in form of commercial DSP Starter Kits (DSK) TMDXDSK6416-TE. In order to make training more efficient, special daughter cards for video processing were purchased. The CCD video camera HDR-SR1E is used as an extended part to all three lab stations. The camera brings to these laboratory stations the possibility of processing of real-time video signals.

The combination of a video daughterboard with DSK forms very strong utility for the development of video signal processing applications such as:

- Video surveillance system
- Security cameras
- Video monitoring system (Process industry)
- Personal video recorder (Set-Top Box)
- Digital video recorder (Security Systems)
- Video phones and video conferencing application
- Networked video application
- Video base station
- Imaging application
- 3-D graphics application

The Video Daughterboard (vDB) presents a modular approach and provides functions to meet the requirements of standard video interfaces compliant to TMS320 crossplatform daughterboard specifications V1.0.

References:

[1] VOLF, J.: *Lab Station for Video Signal Processing,* Proceedings of the conference Research in Telecommunication Technology RTT2006, September 2006, pp. 211-213, ISBN 80-214-3243-8

[2] TI *Semiconductors,* [online], 2006, <www.ti.com>

[3] EI *eInfochips,* [online], 2006, <www.einfochips.com/newsroom/vdb_pr.html>

This research has been supported by by the Ministry of Education, Czech Republic under project No. FRV 1021/G1.

Methodical handbook for creating multimedia courses

M. Fejtová, P. Novák

fejtovam@k333.felk.cvut.cz; novakpe@labe.felk.cvut.cz

Department of Cybernetics, Faculty of Electrical Engineering, Czech Technical University, Technická 2, 166 27 Prague 6, Czech Republic

Due to ever faster development of science and technology, the knowledge acquired during the study before entering the job market is not sufficient for the life-long career. The significance of life-long education is growing. Therefore there are being sought new forms of education that are accessible for broad public and which enable individual approach and optimal utilization of precious time of employed people. These requirements can be reached by combination of classical methods with new information and communication technologies (ICT) – approach nowadays called blended e-learning. This approach is suitable for most of the topics relevant for the life-long learning – the only condition of its utilization is computer literacy of its users. Our aim has been to develop simple, illustrative, well-arranged, structured, and easily understandable teaching materials suitable for combined form of study and for self-study that can be efficiently used by all users who want to acquire practical skills for utilization of modern computer and information technologies.

During last decade in advanced countries stress has been laid on versatile satisfaction of one of the basic human rights – right education. However education is not limited to primary education (continuous education of an individual from kindergarten to university level); education must be offered during the whole life – then we speak about life-long learning. Developed systems of life-long learning enable to individuals to enter the process of self-education any time in their career corresponding with changing tasks or perceived needs in their jobs or personal interests. Lifelong learning means expansion of educational process out of schools.

Concepts about structuring information today stem largely from the organization of printed books and periodicals and the library indexing and catalog systems that developed around printed information. The "interface standards" of books in the English-speaking world are well established and widely agreed-upon, and detailed instructions for creating books may be found in such guides as *The Chicago Manual of Style.* Every feature of the book, from the contents page to the index, has evolved over the centuries, and readers of early books faced some of the same organizational problems that users of hypermedia documents confront today. Gutenberg's Bible of 1456 is often cited as the first modern book, yet even after the explosive growth of publishing that followed Gutenberg's invention of printing with movable type, more than a century passed before page numbering, indexes, tables of contents, and even title pages became expected and necessary features of books. Web documents are undergoing a similar evolution and standardization.

The graphic user interface (GUI) of a computer system comprises the interaction metaphors, images, and concepts used to convey function and meaning on the computer screen. It also includes the detailed visual characteristics of every component of the graphic interface and the functional sequence of interactions over time that produce the characteristic look and feel of educational courses – Web pages and hypertext linked relations. Graphic design and visual "signature" graphics are not used simply to enliven Web pages — graphics

are integral to the user's experience with your site. In interactive documents graphic design cannot be separated from issues of interface design.

Although networked interactive hypermedia documents pose novel challenges to information designers, most of the guidance needed to design, create, assemble, edit, and organize multiple forms of media does not differ radically from current practice in print media. Most Web documents can be made to conform to *The Chicago Manual of Style* conventions for editorial style and text organization. Much of what an organization needs to know about creating clear, comprehensive, and consistent internal publishing standards is already available in such publishing guides as the *Xerox Publishing Standards: A Manual of Style and Design.* Don't get so lost in the novelty of Web pages that basic standards of editorial and graphic design are tossed aside.

We seek clarity, order, and trustworthiness in information sources, whether traditional paper documents or educational courses. Effective page design can provide this confidence. The spatial organization of graphics and text on the Web page can engage readers with graphic impact, direct their attention, prioritize the information they see, and make their interactions with your Web site more enjoyable and efficient.

Graphic design creates visual logic and seeks an optimal balance between visual sensation and graphic information. Without the visual impact of shape, color, and contrast, pages are graphically uninteresting and will not motivate the viewer. Dense text documents without contrast and visual relief are also harder to read, in the case of for example relatively low-resolution screens of personal computers. But without the depth and complexity of text, highly graphical pages risk disappointing the user by offering a poor balance of visual sensation, text information, and interactive hypermedia links.

The content of the methodical handbook is transparently structured into several blocks:

- Introduction
- The CMS system Joomla
- The educational system Moodle
- The design of educational pages
- The work with a pictures
- The video creating

References:

[1] M. FEJTOVÁ, J. FEJT, L. LHOTSKÁ: *E-learning System MultiPeS,* EUNITE 2003, Verlag Mainz, Aachen. ISBN 3-86130-194-6. 2003, pp. 377-383.

[2] M. FEJTOVÁ, J. FEJT, L. SEDLÁČEK, L. LHOTSKÁ: *E-learning Courses in the MultiPeS Systém,* IADIS Press, Lisboa, 2003, vol. 1,2. ISBN 972-98947-0-1., 2003, pp. 949-952.

[3] M. FEJTOVÁ, J. FEJT, P. SMRČKA, L. LHOTSKÁ: *E-learningový kurz základů počítačové gramotnosti v systému MultiPeS,* In E-learning v České a Slovenské republice. Praha: ČVUT, díl 1, ISBN 80-01-02923-9., 2004, pp. 184-189.

This work is based upon work sponsored by the Ministry of Education, Youth and Sports grant No. FRV 2876 F1d "Methodical handbook for creating multimedia courses".

User Modelling in Adaptive Systems

M. Balík, I. Jelínek

balikm1@fel.cvut.cz

Department of Computer Science and Engineering,
Faculty of Electrical Engineering, Czech Technical University,
Karlovo náměstí 13, 121 35 Praha 2, Czech Republic

On the web there is plenty of information and the amount of this information basis is permanently growing. It is convenient to help users to find the appropriate information according to his or her preferences, abilities and limitations. The remedy for these requirements is the system with an ability to adapt its behaviour – adaptive system. The research in the field of adaptive hypermedia has already stared in the early 1900. Since then several models for adaptive hypermedia have been developed. General representatives of these models are for instance the Adaptive Hypermedia Application Model (AHAM), the Munich reference model, the Fundamental Open Hypermedia Model (FOHM) or the Goldsmiths Adaptive Hypermedia Model (GAHM). Unfortunately the existing models were mostly oriented at ad-hoc purposes and are not suitable for general use. Such solutions still need to be developed. Nowadays the research area of adaptive web attracts many researchers from different communities such as hypertext, user modeling, machine learning, natural language generation, information retrieval, intelligent tutoring systems, cognitive science and Web-based education.

In our research we studied the existing models of adaptive hypermedia, compared them and tried to reveal their major disadvantages [1]. As we have already mentioned above, the models do not provide the universality in their expressiveness. The developed adaptive applications are isolated and are not able to interchange data. The user model is created by observing each user individually and the commonalties in user groups and communities are not utilized. On the other hand the adaptation conducted by the system is equal for all of the users. In the time, when adaptive systems are becoming essential in the domain of mobile devices, it is also important to adapt the system to satisfy various limitations of a particular device. Even more it is possible to adapt the application to the user's current location or time. To correctly comply with users needs, some feedback from the user is also necessary.

Although each adaptation model uses different representation of hypermedia structures and different approaches to manipulating them, there are important underlying commonalities in terms of the components found within adaptive hypermedia systems and the interactions between them [3]. We can assume the Generic Adaptivity Model (GAM) [4] to be a partial indication of the universal approach problem solution. The GAM is based on rules like the AHAM model. It extends the classic "user modeling – adaptation" loop proposed by Brusilovsky in 1996 [2]. The part responsible for processing the user model to get the answer that the application wants is called pull adaptation. The other part where the user model is transformed based on the events is called push adaptation. This state-machine model is a theory based on interactive systems. In our research we want to proceed from this proposal and develop necessary extensions.

In our further research we want to find solutions for disadvantages in current adaptive systems. We want to extend the model with an ontology representing semantics of the user model. For this purpose the use of application independent, modular and layered ontologies would be optimal. Such knowledge representation would enable to interchange data between applications. Such approach will also enable to share user preferences in a distributed environment. We will also focus on collaborative modeling of users. To be capable of

separation of users into groups, a metric of similarity needs to be defined. This will enable the classification of users depending on their preferences. The theoretical results will be verified by an experimental system, which we plan to develop.
Results of our research will be utilizable in many hypermedia applications. It will not only facilitate the work of many users, but it will also serve to hypermedia system developers.
The results of our research are part of the work of a special research group WEBING (http://webing.felk.cvut.cz).

References:

[1] BALÍK M. – JELÍNEK, I.: *Modelling of Adaptive Hypermedia Systems* In Proceedings of the Interenational Conference on Computer Systems and Technologies. Varna: Academy of Sciences, 2006, p. V-8-1-V-8-6. ISBN 954-9641-46-5.

[2] BRUSILOVSKY P.: *Methods and techniques of adaptive hypermedia* User Modeling and User-Adapted Interaction, 1996, 6(2-3), 87-129.

[3] OHENE-DJAN J. – GORLE M. – BAILEY CH.P. – WILLS G.B. – DAVIS H.C.: *Is it possible to devise a unifying model of adaptive hypermedia and is one necessary?* AH2003: Workshop on Adaptive Hypermedia and Adaptive Web-Based Systems, 2003

[4] DE VRIEZE P. – VAN BOMMEL P. – VAN DER WEIDE T.: *GAM: A Generic Model for Adaptive Personalization* Technical report: ICIS-R06022, June, Radboud University Nijmegen, 2006

This research has been supported by MSMT under research program No. 6840770014.

This research has been suported by the grant of the Czech Grant Agency No. 201/06/0648.

Constrained Longest Common Subsequence Problem for Generalized Strings

M.Voráček

voracem@fel.cvut.cz

Department of Computer Science and Engineering, Faculty of Electrical Engineering,
Czech Technical University, Karlovo náměstí 13, 121 35 Prague 2, Czech Republic

In this paper, we present a new algorithmic problem – the *constrained longest common subsequence problem for generalized strings* and we present a finite automata based algorithm for solving the presented problem working in $O(|A| n m r)$ time, where $|A|$ is size of alphabet, n and m are the lengths of input generalized strings and r is the length of the input constrained subsequence.

A string is a sequence of symbols from a given alphabet A. A subsequence u of a string x is obtained by deleting some characters from u (not necessarily contiguous). Given two strings x and y, u is a common subsequence of x and y if u is a subsequence of both x and y. u is the *longest common subsequence (LCS)* of x and y if u is the longest among all subsequences of x and y. Let v be a constrained sequence. u is called *constrained LCS (CLCS)* of x and y with respect to v if u is *LCS* of x and y and v is subsequence of u. The *CLCS problem* is to find for given two strings x and y of length n and m, respectively and a given sequence v of length r their LCS with respect to v.

The CLCS problem was introduced by Tsai in [3] and the first algorithm solving the problem with $O(n^2 m^2 r)$ time complexity was presented in the same paper. Later, Chin et al. presented in [4] an algorithm solving the CLCS problem with $O(n m r)$ time and space complexity.

In this paper, we extend the definition of the CLCS problem for generalized strings. Generalized strings are special strings having a set of symbols instead of one symbol in a single position, $x = \{a\}\ \{c, g\}\ \{g\}\ \{a, c, t\}\ \{a, c\}$ is an example of a generalized string. Generalized strings are extensively used in molecular biology to express polymorphism in *DNA* sequences, e.g. the polymorphism of protein coding regions caused by redundancy of the genetic code or polymorphism in binding site sequences of a family of genes.

The CLCS problem for generalized strings is defined as follows: given two generalized strings x and y of length n and m, respectively and given a constrained sequence v of length r, the task is to find the LCS of x and y with respect to v.

Our algorithm solving the CLCS problem for two generalized strings consists of five stages. In the first stage, we construct for generalized string x and y automaton M_1, M_2, respectively, accepting all its subsequences ($Lang(M_1)=Sub(x)$, $Lang(M_2)=Sub(y)$). In the second stage, we create an intersection of automata M_1 and M_2 and we construct thus automaton M_3 accepting all common subsequences of x and y. In the third stage, automaton M_4 accepting all strings containing sequence v as a subsequence is built. In the forth stage, we create an intersection of automata M_3 and M_4 and we get thus automaton M_5 accepting all common subsequences of x and y containing sequence v as a subsequence. In the last step, we find the longest path in the transition diagram of automaton M_5. The concatenation of labels of transitions along the found longest path corresponds to the constrained longest subsequence of x and y with respect to v.

The automata being constructed in the first stage are built using algorithm presented in [1]. The construction requires $O(|A| n)$ time and space and the resulting automaton has $n+1$ states and at most $|A| n$ transitions and its transition diagram is an acyclic directed graph. The

algorithm for construction of an automaton for intersection of the languages represented by two given automata *M', M''* used in the second and the forth stage is the standard algorithm described e.g. in [5] working in $O(|A| |M'| |M''|)$ time and space. The resulting automaton has at most $O(|A| |M'| |M''|)$ states. The automaton used in the third section is built according to the algorithm described as well in [1] in $O(|A| n)$ time and space and it has $n+1$ states and at most $|A|n$ transitions. The fifth steps utilizes the algorithm for creation of topological ordering in directed acyclic graph working in time proportional to the number arcs of the considered graph.

From the previous it follows: the first stage takes $O(|A| n) + O(|A| m)$ time and space, the second stage requires $O(|A| n m)$ time and space, the third stage requires $O(|A| r)$ time and space, the forth stages takes $O(|A| n m r)$ time and space and finally, the fifth space takes as well $O(|A| n m r)$ time and space. Hence, the total space and time complexity of the presented algorithm is $O(|A| n m r)$.

We introduced the *constrained longest common subsequence problem for generalized strings*. We presented a finite automata based algorithm for solving the presented problem working in $O(|A| n m r)$ time, where $|A|$ is size of alphabet, n and m are the lengths of input generalized strings and r is the length of the constrained subsequence.

References:

[1] VORÁČEK, M.: *Searching subsequences in degenerate strings,* Submitted for publication, 2007.

[2] POLCAR, T., MELICHAR, B.: *The longest common subsequence problem - A Finite Automata Approach. In Proceeedings of CIAA 2003.* Berlin Heidelberg: Springer-Verlag, 2003, pp. 294–296.

[3] TSAI, Y. T.: *The constrained longest common subsequence problem. Inform. Process. Lett. 88* . Elsevier, 2003, pp. 173–176.

[4] CHIN, F. Y. L., DE SANTIS, A., FERRARA, A. L., HO, N. L., KIM, S K. : *A simple algorithm for the constrained sequence problem. Inform. Process. Lett. 90* . Elsevier, 2004, pp. 175–179.

[5] HOPCROFT, J. E., ULLMAN, J. D.: *Introduction to automata, langauages and computation.*. Reading: Addison-Wesley, 1997,

Evaluation of 3SQM algorithm performance on fixed point DSP

P. Slepička, Z. Bečvář

slepicp@feld.cvut.cz

CVUT, FEL, Departement of telecommunication technology

Introduction

Especially with transition to packet oriented telecommunication services arises the need to non-intrusively measure, for long periods of time, the quality of transmitted voice signal. The quality of transmitted speech signal allows then the estimation of the quality of the transport (most often IP based) network between the network endpoints. For the telecommunication operator who usually only has access to the one end of the system this can often present the only option of evaluating the quality of the whole communication chain. ITU-T recommendation P.563 [1] specifies the 3SQM algorithm which is intended for non-intrusive voice quality prediction. This recommendation comes with an example C source code of 3SQM algorithm which can be used for evaluation purposes. The C code has been compiled and used to evaluate the possibility of porting the code on widely used Texas Instruments fixed point signal processor C64xx .

Overview of 3SQM algorithm

The 3SQM algorithm, according to ITU-T P.563 is applicable for speech quality predictions without a separate reference signal. For this reason this method is recommended for non-intrusive speech quality assessment, live network monitoring and assessment by using unknown speech sources at the far-end side of a telephone connection. This can provide significant advantage for telecom operators in providing them with a possibility to monitor live calls at all times without the need to insert artificial reference calls into the systems. Earlier methods for speech quality assessment of such systems, such as ITU-T Recommendation P.862 (PESQ) [2] , require either a reference signal or they calculate only quality features based on a restricted set of parameters like level, noise in speech, pauses, echoes or in the case of VoIP on factors like percentage of lost packets and delay [3].

The principle of 3SQM operation is as following. First some signal normalization processing is performed on the input signal. This includes IRS filtering ,signal normalization and voice activity detection. In the second stage of operation , 12 parameters based on the processed input signal are calculated. These parameters take in account speech level, noise, delay, repeated frames, disruptions in pitch period, artificial components in speech signal (beeps, clicks). These 12 parameters are then linearly combined to form the final speech quality prediction (in MOS scale).

3SQM performance on DSP based systems

For evaluating the performance on DSP systems the fixed point signal processor C64xx manufactured by Texas Instruments has been chosen as widely spread processor used in telecommunication systems for speech signal processing. The C code has been compiled in CCStudio, a development tool by Texas instruments, and run on starter kit with C6455 processor clocked 1GHz.

During processing the algorithm always uses floating point representation of the signal. More specifically in C it is 4 byte long type float. This type is not suitable for C64xx type processors as all floating point calculations are done through emulation which is quite slow compared to calculation done in fixed point. 3SQM algorithm operates on the whole length of input signal, which is stored in dynamically allocated memory in several copies for different processing functions. During processing additional memory segments of the size of the input signal are dynamically allocated. This results in very large memory consumption and further slows down the algorithm. That is given by the fact that C64xx can have approximately 1 MB (depending on cache configuration) of fast internal memory used for dynamic memory allocation and additional data has to be stored in about 6x slower external memory. For example 10 second of speech signal in float type need 320kB of memory for one copy only (more then five copies are needed). Without rewriting most of the code and introducing memory management this resulted in the need to place all the speech data into external memory.

When compiled 3SQM code, with all compiler optimalization features turned on, was run on C6455 starter kit, it was found out that real time operation is not possible and DSP and external memory would have to run at more than twice its current frequency for real time performance.

3SQM performance on PC system

3SQM reference implementation performance has also been examined on PC system with Athlon64 3200+ processor and compared to performance of reference implementation of PESQ algorithm (ITU-T P.862). For 17 second input file the calculation took 4.0 second for 3SQM algorithm and 1.6 second for PESQ algorithm. This result shows that current PC based systems are capable of working with better than real time performance and mostly demonstrates the fact that x86 processors come with floating point coprocessor.

Conclusion

The reference C implementation of 3SQM algorithm is not suitable for fixed point signal processors because of performing calculations only in floating point and large memory consumption . To port the code to fixed point processor without fully rewriting it into fixed point arithmetic, which would be a colossal task, the possibility of introducing memory management that would move the data between cache or internal memory and external memory should be investigated as less demanding task.

Floating point DSPs are not so widely used in speech processing however the performance of reference code on floating point DSP should be investigated, because the floating point DSP is a more appropriate platform for code using floating calculations. Estimation based on experience for TI manufactured floating point processors is that floating point calculation are performed about 3x faster than on fixed point processors.

References:

[1] ITU-T *P.563 - Single ended method for objective speech quality assessment in narrow-band telephony applications* ITU-T 05/2004

[2] ITU-T P.862 *Perceptual evaluation of speech quality (PESQ): An objective method for end-to-end speech quality assessment of narrow-band telephone networks and speech codecs* ITU-T 02/2001

[3] TELCHEMY INC. *VQMon algorithm* www.telchemy.com\vqmonep.html

Innovation of subject "Integrated Services Network"

Pavel Bezpalec

bezpalec@fel.cvut.cz

Department of Telecommunication Engineering, Czech Technical University in Prague, Faculty of Electrical Engineering, Technicka 2, 166 27 Praha 6, Czech Republic

For a graduate in our profession it is important to gain not only theoretical foundation through education, but also an adequate practical proficiency. The main aim of the project was to innovate educational process in subject "Integrated Services Network" in practical courses as well as in theoretical level.

Innovation of practical courses

Main work has been done in innovation of practical courses. Refreshed practical courses syllabus contains theoretical workshops as well as four practical tasks.

Task 1 ISDN Basic Access Complementary Services
Task 2 Ref. point S/T – Signalization Analysis
Task 3 B- and D-channel Data Transmission Analysis
Task 4 Terminal Adapters

Innovation of theoretical workshops

Seven theoretical workshops consist of segment of theory and segment of simulation presentation. Simulation should enrich educational process with demonstration of behavior theoretically known methods and principles.

Simulations are mainly in a manner of

- primitives exchange in multilayer reference model
- statistical TDM
- collision avoidance in D-channel
- frame exchange
- message exchange
- call flow

All simulations are done by multimedia presentation.

Innovation of practical tasks

All input study materials for practical tasks have been innovated and transformed into Internet-ready form and then published to server that belongs to our department (www.comtel.cz → Předměty → 32SIS → Materiály pro výuku) and therefore are anytime easily accessible by students.

Innovation of Task 1 – new terminal endpoint as well as material and tools to successful task realization (cables, connectors …) has been bought, repaired and re-measured.

Innovation of Task 2 – new laboratory measurement device that can catch all of event (bits, frames and messages) exchange between communicating parties and well arranged results present on a monitor screen has been bought.

Innovation of Task 3 – old laboratory local private branch exchange (PbX) has been filled in with new equipment that can realize and analyze D-channel data transmissions.

Innovation of Task 4 – new terminal adapters equipped by software analysis tools for detailed analysis of all basic conversional services of data rate adaptation in ISDN has been bought.

Innovation of theoretical lectures

The revised basic of telco knowledge that has been deeply studied has extended a spectrum of lectures. Mainly English written literature has been translated into new lecture base that is in form of MS PowerPoint presentation. This chosen format is able to show new concepts with animated explanation. This is more didactical. An electronic form of new lectures has been placed on Internet (www.comtel.cz → Předměty → 32SIS → Materiály pro výuku) and therefore is easily accessible by students.

Conclusion

Main goals of subject innovation are:

- New knowledge implementation.
- New simulation implementation in theoretical workshops.
- Workplace innovation for practical tasks.
- Practical tasks optimization and material, tools and device complementation.
- New study material creation for theoretical parts of course.
- All study material is now in electronic form of presentation.
- Motivation of students to study modern telco technologies.

References:

This research has been supported by FRVS grant No FRV 867/F1a.

Intelligent web technologies

Ivan Jelínek

jelinek@fel.cvut.cz

Department of Computer Science and Engineering, FEE CTU in Prague
Karlovo nám. 13, Praha 2, 121 35

Present-day web is at the crossroads of development – on one hand the amount of information on the web astronomically grows, on the other hand the number of common web users grows enormously and so the present technologies of data representation and information retrieval angles at their limits. The solution of this situation is not to "educate" more advanced web users but, on the contrary, the solution is: from one side to adapt the communication with web to natural human thinking and human behavior and from the other side to transfer "the thought what the web user searches on the web, indeed" to computer platform. That means the solution is to design such data representation (and access to it) which should respect the semantic of the information in such way that make possible simple semantic processing and that make possible in accordance to abilities and needs of particular user correct information interpretation. And the proposed project deals with these challenges. Expected assets in the frame of information technology are and among investigated areas belong especially:

– research on intelligent and heuristic technique to *support information searching* in web environment,
– research on searching methods on the web with consideration to *the semantics the information* sought,
– investigation on *adaptability of access to information* on web according to the user requirements, types and possibility,
– formulation and implementation of *integrated access to heterogeneous type of information* on the web.

Research team

- Ivan Jelínek, head of the team, associate professor
- Lukaš Bařinka, secretarial assistant, assistant professor
- Miroslav Bureš, head of sub-team, former PhD student + assistant professor
- Martin Švihla, head of sub-team, PhD student
- Martin Ota, head of sub-team, PhD student + assistant
- Martin Balík, member, PhD student
- Tomáš Havryluk, member, PhD student
- Radek Jun, member, PhD student
- Ladislav Čmolík, member, PhD student
- Martin Klíma, member, PhD student + assistant professor
- Michael Valenta, member, assistant professor

The target of the grant project 201/06/0648 is to suggest new intelligent solutions in the web technologies area, which would qualitatively improve the user access to information on the web. By the formulation of the main aspects of proposed solution of the project we put emphasis to structure the main goal to sub-goals not only in the topics but also in the time. *Research covers three basic areas of the web intelligence and eight of its sub-domains*:

Task A. Intelligent methods of information searching on the web
  Subtask A-1) Semantic searching on the web
  Subtask A-2) Intelligent search engine
  Subtask A-3) Heuristic searching methods on the web
Task B. Adaptation of information of hypertext documents
  Subtask B-4 Adaptive navigation on the web
  Subtask B-5) Intelligent hypertext documents
  Subtask B-6) Adaptive hypertext documents for education
Task C. Unification of access to information on the web

Subtask C-7) Integrated access to information on the web
Subtask C-8) Integrated production IS on the web

References - results:

[1] Balík, M. - Jelínek, I.: Modelling of Adaptive Hypermedia Systems. In Proceedings of the Interenational Conference on Computer Systems and Technologies. Varna: Academy of Sciences, 2006, s. V-8-1-V-8-6. ISBN 954-9641-46-5.

[2] Bureš, M. - Jelínek, I.: Decision Theorem for Construction of Adaptive Hypermedia System. In Proceedings of the IASTED International Conference on Web Technologies, Application and Services (WTAS 2006) [CD-ROM]. Calgary: Acta Press, 2006,

[3] Bureš, M. - Jelínek, I.: Integration of User Data in Adaptive Hypermedia System. In Proceedings of the I International Conference on Multidisciplinary Information Sciences and Technologies, InSciT2006. Badajoz: Open Institute of Knowledge, 2006, vol. 1, s. 247-251. ISBN 84-611-3104-5.

[4] Bureš, M. - Jelínek, I.: SACS - Pilot Implementation of System Providing AICC-Compliant Reusable Adaptive Hypermedia E-Learning Content. In Proceeding of IADIS International Conference e-Society 2006. Lisboa: IADIS Press, 2006, vol. 2, s. 44-48. ISBN 972-8924-16-X.

[5] Havryluk, T. - Jelínek, I.: Peer-to-Peer Semantic Search Engine. In Proceedings of the Interenational Conference on Computer Systems and Technologies. Varna: Academy of Sciences, 2006, s. V-10-1-V-10-6. ISBN 954-9641-46-5.

[6] Jun, R. - Jelínek, I.: Adaptive Web based on Semantic Model. In Proceedings of the Interenational Conference on Computer Systems and Technologies. Varna: Academy of Sciences, 2006, s. V-12-1-V-12-6. ISBN 954-9641-46-5.

[7] Ota, M. - Jelínek, I.: Data Exchange in CAD During Iterative Work with Heterogeneous Systems. In Cooperative Design, Visualization, and Engineering. Lecture Notes in Computational Science. 2006, vol. 4101/2006, no. 4101, s. 25-32. ISSN 1439-7358, ISBN 3-540-44494-7.

[8] Švihla, M. - Jelínek, I.: Leveraging Semantic Web Technologies to Integrate Information Related to Academic Papers. In Electronic Publisher of eChallenges e-2006 Conference Proceedings [CD-ROM]. Dublin: IIMC International Information Management Corporation Ltd, 2006, ISBN 1-905824-02-5.

[9] Švihla, M. - Jelínek, I.: Simple Semantic Information Sharing between Websites in one Knowledge Domain. In Proceeding of IADIS International Conference e-Society 2006. Lisboa: IADIS Press, 2006, vol. 2, s. 375-377. ISBN 972-8924-16-X.

[10] Toth, D. - Valenta, M.: Using Object And Object-Oriented Technologies for XML-native Database Systems. In DATESO 2006: Databases, Texts, Specifications, Objects. Ostrava: VSB-TUO, Department of Computer Science of FEI, 2006, s. 6-13. ISBN 80-248-1025-5.

[11] Klima M., Cmolik L., Slavik P. Collaborative Learning in Mobile Environment. In Proceeding of IADIS International Conference CELDA 2006, Barcelona, Spain. IADIS Press, 2006, s. 335-339. ISBN 972-8924-22-4.

[12] Klíma, M. - Slavík, P.: Jabber Based Protocol for Collaborative Mobile Work. In Cooperative Design, Visualization, and Engineering. Lecture Notes in Computational Science. 2006, vol. 4101/2006, no. 4101, s. 9-16. ISSN 1439-7358, ISBN 3-540-44494-7.

[13] Ota, M.: Electronic Service Book. In Proceedings of 13th CIRP International Conference on LIFE CYCLE ENGINEERING . Leuven: Katolieke Universiteit Leuven, 2006, s. 507-512. ISBN 90-5682-712-X.

[14] Richta, K. - Valenta, M. - Vraný, J.: CellStore Project – Object Implemetation of native XML RDBMS. In Objekty 2006. Ostrava: Technická universita Ostrava - Vysoká škola báňská, 2006, s. 51-64., in Czech

[15] Bureš,K.: Formal Description of Adaptive Hypermedia System, Doctoral Thesis, FEE CTU Prague, defended October 22, 2006

This research has been supported by the grant of the Czech Grant Agency No. 201/06/0648.

Improvements of the Subject Digital Signal Processing in Telecommunication

B. Šimák

simak@fel.cvut.cz

Department of Telecommunication Engineering, Faculty of Electrical Engineering, Czech Technical University, Technická 2, 166 27 Praha, Czech Republic

The project deals with the innovation of the subject Digital signal processing in Telecommunication. The changes were introduced in the education starting the winter period 2006. The old syllabus along with the new syllabus of both the lectures and seminars are included. The new topic is represented by the leading edge high performance digital signal processors TMS320C6x from Texas Instruments.

The practical training in the digital signal processing (DSP) in the education of the telecommunication engineering at the department of Telecommunication engineering of the Czech Technical University in Prague was traditionally based mainly on Matlab experiments in the past. Only few seminars were devoted to the old generation of Digital Signal Processors (DSP) TMS320C50. In order to cope with the advances in the DSP technology, the syllabus of the subject was substantially changed. The practical training is based on the Very Long Instruction Word (VLIW) DSPs, both with the floating point (TMS320C6713) and fix point (TMS320C6416) arithmetic in form of commercial DSP Starter Kits (DSK) [1]. In order to make the training more efficient several special daughter cards were designed and realized. The best students can design and realize their own special purpose hardware using our universal daughter cards.

Old Syllabus of the Lectures

Analog and digital signals, conversion
Integral transforms
Implementation of transformation procedures
Design of digital IIR filter
Design of digital FIR filter
Decimation and interpolation filters
Noise properties, stability of digital filters, architectures of the digital signal processors
Adaptive filtering
Digitizing of speech
Parametric coding
Digitizing of broadcast related signals
Digitizing of images and video signals

New Syllabus of the Lectures

Analog and digital signals, conversion
Integral transforms
Implementation of transformation procedures
Design of digital IIR filter
Design of digital FIR filter
Decimation and interpolation filters

Digital Signal Processors, introduction, VLIW architecture
Noise properties, stability of digital filters
DPS TMS320C6x, instruction set, architecture
Design of systems with DSP
Adaptive algorithms in telecommunication
Digitizing of speech, parametric coding
Digitizing of broadcast related signals, images and video signals
Digital image processing, compression

Old Syllabus of the Seminars
Program tools for the analysis and synthesis of discrete systems
Matlab basics
Integral transforms (DFT, FFT, DCT)
Analysis and synthesis of a digital IIR filters
Analysis and synthesis of a digital FIR filters
Decimation and interpolation filters, signal resampling
Development tools for the realization of digital systems using digital signal processors
Instruction sets of digital signal processors
Design and simulation of discrete systems
Realization of discrete system
Speech compression
Test
Evaluation of the properties of the discrete systems

New Syllabus of the Seminars
Program tools for the analysis and synthesis of discrete systems
Matlab basics, advanced topics
Integral transforms, decimation, interpolation, resampling
Analysis and synthesis of digital IIR and FIR filters
DSP VLIW TMS320C6x
Development tools for DSP, Code composer studio, DSK 320C6713
Implementation of convolution and correlation on DSK TMS320C6713
Implementation of echo on DSK TMS320C6713
Implementation of FFT, DFT, DCT on DSK TMS320C6713
Implementation of DTMF coding and decoding on DSK TMS320C6713
Implementation of echo cancelling on DSK TMS320C6713
Implementation of motion detection on DSK TMS320C6416
Implementation of image filtering on DSK TMS320C6416
Presentation of individual projects

References:

[1] WWW.TI.COM

This work has been supported by MŠMT grant No. FRVŠ F1-2520.

Hotel Yield Management Matlab Toolbox

T. Vítek*, D. Pachner*

vitekt2@centrum.cz

*Department of Control engineering, Faculty of Electrical Engineering, Czech Technical University, Technická 2, 166 27 Prague 6, Czech Republic

The tourisms is a very important segment of a grant national product of many European countries. The availability of Internet allows customers to compare and exploit accommodation offers from the whole target region. As the standard and quality of accommodation grew over last years to very high indifferent level, the price seems to attract the customers most. On the side of the providers is the situation not easy. They usually have a good knowledge of their traditional set of customers, however the new trends in business (last minute sales, sales over internet, larger set of potential customers from various countries) stands them in front of many strategic choices that directly impact profit of their accommodation facility. Our project goal is to enhance chances of small and middle size hotel owners to make a good strategic decision. The key idea is to formulate a pricing strategy of a provider as a sequential decision problem, which can be transformed into an optimal control problem. The yield management can therefore be understood as a new application field for the model based prediction control, MPC. It can be shown that the hotel yield management problem can be cast as a MPC feedback control problem. The yield management support product is being developed by the university team in co-operation with Czech hotel association and DataPartner Ltd under the auspices of Czech Ministry of Trade. The product hotelPartner will be commercially available soon.

In general, a yield management system is understood to be a decision tool system aiming to optimize the provider's net revenue. Here, any service or resale business can be the optimized activity of interest. Beside the price, there are always a number of other decisions the provider has to take. By a computer based decision support system, only a few can be optimized algorithmically. These are mainly the numerical decisions such as prices. There are strategic management decisions like what will be the next business market orientation, what services will be offered, which new market segments should be won in the future. These decisions can hardly be described by numbers and are difficult to handle automatically therefore. That is why our approach is confined mainly to the optimal price calculation (Kimes, 2003).

The customers' properties are encoded in the sales data. However the sufficiently large set of data fir economic model identification is just rarely available. Very often the hotel manager knows the every major group of customers very well. He can estimate the price elasticity demand or dependency on the explanatory variables. However to compare individual customers demands and to find the best scheduling for hotel rooms is a very complex tasks. The elements of demand can appear dynamically in time, they can have time dependent customer properties distribution. Also the length of stay can be different for each of the elements. Our approach suggests active manager cooperation. The manager would provide the knowledge of customers needs, possible demand dependency on price and the system should then autonomously decide which combination of customers should be targeted – what price list should be offered. Final task is to create an optimal scheduling for the hotel rooms. The criterion for selection of the best combination is the revenue from the hotel over the period.

The algorithm determines the number of rooms that should be sold to individual customer distribution channels.

From the previous it should be clear, the hotel capacity is shared among demand elements. In fact, there exist a number of room categories, single and double rooms etc. But capacity interactions happen not only among the elements buying the same room type. It is possible to sell higher quality room to person which is interested originally in lower quality one. Thus, the hotel capacity does not provide enough information unless it is defined for all individual room types. Analyzing these facts, we have found the capacity constraints define a partially ordered set structure. The lattice structure enables an effective capacity inequality construction.Supposing the number of sales is a linear function of the sale price, the total revenue is a quadratic function of the price. Moreover, if the number of sales is a decreasing function of the price, the revenue is a negative definite quadratic function of the optimized price. Then the revenue global maximum does exist and it can be found in a finite number of operations (by the quadratic programming algorithm).

We believe the problem formalization is the more complicated part of the solution. The real world problem has to be simplified in many ways, though the key relationships have to be preserved. A number of hotel industry issues cannot be captured by an automated system. Market segment wining is one of them. A real hotel may act sub-optimally in the profit sense in order to increase its market share, credibility, acceptance etc. Such phenomena are difficult to model formally. It is left to the user to modify the profit criteria to achieve the goal. Thus, the yield management support system developed by our project is more a tool. It is believed its user will be able to combine his experience with the numerical optimizations, which in turn can only hardly be performed by a human. The key solution features can be resumed as follows:

1. Adaptive price correction after each reservation.
2. Adaptive price correction based on weather forecasts, snow conditions etc.
3. Optimal prices for non-periodic actions of the congress type
4. Optimal discount space size calculation
5. Over-booking

References:

[1] LUCIANI, S. : *Implementing yield management in the medium sized hotels: an investigation od obstacles and success factors in Florence hotels.* Hospitality management vol.18 1999 pp. 129-142.

[2] KIMES E. S.: *Revenue management: A retrospective* Cornell Hotel and Restaurant Quartery vol. 3 2003 pp. 129-142.

[3] TALLURY K.T., VAN RIZIN G.J.: *The theory and practice of the revenue management* Kluver academic publishers, Norwell, 2004.

[4] WEATHERFORD L. R., KIMES S. E., SCOTT D. A.: *Forecasting for Hotel Revenue management Testing aggregation against disaggregation,* Cornell Hotel and Restaurant Quartery vol. 3 2001 pp. 53-64.

This research project was funded by the Czech Ministry of Trade: project number FI-IM/189. Further information on planned commercial product can be optained on internet pages http://dce.felk.cvut.cz/pachner/yield .

Inovations in The Laboratory of Control Engineering

K. Hyniová

hyniova@control.felk.cvut.cz

Department of Control Engineering, Faculty of Electrical Engineering,
Czech Technical University, Karlovo náměstí 13, 121 35 PRAGUE, Czech Republic

Nowadays, it is desirable for researchers and teachers in engineering to try as much as possible to use some of their more understandable and practical work as teaching materials to give students an insight into areas of science and technology that can be even still under investigation. Partial problems can be offered as mini-projects which may lead to interesting findings depending on the quality of the student undertaking the work. The work carried out as a part of the project offered can be either on a laboratory scale rig or simulation based. In the case of the former, the student gets to develop his/her practical problem solving skills as well as perhaps exploring new ways.

The main goal of the project was to innovate and improve this way the quality of the form and content of the courses on Control Engineering. As the area, modern interactive control circuits have been chosen. Studying modern control tools and control strategies and their variable efficiency in attractive fields in details is extremely interesting and demanding for the students. With the support of the project, four laboratory experimental stands have been introduced. In addition, one experimental stand demonstrating automotive active suspension system designed by the project research team has been added to the learning objectives in the lab.

First experimental stand enables to study theoretical and practical aspects of level and flow PID control. Learning objectives like characteristic features of the tenzometrical pressure transducer of the current level and Hall effect turbine sensor of the current flow, conditioning circuits for sensors, characteristic curves, power amplification of control signals, P, PI, PD and PID control, system stability etc. are the main tasks completed on this model. As the PID regulator of the last generation, digital PID-S/ controller (fy Elettronica Veneta, Ltd., Italy) based on a high performance microcontroller with analog/digital inputs and outputs has been used. Programming of the main control process parameters can be carried out either locally from the keyboard present on the control unit or via serial interface for communication with PCs with the possibility of data acquisition/ programming/ diagnostics. The main function of the controller is to control and monitor the regulation process continuously according to the programmed regulation algorithm. A high resolution graphic controller display provides the numerical or graphical display of the variables behavior during the regulation process.

As the next experimental stand an attractive model of the technological process (color based optimal selection of objects placed on a rotating wheel) has been designed by the project team to support not only various PLCs programming techniques and optimal control strategies but also to introduce OMRON programmable color sensor as a typical member of intelligent sensor family. Special attention is concentrated on the PLC/ sensor communication.

Third experimental stand is focused on control of temperature process. The system has been designed and manufactured with industrial criteria and components to be the instrument necessary to the exhaustive study of temperature control. It consists of a process unit and module with an amplifier for actuator and signal conditioner for thermocouple. On the whole, the system can be used for regulations with PLC type PID or Self Tuning PID. In

this way, it is possible to compare the performances of the different control approaches. The system enables a the theoretical analysis and experiments in the following main exercises: detection of the characteristic curves of the transducer and signal conditioner units, determination of the transducer and signal conditioner linearity, determination of the response delays, analyses of the ON/OFF, hysteretical, proportional, integrative and derivative actions carried out by PLCs, controller set-up according to the response at the maximum stability, detection of the response of closed-loop processes with ON/OFF control, detection of the response of closed-loop processes with P, PI, PD, and PID controls etc.

Fourth experimental stand has been designed to practice fuzzy control applied on a simple air conditioner system using an industrial fuzzy controller. The exercises are concentrated especially on creating control rules, fuzzyfication and defuzzyfication processes, controller set-up and detection and analysis of the system responses. The results can be immediately compared with the control efficiency reached using an industrial digital PID controller.

As mentioned above, one experimental stand demonstrating automotive active suspension system designed by the research team [2], [3], [4], has been added to the learning objectives in the lab. As well known, the main task of a vehicle suspension is to ensure ride comfort and road holding for a variety of road conditions and vehicle maneuvers. In general, only a compromise between these two conflicting criteria can be obtained if the suspension is based on passive components, such as spring and dampers. That is why an active suspension system characterized by a built-in actuator (linear AC electromotor) which can generate control forces (calculated by a computer) to suppress roll and pitch motions and vibrations caused by road unevenness has been designed. The main learning objectives demonstrated on the model are namely new hardware solution of the suspension systems, linear motor as a modern actuator, robust control strategies, energy consumption optimization, and energy storage devices.

References:

[1] K. HYNIOVÁ: *Řídicí technika,* textbook - Faculty of Electrical Engineering - Czech Technical University in Prague, 2006, pp. 151.

[2] K. HYNIOVÁ, J. HONCŮ, A. STŘÍBRSKÝ: *Energy Recuperation and Management in Automotive Active Suspension Systems,* In Proceedings of the 7th International Carpathian Control Conference ICCC 2006, 2006, pp. 185-188.

[3] K. HYNIOVÁ, J. HONCŮ, A. STŘÍBRSKÝ: *Energy Management in Automotive Suspension Systems,* Proceedings of IFAC 6-th Asian Control Conference, 2006, pp.105-110.

[4] K. HYNIOVÁ, J. HONCŮ, A. STŘÍBRSKÝ, A. KRUCZEK: *Energy Management in Automotive Suspension Systems ,* In Proceedings of 10-th Mechatronics Forum Biennial International Conference, 2006, pp. 329–334.

This research has been supported by the FRVS project No. FRV 758/F1a "Inovations in The Subject of Control Engineering".

Innovation of Data Networks

L. Konopka, P. Hampl

konopkl@fel.cvut.cz

Department of Telecommunication Engineering, Faculty of Electrical Engineering,
Czech Technical University, Technická 2, 166 27 Prague 6, Czech Republic

This contribution introduces the project that was focused on the innovation of Data networks which is a mandatory subject educated at CTU in Prague and is settled for students of second term of engineering studies. The main aim of the project was to improve laboratory practices in such way that would prepare graduates for future occupation. In order to accomplished this aim the innovation was focused on modern WAN technologies like Frame Relay, ISDN and ADSL. As there are only a few practices of WAN technologies that respect to economical costs that are accompanied by the operation of FR and ISDN, the design of laboratory practices was focused on highlighting the practical usage. The solution of the project was based on the creation of two case studies that were introduced in [1] [2].

The first case study deals with Frame Relay (FR) and ISDN. As it was mentioned it is necessary to take economical costs that are accompanied by the operation of FR and ISDN in consideration. For instance ISDN is in fact dial up technology and therefore very expensive with respect to telecommunication fees. Therefore ISDN is suitable for remote subscribers that need a connection to headquarter or for the backup of another WAN technology (i.e. FR). It leads us to design a case study that would demonstrate the typical usage of FR and ISDN.

The task of case study is to connect two computers with help of FR. In case of FR network failure the backup technology of ISDN must be designed. Next task of case study is to verify connection over FR network. Than simulate failure in FR network and verify the functionality of ISDN backup. Case study objectives may be resumed:

- Interconnect two routers with the aid of FR technology,
- Verify the functionality of FR network,
- Configure ISDN backup line,
- Simulate a failure in FR network,
- Verify the functionality of ISDN backup line.

The second case study is focused on the configuration of ADSL. As the best way to familiarize students with the ADSL technology is a practical example, the design of case study was aimed to the variety of configuration according to the type of ADSL extension. The task of this case study is to connect a computer network (LAN) to the Internet using ADSL. Next task of case study was to configure DHCP server for clients on the computer network. Students configure the ADSL Cisco router to act as a DHCP server for clients and setup basic ADSL configuration. Students should also determine the upload and download speeds. The summary of the case study steps is following:

- Configure ADSL Cisco router with DHCP service,
- Connect the computer network to the Internet,
- Verify the functionality of ADSL connection,
- Determine the upstream and downstream speeds.

Both case studies are completed by laboratory instructions that contain:

- Motivation,
- Knowledge requirements,
- Theoretical introduction,
- Definition of objectives,
- Topology diagram,
- Technical background,
- Proceeding,
- Controlling questions,
- Resources.

The solution of projects came out the equipment that is owned by the Department of Telecommunication Engineering. The equipment was extended by additional modules that were purchased from the project budget. Also the accent was put on the increasing of qualification of persons that provides the education of Data Networks.

The project brings following outputs:

- New laboratory workplaces were established.
- Case study instructions were created.
- The content of laboratory practice of Data Networks was changed.
- The results were published in [1] [2] [3].

References:

[1] KONOPKA, L. – HAMPL, P.: *Case Study: Frame Relay and ISDN* In: Research in Telecommunication Technology 2006 - Proceedings, Brno: VUT Brno 2006, vol. I, s. 44-48

[2] KONOPKA, L. – HAMPL, P.: *Case Study: ADSL Configuration and Troubleshooting* In: Research in Telecommunication Technology 2006 - Proceedings, Brno: VUT Brno 2006, vol. I, s. 40-43

[3] BOHÁČ, L. – BEZPALEC, P.: *Komunikace v datových sítích. Cvičení. 1. vydání.* Praha: ČVUT, 2006, 151 s.

This research has been supported by FRVŠ 2375/2006.

Lab Station with Communication Processors

V. Doleček

dolecev@fel.cvut.cz

Department of Telecommunication Egineering, Faculty of Electrical Engineering,
Czech Technical University in Prague, Technická 2, 166 27 Prague 6, Czech Republic

Introduction

Significant differentiation in microprocessors for specific use in different areas of engineering occurred in last few years. Next to well-established processors for common use and processors for digital signal processing is detaching specific category of microprocessors for typical use in telecommunications. Because of this incoming trend it is necessary to adjust the content of subject Microprocessor Engineering in Telecommunications, to be corresponding with present state of microprocessor technique for telecommunications. This subject highlights the specifics of communication processors and their differences from processors for common use. It is necessary to familiarize students with programming of communication processors in assembler (for realization of critical parts of code) and in C.

Realization

The project deals with the innovation of seminars in the subject Microprocessor Engineering in Telecommunications. Main goal of the innovation is the preparation of five lab stations for testing of technologies like Ethernet, Wi-Fi, Bluetooth, Voice over IP and other. These lab stations are realized in form of development kits based on IP3023 (Ubicom) [2], with other daughtercards like: Bluetooth extension card based on OPC1601 BlueNiceCom III modules [3], extension card with display, extension card for testing of voice over IP and extension card with CCD camera to test services like webcam.

The IP3023 development kit provides all of the necessary hardware for developing network-enabled devices with the IP3023 multithreaded network processor. The Device Network Kit can be used with Ubicom's Software Development Kit version 6 (SDK6). The development board is designed to provide flexibility for evaluation and extensibility for development work. The IP3023 development board includes LEDs, switches, and buttons to aid in quick evaluation, and provides header connectors for adding daughtercard functionality. Breadboard space is available with all the I/O pins accessible for quick prototyping. An integrated 10/100 Ethernet, MiniPCI connector for 802.11a/g radios and a prototyping daughtercard are included in the Extended Wireless Kit for the IP3023. An Ethernet dongle, which connects to the processor's in-system programming/in-system debug (ISP/ISD) port to enable device programming and debugging, is included.

New Syllabus of the Seminars

1. Introductory seminar, safety instructions for work in lab.
2. IP3023, architecture.
3. IP3023, instruction set, development environment.
4. Exercises with IP3023.
5. Exercises with IP3023.
6. Exercises with IP3023.
7. Exercises with IP3023.
8. Exercises with IP3023.
9. Exercises with IP3023.
10. Exercises with IP3023.
11. Exercises with IP3023.
12. Exercises with IP3023.
13. Exercises with IP3023.
14. Assessment.

The changes were introduced to education in winter semester 2006.

Main benefits from project solution

- Use of new knowledges about modern telecommunication processors in the education.
- Enhancement of study effectiveness about modern telecommunication technologies in the form of lab exercises with develpement kits based on Ubicom processors.
- Creation of five lab stations with communication processors IP 3023 and with different enhancement modules for education in the subject Microprocessor Engineering in Telecommunications.
- Use of these development kits by students in their semester, bachelor or diploma works.

References:

[1] DOLEČEK, V.: *Lab station with communication processors* Proceedings of the conference Research in Telecommunication Technology RTT2006 [CD-ROM]. Nové Město na Moravě, Czech Republic, September 2006, pp. 214-215, ISBN 80-214-3243-8.

[2] WWW.UBICOM.COM

[3] WWW.AMBER-WIRELESS.DE

This research has been supported by FRVŠ grant No. FRV 2286/G1.

Innovation of the Subject Implementation of DSP Algorithms in Telecommunication

P. Slepička, P.Zahradník

slepicp@fel.cvut.cz

Czech Technical University
Department of Telecommunication Engineering
Technická 2
CZ-16627 Praha 6, Czech Republic

1. Introduction

The training in this subject was based on the old generation of Digital Signal Processors (DSP) TMS320C50 and TMS320C6211. In order to cope with new development in the DSP technology, the content of the subject was improved. The new training is based on the fix point Very Long Instruction Word DSPs. Five laboratory setups based on the DSP starter kits TM320C6416 [1] were established. Two setups were completed by the add-on video cards [2]. They allow to digitize and display video signals in real time and make the training in the real time image and video processing possible. Further, in order to make the students familiar with hardware related issues of DSPs, a low cost versatile add-on daughter cards were designed and made. Consequently, each student deals with an individual hardware related problem. It comprises the design and realization of individual add-on hardware. This way, the variety of topics to be solved is practically limitless.

2. Topics of the Subject The subject includes the following topics : development tools for DSP, Code composer studio, DSP programming in C and assembler, mixing of both, programming of the video daughter board, implementation of convolution, correlation, echo generation and canceling, implementation of image filtering, implementation of FFT, DFT, DCT, implementation of DTMF coding and decoding, implementation of motion detection and edge detection.
The innovation of subject can be readily demonstrated by the old and new syllabuses of the subject.

Old syllabus

1.Software for analysis and synthesis of discrete systems.
2. Introduction to using digital signal processors.
3. Basic instruction set of the TMS320C50 digital signal processor.
4. Basic instruction set of the TMS320C6211 digital signal processor .
5. Integral transformations (DFT, FFT, DCT).
6. Integral transformations (DFT, FFT, DCT), implementation on TMS320C50.
7. Integral transformations (DFT, FFT, DCT), implementations on TMS320C6211.
8. Digital filter IIR type , implementation on TMS320C50.
9. Digital filter IIR type , implementation on TMS320C6211.
10. Digital filter FIR type , implementation on TMS320C50.
11. Digital filter FIR type , implementation on TMS320C6211.
12. Decimation and interpolation filters , signal resampling.
13. Decimation and interpolation filters implementation on TMS320C50.
14. Decimation and interpolation filters implementation on TMS320C6211.

New syllabus

1. Software for analysis and synthesis of discrete systems.
2. Integral transformations, decimation, interpolation, signal resampling.
3. Analysis and synthesis of digital filters with finite and infinite impulse response.
4. Digital signal processors VLIW, product line TMS320C6x.
5. development tools for DSP , Code Composer Studio pro TMS320C6x.
6. Implementation of corellation and convolution algorithms on TMS320C6416.
7. FIR and IIR type filters implementation on TMS320C6416.
8. Implementation of algorithms FFT, DFT, DCT on TMS320C6416.
9. Implementation of echo cancellation algorithms on on TMS320C6416.
10. Implementation of digital modulation algorithms on TMS320C6416.
11. Implementation of DTMF algorithms on TMS320C6416.
12. Implementation of motion detection algorithms and video signal compression on TMS320C6416.
13. Implementation of video signal filtration algorithms on TMS320C6416.
14. Demonstration of individual projects.

The main benefits of the subject innovation include

1.Introduction of new fixed point digital signal processor technology into study and possibilities of using this processors in telecommunication applications and systems.

2.Creation of five new laboratory working places for seminars in subject Implementation of DSP algorithms in telecommunication , two of these working places are equipped with video modules making possible the DSP processing of video signals.

3.Higher motivation of students for further study through using up to date technology and signal processors used in modern real world telecommunication system applications and consequent higher possibility of putting acquired skills and knowledge into professional and industrial practice .

4. Because of the newly purchased hardware starter kits, it is possible for students to use these starter kits for their research work outside the scope of the innovated subject as well the possibility for undergraduate student to work on their bachelor and master thesis's.

References:

[1] TEXAS INSTRUMENTS [ONLINE]: *http:\\ www.ti.com*

[2] VDB[ONLINE]: *http:\\www.einfochips.com*

This work was supported by the Ministry of Education, Czech Republic under project No. FRVŠ 2294/G1

Innovation of the Course "Information Security and Secretion of Messages"

Tomáš Vaněk

vanekt1@fel.cvut.cz

Department of Telecommunication Engineering, Czech Technical University in Prague, Faculty of Electrical Engineering

Technicka 2, 166 27 Praha 6, Czech Republic

For professionals in telco domain it is important to have at least general information about network security, basic cryptographic algorithms and protocols. The main goal of the project was to innovate who educational process in subject "Information Security and Secretions of Messages" in theoretical lectures as well as in practical courses. New lectures made students familiar with principles, architecture and applications of modern symmetric-key and asymmetric-key algorithms, hash function and widely used cryptographic protocols.

1. Innovation of the lectures

Main improvements in the course have been done in innovation of the theoretical lectures. A lot of actual English written literature has been studied and transformed into new lectures. Every new lecture comes with presentation in PowerPoint. These presentations illustratively show main ideas of the topics. An electronic form of new lectures is available for the students at www.comtel.cz (section Předměty → X32IBU → Materiály pro výuku)

Lecture 1	Security mechanisms in wireless networks - IEEE 802.11 (802.1x, 802.11i, protocols WEP,WPA,TKIP)
Lecture 2	Digital signature
Lecture 3	SSL/TLS, WTLS
Lecture 4	Protocols for Virtual Private Networks (L2TP, PPTP, GRE, IPsec)
Lecture 5	Certificates, Certification Authority and Time Stamp Authority

2. Innovations of the exercises

1.1. Innovation of theoretical excercises

In the field of theoretical exercises minor changes were done. New scripts for cryptanalysis were prepared in JavaScript and Java. During these exercises the students try to decrypt historical ciphers. These exercises cover:

- Monoalphabetic substitution ciphers
- Polylalphabetic substitution ciphers
- Transposition ciphers

1.2. Innovation of practical tasks

The X32IBU course was transformed from the former 32ODI and 32UDP courses. The main disadvantages of these courses were absence of practical laboratory tasks. Three completely new tasks were created to demonstrate practical aspects of network security and usage of cryptographic algorithms.

Laboratory 1 – Virtual Private Networks in practice. Students will create a secure VPN using IPsec technology and Cisco routers 26xx and VPN using SSL protocol (OpenVPN project).

Laboratory 2 – WiFi networks localization and secure analysis. In this exercise the students will search for wireless networks in designated location. The have to localize the APs (using GPS) and gain as much information as possible about security of found networks by opensource programs (Cain&Abel, NetStumbler,…)

Laboratory 3 – Authentication protocol analysis. In this exercise the student will analyze existing authentication protocol using BAN logic and/or Color Petri Nets. A visual model of broadcast authentication protocol TESLA was created using a tool called "CPN tools" and the student try to search for security wholes that were injected into this protocol.

3. Conclusion

Main goals of subject innovation are:

- Five new theoretical lectures.
- Creation of the new study material for theoretical lectures.
- Three new practical laboratory exercises.
- Crypto portal improvements.
- All study materials are available for students in electronic form.
- Motivation of the students to study modern telco technologies.

This research has been supported by FRVS grant No. FRV 80/F1

Innovation of the subject Artificial Inteligence I.

O. Štěpánková, L. Nováková

step@labe.felk.cvut.cz, novakova@labe.felk.cvut.cz

Department of Cybernetics, Faculty of Electrical Engineering, Czech Technical University, Technická 2, 166 27 Prague 6, Czech Republic

Any modern institution operating in a dynamic environment which aims to use efficiently its resources has to be very careful about its knowledge management and it has to do its best to evaluate its past experience in order to achieve better results in future. The considered knowledge management processes can be supported by the use of knowledge technologies, in particular by data mining and decision support. These technologies have a large potential for knowledge management and they have already proved their advantages in numerous industrial and business problems including applications for networked and distributed organizations. In most domains the use of data mining and decision support remains a great challenge because the target domain is highly knowledge intensive and neither data gathering nor data analysis can be successful unless it is complemented by deep knowledge about both the problem domain and the data analysis process. That is why it is important to offer to the engineering students elements of data-mining and to teach them its theoretical background. With this knowledge they will become domain experts who are able to identify in their working environment those tasks, which can be improved using data mining techniques. In the best or simple case, the graduates acquainted with data-mining technologies will be able to solve the identified problems themselves. If not, they will be ready to specify clearly the task and to communicate with someone (an individual or a company) who is offering data-mining as a service. That is why we have set as the main goal of our project to innovate the subject Artificial Intelligence taught at the Department of Cybernetics of FEE in such a way that the students will get acquainted both with the theoretical foundations of data-mining provided by the machine learning (ML) theory and with the selected machine learning algorithms with high practical potential.

The lectures after explaining the basic definitions (concept, hypothesis, training and test data, background knowledge, etc.) point to the difference between supervised and unsupervised learning and provide overview of main methods which can be used to resolve the respective tasks. The lectures emphasize the theoretical aspects of the treated methods as well as their limits related to the PAC theory while experience in using available SW tools is gained during the exercises. Special attention is given to inductive logic programming (ILP) – a subfield of supervised machine learning which constructs the hypothesis in the language of 1st order logic in the form of a logic program. This paradigm significantly enhances the application potential of ML because it offers natural way how to utilize background (domain) knowledge in the process of hypothesis creation. Moreover, the lectures about inductive logic programming build on the skills acquired in the bachelor subject Programming languages for Artificial Intelligence and they highlight advantages of the corresponding data and knowledge representation.

Special attention has been dedicated to a good choice of practical problems which the students are supposed to solve during their exercises. New datasets (both artificial created by a dedicated SW tool [Vejmelka] and real-life) of different complexity have been prepared to demonstrate the full life-cycle of a data-ming task starting from the data understanding and data preparation, proceeding by hypothesis generation and ending with its evaluation and

testing. Each real-life dataset is complemented by a simple description of the context, motivation for the specified ML task, hints for helping interpretation of the obtained results and some recommendations of useful processing steps.

The main treated topics

- decision trees, algorithm ID3
- overview of symbolic methods of inductive learning – algorithms AQ, CN2, association rules
- testing of hypothesis
- data mining, CRISP methodology, data visualization
- inductive logic programming (ILP)
- Probably Approximately Correct (PAC) learning
- reinforcement learning
- examples of practical applications

All materials for lectures and labs are prepared both in Czech and in English and published on the subject web pages. The subject is also offered for students of the Erasmus program and the outputs of this project are applicable to the course "Data-mining" of life-long education.

References:

[1] BISHOP, CH. *Pattern Recognition and Machine learning* Springer 2006

[2] BERTHOLD, M. HAND, D. J. *Intelligent Data Analysis* Springer 2003

[3] MAŘÍK, V. ŠTĚPÁNKOVÁ, O. LAŽANSKÝ, J. *Umělá inteligence IV.* Academia Praha 2003

[4] VEJMĚLKA, M. *PreDO - Precisely Defined Objects* Research Report GL Praha 2002

This work has been supported by FRVS grant No 832/2006.

Evolutionary Numerical Optimization

M. Lepš, J. Zeman, A. Kučerová

leps@cml.fsv.cvut.cz

Department of Mechanics, Faculty of Civil Engineering, Czech Technical University,
Thákurova 7, 166 29 Prague 6, Czech Republic

In the recent decades, the stochastic evolutionary methods have become very popular within the engineering optimization area. These methods are usually based on simple physical or biological principles, which make them open to relatively easy understanding. Based on the authors' previous research experience, the goal of this project was to create a new elective course "Evolutionary Numerical Optimization" aimed at bachelor- and master-degree students with the course load of three hours per week.

So far, no part of evolutionary optimization area was covered in the curricula of the Faculty of Civil Engineering, CTU in Prague. Therefore, the course is mainly aimed at the basic definitions, classification, applicability, advantages and disadvantages of the abovementioned evolutionary optimization methods as well as traditional methods of mathematical programming. The latter serve mainly as a comparison for the former ones in the terms of performance and applicability. Emphasis is put especially on a thorough explanation of the basic ideas of all the methods using simple and transparent examples. This will make it easier for the students to follow more advanced topics covered in the specialized mathematical and engineering literature. Moreover, we have also tried to maximally incorporate freely available software tools to stimulate future applications of optimization procedures to problems of a Civil engineering design.

Fifteen lecture notes were created in the scope of this project. They include in particular:

1. General introduction into optimization methods – classification of optimization problems and algorithms
2. Mathematical programming methods I – Unconstrained optimization: gradient, Hessian, Newton's method, Conjugate gradients method
3. Mathematical programming methods II – Constrained optimization: KKT condition, insufficiencies of deterministic methods
4. Direct search methods - Monte Carlo method, dynamic Hill-climbing algorithm, Tabu search method
5. Simulated Annealing – basic principles
6. Genetic Algorithms – binary, integer and real-coded genetic algorithms, their history, definitions and basic steps
7. Evolutionary strategies and Differential evolution
8. Evolutionary Algorithms – terms, classification, examples and comparison
9. Parallelization of evolutionary algorithms and NFL Theorem
10. Multi-modal optimization – management of local optima
11. Multi-objective optimization – Pareto-dominance concept, Pareto-optimal set, mathematical programming methods, visualization, multi-objective evolutionary algorithms
12. Solutions to constrained optimization – principles and methods
13. Introduction to Genetic programming – representation of data, genetic operators and problems
14. Meta-modeling – methods and applications

15. Application examples of evolutionary algorithms

All lecture notes are accessible in the open PDF format. The source codes of the notes are available in the (pdf)LaTeX and Microsoft PowerPoint formats. As the complement, ten additional exercises have been prepared:

1. Introduction to computer laboratory
2. Mathematical programming interactive systems
3. Applications of direct search methods to simple examples
4. Applications of simulated annealing and evolutionary strategies
5. Genetic algorithms
6. SADE algorithm and Differential evolution
7. Introduction to the multi-modal system CERAF
8. Multi-objective optimization I – interactive systems
9. Multi-objective optimization II – multi-objective evolutionary algorithms
10. Applications of the Genetic programming

For each topic, all lectures are supported by the database of freely available software tools and benchmark problems. The majority of exercises are based on the MATLAB system platform, which is freely available within the CTU in Prague. During the project, the MATLAB system was also installed at the network of Computing and Information Centre, where the lectures will be held. The remaining exercises are implemented in the C++ programming language or in interactive environments with a user-friendly graphical interface.

In addition, in order to demonstrate the behavior of optimization algorithms, several video sequences were also made available in the AVI format. All project files are currently accessible from internet web-pages:

http://cml.fsv.cvut.cz/~leps/teaching/mmo/index.html

and will be continuously updated together with all lecture notes during forthcoming years.

The course "Evolutionary Numerical Optimization" will start in the summer term 2006/2007 under the name "Modern methods of optimization" with two hour per week load and will be finished by a credit (the change in the name and in the course load was proposed by the Vice-Dean for Education of the Faculty of Civil Engineering, Doc. Ing. Jiří Máca, CSc).

References:

[1] EIBEN, A. E., SMITH, J. E., EIBEN, A.E., SMITH, J. D.: *Introduction to Evolutionary Computing (Natural Computing Series)* Springer, 2003.

[2] BONNANS, J. F., GILBERT, J. CH., LEMARÉCHAL, C., SAGASTIZÁBAL, C. A.: *Numerical Optimization: Theoretical and Practical Aspects* Springer-Verlag, 2003.

[3] HRSTKA, O., KUČEROVÁ, A. *Improvements of real coded genetic algorithms based on differential operators preventing the premature convergence,* Advances in Engineering Software, 35(3-4), 2004, pp. 237-246.

[4] HRSTKA, O., KUČEROVÁ, A., LEPŠ, M., ZEMAN, J.: *A competitive comparison of different types of evolutionary algorithms,* Computers & Structures, 81(18-19), 2003, pp. 1979-1990.

This research has been supported by FRVŠ grant number F1 b 2707.

Subjective Image Quality Evaluation and Enhancement

M. Klíma

klima@fel.cvut.cz

Department of Radioelectronics, Faculty of Electrical Engineering, Czech Technical University, Technická 2, 166 27 Prague 6, Czech Republic

The image quality assessment is a crucial topic in applied multimedia systems. The dramatic development in the field of multimedia technology has brought numerous new approaches and techniques influencing the image quality. The image qualitative aspects in the security field have been extensively studied in our research group [1], [2], [3]. There are several different directions we have to follow. The fundamental item is to establish an observation workplace according to [4] for subjective tests evaluation. We have created such a workplace in a specialized room equipped with the professional TV monitor SONY and the viewing conditions fulfilling the requirements of [4]. The second task was the selection of image tests that are used. We have chosen a set of five typical scenes (SQUARE, GIRLS, POSTERS, GARDEN, and FRUITS). The selected scenes exhibit relevant different properties – large areas of saturated colors, fine details, etc. After initial tests we omitted to apply well known and widely used images such as LENA etc. in order to avoid an excessive fatigue of observers. A special set of image tests have been chosen for the security field – faces, fingerprints and car plates.



Fig.1: Image tests SQUARE, GARDEN and POSTERS



Fig.2: Image tests GIRLS and FRUITS



Fig.3: Security image test – car plate

The second part has been devoted to the image compression and impact of source

image compression. We have tested both compression techniques and standards. Among many compression techniques our attention has been paid to the Karhunen – Loeve transform KLT with suboptimal base and wavelet transform WT. In case of compression standards we have tested JPEG, JPEG 2000 and LuraWave. We have studied the influence of different distortions and artifacts. Apart of the standard subjective tests the masking effects in security tests have been studied. As a measure of masking effect we have evaluated the identification threshold for the correct reading of car plate number. In the first attempt the real car plate has been replaced by a four-digit seven-segment number combined with a masking background.

The third part has dealt with selected image quality enhancing algorithms. These algorithms are well known as a part of standard image processing software packages e.g. Photoshop etc. The attention has been paid to several image quality enhancing tools – edge enhancing (sharpening), de-noising and color saturation. The de-noising and edge enhancing tools have appeared as complementary in such a way that the noise reduction tool is causing a smearing of edges and vice versa. Performing of subjective tests in these cases has been very difficult and we have identified various approaches by different observers. Some of them have been concentrated on the edge sharpness, some of them on the noise level, and the results are questionable. Moreover the results have varied significantly relative to the signal-to-noise ratio. So far we have applied standard sharpening tools (HP filters) and the addition of edge derived information (Sobel, Canny). On the other hand the color saturation shows clear optimum value of saturation achieving a maximum value of subjective image quality. Therefore we have introduced the impressiveness factor showing the relative improvement of subjective quality using a particular enhancing tool.

The last part of the work has been devoted to the Human Vision System HVS modeling and testing of different objective image quality metrics. The objective image quality metrics are extensively studied for long time and there are numerous. We have applied a set of selected metrics and the achieved results have been compared with the subjective tests. Apart of standard metrics MSE and PSNR we have applied a set of others based upon the Sarnoff model of HVS.

References:

[1] PÁTA, P. - KLÍMA, M.: *Efficient Method for Security Image Data Compression,* Proceedings of 37th International IEEE Carnahan Conference on Security Technology,Taipei, Taiwan 2003, pp. 456-459.

[2] KLÍMA, M. - FLIEGEL, K.: *Image Compression Techniques in the Field of Security Technology: Examples and Discussion,* Proceedings of 38th International IEEE Carnahan Conference on Security Technology,Albuquerque, New Mexico 2004, pp. 278-284.

[3] KLÍMA M., FLIEGEL K., ŠVIHLÍK J,: *Quality Enhancement in Security Image Information,* Proceedings of 40th International IEEE Carnahan Conference on Security Technology,Lexington, Kentucky, 2006, pp. 504-509.

[4] ITU-R *Rec. BT 500-10* Methodology for the Subjective Assessment of the quality of television Pictures 2000

This work was funded by the Czech Grant Agency under the projects No.102/02/0133 and No.102/05/2054. The author appreciates very much the support given by dr. Pazderák and Mr Dušek during performing the tests.

Hybrid Approach to HDR Tone Mapping

M. Čadík

cadikm@fel.cvut.cz

Department of Computer Science and Engineering, Faculty of Electrical Engineering,
Czech Technical University in Prague, Karlovo náměstí 13, 121 35 Prague 2, Czech Republic

Merits of high dynamic range imaging (HDRI) are currently widely recognized in computer graphics, high-quality photography, computer vision, etc. However, HDRI becomes popular in interactive and real-time applications as well. Data visualization, computer games and other interactive applications gain new qualities thanks to HDRI. The reproduction of high dynamic (HDR) data on the low dynamic (LDR) output devices requires the reduction of dynamic range, commonly referred to as a *tone mapping* [1]. We can classify the existing approaches according to the transformation they apply to convert input luminances to the output values. *Global* tone mapping methods apply a tone reproduction curve - e.g. a function. Therefore, they transform particular value of the input luminance to one specific output value. *Local* tone mapping operators may on the other hand reproduce particular input luminance to different output values depending on the surrounding pixels.

Although many sophisticated local tone mapping methods were published, these are prevailingly intentional approaches and quite a few of these methods is suitable for interactive and computationally weak applications. Even worse, hardly any of them can be marked as general and scalable. Besides, recent perceptual studies concerning the reproduction of HDR images [2, 3] have shown high importance of preservation of global image attributes (overall brightness, overall contrast). Generally speaking, global methods reproduce overall image attributes well, they are fast to compute, and easy to implement, but may wash away important details. Local approaches excel in reproduction of local contrast (details), but they are computationally intensive and may reproduce overall image attributes poorly.

Motivated by the mentioned findings we present a fast and simple yet powerful general *hybrid approach* to tone mapping issue. This approach takes advantages of both global and local tone mapping approaches to overcome mentioned limitations. Moreover, since the aims of tone mapping can differ among particular applications, the proposed approach can be easily tailored to the miscellaneous goals. The process consists of three steps. First, the input high dynamic range image is transformed using global tone mapping curve. This mapping produces the base of the output low dynamic range image and (if necessary) outputs desired values for the construction of an *enhancement map*. In the second step, the enhancement map is constructed considering the aim of the tone mapping. Finally, the enhancement map is used to guide a local tone mapping method to reconstruct subtle details. It is especially profitable [4] to perform the local enhancement using graphics hardware. The locally enhanced details are then added back to the globally transformed image to improve the final output image.

Besides the choice of the involved methods, the manner of the *construction of the enhancement map* is an essential heart of the hybrid tone mapping. The enhancement map is generally a map of float numbers with the same dimensions as the original HDR image. When we use a linear transform function in a global part of hybrid mapping, the construction of the enhancement map is very simple and effective. Since we know the analytical equation of the transfer curve, the clipping values are then directly known and the enhancement map is constructed effortlessly. For the other approaches (s-shaped curves, log scaling, histogram adjustment, etc.), we propose to use the clip values of 5th and 95th luminance percentiles. However, the manner of the enhancement map construction can reflect a special goal of

hybrid tone mapping, for example the reproduction of details (cognitive dimension of tone mapping). If the running time is not an issue, we can involve more sophisticated criteria to the construction of an enhancement map, e.g. the human visual system properties. Using the visual attention model, for example, we can pass the computational resources to the visually important areas of the image. Another possibility is the usage of contrast sensitivity function (CSF) during the construction of the enhancement map. In this case, the effort of local method will be directed to the areas, where the detail is visible for a human observer.

It is typically advantageous to model the course of visual adaptation over the time for interactive applications. *Time-dependency* of tone mapping is twofold profitable: it increases the perceptual quality on one hand, and it also avoids temporal image artifacts on the other hand. The way of implementation of time-dependency is influenced by the goal of the whole tone mapping method and it is not necessary to realize it at all, in some cases. We use an exponential decay function in our perceptually plausible hybrid approach to model the light adaptation. We omit the simulation of long-term dark adaptation due to its subtle and slow effect and due to efficiency reasons. If the computational cost is the main limitation, the time-dependency may be omitted temporarily with reasonable loss of reproduction quality.

Since one of the goals of the hybrid approach is the reduction of computational complexity, we measured the speedup to original methods using the group of 10 input HDR images. The perception-targeted fast hybrid approach is on average more that 118 times faster than the original local filtering method. Generally speaking, our technique places very small additional load to the system leaving large space for other computations. This is very profitable in interactive applications like the computer games, etc. However, note that besides the performance improvement, hybrid tone mapping can enhance the quality of the output image as well. In the imminent future, we can expect the need of dynamic range reduction even on various portable devices and on small and computationally elementary machines. The hybrid tone mapping will be reasonable in this case as well, thanks to its good scalability. If we face the lack of computational power, we can modify (soften) the criteria of the construction of the enhancement map. Depending on these criteria, we are able to continuously balance the computational load spanning from the complete locally enhanced method up to the factual omitting of the local enhancement (e.g. purely global tone reproduction).

References:

[1] REINHARD, E., WARD, G., PATTANAIK, S., DEBEVEC, P.: *HDRI: Acquisition, Display, and Image-Based Lighting.* Morgan Kaufmann, 2005.

[2] ČADÍK, M., WIMMER, M., NEUMANN, L., ARTUSI, A.: *Image attributes and quality for evaluation of tone mapping operators.* In Proceedings of Pacific Graphics'06, National Taiwan University Press, 2006, pp. 35–44.

[3] YOSHIDA, A., BLANZ, V., MYSZKOWSKI, K., SEIDEL, H., P.: *Perceptual evaluation of tone mapping operators with real-world scenes.* Human Vision & Electronic Imaging X, SPIE, 2005.

[4] FIALKA, O., ČADÍK, M.: *FFT and convolution performance in image filtering on GPU.* Information Visualization'06, IEEE Computer Society Press, 2006, pp. 609–614.

This research has been supported by the Ministry of Education, Youth and Sports of the Czech Republic under the research programs MSM 6840770014 and LC-06008.

Matlab-Aimsun Toolbox

Pavel Dohnal

dohnalp@utia.cas.cz

Department of Control Engineering, Faculty of Electrical Engineering,
Czech Technical University in Prague, Technická 2, 166 27 Prague 6, Czech Republic

Department of Adaptive Systems, Institute of Information Theory and Automation, Academy of Sciences of the Czech Republic, Pod vodárenskou věží 4, 18208 Prague 8, Czech Republic

The aim of AIMSUN–MATLAB interface toolbox is to implement an interface between MATLAB environment and AIMSUN simulator [3] for the purpose of testing of designed traffic control of special macroscopic type. The AIMSUN simulator is powerful tool for simulation of traffic flow while the MATLAB environment provides the rich set of functions that simplify the process of design, optimization and testing of developed traffic control. Toolbox combines together advantages of both of them.

All the actual last data (periodical and global system statistics useful for evaluation of control schemes applied) are gathered in buffer available from MATLAB and stored in their history:

- measure counts, occupancy and speed on detectors and aggregate them. It gathers data for common detection interval for all detectors.
- measure average and maximal queues on sections and aggregate them. It gathers data from common statistics interval (that is different from detection interval in general).
- measure periodical system statistics (total travel time, number of stops, etc.). It gathers data again from common statistics interval.
- measure global system statistics over all experiment (day). It measures the same characteristics as in previous item, but they are agregated for the whole experiment.
- measure applied phase timing for all controlled junctions with all details (start time of junction cycle and length of all phases and interphases.

Make actions:

- generate incidents in selected place and time.
- generate time varying vehicle entrances into the network.
- control length of junction phases in predefined control plan. It means both rates of individual phases and length of cycle of controlled junction can be changed. Even some phases can be skipped by defining their zero time. Though, it is not possible to change order of phases or generate absolutely different control plan.

Besides detection sampling, statistics sampling and junction sampling intervals can be various in general. Also precise data about applied junction phase timing is gathered and can be gained. Toolbox work in more general asynchronous manner.

If external control of junction phases length is used then setting received from MATLAB is not applied immediatelly but each junction waits for begining of new control cycle. So setting

is applied gradually on individual junctions. It hels us to preserve synchronization and offsets among junctions.

AIMSUN-MATLAB interface toolbox implementation comprises three main parts that provide all the functionality:

- the pivotal dynamic library - is written in C and it forms the core of the implemented interface [4]. It has to be linked both to the AIMSUN and MATLAB. While this task is implemented implicitly in MATLAB, it is necessary to link this library explicitly in AIMSUN scenario as one of extensions [2].
- set of MATLAB functions - realize all the necessary function to run AIMSUN simulation with linked AIMSUNMATLAB interface. It comprises preparation of experiment and run of simulation (i.e. manipulation with AIMSUN, obtaining and sending data etc.). All the functions are listed in [2].
- set of MATLAB functions for easier using [1]:
  initArea('AreaName') - initialize and elect current simulation area,
  getActualData(MyArea) - get intensity, occupancy and velocity,
  setActualControl(MyArea, MyControl) - set phases lenghts for junctions,
  demoArea('AreaName') - show area with default control.

The main structure of algorithms of AIMSUN scenario life cycle and main MATLAB function *AimsunSimulationStep* are given close together. In these two algorithms you can follow jumps between algorithms to follow the process of communication and synchronization.

If the low-level logic of communication between AIMSUN and MATLAB stays same, then only the main macro function *AimsunSimulationStep* shall be modified. While macro function is changed its low-level subfunctions need not be modified. All the functions in *AimsunSimulationStep* in part Original basic functions are such low-level functions independent of the logic of macro function. They can be used in new selected manner and even export into independent files. Subfunctions are hidden here in main macro function only for purpose of simplicity of toolbox employment. Changes in low-level logic of communication between AIMSUN and MATLAB require not only modification of basic macro function but also changes in low level m-functions and even in fundamental DLL library.

References:

[1] DOHNAL, P. - DIBELKA L: *MATLAB-AIMSUN Toolbox 2.1 - User's Guide.* Academy of Sciences of the Czech Republic, Institute of Information Theory and Automation, Prague, 2006.

[2] GEBOUSKÝ P.: *AIMSUN-MATLAB Interface - User's Guide.* Academy of Sciences of the Czech Republic - Institute of Information Theory and Automation, 2006.

[3] TRANSPORT SIMULATION SYSTEMS: *AIMSUN Version 4.2 - User manual.* TSS, 2004.

[4] TRANSPORT SIMULATION SYSTEMS: *GETRAM Extensions Version 4.2 - User manual.* TSS, 2004.

This research has been supported by MDČR grant No. 1F43A/003/120 and by MŠMT grant No. 1M0572.

On Relationship between Parallel Reduction and Leader Election Problem in Distributed Systems and Networks

M. Nehéz

nehez@fel.cvut.cz

Department of Computer Science and Engineering, Faculty of Electrical Engineering, Czech Technical University, Karlovo náměstí 13, 121 35 Prague 2, Czech Republic

A *parallel reduction* is a form of applicative order reduction in which all operands in an expression are reduced simultaneously. Variants include parallel outermost reduction and lenient reduction. More precisely, given a positive integer n and an associative binary operation $\otimes$ with an identity element I, the parallel reduction algorithm solves the simultaneous application of the operation $\otimes$ on n elements a[1], …, a[n]. In particular, the operation $\otimes$ may represent operations such as addition, multiplication, max, min, greatest common divisor (gcd), Boolean binary operations, etc. A standard parallel algorithms solves this problem in parallel time O(lon n), [2].

Let us consider a collection of n asynchronous (possible mobile) nodes (agents) dispersed on an arbitrary network. Such collection of nodes can be modeled by a distributed system with connections among the nodes. Let us consider a problem of *distributed leader election* which is a problem of selecting of a one node setting its state as a *leader* among n all nodes. Initially, all nodes have a same state and terminally one node is a *leader* and another $n-1$ nodes are in a state *lost*. This problem is a fundamental problem in distributed systems with many applications such as the *breaking symmetry* of the distributed system [1,4]. It was shown that the problem of leader election is deterministically unsolvable for fully anonymous systems [4]. So, we will consider the distributed systems with distinct labels 1, ..., n.

Our research is focuses on the relationship between the two described problems:

- the parallel reduction and
- the leader election.

The first such question was addressed in [1] where the problem of relation among election, rendezvous and finding of a gcd in anonymous systems with sense of direction was considered.

The results of our research are as follows. The problem of parallel reduction is solvable in distributed systems modeled by point-to-point asynchronous communication networks represented by a simple unoriented graphs consisting of a set of nodes (processors) and edges (communication links). Such a model can be modified to the collection of asynchronous (possible mobile) nodes (agents) dispersed on an arbitrary network. So it represents the computational model considered in this paper.

Consequently, we can posed a crutial question whether the parallel reduction and leader election are computationally equivalent problems in distributed systems with distinct labels (i.e. unanonymous nodes). The answer is that the leader election can be solved by parallel reduction however, the converse implication remains open. The proof of this fact is as follows. Let us consider the distributed system with nodes 1, …, n in which the parallel reduction can be performed. Set the operation min or max for the $\otimes$. Hence, the leader can be obtained as a solution of parallel reduction in described distributed system. The node with minimum (or maximum) label represents the leader.

For possible applications of our computational model we refer the following systems:

- standard communication and interconnection networks [2,4],
- collection of mobile agents [1],
- wireless and ad-hoc networks [3].

Our results can be applied to all latter distributed system hence, the universality of our research is widely useful. As a direction for the future research we address the question of energy-cost measure needed to solve/perform parallel reduction and leader election in radio-networks.

References:

[1 L. BARRIÈRE, P. FLOCCHINI, P. FRAIGNIAUD, N. SANTORO: *Election and Rendezvous in Fully Anonymous Systems with Sense of Direction,* 10th Int. Colloquium on Structural Information & Communication Complexity SIROCCO 2003, Carleton Scientific, 2003, pp. 17-32.

[2] J. JAJA: *An Introduction to Parallel Algorithms,* Addison-Wesley Professional, 1992 .

[3] C. SIVA RAM MURTHY, B. S. MANOJ: *Ad Hoc Wireless Networks: Architectures and Protocols,* Prentice Hall, 2004 .

[4] G. TEL: *Introduction to Distributed Algorithms,* Cambridge University Press, 2000 .

This research has been supported by MŠMT under research program MSM 6840770014.

Usability Testing and Development of Car Simulator - City Rider

I. Malý*, D. Tichý**

malyi1@fel.cvut.cz

*Department of Computer Science and Engineering,
Faculty of Electrical Engineering, Czech Technical University in Prague,
Karlovo Namesti 13, Prague 2, Czech Republic

**Department of Cybernetics,
Faculty of Electrical Engineering, Czech Technical University in Prague,
Karlovo Namesti 13, Prague 2, Czech Republic

In the last couple of years drivers can use much more equipment in their car than ever before. They have mobile phones, car navigations, radio sets and other tools that should help drivers to do their work. Unfortunately, many studies like for example [1] have shown that driving is quite a demanding activity and that drivers should not be distracted for safety reasons. To ensure safe driving, experiments are conducted to measure cognitive load when particular in-car equipment is used. The goal of the experiments is to avoid dangerous setups and to improve user interfaces so that the cognitive load of the driver is maintained at a reasonable level. The experiments are executed either in a laboratory or in the field. Laboratory tests are usually cheaper, easier to prepare and reveal nearly the same issues as the field studies. In the lab we usually do not use real cars but instead we use simulators. Simulators, as an application of virtual reality, are being widely developed in many industries. The most sophisticated simulators have been developed for medical applications, for aerospace and for the car industry. The main objective of the simulators is to create a virtual environment that is as realistic as possible. These virtual environments usually serve for miscellaneous research where the interaction between the virtual environment and the user is examined. Example of such research and development is in [2] and [3].

In previous years, the Car simulator called City Rider has been developed. The purpose of this simulator is to create virtual environment for generation of cognitive load when driving. Cognitive load generation is then used for usability testing of in car equipment. Usability testing is a technique, where users from product target group are trying to fulfill predefined tasks. These tasks are artificial, in order to build controlled environment, but correspond to real life tasks. Usability testing is qualitative method. That means that only limited number of users, usually around 8, is used for testing. It has been demonstrated that such amount of users can reveal about 80% of major problems. Important condition of successful usability test is proper context and realism of the test. Therefore we use the City Rider to generate cognitive load, which should correspond to the same cognitive load generated during real car driving.

Main features of the City Rider simulator are advanced graphics and physical model, then map and landscape generation, and also sufficient, simple and portable setup of the simulator. The simulator environment consists of a LCD monitor, steering wheel with pedals and controlling computer. Developed graphics engine contains some common used optimizations necessary for real-time rendering of large incoming scenes representing different virtual environments like cities or their surroundings with highways. These optimizations, especially frustum culling, are making use of hierarchical system of objects bounding volumes and level of detail. Some advanced techniques like dynamic stencil shadows, multitexturing,

per pixel lighting are used to achieve authenticity of graphical representation. Physical model is based on ODE (Open dynamics engine). Each element in the resulting scene, with which cars or other dynamic objects can interact, has its own physical representation. Accuracy of simulation of vehicle physical behavior is the key parameter for practical usage for usability testing. Real characteristics like acceleration, inertia, brakes, slip were therefore developed. Part of the City Rider is also basic traffic simulator that controls motion of other cars to provide real traffic illusion.

The City Rider simulator was used for usability testing of in-car phone called Car Dialer. Main purpose of the test was to analyze usability of the in-car phone, controlled by voice. During the test we were also collecting the data for further simulator development. Analysis of this data for simulator improvements is the main contribution of this paper.

The results of the usability testing and data analysis lead to new features of the City Rider that are now being implemented. First of all we found, that the standard 19" display is not very suitable for the car simulator, because it does not provide sufficient view angle, comparable to the view angle in the real car. This problem was observed mainly in turnings, where the users wanted to see, what is round the corner. In future, the display must be changed for multiple displays or wide screen projection. Second finding is that for high-quality testing we need much more data from the test than just audio and video from observations. We found that users have problems to rate the usability of the product, because they subjectively tend to improve the quality of the product. We also needed some low level data, like amount and occurrences of pavements hits, speed and position of the car and others to deeply analyze user's problems. These problems are not always caused by parallel control of the in-car phone and may be caused by improper cognitive load of the simulator. Third improvements that are connected with the City Rider are development of additional information shown during the driving. This information like special banners or other disturbances can for example help to change amount of cognitive load or improve task definition and realism. It can also allow new testing techniques, which are similar to ones used in the car industry for the car safety testing, to be performed. The quality of cognitive load and comparison with the real car cognitive load are issues, we want to focus more in further research.

References:

[1] CHITTARO L., DE MARCO L.: *Driver Distraction Caused by Mobile Devices: Studying and Reducing Safety Risks,* Proceedings of International Workshop on Mobile Technologies and Health: Benefits and Risks, 2004.

[2] KJELDSKOV J., SKOV M. B., ALS B. S., HOEGH R. T.: *Is it Worth the Hassle? Exploring the Added Value of Evaluating the Usability of Context-aware Mobile Systems in the Field,* Lecture Notes in Computer Science, Berlin, Springer-Verlag, 2004, pp. 61-73.

[3] KALLMANN M., LEMOINE P., THALMANN D., CORDIER F., MAGNENAT-THALMANN N., RUSPA C., QUATTROCOLO S.: *Immersive Vehicle Simulators for Prototyping, Training and Ergonomics,* Proceedings of the Computer Graphics International (CGI'03), 2003, pp. 90 - 95.

This research has been supported by MŠMT grant No. MSM 6840770014.

Hybrid Real-Time Software Architecture with Low System Overhead and Table Driven FSAs

J. Zdenek

zdenek@fel.cvut.cz

CTU - Czech Technical University in Prague
Faculty of Electrical Engineering
Department of Electric Drives and Traction
Technicka 2, 16627 Praha 6, Czech Republic

Software architecture of real-time, computer controlled systems has many modifications and depends on application size, required speed, hard, soft or mixed real-time model, mono or multi processor design, network type used, optimality of task distribution among hardware nodes, available design time, budget size, experience of software designer and many other factors. Available hardware resources are important software design factor too. Often found limitation are: finite number of hardware interrupt channels, small number of interrupt priority levels, fixed priority levels, very small depth of hardware stack in digital signal processors (DSPs) families, lack of software stack pointer, limited software stack RAM space in microcontrollers, small very fast on-chip RAM with no wait cycles, no possibility to run code from fast RAM data area in some Harvard architecture DSPs etc.

Typical real-time software architectures are:

- Interrupt - no background systems: Simple systems with small user tasks and sufficient number of hardware interrupt resources. No system software available (typically). Application programmer designs all system activity of real-time program.
- Interrupt – background systems: Simple systems with similar feature as this one depicted above. In the background is typically organized only simple infinite loop with group of processing routines running sequentially, no timing, no scheduling. Application programmer again is responsible for all program activity.
- Real-time operating system RTOS: More complex systems with tenths to hundreds application tasks. Operating system has scheduler and dispatcher (executive) and its APIs with many useful services are available to application programmer. Scheduler is fully preemptive priority based [1] or on the same priority levels there can be applied round-robin strategy. Preemptive RTOS can be used as reliable basic layer to schedule and execute application tasks and to support user inter-task and/or inter-node communication [2], [3] including synchronization. As number of tasks goes high overhead of RTOS runs high extensively too and overall throughput and time response of RTOS can be unsatisfactory. RTOS utilizes intensively stack space of computer because typically each user task is equipped with separate stack to be task time behavior management organized easily.
- Hybrid systems – interrupt – background, with task scheduling on background level.

Hybrid real-time system presented here has been designed to be applicable to the real-time systems with many user (application) tasks (hundreds to thousands tasks) organized to complicated and large parallel (semi-parallel) finite state automata (FSA) in multi-node distributed computer systems with asynchronously running communication channels. Each computer network node has client-server architecture. Each node is supposed to be logically single processor unit, but inside one hardware board can be placed several nodes. Node

software consists of FSA clock centre, server channel command processor, master server FSA group, slave client FSA groups, group of FSA tasks executives, channel data synchronizer, master user bit-tasks bank, slave user bit-tasks banks, server processes table-like FSA descriptors, in-node slave processes table-like FSA descriptors, communication channels slave client processes table-like FSA descriptors, time sensitive communication channels interrupt driven services, diagnostic function services and service (debugging) channel interrupt driven routines. Inner software architecture of each node (module) is of mixed-model (hybrid) type – combination of interrupt driven routines and normalized finite state automata (FSA) running on program lowest priority level (background). Individual FSAs are running in semi parallel fashion and have fixed mutual priority. FSAs inside one group are principally synchronous but there is a possibility to run immediately next step if waiting to next synchronization clock has no reason. In each node (module) is one master (server) command processor to process messages from higher level communication channel and one or more active slave (client) FSAs to carry out detailed control and processing functions or to communicate with lower level node (module). Time sensitive actions (clock center, base of communication etc.) are processed by interrupt driven routines. Main functionality is based on action routines (called also bit-tasks) governed by FSAs. Each function is executed by process divided into threads. Each thread is composed from action routines (bit-tasks) executed by related FSA. Processes, threads and sequence of action routine invocations are described by descriptors (1), (2) and (3) respectively. Activity of individual master or slave FSA is defined by (4).

$$PC^{ri}_{j} = \{TH_1, TH_2, \ldots, TH_p\} \quad \text{– Process descriptor} \tag{1}$$

$$TH^{ri}_{j} = \{A_1, A_2, \ldots\ldots\ldots, A_p\} \quad \text{– FSA action descriptor} \tag{2}$$

$$NS^{ri}_{j} = \{N_1, N_2, \ldots\ldots\ldots, N_p\} \quad \text{– Process descriptor} \tag{3}$$

$$\begin{aligned} &\textit{Thread: } j = 0; \\ &\textit{repeat (go} \cap \textit{step)} \\ &\qquad \{ \textit{step=false; Action= F(} TH^{ri}_{j} \textit{); } j = NS^{ri}_{j} \} \end{aligned} \tag{4}$$

All descriptors are in self documented table format fashion (coded in "C" language) and without modification (i.e. error free) are included in final user documentation.

Presented architecture has been proved to be fully functional, maintainable, expandable and relatively application programmer friendly (experienced user) in system model with several hundreds of action routines (bit-tasks) and different FSA sync. clocks.

References:

[1] CHENG, A. M. K.: *Real-Time Systems: Scheduling, Analysis and Verification,* John Wiley, 2002, ISBN 0471184063.

[2] ZDENEK, J.: *Efficient DMA Based Local Computer Network Communication Services for Traction Vehicle,* Proc. of Int. Conf. on Ship Propulsion and Traction Systems SPRTS2005, Oct. 2005, Bologna, 2005 pp.44-51.

[3] ZDENEK, J.: *System Design and Software Architecture of Traction Vehicle Control Computer,* Proc. of 12th Int. Power Electronics and Motion Control Conference, Aug. 2006, Portoroz, pp.1205-1210.

This research has been supported by MSMT grant No. MSM 6840770015.

Cache Misses Prediction by Means of Data Mining Methods

Pavel Kordík, Ivan Šimeček

kordikp, xsimecek@fel.cvut.cz

Department of Computer Science, Faculty of Electrical Engineering, Czech Technical University, Technická 2, 166 27 Prague 6, Czech Republic

We obtained the ”Cache misses” data from the parallel computing group which is experimenting with simulation of cache memories. The goal of this project is to analyze this data and obtain the model of cache misses depending on input features such as associativity of the memory. We also need to determine the significance of input features.

Every modern CPU use a complex memory hierarchy, which consists of levels of cache memories. It is really difficult to predict the behavior of this hierarchy for the given program (for details see [1]). The Cache Analyzer (shortly CA) simulates the behavior of a real microprocessor’s cache and compute the number of cache misses during a computation. All measurements are done in the ”off-line” mode; the CA uses own virtual cache memory for the exact simulation. It also means that another CPU activity doesn’t influence the behavior of the CA. Using this analyzer tool we collected data measuring number of cache misses for various parameters of cache, dimensionality of matrices, etc. These data were essential to make the analytical estimation of the number of cache misses (for details see [2]). The cache misses data were also analyzed by means of data mining methods. This is the main topic of this paper and we will discuss the data mining analysis bellow in the more detailed form.

At first the data had to be preprocessed. It was transformed into the native format of the data mining application WEKA [3] where almost all experiments have been performed. We tried to predict the number of cache misses from input variables (read operations, size of matrices, etc.). The data mining methods from the category of decision trees, Bayes classifiers and neural networks were used. The detailed description of these methods can be found in [4]. Because WEKA is designed to solve mainly classification problems, we had divided the output attribute ”number of cache misses” into 10 intervals (classes). We achieved just 62% classification accuracy by Bayes based methods (Bayes Net, Naive Bayes Simple, etc.). Other methods were unable to give any results because of memory demands. When we studied why the performance is so low, we found out that the data should be further preprocessed. New data set were created from the original one by leaving out redundant measurements with low additional information. It consisted from 1500 records that representatively described number of cache misses (almost uniformly distributed). With this new data set we achieved for data mining methods following classification accuracies:

- MultiLayer Perceptron MLP (92%),
- Radial Basis Function network RBF (93%),
- decision tree C4.5 (95%), etc.

This accuracy is perfect so we can conclude that using data mining methods, we can estimate the number of cache missed with relatively low error.

Data mining also allows us to find out which input variables (features) are most important in estimating the number of cache misses (feature ranking). Again, we performed several experiments with method for feature ranking available in WEKA. The results show that the most important feature is readCount (number of read operations), followed by nonzero (number of nonzero elements in the matrix) and width (the thickness of the strip)

feature. Surprisingly the size (size of the matrix) feature was on the fourth position in average - gaining much lower significance than we expected.

We have loaded the data into the YALE software. To examine the properties of the data set we used self organizing map mapping the space of input features into two dimensional plot. There are several clusters present in the data set. The most important information we can extract from the map is that vectors with high number of cache misses are divided from other vectors.

Our experiments with the projection of raw data revealed that probably the most significant attributes are matrix dimension, distance of non-zero values from diagonal and number of nonzero values. The vectors with high misses rate are separable from other vectors. It means we should be able to get good prediction of cache misses even with these three input features. The diagonal distance feature appears to be the most important when you look at the distribution of the data. To prove our assumptions, we have used the GAME software to extract the significance of the input features and to derive simple predictive model of cache misses rate.

We extracted the math formula from the inductive model. The configuration of the GAME engine was set to default values, just the CombiNeuron units were selected and these units were penalized for complexity with the penalization ratio R=115. The extracted formulae is not in trivial form, it can be further simplified: The most frequented input feature in the formulas are cache block, degree asoc and diag dist. Other inputs do not appear at all - they were not considered significant. To examine the significance of input features we made the following observations.

The significance of input features is derived from niching genetic algorithm (used in GAME to optimize the topology of models). The first layer of the model (units can use just one input) the major feature is cache block. Its significance decreases in further layers, but it is still the most important feature in the fifth layer. The result acquired from 5 GAME models is similar to the one obtained in the previous experiment. The input feature cache block is the most significant and read op is the least significant feature.

We made a lot of experiments in the YALE and GAME software. The results of these experiments indicate that the predication of cache misses is possible given the input features provided. Some of these features are irrelevant (number of read operations). The math equation we obtained from the GAME software can be utilized in prediction of cache misses as well as studying the influence of input features to misses occurrence.

References:

[1] K. BEYLS, E. D'HOLLANDER: *Exact compile-time calculation of data cache behavior,* Proceedings of PDCS'01, 2001, pp. 617-662.

[2] X. VERA, J. XUE: *Efficient Compile-Time Analysis of Cache Behavior for Programs with IF Statements,* International Conference on Algorithms And Architectures for Parallel Processing, Beijing, 2002.

[3] THE UNIVERSITY OF WAIKOTO: *WEKA data mining software,* http://www.cs.waikato.ac.nz/ml/weka/.

[4] I. H. WITTEN, F. EIBE: *Data mining: practical machine learning tools and techniques,* 2nd ed. Morgan Kaufmann series in data management systems, 2005, ISBN: 0-12-088407-0.

This research has been supported by MŠMT under research program MSM6840770014.

A New Format for the Sparse Matrix-vector Multiplication

Ivan Šimeček

xsimecek@fel.cvut.cz

Department of Computer Science , Faculty of Electrical Engineering, Czech Technical University, Technická 2, 166 27 Prague 6, Czech Republic

Abstract

Algorithms for the sparse matrix-vector multiplication (shortly SpMV) are important building blocks in solvers of sparse systems of linear equations. Due to matrix sparsity, the memory access patterns are irregular and the utilization of a cache suffers from low spatial and temporal locality. To reduce this effect, the register blocking formats were designed. This paper introduces a new combined format, for storing sparse matrices that extends possibilities of the diagonal register blocking format.

Introduction

There are several formats for storing sparse matrices. They have been designed mainly for the SpMV. The SpMV for the most common format, the *compressed sparse rows* (shortly CSR) format, suffers from low performance due to the indirect addressing. Many studies were published about increasing the efficiency of the SpMV[1,2].

There are some formats, such as *register blocking*, that eliminate indirect addressing during the SpMV. Then, vector instructions can be used. These formats are suitable only for matrices with a known structure of nonzero elements.

The overhead of a reorganization of a matrix from one format to another one is often of the order of tens of executions of a SpMV. So, such a reorganization pays off only if the same matrix A is multiplied with multiple different vectors, e.g., in iterative linear solvers.

The register blocking formats

These formats are designed to handle randomly occurring dense blocks in a sparse matrix. We will discuss only about *register blocking* (shortly *RB*) [1,3,4]. Nonzero elements of matrix A are grouped into dense diagonal blocks whose sizes can differ.

When we compare our work with similar project SPARSITY [1] (and his successor OSKI) which is based on different ideas:

1. It uses register blocking formats - it handles randomly occurring dense mini-blocks.
2. It uses also a cache optimization, but in completely different approach than in our approach.
3. Author overlooks the matrix transformation time overhead in contrast to our algorithm.

Design of new format for sparse matrices

We include new features to our format:

a) The combined format feature - In the classical RB format, all nonzero elements must be in blocks so blocks of size 1 can exist. Simply speaking, in our format, some elements are stored in the CSR format, while the blocks in the RB format.

b) Cache adaptive feature - We divide matrix A into disjoint nonempty rectangular regions so that the cache can hold all data accessed during the partial SpMV within each region.

c) Partially full blocks feature - To reduce the number of blocks, we omit the assumption of only fully dense blocks and allow also partially full blocks. The maximum sparsity of blocks can be defined by a block heuristic.

Various (even architecture dependent) block heuristics can be designed. We have designed algorithm to find blocks with minimal space complexity. This algorithm uses dynamic

programming so its computational and space complexity for *a* times *b* region is approximately *Theta(a b)*.

Evaluation of the results

All results were measured at Pentium Celeron 2.4 GHz, 512 MB@ 266 MHz, running OS Windows XP with the following cache parameters:
SW: Microsoft Visual C++ 6.0 Enterprise edition and Intel compiler version 7.1
All cache events were monitored by Intel Vtune performance analyzer 7.0.
For testing purposes, we have used 52 real matrices from various technical areas from MatrixMarket and Harwell sparse matrix test collection. We compare performance of CSR format with our format, but it is very hard to conclude the results from our test data set. Speedups depend strongly on the structure of nonzero elements (it means on the "origin" of the matrix).

1) Significant speedups (sometimes over 200%) were achieved for matrices of PDE origin.
2) No speedups were achieved for matrices with the near-random structure.

In this paper, we described a new format for storing sparse matrices that combine advantages of the CSR format and the RB format. This format is also adaptive to the parameters of the CPU cache.

References:

[1] E. IM: *Optimizing the Performance of Sparse Matrix-Vector Multiplication,* Dissertation thesis, University of Carolina at Berkeley, 2001.

[2] J. MELLOR-CRUMMEY, J. GARVIN: *Optimizing sparse matrix vector product computations using unroll and jam,* International Journal of High Performance Computing Applications, 225–236, 2004.

[3] R. VUDUC, J. W. DEMMEL, K. A. YELICK, S. KAMIL, R. NISHTALA, AND B. LEE: *Performance optimizations and bounds for sparse matrix-vector multiply,* Proceedings of Supercomputing,, 2002.

[4] K. R. WADLEIGH, I. L. CRAWFORD: *Software optimization for high performance computing,* Hewlett-Packard professional books, 2000.

This research has been supported by MŠMT under research program MSM6840770014.

An Adaptive Solver for Fluid Dynamics on the GPU

Ondřej Štáva, Ivan Šimeček

xsimecek@fel.cvut.cz

Department of Computer Science, Faculty of Electrical Engineering, Czech Technical University, Technická 2, 166 27 Prague 6, Czech Republic

Abstract

Visualization and simulation of fluid flows has always been one of the most interesting and challenging problem in computer graphics. Fluid dynamics is widely used for simulating of many natural phenomena like fire, smoke, water, or wind and so, a lot of effort has been spent to develop methods for solving it. The methods vary in accordance to the target usage. For engineering applications such as simulation of air flow around a wing, we usually want very precise solvers, whereas in special effects industry, we focus mainly on the visual quality of the result and the simulation does not have to be precise.

This work is focused on a fluid simulation for real time environments such as computer games. This target area has been influenced by a massive enhancement in computer graphics quality in recent years, thanks to the development of dedicated 3D graphics processing units (GPUs). However, when we look on the other aspects, such as game physics, we can see that the development was only minor or none and there is still a big room for improvements.

Introduction

Fluids like smoke or fire have been usually simulated by a particle system, which emits particles in one direction. The particles are usually affected only by the gravity or a wind force, and after some time, they die. This approach is very easy to implement, however it often lacks any possibility of an interaction with an environment. For example, when we put some object into a fire, the fire flow does not change and the simulation looks very unrealistic. To see the expected result, which is fire nicely flowing around the object, we have to compute equations describing the fluid motion. These equations are called the Navier-Stokes equations.

The Navier-Stokes equations cannot be in general solved analytically and we need to find a numerical solution for them. Most of the real-time solutions are based on simulation of fluid dynamics on regular Cartesian grids. One of the first attempts to produce real-time solver was published by Chen et al., however this solver is stable only for very small simulation time steps.

The modern real-time solvers for fluid dynamics are usually based on the work published by Jos Stam[1], where he presented an unconditionally stable solver for Navier-Stokes equations. The simulation of fluid dynamics on regular Cartesian grid can be very well parallelized, as it will be explained later. Due to this fact, there were successful attempts to implement a fluids solver on the GPU, using it as a general stream processor (for details see [2]). The GPU implementation was for example used in a real-time cloud simulation created by Mark J. Harris[16], where the GPU performs all steps of the simulation and the CPU can be used for other tasks.

As it has been mentioned, the real-time methods for simulating fluid dynamics work on regular Cartesian grids. The grid represents an environment where the fluid is simulated and so it has to be big enough to fully cover the whole fluid. However as we can imagine, the fluid usually does not cover the whole environment regularly and so a lot of computational power is wasted to solve the solution on places where it is not needed.

The described problem is solved by refining the grid only on places where the solution is needed. Fluid motion is then computed by so called adaptive solvers. These solvers have to

dynamically update the grid refinement at each simulation step and they have to handle all special cases which occur between cells with different refinement.

Goals

The thesis main goal is to create an adaptive real-time solver for fluid dynamics in 2D based on Stam's method[1], using the modern programmable graphics hardware. When using this method one of the most critical part of the solution is to solve Poisson's pressure equation. When using adaptive solver the best approach is to use a multigrid method[3] which can be easily modified to support adaptive grid refinement. The non-adaptive multigrid method have already been successfully implemented on the GPU for example by Bolz et al. or Goodnight et al. Method used in this thesis differs not only in the adaptiveness but also in other important aspects like discretization scheme or target usage. My work uses cell-centered discretization and is targeted for real-time uid dynamics simulation, whereas the above solutions were using vertex-centered discretization and were targeted for more general usage and their solvers were not particulary optimized for simulating fluid dynamics. When creating the GPU version of the adaptive multigrid method, we are facing several non-trivial problems like dynamic grid refinement without using the CPU, or support for moving obstacles. The other goal is to use this solver for a fluid simulation. For this purpose, I implemented a simple simulation of a smoke-like gas which is flowing around obstacles. The simulation nicely demonstrates how the smoke reacts to the obstacle movements and how the grid is refined on the places where it is necessary. As it has been already mentioned the solver presented in this work is suitable only for 2D grids. Its extension to the 3D is planned for a future work. The necessary changes for the 3D implementation are beyond the scope of this paper.

Conclusions

Many publications about adaptive solutions for fluid dynamics have been published, however most of them were targeted for engineering usage, not for real time applications. My work is based primarily on PhD. thesis published by D. Martin[4] which is focused on adaptive cell-centered methods for incompressible Euler equations in general, and on work published by S. Popinet, who introduces quadtree and octree refinement strategy for regular Cartesian grids.

References:

[1] J. STAM: *Stable fluids,* Siggraph 1999, Computer Graphics Proceedings ACM Trans. Graph., 1999, pages 121-128.

[2] J. D. OWENS, W. J. DALLY, U. J. KAPASI, S. RIXNER, P. MATTSON, B. MOWERY: *Polygon Rendering on a Stream Architecture,* 2000 SIGGRAPH/Eurographics Workshop on Graphics Hardware., August 2000, pages 23-32.

[3] U. TROTTENBERG, C. W. OOSTERLEE, A. SCHULLER: *Multigrid,* Academic Press, 2000.

[4] D. MARTIN: *An adaptive cell-centered projection method for the incompressible euler equations,* PhD thesis, 1998, UC Berkeley.

This research has been supported by MŠMT under research program MSM6840770014.

A New Approach for Accelerating the Sparse Matrix-vector Multiplication

Ivan Šimeček

xsimecek@fel.cvut.cz

Department of Computer Science , Faculty of Electrical Engineering, Czech Technical University, Technická 2, 166 27 Prague 6, Czech Republic

Sparse matrix-vector multiplication (shortly SpMV) is one of most common subroutines in the numerical linear algebra. The problem is that the memory access patterns during the SpMV are irregular and the utilization of cache can suffer from low spatial or temporal locality. Approaches to improve the performance of SpMV are based on matrix reordering and register blocking. These matrix transformations are designed to handle randomly occurring dense blocks in a sparse matrix. The efficiency of these transformations depends strongly on the presence of suitable blocks. The overhead of a reorganization of a matrix from one format to another one is often of the order of tens of executions of a SpMV. For that reason, such a reorganization pays off only if the same matrix A is multiplied with multiple different vectors, e.g., in iterative linear solvers. This paper introduces new approach for the acceleration the SpMV. This approach consists of 3 steps: 1) dividing matrix A into non-empty regions, 2) choosing an efficient way to traverse these regions (in another words choosing an efficient ordering of partial multiplications), 3) choosing the optimal type of storage for each region. All these 3 steps are tightly coupled. The first step divides the whole matrix into smaller parts (regions) those can fit in the cache. The second step improves locality during the multiplication due better utilization of distant references. The last step maximizes machine computation performance of the partial multiplication for each region.

In this paper, we describe aspects of these 3 steps in more detail (including fast and time-inexpensive algorithms for all steps). Our measurements proved that our approach gives a significant speedup for almost all matrices arising from various technical areas.

In general, there is only one way to improve the locality in SpMV [1,2]: by making the multiplication more cache-sensitive. In a typical numerical algorithm, the cache hit ratio is high if the cache can hold data accessed in the innermost loop of algorithms. Memory accesses that do not satisfy this assumption are called distant references. In this paper, we propose and explore a new method for increasing the locality of the SpMV consisting in 3 steps:

1. Dividing matrix A into disjoint nonempty rectangular regions.
2. Choosing a suitable storage format for the regions.
3. Choosing a good traversal of these regions during the SpMV .

We divide matrix A into disjoint nonempty rectangular regions so that the cache can hold all data accessed during the partial SpMV within each region. In this paper, we assume for simplicity that regions are square submatrices of the same size r containing at least one nonzero element. An optimal value of r is hard to predict, because it depends on locations of nonzero elements and cache sizes. Regions are viewed as submatrices. Therefore, we can use common sparse matrix formats for storing nonzero elements inside them. We can use information that an element is inside a region, so we can express all coordinates relatively to the region. All coordinates can be stored by using smaller data-types (char or byte) instead of

long int. It leads to the compressed representation of the input matrix. We call these new formats R-based. In the following text, we will consider only R-CSR and R-XY formats.

For the performance of a program, a high cache hit ratio (high locality) is crucial [3]. Better locality in SpMV is only one step to higher performance of the SpMV [4]. Choosing a good traversal is equivalent to finding a good ordering of regions (partial multiplications). We can simply say that the traversing is good if it leads to a fast SpMV. Now we will discuss this obvious assumption in more formal way with an in-depth analysis. The problem of minimization of L is equal to the problem of optimal indexing of V. It is an NP-complete problem, so finding an optimal solution is hard. To find out whether our approach is vital, we have considered only several standard region traversals.

In this paper, we have presented a new approach for acceleration of the sparse matrix-vector multiplication. This approach consists of 3 steps. Firstly, we divide the matrix A into nonempty disjoint square regions. Secondly, we choose a suitable storage format for each region. We introduce new sparse matrix R-based (R-XY or R-CSR) formats for additional acceleration of the SpMV. These new formats caused much less compulsory misses. Thirdly, we present a methodology for finding a good region traversal. We compare measured and predicted values. For all types of sufficiently large matrices arising from various technical disciplines, our approach gives a significant speedup. The matrix transformation is relatively fast and straightforward. Our measurements prove that matrix transformation pays off for relatively small number of SpMV.

References:

[1] P. TVRDÍK, I. ŠIMEČEK: *Analytical modeling of sparse linear code,* Numerical Analysis and Applications, 3, 2004, pp. 566-573.

[2] K. R. WADLEIGH, I. L. CRAWFORD: *Software optimization for high performance computing,* Hewlett-Packard professional books, 2000.

[3] O. TEMAM, W. JALBY: *Characterizing the Behavior of Sparse Algorithms on Caches* Supercomputing, 1992, pp. 578-587.

[4] J. WHITE AND P. SADAYAPPAN: *On improving the performance of sparse matrix-vector multiplication,* In in Proceedings of the 4th International Conference on High Performance Computing (HiPC '97), IEEE press, 1999, pp. 578-587.

This research has been supported by MŠMT under research program MSM6840770014.

Prototype Implementation of the Execution Engine VPU

M. Dráb, L. Kalvoda, S. Vratislav, M. Dlouhá

drab@kepler.fjfi.cvut.cz

Department of Solid State Engineering, Faculty of Nuclear Science and Physical Engineering, Czech Technical University, Trojanova 13, 120 00 Prague 2, Czech Republic

The actual implementation of the third topmost layer of the Execution Engine, which is the Execution Engine itself, is mostly following the design draft as stated in [1], chapter 3 and 4. The actual instance of the EE is realized by a structure called indecs_ee_t. Among other things it holds a list of contexts, a list of allocated Local Memory Blocks, a structure with the global registers of the EE, the table of targets that are to be considered as a source of the local routing paths, list of input and output instruction streams (connections) and other things important to the fast and possibly simple operation of the VPU (See [1] and [2] for description of the named objects). Let's briefly see some overview of actual implementation of selected parts of the EE (For a bit more information see e.g. [3], where are also described some deviations of the EE implementation from the original draft [1]).

Contexts are defined as a concurrent (though cooperating) sources of instructions. They are instatnitated by a structure called indecs_context_t. These structures are organized in several ways. The first way is the list of contexts available to the particular instance of the EE. It is a dynamically linked list with a header placed in the indecs_ee_t structure and its purpose is to just have all the available contexts listed on one place, so that it is easy to handle them globally, e.g., terminating them properly upon the termination of the EE and such.

The other way of organizing the indecs_context_t structures is of more practical use and is aimed towards speeding up the process of the EE's scheduler to be able to faster decide which context is to be chosen to execute the next virtual instruction. According to [1], chapter 3.2, the whole scheduling scheme of the EE is based on a priority based cooperative multitasking. The next context to be scheduled for executing the next virtual instruction is allways the one, that has the biggest priority number and is ready to execute an instruction, i.e., it has a whole instruction that is to be executed next in within the context available.

To speed up the process of searching the the appropriate context the indecs_context_t structures are also organized in another way. There is a dynamic list of occupied priorities, i.e., each priprity that contains at least one context has an entry in this list. This list is descendently ordered according to the priority. This allows quickly finding the topmost priority context(s) (it takes a constant time) and possibly quickly skip to the next lower priority which also takes a constatnt time and so on. Each entry within this list contains another dynamic list of all contexts (i.e., their indecs_context_t structures) that are currently on that particular priority level. This organization allows us to easily implement the round-robin principle of executing contexts that are on the same (top) priority, according to [1]. The next context to be scheduled on the particular prioriry level is the one that is on the top of the list connected to that priority within the list of occupied priorities. Upon the scheduling the context is moved to the bottom of that list (which is again a constant time operation), which assures the requested round-robin behaviour.

To speed up the searching of appropriate context based on its Context Identification (CID, see [1]), the list of all contexts is hashed according to the CID in addition to the organization in the dynamic list. To speed up the process of searching the lists particular priority level during the operation of reassigning a context's priority, the list of occupied priority levels is hashed as well, this time using the priority level as a hashing key.

The routing mechanism is implemented according to [1], chapter 3.10. However in order to use all of the possibble combinations of the routing registers GREN*i*, GRTE*i* and GRTN*i* and to speed things up a bit, another set of 255 1-bit registers called GRE*i* (Global

Routing Enable) was added. These registers when set to a 0 disable the operation of the particular GREN, GRTE and GRTN registers with the same index, when set to a 1, these are enabled.

To speed up the process of checking which of the 256 targets the routing should apply to, these new 256 1-bit GRE registers are stored as 8 32-bit values which can be tested for non-zero value as a whole and then possibly dig deeper into the individual bits, if it is going to be necessary. Another thing that should speed up this process is a special array of 256 entities held within the indecs_ee_t structure. This array contains for each of the targets a reference counter, i.e., the number of local routing paths that take this particular target as a source for the routing and though are of interest to the routing mechanism, and an index of the first local routing path (by a local routing path in this context we understand the three registers GREN*i*, GRTE*i* and GRTN*i* with the same index *i*), i.e., the one with the lowest index, that takes this target as a source. The searching of the local routing paths for the specific target is then eased in a way, that we explicitly know which is the first one (its index) and that we know how many of such local routing paths there is, so we don't need to go through all of the 256 GREN registers for each executed instruction, in order to see where we need to route it.

The first prototype of the Execution Engine VPU core has been constructed. It yet needs to undergo a series of testing and debugging in order to optimize and determine its characteristics. However the process of integrating it into a full experiment control system still requires a lot of work. First the derivative of the EE, the External Execution Module (EEM) prototype has to be constructed. Next step would be a construction of a simple network consisting of several of these components interconnected together and testing of its operability. Further a series of special EEMs to interact with the actual hardware of the experiment (in this case devices belonging to the KSN-2 diffractometer, whose driving is the ultimate goal of this project) have to be created and tested. Another task would be to create a simple and flexible user interface to let the user actually interact with the experiment control system.

References:

[1] DRÁB, M.: *Project INDECS: The Design of a Superior System of Data Collection and Analysis (Diploma Thesis),* Faculty of Nuclear Science and Physical Engineering, Czech Technical University, Prague, 2003

[2] DRÁB, M. – KALVODA, L. – VRATISLAV, S. – DLOUHÁ, M.: *Execution Engine: The Virtual Processing Unit for Driving Physical Experimental Systems,* Proceedings of Workshop 2004, Part A, Special Issue, Volume 8, Czech Technical University in Prague, 2004, pp. 306–307.

[3] DRÁB, M.: *Prototype Implementation of the Execution Engine VPU Core,* Doktorandské Dny 2006, sborník workshopu doktorandů FJFI oboru Matematické inženýrství, nakladatelství CVUT, 2006, pp. 19–25.

This research has been supported by MSM6840770021 and JINR 22-03007.

Automatic Integration of Ontologies

Radek Jun, Ivan Jelínek

junr1@fel.cvut.cz, jelinek@fel.cvut.cz

Department of Computer Science and Engeneering, Faculty of Electrical Engineering, Czech Technical University, Technická 2, 166 27 Prague 6, Czech Republic

Every day we see the growth of information resources on the web. Together with this growth, the user base and miscellaneous type of terminal devices also grows. In such a situation, the necessity of sorting information for specific group of users arises and the necessity of filtering output information for various types of devices (PDA, mobile phone, TV) becomes an issue. Adapting of these resources could reduce amount of received information, thereby making data searches easy.

Adaptive systems can enhance effective utilisation of huge information resources by reducing the range of information provided to a specific user need. However, the reduction has to be sufficiently smart, neither too little nor too much. A user has to have the chance to change adapted results to non-adapted results and thus control the adaptation process. It should be possible to adapt navigation, content and presentation [5].

We would like to use semantic model for data resources of an adaptive web system. In the HERA methodology [1] it is called *conceptual design*. The semantic model could enable better adaptation process and provide better quality of information. Results from present research in semantic web based on a semantic show that the related complications outweigh the benefits.

Our goal is to search for the right way to use semantics on the web in order to make implementation simple and provide a well arranged user interface. We would like to use the standardised formats, such as *XML*, *RDF*, *RDFS*, *OWL,* which could help share and reuse information sources [1].

Beside adaptation processes there is another major part of a web based system which is data (information) source. If we would like to use some semantics with information, we also need to know how to merge or integrate input sources. We need some semantic metrics [2], which help us to say if some ontologies are same or not. The use of ontologies for resource description seems to be ideal way for data processing by computers. So any web system should be able to work with this type of resources. Namely should be able to merge or to integrate different ontologies.

There we could recognize two basic types of differences on different ontologies. The first type is when each of two ontologies describes different domain. In that case ontologies have to be merged to an one super ontology over common parts (if there is any) or over any more general ontology [3]. The second type is of differences on ontologies is when each ontology describes the same domain, but from different point of view or by a different means. In this case ontologies have to be aligned together in order to make coverage which overlap particular differences on an ontology [3].

Another question is range of integration process automation over all input ontologies. The process of integration has many problems which is not fully solved. This ontology mismatches can be divided into two groups – ontology-level mismatches and language level mismatches [3]. The main problem is with computer understanding of ontology.

Semantic information help to a computer to work with information more efficiently but without any understanding to a text (information) content. This complicate any automation processes because sometimes is very hard to be sure if two nodes (if we look at ontology

definition as at a tree) are the same, similar or different. But a text (information) with semantic information has much more information which really helps to a computer with data processing. It seems that if there is more information about information then it will help with this automation process. But with growth of ontology have to also grow complexity and process time.

To prevent this growth many real projects use some restrictions. A typical restriction is using OWL-DL instead of OWL-Full or using of specific ontology languages. But have to be found balance between amount of restrictions and rest properties of semantic.

We would like to create a web application model which is based on fully automatic ontology integrated data resources. We would like to specify a set of restrictions on input ontologies which guarantee the property of fully automatic integration. All input ontology describes the same domain, but can have small local differences. These small local differences provide dynamic property and could be for example some extra property in ontology definition.

The web application presents input ontology as web pages which can have feedback and the application have to provide safe way back to input (source) ontology (have to cover across small differences). This safe way back is guaranteed by the set of restrictions on input (source) ontologies, because will be possible to say if two ontologies are same (with small local differences) or not. If two input (source) ontologies are not the same, then is impossible to use them with the application. For a set of ontologies which is mark as same will the web application provide full automation integration service.

References:

[1] FLAVIUS FRASINCAR, GEERT-JAN HOUBEN: *Hypermedia Presentation Adaptation on the Semantic Web,* Vydavatel, 2002.

[2] HU B., KALFOGLOU Y., ALANI H., DUPPLAW D., LEWIS P., SHADBOLT, N.: Semantic Metrics Springer-Verlag Berlin Heidelberg, 2006.

[3] PREDOIU L., FEIER C., SCHARFFE F., BRUIJN J., MARTÍN-RECUERDA F., MANOV D., EHRIG M.: *State-of-the-art survey on Ontology Merging and Aligning V2* Digital Enterprise Research Institute, University of Innsbruck, 2005-2006.

[4] KUTZ O., LUTZ C., WOLTER F., ZAKHARYASCHEV M.: *E-connections of abstract description systems* Vydavatel, 2003.

[5] JUN R., JELÍNEK I.: Adaptive web based on Semantic Model, In Proceedings of the Interenational Conference on Computer Systems and Technologies. Varna: Academy of Sciences, 2006, s. V-12-1-V-12-6. ISBN 954-9641-46-5.

This research has been supported by MSMT under research program No. 6840770014. This research has been supported by the grant of the Czech Grant Agency No. 201/06/0648.

Using of Hyperspectral Satellite Data for Environment Monitoring in the Czech Republic

K. Pavelka*, J. Svatušková **

pavelka@fsv.cvut.cz

*Laboratory of Photogrammetry, Dept. of Mapping and Cartography,
**Laboratory of Remote Sensing, Dept. of Mapping and Cartography,
Czech Technical University Prague, Faculty of Civil Engineering,
Thákurova 7, 166 09, Prague 6, Czech Republic

New generations of satellites and entry of the private sector into space research and to the remote sensing data market brought along re-interest in remote sensing. The resolution of contemporary satellites competes with photogrammetry in many respects and development of technologies combining active and passive detectors and also new processing technology can be expected.

Multispectral imaging and processing is a well-developed technology that has been used for many years in environments. The spectral signatures are used for designation of pixels to classes. The spectral information obtained from one image pixel will resemble a spectrum of the same material obtained through laboratory spectroscopy, but atmospheric and terrain corrections must first be done before a direct comparison of image and laboratory spectra can be made. Classical multispectral imaging uses 2-7 spectral channels (Spot, Landsat). The pixel designation to a class is made with explicit probability. With fewer spectral channels and greater width of the spectral channels the findings of the class are worse. For this reason the effort is to increase the number of spectral channels and to reduce their width. However, this activity (called hyperspectral imaging) carries technical problems in construction of devices.

In contrast to classical multispectral instruments, hyperspectral sensors measure hundreds of narrow, contiguous wavelength bands. This type of detailed pixel spectrum provides much more information about the surface than a multispectral pixel spectrum. The number of measured wavelengths is not what defines a sensor as hyperspectral. Rather it is the narrowness and contiguous nature of the measurements. For processing in special software, the spectral libraries are necessary. Spectral libraries are collections of spectral reflectance curves for natural and manmade materials. A reflectance spectrum measures the amount of energy reflected from a surface across a range of wavelengths. As mentioned already, it is the pattern of reflectance and absorption in a reflectance spectrum that enables us to identify spectrally unique materials. Spectral libraries can be made from laboratory or field analysis for materials of known composition. These libraries are a source of reference spectra and aid in the analysis of the hyperspectral dataset. In some projects, the ASTER instrument on Terra-1 satellite can be use as a hyperspectral sensor. ASTER captures high spatial resolution data in 14 bands, from the visible to the thermal infrared wavelengths; and provides stereo viewing capability for digital elevation model creation. The VNIR portion of the ASTER sensor includes two independent telescopes, a Nadir looking one and a backward looking one to help minimize image distortion during data capture. This simultaneous data capture provides true stereo coverage from which a digital elevation model (DEM) can be automatically extracted from using special software.

Sponsored by a grant of the Ministry of Environment, there was a possibility to use and process hyperspectral data by Geomatica 10.01 software and ENVI software. The **EN**vironment for **V**isualizing **I**mages is the most advanced remote sensing software available. ENVI is an extremely powerful tool for analyzing the content of hyperspectral images. The data from Terra/ASTER were processed by using Geomatica. From ASTER data sets the DEM was derived. In the Laboratory of Remote Sensing at the Czech Technical University in Prague, we have 17 scenes from ASTER from the years 2002-2006 for processing and the original spectral library from USGS at present.

Hyperspectral scanning is one of the new lines in remote sensing, it generally consists in reflectivity measurement in tens or hundreds of spectrum bands and in the comparison of the course of reflectivity with reference standards. This way provides significantly better classification of objects of the land surface and their state. In addition to several aerial scanners, there is only one true civil hyperspectral satellite carrier – the satellite Hyperion. In our project, the delivery of Hyperion data was delayed (from meteorological and technical reason); we now have three scenes from the Czech Republic (May and July 2006). The aim of hyperspectral data processing will be a survey of the Neratovice area (40 km north of Prague). This area was heavy polluted by catastrophic flooding in 2002 – in this area the chemical industry near the River Elbe is located. The second aim will be a survey of archaeological interest – this area is rich in findings and some constructional parts (megalithic) can be visible by using hyperspectral data together with very high resolution satellite data (QuickBird). The classical airborne archaeological prospecting depends mainly on vegetation and weather or climate status.

References:

[1] K.PAVELKA,L.HALOUNOVÁ: *Using of high-resolution satellite data for environmental hazard areas monitoring,* ISPRS International Workshop on Processing and Visualization using High-Resolution Images, ISSN 1682-1777 The International Archives of the Photogrammetry,Remote Sensing and Spatial Information Sciences, Vol XXXVI-5/ WG1, 2004, pp. 185-191.

[2] K.PAVELKA,L.HALOUNOVÁ: *Using of TM data and VHR data for reclaimed areas monitoring using vegetation indices,* ISPRS International Workshop on Processing and Visualization using High-Resolution Images, ISSN 1682-1777 The International Archives of the Photogrammetry,Remote Sensing and Spatial Information Sciences, Vol XXXVI-5/WG1, 2004, pp. 259-263.

[3] K.PAVELKA,L.HALOUNOVÁ: *Monitoring of Landslide Using Photogrammetry and Remote Sensing,* Brno GIS 98, Proceedings of Conference,ISBN80-210-1841-0 19982002, pp. 235-243.

[4] M.DANIEL,P.ZEMAN,J.KOLÁŘ,K.PAVELKA,J.SÁDLO: *Tick-Borne Encephalitis and Lyme borreliosis: Comparison of Habitat Risc Assessmant Using Satellite Data,* Central European Journal of Public Health, No.1/Vol.7, 2/1999, ISSN 1210-7778, Czech Medicin Association J.E. Purkyne, 1999, pp-28-35

This research has been supported by the Czech Ministry of Environment within the framework of the program VaV-Grant SM/10/70/04 (CTU 26-41535).

Updated Virtual Control Laboratory

M. Hofreiter, P. Trnka, M. Kopecký

Milan.Hofreiter@fs.cvut.cz

Department of Instrumentation and Control Engineering, Czech Technical University, Technická 4, 166 07 Prague 6, Czech Republic

The increasing use and sophistication of automation in modern engineering systems has created the need for students of all engineering specialization and academic levels to have full working knowledge of the principles and techniques involved in control system design as well as having the practical experience to implement it successfully. This can only be gained by 'hands-on' use of equipment. It is considered essential, therefore, that the training given to all engineering students includes both theoretical and practical aspects of control engineering.

In Czech Technical University in Prague, Faculty of Mechanical Engineering there is a common course Automatic Control for all students in the third study year. Practical training as a component part of the course is realized in the laboratory of Automatic Control, which is one of the laboratories of Department of Instrumentation and Control Engineering.

The laboratory models serve for practicing the fundamentals of logic, analog and digital control (see [1]). To arouse interest in control theory the old laboratory models were removed and substituted by new ones, which are more attractive for students. The apparatuses were manufactured in Department of Instrumentation and Control Engineering with the help of students [3].

With the development of new computer technologies it is now possible to simulate engineering and science laboratory projects on a computer. With Internet access, "virtual laboratories" can be offered to students via the WWW or CD-ROM. Therefore the Virtual Control Laboratory is being gradually developed in Department of Instrumentation and Control Engineering. The portal of the Virtual Control Laboratory is on the address: **http://www.fs.cvut.cz/cz/U210/ar**

The Virtual Control Laboratory [3] is an interactive environment where it is possible

- to design logic circuits
- to find out static and dynamic characteristic of processes and closed-loop systems (e.g. transient responses, frequency responses)
- to select controller (P,I,PI,PD,PID, on-off controller, three positional controller)
- to design controller settings
- to view time courses of the manipulated variable, the controlled variable, the load disturbances and the setpoint
- to design time courses of the disturbances, the setpoint and the manipulated variable (in the manual control)

All virtual models are described and governed in the same manner. Each experimental apparatus contains the following items:

- title
- schematic diagram
- colour photography + video
- description
- tasks
- visual simulation
- literature

WWW pages were built up in the hypertext mark-up language (HTML 4.0). The hypertext of the individual items contains links to additional Web-based resources with related information. The applets for visual simulation were developed in Java 1.5.0 code. Netscape Navigator version 4.6 or Microsoft Internet Explorer version 4.0 and higher may be used to display and execute all actions of the user.

The Virtual Control Laboratory has been updated to correspond with the Real Control Laboratory in the Department of Instrumentation and Control Engineering. Five new virtual models were built up: "Bathyscaph II", "Bathyscaph III", "Ball & Ellipse", "Buggy on the Belt Conveyer" and "Air Levitation", which correspond to four new real models developed in Department of Instrumentation and Control Engineering for education purposes [2].

The laboratory models "Bathyscaph II" (for logic control) and "Bathyscaph III" (for analog and digital control) demonstrate the movement of the hollow cylinder (bathyscaph) in the water tank. The motion of the bathyscaph depends on the pressure above the water surface. The basic aim of the control is to maintain the bathyscaph in a desired position.

The laboratory model "Ball & Ellipse" consists of an ellipse pivoted in its centre. Tilt of the ellipse can be controlled in two perpendicular directions. The steel ball rolls freely on the ellipse railway.

The laboratory equipment "Buggy on the Belt Conveyer" consists of the rail vehicle running on two moving rails (continuous belts). The tilt of the rails, their speed and the speed of the vehicle may be changed. The position of the buggy on the downgrade is controlled variable and the speed of the buggy is actuating signal. In the virtual model the angle of the ascent of the conveyer and the speed of the conveyer are disturbance variables.

The laboratory model "Air Levitation" demonstrates the levitation of the polystyrene ball on the air stream driven by pair of ventilators. The basic aim of the control is to maintain the ball in a desired position.

Nothing can replace the real, hands-on experience of lab work but with the Virtual Control Laboratory

- all students can now do every control experiment in their own time
- virtual experiments can be carried out either as a teaching aid before actual physical lab experiments, or for comparison after these experiments
- if some aspect of the process or system is not understood properly then simulations can be used for clarification
- it is possible to obtain results more rapidly than in a physical laboratory and so more examples can be tried.

References:

[1] HOFREITER, M. ET AL.: *Examples and Exercises from Automatic Control* CTU in Prague, 2006, ISBN 80-01-02447-4

[2] TRNKA, P. – KOPECKÝ, M.- HOFREITER, M.: *Use Internet for Superior Education* In: Advanced Engineering Design AED 2006 [CD-ROM]. 2006, CTU in Prague, ISBN 80-86059-44-8

[3] HOFREITER, M.: *Virtual Control Laboratory,* Praha: Masarykova akademie, 2001, pp. 85-86, ISBN 80-902131-7-0.

This research has been supported by FRVS grant No. 1730/2006.

Section 4

ELECTRICAL ENGINEERING
&
INSTRUMENTATION

Device for Synthetising Optical Holograms

J. Svoboda*, P. Fiala**

jakub.svoboda@fs.cvut.cz

*Division of Precision Mechanics and Optics, Department of Instrumentation and Control Engineering, Faculty of Mechanical Engineering, Czech Technical University, Technicka 4, Praha 6, 166 07

**Department of Physical Electronics, Faculty of Nuclear Sciences and Physical Engineering, Czech Technical University, V Holesovickach 2, Praha 8, 180 00

Optical holography, as we know it since the 1960s, is the method of wavefront reconstruction obtained by interference of two coherent light waves and diffraction. Holography itself was originally established by Dennis Gabor in 1948 as the method of improving resolution of an electron microscope. Since the invention of laser (1959), it has moved to the whole optical branch and many scientists and inventors have focused their minds to improve the technology and find more applications.

In holography we record both the amplitude and phase of light. First, by recording the interference pattern of two coherent light waves to a photographic plate, we obtain a hologram. Then, if we let the reconstruction wave diffract on the recorded pattern, we get the original wavefront from the recorded subject. This means we are realizing the full 3D view. The trouble is that, for such a reconstruction, we need a laser light which would not be any problem in scientific applications, but it can be the problem for common users. Therefore several methods of reconstruction in the white light have been developed. The rainbow process for transmission holograms by Stephen A. Benton, H1-H2 copying process for reflection holograms or Denisyuk reflection holograms.

However, sometimes we can find a subject which can not be, for some reasons, recorded by the standard way (e.g. something big as a house). Or we would like the hologram to have some special additional properties as kinetics, etc. In such cases (and specially in the times of high-capacity computers), we could try to find a way how to synthesize the hologram, i.e. to omit the first step – recording of the interference pattern of two waves and to compute it instead. The thing is, however, that the calculation is so difficult, that it would last days to get the result, even with the today's fastest computers. That is why this method is used only for small holograms and in special cases of security holograms. From a fabrication point of view, even if we get the result, it would not be easy to write the general curves into photoresist by typical lithographic means, since they mostly use x-y positioning stages. However, we could divide the image into single pixels, approximate the pattern by a series of gratings and “fill” each pixel by one of these gratings. By this way, we get a good compromise between the precise approximation of the computed pattern and the limitations of the lithographic device. The overall process can still remain pretty demanding for the computation time. If we want even a faster process, we have to find another way how to synthesize such hologram.

Let us focus on the principles of 3D visual sensation now. The brain interprets the image of a subject from two eyes and each eye sees the subject from a different angle. By assembling both views, the brain gets 3D perception of the subject. So if we can find a method how to make each eye see the view of the subject from a different angle, we would be able to create “artificial” 3D perception from even two views only. This is, in fact, the principle of stereo photography. There are several ways how to implement this idea into a hologram.

The first one, used in dot matrix systems, is that the hologram is divided into pixels. Then a grating is written into each pixel. The pitch and angle of the grating is computed so that if you illuminate such grating under a certain angle, the pixel shines into the designed direction with the designed color. By this method, we can get either 3D impression or kinematic 2D effects.

Another way, the one we want to use in our new device, is a combination of dividing the hologram into subsequent pixels and H1-H2 transmission to reflection copying, mentioned above. First one needs to compute a set of views of the subject to ensure each eye is getting the view from the right angle. Since human eyes are aligned horizontally, we can save some computation time by omitting the vertical parallax. So the subsequent views would look like vertical strips. However, in some cases, we can use both parallaxes, e.g. for kinematic effects or flip/flop effects. In this setup, the spatial light modulator (SLM) with the picture is illuminated by a collimated wave and the image of the subject, with 6.9 magnification, appears approximately about 250 mm behind the objective. A piece of H1 hologram is recorded in the exit pupil of the recording objective. The whole H1 hologram is then obtained by relative shifting of the modulator and the recording plate while the subsequent views are being switched on the modulator. There is a collimated reference beam brought into the exit pupil and the angle of both the reference and signal beam is kept constant for all of the H1 "subholograms". Finally, we get the resulting H2 hologram by illuminating the whole H1 plate by a collimated reconstruction wave and recording the resulting image into a hologram plate.

According to optical setup mentioned above, there has been an optical objective designed, with the field of view large enough to seat the moving SLM and with the aberrations corrected for designed setup. The objective has been manufactured and currently is being tested on the optical desk. According to the results of the tests, there is the final setup and mechanics being constructed. The termination date is supposed to be by the end of this year.

References:

[1] R.J. COLLIER, C.B. BURCKHARDT, L.H. LIN: *Optical holography* Academic Press New York 1971

[2] M. ŠKEREŇ *Computer Generated Optical Diffractive Structures* CTU Reports 1, Czech Technical University in Prague 2006

[3] J. KAMARÁD, J. OTÁHAL, J. PODZIMEK, V. ŠULC *Přesná mechanika a optika* Práce 1974 pp. 257-293.

This research has been supported by CTU0605412 and GA ČR grant No. 102/05/H039

Active Control of Sound Radiation from Vibrating Bodies Using Piezoelectric Actuators

V. Jandák, O. Jiříček

jandav1@fel.cvut.cz

Department of Physics, Faculty of Electrical Engineering, Czech Technical University, Technická 2, 166 27 Prague 6, Czech Republic

Paul Lueg described the principle of active noise cancellation back in 1933. Over the past thirty years, active control has become an easily available method to reduce low frequency noise radiated from structures. The active structural acoustics control (ASAC) approach uses actuators applied directly to the structure with objective of reducing overall sound radiation. The development and testing of new type of such actuators is presented in this paper.

The main component of our active cell is a piezoelectric bending actuator (stripe actuator – piezoelectric bimorph). This type of actuator is designed to produce relatively large mechanical deflection in response to an electrical signal. Two thin ceramic plates are bonded together, with electrodes affixed to each layer to create a parallel bilaminar element. Main characteristics of the various types of stripe actuators are free length, thickness, width, blocking force, resonance frequency, capacitance and total deflection. The resonance frequency f_r of the stripe should be expressed

$$f_r = 0{,}161 \frac{2t}{l_f^{\,2}} \sqrt{\frac{1}{\rho s_{11}}},$$

where l_f is the free length of ceramic plate, t is the thickness of one piezoceramic layer, ρ is density and s_{11} is elastic constant.

Most suitable for our application are the two largest types of the standard five sizes of stripe actuators manufactured by APC International, Ltd. These types provide resonance frequencies 65 Hz and 175 Hz and their dimensions are 60 ×20 × 0,6 mm and 40 × 20 × 0,6 mm (length ×width × thickness). However, the free length of it is about 7 mm smaller. The actuator is made from PZT 856 piezoceramics. Deflection with a stripe actuator can be high (> 2,5 mm) but blocking forces will be low (approximately 0,1–0,5 N). Stripe actuators derive their name from a white stripes that identifies positive surface.

The first concept of active cell was performed with stripe actuators clamped to the vibrating structure vertically. Placed between the stripe actuators was a curved diaphragm. The use of actuators, driven out of phase, produced vibration in the diaphragm. The distance between the actuators was 9 cm. Various materials (paper, aluminum, PVTF leaf of various thickness from 0,05 mm to 0,8 mm, etc.) of various dimensions were tested as a material for rectangular diaphragm. Noise reduction was not negligible, but most of them had susceptibility to undesirable harmonic distortion. This concept of active cell was also fragile, so we have left it.

The second type of active cell consists of four strips described in the previous paragraph (dimensions 40×20×0,60 mm). Two strips are clamped together in a rigid frame (laminate resin) and placed on the thin cork plate in parallel. The other two actuators were placed in a

frame opposite to the first pair on the same thin cork plate. As the stripes vibrate, the oscillating line moment is transmitted to the primary vibrating structure through the laminate frame. So, the sound radiated by the cell is determined by the base structure. The whole active cell has dimensions of 86 × 60 × 10 mm (length × width × thickness). Two identical active cells were constructed for the following testing.

For the testing, we realized a simple radiating structure created from a baffled thin steel plate (300 × 60 × 0,5 mm) clamped to a large rigid desk at both shorter edges. The plate was activated (at its center) by an electrodynamic shaker using a harmonic excitation signal. Two active cells were fixed to the steel plate symmetrically with its center. Each pair of piezoelectric strips of the cell should be activated independently, but we used only monopole type radiation of whole cell, so each stripe vibrates with the same phase and amplitude. The phase shift between the cells and shaker generator was changed, and the attenuation of sound pressure level was measured. The maximum of noise reduction (30 dB) was achieved for a harmonic excitation signal of frequency 200 Hz, hence it is close the resonance of stripe actuators. Overall attenuation in frequency range from 100 to 300 Hz is around 15 dB. This concept of active cell is able effectively to reduce sound radiation to the far field.

The whole testing was performed in an anechoic room at the Department of Physics of Faculty of Electrical Engineering. Development and testing of active cells will be a part of dissertation thesis of this paper's author.

References:

[1] P. ŠVEC, V. JANDÁK, M. BROTHÁNEK, O. JIŘÍČEK: *Weak Radiating Cell for Active Vibration Control: First approach,* Proc. of Inter-Noise 2006, Honolulu, 2006.

[2] C. R. FULLER, S. J. ELLIOT, P. NELSON,: *Active Control of Vibration* Academic Press, London, 1997.

[3] B. D. JOHNSON, C. R. FULLER: *Broadband Control of Plate Radiation Using a Piezoelectric, Double-amplifier Active-skin and Structural Acoustic Sensing,* JASA, 107(2), 1999, pp. 876–884..

[4] Y.-S. LEE, P. GARDONIO, S. J. ELLIOTT *Volume Velocity Vibration Control of a Smart Panel Using a Uniform Force Actuator and an Accelerometr Array* Smart. Mater. Struct. 11, 2002, pp. 863–873.

This research has been supported by CTU grant No. CTU0606013.

Providing of Third Generation Mobile Services via High Altitude Platforms

J. Holis*, P. Pechac*, D. Grace**

holisj1@fel.cvut.cz

*Department of Electromagnetic Field, Faculty of Electrical Engineering,
Czech Technical University in Prague, Technická 2, 166 27 Prague 6, Czech Republic

**Communications Research Group, Department of Electronics, University of York,
York YO10 5DD, U.K.

The third generation mobile system UMTS (Universal Mobile Telecommunications System), especially supplemented with High-speed Downlink Packet Access (HSDPA), should fulfill the increasing requirements for high-speed mobile data communication. The quick deployment of UMTS networks is, among others, limited by coverage possibilities. This is dominant in suburban and rural areas. High Altitude Platforms (HAPs) will be situated in the stratosphere at an altitude from 17 to 22 km and could be used as an alternative to a terrestrial component for third generation mobile networks UMTS or could be a complementary element of terrestrial networks in case of providing telecommunication and data services in sparsely populated areas such as in Africa, during disasters, terrorist attacks, etc. The frequency spectrum in the 3G bands is also allocated for HAPs applications. HAPs in comparison with terrestrial base stations offer many advantages, such as no shadowing at high elevation angles, and can deliver much larger areas of coverage. Essential advantages of HAPs compared with satellites are also the low-cost deployment and the noticeably lower free-space path loss (FSPL). Moreover, the 3G networks provided via HAPs will not require unique user equipment.

First, the propagation prediction methods were investigated. The aim of paper [1] was to introduce propagation prediction methods for High Altitude Platform stations providing the third generation mobile services in suburban and especially in urban areas. Methods of the propagation prediction in urban environment based on ITU-R statistical model describing building deployments and based on Uniform Theory of Diffraction were shown. The probabilities of both Line of Sight connections in streets and additional path losses due to rooftop diffraction were presented. The software tool for HAPs propagation prediction in 3G frequency band for suburban and urban area has been developed.

In the radio network planning of 3G networks the problems of capacity and coverage cannot be separated. To get realistic results of the quality of coverage and cell capacity analysis in real scenarios, where different users employ a range of services which have different processing gain and different receiver *C/I* (Carrier-to-Interference ratio where interference includes both thermal noise and interference) requirements, an iterative simulation approach can give a better insight into performance than an analytical one. Contribution [2] deals with an application of High Altitude Platform stations as an alternative of providing third generation mobile services in suburban and urban areas. It is focused on an impact of circular and elliptical beam antennas on other-to-own cell interference ratio and cell capacity, respectively. Results of system level simulations of UMTS mobile networks operating in WCDMA FDD mode are shown in different simulative scenarios in suburban and urban environments.

An investigation into the impact of antenna radiation patterns on the performance of a 3G mobile communication system provided via a single High Altitude Platform (HAP) was

presented in [3]. Use of elliptical and circular beam antennas is examined for a 91-cell system. Crucial performance parameters are shown to be the main lobe power roll-off and side lobe level. It is presented that the optimum power roll-off from cell center to the cell edge ranges between 10-35dB, which is dependent on the types of antennas used, side lobe level, and antenna gain strategy employed. Elliptical beam antennas are proven to provide the best solution, but circular beam antennas with their gain adjusted to reduce the degree of cell overlap and compensate for increasing path loss are shown to provide similar performance, with the advantage that they are practically more realizable. It is shown that poorer overlap performance can be partially compensated for by an increased power roll-off at the cell edge, a strategy that is employed in the case of the gain adjusted circular beam antennas. The impact of cell radius and elevation angles is also assessed.

One of the factors motivating measurement from low altitude platforms is the lack of propagation prediction models for High Altitude Platforms (HAPs). The Free Space Loss empirical model (FSL) is commonly used for HAPs. This model is sufficient under the Line of Sight (LOS) conditions that are required in the millimetre frequency band. However, HAPs will be also used to provide 3G mobile services in the frequency spectrum allocated to terrestrial 3G networks (around 2 GHz). LOS connections are not required here. The aim of paper [4] was to introduce options for measurements conducted at the CTU Prague using a low altitude airship. Experiments were proposed in the 3G and millimetre frequency bands. An example of measured data at the 2 GHz frequency is presented. An overview of planned experimental work is given. The goal is to obtain experimental data that can be used to plan communication systems delivered via High Altitude Platforms (HAPs).

References:

[1] HOLIŠ, J. – PECHAČ, P.: *Propagation Prediction for High Altitude Platforms in 3G Frequency Band,* The 9th International Symposium Wireless Personal Multimedia Communications – WPMC‘06, San Diego, USA, 2006, pp. 1219-1221.

[2] HOLIŠ, J. – PECHAČ, P.: *Simulation of UMTS Networks Provided via HAP Stations Using Elliptical and Circular Beam Antennas in Urban and Suburban Areas,* The 9th International Symposium Wireless Personal Multimedia Communications – WPMC‘06, San Diego, USA, 2006, pp. 348-351.

[3] HOLIŠ, J. – GRACE, D. – PECHAČ, P.: *The Optimization of Antenna Power Roll-off for High Altitude Platform WCDMA Systems,* First Workshop of COST297 ‘HAPCOS’, York,U.K., 2006.

[4] HOLIŠ, J. – PECHAČ, P. – KOŘÍNEK, T. : *Measurement trial in 3G and millimetre frequency bands using Low Altitude Airship,* First Workshop of COST297 ‘HAPCOS’, York,U.K., 2006.

This research has been supported by CTU grant No. CTU0606613.

Measurement of Small Enclosure Shielding Efficiency

Tomáš Kořínek

korinet@fel.cvut.cz

Department of Electromagnetic Field, Faculty of Electrical Engineering,
Czech Technical University, Technicka 2, 166 27 Prague 6, Czech Republic

Small shielded enclosures are nowadays widely used for measurement of EMS, EMI and sensitivity properties of different devices [1]. Small enclosures can be furthermore utilized as racks for PC servers and different electronic devices placed inside. At present, information security (data protection) imposes requirements on the high values of the shielding efficiency of these small shielded boxes.

Methods for measurement of the shielding efficiency are currently described by standards IEEE Std. 299 [2] and MIL Std. 285. The measurement is performed in two steps. Shielding efficiency is enumerated from transmission between two antennas with setting of an open door and the close door of the enclosure. The shielding efficiency is a difference of these two values (in dB unit). Above mentioned standards describe only measurements of shielding efficiency of enclosures with dimensions greater than 2m such as shielded rooms. Currently, a new standardization working group has been established to develop the standard IEEE 299-2 [3], treating the shielding effectiveness of small enclosures, but specifications for measurement of small enclosure have not been written in Czech Republic and in foreign countries at present.

This project is solved for a frequency band from 0.3GHz to 1GHz. A metallic box with its dimensions 0.84m x 0.77m x 0.64m is chosen as a shielded enclosure. An inner antenna is connected to feed-through SMA/N connector on the top wall of the box. A distance between transmitting and receiving antenna is 0.8m.

The main aim of this work is to highlight drawbacks and advantages of various so far utilized measuring approaches. There are many problems, which have strong influence on measurement results – type of antennas, position of antenna inside the enclosure, measurement of references (in open area or with open door of enclosure), influence of different objects inside the enclosure, location of generator (inside or outside of enclosure), problem of reciprocity theorem. These aspects were investigated by analyses via EM simulation software FEKO and experimental measurements.

The first task that has to be solved out before start of the measurement is the choice of a suitable antenna. The design of the antenna which is being placed inside an enclosure should be tailored to suit the enclosure. Therefore, the effect of the enclosure structure on the response of the antenna should be treated. If possible, the antenna can be designed to minimize this undesirable effect. Measurement configurations including either wire or log-spiral equiangular planar antenna are usually mentioned in literature. That is why the research was mainly concerned with these two types of antenna.

Finally, the log-spiral equiangular planar antenna was chosen, because this antenna can be separated from the enclosure and it is possible to measure of references in the open area (anechoic chamber) or with an opened door. In real scenarios many enclosures don't contain doors and references must be measured in the open area. Shielding efficiencies based on these two measurements of references are different. If the transmitted antenna is placed in the metallic box, the box behaves as a reflector for this antenna and a transmitted power is different at some frequencies. Influences of reference values (measurement in open area or with open door) on shielding efficiency characteristic will be shown.

The next problem, which has been solved, is placing of the transmitting antenna inside or outside of the enclosure. It has been expected, that the configuration of the measurement is reciprocal. This hypothesis has not been confirmed, because the metal enclosure is placed in a near field of both antennas.

The next sphere of interest is a position of the antenna in the enclosure. The shielding efficiency has been measured for three positions of the antenna in the enclosure. The closed enclosure represents a resonator with different quality factors (Q factor) at different frequencies. The inner antenna with different positions generates different distributions of electromagnetic field in the enclosure. Probably, the shielding efficiency values aren't correct at the resonant frequencies. The best method how to eliminate incorrect values of shielding efficiency incorporates either an exclusion of resonances from measured values or covering of inner walls by absorption materials.

The last type of measurement shows an influence of particular object in the enclosure on shielding efficiency. The inserted metallic object has dimensions of 0.37m x 0.34m x 0.18m. Its dimensions are the same as a spectrum analyzer, which is used in special measurement system. This object reduces the inner volume of enclosure and resonances are dramatically changed. The shift of resonances results in change the shielding efficiency throughout whole measured frequency band.

A lot of measurements and simulations for different configuration of transmitting and receiving antenna, references, positions of antenna in the enclosure, positions of some object inside the enclosure and covering inner walls of enclosure with absorption materials have been made. All measured data were compared and the worst case of shielding efficiency was chosen from the measured characteristics. It was found out, that the shielding efficiency of the enclosure is strongly influenced by resonances in the enclosure. Some of results were published at the International symposium on electromagnetic compatibility – EMC Europe 2006 in Barcelona [4].

References:

[1] KOŘÍNEK, T.; PIKSA, P.; MAZÁNEK, M.: *Wideband Measurement in a Small Shielded Box Using Equiangular Spiral Antennas* Radioengineering, December 2006, vol. 15, no. 4, pp. 34–37, ISSN 1210-2512.

[2] IEEE STD. 299: *IEEE Standard Method for Measuring the Effectiveness of Electromagnetic Shielding Enclosures* IEEE, 1997.

[3] CATRYSSE, J.: *IEEE 299-2. Shielding characterisation of small enclosures: actual status and IEEE P299-2 proposal* In Proceedings of the International Symposium on Electromagnetic Compatibility - EMC Europe 2006, Barcelona 2006, pp. 54–63.

[4] ZVÁNOVEC, S.; HAZDRA., P.; KOŘÍNEK, T., PECHAČ, P.; MAZÁNEK, M.: *Measurement of Shielding Effectivenes of Small Shielded Enclosure* In Proceedings of the International Symposium on Electromagnetic Compatibility - EMC Europe 2006, Barcelona, 2006, pp. 249–252.

This research has been supported by CTU grant No. CTU0606813.

A Scalar Microwave Interferometric Measurement System for Nondestructive Testing

J. Zela, K. Hoffmann, P. Hudec

zelaj@fel.cvut.cz

Department of Electromagnetic Field, Faculty of Electrical Engineering,
Czech Technical University, Technická 2, 166 27 Prague 6, Czech Republic

The microwave interferometry is a perspective technique for nondestructive testing in civil engineering, e.g. for measurement of deformations, non-homogenities, etc., [1], [2]. The main advantage of the microwave interferometry is its sensitivity and ability to visualize otherwise hidden undersurface non-homogenities.

A microwave vector phase interferometer based on a multi-port vector network analyzer was published in [3]. An object under test is illuminated by an electromagnetic wave radiated by a transmitting antenna. The wave reflected from the tested object interferes with a direct wave and creates an interferogram. The interferogram is measured by an antenna x-y positioning system. The same arrangement was used for tests on discrete frequencies in the 2 – 50 GHz frequency band using VNA Agilent E8364A.

Majority of results obtained show surprisingly that information provided by amplitude and phase diagrams are very similar. It is a question therefore, whether scalar interferometric measurement only could be sufficient for at least some types of applications. Microwave vector interferometers enable more precise calibration and can have higher dynamic range of course. But microwave scalar interferometers may be sufficient to observe studied deformations and non-homogenities, being substantially simpler and cheaper.

In this contribution is presented design and realization of a new scalar microwave interferometric measurement system and results obtained with this measurement system. For the first tests the 2.45 GHz frequency was chosen. Instead of a slow antenna x-y positioning system an electronic scanning was applied. The key component of the system is a new antenna matrix with 256 antennas. It contains three main parts: surface-mount ceramic antennas with dimensions 5x8 mm, detectors and low-frequency analog multiplexers. All components are mounted on a single layer printed circuit board (FR4), which is fixed on a metal holder. The main advantage of the surface-mount ceramic antennas is their small dimensions. Spacing between two particular antennas are 24 mm (approx. $\lambda/5$), both in vertical and horizontal directions. In order to minimize reflections from the antenna matrix, the holder is covered by absorbers.

Amplitudes of received signals are measured by RF detectors based on zero bias Schottky diodes. Their approx. 50 dB dynamic range seems to be sufficient for the given type of measurement. The mean value of the detector input power can be set by the transmitted output power. Analog multiplexers connect detected voltages to processing circuits (amplifiers, selective voltmeter). Transmitted signals are amplitude modulated (1 kHz), all signal paths behind RF detectors are AC coupled. A 1 kHz band-pass filter removes all unwanted signals.

Technique of creating interferograms is the same as in experiments described above: an electromagnetic wave reflected from a tested object interferes with a direct wave from transmitting antenna and creates an interferogram. The interferogram is measured with the antenna matrix.

Measurements with the developed system need a calibration. Since there is no direct access to the antenna matrix detectors, the system was calibrated (normalized) by a semi-planar known wave.

A measurement of deformation of a plain steel sheet was used as a reference measurement. Dimensions of the measured steel sheet were 100 x 50 cm. Firstly, interferometric measurement by VNA and antenna x-y positioning system on frequency 2.45 GHz was performed. The resolution of these measurements was 36x36 points. The distance between two measurement points was set on the positioning system to 12 mm (approx. $\lambda/10$). A double ridged waveguide horn with the dimensions of the aperture 104x78 mm was used as a receiving antenna.

The same measurement with the new scalar system was repeated using the antenna matrix with 256 antennas. In this case the distance between two measurement points was 24 mm.

There can be seen shifts of interference stripes in interferograms with respect to the sheet deformation as well as in the measurement with the VNA and the x-y positioning system. Greater shifts of interference stripes correspond to greater deformations of the sheet. However scalar measurement data show significantly greater point to point differences compared to smooth data obtained by the VNA and the positioning system. Namely the differences in horizontal direction are surprising. These differences are reproducible and systematic. They are too sharp to be explained by greater distances between measurement points of the antenna matrix. Since there was no mechanical motion during scalar measurement, measurement was about 60 times faster than the measurement with the positioning system.

The new scalar system for microwave interferometry using an antenna matrix makes possible significantly faster measurement compared to the system using an antenna positioning system. The results obtained were compared to the results of measurement using VNA and antenna positioning system. There is a reasonable global agreement between both measurements but there are significant local differences. An extension to higher frequencies is supposed.

References:

[1] PIERACCINI, M. - LUZI, G. - MECATTI, D. - FRATINI, M. - NOFERINI, L. - ATZENI, C.: *A microwave interferometer with imaging capability for remote measurements of building displacements.* Materials and Structures, Materials and Structures, 2005, vol. 38, no. 283, pp. 795-800.

[2] PIERACCINI, M. - TARCHI, D. - RUDOLF, H. - LEVA, D. - LUZI, G. - ATZENI, C.: *Interferometric radar for remote monitoring of building deformations.* Electronics Letters, 2000, vol. 36, no. 6, pp. 569 - 570.

[3] ZELA, J. - HOFFMANN, K. - HUDEC, P.: *A Novel Vector Microwave Phase Interferometer.* In: Proceedings of the 36th European Microwave Conference [CD-ROM]. Piscataway: IEEE, 2006, pp. 1025-1027.

[4] ZELA, J. - HOFFMANN, K. - HUDEC, P.: *A New Scalar Microwave Interferometric Measurement System.* In: 68th ARTFG Conference Digest, Automatic RF Techniques Group [CD-ROM]. Piscataway: IEEE, 2006, pp. 164–168.

This research has been supported by CTU0607113.

Satellite Navigation Applications in Indoor Environment

P. Puričer

puricep@fel.cvut.cz

Department of Radio Engineering, Faculty of Electrical Engineering, Czech Technical University, Technická 2, 166 27 Prague 6, Czech Republic

In the recent decade, Global Navigation Satellite Systems (GNSS) dominated the area of position determination and navigation. Their use dates back to last century when two main systems, GPS NAVSTAR and GLONASS, were brought alive. In the next few years the new GNSS Galileo will accompany them. Its predecessor, EGNOS (European Geostationary Navigation Overlay Service), is already in operational status. It belongs under satellite based augmentation systems (SBAS) that offer improvement of present GNSS systems [1]. Position and integrity enhancement of GNSS is even more important in the safety critical applications operating under difficult conditions, for example in dense urban areas or indoor.

If we consider for example use of EGNOS signal in the land applications we have to deal with the problem of user movement in the environment. The signal is affected by this environment which can lead to EGNOS satellite signal absence for augmentation. Such difficult environment can be for example terrain cuts for rail tracks, urban canyons with low visibility to satellites, signal attenuation by building walls, etc. It will result in degradation of the positioning service quality. Besides that, SBAS usually provide information about health and integrity of the navigation system. The absence of this information can affect usability of satellite navigation in the safety critical applications, for example in railway signalling system or E112 emergency service. Therefore it is necessary to investigate influences of environment to the augmentation systems signals and suggest possible solution.

The analysis of the signal availability started with investigation of the main phenomenon related to user movement in the environment, a shadowing of the satellite signal path. A set of experimental measurements was done to get knowledge of satellite signal behaviour and GNSS and/or SBAS signal quality in different typical environments.

The measuring equipment was based on experimental GNSS software receiver, developed at the Department of Radio Engineering of the Czech Technical University in Prague. The measurements were realized in typical environments: city of Prague, industrial town, village, highway, main and secondary roads in the country. In the next step, the measurements of GNSS signal reception were done for difficult environments (urban areas, indoor) for the case of non-augmented and augmented mode of operation.

The experiments [2] have clearly shown that availability of SBAS signal in some types of environments is problematic. The signal and data reception of the signal typically in industrial town and big city based solely on reception of the original satellite signal cannot provide sufficient quality of service. The same situation is in the case of indoor reception. The reception has to be complemented by other methods.

The dissemination of SBAS augmentation data can be realized by various means. However, the chosen method has to be available in the sufficient quality in locations where the difficulties with standard satellite signal reception fails. The microwave data links suffer from similar problems as satellite signals (visibility). A network of FM transmitters can be used for better coverage but it will not be wide enough to respect global nature of SBAS service, besides that the operational costs of continuous service would be very high.

Very prospective solution seems to be use of Internet for EGNOS data dissemination. The European Space Agency (ESA) supported these activities by realizing project SISNET (Signal in Space through Internet). The EGNOS data are distributed by TCP/IP connection to the users. Similar approach uses another network EUREF-IP, disseminating differential GNSS data from the several permanent stations of EUREF network.

The above described solution establishes common universal layer of data provision. The connection of the user to the Internet data can be solved according to the particular needs, i.e. it is available even for mobile applications. The classical solution of the "last mile" access is a use of cellular network with GPRS or UMTS capability. Such a connection can be established only in case of need, therefore it can save power of the device and operation costs for the user. Another advantage of the Internet use is in the fact, that it enables use of EGNOS data even for receivers that are not capable to receive and process EGNOS satellites signals, the data can be preprocessed and provided to the receiver in the standard RTCM format for differential corrections. Therefore the architecture of such a receiver consists from three main blocks, GNSS receiver itself, communication block for Internet connection, and data processing and control block that ensures augmentation data preprocessing for GNSS receiver, controls connection to the network in case of lack of EGNOS data from space (for example during indoor use).

The blocks can be either independent (they can even be stand alone devices) or they can be integrated in various levels. Two concepts of such system were developed at the Department of Radio Engineering. First one uses experimental GNSS software receiver concept described above in the EGNOS reception test measurements. The receiver is integrated to the eurocard (160 mm × 110 mm) PCB OEM module with network connection capability. The second one, more versatile, consists of eurocard 3U format PCB populated with independent processing control unit, communication OEM module, and navigation module, realized by OEM GPS receiver.

This architecture was chosen to serve as a testing platform for various combinations of devices, not only OEM modules but for example for testing of common GNSS user receivers. The processing control unit, based on PowerPC architecture running under real-time Linux kernel, provides decoding of the augmentation data. GPRS module can be easily changed with other ones using UMTS or WLAN technologies.

The presented experimental study and receiver design was used for analysis of indoor GNSS signal availability and parameters that will help in specification of indoor based GNSS reception and processing improvement as a part of author doctoral thesis.

References:

[1] SEIDL, L. – KOVÁŘ, P. – PURIČER, P. – VIČAN, M. – VEJRAŽKA, F.: *Local Augmentation in GNSS.* In Transport Systems Telematics 5th International Conference Proceedings. Ustron: Wydawnictwo Politechniki Slaskiej, 2005, pp. 353–362.

[2] PURIČER, P. – ŠPAČEK, J.: *EGNOS Augmentation for Difficult Environment.* Advances in Transport Systems Telematics, Silesian universty of Technology, 2006, pp. 131–136.

This research has been supported by grant CTU0610013.

EGNOS Signal Monitoring Station

J. Špaček, P. Kovář

spacekm@fel.cvut.cz

Department of Radioelectronics, Faculty of Electrical Engineering, Czech Technical University, Technická 2, 166 27 Prague 6, Czech Republic

The satellite navigation systems monitoring has long tradition at our department. We continuously monitor GPS and GLONASS systems since 1996 and also share data from this monitoring via internet. In the last years our team has been building the experimental GNSS receiver based on software defined radio architecture. Current second generation receiver consists of a compact RF front-end and a digital processor based on programmable logic FPGA Virtex II Pro by Xilinx with integrated PowerPC processors. The signal processing programmed into the FPGA ensures transformation of the intermediated frequency signal to the base band and correlation reception algorithms. These algorithms have low complexity, but they require high numerical power. The remaining high complexity but less numerical demanding algorithms are executed in PowerPC processor. The receiver is suitable for experiments with signal processing and further allows more detailed access to the signals of satellite navigation systems.

Monitoring station with experimental GNSS receiver provides more information about GPS system signals and recently in addition signals of the European Geostationary Navigation Overlay Service (EGNOS). The EGNOS system is a kind of Satellite-Based Augmentation System (SBAS) covering Europe. Geostationary satellites broadcast a GPS-like ranging signal with embedded corrections, providing improved accuracy, availability and integrity over GPS and GLONASS. Monitoring station is also capable to receive signals of constructed European navigation system Galileo [1]. The Galileo system and modernized GPS are coming with new services for safety-of-life applications.

The development of the GNSS systems and introduction of the new guaranteed services performance requires the development of the GNSS monitoring system. The basic requirements on the provider-independent monitoring system are [2]:

1. Measurement and storage of signal or data on very low level, to be able to reconstruct the anomalous behavior of the navigation system and simultaneously eliminate mistakes in the monitoring system.
2. Support the investigation of the anomalous status of the navigation system and secure data for reconstruction of the anomalous behavior of the navigation receiver.
3. Support transformation of the low level data and signal to the widely used format for other analyses.
4. Share monitoring data via internet.

This requirement respects designed GNSS monitoring station architecture. The construction of the GNSS monitoring station was planned in several phases. Now is the monitoring station in the first phase and provides monitoring all in view GPS, EGNOS, and Galileo satellites on L1 frequency. In the next phase the capability of monitoring of the Galileo E5, GPS L2 CA, and GPS L5 signals will be progressively implemented.

Monitoring station consists of the second generation experimental GNSS receiver equipped with the L1 front end. For this purpose the 16 identical GPS/EGNOS/Galileo correlators capable to process BPSK and BOC(1,1) modulation were programmed to the receiver FPGA. The PRN code is stored in the correlator 16 Kbits RAM memory and can be downloaded from the receiver computer.

The requirements on transparency and capability of the post processing investigation of the non standard system and receiver states were taken in account in development of the data format and communication protocol for GNSS monitoring station. From this reason the monitored data are stored in PC workstation in raw form to keep available all information for measurement analyses and elimination of the errors in the monitoring station. Monitoring station raw data content: raw carrier phase measurement, extended PLL status (actual tracking error, and detailed PLL status indicators), raw code measurement, extended DLL status (actual tracking error, signal to noise ratio, and detailed DLL status indicators), and IQ signal samples wide one bit (20 ms for GPS, 2 ms for EGNOS, and 1 ms for Galileo).

Further on the attached PC workstation runs software for analyses of the stored data and software for transformation of this raw data to the "Receiver Independent Exchange Format" (RINEX). For analyses of the RINEX data can be used some navigation or surveillance software packages like PEGASUS (Prototype EGNOS Analysis System Using SAPPHIRE) by Eurocontrol. The PEGASUS software is a tool which allows analysis of data collected from the EGNOS. The tool analyzes raw GNSS and SBAS data streams using only algorithms contained in the published standards and giving the possibility of easy access to the data processing with graphical presentation of the results. The other possible way how to analyze the monitored data is to develop special software. This software targeted for Matlab environment is under development. The software will directly process raw data measurement, because RINEX format supports only subset of the raw measurement information. The PC workstation also provides this data via internet.

In the frame of this project we plan to upgrade GNSS monitoring station to all Galileo frequencies. The second version of the experimental GNSS receiver has not sufficient performance of the FPGA for implementation of the approximately 100 correlators including Galileo E5 correlators, which should process extra wideband signals. Our plan therefore supposes the design of the third version of the experimental GNSS receiver based on latest Virtex 4 FPGA by Xilinx with higher performance. The goal of this receiver is sufficient power for processing of all Galileo signals in space.

References:

[1] SEIDL, L: *Snapshot Receiver for GPS and Galileo.* In Transport Systems Telematics 6th International Conference Proceedings [CD-ROM]. Katowice: Silesian University of Technology, 2006, pp. 427–433.

[2] KOVÁŘ, P. – SEIDL, L. – ŠPAČEK, J. – VEJRAŽKA, F.: *Software GNSS Receiver for Signal Experiments.* In Proceedings of IAIN/GNSS 2006. Jeju: Korean Institute of Navigation and Port Research, 2006, pp. 391–394.

This research has been supported by CTU grant No. CTU0610113.

Noise Removing from an Image Data Based on Bayesian Statistics

J. Švihlík

svihlj1@fel.cvut.cz

Department of Radioelectronics, Faculty of Electrical Engineering, Czech Technical University in Prague, Technická 2, 166 27 Prague 6, Czech Republic

This paper deals with advanced image noise removal methods based on the Bayesian statistics. There will be discussed some algorithms for additive image noise suppression and also algorithm for the elimination of the thermally generated charge in the astronomical images, which were acquired by CCD (Charged Coupled Device sensor).

Generally, for the additive noise suppression a number of algorithms can be used. These algorithms should be firstly divided to the methods, which are processed in spatial domain or in the transform domain. The spatial domain noise removal methods (convolution or median filtering) belong to the one of the simplest methods. For the considerable noise contamination, the results obtained by these methods are not so favourable. Fortunately, the transform domain methods were developed. There can be used a number of transforms, for instance the 2D Fourier Transform or The Wavelet Transform. The Wavelet Transform transforms analyzed signal to the different frequency bands. Nowadays the methods processed in the wavelet domain using statistical model of the wavelet coefficients to the most powerful algorithms can be involved.

It is generally known that every astronomical image which was acquired by CCD sensor, have to be corrected by dark frame. The Dark frame maps the thermally generated charge of the CCD. May become that we don't have the dark frame image and we cannot directly to correct the astronomical images. It is good to note that uncorrected images are not suitable for subsequent investigation. There exist simple nonlinear filtering methods, e.g. median filtering, but the obtained results are not so satisfactory. So, similarly as in the before item, the statistical methods were proposed.

As was mentioned above the most powerful additive noise removal methods are based on the Bayesian estimators in the wavelet domain using statistical model of the wavelet coefficients as prior information about images. During the IG project-solving certain noise removal algorithms were implemented. All these additive noise removal algorithms use The Discrete Wavelet Transformation (DWT). The DWT transforms image to the different frequency bands. The high frequency bands have a special shape of the histogram with heavy tails and with the maximum at the zero. Furthermore, wavelet coefficients histogram should be modeled by generalized Laplacian probability density function (PDF) [1]. This model has two parameters, the first controls the shape and the second one controls the width of the PDF. It is quite evident that the value of these parameters has to be estimated. There exist a number of the statistical methods for parameters estimation, but many of these are suboptimal. It means that it is impossible to estimate parameters value directly from noisy wavelet coefficients. So, as the best method for parameters estimation the moment method was chosen. Furthermore, the images, where the noise was suppressed, were estimated using Bayesian Least Square Error (BLSE) Estimator and Maximum A posteriori estimator. The obtained results were compared with other methods processed in the wavelet domain based on the suitable thresholding of the wavelet coefficients. The best results were obtained by Bayesian estimators [2], [4].

As was mentioned in the third item, the astronomical images acquired by CCD sensor for the thermally generated charge have to be corrected. During the IG project-solving the algorithm for the thermally generated charge elimination was proposed. This algorithm [3] is based on the BLSE or MAP estimator. The generalized Laplacian model for the signal and for the noise description is used. The model parameters can be estimated using Least Square Error (LSE) method or by the moment method. The LSE method is quite suboptimal, but the derived equations for the moment method are hardly solved. This algorithm will be in the future improved, but now to the promising eliminating algorithm should be involved.

References:

[1] ŠVIHLÍK, J. – PÁTA, P.: *PDF Model of Multimedia and Scientific Images in the Wavelet Domain.* In Proceedings ELMAR 2006. Zadar: Croatian Society Electronics in Marine - ELMAR, 2006, pp. 17–20, ISBN 953-7044-03-3.

[2] FLIEGEL, K. – ŠVIHLÍK, J. – ŘEŘÁBEK, M.: *Design of CMOS-APS smart imagers with mixed signal processing and analysis of their transfer characteristics.* In Infrared Detectors and Focal Plane Arrays VIII. Bellingham: SPIE, 2006, pp. 1–12, ISBN 0-8194-6374-4.

[3] ŠVIHLÍK, J. – PÁTA, P.: *Dark Frame Correction via Bayesian Estimator in the Wavelet Domain.* In 2006 IEEE International Symposium on Signal Processing and Information Technology [CD-ROM]. Madison: Omnipress, 2006, pp. 55–58, ISBN 0-7803-9754-1.

[4] KLÍMA, M. – FLIEGEL, K. – ŠVIHLÍK, J.: *Quality Enhancement in Security Image Information.* In Proceedings of the 40th International Carnahan Conference on Security Technology. Piscataway: IEEE, 2006, pp. 60-67, ISBN 1-4244-0174-7.

This work has been supported by the grant CTU0610213 "Noise Removing from an Image Data Based on Bayesian statistics" of the CTU Prague. This research has been also supported by the grants No.102/05/2054 and No.102/03/H109 of the Grant Agency of the Czech Republic and by the research project MSM 6840770014 of the Ministry of Education, Youth and Sports of the Czech Republic.

Modelling of the system for dynamic ADC parameters measurement

P. Česák

cesakp1@fel.cvut.cz

Department of Measurement, Faculty of Electrical Engineering, Czech Technical University, Technická 2, 166 27 Prague 6, Czech Republic

A significant number of ADC dynamic test methods are based on ADC sine-wave stimulus. Generally, the signal quality (namely THD and SNHR) of such signal is recommended to be at least 10 dB better than that of the measured ADC. In practice, this requirement is very difficult to achieve particularly for testing of 12–16 bit ADCs in the frequency range from hundreds of kHz to several tens of MHz. No commercially produced generator reach sufficient signal quality (phase noise, spectral purity) in this frequency range; their THD do not exceed -50 dB what is enough only for 8 bit ADCs.

The system for dynamic ADC parameters measurement (developed at the CTU in Prague [1]) is based either on high-quality low-distortion band-pass filters or on common low-cost band-pass filters. While the high-quality filters are suitable for testing of ADCs with the ENOB up to 20 bits, low-cost filters can be applied for the direct testing of ADCs with the ENOB up to 13 at the frequencies bellow 10 MHz and of ADCs with the ENOB up to 11 at the frequencies bellow 20 MHz.

Each analog filter used in the measurement system is tuned up at one discrete frequency. The choice of system frequencies was performed accordingly to the recommendation of IEEE Std 1241–2000 [2]; the optimal frequency f_{opt} should fulfill the condition of M equally spread phases in the range from 0 to 2π (M is the number of samples in a record). It is also important to ensure that higher harmonic components in the basic frequency band and the components mirrored around the frequency of $f_s/2$ and 0 do not overlap. Taking these rules into account, the following frequencies were chosen: 4.4156 MHz, 9.48416 MHz and 19.5076 MHz.

The system for dynamic ADC parameters measurement contains these components: signal generator, band-pass filter (high-quality low-distortion or common low-cost), ADC module (PXI, VXI). ADC data is processed by a software package called Digester (also developed at the CTU in Prague). Matlab was selected to create the model of the system for dynamic ADC parameters measurement.

Several issues had to be overcome to start creating a model. Firstly, it was required to control Digester directly from Matlab by simple commands – to obtain data from ADC by a script file for the model identification purpose. Secondly, it was required to process data by a script file by the algorithms embedded in Digester. The development of these new features (and another ones) in Digester took a long time and often it was required a few programmers to cooperate. It was impossible to avoid problems (run-time errors, logical mistakes, etc.) when implementing a new feature. The structure (source codes, data flow) of previous Digester was found insufficient for future development and extension. Therefore, a new structure of the application and its development were proposed this year [3]. Digester has now being rewritten, which will continue in the year 2007.

Regarding the rewriting process, it was also impossible to handle all versions of the Digester manually. So there was conducted a study about a system that would control versions of the application. It is indeed needed because a lot of programmers have been working on the application and modules. The version control system is a good way to avoid problems.

The requirements put to the version control system were to be available as Freeware (neither client nor server must be limited by license), easy user interface (the programmers shouldn't spent much time to understand the version control system itself) and available Windows client (developed application will be used under Microsoft Windows OS). According to these requirements the Subversion software was chosen. The main advantage is a user-friendly client called TortoiseSVN integrated into Microsoft Windows OS.

Subversion is a server based application, thus it was installed on a new dedicated server. Connection to this server is also available from the Internet. The server is running on Debian operation system – it was selected because of easy administration and better security. The source codes of the newly developing Digester are shared by this server. There will also be a website to host additional information about this project. Digester and its new conception will be presented at the conference IMTC 2007; the paper was already accepted [4].

The model of a test apparatus is composed from the signal generator, noise generator, band-pass filters and the ADC. Each component is usable as a standalone module. This enables to use these components by other scripts. The main purpose is to use the model for easy understanding how the system works. So it was accompanied by a graphical user interface in Matlab. It enables the user to easy setup the parameters of each components. During development of the model it was required to improve quality and expand the system for dynamic ADC parameters measurement – the system was equipped by high-quality cables, splitters, combiners and terminators. This enables additional expansion of the system for dynamic ADC parameters measurement in future.

Additional improvements of the system for dynamic ADC parameters measurement based on the created model were proposed. One of the required components was the Altera Cyclone II board with EP2C5 that was designed and developed as a four-layer printed circuit board. It is assembled by four independent 40-pin connectors to connect all available input/output pins from EP2C5 to external boards. The development board contains adjustable internal voltage selected by jumpers. The EP2C5 has the possibility to connect four different power supplies for each side of the chip. This makes the board universal for general purposes.

References:

[1] HAASZ, V. – KOMÁREK, M. – ROZTOČIL, J. – SLEPIČKA, D. – SUCHÁNEK, P.: *System for Testing Middle-Resolution ADCs Using Test Signal up to 20 MHz,* In IMTC/06 Proceedings of the 23rd IEEE Instrumentation and Measurement Technology Conference, 2006, pp. 266–270.

[2] IEEE STD 1241-2000: *IEEE Standard for Terminology and Test Methods for Analog-to-Digital Converters* The Institute of Electrical and Electronics Engineers, Inc., New York, 2000, pp. 29–30.

[3] ČESÁK, P.: *The Structure of a Large Application,* POSTER, 2006, [CD-ROM].

[4] ČESÁK, P. – ROZTOČIL, J.: *Development of large software for the ADC testing,* IMTC, Submitted 2006.

This research has been supported by CTU0610413.

Dual-Mixer Time-Difference Multiplier

A. Kuna, J. Roztočil

kunaa@fel.cvut.cz

Department of Measurement, Faculty of Electrical Engineering, Czech Technical University, Technická 2, 166 27 Prague 6, Czech Republic

As the sampling rate of the Analog-to-Digital Converters increases the frequency stability of both the testing and sampling signals comes into the account for evaluation of ADC parameters. In the Laboratory of ADC testing of the Department of Measurement FEE CTU a frequency stability measurement system is being developed. At the present time the system is based on the direct measurement of time-difference using the SR620 universal time interval counter. Assuming intervals short enough to neglect the impact of time-base instability and assuming that the noise is white phase modulation, we have the limiting background instability in terms of Allan deviation as $\sigma_y(\tau) = \sqrt{3}\text{x}10^{-11}/\tau$ i.e. at 1 s of $1.7\text{x}10^{-11}$. The laboratory has been equipped with a pair of 5 MHz Milliren MTI-260 quartz oscillators used as a sampling reference which show σ_y ($\tau = 1$ *s*) = $6\text{x}10^{-13}$ and $9\text{x}10^{-13}$, respectively. Therefore the current measurement system needs to be upgraded to evaluate such performance.

The principle of dual-mixer time-difference multiplication for the time domain frequency stability measurement has been known and used for years [1 – 3]. Assume that $\varphi(t)$ is time-dependent phase difference between two sinewave signals from oscillator 1 and 2, both with carrier frequency v. The two signals are mixed with a third sinewave signal from common oscillator to provide two beat notes at frequency v_B. Assume further that $x_B(t_0)$ is the beat time-difference between the zero crossings at instants t_0 and $t_0 + x_B(t_0)$. Since the input time-difference at frequency v is $x(t_0) = \varphi(t_0)/2\pi v$ we get $x_B(t_0) = mx(t_0)$ where $m = v/v_B$ is the multiplication factor.

In the design of FEE DMTD multiplier each channel includes a chain with a mixer, low-noise preamplifier and two limiter amplifiers.

The common frequency source is one of the MTI-260 quartz oscillators that provide nominally 5 MHz at +9 dBm power. The oscillator frequency is offset 5 Hz which gives v_B = 5 Hz at 5 MHz and thus the multiplication factor is 10^6.

The mixer is a double balanced Minicircuits SRA6. It does not provide lower flicker phase modulation compared to HP10514A (assembled from separate diodes) which is unfortunately no more commercially available.

The low pass filter following the mixer is two-stage LC filter with 100 kHz cutoff frequency used to efficiently suppress the RF component in the output from the mixer.

The low-noise amplifier is a LT1028 with gain A = 28. The LT1028 exhibits a voltage noise of less than 1 nV/√Hz, the $1/f$ corner frequency of 3 Hz and gain-bandwidth product GBW = 75 MHz. It is followed by single-pole RC filter with cutoff frequency 15 Hz.

The limiter amplifiers are the Analog Devices OP27. It exhibits the voltage noise of 3 nV/√Hz, the $1/f$ corner frequency of 3 Hz and GBW = 8 MHz. The voltage gains are set to 130 and 100, respectively. The first limiter amplifier contains a single-pole RC filter in the feedback with a bandwidth of 160 Hz in the zero-crossing area. The 2nd limiter amplifier provides a trapezoidal waveform with a slope of $7\text{x}10^5$ V/s at the zero crossings.

A comprehensive analysis of the impact of phase noise in common oscillator to the background noise of a DMTDM system has been made in [4]. It has been shown that for $x_B \rightarrow 0$ also residual Allan deviation of the relative fractional frequency $y_C(t)$ $ADEV_{CR} \rightarrow 0$. Due to the system symmetry the noise contribution of the test oscillator is described the same

way as that of the common oscillator. Since the same MTI-260 oscillator with similar noise performance has been used as the test oscillator, its noise contribution cannot be neglected.

The multiplied time-difference x_B is measured with a time interval counter whose noise impact on the DMTD multiplication has to be evaluated. It can be done experimentally applying one of the beat signals to both the start and stop inputs of the counter. A suitable delay in stop input can be obtained by small voltage offset in the trigger level. For the input slope of $7\text{x}10^5$ and the beat period $T_B = \tau_0 = 0.2$ s the SR620 counter provides white phase noise modulation with corresponding $ADEV(\tau) \approx 1\text{x}10^{-15}/\tau$. The noise contribution of the counter is then negligible.

The overall noise in a single channel of DMTDM includes two main components: the noise in the first elements of the channel with a narrow bandwidth, and the noise in the limiter amplifiers with a wide bandwidth. The first case concerns the noise in the mixer, the noise of the loss elements used to filter the RF product at the output of the mixer, the noise in resistors around the low-noise preamplifier and the proper voltage noise of the low-noise preamplifier. The wideband noise comes from all the elements located after the low noise preamplifier. First limiter amplifier increases the slope in the zero crossing area; therefore the higher bandwidth in the linear zone is required. If the slope of the second limiter amplifier reaches the slew rate of the OP27 amplifier ($2.8\text{x}10^7$), additional non-linear effects may be observed. These may reduce the system background noise as well as the noise that is an object of our measurement. Currently the slope at the output of the second limiter amplifier is about $7\text{x}10^5$ and this effect need not to be considered.

Concerning the other noise sources such as ground loops, electromagnetic interference, environmental effects, vibrations and temperature drift the proper mechanical construction is important. It includes the grounding and shielding, the SMA and N type connectors have been used instead of BNC and two separate DC power supplies have been used to avoid the crosstalk between the channels. The previous system for frequency stability measurement has been improved with a dual-mixer time-difference multiplier with system background noise reduced to $ADEV(1\text{ s}) \approx 3.1\text{x}10^{-14}$.

References:

[1] HOWE, D. A. – ALLAN, D. W. – BARNES, J. A.: *Properties of Signal Sources and Measurement Methods* Proc. 35th Annu. Symp. Frequency Contr., 1981.

[2] ALLAN, D. W. – DAAMS, H.: *Picosecond Time Difference Measurement System* Proc. 29th Annu. Symp. Frequency Contr., Atlantic City, USA, 1975, pp. 404–411.

[3] STEIN, S. R.: *Frequency and Time - Their Measurement and Characterization* Precision Frequency Control, volume II 1985, pp. 229–231.

[4] SZE MING, L.: *Influence of Noise of Common Oscillator in Dual-Mixer Time-Difference Measurement System* IEEE Trans, on Instr. and Meas., vol. IM-35, 1986, pp. 648–651.

This research has been supported by CTU grant No. CTU0610513.

The Methods of random signals generation with given distribution of amplitudes

Jan Neškudla, Josef Vedral

neskudj@feld.cvut.cz

Department of Measurement, Faculty of Electrical Engineering
Czech Technical University, Technicka 2, CZ 166 27, Praha 6, Czech Republic
tel. +420 2 2435 2120, fax: +420 2 311 99 29

1 INTRODUCTION

Digital-to-Analogue (DAC) is the key device of contemporary measuring devices while it provides an interface between analogue and digital areas. It must be considered as a non-ideal device that errors are to be measured by manufacturers as well as by application engineers. There are several basic methods that are commonly used for ADC and DAC testing. Sine fit test [1], [5] stands for an example of time-domain testing while single- and dual-tone FFT test [5] can be considered as the frequency-domain test method. Such standard methods are well described in IEEE-STD-1241 Standard for Terminology and Test Methods for Analog-to-Digital Converters or in IEEE-STD-1057 Standard for Digitizing Waveform Recorder. The typical example of statistical approach is histogram test that can use various input signals. Nevertheless, sine-wave full-scale input signal is mostly used, too. Not only sine wave but any deterministic input signal requires accuracy (linearity, signal to noise ratio, etc.) of such signal higher than expected accuracy of tested AD converter. This fact becomes problem when low sampling frequency, high-resolution AD converters (e.g. ∑-Δ or dither-based) or on the contrary very high-speed AD converters like these of digitizing oscilloscope are to be tested. In such cases, stochastic input signal must be used for test [2], [3], [4].

2 DETERMINISTIC VS STOCHASTIC TESTING SIGNALS

The histogram test method [5] allows use noise as the input signal. One can use uniformly or Gaussian distributed noise. Uniformly distributed noise enables easier and more accurate histogram processing but it is difficult to generate such noise. There is not any suitable „physical source“ of large scale uniformly distributed noise.

3 M-SEQUENCES AND ITS GENERATION

M-sequences are pseudorandom sequences of maximal period, and now days it's a mainly used part of pseudorandom family, because their good theoretical knowledge. They are generated by primitive irreducible polynomial over Galois Field GF(q) degree q. In this exploration we are using GF(2) and thus binary m-sequences are generated. Used hardware implementation structure is LFSR of degree n, where the feedbacks taps are well known and can be easily found on many books [6]. By proper setting of those feedbacks, maximally length uniformly distributed pseudorandom sequence of period 2^n-1 is generated. When the parallel output signal from LFSR is converted by DAC, its linearity change distribution of amplitudes and thus no exact uniform distribution is obtained. Followed technique show how to linearize DAC in this case.

4 DECOMPOSITION AND INTERALACING OF M-SEQUENCES

If the period of an m-sequence is 2^n-1=k.l with k relative prime to l, then the vector e, a period of the m-sequence, can be decomposed in a special way into two sequences of lengths k and l (see table 1). The properties and structures of those m-sequences are well known [7]. This technique is possible to

use for a designing new pseudorandom sequence with desirable weights in distribution. Whole exploration is directed to single period of the m-sequence, which can be more conveniently represented by vector *e*, *e*=(e0,e1,.....,ep), where *p* is index from 0 to *n*. Elements of that vector is consequently organized into an *l x k* matrix. The k columns of obtained matrix represent either an m-sequences of period *l* or an all-zero sequence. Given the above matrix structure, a binary m-sequence {ai} of period *l* . *k* can be based on sampling a binary m-sequence {bi} of period *l* with decimation value r=*k*. By suitable initial conditions, it is possible to establish a set of *k* sampled m-sequences which are used as the columns of above *l x k* matrix to produce desired m-sequence with demanded distribution of amplitudes in output sequence. That's because we can interlace a sequences from matrix *l x k,* and we can exploit the same sequence several times or even include the all-zero sequence, which is problematic to obtain with classical LFSR pseudorandom generator. The second advantage is possibility of generating long period pseudorandom sequence based on smaller one.

Table. 1

n	N	Factorization
8	255	$3 \cdot 5 \cdot 17$
10	1023	$3 \cdot 11 \cdot 31$
16	65535	$3 \cdot 5 \cdot 17 \cdot 257$
22	4194303	$3 \cdot 23 \cdot 89 \cdot 683$

ACKNOWLEDGENENT
This project is supported by IG ČVUT No. CTU0610613.

REFERENCES

[1] Seitzer,D., Pretzl, G., Hamdy, N.A.: Electronic analog-to-digital converters. John Wiley, Chichester 1983. ISBN 0471 901989
[2] Carbone, P.,Petri, D.: Noise Sensitivity of the ADC Histogram Test, IEEE Instrumentation and Measurement Technology Conference, St. Paul, Minnesota, May 1998.
[3] Vedral, J. - Holub, J.: Statistical Testing of Sigma Delta ADCs. In: Proceedings of Workshop 2000. Prague : CTU, 2000, vol. A, p. 200. ISBN 80-01-02229-3.
[4] Holub, J., Vedral, J.: Signal Source for Statistical Testing of ADC. XVI.Congress IMEKO. 5th Worshop on ADC Modelling and Testing. Wien 2000, vol. 10, p. 177-181. ISBN 3-901888-12-8.
[5] IEEE-STD-1241 Standard for Terminology and Test Methods for Analog-to-Digital Converters.
[6] Zepernick H.-J., Finger A. : Pseudo Random Signal Processing – Theory and Application, John Wiley & Sons, Ltd, 2001, ISBN-10 0-470-86657-8 (HB)
[7] LIH-JYH WENG: Decomposition of M-sequences And Its Applications, IEEE Transactions of Information theory, vol. IT-17, no. 4, July 1971
[8] NESKUDLA J., VEDRAL J.: DIGITALLY CONTROLLED WHITE NOISE GENERATOR, IMEKO XVIII World Congress, Rio De Janeiro, Brasil, 2006

Flight Data Measurement System for Small Airplanes

P. Pačes

pacesp@feld.cvut.cz

Department of Measurement, Faculty of Electrical Engineering, Czech Technical University, Technická 2, 166 27 Prague 6, Czech Republic

Introduction: The final product of this work, supported by the Czech Technical University internal grant, was to find out next direction of study in area of small aircraft flight and guidance electronic systems. This paper is focused on problem around small, hobby and ultralight aircraft instruments and their interconnection – i.e. small aircraft avionics. Common solution consists from transducer of scanned quantity which is connected to appropriate indicator–gauge. This solution has some advantages and also disadvantages. Modern systems usually uses complex avionics system based on the MEMS (Micro-Electro-Mechanical Systems) sensors and modern display technology (LCD). The MEMS type of sensors allows holding low manufacturing cost and the LCD displays allows achieve high flexibility in displayed data. The LCDs also have lower weight then common mechanical instruments.

The suggested solution in this paper has some difficulties that have to be overcome. The aircraft industry is very slow in changing working things and putting some new substitution for them. The software of the new device must be certified. The hardware must be certified. The developer has to take care of a lot of things that are related with another. For example a battery backup of the electronic avionic system is also a big challenge. Main part of work supported by CTU IG CTU0610713 was done in these areas: pressure measurement, software and hardware certification and sensor connection and interconnection.

Pressure measurement: Pressures are important quantities in all aircraft industry. The air speed, vertical speed and altitude are quantities that can be measured by pressure. The small aircrafts use altitude in range from 0 to 5 km above Earth surface and horizontal speed in range from 0 to 350 km/h. The outcome of this research also was a study of suitability of use MEMS pressure sensors in the small aircraft avionics system and estimation of their precision and limit values [2]. Following MEMS pressure sensors were measured: Memscap SP82, Honeywell 19U, Freescale MPX4115A, Freescale MPXAZ6115AC6U, Freescale MPXV5100DP and Intersema MS5534-BM. The Memscap SP82 sensor was chosen for another work. Following particulars led to this choice: sensor already has several certification marks for use in aircraft industry; it is possible to heat sensor in the application; the sensitivity and range are sufficient. The main disadvantage of this sensor is its price that is at the limit for using in small aircraft area.

The second prototype of an aerometrical system was designed and manufactured with Memscap SP82 sensor.

Software certification: Aircraft industry and especially aircraft electronics is in most cases connected with expression “safety critical” or “life critical”. These systems are systems whose failure or malfunction may result in: death or serious injury to people, or loss or severe damage to equipment or environmental harm. Part of the time put into this project was spent to study several standards used for hardware and software testing and for software and hardware certification.

One paper [3], that in general layer describes the actual situation around aviation and airborne electronic equipment certification in the Czech Republic, was written and presented. The paper points at the legal basis of the certification situation in the Czech Republic.

The differences between certification of small-sport aircrafts and general aviation category are highlighted. The next aim of that article is to introduce software and hardware certification standards and recommendation. In the end the article depicts a design of some airborne electronic equipment developed in the laboratory of airborne control and information instruments.

Sensor connection and interconnection: In modern avionics systems all sensors and display systems are connected by some kind of the bus. The most famous airborne buses are ARINC 429, ARINC 629 and MIL-STD-1553. In case of application in the area of small aircraft the good solution is to use CAN based network. CAN bus is widely dispersed in the automotive industry. A lot of very cheap microcontrollers contain CAN controller unit. There is a CANaerospace project available in the Internet.

For sensor maintenance and hot-plug ability the IEEE 1451 family of standards were studied. These five standards define how transducers can be mapped to a target network based on an object model defined independently of the network physical bases.

Also exact definition of time is very important part of every measurement. The time synchronization protocol should be implemented according to the IEEE 1588 standard. This standard describes message exchange routine that allows time synchronization in a packet oriented networks.

Conclusion

The main part of work involved in this project was aimed on the field of small aircraft, especially on the pressure measurement, software certification and sensors connection. The attention was put on the reusability of done work. A number of papers were presented on several places. One article was printed in the Automatizace magazine. That article describes interoperability between GPIB measurement bus and MS Excel environment using COM objects. The same guide can be used for measuring with RS232 connection. The IEEE 1451.2 and IEEE 1588 standards were implemented on the Motorola MC9S12XDT256 microcontroller with XGATE capability. The IEEE 1588 implementation source codes are ready to use in another solutions as the C file implementations and also as MS Windows DLL library. The LabView software development environment was used in some parts of the project solving because of fast development process. The all work included in this project allowed to learn a lot of new, useful things and shifted limit of the article author skills.

References:

[1] P. PAČES, - K. DRAXLER: *The Small AircraftAltimeter,* New Trends in Civil Aviation 2006, International Conference, VUT Brno, University of Defense. 2006 pp. 117–122.

[2] P. PAČES: *Utilization of Low Cost MEMS Pressure Sensors in Small and Ultralight Aircraft Avionics,* POSTER 2006, CTU Prague, 2006 CDROM.

[3] P. PAČES: *The Certification of Aircraft Electronic Devices and Software Equipment in the Environment of the Czech Republic,* Slovak Air Force Institute of Research and Testing Košice 2006, 7th International Conference, 2006 CDROM.

[4] H. RAMOS, - P. RAMOS, - P. PAČES: *Development of a IEEE 1451 Standard Compliant Smart Transducer Network with Time Synchronization Protocol,* IMTC, Poland, 2007 .

This research has been supported by Czech Technical University internal grant No. CTU0610713. The work described in this paper was supervised by kind patronage of Associate Professor Karel Draxler. The author very appreciates his help and support.

Dynamical testing of ADCs with digitally generated testing signals

Suchánek P.

suchanp3@fel.cvut.cz

Department of Measurement, Faculty of Electrical Engineering, Czech Technical University, Technická 2, 166 27 Prague 6, Czech Republic

Testing of analog-to-digital converters (ADC) can be carried out in two ways. One group of tests is in the time domain, where the sinewave fitting is used prio to any calculations, while the other group of tests is in the frequency domain, where the power spectrum is calculated first. The former include histogram test, sine-wave fitting, Integral Nonlinearity (INL) or Diferential Nonlinearity (DNL) estimation. The latter include Spurious-free Dynamic Range (SFDR) or Total Harmonic Distortion (THD).

A typical test-bed consists of a signal source, optional filters for the test signal and a device under test (DUT). An amplifier may be needed in some configurations. For many test scenarios only a single-tone test signal is needed especially when testing nonlinearities induced by the DUT. In this case, the test signal must be spectrally purer that the DUT. As there are no high quality signal generators for testing high-speed high-resolution ADC a single-tone test scenarios lead to using filters. Another way is to use dual-tone test signals, where common generators can be used.

When evaluating DUT parameters in the frequency domain tests, any other products apart from the fundamental found later in the power spectrum are to be assigned to the ADC under test. However, any nonlinearity, either in the generator output, in the devices along the signal path or in any active component (the amplifier) results is additional harmonics component. Then, depending on the amplitudes of these it may severely affect the estimation of parameters of the tested ADC as we can not distinguish, whether the nonlinearities arose in the ADC or were already present in the test signal. To deal with this and obtain a spectrally pure signal, there are two ways, both resulting in a clear test signal spectrum containing only needed signals (the fundamental).

The first method is to use a filter, again more linear then DUT as the last device in the signal path before entering a DUT. Some specially designed nearly linear filters with air coils were manufactured at the Department of Measurement in last years [1]. The filters are placed in robust cooper boxes. On the opther hand, in the case of dual-tone test signals a power combiner is used.

The other method to achieve a spectrally pure test signal is to use digital pre-distortion (denoted as DPD) [2]. The distortion present in the test signal is measured before real testing and all unwanted components are eliminated. They can be harmonics, intermodulation products or spurious. The elimination is conducted by adding signals with the same parameters as the distortion but with the opposite phase. The essential point is that it should be measured by a device that would not induce further errors into the signal. If that happened, the pre-distortion would not work correctly and the process of elimination could diverge.

In our case, the procedure to find pre-distortion can be described in several steps. Firstly, the desired level for spurious-free dynamic range of the test signal was set (the target). Secondly, the signals exceeding the level set by the user were found. Lastly, appropriate signals with opposite phase were calculated and added up to the original signal. The last two steps are iteratively looped, until the target is achieved. The most crucial part is to find a phase of the unwanted components to eliminate them. The spectrum was measured by a spectrum

analyzer that does not provide the phase information. So the phase information had to be found iteratively. The phase search tried 3 different signals with mutual phase shift by 120°. The best result was kept for further iterations. For this method, a state-of-the-art arbitrary waveform generator (AWG) and spectrum analyzer were used. Of course, this method has some limitations. One of them is a finite resolution of the generator causing some spectral line to uncompensatable. The iterative algorithm is general and can be applied for any application.

Another improvement would be a phase locked loop used to provide coherent sampling frequency for the test. This should eliminate the need to window measured data when frequency spectra calculations are desired. The printed board was designed with interface to a Altera FPGA board also designed within our laboratory. With this device we would like to test a new method of generating a signal by a closed loop where more crossing-level are used. Multiple crossing levels can be used for sophisticated evaluation of zero-level crossing. The proposed PLL can be turn off during sampling data as any change in sampling frequency would distort measurement and induce phase noise.

During the conducted tests, applicability of the filter method was approved. When evaluating the system other digitizers available in our laboratory, a problem with improper signal conditioning and problem with disturbance from ground loop was analyzed. The test system uses band-pass and band-stop filters. When the cases of the filters are connected by parasitic impedance or when all devices are powered from the same power supply line a ground loop is created. These ground loops induce distortion. A simple guide was proposed to locate the ground loops [3]. On the other side, there should be an attenuator in between the two filters to match the output. When this is not present reflections occur and the amplitude transfer function on the band-stop output is significantly reshaped.

The planned USB interface is not needed and the effort was more put into extending the software package Digester. During work on the topic it was proposed to carry out new development as this package has been modified by many authors and has become very difficult to add new features. Therefore, a new modular conception was proposed and programming of several modules has already been carried out. This was carried out during a bachelor thesis [4].

References:

[1] KOMÁREK, M. – PAPEŽ, V. – ROZTOČIL, J. – SUCHÁNEK, P.: *Sine-Wave Signal Sources for Dynamic Testing High-Resolution High-Speed ADCs,* XVIII IMEKO World Congress and Brazilian Congress of Metrology [CD-ROM] 2006, pp. ???–???.

[2] BJÖRSELL, N. – SUCHÁNEK, P. – HÄNDEL, P. – RÖNNOW, D.: *Measuring Volterra Kernels of Analog to Digital Converters Using Stepped Three-tone Scan,* IEEE Transaction on Instrumentation and Measurement Technology, Submitted 2006

[3] SUCHÁNEK, P. – KOMÁREK, M. – HAASZ: *Practical Aspects of Dynamic ADC Testing in Frequency Range 1 to 20 MHz,* In BEC 2006 - 2006 International Baltic Electronics Conference, 2006, pp. 167–168.

[4] VLČEK, T. *Možnosti komunikace se vzdálenými měřícími systémy, Bakalářská práce.* In Czech language. 2006

This research has been supported by CTU0610813.

Basic Intelligent Image Sensors Systems and Dedicated Image Gauging Methods

J. Třešík, J. Fischer

trestj1@fel.cvut.cz

Department of Measurement, Faculty of Electrical Engineering, Czech Technical University in Prague,
Technická 2, 166 27, Prague 6, Czech Republic

The aim of this project was design an intelligent basic image processing system, search out typical application of use and develop suitable group of gauging methods.

The project was solved in several phases. At the beginning it was necessary to develop hardware of the image processing system. The basic intelligent image sensor was designed and several elementary gauging tasks was developed and checked. The dimension measurement, area measurement, optical centroid measurement and barcode reading are examples of typical image processing tasks that are suitable for basic intelligent image sensors.

The new problems arise from the first developed system and the new advance basic image processing system had to be developed.

The CMOS image sensor KAC 9218 from Kodak was used like a source of image signal in booth systems. The first system was based on Complex Programmable Logic Device (CPLD) Altera-MAX II. The KAC 92XX image sensor offers twelve data byte and group of synchronization signals. The sensors setup is prepared by means of I^2C bus after power up. The AVR microcontroller from Atmel was used for communication with PC and sensor initialization setup. The USB full-speed interface was selected for the firs implementation of the system. Capability of the Full-Speed interface is not enough for user friendly setup of target system (focusing and exposition of objective) hence the High-Speed interface was included in to the second version of the sensor. The group of elementary gauging tasks was developed for the first implementation of the system. The system is able to measure objects dimensions in the line direction, area of the object in the image, the position of the centroid in the image. The reading of EAN 13 barcodes is implemented for demonstration of low powered system abilities.

The varying lighting conditions can causes complications during measurement. The accurate edge detection can be disturbed. Dimensions of measured object can be dependent on the lighting conditions if the static threshold level is used. The missing of measured object is the worst case of varying lighting condition and can occurs. The superior edge detection method has been developed. Described method is based on the first and second derivation. The first derivation is useful for the maximal gradient finding. The complications can arise in the following peak localization. The maximum localization task can be converted to the zero cross task by means of the second derivation. However the second derivation is more noise sensitive. Many wrong zero crossing events can occurs.

The modified second derivation based method arises from Canny single dimensional edge detection method. The Canny 1D edge detector uses Gaussian smoothing and derivation. The Gaussian operator function with zero mean value is defined by equation (1), where σ is

$$G(x) = \frac{1}{\sqrt{2\pi}\sigma} e^{\frac{-x^2}{2\sigma^2}} \tag{1}$$

$$\frac{dG(x)}{dx} = \frac{-\sqrt{2}x}{2\sqrt{\pi}\sigma^3} e^{\frac{-x^2}{2\sigma^2}} \tag{2}$$

standard deviation. Input signal is convoluted with the Gaussian impulse response. The derivation follows convolution of the signal and the Gaussian filter. The positions of edges are represented by minimums and maximums in output signal.

The process of convolution and process of derivation can be swapped. Edges can be detected by mean of convolution the input signal with derivated Gaussian (2).

The second derivation can be included into the convolution operator too. Insertion the threshold unit between the first and second convolution (derivation) is more suitable. The problem of the great noise sensitivity can be solved by convenient threshold level. The threshold level setting is not critical in this case and can be static for the most real images. Implementation of the single dimensional edge detection method and real checked application on low powered CPLD based system is described in [1].

The basic problems can be solved by above mentioned low powered CPLD based intelligent image sensor. For more sophisticated image processing tasks the more powerful system had to be developed.

The second developed system is based on Xilinx Spartan 3 FPGA (field programmable gate array). One of great advantage of new the system is USB2.0 – High Speed interface that offers life image on the computer screen. Used Spartan 3 FPGA offers enough power abilities for more demanding image processing tasks. It contains DSP bocks with 18 bits hardware multiplier units and memory blocks. Enough power abilities is important for the necessary modular solution of the firmware. The well prepared modular blocks of image processing task can significantly simplifies and accelerate the process of result measurement problem solving.

Possibility of basic intelligent image sensor implementation was checked. Target image processing tasks are basic gauging tasks like dimension and position measurement. More complex image processing tasks development is aim of near feature. Any direction dimension measurement, adaptive threshold level computing, basic regulators and surface quality check routines are examples of now prepared more complex image processing tasks. The main advantage of programmable logical device solution in comparison with processor solution is possibility of parallel processing. Several measurement units can operate at the same clock frequency without synchronization needing. The maximum information can be directly extracted from the image “on the fly”. It means that picture memory needn’t be used. All information can be selected directly from image sensor.

References:

[1] TŘEŠTÍK, J.: *The Single Dimensional Edge Detection Method for the Intelligent Image sensor* Baltic Electronics Conference - Tallinn, ISBN: 1-4244-0414-2 2006

[2] HECHT, E.: *Optics* 4th edition, ISBN: 0-8053-8566-5 Addison Wesley, San Francisco, 2002

[3] TŘEŠTÍK, J.- FISCHER, J.: *Binary Pre-processing the Videosignal from CCD Camera,* IWCIT 2005 - International Workshop Control and Information Technology. Ostrava: Technická univerzita, 2005, s. 347-350. ISBN 80-248-0906-0. 2005

The research was supported by the CTU internal grant No. CTU0610913 “Methods of Synthesis the CMOS Image Sensor Based Measurement Equipments for the Dedicated Applications” and the research program No. MSM6840770015 "Research of Methods and Systems for Measurement of Physical Quantities and Measured Data Processing" of the CTU in Prague sponsored by the Ministry of Education, Youth and Sports of the Czech Republic.

Implementation of New Practice Exercises into the Digital Signal Processing in Telecommunications

Z. Bečvář

becvaz1@fel.cvut.cz

Department of Telecommunication Engineering, Faculty of Electrical Engineering,
Czech Technical University in Prague, Technická 2, 166 27, Praha 6, Czech Republic

The main objective of this project was the innovation of the subject "Digital Signal Processing in Telecommunications" at Czech Technical University in Prague. There were implemented two practice exercises focused on image and video processing. The Texas Instrument's fixed point digital signal processors TMS320C6416 and Einfochips daughter card were used as main laboratory equipment in these exercises. The changes were introduced into the education in the winter semester 2006.

The main goal of the subject "Digital Signal Processing in Telecommunications" is acquaint the students in Master study program with principles and methods used for processing of digital signals including sampling of analog signals, application of integral transformations, digital filtrations, adaptive filtration methods and methods for low bit rate audio and video coding. This is focused on the usage of these methods for realization of the telecommunications equipments with Digital Signal Processors (DSP). The students deal with analysis of digital filters, discrete systems and voice signals in the practical training. The absence of practice experience with processing of video signals was the biggest problem of this subject.

There were need of originate new experimental workplace, which can be used by the students to get a practice experience with implementation of an algorithms associated mainly with coding and compression of the images and the videos. These workplaces are equipped with:

- Starter Kit mounted with Texas Instruments TMS320C6416 DSP [1]
- Einfochips Video Daughter Board (VDB) for C6000 EVM/DSK card [2]
- OLED graphic display
- Oscilloscope Owon 20 MHz.

The TMS320C6416 DSP is the high performance fixed point processor with Very Long Instruction Word (VLIW) architecture. The wide of word is 256-bits. This architecture allows supply up to eight 32-bits instructions to the eight functional units during each cycle. The TSM320C6416 provide performance of up to 8000 million instructions per second (MIPS) at a clock rate of 1000 MHz. The C6416 has two embedded coprocessors – Viterbi Decoder Coprocessor (VCP) and Turbo Decoder Coprocessor (TCP). Those coprocessors significantly speed up channel decoding operations on-chip. This DSP's core processor (CPU) has 64 general-purpose registers with thirty-two 32-bit word length and two sets of independent functional units. Each set contains 4 units (.L, .S, .M, .D). The two sets of functional units, along with two register sets are composed sides A and B of the CPU. Each side of CPU can share 32 registers belonging to this side.

For video processing are some video inputs and outputs needed. Those Starter Kits have no video interface. Video input/output must be supplemented with a daughter board equipped with video inputs and outputs. The Einfochips VDB for C6000 EVM/DSK cards is

used as the daughter boards. This daughter board presents a modular approach and has NTSC/PAL and S-video input and NTSC/PAL and S-video output. The digital interface to the DSP is via Xilinx Spartan-II FPGA. VDB is equipped with two extension connectors compliant to TMS320 cross-platform daughter board specification V 1.0 that allows to be connected to the EVM board. Further is the VDB equipped with one expansion connector provides access to the DSP's asynchronous External Memory Interface (EMIF).

With it is modular approach, the core DSP and memory design of the EVM/ DSK can be leveraged across several multi-channel, multi-function and advanced applications such as image applications, video surveillance system, security cameras, video monitoring system, personal or digital video recorder, 3-D graphics application, etc.

The new workplaces are equipped with oscilloscopes and OLED displays (together with DSP and VDB). The oscilloscope allows to the students get new practice experience not only with signal processing, but they can deals with the DSP's hardware architecture. The OLED displays are used as a signaling component.

There were originating two modern practice exercises that deal with image and video processing. The new exercises are follows:

- Image compression
- Video compression and motion detection

The first one is focused on the processing, coding and compressing of a static image. The students try implementation of Run Length Encoding (RLE) algorithm. The second one is aimed on the compression of video signals and motion detection. There are tested functions of basic video compression algorithms and further there is implemented algorithm for motion detection in video signal. The study materials belonging to this practice exercises have been created and are available at the official department webpage (www.comtel.cz) in the section "Exercises" in the subject "Digital Signal Processing in Telecommunications".

The created workplaces are used in addition for experiments in frame of solving bachelor and diploma thesis of students in bachelor and master study program and for experimental research and development works of postgraduate students.

References:

[1] TEXAS INSTRUMENTS: *www.ti.com.*

[2] EINFOCHIPS: *www.einfochips.com.*

[3] QURESHI, S.: *Embedded Image Processing on the TMS320C6000DSP: Examples in Code Composer Studio and Matlab* Springer, 2005.

[4] BECVAR, Z.: *Implementation of New Practice Exercises into the Digital Signal Processing in Telecommunications* Research in Telecommunicaton Technology, 2006.

This research has been supported by grant FRVŠ No. 2125/2006/G1.

Compact Control Circuit of the InGaAs Photon Counter

J. Kodet, I. Prochazka, K. Hamal

prochazk@mbox.cesnet.cz

Department of Physical Eletronic, Faculty of Nuclear Sciences and Physical Engineering, Czech Technical University in Prague, Brehova 7, 115 19 Prague 1, Czech Republic

We are presenting the design, construction and performance of the compact control circuit of the InGaAs photon counter. The main design goals were to construct detector control circuit, which enables the InGaAs photon counters to operate in a gated mode. The main application for the detector will be quantum cryptography, where the detection of single photons of wavelength 1.55 micrometers is needed. This wavelength is suitable for communications purposes with optical fibers [1]. The photodiode structure will be pulse biased 2 to 4 Volts above its breakdown voltage for a short time interval in which the arrival of photon of interest is expected. The photon detection will cause an avalanche multiplication of carriers, which will cause the current flowing cross the structure. This avalanche current flow will be terminated by lowering the bias below the break down voltage. The time, for which the avalanche current flows, must be short, in the range of several nanoseconds only to avoid detection structure damage and to limit the afterpulsing effects. Additionally, the bias source must be equipped with fast current limiting option, since the stationary current through InGaAs structure might cause its non-reversible destruction. The avalanche current – the photon detection event - will be detected by fast ECL comparator. The quantum cryptography requires very short adjustable detecting window width in range of 3 to 10 nanoseconds. The repeating frequency of detection windows is required to be up to 2 MHz. The maximum detection rate is limited by intrinsic detection noise and the after-pulsing effects. The very short detecting window requires nanoseconds rise and fall times of gating pulses. The gating pulse minimum amplitude required is 5 volts. Gate pulse forming circuit design was the most challenging task in the device design and construction.

The entire control circuit consists of five blocks. First is the gate signal receiver, which works with ECL input voltage levels and TTL voltage levels in output. The receiver drives the gate window generator composed of C-MOS gates. The gate window pulse is level shifted by the voltage level converter to match the fast ECL comparator input voltage range. This comparator works as a breakdown sensor of the InGaAs photon counter. The detector bias control circuit is equipped with fast current limiting option for protection of photodiodes against destruction, it stabilizes the bias voltage in range of 25 to 55 Volts. The pair of integrated DC/DC converters 5V to 2x15V [2] is used. The current limiting option is set to value 1 milliampere and the limitation of current reacts in range of hundreds of nanoseconds.

The core of the circuit, which consists of gated signal receiver, generator of fast rise/fall edges and fast ECL comparator, is designed using the SMD technology. That enabled to create the entire device very compact 60 x 60 mm in size. The circuit is powered with external stabilized supply providing +5 and –6 volts, the input and output signals are connected via SMA connectors.

The entire circuit has been tested in first step with silicon avalanche diodes K14. These diodes have been developed in our labs in early nineties [3] and were dedicated for high precision satellite laser ranging. For our group well known diodes let to confirm nanoseconds rise/fall edges and to tune the device. The shortest detecting window width achieved was 2.7 nanoseconds with repetition rates 2 MHz at a room temperature. In second step was control

circuit tested with different InGaAs detection chips. The chips were operated at room temperature and thermoelectrically cooled temperatures, as well. The gated window width was set in the range of 3 to 10 nanoseconds and the repetition rates up to 5 MHz were tested. The timing resolution of the photon detection was tested in the Time Correlated Photon Counting (TCPC) experiment. As a photon source was used laser diode, which generated 40 picoseconds long laser pulses at the wavelength of 1.55 micrometers. The individual photons were detected with timing resolution in the range of 200 to 500 picoseconds and with the detection probability 5 – 15 % depending on the detector bias voltage.

The main foreseen application of the detector is quantum cryptography, but the control circuit can be used in connection with various avalanche photodiodes hence it can be applied in different applications.

References:

[1] SENSORS UNLIMITED, INC. *Photon-Counting APD, Inc. [online].WWW: <http://www.sensorsinc.com/downloads/4110-0036_6_SU055.pdf>.* 2005 [cit. 2007-01-02].

[2] HN ELECTRONIC COMPONENTS GMBH & CO. KG *[online]. WWW: <http://www.hn-electronic.de/pdf/sim1dil8.pdf>.* 2006 [cit. 2007-01-02].

[3] PROCHAZKA, IVAN.: *Semiconducting single photon detectors: the state of the art* In physica status solidi (c). Volume 2, Issue 5, 2005, 1524-1532.

This research has been supported by conctract CTU - FNSPE No. 40-06-010, Duepigreco s.p.a., Napoli, Italy.

Planar Lightwave Hybrid Integration Circuits

V. Jeřábek, I. Hüttel **, V. Prajzler, Z. Burian, J. Armas

jerabek@fel.cvut.cz – fax:+420224310792

Department of Microelectronics, Faculty of Electrical Engineering,
Czech Technical University, Technická 2, 166 27 Prague 6, Czech Republic

** Institute of Chemical Technology,
Technická 5, 166 28, Prague 6, Czech Republic

Introduction

A new field which arose throughout the past few years is the field of integrated optoelectronics. Within this field of hybrid or even monolithic structures of optics, optoelectronic and electronic components are becoming useful for the transmission of information in the increase of speed up to hundred gigabits per second.

Planar lightwave circuit (PLC) hybrid integration technology enables us to construct component by combining PLC with passive function (fiber and planar optical waveguides) and active optoelectronics devices (laser diodes, optical amplifiers and photodiodes) hybridized on a PLC [1], [2].

Polymer or silica-based planar lightwave circuit (PLC) hybrid integration is a promising way to provide highly functional photonic components. The major advantage of hybrid approach is that the PLC can be fabricated using existing technology piecing together with devices which have been substantially optimized in a given material [3].

This paper describes research works realized at the Czech Technical University in Prague by microelectronics department and the Chemical Technology Institute in Prague. The paper is an overview of the progress in some optoelectronic element for PLC hybrid integration technology and describes first experiment which led to the construction hybrid integrated PLC for optoelectronics information transmitting and receiving and description of their properties.

OE devices for PLC hybrid integration

OE devices – laser diodes, optical amplifiers and waveguide photodiodes in which spot size of radiation is expanded to match an optical fiber are attractive for providing low – loss coupling to optical fibers and waveguides without lenses as well as offering an alignment when assembling optical modules.

Laser diodes are key components in the economical optic transmission systems. For PLC transmitters are used the spot-size converter integrated laser diodes SS-LD having a vertically tapered waveguide which is butt-jointed to a strained active region. The thickness of tapered waveguide at the facet and the joint portion is from 0.1 to 0.3 μm. The wideness stripe is 1 or 2 μm. The vertical tapered passive waveguide with a bandgap wavelength material smaller than the oscillating wavelength is suitable for very low loss.

For construction PLC and low-loss optical coupling without lenses and optical mirrors is suitable use a waveguide photodiode (WG-PD). A WG-PD has a structure suitable for flip-chip bonding directly on to the PLC platform. The WG-PD combining the selectivity of an impurity-diffused pn-junction and planarity of a slab waveguide. The structure incorporate multimode double-core structure consisting of an InGaAsP photoabsorption layer and upper and lower transparent InGaAsP intermediate-bandgap layers. The photoabsorption layer thickness is 3 μm and two intermediate layers have thickness 2 μm. For high responsivity at a low operation voltage p-type doping is introduced using of Zn-diffusion in a part of the photo-absorption layer.

Fabrication of PLC hybrid integration

Our works will first concentrate on design and construction of a PLC ridge and channel waveguide, which was made from dielectric (Si, SiO_2, Si_3N_4) and organic (PMMA, SU-8) materials, prism and mirror coupling radiation into a PLC waveguide and standard PIN InGaAsP photodiode. The Si_3N_4 optical planar waveguides was fabricated by using Plasma Assisted Chemical Vapor Deposition (PACVD) on silica on silicon substrate. The ridge or channel waveguides would be fabricated by using standard UV lithography.

The polymer layers were deposited by using spin coating method on silica on silicon. As polymer we choose NANO^{TM} SU-8 2000 polymer from MicroChem Corp. due to good optical and mechanical properties (this polymer has optical losses less than 1 dB/cm at the key communication wavelengths of 1 300 and 1 550 nm). Before UV lithography the samples were prebake for 10 min. at 90°C. The channel waveguides would be fabricated by using UV lithography. As a last step the post backing (200 °C at 120 min or 90°C at 15 min.) would be carried out to stabilize optical properties.

Conclusion

We have described recent progress made in first stage of research PLC hybrid integration technology realized at the Czech Technical University in Prague. In near future we plan to work on the second stage and third stage of the research. The second stage will be a design and fabrication of the platform technology for classical and spot-size optoelectronics elements. The third stage will be evaluation a chip and a half-encapsulated chip bonding technology.

References:

[1] K.KATO AT ALL: *PLC Hybrid Integration Technology and Its Application to Photonic Components* IEEE J.of Selected Topics in QE, 2000, pp.č.4-č.13

[2] T.HATTA AT ALL.: *Hybrid Integrtion of WaveguidePhotodiode and Preamlifier IC Using Au Stud Bump* J. of Lightwave Technology, 2006 pp.č.3187-č.3194

[3] L.ELDADA AT ALL.: *Avances in Polymer Integrated Optics* IEEE J.of Selected Topics in QE, 2000 pp.č.54-68

This research has been supported by GA ČR grant Nos. 102/06/0424 and the research program MSM6840770014 of the Czech Technical University in Prague.

Innovation of Courses on Design of Integrated Electronic Systems

P. Hazdra

hazdra@fel.cvut.cz

Department of Microelectronics, Faculty of Electrical Engineering, Czech Technical University in Prague, Technická 2, 16627 Prague 6, Czech Republic

Semiconductor electronics has experienced drastic expansion and improvement in the last forty years. Since the introduction of the first integrated circuit, the number of transistors in a single chip has grown exponentially, and a silicon chip now routinely contains hundreds of thousands or even hundreds of millions of transistors. Increasing complexity of integrated circuits, widening of their application field and permanent pressure on time-to-market shortening, necessitated in new approaches in integrated electronic system design. Nowadays, design methodology shifts towards to higher levels of abstraction (behavioral and system level) which show only selected key features of the system and ignore associated details [1,2]. For this purpose, several hardware description languages (HDL) were developed to move from gate to register transfer level (RTL). Now, the advanced HDL (SystemVerilog, SystemC, etc.) attack the system levels and C++ is also being utilized for hardware/software co-design. Another way how to handle design of complex system is to re-use successful and already tested designs since it is nearly impossible to create a contemporary integrated electronic system from scratch. These existing functional blocks, usually referred to as Intellectual Property (IP) macrocells, provide the designer with a collection of predefined and already tested functions, such as microprocessors, DSP functional blocks, etc. It is evident that education of integrated electronics systems performed at technical universities has to cope with these new phenomena.

The main aim of the presented project was to create a new, obligatory subject X34SIE "Synthesis of Integrated Electronic Systems" dedicated to advanced design of electronic systems to be taught at the Department of Microelectronics, CTU in Prague as a part of the master course in Electronics. Before realization of the project, the education in integrated circuits design was mainly focused on device and circuit level and only a limited space was dedicated to higher levels (behavioral and RTL) and design of complex integrated systems. The design proceeded mainly in virtual reality since it is impossible to realize designed systems during the semester where the IC's design is being taught. For this reason, we focused on design of programmable devices (Field Programmable Gate Arrays) which exploit nowadays the most advanced technologies (90 and 60 nm nodes), provide highest system complexity and their design can be completed quickly without excessive NRE costs. Since we had to migrate to a completely new area of design, the innovation of the software and hardware design platform was a primarily task.

According our previous experience, we selected ISE (Integrated Software Environment) Foundation design package from Xilinx, Inc. as a basic design system. The ISE Foundation is the industry's most complete programmable logic design environment and includes the most advanced timing driven implementation tools available for programmable logic design, along with design entry, synthesis and verification capabilities. It offers design entry in higher HDL language as VHDL and Verilog together with hundreds of IP cores, including PCI, DSP and other pre-designed and tested solutions. We completed the ISE

system with EDK (Embedded Development Kit for soft- and hardprocessor design) and SysGen (System Generator for direct synthesis of DSP circuits from Matlab) software. Twelve PC based workstations were equipped with the full version of the software and design facilities wer further completed with two new workstations to allow education of postgraduate students and realization of diploma works.

Three hardware platforms from Xilinx, Inc., the top producer of advanced programmable logic devices, were selected for design implementation and testing: the Spartan-IIE, Spartan-IIIE and Virtex-4 Field Programmable Gate Arrays (FPGA). While, the Spartan-IIE family and CoolRunner-II CPLDs will be used for basic digital circuits design and verification (obligatory starting project), Spartan and Virtex FPGAs represent two distinct classes of high density FPGAs for implementation of integrated systems with the highest complexity. Spartan series devices represent the first FPGAs specifically optimized for the low-cost, rapidly changing consumer market. In contrast with it, the Virtex-4 FPGAs are the highest density FPGA in the industry, which are moreover furnished with PowerPC 450 processor core to provide system on chip design capability and DSP solutions. The laboratory for integrated electronic system design was furnished with development boards for each type the device. The development boards are equipped with different peripherals, e.g. pushbuttons, keyboards, LEDs, LED and LCD displays, ADCs, DACs, Ethernet, USB and RS-232 interfaces allowing their communication with other boards or peripheral devices (PC mouse, PC keyboard, VGA monitor, etc.). Within the framework of the project, several peripheral drivers were developed (VGA, LCD, PS2 keyboard, PS2 mouse, etc.) to serve students as a platform for their semestral projects. In this way, it is expected, that complex designs (e.g. a full-function calculator, a complete computer, a video game, as well as other circuits and systems) can be designed and verified by students within one semester. The laboratory for integrated circuit design was also equipped with a specialized library consisting of books dealing with the design and verification of complex electronic systems. This library is mainly intended for postgraduate students to deepen their knowledge in the field.

The inherent part of the project was the innovation of the curriculum of the subject "Synthesis of Integrated Electronic Systems". The new software and hardware equipment of the labs enabled to introduce the education on highest worldwide standards. The VHDL language is now being used for design entry and test. Design of electronic systems containing hundreds of thousands system gates and different hardware blocks (RAM, DSP blocks, etc.) can be made by students in the master's course.

The acquired software and hardware platforms, especially Virtex-4 kits, will be also used for education of PhD students within the subject *"Design of Programmable Integrated Circuits"*. This allows realization of complex designs and reconfigurable systems on chip.

References:

[1] WOLF W: *Modern VLSI Design: System-on-Chip Design,* Prentice Hall, 2002, ISBN 0 13-061970-1

[2] DESCHAMPS J.-P., BIOUL G.J.A., SUTTER G.D. : *Synthesis of Aritmetic Circuits: FPGA, ASIC and Embedded Systems,* Wiley Interscience, 2006, ISBN 13-978-0471-068783-2

This research has been supported by the grant No. FRV 886 F1b/2006.

Wavefront Aberrations in the Ultra Wide-Field Camera and Shift Variant Image Data Processing

M. Řeřábek

rerabem@fel.cvut.cz

Czech Technical University in Prague, Faculty of Electrical Engineering,
Department of Radioelectronics,
Technická 2, 166 27 Praha 6

Automatic optical systems used in astronomy find the growing importance in last several years. These systems are often used as a ground based supporting experiments for the special satellites (e.g. INTEGRAL, BeppoSAX). The application of the optimization of the similar experiments BOOTES (Burst Observer and Optical Transient Exploring System - http://www.laeff.esa.es/BOOTES/ing/introd.htm) and BART (http://lascaux.asu.cas.cz/en/) is described.

The main idea of these automatic astronomical optical systems is based on the long-term image data collection. Data have been acquired with specific characteristics. They include especially focal length, spectral bands and sensor parameters. Image data can be divided into three main groups. First one concludes data acquired in the primary focus of the big telescope (deep sky), wide-field lens and as well as "fish-eye" all sky data imaging. There are a lot of different kinds of optical aberrations and distortion in these systems.

Optical aberrations negatively effect to the image quality and imaging system transfer characteristics and cut precision of other measurement. Especially the ultra wide field camera (UWFC) systems contain high order aberrations. High order aberrations cause a nonlinear shift variant dependence of the imaging system point spread function (PSF).

Simulations and modelling of different optical aberrations influence on the astronomical measurement accuracy are described. The Seidel or Zernike polynomials are used for precise calculation of the wavefront aberrations of the optical system. Seidel aberration polynomials are convenient for serving as a primary aberrations interpreter. Even high order wavefront aberrations with higher precision can be described using the Zernike polynomials.

Described aberrations include above all the third order aberration, i.e. spherical aberration, coma, astigmatism, field curvature and distortion or tilt. These five basic aberrations have a most fundamental influence to the transfer characteristics of imaging system.

Relation between high order aberrations influence and measurement precision is discussed. The most important methods for astronomical image data processing contain photometric and astrometric (positional) measurement, point spread function (PSF) profile deformation of objects, false objects detection and their classification, MSE, SNR and subjective evaluation.

The real data from the BOOTES experiment (wide and ultra wide field cameras - UWFC) are used for our simulations and modelling and also for very interesting application "fish-eye" image processing. Objects on this ultra wide field images are really small (a few pixels per object) and therefore all measurements are difficult and contain many aberrations. MATLAB and OSLO software is used for simulations and modelling.

Higher quality and precision of image data can be obtained with deconvolution of the acquired images and system point spread function. The point spread function can be modelled as a space variant function from the estimation of optical system wavefront aberrations. Similar approaches have not been often used for image data processing from UWFC.

The main goal of this project is the precise description of the wavefront aberrations by using Zernike polynomial expression. That will enable us to optimize the image post-processing procedure.

References:

[1] BORN, M., WOLF, E.: *Principles of Optics* Pergamon Press London, 1993.

[2] GOODMAN, J.W..: *Introduction to Fourier Optics* McGraw-Hill Boston, 1996.

[3] HOPKINS H.H..: *Wavetheory of Aberrations* Oxford University Press London, 1950.

[4] WELFORD, W.T.: *Aberrations of the Symmetrical optical System* Academic Press London, 1974.

[5] POON, T.CH., BANERJEE, P.P.: *Contemporary Optical Image Processing with MATLAB* Elsevier, 2001.

[BOOTES] de UGARTE POSTIGO, A., MATEO SANGUINO, T.J., CASTRO CERÓN, J.M., PÁTA, P., BERNAS, M., et. al.: *Recent Developments in the BOOTES Experiment*, In AIP Conference Proceedings 662. Cambridge: Massachusetts Institute of Technology, pp. 553-555, 2003.

This research has been supported by GA ČR grant No. GA 102/05/2054.

OPTICAL CHARACTERISATION OF MOVPE GROWN ENGINEERED InAs/GaAs QUANTUM DOT STRUCTURES

P. Hazdra, J. Voves, J. Oswald*, K. Kuldová*, A. Hospodková*, E. Hulicius*, J. Pangrác*

hazdra@fel.cvut.cz

Department of Microelectronics, Faculty of Electrical Engineering, Czech Technical University in Prague, Technická 2, 166 27 Prague 6, Czech Republic

*Institute of Physics, Academy of Sciences, Cukrovarnická 10, 162 53 Prague 6, Czech Republic

Self-assembled InAs/GaAs quantum dots (QDs) are a subject of intense research due to their unique atomic-like properties and potential device applications. A part of the research activities in this field is driven by the idea to bring the emission wavelength of the QDs up to the values of 1.3 μm and 1.5 μm important for telecommunications. The performance of the QD-based light emitting structures is determined by the dot size, their density and by the difference between the transition energy of the first excited state and that of the ground state. The emission wavelength of the QDs can be changed by changing their size and the composition of the dots and of the barriers [1]. Another way to achieve higher values of the wavelength consists in using vertically stacked multi-layer QD structures. During the growth, the QDs form preferentially just above those in the previous layer. As a result, the multilayer contains column–like structure of stacked QDs. Such structures possess high deformation energy, which can lead to the formation of defects. On the other hand, these vertically correlated QDs have many advantages in comparison with single-layer QD structures. Most importantly, the size of the QDs increases considerably when going from the bottom to the top layer, leading to a red shift of the emission wavelength. Control of the MOVPE growth and further optimisation of advanced QD structures necessitates application of adequate diagnostic techniques capable to characterise them quickly and accurately. Optical methods offer fast, non destructive and contactless option. The most popular technique, photoluminescence (PL), works best at low temperatures and yields mainly ground state interband transitions. On the other hand, photomodulated reflectance (PR) spectroscopy, which is rarely used experimental method for checking of QD structures, provides equivalent energy resolution to that of PL at low temperatures and probes wider range of critical points, highlighting the ground state and also many high order interband optical transitions from which band structure, especially of the wetting layer, can be deduced.

In our work, we focused on PL and PR characterisation of various types of MOVPE grown InAs/GaAs QD structures prepared by LP MOVPE technique in an AIXTRON 200 machine using Stranski–Krastanow growth mode on semi-insulating (100) GaAs. The growth started by the first GaAs buffer layer at 650°C. Then, the temperature was decreased to 500°C for the growth of the rest of the structure, consisting of the second GaAs buffer layer, the InAs QD layer and 15 nm GaAs capping layer. We studied the influence of the growth conditions on the QD properties. Namely, the growth interruption time (GIT) was changed from 30 s to 7.5 s for single layer structures and the number of QD layers was changed from 1 to 7. PL of these QD/WL structures was measured at 7 and 300 K. PL was excited by an Ar and a

semiconductor lasers (488 nm and 808 nm) with excitation density ~ 5 Wcm^{-2}. Standard lock-in technique with Ge detector was used for detection. PR spectra were measured using a setup where a 5 mW HeNe laser was used as the modulating source and a 30 W tungsten halogen lamp filtered by a JY640 grating monochromator provided the monochromatic light. The reflected light was detected by a cooled Ge detector and the resulting signal was processed by PAR5210 lock-in amplifier. Optical transitions were interpreted using simulation of electronic states in InAs and InGaAs by the nextnano^3 simulator.

First we studied the effect of growth interruption time change on QD properties. The growth interruption after the InAs layer growth, which is needed to complete QDs formation, was changed from 7.5 to 30 seconds. PL spectra measured at 7 K showed that emission from QD is shifted towards lower energy with increasing GIT. The PL red shift can be explained by increase of QD size with increasing GIT. These results show that QD formation is very slow process. To study corresponding change of WL thickness, we monitored optical transitions by PR measurements. Spectra were dominated by GaAs band gap bulk like signal at the energy of 1.42 eV. Below this energy the spectrum exhibited a broad resonance in the band of QDs transitions and sharp resonances corresponding to the optical transitions in the WL. The strongest resonance at lowest energy was attributed to e1h1 transition and the weaker one to e1lh1 transition. PR clearly showed that increasing of the GIT caused blue shift and lower splitting of e1h1 and e1l1 transitions. This means attenuation of WL thickness. To get exact magnitudes of WL thickness, we compared the measured e1h1 and e1l1 transitions with those received on ultrathin InAs quantum wells (QW) grown by the same apparatus. Result show that increasing of the GIT decreases the apparent WL thickness (from close to relaxation limit of 1.4 ML for GIT=7.5s to 1.05 ML for GIT=30s) and corresponding strain in the structure.

Preparation conditions of vertically stacked structures were optimised for 3 InAs QD layers. PL showed that emission maxima shifted towards low energy in comparison with the single layer sample. This PL red shift is caused by increase of QD size with increasing of layer number. Increasing the number of QD layers also causes coupling of QW formed by their WLs. PR measurement on these structures provided valuable information even for samples with low luminescence intensity (higher number of QDs layers) - a red shift all resonances originating from the WLs which is due to the coupling of the electronic states in QWs formed by WLs. Close agreement between experiment and simulation for the magnitude of GaAs separation layer thickness of 7.5 nm, which was confirmed XRD measurement, indicate on the validity of the model which was used for simulation of multi-QWs formed by WLs. In this way, we showed [2] that the PR measurement supported by calibrated simulation can provide valuable information about growth and optimisation of vertically stacked QDs layers.

References:

[1] D. BIMBERG, M. GRUNDMANN, N.N. LEDENTSOV: *Quantum Dots Heterostructures,* Wiley, Chichester, 1999.

[2] HAZDRA, P. – VOVES, J. – OSWALD, J. – KULDOVÁ, K. – HULICIUS, E. – PANGRÁC, J.: *Optical characterisation of MOVPE grown vertically correlated InAs/GaAs quantum dots,* European Nano Systems 2006, Paris, 2006, pp. 9-13.

This work was supported by the grant No. 202/06/0718 of the Grant Agency of the Czech Republic, by the Research Programme MSM 6840770014, the GAAV grant No. B101630601, and the project AV0Z 10100521.

Low-Temperature Radiation Enhanced Diffusion of Palladium and Platinum in Silicon

P. Hazdra, J. Vobecký

hazdra@fel.cvut.cz

Department of Microelectronics, Faculty of Electrical Engineering, Czech Technical University in Prague, Technická 2, 16627 Prague 6, Czech Republic

Diffusion of gold, platinum and palladium has been used for years to control carrier lifetime in semiconductor technology. In the last decade, it was outperformed by electron, proton, and especially helium irradiation because they offer better reproducibility, capability of defect localization, several degrees of freedom in profile shaping, and "off-line" application after contact processing [1]. However, radiation defects anneal out at relatively low temperatures (~350°C) and they are not ideal recombination centers - in high concentrations, they increase device leakage and cause parasitic doping. On the contrary, platinum (palladium) atoms at substitutional position in silicon lattice Pt_s (Pd_s) are ideal recombination centers, but shaping of their profile is difficult. Combination of both approaches, i.e. application of radiation damage to guide the in diffusion of noble metals is one possibility how to get an arbitrary profile of ideal recombination centers [2].

In this project [3], we compared the effect of high-energy helium implantation on guided in diffusion of platinum and palladium in the temperature range from 600 to 800°C. Local lifetime killing using this approach was then used for optimization of turn-off properties of high power PiN diodes and compared with the traditional helium implantation. The diffusion of platinum and palladium was studied on 2.5kV/100A high power diodes (area 2 cm^2, thickness 370 μm) fabricated on <111> 130 Ωcm n-type float zone silicon having 10 μm thick aluminum (Al) anode and cathode contacts. The reference diodes (standard He) were implanted through the anode contacts by 11 MeV He^{2+} ions with fluences $1x10^{10}$, $3x10^{10}$, $5x10^{10}$, and $2.5x10^{11}$ cm^{-2} and subsequently annealed at 200°C to remove unstable defects. Diodes for in diffusion of platinum were removed from the standard process flow prior to the processing of contacts to sputter Pt layer at anode surface subsequently sintered to platinum silicide (PtSi) at 450°C for 60 minutes. In some devices, the formation of PtSi layer was substituted by 19 MeV Pt^{6+} implantation at fluence of $5x10^{12}cm^{-2}$. The palladium was sputter deposited at anode, but not sintered. Afterwards, 10 MeV He^{2+} implantation was applied through anode with a fluence of $1x10^{12}$ cm^{-2} on both Pt and Pd devices. This produced the maximal concentration of vacancy related defects at the end of the helium range about 70 μm from the anode surface, i.e. at the same position as in the standard He device. Diodes were then annealed for 20 minutes in vacuum at temperatures 600 - 800°C to promote the diffusion of Pt (Pd) from surface into the position of radiation defects. Diodes were then provided by 10 μm thick Al contacts. Electrically active defects were characterized by Capacitance Deep Level Transient Spectroscopy (C-DLTS), High-Voltage Current Transient Spectroscopy, C-V profiling and Spreading Resistance Profiling. The forward and reverse I-V curves of modified diodes were measured in four point arrangement at constant temperatures. The reverse recovery waveforms were recorded at 30°C in the conditions of resistive switching.

C-DLTS measurement on diodes with PtSi layer shows that helium implantation substantially enhances low-temperature in diffusion of platinum evidenced by the presence of the deep level at E_C-E_T= 0.23 eV corresponding to the acceptor state of the substitutional platinum $Pt_s^{-/0}$. The signal of this level significantly increases with helium implantation and

increasing diffusion temperature. Although helium implantation at doses of $10^{12}cm^{-2}$ produces significant amount of radiation damage, no additional electrically active defects were observed in diodes after annealing at temperatures above 650°C. Pt_s preferentially decorates the region of radiation damage maximum which is located at the projected range R_{pHe} of 10 MeV He^{2+} ions. In this way, the lifetime in the vicinity of the anode junction is killed locally as after helium implantation to equivalent depth. Although, Pt_s can be precisely localized by radiation damage, the peak concentration of Pt_s is limited to about $10^{14}cm^{-3}$ for optimum in diffusion temperature (700°C). This limits the capability of lifetime reduction.

C-DLTS spectra recorded on diodes where palladium was introduced from the Pd layer exhibited a peak at 124 K corresponding to the level at E_C-E_T= 0.224 eV which appeared when annealing overcame 700°C. Signal of this level, which is identical with the acceptor state of the substitutional palladium $Pd_s^{-/0}$, also significantly increases with He^{2+} implantation. Although the electrically active palladium exhibits lower solubility in silicon than platinum, radiation damage enhances its in diffusion already at lower temperatures (<700°C) when Pd peak concentration exceeds that of platinum. This was explained by higher affinity of Pd to make complexes with vacancies.

Measurement on devices showed that I_{RRM} of untreated device is significantly reduced using both the standard and novel techniques. Due to the broader peak of the recombination centers and their electronic properties, the novel technique avoids a current swinging which is typical for standard He^{2+} implanted devices. The same reason makes the devices more resistant against dynamic avalanche, the most frequent failure mechanism, so the Pd devices survive even the turn-off above 2 kV. It was shown that all presented techniques follow the same trade-off between dynamics (I_{RRM}) and static (V_F) losses. That of the standard He^{2+} implantation shows very high span towards high V_F and low I_{RRM} that cannot be achieved by the diffusion techniques due to the limited solubility of either Pt or Pd at low temperatures. The advantage of the new techniques is that it gives two times lower leakage current compared to the standard He implantation for equivalent reduction of I_{RRM}. In Pd devices, this is true in the range of optimal annealing temperatures, where the amount of Pd_s is higher than that of deeper levels. Together with about two time higher thermal budget and ruggedness under fast turn-off, this feature represents the third advantage of the new techniques.

References:

[1] HAZDRA, P. – VOBECKÝ, J. – BRAND, K.: *Optimum Lifetime Structuring in Silicon Power Diodes by Means of Various Irradiation Techniques,* Nuclear Instruments and Methods in Physics Research B 186(1-4), 2002, pp. 414–418.

[2] SCHMIDT D.C., SVENSSON B.G., GODEYS., NTSOENZOK E., BARBOT J.F., BLANCHARD C.: *The Influence of Diffusion Temperature and Ion Dose on Proximity Gettering of Platinum in Silicon Implanted with Alpha Particles at Low Doses,* Appl. Phys. Lett. Vol. 74, 1999, pp. 3329–3331.

[3] J. VOBECKÝ, P. HAZDRA: *Low-Temperature Radiation Controlled Diffusion of Palladium and Platinum in Silicon for Advanced Lifetime Control,* Nuclear Instruments and Methods in Physics Research B 253, 2006, pp. 162-166.

This research has been supported by the project of the Ministry of Education, Youth and Sports of the Czech Republic LC06041 and the Research Programme of the Czech Ministry of Education MSM6840770014.

Verification of Laser Scanning Systems Quality

T. Křemen, B. Koska, J. Pospíšil

tomas.kremen@fsv.cvut.cz

Department of Special Geodesy, Faculty of Civil Engineering, Czech Technical University in Prague, Thákurova 7, 166 29, Praha 6, Czech Republic

The terrestrial laser scanning systems are a relatively new measurement technology used in geodesy. It serves for contactless collection of space data, modelling and visualization. Our work focused on verifying quality of the measured data by the scanning systems that use the space polar method. The laser scanning system Leica HDS 3000 was used as a representative of the stated scanning systems in the accomplished experiments. To the current user, the terrestrial laser scanning systems are a black box, where the measurement procedure and processing data is covered with a trade secret. The information stated in the technical parameters of the single scanning systems are reliable, but in many cases they are insufficient and their practical verification is complicated. That is why the experiments that we carried out were focused on verifying quality and reliability of the measured data and determination of some scanner parameters. Two accomplished experiments were carried out. The first experiment dealt with verifying abilities of the scanning system to measure of various material types under various incidence angles in several distances and the second experiment dealt with testing a new method of direct measurement standard deviations of horizontal directions zenith angles of the laser scanners.

Quality of the measured data of the terrestrial laser scanning systems, the principle of which is the space polar method, is influenced by several significant factors. We concerned about influences of geometric configuration and physical characteristics of the measured surface. When determining position of a point, the scanning system measures length between the scanner and the point, assigns horizontal and vertical direction to this joint and calculates position of the point. Whether length will be measured and with what quality it will be measured, depends on telemetric signal that will fall on the sensor of the scanner [1]. Quality of the falling telemetric signal is influenced especially by physical characteristics of the surface that do not participate in quality of the measured angles. We distinguish several basic types of surfaces according to form of their reflectivity diagram, which states direction dependence of amount of reflected radiation for the given position of source of falling radiation. Diffusion surface reflects radiation proportionally in all directions. Ideal specular surface reflects falling radiation according to the reflection law. Chequered surfaces reflect radiation most in the direction from which radiation falls on the surface. Ability of the HDS 3000 laser scanning system to measure surfaces of different types of materials under different incidence angles in two distances was tested in this experiment. Influence on quality and accuracy of measured points were observed. Forty-six materials were tested. Surfaces were measured under six incidence angles in distances 15 m a 25 m from the scanner. The results of the accomplished experiments confirmed that the most suitable surfaces for scanning are light surfaces with diffusion reflection of falling radiation. For surfaces with specular reflection of falling radiation it came to multiple reflection of telemetric signal for steeper incidence angles. For surfaces with specular reflection and high absorbability of the falling signal, the amount of signal reflected back into scanner sensor was so small that the length was not measured in many cases.

From the viewpoint of determination of angle errors of scanning systems, the number of publications is small, for example [2]. These publications do not deal with determination of standard deviations of horizontal directions and zenith angles, but only with assessment of a transverse error between the measured and modeled objects. This method can be used only for relative accuracy assessment of different laser scanning systems. That is why the new method of direct determination of standard deviations of horizontal directions and zenith angles of laser scanners was proposed. Because of using a digital camera, the method can be used only for scanning systems with a distance meter with a wave length of a visible area of electromagnetic radiation. The method assesses only interior accuracy of the scanning system within a small field of view (1x1 gon) and therefore the results are not influenced by systematic errors of the device as a collimation error, index error and other errors. On the other hand, the method shows real measurement accuracy for modelling of smaller objects. The method is based on a modified photogrammetric method of directive linear transformation (DLT) in 2D [3]. A calibration field is created, which is placed across to the measurement direction. The field is photogrammetrically measured. After switching the lightning off, the plane with a calibration field is measured with a laser scanning system, during which it is photogrammetrically measured. On the basis of the photogrammetric method, it is possible to determine a plane position with a scanner of the measured points with accuracy approximately 0.1 mm to each coordinate. The measurement is transformed from the scanner into the plane system of the calibration field (x axis vertical, y axis horizontal and z axis is perpendicular to the field plane) [4]. Real errors of the scanner are assessed, as differences of the coordinate differences of photogrammetric method and scanning method. This method can be used for all laser scanners the distance meters of which use electromagnetic radiation with wave length in visible spectre. The method judges only internal accuracy of the scanning system within small field of view (1x1 gon). In our concrete realization, the method is suitable for scanners with standard deviation in direction 1.3 mgon and higher because it is ten times lower accuracy than the accuracy of the photogrammetric method. The angle standard deviation stated by the manufacturer for the Leica HDS 3000 scanner (exactly as for the HDS 2500 model) is 60 micro-radians, which represents standard deviation in direction 2.7 mgon. That is why the result of experiments can be considered very surprising, where standard deviation in horizontal direction and also zenith angle comes from approximately between 0.2 to 0.3 mgon, which is roughly ten times more accurate.

References:

[1] KŘEMEN, T.: *Testing of Terrestrial Laser Scanners* The Proceedings of Optical 3-D Measurement Techniques VII, Wien, Austria 2005 pp. 329-334.

[2] BOEHLER, W. – VICENT, M. B. – MARBS, A.: *Investigating Laser Scanner Accuracy* The Proceedings of The XIXth CIPA Symposium at Antalaya, Turkey 2003

[3] HTTP://KWON3D.COM/THEORY/DLT/DLT.HTML *[cit. 1.6.2006]*

[4] KOSKA, B.: *Project alltran* [cit. 2.1.2007] k154.fsv.cvut.cz/~koska/

This research has been supported by MŠMT grant No. MSM 6840770005.

Laboratory Models for Students of the Subject Automation Control

P. Jakoubek, P. Trnka

pavel.jakoubek@fs.cvut.cz
pavel.trnka@fs.cvut.cz

Department of Instrumentation and Control Engineering, Faculty of Mechanical Engineering, Czech Technical University, Technická 4, 166 27 Prague 6, Czech Republic

In last months, some exemplars of the laboratory model Bathyscaphe (www.ar–batyskaf.wz.cz), were sent to four partner technical laboratories. In return for the laboratory model Bathyscaphe, which was designed and constructed at the Faculty of mechanical Engineering, Czech Technical University in Prague [2], we obtained the laboratory model Hydro-Pneumatic Model from the University of Pardubice, the Time Delay Model from the Tomas Bata University Zlín, the Temperature Air Model from the VSB – Technical University of Ostrava and the Model with an elastic Clutch from the Technical University of Liberec. All these Models are particularly described in [3].

To take use of all these models it was necessary to create some exercises for Student of the subject Automation Control [1], one of the subjects that are thought at Faculty of Mechanical Engineering as a part of the basic study. The purpose of these exercises was to take the student with the basics of automation control up and to help them to understand the subject matter of lectures. The emphasis lies on understanding and constructing of time-response characteristics, static characteristic and on the familiarization with some methods of setting the controllers to control the system properly.

The submissions of these exercises are placed on web (http://www.fs.cvut.cz/cz/U210/ar/) and should give an afford to students to see the requirements and to simulate the exercise before the lesson starts. Students can also download a short movie file, to see the models running.

Hydro-Pneumatic Model

The Hydro-Pneumatic Model combines both hydraulic and pneumatic components in order to stress coupling between water tanks. The model consists of four water tanks, grouped in two couples. In every section, water is pumped through a valve into the upper tank, flows into the lower tank through an orifice and from here through a second orifice back into the reservoir. Air spaces above the water are connected together by pneumatic volumes and valves with the possibility to release air to the atmosphere. These pneumatic connections create a cross coupling between each section. System properties and structure may be manually changed by the size of the orifices and by the valves in the pneumatic loops. The water levels in all tanks are measured by difference in pressure sensors. Pressures in pneumatic volumes, atmospheric pressure and inlet water pressure are measured too.

Students should find appropriate parameters of the PID controller, using two modified Ziegler-Nichols methods and control the system by PID controller, whose parameters were to be found and set by the input function in Matlab, where the PID algorithm was realized.

Time Delay Model

The time delay is realized by measuring the temperature of the media at several places in the interconnecting pipeline. The model contains a safe hot water source with electric heating and thermostat-based regulation in the range between 30 and 85±C. Hot water is transported by a variable-speed pump into the interconnecting pipeline ending in a heat exchanger. The pipeline is connected through an intercepting valve, where the flow is divided between the pipeline and a reversing coupler. The pipeline itself is composed of several meanders where it is possible to place thermometers and thus to obtain various values of the time delay. The time delay can also be affected by changing the speed of the pump and position of the valve.

Communicating with Matlab by the GUI (Graphical User Interface) student should calculate, using the Method of Desired Model and set PS or PSD controller parameters, in dependence of mathematic model, given by assistant.

Temperature Air Model

The Temperature Air Model is a physical model of air-conditioning. There are the source of heat air (the small bulb) with quick dynamic response and two ventilators as the sources of air flow. Together in the model, there are six transducers measuring the temperature of hot air flow at three different positions from the bulb, two flow meters (propeller turbine and thermo anemometer) for volume flow measurement and one photo resistor sensor of bulb luminance.

Student should measure several time-response characteristics, find out and register some specifics and upon these construct a static characteristic.

Model with an elastic Clutch

Model with an elastic Clutch enables rotation speed control of an industrial DC-motor with the load and elastic clutch. It consists of a DC-motor with load and measuring devices. A dynamo that can be brought into an effect creates the load disturbance. The latter is signalized by lights. The load is connected with the DC-motor by a clutch which can introduce elastic or coupling muff. The measure device is the speedometer which is calibrated by an incremental speed sensor.

Students should measure several time-response characteristics and then construct static dependences of the output revolutions on the input voltage and disturbance.

References:

[1] P. ZÍTEK, M. HOFREITER, J. HLAVA: *Automatické řízení,* Vydavatelství ČVUT, 1999

[2] J. JIRKOVSKÝ, J. PODSTATA, M. HOFREITER: *Advanced Engineering Design AED 2006,* CTU Prague 2006

[3] P. KLÁN, M. HOFREITER, J. MACHÁČEK, O. MODRLÁK, L. SMUTNÝ, V. VAŠEK: *Process Models for a new Control Education Laboratory,* IFAC, 2005

This research has been supported by MŠMT RP grant No. 642.

Section 5

MATERIALS ENGINEERING

Experimental Method for Monitoring Salt Transport Induced by External Electric Field

L. Fiala

fialal@fsv.cvut.cz

Department of Building Materials, Faculty of Civil Engineering, Czech Technical University, Thákurova 7, 166 29 Prague 6

The simplest way how to assess the salt induced damage of building material is to analyze the specimens of the studied material in laboratory. This provides information on water content and on the type and amount of particular ions in material which is useful for appreciation of the current state. However, it is very difficult to make reliable predictions of further damage on the basis of these data. It requires years of on site measurements of salt transport and storage.

Prediction of water and salt movement and salt crystallization in building materials can be effectively done by mathematical and computational modeling. In this way, the time development of water and salt concentration fields can be obtained which is fundamental information for the assessment of possible future damage. The accuracy of simulated water and salt concentration fields critically depends on the availability of all input parameters. The most important input parameters for computational modeling are water and salt transport and storage parameters of the studied materials which appear in water and salt mass balance equations. For the problem of coupled water and salt transport, these parameters include moisture diffusivity and sorption isotherm as water transport and storage parameter, ion binding isotherm as salt storage parameter and salt diffusion coefficient as salt transport parameter [1, 2]. These parameters can be effectively determined by common laboratory methods. Due to the fact that diffusion experiments for measuring salt concentration profiles are very time-consuming, various acceleration methods are applied. One of these methods is the steady-state migration experiment that is presented in this paper. It is based on acceleration of salt ions caused by external electric field. For the measurement of salt flux, two basic principles can be applied. The first possibility is to measure salt concentration in the downstream cell at the anode. This measuring procedure is based on many assumptions, e.g. on the establishment of a steady state salt flux. It means constant concentration gradient during the test what requires frequent renewal of the upstream and downstream solutions. Salt ions also interact with the material and this leads to a decrease of salt ions penetration rate within the material sample. Even though this phenomenon does not affect the value of the effective diffusion coefficient it increases the time lag.

In the experiment performed in this work, we have used another procedure to the assessment of the salt flux. It is based on measuring the drop in salt concentration in the upstream cell.

The flux of ions through the saturated sample of porous building material induced by electric field can be expressed as

$$-J(x) = D_e \frac{\partial c}{\partial x} + \frac{zF}{RT} D_e c E \text{ [3].} \quad (1)$$

During a migration test, assuming that the upstream side of the material sample is very quickly saturated with salt ions, we can neglect the diffusion term since there is no concentration gradient at x = 0. Then the flux of chlorides through the upstream side is constant and can be described by following equation

$$J_{up} = \frac{F}{RT} D_{e,up} c_{up} E \,, \tag{2}$$

where E is intensity of electric field [V/m], J_{up} chloride ion flux through the upstream side of the sample [mol/m^2/s] and c_{up} is average concentration in the upstream cell [mol/m^3]. The chloride ion flux J_{up} was determined after the achievement of the steady state salt transport according to the equation

$$J_{up} = \frac{c_{up1} V - c_{up2} V}{St} \,, \tag{3}$$

where c_{up1} is concentration at time t_1 [mol/m^3], c_{up2} concentration at time t_2 [mol/m^3], V volume of salt solution in the upstream cell [m^3], S sample surface exposed to the salt solution [m^2], $t = t_1 - t_2$ time interval [s] corresponding to the salt flux J_{up}. From this equation, effective diffusion coefficient can be expressed, and for measured input data calculated.

In the experimental work we have used measuring apparatus consisting of plastic container that was divided into two parts. In the middle of the container, there is the plastic barrier with the hole where the sample isolated by silicone gel is fixed. Thickness of the sample was 10 mm, width and height 50x50 mm. Into the compartments, 2.5 litres of distilled water and 2.5 litres of 0.65M NaCl solution was poured. After that, the electrodes were placed into the both compartments. For the sake of homogenous field need, electrodes were plane shaped having dimensions 50x50 mm and made of bronze. Cathode was placed into the solution of NaCl and anode into the distilled water. The distance of electrodes from the central barrier was 20 mm. Electrodes were connected to the source of direct electric voltage of 4V. Experiment was carried out at constant laboratory temperature 22±1°C.

As the main aim of the presented work was to verify the designed experimental setup, cast flue gas desulfurization (FGD) gypsum was chosen as the studied material. The main reason of this option was expected duration of migration experiment that is shorter than for other materials like concrete or sandstone. On the basis of performed experiment and calculations, the value of apparent chloride diffusion coefficient was determined. This parameter will be used as input data for modeling salt transport by computational modeling methods. In future work we will focus on improving the measuring apparatus and on investigation of more common building materials like concretes and bricks.

References:

[1] ČERNÝ, R. – PAVLÍK, Z. – ROVNANÍKOVÁ, P.: *Experimental Analysis of Coupled Water and Chloride Transport in Cement Mortar.* Cement and Concrete Composites, 2004, pp. 217–226.

[2] JIŘIČKOVÁ, M. – PAVLÍK, Z. – ČERNÝ, R.: *Free and Bound Chloride Concentration in Concrete: Analysis of Applied Techniques,* Proceedings of the International Conference Life Cycle Assessment, Behaviour and Properties of Concrete and Concrete Structures, Brno, Technical University, 2004, pp. 160-165.

[3] TRUC, O. – OLLIVIER, J.P. – CARCASSES, M.: *A new way for determining the chloride diffusion coefficient in concrete from steady state migration test.* Cement and Concrete Research, 2000, pp. 217-226.

This research has been supported by CTU grant No. CTU0601511.

Dependence of Ductility of FRC on Strenght of Fibres

Golmadingar Djimalde, Jan Vodička

djimalde@seznam.cz, jan.vodicka@fsv.cvut.cz,

Department of Concrete and Masonry Structures, Faculty of Civil Engineering, Czech Technical University, Thákurova 7, 166 29 Prgue 6, Czech Republic

This contribution presents results of destructive tests, which were performed with financial support of the Faculty of Civil Engineering, Czech Technical University in Prague. The experiments, which were conducted within the scope of the project, focused on ductility of fiber concrete. This property of fiber concrete, which characterizes toughness of material, is the most important property of fiber concrete, which allows not only greater strains but also helps to transfer tensile stresses after a crack occurs.

Ductility of fiber concrete depends mainly on the type and volumetric amount of the used fibers. Therefore, ductility is influenced by the strength, geometric parameters and the shape of the fiber ends, where all those influences predetermine the forces, which can be transferred within the microstructure of the fiber concrete. If the parameters of the fibers are not suitable, the fiber concrete shows almost no capacity of extra ductility and ultimately it behaves as ordinary plain concrete, which is a rather brittle material.

Proving ductility of fiber concrete is quite demanding compared with proving of common measured strength characteristics. The most common test arrangement is the bending of test beams when loading is controlled by deformation. These days only a limited number of laboratories are equipped with necessary technical systems capable of conducting such experiments. For less precise verification of ductility of fiber concrete or for verification of suitability of used fibers, one can conduct the splitting tensile test. At splitting of the test specimen into two sections, it can be assumed that fiber concrete has zero ductility and behaves as a brittle material. Low ductility of fiber concrete is evidenced by a sound effect when the test specimen splits. On the contrary, high ductility of fiber concrete is proved by no sound whatsoever, but a gradual broadening of the crack, which is typical for the splitting tensile test.

The program of the project was set so that it was possible to assess and verify the ductility of fiber concrete when using the steel fibers FIBREX and DRAMIX, which differ significantly in the decisive parameters, being the strength, length and end arrangement.

With respect to the financial sources and provided time, fiber concrete with only the mass concentration corresponding to 1 % of volumetric reinforcement, which represents a batch of 78.5 kg/m^3, was tested. Due to the length of the DRAMIX fiber, which is 60 mm, the test specimens with the edge dimension of at least 150 mm were selected, which allowed elimination of the wall effect during production and thus ensured homogeneity of fiber concrete. It is recommened that test specimens of such dimensions are used always for testing fiber concrete so that the assumption of homogeneity is fulfilled.

The results of the conducted tests are summarized below:

- compressive strength measured on cubes (150 x 150 x 150 mm)
  Dramix – 69.3 MPa , FIBREX – 86.6 MPa,

- splitting tensile strength measured on cubes (150 x 150 x 150 mm)

Dramix – 7.69 MPa , FIBREX – 6.28 MPa (slight sound effect detected),

- force recorded at crack initiation on beams (150 x 150 x 700 mm) subjected to bending
  Dramix – 36 kN , FIBREX – 34 kN,

- force recorded at 1 mm deflection of beam
  Dramix – 32 kN , FIBREX – 10 kN.

Comparison of recorded strengths and ductility of the two types of fiber concrete:

1. The FIBREX fibers whose length is 25 mm are significantly shorter than the DRAMIX fibers and their influence on cement stone is greater than that of the long fibers when subjected to compression.
2. The FIBREX fibers whose length is 25 mm are significantly shorter than the DRAMIX fibers and their influence on fiber concrete microstructure is less prominent when subjected to splitting tension.
3. When subjected to bending, both types of fibers showed almost identical bending tensile strength at crack initiation, which was determined from the recorded forces.
4. After crack initiation at the deflection of the beam of 1 mm, the type of fiber influences the ultimate force, which can be carried by the beam, significantly.

The conclusion drawn from the above results and the comparison of the recorded values is that selection of fibers affects ductility of fiber concrete. However, the degree of influence does not depend on the selected fibers only, but also on the composition of cement matrix, or simply on the concrete class, as evidenced in literature [1, 2].

The proved influence of short fibers on compressive strength can be utilized in application of fiber concrete to some structures.

References:

[1] DJIMALDE G. - KOLÁŘ K. - VODIČKA J.: *Strenght of FRC in Dependence on Length of Fibres* SEKURKON Ostrava, 2006, pp. 109-113.

[2] VODIČKA J., KOLÁŘ K., DJIMALDE G.: *Reference Strenght of FRC in Dependence on Low Content of Different Steel Fibres* SEKURKON Ostrava, 2006, pp. 102-108.

This research has been supported by IGS ČVUT, grant number CTU0601611.

The Study of The Surface Properties of C/C composites

Z.Tolde,V.Starý, M.Douděrová

tolde@seznam.cz

Czech Technical University, Karlovo nám. 13, Praha 2, 121 35, Czech Republic

INTRODUCTION:

We measured the coefficient of friction and wear resistance on 2D carbon-carbon composites and on the surface layer of pyrolytic carbon (graphite). To explain these measurements we also measured the surface roughness and microhardness of both the composite and the layer. Due to its exclusive properties, this material system is often used in biomedical applications (bone and joint implants), machinery (friction-bearing parts) and in the aircraft industry (parts of the braking system). We studied the samples both with native ("as prepared") surfaces and also with surfaces prepared by grinding and polishing, to obtain samples with various roughnesses. The measurements demonstrate the excellent tribological properties of the surfaces, especially the very low friction coefficient and the very good wear resistance of the surface of the pyrolytic carbon layer on the polished 2D C-C composite. Pyrolytic carbon (graphite) forms as result of pyrolysis, a chemical process where the bonds among the atoms of hydrocarbon molecules are broken due to high temperature. The process temperature is about 1200 - 1300^{o}C for amorphous low temperature pyrolytic carbon (LTI, low temperature isotropic), and about 2000^{o}C for partially crystalline pyrolytic carbon (pyrolytic graphite).

CONTACT ANGLES AND WETTING INHOMOGENEOUS SURFACES:

The roughness and heterogeneity are common features of all real surfaces even if they were prepared very carefully. Every scratch on the surface can play the role of a capillary in which a liquid rises up. This happens if the contact angle θ is acute. At the other side the liquid decreases in the capillary for obtuse contact angles θ. In other words the rough surface has usually a good wettability in comparison with smooth surface, if we presume use of liquid with good wetting ability. We will get opposite results by use of liquids with bad wetting ability. Both of these factors are proved in the magnitude of the contact angle – wetting angle θ.

DEFINITION OF THE SAMPLES SETS:

In this way, four sets of samples were prepared, with various states of the surface. SET I C-C (composite) samples without surface treatment, SET II surface C-C (composite) samples were ground by metallographic paper samples, SET III C-C (composite) samples without surface treatment were covered by a layer of pyrolytic graphite and SET IV surface C-C (composite) samples ground by metallographic paper were covered by a layer of pyrolytic graphite.

CONCLUSIONS:

- the lowest friction coefficient was observed in the ground samples without a PyG layer

- the highest friction coefficient was observed in the unground samples with a PyG layer
- the best wear resistance was observed in the samples covered by PyG layers, almost independently on the substrate grinding (under the layer)
- the lowest contact angels was observed in the samples with a PyG layer

References:

[1] 1. CHERRY B.W. *Polymer surfaces* Published by the Press Syndicate of the University of Cambridge 1981,

[2] 2. ADAMSON A.W: *Physical chemistry of sourfaces* A Wiley-Interscience publication, 1979,

[3] 4. VITALE, E, GIUSTI, P.: *of the resistance of pyrolytic carbon to abrasive wear* International Journal of Artificial Organs, 1975, 777-785.

[4] 6. OLIVA V., OLEXA J.: *Introduction to the theory friction, abrasion and contact wear* , ČVUT, 1978,

No. CTU0605912

Development of Fiber Optic Sensor of Alkali Ions in Water

R. Klepáček, L. Kalvoda

rudolf.klepacek@seznam.cz

Department of Solid State Engineering, Faculty of Nuclear Science and Physical Engineering, Czech Technical University, Trojanova 13, 120 00 Prague 2

Analysis of alkali ion contents in aqueous solutions attracts a considerable attention nowadays within the community of sensor developers. Information about an instant concentration of Na^+, K^+, Mg^{2+} and Ca^{2+} ions has relevance for assays of organic solutions, such as human, animal, and plant blood, and is fundamental in tests of drinking water, underground water, water used in food-processing industry, and all sorts of waste water. Two experimental methods are widely applied for the alkali ion analysis at present: the absorption and emission flame spectrophotometry, and the potentiometry utilizing ion selective electrodes. Both the methods allow for the selective determination of alkali ions concentrations within a ppm range, but at the expense of relatively high instrumentation and labor costs. Thus, there is still a practical interest focused on the development of a portable cheep sensor suitable for continuous, in-situ analysis of alkali ion concentration.

Our research concentrates on development and design of an intrinsic fiber optic sensor of alkali ions in water environs. Physical and chemical principles of the sensor operation have been already given elsewhere [1, 2]. The research work presented in this contribution deals with the following two partial problems: (i) The immobilization of a suitable reagent within a cladding polymer layer of the sensing fiber [3], and (ii) the interaction mechanism of a typical alkali ion ionophore, calix[4]arene, with the target ions [4].

The design of a sensing optical fibre, i.e. in our case the sensitization of the fiber cladding, must preserve good waveguide properties of the fiber as well as assure the desired sensor properties, such as a fast response time, good reversibility, long time stability, and appropriate sensitivity. Two approaches are generally applicable for preparation of the sensitive cladding layer: coating a bare fiber core with a special formulation containing the necessary reagents, or diffusing the reagents mixture from a suitable solution into an already prepared cladding layer. The measurements performed in [3] showed that for a standard siloxane cladding (Dow Corning Optigard formulation), a mixture of ethanol and chloroform (1:1 wt.) provides a good polymer swelling and reagent diffusivity. We have proved that a long sensing fiber appropriate for distributed sensing can be prepared by this procedure.

The second working task was concentrated on the investigation of the reaction mechanism ionophore – target ion taking place at an interface between aqueous and lipophilic phases. 4-tert-Butylcalix[4]arene-tetra(ethyl-acetate) (TEAC) was at first used as the ionophore. The lipophilic sensing cladding layer was in this case simulated by a TEAC solution in hexane (1mM). The course of the reaction was checked by means of specific conductivity and pH measurements providing information about the concentration changes of the target alkali ions and protons within the tested aqueous solutions. The data collection was performed with a new experimental setup built up in frame of the current project. The core part is a home-made measuring chamber having a quartz interior cuvette and a thermostatic shell attached to an external Haake F423 thermostat. The temperature was kept at 20^o C during the experiments. The cuvette was filled with argon gas to reduce the influence of atmospheric CO_2 dissolution in the tested solutions. A Gryf Magic XBC control unit equipped

with a conductometric XBK-1 probe (3 Pt electrodes) and a XBK-3 pH measuring head was used to collect the data and to transfer them to the attached PC. The experimental procedure was as follows: at first, the aqueous solution was added into the measuring chamber and the conductivity or pH value was measured until a steady state was reached. Then, a lipophilic hexane solution containing the tested ionophore was added and the temporal changes of the measured parameter were recorded. The obtained steady state values were used for calculations of the corresponding reaction stability constants and extraction coefficients.

We have already reported that under conditions of a restricted proton exchange between an aqueous alkali solution and a lipophilic TEAC solution, a hydrolytic attack on the TAEC reagent dominates both for alkali chlorides and alkali hydroxides [1]. For the basic testing solutions, the reaction stability constants could be calculated from the obtained specific conductivity data corrected on the supposed change in the OH^- ions concentration: $K_{Na+} = 3.7 \times 10^{-6}$, $K_{K+} = 3.3 \times 10^{-7}$, $K_{Ca2+} = 8 \times 10^{-5}$ [4]. Thus, the highest selectivity (~ 1/K) was obtained for the K^+ ions what was in contradiction to the known selectivity of the TEAC reagent towards Na^+ ions.

Further experiments were therefore performed with aim to understand the process of ions migration over the interface between the aqueous sample solution and the liquid membrane, the consecutive complex creation, and the conditions leading to the hydrolytic attack on TEAC structure [4]. At first, an efficient lypophilic proton donor, myristic acid (MA), was added to the TEAC solution in hexane (1 : 1 molar ratio) and conductivity of the aqueous phase containing 1mM solution of one of the tested alkali chlorides and hydroxides was recorded for 24 h. Similar behavior as without MA addition was observed, i.e. the hydrolysis of TEAC molecules could be again identified, the reaction being much stronger for the alkaline samples. Thus, the hydrolysis seemed to be preferentially induced by the contact with the sample phase then by the lack of available proton donor inside the lipophilic reagent solution. For the hydrolysis lead to dissidence of ethyl groups from TEAC, we tested the extraction behavior of a 4-tert-Butylcalix[4]arene (TBC) – a derivative which is un-substituted at the lover calix[4]arene rim. As expected, no extraction into TBC toluene solution (1mM) was observed. The hydrolysis was absent in case of TBC, in agreement with the proposed mechanism of the TEAC hydrolysis.

The further research will be focused on application of the built-up conductometric setup and the related methodology to investigation of other ionophores, chromo-ionophores, and their mixtures with chromogenes, suitable for application in intrinsic, absorption-based fiber optic sensors.

References:

[1] KLEPÁČEK, R. – KALVODA, L.: *Novel sensors of alkali metal ions based on optical fibers,* In: Proceedings of Workshop 2005, CTU Report 9, 2005, pp.512-513.

[2] KLEPÁČEK, R. – KALVODA, L.: *Development of Fiber Optic Sensor of Alkali Ions in Water*, In: Proceedings of Workshop 2006, CTU Report 10, 2006, pp. 406-407.

[3] KALVODA, L – AUBRECHT, J. – KLEPÁČEK, R.: *Fiber Optic Detection of Ammonia Gas*, Acta Polytechnica 46(2), 2006, pp. 41-46.

[4] KALVODA, L – KLEPÁČEK, R.: *Extraction of Alkali Ions into Lipophilic Solutions Studied by Conductometric Method*, to be published.

This research has been supported by grant CTU0611014

The Comparision of Testing Methods Dealing with Open Porosity Determination of Hydrophobic Mortars

M. Ibehejová, J. Kolísko, L. Balík

ibehejo@klok.cvut.cz

Department of Experimental and Measurement Methods, Klokner Institute,
Czech Technical University,
Šolínova 7, 166 08 Prague 6, Czech Republic

In practice building materials are often exposed to various moisture impacts which can lead to the total deterioration of structures. In the mechanisms of deterioration the uptake water or aqueous solutions by capillary suction play an important role. The durability of the construction is significantly influenced by the material open porosity.

The water uptake and capillary suction can be reduced drastically by impregnation carried out with the hydrophobic agent, which changes the active pore structure surface into the inactive – hydrophobic and reduces diffusive mass transport in materials.

Hydrophobic coating are based either on chemical way i.e. that material reacts with the hydrophobic agent (e.g. silicone, silane) or on physical way i.e. inactive hydrophobic agent does not react with the substance (e.g. metallic stearate).

The main and final objective of the project was the comparison of testing methods dealing with open porosity by internal hydrophobic model mixes and non-hydrophobic model. Also following corresponding parameters by hydrophobic and non-hydrophobic materials were provided: capillarity moisture absorption capacity, water vapour permeability, bulk density, pressure strength, pore-size distribution.

In the project we used model mortar, which contained binder as Cement I 42,5 R, sand 1 (with grading 0-0,5), sand 2 (with grading 1-1,6) and foamer in relation 56:30:14:0,16. This model mortar was modified by use of silane and zinc stearate as hydrophobic admixtures in the amount of 0.5% by mass. The amount of water was between 11% and 16% multiple of amount of dry mix.

The open porosity was experimentally determined by fresh mixes (ČSN EN 1015-7) and by hardened mortars (isopropanol absorption, mercury porosimetry, water absorption).

Table 1 presents changes of mortars properties in the relation of hydrophobization of mixes. The open porosity of model mortar and mortar with zinc stearate achieved against mortar with silane significantly higher values by all testing methods due to reaction of foamer and silane admixture. This fact reflects also in the bulk density, bending strength and pressure strength values.

The open porosity tested by isopropanol absorption achieved the highest values of all testing methods (23%-38%) whereas water absorption test values decreased significantly (17%-24%). The results confirmed the effect of water repellent treatment of two used mortars.

Open porosity values presented by mercury porosimetry decreased in the range of 14% compared to isopropanol absorption test by model mortar and mortar with zinc stearate whereas by mortar with silane provided both methods identical value. The cause of the results is the pore size distribution: model mortar and mortar with zinc stearate contain considerable pore volume with pore radius bigger than 170μm, which was not possible to measure with mercury porosimetry reliably by used materials.

Mortar	Bulk density	Open porosity determination to following methods				Bending strenght	Pressure strenght
		Porosity in fresh mortar	Isopropanol absorption	Mercury porosimetry	Water absorption test	(28 days)	(28 days)
	[kg/m^3]	[%]	[%]	[%]	[%]	[MPa]	[MPa]
Model mortar	1399	40	38	33	24	2,1	5,8
Mortar with silane	1829	12	23	23	17	3,8	10,2
Mortar with zinc stearate	1499	35	36	32	20	2,3	6,4

Table 1: Basic properties of model mortar and hydrophobic mortars with 0.5% silane and zinc stearate.

It can be concluded that open porosity values of hydrophobic and non-hydrophobic mortars depends significant on used testing method. By all three tested mortars were achieved highest open porosity values by isopropanol absorption testing method, whereas water absorption testing method provided the lowest values. The open porosity results achieved by mercury porosimetry were the same or 14% lower than values of isopropanol absorption testing method.

References:

[1] MODRÝ, S. – BAŽANTOVÁ, Z. – SCHNEIDER, P. – SPITZER, Z.: *Porometrické metody a jejich použití ve výzkumu, vývoji a kontrole jakosti surovin a výrobků* ČSVTS, Praha, 1985 .

[2] FRANKE, L. – REIMANN-ÖNEL, R.: *Observation of Mass Transport and Related Deterioration Mechanisms in Porous Building Materials* International Journal for Restoration of Buildings and Monuments, Vol 6, No 4, 2000, pp. 451–462.

[3] GERDES, A.: *Hydrophobierung von Stahlbetonbauwerken - Theoretische Grundlagen und praktische Anwendung* International Journal for Restoration of Buildings and Monuments, No 2, 2005, pp. 185–207.

[4] KRIEGEL, R. – BUCHWALD, A. – KAPS, CH.: *Material Structure and Diffusive Mass Transport as Pointed out by Means of Selected Examples* International Journal for Restoration of Buildings and Monuments,Vol. 6, No 4, 2000, pp. 429–449.

This research has been supported by CTU0612731.

Modeling of Microstucture of Cement Paste Using Image Analysis

K. Forstová, J. Němeček

katerina.forstova@fsv.cvut.cz

Department of Mechanics, Faculty of Civil Engineering, Czech Technical University in Prague,Thákurova 7, 166 29 Prague 6, Czech Republic

Presented work deals with the modeling of cement paste microstructure for the purpose of simulation of its micromechanical behavior. Microstructural model is required for validation of experimental data from nanoindentation measurements. During nanoindentation, mechanical properties are obtained from indent neighborhood in the scale of nanometers to micrometers. From the microstructural point of view, the hydration of cement clinkers results in the formation of cement paste. Several known models, like Power's model, describe an origin of new phases, however such model estimates phases only quantitatively. In order to reconstruct the cement microstructure spatially, discrete cement hydration model (NIST model Cemhyd3D – resolution 1 μm) can be used. Statistical descriptor in the form of autocorrelation function is employed for microstructure reconstruction in CEMHYD3D. Presented microstructure reconstruction is based on 2D images from electron microscope. The surface of sample is segmented in different phases: clinkers, capillary pores and hydrated products. Computed functions are used also for 3D reconstruction of periodic microstructure of the cement paste.

Images were captured by back-scattered detector of environmental scanning electron microscope (ESEM). Contrast in these images is produced by variations in atomic number within the specimen, the resulting image displays in grey scale the shape and possible phase of microstructure surface. Typical image contains black color which represents empty pores (they have zero reflectivity), white color of mainly unhydrated clinker minerals (they contain calcium and silica, have high reflectivity). Gray levels can be assigned to hydration products (C-S-H gel, calcium hydroxide, ettringite etc.) but there has not been found a way how to distinguish these phases according to the grey level. Successful outcome that lies within accepted limits is strongly dependent on threshold level, i.e. separation of pores from the rest of phases. There are a number of approaches that have been taken to reconstruct random media. One of the approaches is available when the real microstructure is replaced by its binary image. To provide a general statistical descriptor of such a system it is useful to characterize each member of ensemble by a random stochastic function – characteristic function $\chi_r(x, \alpha)$, which is equal to one when point x lies in the phase r in the sample α and equal to zero otherwise [1].

Then, the one-point probability function gives the probability that a point x will be found in a given phase r and the two-point probability function S_{rs} stands for the probability that the points x and y will be located in phases r and s, respectively:

$S_r(x) = P(\chi_r(x) = 1), \qquad S_{rs}(x, y) = P(\chi_r(x)\,\chi_s(y) = 1).$

For the case of statistically homogeneous and ergodic media, information contained in the one-point probability function reduces to the volume fraction of a given phase. In addition, the two-point probability function then depends on (x−y) only and can be obtained from the relation $S_{rs}(x,y) = \frac{1}{WH} IDFT\left\{DFT\{\chi_r(x,y)\}\overline{DFT\{\chi_s(x,y)\}}\right\}$ where W is the width of image, H is the height of image, $\chi_r(x, y)$ is the characteristic function of phase r, $\chi_s(x, y)$ is the

characteristic function of phase *s* (other than phase *r*), DFT and IDFT stand for the direct and inverse Fourier transform and overline denotes the complex conjugate [1].

The process of the reconstruction of microstructure according to real images starts with the replacement of a real microstructure with a binary image. In this way a two-phase reference system is created. For this image the two point probability function is calculated. An effective reconstruction procedure enables one to generate arbitrarily accurate structures. The second step of the reconstruction process is to use a random checkerboard with volume fraction of the reference system as the initial structure. The structure is then altered by a phase interchange of two randomly selected pixels within the system. The resultant two-point probability function of this intermediate system is calculated. This procedure is carried out successively until the evolving system's two-point probability function matches the reference two-point probability function within a tolerance limit [2].

To summarize, the principle of 2D reconstruction of random media using image analysis and two-point probability function was presented. However, it is clear that even if the correlation function of the reference and reconstructed images are in good agreement, it is not ensured that both images will match each other. Next step will be extension to other correlation functions and boundary conditions to find such resulting system, that will match better with the reference image. Another useful application is the reconstruction of a three-dimensional structure using information obtained from two-dimensional image. The result of this work is 2D configuration of cement phases applicable for the simulation of mechanical properties on microscale and macroscale with FE analysis

References:

[1] SEJNOHA M., ZEMAN J. : *Micromechanical Analysis of Random Composites* CTU Reports, vol 16, 2002

[2] TORQUATO S., YEONG C. L. Y. : *Reconstructing random media* Physical Review E vol. 57 1998 pp. 495 - 506

This research has been supported by CTU 11-86134 and by GACR 103/06/1856.

Properties of Alkali Activated Aluminosilicate Materials with Different Aggregates

L. Zuda, R. Černý

cernyr@fsv.cvut.cz

Czech Technical University, Faculty of Civil Engineering, Department of Mechanics, Thákurova 7, 166 29 Praha 6, Czech Republic

Alkali-activated aluminosilicates form high-strength materials [1]. They also exhibit remarkable high-temperature resistance which makes them perspective materials for high-temperature applications, for instance as fire protecting layers in buildings and tunnels. A successful application of these materials in building structures is, however, not straightforward and requires a sufficient knowledge of their mechanical, hydric and thermal properties. This, unfortunately, is not always the case in the current practice because properties of alkali-activated aluminosilicates were studied only relatively seldom to date. When some parameters were measured, then it was mostly just mechanical properties. Hydric properties such as moisture diffusivity, water vapor permeability and water vapor adsorption capacity depending on the moisture content were not yet measured even in normal conditions (on the basis of water permeability and air permeability it is possible to get some estimates but serious data not at all), for the thermal parameters the situation is very similar. The effect of high temperatures on hydric and thermal properties was not studied yet as well.

In this paper, basic hydric and thermal properties of two alkali activated aluminosilicates with sand aggregates and with electrical porcelain filler, namely moisture diffusivity, water vapor diffusion coefficient, thermal conductivity and specific heat capacity, are determined on the samples subjected to thermal loads of 200^0C, 400^0C, 600^0C, 800^0C, 1000^0C and 1200^0C and compared to the reference material data.

Fine-ground slag of Czech origin (Kotouč Štramberk, Ltd.) was used for sample preparation. As alkali activator, water glass solution was used. It was prepared using Portil-A dried sodium silicate preparative (Cognis Iberia, s.l. Spain). The sand aggregates were normalized according to EN 196-1. Electrical porcelain was provided by P-D Refractories CZ, Velké Opatovice. Its porosity was 0.3%, water absorption at saturation 0.1%, bulk density 2350 kg/m^3. The composition of the mixture for sample preparation is presented in Table 1.

Table 1 Composition of mixture for sample preparation

Sand or electrical porcelain [g]	Slag [g]	Alkali-activation silicate admixture [g]	Water [ml]
1350	450	90	190

The technology of sample preparation was as follows. First, the silicate preparative was mixed with water. The solution was then mixed in the homogenized slag-filler mixture. The final mixture was put into molds and vibrated. The specimens were demolded after 24 hours and then stored for additional 27 days in a water bath at laboratory temperature.

After the 28-day curing period, the specimens were dried at 110^0C and after drying subjected to thermal load. Heating of the samples to the predetermined temperature was always done with the rate of 10 K/min, then the specimens remained at that temperature for

the time period of two hours and finally they were slowly cooled. The chosen pre-heating temperatures were 200^0C, 400^0C, 600^0C, 800^0C, 1000^0C and 1200^0C.

In the experimental work, the following samples were used for every pre-treatment: basic properties - 3 specimens 50 x 50 x 23 mm, water absorption - 3 specimens 50 x 50 x 23 mm, water vapor diffusion resistance factor - 3 cylindrical specimens with the diameter of 120 mm and height of 20 mm, thermal conductivity and specific heat capacity - 3 specimens 70 x 70 x 70 mm. The samples for determination of water absorption and water vapor diffusion parameters were provided on all lateral sides by water- and vapor-proof plastic foil insulation.

Basic characteristics of the studied aluminosilicate materials were determined by water vacuum saturation method. The porosity and bulk density were changed only moderately for heating up to 600^0C. However, heating to 800^0C and 1000^0C led to a decrease of bulk density down to 10% and increase of porosity up to 40% in comparison with reference room temperature data.

The apparent moisture diffusivity was determined using the water absorption experiment. It increased already from 600°C loading temperature for both studied materials but then for the aluminosilicate with electrical porcelain filler was stabilized at almost constant values roughly corresponding to moisture diffusivity of ceramic brick. This can be considered as a very good result. The apparent moisture diffusivity of the material with sand aggregates increased for the pre-heating temperatures of 800°C and higher by an additional order of magnitude in a comparison with the pre-heating temperature of 600°C. Water vapor diffusion resistance factor decreased with increased loading temperature for the material with electrical porcelain filler only moderately, 30% in maximum, and for 1200^0C it slightly increased. The decrease of the water vapor diffusion resistance factor of the material with sand aggregates was more remarkable, down to three times in a comparison with the reference data. Both these results roughly correspond with the porosity data.

Heating above 400°C led for the material with electrical porcelain filler to a certain, not very significant decrease of thermal conductivity which was 10% in maximum. However, the subsequent increase of thermal conductivity for the heating temperature of 1000^0C cannot be explained in this simple way any more. One of the possibilities how to explain this seeming anomaly is that the increasing amount of larger pores probably led to a change of the initially almost homogeneous pore distribution in the material and some thermal bridges could appear.

References:

[1] ROY, D.M.: *Alkali-activated cements. Opportunities and challenges.* Cement and Concrete Research 29, 1999, pp. 249–254.

This research has been supported by the Czech Ministry of Education within the framework of the KONTAKT program, under the Czech-Greek bilateral cooperation project No. 7-2006-29

High-Temperature Properties of Alkali Activated Aluminosilicates

L. Zuda, R. Černý

cernyr@fsv.cvut.cz

Czech Technical University, Faculty of Civil Engineering, Department of Mechanics, Thákurova 7, 166 29 Praha 6, Czech Republic

Alkali-activated aluminosilicates belong to perspective materials in the field of fire protection because they exhibit remarkable high-temperature resistance and very favorable mechanical properties. Therefore, this type of materials is capable of replacing classical Portland or blended cement as traditional binder in concrete in the situation where high temperature resistance of the material is required [1].

In this paper, high temperature values of thermal diffusivity and specific heat capacity of an alkali activated aluminosilicate material are measured in the temperature range up to 1200^0C.

Fine-ground slag of Czech origin (Kotouč Štramberk, Ltd.) was used for sample preparation. As alkali activator, water glass solution was used. It was prepared using Portil-A dried sodium silicate preparative (Cognis Iberia, s.l. Spain). The sand aggregates were normalized according to EN 196-1 with the granulometry PG1, PG2, PG3. The composition of the mixture for sample preparation is presented in Table 1.

Table 1 Composition of the alkali activated slag material

Sand aggregates [g]			Slag [g]	Alkali-activation silicate admixture [g]	Water [ml]
PG1	PG2	PG3			
450	450	450	450	90	190

The technology of sample preparation was as follows. First, the silicate preparative was mixed with water. The solution was then mixed into the homogenized slag-sand mixture. The final mixture was put into 71x71x71 mm molds and vibrated. The specimens were demolded after 24 hours and then stored for further 27 days in water bath at laboratory temperature. Three specimens were studied for every measurement.

The determination of high-temperature thermal diffusivity was performed by the double integration method. It was calculated using the results of experimental measurements of temperature fields in the sample at one-sided heating in the solution of the inverse heat conduction problem. As the adiabatic methods are not very suitable for measuring high-temperature specific heat capacity of building materials, mainly because of the necessity to use relatively large samples, a nonadiabatic method was employed for the determination of temperature-dependent specific heat capacity.

Bulk density and open porosity of the studied aluminosilicate material in dependence on temperature are presented in Table 2. The data were obtained using the common water vacuum saturation method. We can see that the porosity began to increase significantly after heating to 600^0C, achieved its maximum at 800^0C, and at 1000^0C and 1200^0C it was not changed significantly.

Table 2 Porosity and bulk density of the studied aluminosilicate material as functions of temperature

Temperature [^{0}C]	Porosity [m^3/m^3]	Bulk density [kg/m^3]
25	0.18	2170
200	0.22	2100
400	0.17	2170
600	0.22	2070
800	0.24	2030
1000	0.24	2050
1200	0.23	2050

The dependence of specific heat capacity of the studied aluminosilicate material on temperature exhibited a maximum between 400^{0}C and 500^{0}C and after decreasing a little at 700^{0}C it began to increase very sharply, with a maximum at about 1100^{0}C. This last maximum was too high for any pure specific heat capacity considerations. However, it should be noted that the result of the applied method is in fact a value of "effective specific heat capacity" which may also reflect some other changes in enthalpy as for instance the enthalpy of chemical reactions taking place in a particular temperature range or enthalpy of phase change. In our case it means that a highly exothermal reaction could take place in the temperature range of approximately 800-1100^{0}C.

The thermal diffusivity vs. temperature function determined by the double integration method increased about three times between 150^{0}C and 400^{0}C and then it began to decrease. The observed increase in thermal diffusivity may be related to the increase in porosity in the temperature range of 25-600^{0}C (see Table 2). The later decrease may be caused by the structural changes in the material resulting in variations of the porous structure.

The measurements of specific heat capacity and thermal diffusivity of the alkali activated slag based material in the temperature range up to 1200^{0}C in this paper have shown that the material has a good potential for its future high-temperature applications in civil engineering. The material was found to be very stable up to 1200^{0}C, and its thermal diffusivity decreased with the increasing temperature for the temperatures higher than 400^{0}C which is a very positive feature for a material potentially applicable as fire protecting layer in building structures.

References:

[1] DAVIDOVITS, J., DAVIDOVITS, R., JAMES, C.: *Geopolymere.* Saint-Quentin, 1999.

This work was funded by the Czech Ministry of Education within the framework of the KONTAKT program, under the Czech-Slovak bilateral cooperation project No. 2.

Mechanical Properties of High Strength Steel Sheets

R. Mušálek, P. Haušild, J. Siegl, J. Bensch, J. Sláma*

Radek.Musalek@fjfi.cvut.cz

Department of Materials, Faculty of Nuclear Sciences and Physical Engineering,
Czech Technical University, Trojanova 13, 120 00 Prague 2, Czech Republic

* ŠKODA AUTO, a. s., TKI-3/6, V. Klementa 869, 293 60 Mladá Boleslav, Czech Republic

High strength steel (HSS) sheets are nowadays widely used for the construction of reinforcement parts in the car body. These materials have high tensile strength (up to 1800 MPa) and are capable of withstanding extensive plastic deformation. Therefore a large amount of impact energy during a crash-test or a collision can be absorbed, which increases the safety level of the car crew. It is important to have appropriate testing methods available so that different grades of high strength steels can be compared.

Typical thicknesses of HSS used in the car industry do not allow using of some standardized testing procedures. Current testing methods of these materials are mainly based on static loading tests. It turns out to be insufficient because the loading of the material during a collision is dynamic. The aim of our study was to propose and verify an appropriate methodology for testing of the thin HSS sheets by the means of fracture mechanics and fractographic analysis [1], [2].

Different approaches to the HSS sheets testing are nowadays being developed worldwide, e. g., modified Charpy impact test or Erichsen cupping test. It is possible to examine thin sheet specimens or assemblies of several layers of the sheet. It is assumed that thicknesses which are demanded by the standardized testing method for bulk materials can be obtained in this way. The modified Charpy impact test which we carried out on several assembled specimens (5 x 2 mm = 10 mm) indicated that each layer tends to behave like an individual entity. Therefore the single-layer specimens were used for further research.

Mechanical properties of three HSS sheets (DOCOL 1200 M, Multiphase 1200 and BTR 165) were tested. The microstructures were observed by the means of the light and scanning electron microscopy in three perpendicular directions. The specimens were grinded, polished, and etched using 3% Nital. A fine microstructure of mixed ferrite-martensite was observed for every specimen. It is supposed that forming has relatively small influence on the isotropy of observed materials due to thermomechanical treatment during the manufacturing process.

Tensile tests were carried out to obtain input data for a finite element method simulation of the modified Charpy impact test and fracture toughness test. Finite element method software (package Abaqus ver. 6.5.1) was used. These simulations provided some better insight in the loading process of the specimens with thicknesses $B = 2$ mm.

Modified Charpy impact test was based on the standardized Charpy impact test (ČSN EN 10 045-1). The thickness of the specimen was given by the thickness of available steel sheets. The impact energy needed to break specimens into two pieces was measured at different temperatures. Specimens were cooled down in the mixture of liquid nitrogen and ethanol. The temperature of the mixture was determined by a thermocouple. Ductile-to-brittle transition curves were measured. It was observed that tested materials remained ductile even at rather low temperature (-100 °C).

Fracture toughness tests (ASTM Standard E 1820-99) were conducted on the CT specimens at room temperature. A sharp fatigue crack was prepared using cyclic loading machine. Then the dependency of applied load vs. displacement was measured and the growth of the crack was measured by the light microscope. Determined values of the fracture toughness K_q are linked to the specimen thickness. The fracture toughness under the condition of plane strain K_{IC} was estimated [3]. A good agreement between our experimental results and the fracture toughness values of martensitic materials given in handbooks can be mentioned. The tearing resistance (J-Δa) curves were measured.

Fractographic analysis using light and scanning electron microscopy was carried out on the fracture surfaces of broken specimens. Observation of the Charpy impact test specimens confirmed that fracture mechanisms of HSS remain ductile even at low temperature. Due to the small thickness, shear lips covered fracture surfaces of all specimens tested above the transition temperature. Ductile dimples were observed on the whole fracture surface of every specimen broken above the transition temperature. Below the transition temperature both signs of cleavage and ductile dimpled fracture were observed.

With respect to the slight differences in the specimen thickness for different materials, it was observed that all three observed steels have very similar mechanical properties.

It was confirmed that a new approach to the thin HSS sheets testing by the means of fracture mechanics can be valuable and can provide new information about the behaviour of high strength steel materials under the dynamic loading. Designed methods are nowadays being used for further materials testing of HSS [4].

References:

[1] MUŠÁLEK, R.: *Studium vybraných materiálových vlastností vysokopevnostích plechů pro automobilový průmysl, Master's Thesis,* KMAT-FNSPE-CTU Prague, 2006, 115 p.

[2] MUŠÁLEK, R. – HAUŠILD, P. – BENSCH, J. - SIEGL, J. - SLÁMA. J.: *Studium mechanických vlastností a lomového chování vysokopevnostních plechů,* Proceedings of Fractography 2006, 2006, pp. 247 - 254.

[3] IRWIN, G. R.: *Fracture Transition for a Crack Traversing a Plate,* J. Basic Engineering 82, ASME, 1960, pp. 417-425.

[4] MUŠÁLEK, R. – HAUŠILD, P. – SIEGL. J.: *Hodnocení vrubové houževnatosti vybraných vysokopevnostních plechů,* Výzkumná zpráva V-KMAT-669/06, KMAT-FNSPE-CTU Prague, 2006, 14 p.

This research has been financially supported by project MSM 6840770021 Diagnostika materiálů. Support by ŠKODA AUTO, a. s. is gratefully acknowledged.

Detection of Gaseous Ammonia Using Evanescent Optical Sensor

J. Aubrecht, L. Kalvoda

aubrechtj1@km1.fjfi.cvut.cz

Department of Solid State Engineering, Faculty of Nuclear Sciences and Physical Engineering, Czech Technical University, Trojanova 13, 12000 Prague 2, Czech Republic

The presented research is focused on development of distributed fiber optic sensor for detection and location of ammonia leaks. The later establish a serious problem for all the industrial facilities utilizing large-scale cooling systems, cold-storage rooms and ammonia reservoirs. The sensing system is invented primarily for location of large scale, potentially harmful ammonia leaks, featuring concentration of ammonia in air close to the lethal levels (0.5 - 1 pph). In the following, the research related to preparation and tests of prototype sensing fibers by means of optical spectroscopy and optical time domain reflectometry (OTDR) is described. In our investigations, we used custom-made multimode fiber (core reflective index - 1.458, 230/260 μm core/cladding diameter, commercial title Optigard Q3-6662), which consist of silica core and polymer clad. The light propagates through the fiber core by means of total reflections, which happen at core and cladding interface. The total reflections at interface are attended by formation of evanescent field components, which propagate through interface into the cladding. This field creates the optical contact between the core and cladding layer of the fiber. The physical principle of the detection is combined with a chemical reaction between gaseous ammonia and a reagent - an organometallic complex dye. The reaction mechanism is based on a ligand exchange process accompanied by changes of optical absorption spectrum within the VIS-NIR range. The experimental setup used for absorption measurement consisted of a halogen lamp, a focusing microscopic lens, an ammonia injector, an optical pigtail with an integration sphere, a testing gas chamber and a source of dry ammonia/nitrogen and plain nitrogen gas. The absorption spectra were recorded with Ocean Optics S1000 fibre optic spectrometer (200 - 1200 nm detection range). The OTDR setup used in experiments consisted of Photodyne 5500 XFA OTDR unit (λ= 850 nm, pulse duration 20 ns, average pulse power 30 μW, repeating frequency 3.1 kHz), and HP 54615B digital oscilloscope (sampling speed 1 GSa/s, 500 MHz signal bandwidth). OTDR unit launched the pulses into the tested fibre, registered the intensity of the back-coming light using a Si-PIN diode, logarithmically amplified the intensity and provided the output signal to the oscilloscope. Parts of the fibers exposed to the analyte gas were placed in a special sealed chamber. The ammonia gas was prepared by evaporation of an ammonia/water solution in vacuum, drying it in a column filled with sodium hydroxide, and then mixing it with nitrogen gas. For measurements, the mixture was pumped into one of the testing chambers. The organic ligands (5-(4′-dimethylaminophenylimino)-quinolin-8-1 (L1) and (7-chloro-5(4′-diethylamino-2′-methylphenylimino)-quinolin-8-1 (L2) were synthesized as described in [2]. Other chemicals (analytical grade) were obtained from Sigma-Aldrich and Lach-Ner. Practical realization of the proposed detection principle requires full understanding of the ligand complexion reaction with ammonia leading to achievement of its high reversibility (driven only by the ammonia concentration changes), and the high reaction speed. In the same time, the VIS-absorption bands of the ligand and the complex must show a remarkable difference of their characteristic wavelengths, to provide a suitable basis

for the optical detection. Achievement of the reversible formation of the complex within the particular polymer cladding matrix is a very complicated task for it is necessary to tailor the micro-conditions of the sensing chemical reaction (type of the central metallic cation, lipophilicity of the counter-anion, solvability of the ligand within the polymer, etc.), and the high ammonia permeation together. In the reported research, we firstly focused on analysis of the VIS spectral shifts accompanying the complex creation for set of bivalent cations [1, 2]. Later the influence of time degradation on properties of reagents and prototype fibers was tested and a reaction time, saturation time, concentration sensitivity and coefficient of ammonia gas diffusion through the cladding were investigated. Parameters of the sensing reaction were gradually studied in a liquid phase (in solutions of ethanol with ammonium hydroxide added) and on samples of short sections of siloxane-clad optical fibers (10 cm in length) by VIS-NIR spectroscopy. In the later case, the fibre cladding layer was sensitized by the reagent diffusion from its solution. The solutions of ethanol, chloroform, dichloride methane, acetone, higher alcohols, and their mixtures were tested [1]. The best results were obtained with the 1:1 (wt.) mixture of ethanol and chloroform. The superior reaction properties with ammonia were in ethanol solutions observed for Cu^{2+} and Co^{2+} complexes with the L1 ligand. Sulphate, bromide and nitrate counter-anions were tested. Slightly superior results were obtained with the bromides and nitrates [1, 2]. The upper results were employed for preparation of longer sensing fibre sections (featuring $\sim 15/100$ m the sensitized/full length) tested as distributed sensors of ammonia leaks. The localization method was based on the OTDR technique allowing for analysis of optical attenuation over the full length of the sensing fibre. A pulse of light is transmitted down the fibre and the light intensity which is back-scattered within the numerical aperture of the fibre is measured. The time between launching the pulse and detecting the signal provides a measure of the distance, whilst the signal intensity gives the local fibre properties-related information. Using a simple theoretical model considering the Raleigh scattering mechanism only [2], it is then possible to identify optional ammonia attacks (leak position, gas concentration) from observed changes of the recorded OTDR curve. In addition to the Raleigh back-scattered signal, the OTDR spectrum includes also two Fresnel reflections originating respectively from the front and free end of the fibre. The obtained results showed a well-resolved and relatively fast response of the tested fibres when exposed to the ammonia/nitrogen gas mixtures within the concentration range 200 - 10 000 ppm [2]. The theoretical concentration sensitivity derived from the observed S/N ratio of the employed OTDR system was ~ 50 ppm. The fast reaction time $\tau_{90} \approx 30$ sec. was observed. However, the regeneration of the tested fibers following their exposure to ammonia was not complete. Therefore, the later will be the main subject of the forthcoming research.

Reference

[1] Aubrecht, J.: *D*etection of gaseous ammonia using evanescent optical sensor, Diploma Thesis, FNSPE CTU Prague, 2006.

[2] Kalvoda, L.,Aubrecht, J., Klepáček, R.: *F*iber Optic Detection of Ammonia Gas, Acta Polytechnica 46(2) (2006) 41-46.

Alkali Activated Slag as Cement Replacement in High-Temperature Applications

J. Toman*, R. Černý

toman@fsv.cvut.cz

*Czech Technical University, Faculty of Civil Engineering, Department of Physics, Thákurova 7, 166 29 Praha 6, Czech Republic

Czech Technical University, Faculty of Civil Engineering, Department of Mechanics, Thákurova 7, 166 29 Praha 6, Czech Republic

The last century has focused quite properly its technology on Portland cements, concentrating on the development of binding systems consisting of the high calcium content minerals, C_3S, C_2S, C_3A, and C_4AF. These systems have served well, but not without some drawbacks (see, e.g. [1]). Production of Portland cement involves the grinding of raw materials, the calcination of raw materials at 1500°C and the grinding of cement clinker and gypsum. It is an energy-intensive process and requires approximately 4000 MJ/t of cement. Because Portland cement and concrete derived from it constitute the largest volume manufactured material in the world, it is also a significant source of carbon dioxide. This is the result of decarbonation of limestone in the kiln during manufacturing,

$$5CaCO_3 + 2SiO_2 \rightarrow 3CaO \cdot SiO_2 + 2CaO \cdot SiO_2 + 5CO_2,$$

and the use of fossil fuel in the kiln. The production of 1 ton of Portland cement accounts for 1 ton of CO_2. Furthermore, there are certain limitations regarding the durability of the concrete products. Therefore, it is appropriate that now more attention should be given to more conservative systems.

Waste utilization is an attractive alternative to disposal in that disposal cost and potential pollution problems are reduced or even eliminated along with the achievement of resource conservation. Nevertheless, the utilization strategy must be coupled with environmental and energy considerations to use available materials most efficiently.

Properly fast cooled iron blast furnace slag, steel slag, phosphorus slag, copper slag and lead slag have cementitious or pozzolanic properties. As the use of these slags as cementing components needs only grinding, it saves substantial amounts of energy compared with the production of Portland cement. For example, the energy required to grind granulated blast furnace slag is only approximately 10% of the total energy required for the production of Portland cement.

At the present, most industrial slags are being used without taking full advantage of their properties or disposed rather than used. Mostly, they are used as aggregates for different applications or ballasts. Only a small portion of ground granulated blast furnace slag is used for a partial Portland cement replacement. The partial replacement may decrease the early strength, but increase the later strength and improve microstructure and durability of hardened Portland cement and concrete very significantly [2]. Many research results have indicated that clinkerless alkali-activated slags show higher strengths, denser structure and better durability than Portland cement under both normal and hydrothermal conditions. Thus, the optimum use of these slags is as cementing material components rather than as aggregates or for base stabilization.

The principle of alkaline activation of blast furnace slag has been known since the 1940s [11]. However, systematic studies on alkali-slag cement were not carried out until in the early 1960s. This type of cement is simply obtained by mixing ground slag and a proper alkali activator.

Generally, the reaction mechanism of alkali activated materials can be described in two steps. The first is the generation of reactive species (alkaline activation). The alkaline pore solution disintegrates the solid network to produce reactive silicate and aluminate species with low molecular weights. The activation of the solid is achieved with alkaline solutions containing alkali hydroxides, alkali silicates and/or alkali carbonates. The second step is the setting reaction. Pure aluminosilicate materials, e.g., metakaolin and some types of fly ash, set by a condensation reaction which leads to the formation of aluminosilicate polymers. Typically, aluminosilicate polymers are forming three-dimensional networks in a similar structure than zeolites, but are almost completely amorphous. As shown by several authors, the setting of alkali activated slag and calcium-containing materials can be characterized by both a condensation reaction and a hydration reaction forming CSH (or Al-substituted CSH) and CAH phases, depending on calcium content and alkalinity.

Slags are mostly activated with sodium silicate (waterglass) which has been widely reported to give rise to rapid hardening and high compressive strengths. Problems, however, can be experienced with very short set times and subsequent shrinkage, and the activators used are often highly corrosive and would be difficult to handle safely outside of the laboratory. Therefore, a sodium silicate with higher modulus (silica-to-alkali ratio) is often used that is less corrosive and thus safer, and also partly alleviates the set time difficulties.

Alkali-activated slags belong to perspective materials in the field of fire protection because they exhibit remarkable high-temperature resistance and very favorable mechanical properties. Therefore, this type of materials is capable of replacing classical Portland or blended cement as traditional binder in concrete in the situation where high temperature resistance of the material is required.

Although the potential for high-temperature applications of aluminosilicate materials is obvious for years, the measurements of their properties in high-temperature range are very sparse in the scientific literature. Thermal parameters such as thermal conductivity and specific heat capacity were not yet measured even in normal conditions. The dependence of thermal and hydric properties on temperature in the high-temperature range was not studied as well. Therefore, analysis of both thermal and hydric properties of these materials, particularly in high-temperature conditions and after high-temperature exposure is very desirable.

References:

[1] ROY, D.M.: *Alkali-activated cements. Opportunities and challenges.* Cement and Concrete Research 29, 1999, pp. 249–254.

[2] SHI C, QIAN J.: *High performance cementing materials from industrial slags — a review.* Resources, Conservation and Recycling 29, 2000, pp. 195–207.

This work was funded by the Czech Ministry of Education within the framework of the KONTAKT program, under the Czech-Polish bilateral cooperation project No. CZ - 31.

Properties of Concrete Damaged by Salt Action

E. Mňahončáková, M. Pavlíková*, R. Černý**

eva.mnahoncakova@fsv.cvut.cz

Department of Physics, Faculty of Civil Engineering, Czech Technical University, Thákurova 7, 166 29 Praha 6, Czech Republic
*Department of Building Materials, Faculty of Civil Engineering, Czech Technical University, Thákurova 7, 166 29 Praha 6, Czech Republic
**Department of Mechanics, Faculty of Civil Engineering, Czech Technical University, Thákurova 7, 166 29 Praha 6, Czech Republic

The progressive building materials development improves their quality and utility value. In order to achieve better material properties, besides the new technologies also specific admixtures are employed. The accurate admixtures dosage and technological conditions observation can improve the material parameters like strength and durability. Most frequently, the mineral admixtures, for example pozzolana, fly ash or flue cinder, are used in concrete production. Fine siliceous materials usually called silica fume belong to relatively newly applied materials improving concrete quality. Concrete belongs to the most extensively used materials in construction industry. Requirements on increasing load or on reduction of the construction thickness become highly actual. In particular, extension of concrete durability lies in focus of interest. The storage of chemicals in concrete silos often presents durability problems due to chemical attack, the high concentration encountered inevitably causes severe conditions. Principal aim of this study is to examine the influence of the physicochemical changes on basic hygric and thermal properties of high-performance concrete that occur in concrete exposed to ammonium salts, notably ammonium sulphate and nitrate, which are noted for their aggressivity. The obtained data can be applied as input parameters for computer simulations aimed to the prediction of concrete service life.

The high performance concrete of two basic compositions C90/105 and C60/75, marked as BI and BII, respectively, was chosen as a basic tested material. The first one, BI, was composed of cement CEM I 52.5 R, silica fume suspension, aggregate of 0-16 mm granulity, accelerant Lentan VZ33, larry Woerment FM794, and water of given proportion. The second one, BII, had the same composition as BI except for the silica fume suspension. To analyse the effect of aggregates on heat and moisture transport parameters, the cement pastes marked as PI and PII, and concretes without the aggregates of 8-16 mm granulity marked as BBI and BBII, were also studied. All the specimens were left in 3-M NH_4NO_3 solution for three months. The samples for measuring hygric and thermal parameters were stored at 25 °C in usual laboratory conditions (relative humidity about 30-35%); another set of measurements was done with the various values of relative humidity. The sample sizes depended on the type of measurement.

Some of the basic material properties, namely vacuum saturation moisture content, bulk density, and open porosity were studied first. Each sample was dried in an oven to remove majority of the physically bound water. After that the samples were placed into the desiccator with deaired water. During three hours air was evacuated with vacuum pump from the desiccator, the specimen was kept under water not less than 24 hours. The so-called "Archimedes weight" was determined by weighing immersed water-saturated samples.

Hygrothermal behaviour of building materials is described by thermal and hygric properties. The one of the common material properties is water vapour diffusion resistance factor, basically measured according to the standard ČSN 72 7031 [1]. The measurement is

carried out in steady state under isothermal conditions. It is based on one-dimensional water vapour diffusion, measuring the diffusion water vapour flux through the specimen and on measuring partial water vapour pressure in the air under and above specific specimen surface. Water vapour transmission properties of a material are obtained by placing a specimen of the material on the top of a cup and sealing it. The cup should contain sorption material (desiccant, saturated salt solution or water). The sealed cup is placed in a controlled climate chamber and weighed periodically. The steady state values of mass gain or mass loss are utilized for the determination of the water vapour transfer properties. The simplest way, how to describe liquid water transport through a porous material, is using a water suction experiment. Set up for measuring the water absorption coefficient consists of tank filled with water, and the specimen, water and vapour-proof insulated on four lateral sides, fixed on automatic balances and immersed 1-2 mm in the water [2]. The water absorption coefficient, A, is calculated from the linear part of the dependence of the increase of tested sample's mass on the square root of time. Then moisture diffusivity can be calculated from the vacuum saturation moisture content and water absorption coefficient according a simple equation [3]. Among the thermal properties, the thermal conductivity, thermal diffusivity and specific heat capacity were measured using the commercial device ISOMET 2104 (Applied Precision, Ltd.).

Our experimental results confirm literature data [4]. In a comparison with reference specimens not exposed to salt action, the porosity is lowered, as well as the ability of water and water vapour transport, contrary to bulk density and heat transport parameters, which are increased. These phenomena have been observed in materials damaged by salt after their three months action.

The measurements of thermal and hygric parameters of a high performance concrete damaged by salt action were done with the primary aim to obtain the input data for computer simulation. Therefore, the different concrete components were mixed and consequently the basic parameters of the prepared samples were tested. The results show effect of aggregate granularity but the influence of silica fume suspense addition is not so significant.

References:

[1] ČSN 72 7031: *Měření součinitele difúze vodní páry stavebních materiálů metodou bez teplotního spádu.* ÚNM Praha, 1974, pp. 1-7.

[2] S. ROELS, J. CARMELIET, H. HENS, O. ADAN, H. BROCKEN, R. ČERNÝ, Z. PAVLÍK, C. HALL, K. KUMARAN, L. PEL, R. PLAGGE: *Interlaboratory Comparison of Hygric Properties of Porous Building Materials.* Journal of Thermal Envelope and Building Science, 27, 2004, pp. 307-325.

[3] M.K. KUMARAN: *Report on Measurements to Determine Moisture Diffusivity of Eastern White Pine.* IEA Annex XXIV Report T3-CA-92/04, 1994.

[4] A. BAJZA, I. ROUSKOVÁ, S. UNČÍK, LE Q. HUNG: *Vlastnosti a struktura cementových kaší korodovaných roztokami NH4NO3,* Stavebnícky časopis, 37, č. 8, VEDA, Bratislava, 1989.

This work was funded by the Czech Ministry of Education within the framework of the KONTAKT program, under the Czech-Polish bilateral cooperation project No. CZ - 3.

Properties of Lightweight Carbon Fiber Reinforced Cement Composite

E. Mňahončáková*, P. Tesárek, P. Konvalinka, R. Černý**

eva.mnahoncakova@fsv.cvut.cz

*Czech Technical University, Faculty of Civil Engineering, Department of Physics, Thákurova 7, 166 29 Praha 6, Czech Republic

Czech Technical University, Faculty of Civil Engineering, Department of Mechanics, Thákurova 7, 166 29 Praha 6, Czech Republic

**Czech Technical University, Faculty of Civil Engineering, Experimental Center, Thákurova 7, 166 29 Praha 6, Czech Republic

Cement-based materials are characterized by very good properties in compression but their brittle manner of failure under tensile or impact load was a limiting factor for their applicability range from the very beginnings. Fiber reinforcement is a traditional and effective method how to improve the toughness and durability of cement based products. The steel rod reinforcement became very popular during the whole last century and remains the most frequently used type of concrete reinforcement until now. However, in the second half of the 20th century, an application of uniformly dispersed short fibers strengthening the brittle cementitious matrices appeared with an increasing frequency. In the current practice, steel, glass, carbon and various polymeric fibers such as polyethylene, polypropylene, nylon, polyester, polyurethane, cellulose, etc., are commonly used in cement-based materials.

Carbon fiber reinforcement has found its application first in polymeric matrices for automotive and aircraft industry. It partially replaced previously used glass fibers in such situations where superior strength properties, very low tensile strains and mass savings were necessary. The initial phases of utilization of carbon fibers in the production of composite materials were affected by their high price. Carbon fibers are produced by the controlled oxidation, carbonization and graphitization of carbon-rich organic precursors, which are already in fiber form. In the beginnings of carbon fiber production the most often used precursor was PAN (polyacrylonitrile) that gave superior carbon fiber properties but was quite expensive. The appearance of low-cost pitch based carbon fibers in 1980s has led to a significant increase of various applications of carbon fibers. In the construction industry it resulted in an increasing use of carbon fiber reinforced cement composites.

Similarly as with the other fiber reinforced cement composites, also the properties of carbon fiber reinforced cement composites were studied in an insufficient way until now. The most frequently analyzed were the mechanical properties. The hygric and thermal properties were measured only rarely. In addition, the specimens were tested mostly in the reference state, i.e., in room temperature conditions. The properties of this type of materials in high-temperature conditions or after high-temperature loading were studied only exceptionally.

In this paper, basic thermal and hygric properties of carbon fiber reinforced cement composite were measured in both reference state and after pre-heating up to 1000^0C.

The samples were produced in the laboratories of VUSTAH, SA using a successive homogenization procedure. First, Casiflux (40 % by mass of dry substances), microdorsilite (17 %) and microsilica (2 %) were homogenized in a mixing device, then cement (40 %) was added and the dry mixture was homogenized again. The dry well homogenized mixture was thoroughly mixed with water (w/c = 0.85). Then, the carbon fibers (1 % by mass) were added

and the mixture shortly mixed again. Finally, the prepared mixture was autoclaved. After the time period of 28 days after mixing, the samples were dried and prepared for testing.

In the experimental measurements, four various sample pre-treatment conditions were tested: reference specimen not exposed to any load, specimen exposed to a gradual temperature increase up to 600, 800 and 1000^0C during two hours, then left for another 2 hours at the final temperature and slowly cooled.

Experimental results showed that two principal changes in porosity appeared, namely between the reference state and the loading temperature 600^0C when the increase of porosity was 12%, and between 800^0C and 1000^0C when the porosity increased by 9%. This indicates significant structural changes due to chemical reactions after high-temperature loading.

The diffusion coefficient of water vapor increased significantly with the increasing pre-heating temperature which is in an agreement with the increasing porosity. After 1000^0C pre-heating the diffusion coefficient of water vapor was four to five times higher than in the reference state.

The water transport in the perpendicular direction to the board was in the reference state significantly slower than in the direction of the board, the moisture diffusivity κ was approximately six times lower, the water absorption coefficient A about two times lower. This was probably due to the more compact structure of the board near the board surface. For the thermally loaded specimens the differences between the two orientations were much lower and for the pre-heating temperatures higher than 600^0C they were within the error range of the measuring method. These findings were probably due to the damage of the structure after heating to high temperatures and the consequential opening of the preferential paths for water transport in both principal directions which was indicated by the increase of the saturated water content w_{sat} with increasing pre-heating temperature. The increase of moisture diffusivity up to three orders magnitude in a comparison with reference specimens means that the structural damage was very significant.

The thermal conductivity in dry state after pre-heating to the temperatures of 600^0C and 800^0C moderately decreased (down to 15%) but for 1000^0C it slightly increased. This finding is not in a direct correlation with the porosity measurements because with the increasing temperature the volumetric fraction of air increased which should lead to a decrease in thermal conductivity. The most probable reason of the measured changes of thermal conductivity was a change in the character of the porous structure after heating which was indicated also by a significant increase of matrix density after pre-heating to 1000^0C.

The thermal conductivity in fully water saturated state was affected by the presence of water in the most significant way so that it increased up to 35%. This is in accordance with the increase of porosity after heating. A similar effect was observed for the volumetric heat capacity which increased up to 10%.

References:

[1] OHAMA Y.: *Carbon-cement composites.* Carbon, Vol. 27, 1989, pp. 729-737.

[2] CHUNG D.D.L.: *Carbon Fiber Composites.* Butterworth-Heinemann, London, 1994.

This research has been supported by the Ministry of Industry and Trade of Czech Republic, under grant No. FT – TA/019.

Plastics welding – welding parameters optimalisation through the use of statistical software

J. Beránek

beranekj@fs.cvut.cz

Department of Mechanics, Klokner Institute, Czech Technical University,
Šolínova 7, 166 08 Prague 6

This study deals with heated tool welding of polyoxymethylen (POM), with impact of welding parameters on the quality of produced joints and consequential optimalization of these parameters.

As a surveyed material in this study was used polyoxymethylen Ultraform N2320 C (product of BASF Corporation). This is a special copolymer of POM filled with carbon nano-fibres which can conduct electric current. From these material were produced standardised test specimens for tensile test (viz. ISO 3167). Before welding, test specimens were divided into halves and worked the accurate dimensions. Finally, specimens were welded by using heated tool welding technology.

Implementation:

The optimisation of welding parameters was accomplished by using statistical software MINITAB Release 14.20. First step in optimizing is design of experiment. It consists of significant welding parameters determination and assignment of marginal conditions for these variable parameters. Significant variable parametrs of heated tool welding are indicated in Table 1.

variable parameters	unit	lower limit	upper limit
temperature	[°C]	200	240
heating time	[s]	13	23
welding path	[mm]	0,5	1
smoothing path	[mm]	0,2	0,5

Table 1 Variable parameters of heated tool welding.

It is obvious there are four variable factors entering in the experiment. Account on that the half-factorial experiment (2^{k-1} design) was chosen as most suitable because 8 combinations of these variables will be proposed. Otherwise, for full-factorial design (2^k) would be proposed 16 combinations and it would be material- and time-consuming.

Second step in this experiment is testing of welded specimens. For any of these 8 combinations was welded a set of 11 specimens, 5 of them were utilized for tensile test, 5 of them for Charpy impact test. Tensile test (ISO 527-2) was accomplished at testing machine INSTRON 1273 by the testing speed of 10 mm/min. Charpy impact test (ISO 179) was accomplished at hammer CEAST (energy of pendulum hammer 7,5 J, weight 1,096 kg, lenght 370 mm, speed 3,70 $m.s^{-1}$, angle 150°). Impact was taken at the narrow side of the unnotched test specimen.

Final step is data evaluatin and interpretation the results. On the basis of statistical methods is possible to get assorted dependences of quality of welded joints on single

parameters and mutual interactions of them. These advices make us possible to estimate the importance of any variable factors and optimize values of welding parameters.

Results:

Dependance welded joints quality on combinations of welding parameters is very complicated. Hence, the application of any statistical software is necessary for comprehensive interpretation of these dependences and welding parameters determination.

The result of this experiment is optimal combination of welding parameters for welding Ultraform N2320 C using the heated tool welding technology. It is summarized in Table 2.

welding temperature	heating time	welding path	smoothing path	failure strength	impact resistance
[°C]	[s]	[mm]	[mm]	[MPa]	[kJ/m2]
240	13	1	0,2	64,76	26,85

Table 2 The result of experiment – optimal welding parameters.

Conclusions:

- Optimal welding parameters for welding Ultraform N2320 C by heated tool technology are mentioned in Table 2.
- Resulting values of welding parameters are optimal with respect to initially variable limits in which the experiment was designed. With respect to results of the experiment it is imposible to get much better values of mechanical properties changing these limits.
- With using suitable welding parameters it is possible to reach for nearly 90% strength of base material in weld joint. Simultaneously, it is possible to reach sufficient values of impact resistance.
- Optimisation of welding parameters is necessary both for achievement of quality and for minimisation cost of real products manufacture.
- Influence of heating time is essential for final cost of the welded product, especially in a lot manufacture. That is why the maximum reduction of time for heating material is very desireable.

References:

[1] COX, D.R. – REID, N.: *The Theory of the Design of Experiments,* Chapman & Hall/CRC 2000.

[2] TKÁČ, M.: *Náštroje štatistického riadenia kvality,* Košice 2001.

[3] BRYDSON, J.A.: *Plastics Materials,* Butterworth - Heinemann 1999.

This research has been supported by MŠMT grant No. MSM6840770015.

Corrosion and Fatigue Degradation of Stainless High Alloyed Steels and Nickel Alloys

K. Dalíková*, J. Kunz*, V. Číhal**

klara.dalikova@fjfi.cvut.cz

*Department of Materials, Faculty of Nuclear Sciences and Physical Engineering, Czech Technical University, Trojanova 13, 120 00 Prague 2, Czech Republic

**SVÚOM Ltd., K Měšťanskému pivovaru 934/4, 170 00 Prague 7, Czech Republic

The research has been carried out within the cooperation of Department of Materials - Faculty of Nuclear Sciences and Physical Engineering - CTU in Prague and research institute SVUOM Ltd. The experimental programme was dealing with six very noble, highly alloyed materials, namely: austenitic stainless steels Uranus SB8 and Uranus B26, duplex stainless steels Uranus 45N and Uranus 52N+, nickel alloys Nicrofer 3127 hMo and Nicrofer 5923 hMo, which are often used in the power, chemical and food-processing industry. The aim of the research is to verify the most important characteristics quantifying the degradation properties (failure mechanisms, corrosion mechanisms, degradation types and processes etc.).

All materials under study are characterized by very low content of carbon (0.007÷0.026%) as a prevention of intergranular corrosion, nitrogen (0.172÷0.248%, except Nicrofer 5923 hMo) for the increasing of strength properties, relatively high content of chromium (20.4÷26.65%) and nickel (24.75÷60.9% for austenitic steels and nickel alloys, 5.07÷6.02% for duplex steels), which are the essential elements ensuring corrosion resistivity (see Tab.1). The yield limit $R_p0.2$ and ultimate strength R_m of all investigated alloys are in the range (300÷560) MPa and (600÷800) MPa respectively.

Tab. 1 – Chemical composition of investigated alloys

Alloys	*Ni*	*Cr*	*Mo*	*Cu*	*Mn*	*Si*	*N*	*C*	*S*	*P*	*Fe*	*Co*	*V*	*W*
UR SB8	**25.90**	**25.05**	**4.73**	**1.45**	**0.936**	**0.246**	**0.2144**	**0.01**	**0.0008**	**0.014**	**-**	**-**	**-**	**-**
UR B26	**24.75**	**20.40**	**6.30**	**0.86**	**0.88**	**0.22**	**0.198**	**0.009**	**0.0004**	**0.016**	**-**	**-**	**-**	**-**
UR 45N	**5.07**	**21.80**	**3.13**	**-**	**1.343**	**0.356**	**0.172**	**0.026**	**0.0005**	**0.021**	**-**	**-**	**-**	**-**
UR 52N+	**6.02**	**24.90**	**3.74**	**1.65**	**1.13**	**0.335**	**0.248**	**0.015**	**0.001**	**0.014**	**-**	**-**	**-**	**-**
3127 hMo	**31.05**	**26.65**	**6.34**	**1.16**	**1.51**	**0.04**	**0.207**	**0.008**	**0.005**	**0.01**	**-**	**-**	**-**	**-**
5923 hMo	**60.90**	**22.50**	**15.50**	**0.01**	**0.15**	**0.04**	**-**	**0.007**	**0.003**	**0.002**	**0.34**	**0.02**	**0.15**	**0.01**

One part of the experimental programme was the slow strain rate test (SSRT). The resistivity against mechanical stress and aggressive media was studied. Cylindrical test specimens with diameter 2 mm and working part length 10 mm were used for the experiments. Corrosion media containing chloride ions ($CaCl_2$, $CaCl_2$+$FeCl_3$, $CaCl_2$+ $FeCl_3$+KSCN, etc.) were suggested; the alloys under study should be with similar substances in contact in practice. For the comparison, the same tests were realized in the inert medium – glycerol. The specimens were loaded at the strain rate 2.56 x 10^{-6} s^{-1} and at the temperature the value of which depends on the bubble point of each medium: $T = (105 \div 120)$ °C. During the testing, the load vs. time was monitored. Time and load to the failure were the main output parameters for the evaluating criteria. The test results were presented in the relative form as a ratio between the corresponding values ascertained in aggressive and inert mediums. After the slow strain rate test, all specimens were examined by stereomicroscope. The investigation was completed by fractographic analysis of fracture surfaces of failed test

bodies. By means of scanning electron microscopy, the large photodocumentation was made. For the both duplex steels tested, intergranular decohesion is predominant failure micromechanism in corrosion media, while in inert medium, it is transgranular one. Numerous secondary microcracks were observed both on the specimen surfaces and on the fractures - they are the results of the influence of aggressive medium and mechanical stress. By the SSRT, it was found out that both duplex steels are relatively very sensitive on the media containing chloride ions. At the austenitic steels and nickel alloys under study, the attention has been paid to the finding such corrosion medium which enables the study of their stress corrosion cracking. More aggressive media (e.g., according to ASTM G28B) simulating an environment in the scrubbers, where the alloys should be used, are also applied in the tests.

The measurement of polarization curves by means of potentiodynamic method was the next part of the research. The aim of these experiments was to characterize the corrosion behaviour of passivative metals in electrolytes, i.e., the assessment of the characteristic potentials and current densities quantifying the degradation processes. Few laboratory measurements were carried out so far. This experimental will continue in near future and will be completed.

By means of servo-hydraulic machine INOVA ZUZ 50, the fatigue tests of CT-specimens (width $W = 38$ mm, length $L = 45.6$ mm and thickness $t = 4$ mm) at constant stress range were carried out. By both optical and potential method, the crack length vs. the number of applied cycles was monitored during the testing. The data obtained enable to determine the fatigue crack growth rate da/dN as a function of the stress intensity factor range ΔK and to estimate the fatigue threshold ΔK_p of all investigated materials. One set of the specimens was tested until the final failure of whole cross-section. These specimens will be subjected to the detail fractographic analysis focused on the fatigue failure mechanism study. The testing of the second set of CT-specimens was terminated in the moment when crack of length about $a = 21.5$ mm was created.

The mentioned second set of pre-cracked CT-specimens will be subsequently used in the next part of experimental programme – tests of stress corrosion cracking at the constant load. The same corrosion media as for the SSRT and elevated temperature in dependence on medium and possibilities of experimental equipment will be used with aim to assess conditions and kinetics of the crack growth in specific environment.

The metallographic analysis of structure and texture of all six investigated alloys was integral part of the research. It brings the information about initial materials characteristics, e.g., microstructure, grain size, rolling direction etc. Obtained results will be included in the database of properties of these top corrosion-proof materials. This source will provide the objective data for optimal selection of suitable structural material for some specific application in engineering practice.

References:

[1] Dalíková, K. – Kunz J. – Číhal, V.: Korozní zkoušky vysocelegovaných duplexních ocelí při pomalé rychlosti deformace. In: *Fractography 2006*. Institute of Materials Research SAS Košice 2006, s. 263-270.

[2] *Corrosion of Metals and Alloys – Stress Corrosion Testing – Part 7, Slow Strain Rate Testing.* ISO/CD 7539-7, ISO 2005, 12 p.

[3] Koroze kovů a slitin – Zkoušky koroze za napětí. Část 6: Příprava a používání vzorků s předem vytvořenou trhlinou za konstantního zatížení nebo za konstantního rozevření trhliny. ČSN EN ISO 7539-6, 2003, 41 s.

This research has been supported by projects MSM2579478701 a MSM6840770021.

Metakaolin - Active Micro-filer for High Performance Concrete

P. Konvalinka, K. Kolář, J. Kolář

conwa@fsv.cvut.cz

Experimental Centre, Faculty of Civil Engineering, Czech Technical University, Thákurova 7, 166 29 Prague 6, Czech Republic

Metakaolin is known as latent hydraulic admixture for cementitious composites. Metakaolin is produced by burning of kaolinitic clay at temperature 600-800 °C. Metakaolin reacts with calcium hydroxide when is ad to cement based composition and product of this reaction is close to product of hydration of silicate cements. This process increase density of cementitious paste and consequently the strength and modulus of elasticity of concrete are increased. Presented result describe influence of metatakaolin produced by company Keramost and used as admixture to concrete with cement CEM I 42,5. Three types of mixtures (see table 1, 2, 3) were compared. Tested parameters were workability, compression strength (1, 2, 3, 7, 28 days) and modulus of elasticity (28 days).

Table 1: Mixture 1 – Reference mixture without metakaolin

Material	Dosage [kg/m^3]
Cement CEM I 42,5 R	440
Aggregates – sand 0-4 mm	795
Crushed gravel 4-8 mm	315
Crushed gravel 8-16 mm	670
Plasticizer (carboxylether) Stachement 2090	4,4
Water H_2O	177

Workability - slump S3 - up to 150 mm – EN 206-1.

Table 2: Mixture 2 – Concrete with metakaolin – dosage 10% of weight of cement

Material	Dosage [kg/m^3]
Cement CEM I 42,5 R	400
Metakaolin	40
Aggregates – sand 0-4 mm	795
Crushed gravel 4-8 mm	315
Crushed gravel 8-16 mm	670
Plasticizer (carboxylether) Stachement 2090	4,4
Water H_2O	177

Workability … until 6 min. after mixing was concrete very liquid (slump S4 - more than 160 mm), after 6 min. there was rapid reduction of workability, mixture was very dry and long vibration must be applied to prepare testing specimens.

Table 3: Mixture 3 – Concrete with metakaolin – dosage 10% of weight of cement and plasticizer – dosage 2% of weight of fine material = cement + metakaolin

Material	Dosage [kg/m^3]
Cement CEM I 42,5 R	400
Metakaolin	40

Aggregates – sand 0-4 mm	795
Crushed gravel 4-8 mm	315
Crushed gravel 8-16 mm	670
Plasticizer (carboxylether) Stachement 2090	8,8
Water H_2O	160

Workability – flow test according to ČSN EN 206-1:
After 15 min … result 540 mm
After 30 min … result 540 mm
After 60 min … result 490 mm
After 90 min … result 460 mm

Table 4: Test results - Compression strength = mean of 3 cubes 150 mm, Modulus of elasticity = mean of 3 beams 100×100×400 mm

Age of specimens [days]	Bulk density [kg.m^{-3}]	Compression strength [MPa]	Modulus of elasticity [GPa]
Mixture 1			
1	2345	35,2	
3	2350	46,3	
7	2375	57,7	
28	2388	63,7	38,5
Mixture 2			
1	2415	36,5	
3	2425	54,5	
7	2427	61,0	
28	2415	75,0	40,4
Mixture 3			
1	2410	31,2	
3	2415	57,5	
7	2420	72,0	
28	2428	90,0	44,0

High values of strength and modulus elasticity at age 28 day after mixing show very positive influence of metakaolin admixture on those parameters.

References:

[1] K. KOLÁŘ, T. KLEČKA, J. KOLÍSKO, N. DUBSKÝ: *Time Development of Static Modulus of Elasticity of HPC with Application of Superplasticizers on Carboxylether base,* Innovations and Structural Implications and Mindess Symposium, The University of British Columbia, 2005, pp. 55.

[2] T. KLEČKA, K. KOLÁŘ, J. VODIČKA, P. BOUŠKA: *Long-term Durability of Special Composite Materials,* Scientific Conference Quality and Reliabilty in Building Industry, TU Košice, 2006, pp. 189–196.

This research has been supported by company KERAMOST, a.s.

Coupled Water and Salt Transport with Crystalization: Calibration of the Computational Model

J. Kelnar, J. Maděra, R. Černý

jan.kelnar@fsv.cvut.cz

Department of Mechanics, Faculty of Civil Engineering, Czech Technical University, Thákurova 7, 166 29 Praha 6, Czech Republic

A diffusion-advection model was used for basic description of coupled water and salt transport in porous building materials, taking into account both water movement due to the moisture gradient and dispersion effects within the liquid phase due to the concentration gradient. Salt crystallization in the porous body was modeled using an equilibrium model. The effect of salt bonding on the pore walls was taken into account as well. The original moisture and salt transport modeling treatment chosen by Pel et al. [1] was modified and extended in order to avoid the apparent problems with the model. The basic idea that the mechanism of salt solution transport can be described by Bear and Bachmat diffusion-advection model [2] taking into account not only the influence of moisture flow on salt transport but also the effect of salt bonding on pore walls was preserved. In addition to the effects taken into account in the original model from [1], salt crystallization and water vapor transport were introduced into the model in order to facilitate modeling of drying experiments. Also, contrary to the model from [1], the dispersion effects in the liquid phase were considered as significant and included into the parameter identification process.

The modified mathematical model was then formulated as follows:

$$\frac{\partial\left(wC_f\right)}{\partial t}H\left(C_{f,sat}-C_f\right)=\frac{\partial}{\partial x}\left(wD\frac{\partial C_f}{\partial x}\right)+\frac{\partial}{\partial x}\left(C_f\kappa\frac{\partial w}{\partial x}\right)-\frac{\partial C_b}{\partial t}-\frac{\partial C_c}{\partial t}$$

$$\frac{\partial w}{\partial t}=\frac{\partial}{\partial x}\left(\kappa\frac{\partial w}{\partial x}\right)+\frac{\partial}{\partial x}\left(\frac{\delta}{\rho_w}\frac{\partial p_v}{\partial x}\right)$$

$$\frac{\partial C_c}{\partial t}=\frac{\partial\left[w\left(C_f-C_{f,sat}\right)\right]}{\partial t}H\left(C_f-C_{f,sat}\right)$$

where C_c is the amount of crystallized salt [kg/m^3$_{\text{sample}}$], $C_{f,sat}$ is the saturated free salt concentration [kg/m^3$_{\text{solution}}$], H is the Heaviside step unit function, H(x≥0)=1, H(x<0)=0, δ the water vapor diffusion permeability [s], p_v the partial pressure of water vapor [Pa], and ρ_w the density of water [kg/m^3].

The mathematical model was solved using the Galerkin finite element approach, and a computational implementation is performed. In the parameter identification process, a salt solution suction experiment from a free salt solution level into a dry specimen was proposed for the determination of moisture diffusivity as a function of moisture content and salt diffusion coefficient as a function of salt concentration.

The computational model was then verified in both wetting and drying experiments, which were performed partially by Z. Pavlík and M. Pavlíková at CTU Prague and partially by L. Pel at TU Eindhoven (see [3] for details).

In the wetting experiment, 1M-NaCl solution suction into sandstone samples was chosen. The chloride binding isotherm of sandstone was measured first. The samples of sandstone with the dimensions of 20 x 40 x 160 mm were then subjected to 1-D chloride solution penetration and moisture profiles and chloride concentration profiles were determined for the suction times of 30, 60 and 90 minutes. Moisture diffusivity and chloride diffusion coefficient were then calculated. At the verification of the numerical stability of the parameter identification process of the applied coupled moisture and salt transport model, a forward analysis was performed. The moisture diffusivity and chloride diffusion coefficient were substituted into the computational implementation of the model and moisture and free chloride concentration profiles were calculated for the suction times of 30, 60 and 90 minutes exactly as in the experiments. The results showed that the calculated moisture and chloride concentration profiles agreed reasonably well with the measured profiles, the differences were well within the error range of the measuring methods.

In the drying experiment, the sandstone samples were saturated first by 3M-NaCl solution. Then, the drying process was started in an environment with a relative humidity close to 0%. Moisture and free chloride concentration profiles were measured every two hours using the NMR technique. In the computational simulations, moisture diffusivity, chloride diffusion coefficient and moisture transfer coefficient were the free parameters which were supposed to be fitted according to the experimental data. The least square method was used for the assessment of simulated data in the particular cases. The agreement between the measured and calculated moisture and chloride concentration profiles was in the drying experiment worse than in the wetting experiment which was an expected result, taking into account the uncertainties in the parameter identification process in the drying phase. However, still the differences were within reasonable limits so that the model could be considered as applicable for the prediction of moisture and salt concentration profiles.

It can be concluded that the modified diffusion-advection model of coupled moisture and salt transport in porous materials including water vapor transport and salt crystallization presented in the paper seems to be the most suitable option in the current state of modeling salt transport, particularly taking into account the availability of the necessary input data for computational modeling. The model can avoid both the oversimplifications such as the assumption of linear salt diffusion problem without water flow effect which application could result in significant distortion of physical reality and the too high complexities connected with an application of fully coupled heat, moisture, salt and momentum transport models which could face almost irresolvable problems with the accuracy of necessary input parameters.

References:

[1] PEL L., KOPINGA K., KAASSCHIETER E.F.: *Saline absorption in calcium-silicate brick observed by NMR scanning.* J. Phys. D: Appl. Phys, Vol. 33, 2000, 1380-1385.

[2] BEAR J., BACHMAT Y.: *Introduction to Modelling of transport Phenomena in Porous Media.* Dordrecht, Kluwer, 1990.

[3] PEL L., ČERNÝ R., PAVLÍK Z.: *Moisture and Ion Transport. WP5 2-Years Report of the EU 6 th Program Project SSPI-CT-2003-501571.* TU Eindhoven, 2006.

This research has been supported by EC within the 6th Framework Programme, under contract No SSPI-CT-2003-501571 .

Modeling of hardening, softening and critical state of fine grained soils

T. Janda

tomas.janda@fsv.cvut.cz

Department of Mechanics, Faculty of Civil Engineering, Czech Technical University in Prague, Thákurova 7, 166 27 Prague 6, Czech Republic

Apart from almost classical models such as Mohr-Coulomb or Drucker-Prager elasto-plastic models, there exists a number of more advanced constitutive models enable to predict fundamental aspects of grainy materials. The widely used approach for the prediction of mechanical response of fine grained soils is to follow the concept of critical state. This concept suggests that for every stress state there is a certain critical void ratio the soil reaches after sufficiently large shearing. To arrive at the critical state the material can either contract or dilate depending on the value of the initial void ratio. The contraction or dilatation behavior results in hardening or softening change of the elastic stiffness.

The concept of the critical state of soil material was first introduced by Hvorslev and further developed by Roscoe and his co-workers to eventually arrive at the formulation of modified Cam clay model (MCC) [1]. The model can address, at least qualitatively, most of the characteristics of the real soil behavior including hardening or softening and the final collapse of soil when reaching the critical state. Nevertheless, it has been suggested in the literature that the original formulation suffers from a number of drawbacks particularly on the dilation part predicting unrealistic softening behavior that occurs for heavily overconsolidated materials.

The motivation for the formulation of the generalized Cam clay model (GCC) is to eliminate some of the drawbacks that modified the Cam clay suffers from. The major limitation of the modified Cam clay model is the unrealistic softening predicted for heavily overconsolidated soils. In such conditions a more reliable results are provided by the Mohr-Coulomb model. Therefore the natural approach is to combine these two failure criterions to create a new yield surface.

Generalized Cam clay model introduces a reduced the yield surface at the supercritical side. Since for the overconsolidated soils the Mohr-Coulomb model gives reasonable results the shape of the yield surface is changed in the way to fit approximately the Mohr-Coulomb hexagonal cone. In particular, the proposed yield surface is composed of two smoothly connected surfaces. The smooth connection is located on the critical line, thus the softening behaviour found for heavily overconsolidated soils is govern by different yield function and plastic potential than for normally consolidated material. The features introduced into the generalized Cam clay model cover only the changes of the yield function and plastic potential. The stress strain relationship - the bilinear diagram of isotropic consolidation - remains unchanged. Since the stress strain relationship is identical for both models, the hardening/softening rule remains unchanged too. The formulation of hardening/softening modulus differs for the subcritical (compression) and supercritical (dilatation) sides. One of the advantages of the generalized formulation lies in the use of standard material parameters. In the new formulation the parameters of modified Cam clay model - compression modulus, swelling modulus, initial void ratio and inclination of the critical state line are supplemented by peak friction angle and cohesion well known from the Mohr-Coulomb model.

The implementation of plasticity model into the finite element program requires an algorithm that evaluates stress increment for a given strain increment. This procedure, known

as the stress-return algorithm, should also find the elastic and plastic parts of the strain increment and ensure the satisfaction of consistency condition. Because the set of equations which have to be satisfied at the end of the load step is nonlinear the stress-return algorithm can not be expressed explicitly and performed in a single step. The usual way to carry out the stress-return in such a case is to employ one of the numerical approaches. Here the Newton-Raphson iteration scheme is used for both models [4].

To verify the predictive capabilities of the new formulation a number of examples was performed. The conventional triaxial shear test is carried out to highlight the major differences in the MCC and GCC models. The triaxial shear test has several advantages. First, there exists an analytical solution for the modified Cam clay and thus the numerical implementation can be compared to the accurate results. Next, the stress and strain fields are homogenous all over the soil sample and the attention can be focused only on the material point. Finally, the stress path during triaxial shear test is known in advance, which allows to control the position of its intersection with the yield function. To clarify the development of the yield surface during the tests it is convenient to plot the results in the stress space. Particularly the path of the total and effective stress, the pore pressure and the yield function can be drawn in the space σ_m - J. In the case of triaxial extension, the slope of critical state line of the generalized Cam clay model is less steep. This relates to the fact that the surface depends on the Lode angle [3] and is inscribed to the modified Cam clay model. As the normally consolidated soil started to yield the negative plastic strain appeared and the material started to harden. The yield surface expands to finally arrive at the critical state. The effective stress path bends to the right and ends at the critical state line. For a heavily overconsolidated sample the stress path reaches the yield surface at the supercritical side. Here a positive volumetric plastic strain is generated and the material softens. The dilatation causes the decrease in pore pressure and the effective stress path bends to the right. Such a qualitatively various behavior for differently consolidated soils was observed experimentally in [2].

The influence of shape of the yield function in the deviatoric plane [3] is examined next by solving the problem of foundation strip settlement. The result of this analysis provides the variation of the vertical displacement as a function of the applied load. The collapse load predicted by the GCC modeling is considerably smaller when compared to that one found with the MCC model. This is attributed to the fact that the Lode angle dependent yield surface of the GCC model turns on the plastic deformations at much early stages of loading since being essentially inscribed into the circular surface of the MCC model. The obtained results demonstrate the importance of the shape of the yield function in the deviatoric domain. Similar analysis in this field is provided in [2].

References:

[1] ROSCOE, K. H. – BURLAND, J. B.: *On the generalised behaviour of 'wet' clay* Cambridge University Press, 1968, pp. 535–609.

[2] POTTS, D. M. – DRAVKOVIČ, L.: *Finite element analysis in geotechnical engineering - - theory* Thomas Telford, London, 1999.

[3] LADE, P. V. – KIM, M. K.: *Single hardening constitutive model for frictional materials I. Plastic potential function* Computers and Geotechnics, 1988, pp. 307–324.

[4] GROEN, A. E.: *Three-dimensional elasto-plastic analysis of soils* Technical University Delft, 1997.

This research has been supported by AV ČR grant No. 1ET410430156.

Properties of Fiber Reinforced Cement Composites during High-Temperature Exposure

E. Mňahončáková*, P. Tesárek, P. Konvalinka, R. Černý**

tesarek@fsv.cvut.cz

*Czech Technical University, Faculty of Civil Engineering, Department of Physics, Thákurova 7, 166 29 Praha 6, Czech Republic

Czech Technical University, Faculty of Civil Engineering, Department of Mechanics, Thákurova 7, 166 29 Praha 6, Czech Republic

**Czech Technical University, Faculty of Civil Engineering, Experimental Center, Thákurova 7, 166 29 Praha 6, Czech Republic

Glass-fiber reinforced cement composites (GFC) are produced by incorporating a small amount of alkali-resistant glass fiber in cement mortar to overcome the traditional weakness of inorganic cements, namely poor tensile strength and brittleness (see, e.g., [1]-[3]). The length and content of the glass fiber reinforcement can be chosen to meet the strength and toughness requirements of the product. Also, the type of aggregates can be varied in order to control thermal properties. GFC are often employed in severe conditions. These might be exposed for instance to high temperatures and/or high mechanical loads. However, their thermal and hygric properties are mostly measured in laboratory conditions only, so that designers cannot take into account the changes in their material parameters during and after loading. In this paper, basic thermal properties, namely, the thermal diffusivity, specific heat capacity, thermal conductivity and linear thermal expansion coefficient of high-density glass fiber reinforced cement composite are determined as functions of temperature up to 1000^0C.

The specimens of the glass fiber reinforced cement composite were produced in the laboratories of VUSTAH Brno. The composition of the material was as follows (calculated among the dry substances only): Portland cement CEM I 52.5 54%, sand 0-1 mm 40%, microsilica 3%, alkali-proof glass fiber 12 mm long 3%. Water in the amount corresponding to the w/c ratio of 0.33 was added to the mixture. The samples were produced using a successive homogenization procedure. First, sand and microsilica were homogenized in a mixing device, then cement was added and the dry mixture was homogenized again. The dry well homogenized mixture was thoroughly mixed with water. Finally, the glass fibers were added and the mixture shortly mixed again. The prepared mixture was cast into the molds and vibrated. The samples for the measurement of particular material parameters had the following dimensions: thermal diffusivity and specific heat capacity - 71x71x71 mm, linear thermal expansion – 40x40x120 mm. For every pre-treatment, 3 specimens were used for testing. Before the measurements of all parameters, all specimens were dried in an oven at 110 °C. In the experiments, four various sample pre-treatment conditions were tested: reference specimen not exposed to any load, specimen exposed to a gradual temperature increase up to 600, 800 and 1000^oC during two hours, then left for another 2 hours at the final temperature and slowly cooled.

The measurements of basic parameters of the studied material depending on the loading temperature were done using the vacuum water saturation method. The most important change in porosity occurred between the unloaded state and the loading temperature of 600^0C where the increase of porosity was as high as 40%. Later porosity changes were lower than 10%. This is in accordance with the behavior of most Portland cement based

composite materials where the most important chemical reaction in the high temperature range is decomposition of calcium hydroxide at about 460-480^{0}C.

High-temperature measurements of thermal diffusivity were performed using a double integration method which employs measured temperature profiles at one-sided heating. The values of thermal diffusivity increased with both the increasing actual temperature and the increasing pre-heating temperature, particularly in the range of higher temperatures. The most probable reason for these findings was an inclusion of the convective and radiative modes of heat transfer into the values of thermal diffusivity which, due to the transient character of measurements and the occurrence of high temperature gradients in the measured specimens, was not a common Fourier thermal diffusivity but an apparent thermal diffusivity. However, from a practical point of view this does not seem to be a flaw because any appearance of high temperatures in a building structure is often accompanied by high temperature gradients.

The specific heat capacity vs. temperature relation was determined using a nonadiabatic technique. In the low-temperature range to approximately 300^{0}C, an increase of specific heat capacity was observed but for higher temperatures the changes were very low and the specific heat capacity remained almost constant. The small decrease of specific heat capacity for temperatures higher than 400^{0}C can be attributed to the partial loss of mass due to the decomposition of calcium hydroxide.

The thermal conductivity as function of temperature $\lambda(T)$ was calculated on the basis of measured thermal diffusivity $a(T)$, specific heat capacity and bulk density. The shapes of the $\lambda(T)$ functions were very similar to those of $a(T)$ functions. This is a consequence of the more remarkable dependence of thermal diffusivity on temperature in a comparison with the specific heat capacity and bulk density.

The results of measurements of the linear thermal expansion coefficient α showed that in the range of lower temperatures the measured data corresponded well with the common α values known for cement mortar and concrete, and also for higher temperatures the observed changes were not very dramatic. The minima at approximately 500^{0}C and 800^{0}C may be a consequence of decomposition reactions in the cement binder, namely calcium hydroxide in the first case and calcium carbonate in the second.

It can be concluded that the measurements of temperature dependence of the thermal conductivity and specific heat capacity of the glass fiber reinforced cement composite in this paper have shown that the decomposition of calcium hydroxide was the principal factor affecting the behavior of thermally loaded specimens. For the fire protection of building structures, the measured results indicate that the heat transfer in the studied material was accelerated once temperature achieved 500-600^{0}C which might be dangerous because the fire-protecting ability of such a structure decreases compared to the values calculated with data measured at lower temperatures. Using the high-temperature data in the evaluation of fire-protecting abilities of such structures is therefore highly recommended.

References:

[1] MAJUMDAR A.J., V. LAWS: *Glass Fibre Reinforced Cement.* BSP, Oxford 1991.

[2] YOUNG J.: *Designing with GRC.* Architectural Press, London 1978.

[3] TRUE G.: *GRC Production and Uses.* Palladian Publications Ltd., London 1986.

This research has been supported by the Czech Science Foundation, under grant No. 103/06/1474.

Carbon Layers Doped with Erbium or Erbium and Ytterbium Ions

V. Prajzler, I. Hüttel*, J. Špirková*, J. Oswald,
V. Peřina ***, Jiri Zavadil****, Z. Burian**

Vasek.Prajzler@email.cz

Department of Microelectronics, Faculty of Electrical Engineering,
Czech Technical University,
Technická 2, 166 27 Prague 6, Czech Republic

* Institute of Chemical Technology,
Technická 5, 166 28, Prague 6, Czech Republic

** Institute of Physics, Academy of Sciences,
Cukrovarnická 10, Prague 6, Czech Republic

*** Institute of Nuclear Physics, Academy of Sciences,
Řež near Prague, Czech Republic

**** fInstitute of Radio Engineering and Electronics, Academy of Sciences of the Czech Republic, Chaberska 57, 182 51 Prague, Czech Republic;

Carbon layers have attracted the attention of various investigators due to their unique optical, electrical and mechanical properties [1], [2]. The research on deposition of carbon layers is mainly focused on fabrication of diamond-like carbon (DLC) or carbon nanotubes. In this case the research was focused on development of carbon layers which ought to have good optical properties in potential application for integrated optics. In the publication [3] was shown that it is possible to prepare carbon planar waveguides with attenuation less than 1 dB/cm. Low optical losses of the optical materials are one of the most important preconditions for using this material in integrated optics and for doping this material by active ions such as erbium.

Erbium doped materials exhibits luminescence at 1 530 nm which overlaps the minimum loss region of silica-based fibers used in optical communications. This wavelength is commonly used in the fiber optics telecommunication systems. For this purpose the research was focused on the preparation and the investigation of carbon layers containing erbium ions. For this reason it was decided to investigate the preparation of carbon layers containing erbium or erbium and ytterbium ions.

The carbon layers were deposited by RF magnetron sputtering (*Balzers Pfeiffer PLS 160*) using carbon target of 99.9999% purity. The typical growth parameters were: the deposition temperature 300 K, Ar or Ar + CH_4 gas mixture, total gas pressure from 1 to 4 Pa and the growing time ranged from 30 min to 4 hrs at power from 50 W to 150 W (13.56 MHz). For Er^{3+} and Yb^{3+} doping into the carbon samples the powder of Er (99.9% purity) and Yb (99.9% purity) was placed onto the top of the carbon target.

The compositions of the fabricated samples were determined by nuclear chemical analysis as Rutherford Backscattering Spectroscopy (RBS) and Elastic Recoil Detection

Analysis (ERDA). The evaluations of RBS and ERDA spectra were done by GISA3 and SIMNRA code, respectively. The analysis proved that the samples contained carbon, argon, oxygen, hydrogen, erbium and ytterbium ions. As Er and Yb have very close values of atomic weights these two elements cannot be distinguished in the RBS spectra, thus only sum of both elements can be obtained. The amount of the incorporated erbium and ytterbium ions differed depending on the area of the target covered by erbium powder laid on the target as well as on the erosion area represented by the part of the surface covered by the RE ions. The samples had a total erbium + ytterbium content ranged from 1 to 20 at %. The highest concentration (20 at %) of erbium and ytterbium ions was found in the sample doped using the mixture of 0.0502 g of erbium and 1.0001 g of ytterbium powder.

Transmission spectra of the samples were measured in the spectral region from 400 nm to 1100 nm under room temperature. The transmission spectra shown typical strong $^2H_{11/2}$ transitions which correspond to optical materials doped with erbium ions. There was not observed peak around 980 nm in carbon layers co-doped by Yb^{3+}. This wavelength corresponds to $^2F_{5/2}$ transition (the strongest transition for Yb^{3+} doped optical materials). It assumes that it is due to the low Yb^{3+} concentration. The photoluminescence measurement was carried out at two excitation wavelengths: Ar ion lasers operating at λ_{ex} = 514.5 nm (under temperature 4 K), E_{ex}= 300 mW and semiconductor laser P4300 operating at λ_{ex} = 980 nm, E_{ex}= 500 mW (under room temperature). The FEU62 photocell was used for detection of the wavelength from 500 nm to 1 000 nm, while the Ge detector was used for the wavelength from 1 000 nm to 1 600 nm. The reference chopper frequency was 75 Hz. Er^{3+} doped carbon layers exhibited photoluminescence peak at 1 530 nm under optical pumping at 514.5 nm. This peak corresponds to Er^{3+} to the $^4I_{13/2} \rightarrow {}^4I_{15/2}$ transition. There was observed only a weak peak at 1 530 nm under the optical pumping at 980 nm. It was also observed that Yb^{3+} co-doping does not increase the photoluminescence intensity. This result was not expected and it was supposed it was due to a low Yb^{3+} concentration.

One of the major problem encountered in our research was that fabricated erbium doped carbon layers contained oxygen and hydrogen traces. OH impurities are known to be a strong quencher of Er^{3+} luminescence. The next research will be focused on the fabrication of carbon layers with a lower level of oxygen and hydrogen contamination. It is expected that the lower content of the contaminants will improve the photoluminescence at 1 530 nm.

References:

[1] A.R. ALVES, J.F. ROSSETTO, O. BALACHOVA: *Some Optical Properties of Amorphous Hydrogenated Carbon Thin Films Prepared by RF Plasma deposition using Methane,* Microelectronics Journal (32): 9, 2001, pp. 783-786.

[2] E. TOMASELLA, C. MEUNIER, S. MIKHAILOV: *a-C:H Thin Films Deposited by Radio-Frequency Plasma: Influence of Gas Composition on Structure, Optical Properties and Stress Levels* Surface and Coatings Technology (141): 2-3, 2001, pp. 286-296.

[3] I. HÜTTEL, J. GUROVIČ, F. ČERNY, J. POSPIŠIL: *Carbon and carbon nitride planar waveguides on silicon substrates* Diamond and Related Materials 8, 1999, pp. 628–630.

Our research is supported by the Grant Agency of the Czech Republic under grant number 102/06/0424 and the research program MSM6840770014 of the Czech Technical University in Prague.

Polymer Optical Planar Waveguides Doped by Erbium Ions

V. Prajzler, I. Hüttel*, J. Špirková*, M. Myslík, O. Hlaváč, L. Oleksiy* Z. Burian, V. Jeřábek

Vasek.Prajzler@email.cz

Department of Microelectronics, Faculty of Electrical Engineering,
Czech Technical University,
Technická 2, 166 27 Prague 6, Czech Republic

* Institute of Chemical Technology,
Technická 5, 166 28, Prague 6, Czech Republic

Photonics devices and optical waveguides play very important role in integrated optics and optoelectronics. Up to now many different waveguide materials have been used for these purposes. The most often used materials are semiconductors such as silicon, gallium arsenide, gallium phosphate, gallium nitride, indium phosphate and etc., also dielectric materials such as lithium niobate, sapphire, lithium tantalite and optical glasses. These materials have suitable properties for the thought applications but the fabrication process of the optical devices is not simple and it is also rather expensive. Nowadays photonics devices are based on new materials such as organics and polymers like Polymethylmethacrylate (PMMA), Polysthyrene (PS), Polyfluoromethacrylate (PFMA), Polydimethylsiloxane (PDMS), Epoxy Novolak Resin (ENR, formally named as NANOTM SU8 2000) and etc. [1] and new methods are used to fabricate polymer optical devices include photocrosslinking, photobleaching, reactive ion etching, photolocking, laser/electron beam writing, and nowadays also LIGA-like process [2]. Optical components based on polymers are specially attractive due to simple fabrication process and low cost. Erbium doped optical materials are of great interest in field of optical communications because they operating at 1 550 nm. This wavelength is a standard telecommunication wavelength with a big potential on a data communication field.

Our polymer optical waveguides were theoretically designed by using mathematical modification of the dispersion equation [3]. We determined the number of guided modes and critical thickness of the waveguides. After that the polymer layers were fabricated by spin coating on silicon and silica-on silica substrates.

Present experiments were performed on Polymethylmethacrylate (PMMA). For the coating the small pieces of PMMA (Goodfellow) have been melting in chloroform for a few days. For erbium doping it was used $ErCl_3$ or ErF_3 melting in C_5H_9NO. The drawing of the spin-coating set-up and the design of the optical waveguides were previously described in [4].

The properties of the fabricated layers were analyzed by various methods. The refractive indices of the samples were determined by refractometer at wavelength range from 200 nm to 800 nm and by a prism coupling method at 632.8 nm. The optical losses were evaluated by scanning the light scattered from the waveguides by the CCD camera. The absorption spectra were taken at wavelength range from 300 nm to 600 nm. The film thickness was measured by a profilmeter Talystep (Taylor&Hobson).

The photoluminescence measurement was carried out at two excitation wavelengths:

- Ar laser ILA-120 operating at λ_{ex} = 488 nm, E_{ex}= 100 mW,
- Semiconductor laser P4300 operating at λ_{ex} = 980 nm, E_{ex}= 500 mW.

The FEU62 photocell was used for detection of the wavelength from 500 nm to 1 000 nm, while the Ge detector was used for the wavelength from 1 000 nm to 1 600 nm. The reference chopper frequency was 75 Hz. All the luminescence measurements were performed at the room temperature.

The fabricated samples had a thickness around 1 μm and had a good optical quality. It was observed a peak attributed to the Er^{3+} transition at wavelength around 530 nm. The polymer layers doped with $ErCl_3$ melting in C_5H_9NO did not exhibit the emission at 1 530 nm. Better results were achieved with polymer samples doped with ErF_3. The samples exhibited the typical emission at 1 550 nm due to the Er^{3+} intra-4f $^4I_{13/2} \rightarrow {}^4I_{15/2}$ transition. The next research will be focused on the investigation of optical properties erbium doped polymer layers co-doped with ytterbium ions.

References:

[1] H. MA, A.K.Y. JEN, L.R. DALTON: *Polymer-Based Optical Waveguides: Materials, Processing, and Devices,* Advanced Materials (14): 9, 2002, pp. 1 339-1 365.

[2] B.L. BOOTH: *Low-Loss Channel Wave-Guides in Polymers,* Journal of Lightwave Technology (7): 10, 1989, pp. 1 445-1 453.

[3] R.G. HUNSPERGER: *Integrated optics Theory and Technology,* Springer, fifht Edition 2002.

[4] M. PRAJER, V. PRAJZLER: *Polymer Optical Planar Waveguide,* 8th International Student Conference on Electrical Engineering, POSTER 2004 pp. NS19.

This research has been supported by GA ČR grant No. 102/06/0424 and the research program MSM6840770014 of the Czech Technical University in Prague .

Gallium Nitride Layers Doped by Er3+ or Er3+ / Yb3+ by Ion Implantation

V. Prajzler, I. Hüttel*, E. Alves, Ch. Buchal ***, J. Špirková*, J. Oswald****, V. Peřina *****, H. Boldyryeva*****, V. Machovič*, Z. Burian**

Vasek.Prajzler@email.cz

Department of Microelectronics, Faculty of Electrical Engineering,
Czech Technical University,
Technická 2, 166 27 Prague 6, Czech Republic

* Institute of Chemical Technology,
Technická 5, 166 28, Prague 6, Czech Republic

** Instituto Tecnológico e Nuclear, EN10, 2686-953 Sacavém, Portugal

*** Institut für Schichten und Grenzflächen (ISG1), Forschungszentrum Jülich,
D-52425, Julich, Germany

**** Institute of Physics, Academy of Sciences,
Cukrovarnická 10, Prague 6, Czech Republic

***** Institute of Nuclear Physics, Academy of Sciences,
Řež near Prague, Czech Republic

Gallium Nitride (GaN) became one of the most promising wide band gap (3.4 eV) direct semiconductor materials for use in high power and high frequency transistors, UV photo detectors, light emitting diodes (LEDs) or laser diodes (LDs) [1], [2]. It was shown in [3] that the thermal quenching in Er-doped semiconductors decreases with increasing bandgap. Therefore, wide-bandgap semiconductors such as GaN are attractive hosts for the Rare Earth (RE) elements. There are three possibilities how to obtain GaN layers doped by RE ions. The first possibility is to use the process called "doping in situ". For this purpose is used Molecular Beam Epitaxy (MBE). When it is used MBE it is necessary used Ultrahigh-Vacuum (UHV). The second possibility is to fabricate GaN layers by Metal Organic Chemical Vapor Deposition (MOCVD) and then to dope these layers by using ion implantation. The next method for doping GaN layers by RE ions is diffusion. But this method has a limited use mainly due to a low diffusivity of RE ions and that is why this technique is not commonly applied.

In our case we used GaN layers (TDI Inc. Company) deposited by MOCVD on sapphire substrate and doped with Er^{3+} or Er^{3+} and Yb^{3+} ions by ion implantation. The doping was done by implantation energy of 190 keV or 210 keV at room temperature or 300 keV at temperature of 450 °C. With applied doses from $1 \cdot 10^{13}$ Er·cm^{-2} to $5 \cdot 10^{15}$ Er·cm^{-2} and from $1 \cdot 10^{14}$ Yb·cm^{-2} to $5 \cdot 10^{16}$ Yb·cm^{-2}. After the implantation the samples were annealed at temperatures around 800 °C under flowing nitrogen for 30 minutes.

The structure of GaN layers was investigated by XRD and samples had single crystalline hexagonal wurtzite structure. GaN sample doped by erbium or erbium and

ytterbium did not imply any structural changes. The compositions of the fabricated samples were determined by Rutherford Backscattering Spectroscopy (RBS) and Elastic Recoil Detection Analysis (ERDA). The erbium and ytterbium ions have very close values of atomic weights. These two elements cannot be distinguished in the RBS spectra, thus only sum of both elements can be obtained. Therefore, erbium and ytterbium concentrations were simulated by using the GISA program as Thulium (Tm; $M_{Er} + M_{Yb} = M_{Tm}$) and the range of the RE total content (sum of Er and Yb) spread from 0.02 to 3.38 at %, depending on the actual Er or Yb implantation dose.

Transmission spectra of the samples in the spectral region from 400 nm to 1 000 nm at room temperature were taken as well. We observed only a weak peak attributed to the Er^{3+} transition. There was not noticed any transition of the Yb^{3+} ions at 980 nm ($^2F_{5/2}$) with the erbium doped GaN layers co-doped by Yb^{3+} ions, probably because the absorption coefficients for ytterbium ions were very low. The optical losses were measured by a scattering detection method. The reference (un-doped) GaN had the optical losses lower than 2 dB/cm. The optical losses after the ion implantation and subsequent annealing increased above 10 dB/cm. It was expected that optical losses will be lowered again after annealing at temperature 1000 °C, as it will result in more homogeneous distribution of the incorporated ions. This will be put under further investigation. The photoluminescence measurement was carried out at two excitation wavelengths: He-Ne ion lasers operating at λ_{ex} = 632.8 nm and semiconductor laser P4300 operating at λ_{ex} = 980 nm. The samples exhibited typical photoluminescence bands attributed to erbium $^4I_{13/2} \rightarrow {}^4I_{15/2}$, which intensities increase with increasing implantation dose. Obviously, co-doping with ytterbium ions increases the intensity of the luminescence. The best results were obtained when it was used an implantation dose $1 \cdot 10^{15}$ Er·cm^{-2} and $1 \cdot 10^{15}$ Yb·cm^{-2} and applied energy of 300 keV.

The next research will be focused on the investigation of the post-implantation annealing of the samples at the temperature above 900 °C. It is supposed that it will help to improve the intensity of the luminescence. The properties of erbium or erbium and ytterbium implanted into GaN samples we were presented in paper [4].

References:

[1] S.J. PEARTON, J.C. ZOLPER, ET AL.: *GaN: Processing, Defects, and Devices,* Journal of Applied Physics (86): 1, 1999, pp. 1-78

[2] H. MORKOC, S. STRITE, ET AL.: *Large-Band-Gap SiC, III-V Nitride, and II-VI ZnSe-Based Semiconductor-Device Technologies,* Journal of Applied Physics (76): 3, 1994, pp. 1 363-1 398.

[3] P.N. FAVENNEC, H. LHARIDON, ET AL.: *Luminescence of Erbium Implanted in Various Semiconductors - IV-Materials, III-V-Materials and II-VI Materials,* Electronics Letters 25: (11), 1989, pp. 718-719.

[4] V. PRAJZLER, E. ALVES, CH. BUCHAL, ET AL.: *Optical Properties of Er3+ + Yb3+ Doped Gallium Nitride Layers,* SPIE Optics&Photonics, San Diego, (6286), ISSN 0277-786X, ISBN 0-8194-6365-5, 2006, pp. 62860K-1 - 62860K-10.

This research is supported by the Grant Agency of the Czech Republic under grant number 102/06/0424 and the research program MSM6840770014 of the Czech Technical University in Prague and partly also by Ministry of Education, Youth and Sports of the Czech Republic number LC6041.

Fracture Toughness Testing of Iron Aluminides Based Intermetallic Alloys

P. Haušild*, M. Karlík*, A. Kubošová*, J. Prahl*, M. Ropars**

Petr.Hausild@ fjfi.cvut.cz

* Department of Materials, Faculty of Nuclear Sciences and Physical Engineering, Czech Technical University, Trojanova 13, 120 00 Praha 2

** Laboratoire Génie Mécanique et Matériaux, Université de Bretagne Sud, Rue Saint Maudé, 56321 Lorient, France

Iron aluminides based on FeAl and Fe_3Al exhibit superior corrosion resistance to high-temperature oxidation and sulfidation, good wear resistance, low density of ~5.6 $g.cm^{-3}$ (FeAl) and 6.7 $g.cm^{-3}$ (Fe_3Al) respectively, ease of fabrication and relatively low cost reducing the amount of Ni and Cr indispensable in common high-temperature stainless steels or nickel superalloys. These properties offer a potential for several uses such as heating elements, furnace fixtures, heat-exchanger piping, sintered porous gas-metal filters, automobile and other industrial valve components, catalytic converter substrates and components for molten salt applications [1].

The potential applications of iron aluminides were limited for a long time by their poor room temperature (RT) ductility resulting mainly from environmental hydrogen embrittlement. The RT ductility can be enhanced by chromium alloying with a usual amount ranging between 2 and 6 at.%. Chromium decreases the energy of antiphase boundaries and improves mobility of dislocations resulting in the increase of ductility. The addition of chromium also results in the formation of a protective Cr_2O_3 oxide layer on the surface. Consequently, the environmental embrittlement is softened.

Although the influence of the environment and alloying elements on tensile properties of iron aluminides such as strength and ductility is widely reported, very little work has been published on the fracture toughness. In this paper, the methodology of fracture toughness testing of intermetallic alloys based on FeAl and Fe_3Al has been developed. The preliminary study was undertaken on the alloy with the chemical composition of Fe-16.8Al-2.58Cr-1.21Zr-0.05C (wt.%) [2,3].

The fracture toughness tests were performed on a computer–controlled servohydraulic loading machine INOVA ZUZ 50 equipped with a resistance-heated furnace. The tests were performed at the constant crosshead speed of 0.25 mm/min according to the norm ASTM E 1820. Half inch Compact Tension (CT) specimens of thickness B=12.5mm and width W=25mm were machined in perpendicular to the rolling direction. The specimens were annealed for 2h at 700°C before testing. The experiments were performed at 20, 200, 400, and 600 °C. At RT the specimen thickness varied from 3.5 to 12.5mm in order to account for the effect of size on fracture toughness. Since the material is coarse grained and it is very difficult to distinct the boundary between fatigue crack propagation and final static rupture (fracture morphology of final static failure is very similar to the morphology of fatigue fracture), the specimens were not precracked using cyclic loading but using electroerosion by a wire of diameter 0.3 mm. The crack length-specimen width ratio a/W was about 0.55. The crack growth during the fracture toughness test was monitored by temperature independent potential method using TECHLAB SRT-2K device controlled by Fatigue Crack Growth Monitor software.

The fracture toughness K_Q has been measured from the load *vs.* load-line displacement. The values of fracture toughness are given in table 1. The fracture toughness increases from about 27 MPa.m$^{1/2}$ at RT to about 42 MPa.m$^{1/2}$ at 400°C. With further increase of temperature, the fracture toughness decreases (at 600°C K_Q=30.5 MPa.m$^{1/2}$).

The specimen dimensions did not allowed to fulfill the plane strain conditions during the tests. However, at RT the specimen thickness has only very low effect on the fracture toughness values.

Table 1 Values of fracture toughness K_Q measured at 20, 200, 400, and 600°C

T (°C)	a (m)	a/W	K_Q (MPam$^{-1/2}$)
20	0.014	0.56	26.51
20	0.01445	0.578	28.20
200	0.0137	0.548	34.30
200	0.01375	0.55	30.48
400	0.0136	0.544	39.70
400	0.0139	0.556	42.74
400	0.0137	0.548	41.77
600	0.01425	0.57	30.83
600	0.01385	0.554	30.49

The fractographic analysis showed that the fracture surfaces of specimens fractured at 20, 200 and 400°C exhibit transgranular cleavage facets, while on the fracture surfaces of specimens fractured at 600°C the ductile dimpled fracture predominates.

The developed methodology of fracture toughness testing will be used for testing of new alloy for high temperature applications based on Fe-40(at.%)Al.

[1] WESTBROOK, J. H. – FLEISHER, R.L.: Intermetallic Compounds. John Wiley, New York, 1995.

[2] PRAHL, J. – HAUŠILD, P. – KARLÍK, M. – CRENN, J.-F.: *Fracture behaviour of Fe_3Al alloy with additions of Zr and C at different temperatures*, Kovové materiály – Metallic Materials, 43, 2005, pp. 134-144.

[3] KUBOŠOVÁ, A.: *Lomové vlastnosti uspořádaných slitin na bázi Fe_3Al,* Diploma thesis - Department of Materials, Faculty of Nuclear Sciences and Physical Engineering, Czech Technical University, 2006.

This research has been financially supported by the Grant Agency of the Czech Republic in the frame of the project No. 106/06/0019.

Comparison of Several Computational Models of Coupled Heat and Moisture Transport

J. Maděra, R. Černý

madera@fsv.cvut.cz

Department of Mechanics, Faculty of Civil Engineering, Czech Technical University, Thákurova 7, 166 29 Praha 6, Czech Republic

According to the supposed main transport mechanism and the corresponding mathematical description, three basic groups of water and water transport models can be distinguished, namely the diffusion models, the convection models and the hybrid models. Convection models describe water transport in porous materials in a way, that water in the porous system flows through the particular channels similarly as for instance in pipes, where convection is the main transfer mechanism and gradient of pressure acts as the main driving force. This is probably the most natural way of describing this phenomenon. Therefore, this type of models appeared historically as the first. The diffusion theory of moisture transfer in porous materials is based on the assumption that moisture in liquid or gaseous phase penetrates through the porous system by a diffusion mechanism in a similar way as for instance in a system of two gases.

The first diffusion model used in the computational implementation of the problem of coupled heat and moisture transport was the model by Künzel [1]. The moisture and heat balance equations were formulated as

$$\frac{d\rho_v}{d\varphi}\frac{\partial\varphi}{\partial t} = div\left[D_\varphi grad\varphi + \delta_p grad(\varphi p_s)\right],$$

$$\frac{dH}{dT}\frac{\partial T}{\partial t} = div\left(\lambda gradT\right) + L_v div\left[\delta_p grad(\varphi p_s)\right],$$

where ρ_v is the partial moisture density, φ the relative humidity, δ_p the water vapor permeability, p_s the partial pressure of saturated water vapor in the air, H the enthalpy density, L_v the latent heat of evaporation of water, λ the thermal conductivity, and T is the temperature.

The simplified version of the general heat, moisture, air and salt transport model by Grunewald [2] was chosen as the second model which was also of diffusion-type. The moisture and heat balance equations were formulated as

$$\left[\rho_w - \rho_v + \frac{a}{R_v T}p_{vs}\frac{d\varphi}{dw}\right]\frac{\partial w}{\partial t} + \left[w\frac{d\rho_v}{dT} + \frac{a}{R_v T}\left(p_{vs}\frac{d\varphi}{dT} + \varphi\frac{dp_{vs}}{dT} - \frac{p_v}{T}\right)\right]\frac{\partial T}{\partial t} =$$

$$div\left[\left(\rho_w D_w + p_s\delta_p\frac{d\varphi}{dw}\right)grad\ w\right] + div\left[\left(\delta_p\frac{dp_s}{dT}\varphi + p_{vs}\delta_p\frac{d\varphi}{dT}\right)grad\ T\right]$$

$$\left[\rho_w u_w + u_v\left(\frac{a}{R_v T}p_{vs}\frac{d\varphi}{dw} - \rho_v\right)\right]\frac{\partial w}{\partial t} +$$

$$+\left[\rho_m\frac{du_m}{dT} + \rho_w w\frac{du_w}{dT} + \rho_v\frac{du_v}{dT}a + u_w w\frac{d\rho_w}{dT} + u_v\frac{a}{R_v T}\left(p_{vs}\frac{d\varphi}{dT} + \varphi\frac{dp_{vs}}{dT} - \frac{p_v}{T}\right)\right]\frac{\partial T}{\partial t} =$$

$$= div\left[\left(\rho_w D_w u_w + h_v p_{vs}\delta_p \frac{d\varphi}{dw}\right) grad\ w\right] + div\left[\left(\lambda + \delta_p \varphi h_v \frac{dp_{vs}}{dT} + \delta_p p_{vs} h_v \frac{d\varphi}{dT}\right) grad\ T\right]$$

where ρ_w is the water density, ρ_m the material density, δ_p the water vapor permeability, p_{vs} the partial pressure of saturated water vapor in the air, p_v the partial pressure of water vapor in the air, R_v the gas constant of water vapor, u_m the specific internal energy of the solid material, u_w the specific internal energy of the liquid water, u_v the specific internal energy of water vapor, a the relative volume ratio of the air in partially saturated material.

The third model used in the computational implementation of the problem of coupled heat and moisture transport was formulated according to the convection model of Philip and de Vries [3] which is based on the description of liquid water transport by the Darcy's equation. In the computational implementation, the innovated de Vries [4] version of the model where the heat flux was considered in a more complicated form was used. The balance equations in this innovated model look as follows:

$$\frac{\partial}{\partial t}\left(\rho_l w + a\rho_v\right) = div\left[\rho_l\left(D_{wl} + D_{wv}\right) grad\ w\right] + div\left[\rho_l\left(D_{Tl} + D_{Tv}\right) grad\ T\right] + \frac{\partial}{\partial z}\left(\rho_l K_l\right)$$

$$\frac{\partial}{\partial t}\left(\rho_s h_s + \rho_l h_l w + a\rho_v h_v\right) = div\left(\lambda\ grad\ T\right) - div\left[\rho_l h_l\left(D_{wl} grad\ w + D_{Tl} grad\ T\right)\right] -$$

$$- div\left[\rho_l h_v\left(D_{wv} grad\ w + D_{Tv} grad\ T\right)\right] - \frac{\partial}{\partial z}\left(h_l \rho_l K_l\right)$$

where h is the specific enthalpy and the diffusion coefficients D_w and D_T are formulated as

$$D_w = D_{wl} + D_{wv},\ D_T = D_{Tw} + D_{Tv},$$

where D_{wl} and D_{Tl} are the coefficients of water diffusion in the porous body induced by moisture gradient and temperature gradient, D_{wv} and D_{Tv} are the coefficients of water vapor diffusion induced by moisture gradient and temperature gradient.

The models described above were included into the computer simulation tool TRANSMAT.

Comparison three mathematical models were chosen simply computational analysis for brick wall. Results of analysis in this paper were showed significant differences in profiles relative humidity for diffusions models and convection model within the range 10 – 15%. These differences were caused very small accuracy measuring of hydraulic conductivity comparison with moisture diffusivity. Hydraulic conductivity is basic parameter of convective model and moisture diffusivity of diffusion models. Temperature profiles were very similarly for analysis three models.

References:

[1] KÜNZEL H.M. *Simultaneous Heat and Moisture Transport in Building Components* IRB Verlag 1995

[2] GRUNEWALD J. *Diffusiver und konvektiver Stoff- und Energietransport in kapillarporösen Baustoffen* TU Dresden 1997

[3] PHILIP J.R.,DE VRIES D.A. *Moisture movement in porous materials under temperature gradients* Transactions of the American Geophysical Union 1957 pp. 222-232

[4] DE VRIES D.A. *The theory of heat and moisture transfer in porous media revisited* International Jouranl of Heat and Mass Transfer 1987 pp. 1343-1350

This research has been supported by the GA ČR, under gran No. 103/06/P021 .

The Influence of Salt Ionic Concentration on Electro-osmotic Flow

L. Balík, T. Mejdr

balik@klok.cvut.cz

Department of Experimental and Measurement Methods, Klokner Institute, Czech Technical University in Prague

When electrodes are placed across clay mass and direct current is applied, water in the clay pore space is transported to the cathodically charged electrode by electro-osmosis. Electro-osmosis transport of water through clay is a result of diffuse double layer cations in the clay pores being attracted to a negatively charged electrode or cathode. As these cations move toward the cathode, they bring with them water molecules that clump around the cations as a consequence of their dipolar nature. In addition, the frictional drag of these molecules as they move through the clay pores help transport additional water to the cathode. The macroscopic effect is a reduction of water content at the anode and an increase in water content of the clay at the cathode. In particular, free water appears at the interface between the clay and cathode surface.

Six samples were tested. All samples were composed of solid and cohesionless phase and both phases were moistened by saltwater. Solid and cohesionless phases were placed in intercommunication position. Higher humidification was brought in cohesionless part of samples. Samples were embedded between positive and negative electrodes and the current voltage of 6 V was applied. Comparable initial values were moisture of cohesionless phases, moisture of solid phases, applied voltage, arrangements and material base of samples. Dissimilar initial values were salt concentration of embedded solutions into samples. Three type of saltwater (marked 1, 2, 3) were used for experiment. Saltwater were solution of salt ions (Cl^-, NO_3^{1-}, SO_4^{2-}) in distilled water. The concentration for type 1 was 0,075 % NaCl , 0,1% $NaNO_3$ and 0,5 % Na_2SO_4, for type 2 was 0,2 % NaCl , 0,25% $NaNO_3$ and 2 % Na_2SO_4 and for type 3 was 0,5 % NaCl , 0,5% $NaNO_3$ and 5 % Na_2SO_4. Samples 1 and 2 (brick 42 and 44) were moistened by solution 1 (test 1), samples 3 and 4 (brick 46 and 43) by solution 2 (test 2) and samples 5 and 6 (brick 45 and 41) by solution 3 (test 3). The capital evaluative criteria were total passed electric charge, total moisture decrease of solid phases and moisture decrease of solid particle which is in contact with anode.

Data evaluation didn´t approve explicit dependence between concentration of salt and transported water content. Total electric charge and moisture degrease of solid phases refer to possibility of increasing electro-osmotic flow with rising salt concentration, but this contention isn´t supported by moisture degrease in the area near the anode. The maximum volume of transported saltwater was in test 1 - 0, 9 g (it means 1, 2 % of inlayed moisture), in test 2 - 3, 59 g (it means 4, 7 % of inlayed moisture) and in test 3 - 7, 2 g (it means 9,4 % of inlayed moisture). Maximal passed charge in test 1 was 587 C, in test 2 was 663 C and in test 3 was 1027 C. Maximal moisture degreasing in area near anode was in test 1 - 0,43 g, in test 2 - 4,33 g and in test 3 - 3,54 g. The concave shape of moisture distribution in solid phase and great moisture degreasing was found in all tested samples. Drying detected near phase boundary can be explained either enhanced evaporation in this local area in time of electro-osmotic action or increase electro-osmotic activity in cohesionless phase. In that case considerable sucking accrued from immediate area of solid phase. The total charge which passed through arrangement increased with salt concentration. Double increasing of passed charge was charted in samples from 1 to 6 and his rate monotonously grew from 1 to 6

(except sample 4, which was cut off from analysis). Evaluation of current curve shows great correlation between samples 1 and 2. Initial current increases with salt concentration of dilution. Current in time of test ending (approximately 50 days) was in all cases in narrow area between 16 and 37 μA. Uniform current decline was noted in case of samples 1, 2 and 3. The current curve of sample 5 (the highest concentration) has considerable cavity between 12^{th} and 14^{th} day from 400μA to 150μA. The current curve of sample 6 (the highest concentration) has considerable irregularity from 42^{th} day to the end. The great irregularity was noted in case of sample 4 during electro-osmotic action. This sample was disabled from all the valuation.

Results which were concluded didn´t prove dependence of volume transported saltwater on solution concentration. This conclusion stems from evaluation of all pre-arranged criteria It is true that two from three pre-arranged criteria showed monotone increase in dependence on increasing of concentration. Third criteria (moisture degrease near anode) didn´t prove dependence in case of dilutions 2 (degrease 4,33g) and 3 (degrease 3,54g). We can anticipate, that electrical field of solid phase was largely influenced of enormous moisture degreasing in middle part of tested samples. This fact could influence electro-osmotic flow. The drying of middle part of samples is a new effect, which wasn´t detected in previous measurements. The second alerting coefficient is the eminent evaporation of samples. The evaporation was comparable with the electro-osmoticly transported solution. The data evaluation was complicated by difficult assignment of evaporation to solid and to cohesionless part of sample. The aim of next tests will be analyses of predicative value of third criteria. On the base of past experience the next effort must be oriented on maximal degreasing of evaporation.

Results of tests which were carried out till now and which belong into more extensive project dealing with electro-osmotic effects in building materials can be compiled into next sentences.

Capacity of electro-osmotic flow rises with value of applied voltage and current density.

Capacity of electro-osmotic flow isn´t influenced by initial dampened of sample in the range of 4,87 to 8,6 %.

It wasn´t explicit approve dependence of capacity of electro-osmotic flow on concentration of salt in the range of solutions 1, 2, 3 described above.

References:

[1] BALÍK, L: *Využití elektroosmózy k dodatečnému vysušování zdiva.* Ph.D. Thesis. Praha ČVUT, 2004, 242 p.

[2] BALÍK, L. – SVOBODA, L.: *Studium podmínek pro efektivní použití elektroosmotického vysoušení In: Construmat 2002* ČVUT Praha, 2002, pp. 8-9.

[3] BALÍK, L. – SVOBODA, L.: *Electro-Osmotic Flow in Building Materiále II. In: Proceedings of Workshop 2004 Part A. Prague* Czech Technical University in Prague, 2004, pp. 594-595.

[4] BALÍK, L. – MEJDR, T.: *Vliv počátečního zvlhčení cihelných vzorků na elektroosmotický transport vlhkosti In: Sanace a rekonstrukce staveb 2006* Česká stavební společnost, WTA CZ, 2006 pp. 282-285.

This research has been supported by GA ČR grant No. 130/06/P456.

Computer Analysis of Heat Conduction in Concrete

P. Rybár, T. Doležel, P. Konvalinka

pavel.rybar@fsv.cvut.cz

Department of Mechanics, Faculty of Civil Engineering, Czech Technical University, Thákurova 7, 166 29 Praha 6, Czech Republic

1. Introduction

Concrete is the one of most commonly used structural material. Its mechanical and termophysical properties should be known at the best level of knowledge to achieve economically designed constructions. Concrete is a very heterogeneous material and the macroscopic characteristics are influenced with components used in mixture. For mathematical description of such material, many parameters must be known.

This article is focused on determination of thermal diffusivity of differently moist concrete specimens depending on ambient temperature. Accurate calculation of temperature-moisture field requires considering material characteristics as a function of temperature, time or moisture, not only being constant. Ideal solution of transport processes would be a mathematical model which is based on a microscopic level. Such model would consider single atoms and their mutual interactions. This is not possible due to computational complexity. A reasonable approach is a simulation at a mezoscopic level which means that accomplished calculation on adequate sample could be used as solution on whole material as if it was homogenous.

2. Experiment and Specimens

A concrete cylinder with diameter 150 mm and height 300 mm (standard sized cylinder specimen which is used for compression strength tests) was used as a specimen for all experiments. The specimen was equipped with four digital thermometers in the middle of height. The specimen was loaded with three temperature cycles, which simulated normal temperature loading of real constructions. The first part of experiment represents freezing the cylinder from temperature of 23°C to -17°C. In the second part, the specimen was thawed from -17°C to 16°C. During the third part of experiment, the concrete sample was cyclically cooled down and warmed up between -17°C and 16°C. Measured temperatures were recorded and stored every 30 seconds for later evaluation with computer.

3. Mathematical Solution of Experiments

Mathematical model of heat transport uses common heat conduction equation (moisture and chemical compound transport is not included).

$$c\rho\frac{\partial T}{\partial t} - div(\lambda grad T) = G(x,t)$$

For mathematical calculation of 1D heat transport without internal heat source, the original formula might be modified to

$$a\frac{\partial^2 T}{\partial x^2} = \frac{\partial T}{\partial t}.$$

After replacing the derivations with difference approximation and substitution we get

$$a\left(T_{i-1,j}\right)=\frac{h^2\left(T_{i,j}-T_{i-1,j}\right)}{\tau\left(T_{i-1,j+1}-2T_{i-1,j}+T_{i-1,j-1}\right)}.$$

With the above-mentioned mathematical formula, the course of thermal diffusivity depending on temperature was determined from experimentally measured data.

4. Result and Discussion

Thermal diffusivity evaluation has been carried out for positive temperatures and for temperatures below zero. There is evident difference between courses of thermal diffusivity for each of measured sensor place. This could be caused by an unequal content of moisture or by distinctive non-homogeneity of material. Zero values of thermal diffusivity are caused by two consecutive identical measured values. This is not possible for steady temperature field. It is caused by measurement error of the thermometers. On the basis of executed experiment, thermal diffusivity of plain concrete equals to 1,256.10-6 m2.s-1 for 15°C and 1,532.10-6 m2.s-1 for -8°C. Thermal diffusivity is then greater for temperatures below zero. This evidently causes the disparity in thermal conductivity of water (0,55 W.m-1.K-1) and ice (2,3 W.m-1.K-1). That means the more liquid water the material contains the more thermal conductivity will be influenced, especially when ambient temperature is below freezing point.

Comparison between calculated value of thermal conductivity 2,38 W.m-1.K-1 and value from Czech code 1,3 W.m-1.K-1 (ČSN 730540-3) or in accordance with European one EN 1992-1-1 shows wide difference between measurement and code suggestions.

5. Conclusions and Recommendations

It is obvious that it is not needed to calculate with thermal diffusivity as a temperature function when are designed or criticized common engineering constructions that are exposed to minimal temperature loading. In this case it is adequate to consider thermal diffusivity as a constant.

Conversely using the thermal diffusivity as a constant cannot be recommended for structures loaded with extreme temperature differences e.g. fire and other extraordinary cases when underestimating thermal diffusivity as temperature function can evoke incorrect temperature field calculation in material.

It is useful to consider changing value of thermal diffusivity for special situations e.g. moist material exposed to temperatures below zero Celsius degree. Change of state of water affects value of thermal diffusivity (ice has higher value of thermal diffusivity then water).

References:

[1] S. MÍKA, P. PŘIKRYL: *Numerické metody řešení parciálních diferenciálních rovnic, Stacionární rovnice,* ZČU., 1997.

[2] F. MRLÍK: *Stavební fyzika 2, stavební tepelná technika,* VUTIM Brno, 2000.

[3] P. RYBÁR: *Experimentální a počítačová analýza přenosu vlhkosti ve stavebním materiálu s povrchovou úpravou,* Diplomová práce. ČVUT Praha, 2004.

[4] P. KONVALINKA, T. DOLEŽEL: *Vliv cyklů zmrazování a rozmrazování na materiálové vlastnosti beto,* Závěrečná zpráva projektu FRVŠ G1 1943, 2004.

This research has been supported by GA ČR grant No.: 103/06/1474.

Modeling and Analysis of Prestressed Lightweight Aggregate Concrete Beams - Time Dependent Deformations

Omar Bacarreza

Omar.Bacarreza@fsv.cvut.cz

Department of Mechanics, Faculty of Civil Engineering, Czech Technical University,Thákurova 7, 166 29 Prague 6, Czech Republic

Three beams were produced from light weight aggregate concrete. After seven days of the concreting the samples were prestressed, and finally loaded after 28 days by loading blocks. A computer model was created and the results from this model and experiments were compared.
To obtain the computer model as close as possible to the reality, all the material properties (modulus of elasticity, ultimate strength, etc.) used in the computer model were obtained from the experimental data. The values obtained from the measurements were calculated according to the Czech National Standards. The deformations are measured using the strain gauge technique and the deflections with dial gauges.
The computer model uses a linear geometric and linear elastic material model, the general-purpose finite element code ANSYS was used.

EXPERIMENTAL SAMPLES

The experimental samples are three simply supported beams with a density ρ=2000 kg/m^3. The nominal dimensions of the beams are 6600 mm long x 600 mm wide x 260 mm deep. The clear span of the beams is 6000 mm between supports.
They are prestressed by two strands placed at 80 mm from the bottom fibers and 150 mm from the sides. The beams are post-tensioned.
The beams were loaded symmetrically, in four-point bending, with point loads 0.7m either side of the mid-span location with a load of 13 kN by a loading block.
To measure the deflections seven dial gauges were placed on the beam every meter and four strain gauges were installed to measure the strains in the middle of the span and on one support.

THE COMPUTER MODEL

The finite element code ANSYS has been used for the computer model, due to symmetry about the longitudinal axis, only one half of a beam is modeled and symmetry boundary conditions applied.
The elements used to model the concrete were the SOLID186 element, which is a higher order 3-D 20-node structural solid element. It has quadratic displacement behavior. The element is defined by 20 nodes having three degrees of freedom per node: translations in the nodal x, y, and z directions. The element supports plasticity, hyperelasticity, creep, stress stiffening, large deflection, and large strain capabilities.
For modeling the concrete material, a linear elastic material model was used, with the modulus of elasticity and Poisson's ratio obtained from the laboratory tests.
Two different creep models were used: the "Modified Time Hardening" model defined in Eq.(1) and the "Primary + Secondary Time hardening" model defined in Eq.(2) .

$$\varepsilon_{cr} = \frac{C\sigma^{C_2} t^{C_3 +} e^{-C_4/T}}{C +} \tag{1}$$

$$\varepsilon_{cr} = \frac{C\sigma \quad t \quad ^{+} e^{-}}{C +} + C\sigma \quad te^{-C_7/T} \tag{2}$$

It can be seen that both models are dependent on the equivalent stress, time and temperature, the effects of temperature can be neglected and the creep strain is assumed to be linear dependent on the stress. (So that C2 = C6 = 1, and C4 = C7 = 0).
To obtain the remaining coefficients the data measured in the laboratory is input into the program and curve fitting is performed (Creep curve fitting is a nonlinear regression process. A successful curve fit depends greatly on the initial coefficient values).
For modeling the prestressing steel, the material characteristics were taken from tables provided by the producer.
The elements used to model the steel elements were the LINK180 element which is a spar. This 3-D spar element is a uniaxial tension-compression element with three degrees of freedom at each node: translations in the nodal x, y, and z directions. Plasticity, creep, rotation, large deflection, and large strain capabilities are included. Prestressing can be easily applied on this element type.
Due to problems with the mix and the pouring, the light weight aggregate started to float to the top of the samples, so that the upper part is not uniformly compacted, and it is neglected in the geometry (cross section) of the model (it is considered to be non load bearing), and it is only assumed to be part of the permanent load.
The prestressing stress is assumed to be constant throughout the whole beam, and it is applied after the loss from anchorage slip (reduced).
.

RESULTS AND DISCUSSION

The obtained results from the computer model were compared with the experimental results and it was found that the “Primary + Secondary Time Hardening Creep” model fits better to the experimental results.
The discrepancy in the results can be explained due to the non-homogeneity of the mix; in the computer model it is assumed a linear elastic homogenous material, but the samples are not homogenous at all, since it can be seen that the lower part of the beams is always more compacted (so it is more dense and stiff) than the upper one.
Another possible reason is due to fact that the given formulas can describe only the basic creep, neglecting the drying creep and shrinkage.

ACKNOWLEDGMENTS

Financial support for this work was provided by the Czech Science Foundation, grant No. GAČR 103/06/1474

REFERENCES

[ČSN ISO 6784] – Stanovení statického modulu pružnosti v tlaku.
[ČSN ISO 4012] – Stanovení pevnosti v tlaku zkušebních těles.
ANSYS, ANSYS Manual Set, 1998, ANSYS Inc., Southpoint, 275 Technology Drive, Canonsburg, PA 15317, USA.

Modeling of deformation processes in Fe-3%Si single crystals

J. Prahl*, M. Karlík*, C. Rey, M. Clavel**, P. Haghi-Ashtiani****

Jakub.Prahl@fjfi.cvut.cz

*Department of Materials, Faculty of Nuclear Sciences and Physical Engineering, Czech Technical University in Prague, Trojanova 13, 120 00 Prague 2, Czech Republic

**Ecole Centrale Paris, LMSS-MAT, 92295 Châtenay-Malabry, France

The ductile to brittle transition in ferritic steels [1] is a widely studied phenomenon. The fundamentals of its mechanisms are often investigated on a model alloy Fe-3wt%Si [2]. In order to simulate complicated processes in this material, sophisticated computer modeling methods are used. At the atomic scale, molecular dynamics simulations describe behaviour of individual atoms, capable to estimate the stress for dislocation emission or for mechanical twinning [3]. On the other hand, the mesoscopic finite element modeling (FEM) takes into account pre-existing dislocations in the crystal and the evolution of their density on different slip systems during plastic deformation [4]. This paper reports results of the mechanical testing of single crystals in two different crystallographic orientations as well as the FEM modeling of their behaviour.

Single crystals of the Fe-3wt%Si alloy were prepared by the method of zonal melting. Two different crystallographic orientations of single crystals were chosen – the first single crystal has got its axis oriented in the direction [100], the other one in the direction [110]. Two kinds of tensile test samples were used in the experiments: unnotched test samples of the following dimensions: the length L = 26 mm, width W = 9.4 mm, and thickness B = 1.7 mm (length and width of the active part were L_0 = 14 mm and W_0 = 2.7 mm), and rectangular single edge notched (SEN) test samples of dimensions 50 mm x 10 mm x 2 mm (active length 28 mm). The crack propagated in the <1 1 0> direction on the plane (1 0 0), or (1 0 -1) for the second orientation.

Tensile tests were carried out at room temperature on the deformation machine INSTRON in the laboratory MSS-MAT at Ecole Centrale Paris. During the tests constant crosshead speed was used (0.0015 to 0.0055 $mm.s^{-1}$).

The fracture of the unnotched test samples of orientation <1 0 0> occurs on crystallographic planes (1 0 0) by cleavage mechanisms (after deformation of about 3%), even before reaching the plastic instability (necking). On the other hand, test samples of the other orientation withstood the deformation of about 15% or even more. Critical resolved shear stress was estimated as about 145 MPa for both orientations. The results from the experiments of single edge notched (SEN) test samples are reported in [5].

The computer simulations were performed in software ABAQUS/Standard 6.5.1 using the user subroutine UMAT allowing to take into account the real crystal structure (with preexisting dislocations). The fundamentals of the model are three laws of theory of plasticity: the flow rule, hardening law, and the law of evolution of dislocation density. Model specimens fulfilling the geometry, material parameters, crystallographic orientation, and

boundary conditions of the test samples were created using 22 input parameters. These parameters were found to fit the experimental results. As output parameters it was possible to observe all stress and strain, activated slip systems (of 24 possible), and densities of dislocations on these slip systems.

The input model parameters providing good agreement between experimental and computed stress-strain curves have been found in the case of the orientation <1 1 0>. In the case of the orientation <1 0 0>, 4 equivalent slip systems [1 1 1](2 -1 -1), [1 1 -1](2 -1 1), [1 -1 -1](2 1 1), and [1 -1 1](2 1 -1) were identified, while for orientation <1 1 0>, 2 major slip systems [-1 -1 1](1 -2 -1), [-1 1 1](1 2 -1), and 4 secondary slip systems [-1 1 1](1 1 0), [-1 -1 1](-1 1 0), [-1 1 1](0 -1 1), and [-1 -1 1](0 1 1) were observed. For both orientations, the modeled activated slip systems were in agreement with the experimental results (light microscopy observations).

The values of total densities of dislocations for orientation <1 1 0> (4.0×10^{13} m/m^{-3} after deformation of 2%, and 2.0×10^{13} m/m^{-3} after deformation of 10%) determined experimentally from the TEM micrographs are also in a good agreement with the computed values. The simulations have also showed the influence of macroscopic orientation of the specimens (given by Euler's angles) on the evolution of dislocations on the slip systems. The model of SEN test sample confirmed the experimental results as well.

References:

[1] SMITH, E.: *The physical basis of yield and fracture,* In: Proceedings of Inst. of Physics and Phys. Soc., Oxford, 1966, pp. 36-46.

[2] SPIELMANNOVÁ, A - LANDA, M. - MACHOVÁ, A. - HAUŠILD, P. – LEJČEK, P.: *Influence of crack orientation on the ductile-brittle behavior in Fe-3wt%Si single crystals*, Material Characterization, in press.

[3] MACHOVÁ, A. - BELTZ, G.E.: *Ductile-brittle behaviour of (001)[110] nano-cracks in bcc iron*, Material Science and Engineering A 387-389, 2004, pp. 414-418.

[4] ERIEAU, P. - REY, C.: *Modeling of deformation and rotation bands and of deformation induced grain boundaries in IF steel aggregate during large plane strain compression*, International Journal of Plasticity 20, 2004, pp. 1763-1788.

[5] LANDA, M. - MACHOVÁ, A. - PŘEVOROVSKÝ, Z. - ČERV, J. - ADÁMEK, J.: *Crack growth in single crystals of α-iron (3wt.% Si)*, Czechoslovak Journal of Physics 48, 1998, pp. 1589-1606.

This research has been supported by the Czech Science Foundation (Project GACR 106/04/066).

Heat Feedback System for Curing Concrete Specimens under Prescribed Temperature History

P. Štemberk, N. Pokorná, A. Kohoutková

stemberk@fsv.cvut.cz

Department of Concrete and Masonry Structures, Faculty of Civil Engineering, Czech Technical University, Thákurova 7, 166 29 Praha 6, Czech Republic

The majority of very early age defects in concrete is attributed to incapability of the hardening concrete to cope with increasing differences in stress distributions, mainly caused by the non-uniform temperature fields. This effect becomes of importance in massive concrete structures where the heat generated by hydrating cement is constrained by the surrounding mass. Since massive concrete structures are usually unique in shape, direct measurements of temperature and other measurable quantities acquired from precedent cases are not available, therefore, it is desired to develop a system for simulating a temperature history at arbitrary location in the concrete structure on a specimen which can provide valuable experimental information on the effects related to the hydration of mass concrete. In numerical analysis of a massive concrete structure, the effect of elevated temperature due to hydration can be taken into account by applying, e.g., the equivalent age concept using the Arrhenius reaction-rate equation, whose parameters are available for commonly used cements. However, in the case of special structures, new materials may be used for which relevant experimental data are not at hand, such as time-dependent deformation of solidifying concrete at elevated temperature, which come into play with the considerable selfweight of the concrete mass. Further, acquiring experimental data on the specimens obtained directly from the actual structures has its limitations regarding the retrieval of the specimens. Therefore, it seems reasonable to prepare a test specimen outside the actual structure by curing the specimen under the same conditions as it would be subjected to in the mass of the actual structure. This approach has been attempted by researchers and practicing engineers with various success. The usual drawbacks are represented by too expensive and complicated equipment on one side and excessive inaccuracy in the curing conditions on the other.

In this study it was attempted to develop a heating system for curing specimens under prescribed temperature history which overcomes the above mentioned drawbacks in the systems of this sort. For the sake of generality in application, it was decided to employ a decision-making mechanism based on the fuzzy logic, [1]. This approach proved to be effective in treating the uncertainties related to heat losses, the rate of heat supply and the actual temperature measurement while providing very acceptable accuracy. Another advantage of this approach is the zero requirement to know any exact characteristics related to the performance of heaters, heat losses and the thermal properties of the materials used in the system. Instead, the parameters required for fuzzy decision making are obtained from few preliminary tests of the system which address its overall performance. The controlling units of heating systems in general have to overcome the difficulties with a delay in response to heating which is due to the thermal conduction, convection and radiation characteristics of materials. For the conventional convection-conduction systems, an efficient stirring is essential to reduce this effect. The controlling units can be divided into two classes, first, those with simple on/off switches controlling a constant rate of heat supply and, second, those capable of changing the rate of heat supply. Obviously, the second class has a greater potential to ensure a good accuracy. However, the final accuracy and stability of a heating system depend on the decisions

when or how much heat should be supplied. The ruling based on the fuzzy set theory a priori assumes occurrence of not precise input data and so the decision making is formulated in a very general form, mainly derived from observed tendencies, with the rulings based on the maximum of minima principle [2]. Of course, such a controlling unit cannot maintain the desired value precisely, but, if a small reasonable inaccuracy is allowed deliberately, the controlling unit gives stable rulings which ensure a good accuracy even for systems with varying parameters. So, the objective in development of the heat controlling system was a general controlling unit which could be applied to an arbitrary set of a heat source with a constant rate of heat supply (on/off switch), stirring device, thermocouples, a container and a heated medium. This was achieved by choosing the target temperature history, the temperature of a concrete specimen and the temperature of the medium surrounding the concrete specimens (water in our case) as the ruling quantities and the duration of heating and the duration of waiting for recognition of an action as the acting quantities. Based on the inaccuracy among the target history temperature, the temperature of concrete and water, and their rates of change, the decision on heating duration and corresponding waiting time are made. The calibration of the above fuzzy quantities is made on three tests where the first is focused on the performance of the heater and the response of the system, the second on the heat losses and the third on the interval after which an action can be recognized. It should be noted that no exact information on the parts of the system is necessary, that means the volume of the medium and its thermal properties do not have to be measured, the type and nominal performance of a heat source does not have to be known and the dimensions and material properties of a container also do not have to be considered. The rulings in the decision-making mechanism, which will call upon appropriate actions, are defined linguistically as, e.g.: IF “temperature of water is lower than that of concrete specimen” and “temperature of concrete specimen is lower than target temperature“ THEN “keep the heater on for long time”. The heating system provides an accuracy of less than 5 % even when the target temperature is equal to the room temperature, which means, one cannot rely on any rectification of an improper ruling by natural heat losses. The target temperature history can be obtained either from real measurements or from a thermal analysis, [3], where the function of heat generation is the influencing factor. The adiabatic test conducted with the actual concrete to be used is the most convenient source of the heat generation function. In the cases when the adiabatic test is not possible, a recommended form of the heat generation function can be adopted from standards and provisions, where the thermal parameters of typical concrete at the very early ages are also available.

References:

[1] G. J. KLIR, B. YUAN: *Fuzzy Sets and Fuzzy Logic: Theory and Applications,* Prentice-Hall, Inc., 1995.

[2] L. A. ZADEH: *Fuzzy Sets,* Information and Control 8, 1965, pp. 338-353.

[3] R. W. LEWIS, P. NITHIARASU, K. N. SEETHARAMU: *Fundamentals of the Finite Element Method for Heat and Fluid Flow,* John Wiley & Sons, Ltd., 2004.

This research has been supported by Czech Science Foundation, project number 103/05/2244, which is gratefully acknowledged.

Properties of Silicate Protecting Layers of Concrete Structures

M. Pavlíková, R. Černý

milena.pavlikova@fsv.cvut.cz

Department of Building Materials, Faculty of Civil Engineering, Czech Technical University, Thákurova 7, 166 29 Prague 6

The properties of silicate protecting layers were studied for fine-grained concrete substrates with and without superplasticizer addition, and different water cement ratio. Basic material characteristics, water and water vapour transport and accumulation parameters of fine-grained concrete were measured to obtain information about behaviour and properties of the tested basic substrates. To protect concrete surface against aggressive substances, the silicate layer was proposed. The measured data showed that silicate layer could protect concrete surface against water and aggressive solutions penetration.

Concrete structures are exposed to unfavourable external conditions, which can negatively influence their properties and service life. Degradation processes, such as frost attack and steel corrosion in cement-based materials, cause society considerable costs yearly. From that reason, the concrete protection is very important to extend the time period between concrete structure reparations.

Many of the durability problems of concrete structure are directly or indirectly associated with pore solution condition, for example reinforcement corrosion, salt-frost scaling, carbonation and salt attack. Today, constructions are indeed designed using powerful computer tools where deformations and stresses may be calculated with acceptable accuracy for both static loads and more complex dynamic load cases. The service life of a structure is not, however, determined solely by its resistance to maximum possible loads in its initial virgin state. Instead, degradation of the bulk material and material surfaces caused environmentally induced effects determines the service life.

The concrete protection against corrosion can be divided into two basic types, the first one is called primary protection, for example concrete with great useful properties production like as high performance concrete. The next secondary protection consists in surface constructions treatment. The surface modifications embody proofing, painting, insulations and sealing of high porous concrete using grouting [1].

The silicate protecting layers can be applied in the most cases, like as sealing of roofs, parking places, surfaces of roads, railway bridges, docks and water proofing constructions [2]. This cheap damp proofing can preserve concrete construction during the whole service life. It is based on formation of hydrated calcium silicates in pores and cracks to the 20 mm depth. This silicate layer can seal cracks up to 2 mm width. In the case of secondary cracks formation in treated concrete surface, the silicate layer can react again with water and reactive products fill in new cracks up to 1 mm width. This phenomenon is called autogenously treatment.

At the present time, it is not a lot of information and dates about behaviour and properties of this silicate hydro isolation. However CSIRO [3] deals with the water and

chloride penetration to the concretes treated by silicate protecting layer, porosity, micro structure, salt transport parameters, hygric transport parameters etc. were not studied yet.

In this paper, density, bulk density, porosity, compressive and bending strength, water vapour diffusion coefficient, water vapour diffusion resistance factor, apparent moisture diffusivity, and water absorption coefficient of five different types of fine- grained concrete are determined. The silicate protecting layer is applied on the sample surface to quantify the effect of applied protection on water vapour and liquid water transport to background material.

Basic material parameters were obtained in quite common way using vacuum saturation method. Mechanical parameters were tested with testing device DSM25000, INOVA Praha. Water transport was characterized with apparent moisture diffusivity and water absorption coefficient using simple water suction experiment [4]. The cup method was employed in the measurements of the water vapour transport parameters.

To determine the influence of concrete composition on measured parameters, five different concrete mixtures were mixed. Three mixtures had the same composition but different water/cement ration, one mixture was prepared with addition of superplasticizer and the last one with fly ash addition. Tested samples were mould in the form of standard prisms of size 100x100x400 mm or 40x40x160 mm. Prisms were stored in water during 28-day curing period and then 7 days at 50% relative humidity. The experimental specimens were cut to required sizes depending on the experimental measurement. One set of each tested materials was heated up to 600°C to simulate micro cracks. Silicate damp proofing was painted on the surface of samples with and without micro cracks. After that, surface was sprayed with water three times to form hydrated calcium silicates, so-called “CSH-gel”, in silicate layer. Specimens were dried in a vacuum oven at 70°C before measurements. The experiments were carried out in laboratory conditions at 25±2°C and 30±5% relative humidity.

The experimental results presented in this paper showed that the analyzed silicate protecting layer may potentially become a good solution how to prevent concrete from water penetration. However, its application technology was proved not to be very effective although all recommendations of the producer were exactly followed. The main problem which was identified on the basis of analysis of water suction measurements was the insufficient thickness of the protecting layer.

References:

[1] P. ROVNANÍKOVÁ, D. JANÍČEK: *Injektáže polyuretanovými pryskyřicemi ve stavební praxi,* Sborník konference Sanace a rekonstrukce staveb, Prague, 1998, pp. 122-127.

[2] P. ČELIŚ: *Celoživotní hydroizolace mostních konstrukcí,* Stavitel, 2004, pp. 36.

[3] CSIRO: *Building,* Construction and Engineering. NSW, Australia, 1999.

[4] R. ČERNÝ, P. ROVNANÍKOVÁ: *Transport Processes in Concrete,* Spon Press, London, 2002.

This work was funded by the Czech Sience Foundation under project No.103/05/2376 .

Moisture and Salt Transport and Storage Parameters of Materials Used in Historical Buildings

M. Pavlíková, Z. Pavlík*, R. Pernicová, R. Černý*

jiricko@fsv.cvut.cz

Department of Building Materials, Faculty of Civil Engineering, Czech Technical University, Thákurova 7, 166 29 Prague 6

* Department of Mechanics, Faculty of Civil Engineering, Czech Technical University, Thákurova 7, 166 29 Prague 6

Prediction of water and salt movement and salt crystallization in the walls of historical buildings can be done effectively by means of mathematical and computational modeling. In this way, the time development of water and salt concentration fields can be obtained which is crucial for a proper assessment of possible future damage. However, the accuracy of simulated water and salt concentration fields critically depends on the availability of all input parameters.

In this paper, water and salt transport and storage parameters of sandstone from the Mšené-lázně quarry in Czech Republic are determined. The main aim of this experimental work is to obtain sufficiently accurate input data for the computational model of coupled water and salt transport which is to be used for damage assessment of parts of historical buildings or sculptures built from the Mšené sandstone.

Water transport was characterized in quite common way using the sorptivity and apparent moisture diffusivity [1]. The wet cup method, dry cup method and wet-dry combined method were employed in the measurements of the water vapor diffusion coefficient. For description of water storage parameters, the sorption isotherm and water retention curve were measured. The sorption isotherms were measured employing desiccators with different salt solutions for simulation of specific relative humidities. The water retention curve was determined using an ordinary pressure plate device [1]. In the determination of ion binding isotherm as the main salt storage parameter, a modified Tang and Nilsson adsorption method [2] was applied. Using the Bear and Bachmat diffusion-advection model [3] taking into account (in addition to salt dispersion in the liquid phase) the influence of moisture flow on salt transport and also the effect of bound salt on pore walls, the moisture diffusivity κ (in m^2s^{-1}) and the salt dispersion coefficient D (in m^2s^{-1}) appear as the main salt solution transport parameters. In this way, system of two parabolic differential equations is used for description of water and salt mass balance. The system of two parablic equations was solved by an extension of the Boltzmann-Matano treatment (see [4] for details of the original procedure).

The measurements of water and salt transport and storage parameters of Mšené sandstone determined in this paper can be utilized in the practice in basically two ways. The first is their direct use in computational models of coupled water and salt transport. Reliable input parameters make possible reliable computational predictions of water and salt movement in envelope parts of historical buildings. The predicted moisture and salt concentration fields can then be used for instance at planning the necessary maintenance of surface layers or at avoiding excessive damage of a historical material due to salt crystallization by designing proper time schedule of conservation measures in advance.

The second benefit of accessed material parameters is immediate because in many cases they enable reliable qualitative estimates of the material behavior in a historical building. As for the Mšené sandstone analyzed in this paper, its most important characteristic following from the measured material parameters is the very fast water transport capability. This is an ambivalent feature. On one hand it makes possible fast water redistribution for instance after rain. This reduces possible hydric strains and prevents from water accumulation in topmost surface layers which often plays a significant role in material damage. On the other hand, with the nonexistent horizontal water-proof insulation in a majority of historical buildings the fast water transport capability leads to fast water uptake from the subsoil.

Mšené sandstone was found to be open for water vapor transport which is definitely a good feature. In particular, in the winter period the high water vapor diffusion coefficient is a necessary condition for free water vapor removal from the interior of a historical building, avoiding water condensation in the envelope.

The fast salt transport capability of Mšené sandstone within the liquid phase cannot be considered as positive, in general. In practice it means that salt can be transported rapidly from the subsoil into vertical structures, and in the particular case of chlorides studied in this paper its movement is almost as fast as the movement of liquid water. However, for an application of desalination procedures the fast salt transport capability can result in faster salt removal from a material. Thus, if desalinations of structures built from Mšené sandstone are supposed to be performed, they have to be done more frequently but can be finished in shorter time.

The salt bonding in Mšené sandstone can be potentially dangerous if nitrates are present. Bonding of a high amount of ions on pore walls can lead to tensile stresses which increase the risk of damage. The high difference between the bonding capacity of nitrates and chlorides observed in the experiments may indicate that the character of bonding was more physical in the case of chlorides and more chemical in the case of nitrates.

Analysis of water storage parameters showed that Mšené sandstone contains mainly large pores; small pores are present in negligible amount. This is a very positive feature as a risk of damage due to salt crystallization (and due to ice formation as well) is low for this kind of materials. Open pore structures with large pores have enough free space for crystal growth so that crystallization does not lead to damage of internal structure.

References:

[1] M. JIŘIČKOVÁ: *Application of TDR Microprobes, Minitensiometry and Minihygrometry to the Determination of Moisture Transport and Moisture Storage Parameters of Building Materials* Prague: Czech Technical University, 2004.

[2] M. JIŘIČKOVÁ, R. ČERNÝ: *Chloride Binding in Building Materials,* Journal of Building Physics, No. 29, 2006, pp. 189-200.

[3] J. BEAR, Y. BACHMAT: *Introduction to Modeling of Transport Phenomena in Porous Media,* Vol. 4, Kluwer, Dordrecht, 2004.

[4] R. ČERNÝ, P. ROVNANÍKOVÁ: *Transport Processes in Concrete,* Spon Press, London, 2002.

This work was funded by the Czech Science Foundation under project No. 103/06/0031.

Numerical Modelling of Timber Reinforced with Carbon

L. Hluší, P. Konvalinka

lenka.hlusi@fsv.cvut.cz

Department of Mechanics, Faculty of Civil Engineering, Czech Technical University, Thákurova 7, 166 29 Prague 6, Czech Republic

Timber is organic, anisotropic and inhomogeneous material. It has different characteristics in different directions, distinctive are the differences in the direction parallel to fibres and across the fibres. In the direction parallel to fibres it achieves higher values of strenght, stiffness and lesser values of temperature and moisture deformations than across the fibres. For example the tensile strength in the direction parallel to fibres is $f_{t,o}$= 13 MPa, the tensile strength across the fibres is $f_{t,90}$ = 0,3 MPa (these values are from Czech codes for natural timber of strength class SI). Because of these features it is very difficult to describe the behavior of timber in constructions under load. There are efforts to ensure the best material characteristics of the timber members and it means to improve the material itself and to learn how to determine the characteristics of the composite material.

The common present method of improving is the method of the glued laminated timber. Single lamellas are lengthened through indented joint and then glued together. It is possible to produce big cross-sections limited only with machine capabilities. Incoming attempts are aimed at composite materials - timber and concrete or timber with fibre reinforcement. There are many types of fibre materials, e.g. glass fibres, aramid fibres or carbon fibres. The fibres are processed into fabric layers and bond together with the epoxide resin, then are compressed and hardened.

For this research the carbon fibres were chosen because of their good loading capacity, the stability to chemical attack and water attack. The thickness of the reinforcement was 2 mm and it was made of eight fabric layers bonded with epoxid resin. It was necessary to choose the type of the experimental test. Timber members are in most cases strained in bending or in compression. That's why the four-point bending test was chosen. The specimens were divided into four sets – natural timber, reinforced natural timber, glued laminated timber and reinforced glued laminated timber. The cross-section of the specimens was 30x30 mm and the length was 600 mm. The specimens were made of spruce timber of category SI and the reinforcement was glued with the epoxide glue to the bottom side of the beams. Practically the carbon lamella should be covered with at least one timber layer due to fire prevention, but for the determination of the material characteristics it was better to put the layer in this location because of the arm of the inner forces.

In general for load-bearing cross-section can come four stress states: the elastic state, the ultimate elastic state, elastic-plastic state and plastic state. For all states two basic conditions are considered:

$N_x = 0$, where $N_x = \iint_A \sigma_x dA$, then $\iint_A \sigma_x dA = 0$

$M_y = M_{el\ (elpl,\ pl)}$, where $M_y = \iint_A \sigma_x z dA$

for two unknowns:

- the location of the neutral axis
- the moment of capacity for the cross-section

The calculation of all states is known and is described in detail in [2]. The plastic behavior is not usual for timber beams. When reinforced, the situation changed. Timber was not supposed to reach the plastic state, but it was necessary to calculate both limitary values – the ultimate elastic state and the plastic state – to compare the results from experimental tests and the theoretical values. The assumption was proved. The reinforced specimens performed the elastic-plastic behavior: ($M_{el} < M_{ex} < M_{pl}$):

Natural timber: 388,313 Nm < 524,97 Nm < 699,390 Nm

Glued laminated timber: 522,382 Nm < 594,0 Nm < 932,514 Nm

For practical application was necessary to create a model which was suitable for the experimental tests. Then the use of the reinforced beams could be easier when the behavior of the beams was known. The numerical model was created during my intership in France. The used program called Code Aster is a program which uses the finite element method and was developed by a team of researchers of Laboratoire de la Mécanique et Technologie at École Normale Superiére in Cachan, Paris, when I went through the intership.

In accordance with the principal of virtual work the modulus of elasticity was calculated for all specimens. These values were used as input data for the program together with the information about the layout of the experimental test and the loading. The effort was aimed at the approximation to the work diagrams determined from the experimental tests. For both types of unreinforced timber the model worked perfectly and that was the first step for making the model of the reinforced timber. It was an iterative process – the elastic-plastic behavior was known but the curve for it wasn't (for example, for concrete the bilinear model is often used, but for this purpose it was inappropriate).

The failure of the beams was naturally different for unreinforced and for reinforced timbers. The reinforced specimens mostly broke in shear. This piece of knowledge was supported with the model. The timber went to the elastic-plastic state and although the capacity in compression wasn't used completely, the timber exceeded the limitary value of the capacity in shear and the beam failured.

The final model works for all specimens. The capacity of the reinforced beams is higher than of the unreinforced beams. The deflection of the reinforced beams is so big compared to unreinforced that in constructions the people would be warned before the collapse of the building.

References:

[1] HLUŠÍ, L.; KONVALINKA, P.: *Analysis of Reinforced Timber Members,* Acta Mechanica Slovaca, Košice 2006, ISSN 1335-2393

[2] HLUŠÍ, L.; KONVALINKA, P.: *Numerical Model of Timber Cross-section Reinforced with an Carbon Lamella,* ČVUT Praha, 2006, ISBN 80-01-03574-3, pp. 117-129

[3] HLUŠÍ, L.; KONVALINKA, P.: *Experimental Tests for Determination of Material Characteristics of Reinforced Timbers,* ČVUT Praha 2005 ISBN 80-01-03348-1, pp.69-76

This research has been supported by GACR grant Nr. 103/06/1474.

Physical Aspects of the Transition Behaviour of Ferritic Steels

M. Karlík*, P. Haušild*, B. Strnadel, M. Kytka*****

Miroslav.Karlik@fjfi.cvut.cz

*Department of Materials, Faculty of Nuclear Sciences and Physical Engineering, Czech Technical University in Prague, Trojanova 13, 120 00 Prague 2, Czech Republic

**Department of Materials Engineering, Technical University of Ostrava, 17. listopadu 15, 708 33 Ostrava, Czech Republic

***Integrity and Technical Engineering Division, Nuclear Research Institute, Husinec – Řež 130, 250 68 Řež, Czech Republic

Although it has been subjected to an extensive research, the ductile-to-brittle transition DBT in steels remains one of important issues in materials science. The integrity of key safety components made of steel such as reactor pressure vessels, depends on the material's resistance against brittle fracture. Cleavage, characteristic for fracture of steels at low temperature, is a sequential stochastic process of crack nucleation and crack propagation by a local reinitiation of cleavage facets. Cleavage in steels is usually assumed to be induced by carbide cracking [1]. The role of other isolated second phase particles or clusters of inclusions such as MnS in cleavage fracture was also mentioned [2]. However, the situation in steels with lath microstructure such as bainite, containing only fine carbides is more complex. Several cleavage initiation mechanisms were observed for one kind of steel with similar or even with the same thermal treatment [3]. This uncertainty complicates using of obtained information in further research of mechanisms of cleavage in steels.

This paper summarizes results of the research carried out in the frame of the project "Physical Aspects of the Transition Behaviour of Ferritic Steels" supported by the Czech Science Foundation. The research works on nuclear reactor pressure vessel steels A508 and 15ChMFA, high carbon ferritic-pearlitic steel and Fe3wt%Si single crystals were organized in an international collaboration with partner laboratories in France (MSSMAT, Ecole Centrale Paris, Electricité de France, MMC Renardières) and in Austria (USTEM, Vienna University of Technology, and FELMI-ZFE, Graz University of Technology).

Furthermore, we participated in an international benchmark "Micromechanisms of Fracture" comparing fractographic analyses provided on selected specimens of reactor pressure vessel steel by several other laboratories in France and in Germany (CdM ENSM Paris, MMSMAT EC Paris, LML EC Lille, CEA Saclay, EdF Renardières, ENSAM Metz, GEMPPM INSA Lyon, and FIW Freiburg) [4].

The mechanical properties of non-irradiated and irradiated 15Ch2MFA pressure vessel steels were characterised by means of tensile and instrumented Charpy tests. The Charpy tests revealed a shift of DBT temperature of about 65 °C after neutron fluence 10^{24} nm^{-2}. The ductile crack situated in the zone next to the V-notch of Charpy specimens displayed a high degree of correlation between the fracture energy and the ductile crack length. No significant acceleration in ductile crack initiation or growth was observed in the irradiated specimens [5].

A transmission electron microscopy study of tempered bainitic nuclear reactor pressure vessel steel A508 Class 3 was carried out. Cross-section thin foils from nickel

electroplated Charpy V-notch specimens fractured in impact and quasi static loading at -30°C and a CT25 specimen fractured in quasi static loading at 0°C were prepared in the ductile tearing and cleavage regions of the fracture surface. In the ductile tearing zone, the microstructure was very heterogeneous. In the cleavage zones of both types of specimens, high dislocation density was found. An isolated twin was observed in the CT25 specimen [6].

The effect of microstructure on fracture characteristics of high carbon hypo eutectoid steels used for railway wheel sets have been studied under conditions of quasi-static and dynamic loading. Experimental sets of fracture toughness and Charpy impact energy values have been statistically treated. The fracture occurred almost exclusively by cleavage. Mechanisms of cleavage initiation have been revealed from fractographical analysis of fracture surfaces. Whereas fracture surfaces of broken CT specimens exhibit a number of cleavage origins on fracture surface of CVN specimens there is usually only one [7].

The ductile to brittle transition (DBT) in α-iron was studied on oriented single crystals of a Fe-3wt%Si alloy using tensile testing, scanning and transmission electron microscopy. The experimental results are compared with molecular dynamic simulations. Single-edge notched specimens were loaded in tension at room temperature, the crack propagated in a (001) plane and in the [110] direction. At a slower loading rate, the crack growth is more difficult since it is impeded by emission of shielding dislocations from the crack tip in the <111> {112} slip system. Twin formation at the crack front was detected in simulations with edge cracks [8].

References:

[1] SMITH, E.: *The physical basis of yield and fracture,* In: Proceedings of Inst. of Physics and Phys. Soc., Oxford, 1966, pp. 36-46.

[2] ROSENFIELD, A.R. - SHETTY, D.K. - SKIDMORE, A.J.: *Fractographic observations of cleavage initiation in the ductile-brittle transition region of a reactor-pressure-vessel steel,* Metall. Trans. A 14, 1983, pp. 1934-1937.

[3] ROSSOLL, A.: *Détermination de la ténacité d'un acier faiblement allié à partir de l'essai Charpy instrumenté,* PhD thesis, Ecole Centrale Paris, France, 1998.

[4] BOUCHET, C.- HAUŠILD, P.- NEDBAL, I.: *Benchmark on the determination of the cleavage triggering site in a RPV steel in the DBT range,* In: Proc. 11th Int. Conference on Fracture ICF 11 Turin, Italy, 20-25 March, 2005. CD-ROM.

[5] HAUŠILD, P. – KYTKA, M. – KARLÍK, M. – PEŠEK, P.: *Influence of irradiation on the ductile fracture of a reactor pressure vessel steel*, J. Nucl. Mater., 341, 2005, p. 184.

[6] KARLÍK, M. – HAUŠILD, P. – PRIOUL, C. – STOGER-POLLACH, M.: *Microstructure of low alloyed steel close to the fracture surface*, Mater. Sci. Eng. A**,** 2007, in press

[7] STRNADEL, B. – HAUŠILD, P. – KARLÍK, M. (2006), *Quasistatic and dynamic fracture of pearlitic steel*, in: E.E. Gdoutos (Ed.), Fracture of Nano and Engineering Materials and Structures, Proc. 16th European Conference on Fracture (ECF16), Alexandropoulis, Greece, July 3-7, 2006, Springer, 2006 p. 495.

[8] PRAHL, J. – MACHOVÁ, A. – LANDA, M. – HAUŠILD, P. – KARLÍK, M. – SPIELMANNOVÁ, A. – CLAVEL, M. – HAGHI-ASHTIANI, P.: *Fracture of Fe-3%Si single crystals*, Mater. Sci. Eng. A**,** 2007, in press

This research has been supported by the Czech Science Foundation (Project GACR 106/04/066).

Monitoring of Salt Imbibition Using TDR and Electrical Conductivity Method

M. Pavlíková

milena.pavlikova@fsv.cvut.cz

Department of Building Materials, Faculty of Civil Engineering, Czech Technical University, Thákurova 7, 166 29 Prague 6

Deterioration of porous building materials is strongly related to the presence of moisture. Many chemical degradation processes such as dissolution and leaching of calcium in concrete, transformations of material forming compounds, and crystallization of salts are induced by moisture. The reasons for the moisture presence are various. Water comes to the porous building materials by capillary suction of driving rain and run off water, by condensation, by capillary rise of groundwater, etc. Rarely pure water is involved. Mostly the water transports dissolved contaminants, e.g. salts. If the material dries out again, salt crystallization may occur. As the results of salt crystallization, disintegration of porous structure can be observed. In recent years, several numerical models have been developed for the simulation of moisture and salt transport in porous materials as a reliable tool for prediction of salt induced damages of building materials and structures.

The advanced experimental laboratory methods together with generally employed ones allow development of more precisely formulated physical models, to simulate moisture and salt transport, to describe the hygric properties of porous building materials, to understand deterioration mechanisms and to anticipate materials destruction. In computational modelling of salt transport, the determination of moisture and salt storage and transport parameters is considered to be crucial point. Because the determination of material parameters describing the salt movement is often difficult and time-consuming, there were developed sophisticated instantaneous profile methods for simultaneous determination of these parameters.

The Time Domain Reflectometry (TDR) is method for estimating volume fraction of water in material by measuring time that takes to an electromagnetic pulse to travel along a transmission line buried in the material [1]. The measured time is time it takes pulse to travel from the beginning of the probe to the end of the probe, reflect from the end and to travel to the beginning of the probe (the round trip time). This time is directly related to the velocity of propagation of the electromagnetic pulse travelling along the probe, and the velocity of propagation is related to the average dielectric constant of the material in contact with the probe [2]. The permitivity of air is 1, of dry material 2-3, and of water approximately 80. Therefore, the presence of water in the material heavily influences the measured relative permitivity of the material. The TDR method is applicable to all types of materials, except of material having large bulk electrical conductivity [3]. Its using is also restricted by temperature; the device cannot be used at or below freezing point of water. Because of a wide range of different materials, the accurate relationship between relative permittivity and water content does not exist. However a lot of calibration or conversion functions were developed, tested and reported by numerous researchers, the individual calibration curve for the studied

material is probably the most precise solution in the evaluation of moisture content from the measured dielectric constant.

In this work, measuring equipment LOM/RS/6/mps produced by EASY TEST, Poland, was employed. The applied equipment is based on the TDR technology with $\sin^2$-like needle pulse having rise-time of about 200 ps. It periodically records relative permitivity, moisture and bulk electrical conductivity with help of LP/ms – minihygrometry probes to obtain the instantaneous profiles of moisture and salt in chosen time intervals. In the experiment, it was first necessary to calibrate the measuring system to the studied material. Moisture content was determined by gravimetric method and ion concentration content in material using pH/ ION measuring device with ion selective electrodes. The sufficient space holes were bored into the samples cut out of measured materials. Then, the samples were water and water vapour proof insulated using epoxy resin and after hardening, the samples were dried in an oven. After that, the probes were placed into the prepared parallel holes. Because there should be no air gaps around the probe as this can result in large, fluctuating errors, the ECG conducting gel was applied on sensors rods. The probes were fixed using the technical plasticine and the samples were installed into the measuring place.

The measurements of moisture and salt profiles were done on three different types of porous building materials. There were measured the vertical NaCl solution suction profiles of aerated autoclaved concrete, calcium silicate, brick, and sand stone. The volumetric moisture content in all cases of TDR measurement was calculated according to basic Malicki equation.

The measured results will find use in computer modelling of moisture and salt transport. The highly sensitive TDR technique, currently especially used in soil measurement, will allow many applications in studying structure of porous materials and their behaviour. The application of TDR technique makes possible to explore water content profiles with the resolution 0.1% from the measured value of moisture content with use of small sensors. In addition to the moisture content determination, the utilized combined LP/ms sensor can be employed for measurement of bulk electrical conductivity. Therefore, salt concentration and moisture profiles can be measured at once. This measuring technology is advantageous for monitoring salt transport in porous building materials, and in combination with chemical analytical methods applied on the investigated material after the experiment it can be used for determination of ion-binding isotherms, the critical parameter for description of salt storage.

References:

[1] Z. PAVLÍK: *Development of a Semi-scale Technique for the Assessment of Hydro-thermal Performance of Multi-layered System of Building Materials,* CTU Reports, 1,Vol. 8, Praha, 2004.

[2] G.C. TOPP, J.L. DAVIS, A. ANNAN: *Electromagnetic Determination of Soil Water Content: Measurements of Coaxial Transmission Lines,* Water Resour. Res. No. 16, 2006, pp. 574-582.

[3] M.A. MALICKI, R. PLAGGE, C.H. ROTH: *Reduction of soil matrix effect on TDR dielectric moisture determination by accounting for balk density or porosity,* European Journal of Soil Science, Vol. 47, 1996, pp. 357-366.

This work was funded by the Czech Sience Foundation under project No.106/04/P255 .

Optical Properties of Thin Nanodiamond Films

Z. Bryknar, Z. Potůček

bryknar@troja.fjfi.cvut.cz

Department of Solid State Engineering, Faculty of Nuclear Sciences and Physical Engineering, Czech Technical University, Trojanova 13, 120 00, Prague 2, Czech Republic

Thin films of nanocrystalline diamond can become a preferred diamond form for many future applications. They exhibit excellent optical and electromechanical properties, low surface roughness, and can be deposited at low cost over large area by microwave plasma-enhanced chemical vapor deposition (MWPE CVD) in hydrogen-methane plasma. However, nanocrystalline diamond films grown by MWPE CVD consist of small grains with large amount of grain boundaries resulting in increased defect density. Thus, their properties differ in some aspects from those of perfect single crystal diamond and polycrystalline CVD diamond thick layers.

In this study, absorption and photoluminescence spectroscopy have been used in order to investigate the electronic properties of defects in the energy gap.

Nanodiamond films with thicknesses within the range of 250-1650 nm were grown by MWPE CVD on silicon (100) substrates. Nanocrystalline diamond films of different structural properties have been obtained by using a bias enhanced nucleation for nucleation density over 10^{10} cm^{-2} and by changing the deposition conditions. The nucleation process and growth were monitored with scanning electron microscopy. Then, windows of (4-6) x (4-6) mm^2 were opened in the substrate by directional etching, leaving perfectly transparent, self-supporting nanodiamond membranes [1]. Some membranes were warped. This behavior depends on the grain size and seems to be also influenced by residual nitrogen contamination, the internal stress, and thickness inhomogeneity. Typical nanograin sizes have been observed in the range 20-100 nm.

The refractive index and the thickness of the nanocrystalline diamond thin films were calculated from the measured spectral dependence of their transmittance and interference fringes using a procedure described in [2]. Transmittance in the interference maximum in the NIR (where the films of good optical quality have no absorption), does not reach 100 %. Suppression of interference fringes in the visible spectral region and disappearance in UV region is due to light scattering, the roughness to wavelength ratio being the decisive parameter.

Photoluminescence emission and excitation spectra were studied within a wide temperature range (12 – 300 K) and spectral (220 – 900 nm) region. They do not depend markedly on temperature. PL spectra exhibit a structure of different origin. A nearly regular modulation of PL intensity measured on thick films (>700 nm) is related to interference effect nevertheless composite character of PL is clearly seen on thin films. PL emission spectra consist of two main broad emission bands distributed near 2.2 and 1.8 eV. The luminescence mechanism is supposed as follows: Excitation light generates the electron-hole pairs localized spatially at luminescence centers. These pairs recombine radiatively and emit luminescence. The sp^2 hybridized carbon sites presented in grain boundaries are supposed to behave as luminescence centers. These carbon atoms form π bonds and give rise to electronic density of states. Extent of π electron localization is closely related to the size of structural units

containing sp^2 carbon sites [3]. Radiative recombination through these sp^2 hybridized carbon sites depends on the localization extent of π electronic states. Therefore, it is reasonable to suppose changes in the PL emission spectra due to changes of film thickness and excitation energy as it was observed.

References:

[1] V. MORTET, J. D'HAEN, J. POTMESIL, R. KRAVETS, I. DRBOHLAV, V. VORLICEK, J. ROSA, M. VANECEK: *Thin nanodiamond membranes and their microstructural, optical and photoelectrical properties,* Diamond Relat. Mater. 14, 2005, pp. 393-397.

[2] R. SWANEPOEL: *Determination of the thickness and optical constants of amorphous silicon,* J. Phys. E 16, 1983, pp. 1214-1222.

[3] T. HEITZ, C. GODET, J. E. BOURÉE, B. DRÉVILLON.: *Radiative and non-radiative recombination in polymer-like amorphous carbon films,* Phys. Rev. B 60, 1999, pp. 6045-6052.

This research has been supported by GA ČR grant No. GA 202/05/2233 and MŠMT grant No. MSM 6840770021.

Study of Transition Metal Oxides: the Mixed-Valent Cobaltite Perovskites

A. Chichev

politruk@nm.ru

Department of Solid State Engineering, Faculty of Nuclear Sciences and Physical Engineering, Czech Technical University, Trojanova 13, 120 00 Prague 2, Czech Republic

Transition metal oxides (TMO) are systems with large variability of structures and chemical bonding, which brings about an alluring range of magnetic, electrical and optical properties. A strong interaction between chemical compositions of TMO, their transport characteristics, magnetic orders and crystal structures produce a rich field for fundamental research and technological applications.

Magnetic oxides like cubic ferrites or hexaferrites are commonly used for decades as permanent magnets, materials for the radiofrequency and microwave applications or, more recently, for the perpendicular magnetic recording . The piezo- and ferro-electric oxides, often based on early transition metal oxides, find applications in sensors, actuators and transducers, but also as non-linear optical elements . Possible use of transition metal oxides in devices includes spin valves, nonvolatile memory, spin-based field-effect transistors (FET), spin-based light emitting diodes (LED), and spin resonant tunneling diodes (RTD) [1].

Many properties of TMO have been studied in recent years: the high- temperature superconductivity [2] and of other spectacular phenomena such as large magnetoresistance [3] and high-efficiency thermoelectricity [4]. In last two decades, a great attention was attracted to the conducting transition metal oxides with mixed-valent cations [5]. Many of systems with prospects for application belong to a structural class of perovskite or perovskite-like compounds which are members of a large family of crystals known as Ruddlesden-Popper phases [6]. We may note especially the cuprates of the $La_{2-x}Sr_xCuO_4$ of $YBa_2Cu_3O_7$ types with occurrence of superconductivity at relatively high temperatures compared to alloys, critical point reaching to about 100 K. The superconductivity in these so-called high-temperature superconductors is associated with charge carriers in the perovskite planes CuO_2 with a non-integer valence Cu^{2+}/Cu^{3+}. Extensive studies were done on the Mn^{3+}/Mn^{4+} perovskites of composition $Ln_{1-x}A_xMnO_3$ where Ln represents trivalent rare earth, La, Y or Bi, A is generally divalent alkaline earth or Pb. The prospects for application come from the occurrence of the ferromagnetic metallic state (electronic conductivity with spin polarized carriers) and, for samples in the non-conducting paramagnetic or antiferromagnetic state, from the possibility to induce a transition to the ferromagnetic metallic conductor by external magnetic field (so-called colossal magnetoresistance – the CMR effect) [7]. The detailed studies of CMR in manganites by diverse experimental means have shown that the Mn^{3+}/Mn^{4+} charge and orbital (Jahn-Teller) ordering plays a critical role in the electronic transport and, moreover, revealed other colossal effects associated with the ordering phenomena, such as the anomalies in sound velocity, specific heat or thermopower.

Present study is focused to perovskites and perovskite-like systems with Co^{3+}/Co^{4+} valency. Their unusual magnetic and electronic properties come from possibility of several ionic states that generally violate Hund rules. This is caused by the fact that increased electron correlation effects (intra-atomic Coulomb repulsion) can be overcome by the effects of crystal fields. In

particular, the octahedrally coordinated Co^{3+} ions in perovskites can exist in three spin states - the non-magnetic low spin state that corresponds (in the limit of fully localized electrons in strong crystal field) to filled t_{2g} levels and empty e_g states (LS, $t_{2g6}e_{g0}$, S = 0), and two magnetic states that correspond either to the intermediate spin (IS, $t_{2g5}e_{g1}$, S = 1) or to the high spin state (HS, $t_{2g4}e_{g2}$, S = 2). Similarly for Co^{4+}, two spin states are possible, LS ($t_{2g5}e_{g0}$, S = 0.5) and IS ($t_{2g4}e_{g1}$, S = 1.5) while Co^{2+} ions are reported always as HS ($t_{2g5}e_{g2}$, S = 1.5).

The objective of this thesis is to investigate two series of cobalt oxides materials. The first one is $Pr_{0.5}Ca_{0.5}CoO_{3-y}$ (y=0.07 and y=0.00) that is a member of "half-doped" perovskite cobaltites. There are two topics in their studies that attract particular attention - the microscopic description of the ferromagnetic and paramagnetic metallic phases (typical example is $La_{0.5}Sr_{0.5}CoO_3$), and the occurrence of the low-temperature metal-insulator (M-I) transition that was firstly reported for $Pr_{0.5}Ca_{0.5}CoO_3$ by Tsubouchi et al. [8].

The other series are the single-layered perovskites $La_{2-x}Sr_xCoO_4$ ($1.0 \leq x \leq 1.4$). This system has been studied less intensively than the first one, among other reasons due to its more difficult preparation, especially for the phases with higher oxidation state of Co. But the possibility to vary the valence of Co over much larger range, hypothetically from Co^{2+} for x=0 to Co^{4+} for x=2, which lead to modification some system properties, has made these compounds the subject of interesting research.

References:

[1] S. A. Wolf, D. D. AWSCHLOM, R. A. BUHRMAN, J. M. DAUGHTON, S. von MOLNAR, M. L. ROUKES, A. Y. CHTCHELKANOVA, D. M. TREGER: Science **294**, 2001, p. 1488.

[2] J. G. BEDNORZ, K. A. MUELLER : Z. Phys. B: Condens. Matter **64**, 1986, p. 189.

[3] R. M. KUSTERS, J. SINGLETON, D. A. KEEN, R. McGREEVY, W. HAYES: Physica B **155** , 1989, p. 362.

[4] I. TERASAKI, Y. SASAGO and K. UCHINOKURA, Phys. Rev. B **56**, (1997),p.R12685

[5] Y. MORIMOTO, A. ASAMITSU, H. KUWAHARA, Y. TOKURA : Nature **380**, 141 1996, p. 141.

[6] S. N. RUDDLESDEN, P. POPPER : Acta Crystallogr. **10**, 1957,p. 538.

[7] S. JIN et al., Science **264**, 1994, p. 413.

[8] S. TSUBOUCHI et al., Phys. Rev. B **66**, 2002 , p. 052418.

This work was funded by the Czech Ministry of Education No. 2027 G 6.

Homogenization Techniques for TDR Calibration

Z. Pavlík. L. Fiala, R. Černý

pavlikz@fsv.cvut.cz

Department of Building Materials, Faculty of Civil Engineering, Czech Technical University, Thákurova 7, 166 29 Prague 6

The application of TDR method for measuring moisture content in porous building materials is presented in the paper. As the basic technological problems related to the use of TDR for building materials were already solved before [1, 2], the main attention is paid to the evaluation of moisture content from the measured permittivity values.

There are in principle three basic approaches to the determination of moisture content from measured relative permittivity. The first approach consists in empirical calibration for the particular material using reference method. Another possibility is utilization of empirical conversion functions generalized for a certain class of materials, which, however, are always limited to specific groups of materials only, for which they were proposed. The third possibility is application of dielectric mixing models, which assumes knowledge of the relative permittivities of the material matrix, water, air and other parameters, that can not be measured directly but have to be determined by empirical calibration of the model.

In this paper, the empirical calibration was done using the gravimetric method. The empirical calibration curve was then used for the assessment of two other empirical conversion functions frequently used is soil science designed by Malicki and Topp.

In terms of homogenization, a porous material can be considered as a mixture of three phases, namely solid, liquid and gaseous phase. For the building materials, the solid phase is formed by matrix depending on material composition, liquid phase is represented by water and gaseous phase by air. In the case of dry material, only the solid and gaseous phases are considered. The volumetric fraction of air in porous body is given by the measured total open porosity. In case of penetration of water, part of the porous space is filled by water. For the evaluation of relative permittivity of the whole material, the permittivities of the particular constituents forming the porous body have to be known. In this work, we have employed several different homogenization techniques, among them formulas proposed by Dobson et al., de Loor, Looyenga, Birchak, Polder and van Santen, and Lichtenecker. For verification of obtained results, the Wiener's upper and lower bound were used. In our calculations we have introduced also the fourth phase that is represented by bound water showing different physical properties compared to the liquid free water.

Measurements were done on calcium silicate samples produced by Calsitherm, Germany using TDR technology working apparatus LOM/RS/6/mps produced by Easy Test, Poland. The experiment was done on 20 samples having dimensions of 40 x 40 x 100 mm. At first, two parallel holes having the same dimensions as the sensor rods were bored into each sample. Then, the sensors were placed into the samples and sealed by silicon gel. The samples were partially saturated by water and insulated to prevent water evaporation. The relative permittivity of wet samples was then continuously monitored until the measured values reached the constant value. Then, the experiment was interrupted, sensors removed from the samples and moisture content in the samples was determined using gravimetric method. Finally, the measured values of permittivity were assigned to the gravimetric moisture

content. As the application of homogenization techniques and empirical functions for evaluation of moisture content from measured relative permittivity assumes the knowledge of material properties, the measurement of porosity, bulk density and matrix density were carried out as well. The measurements were done on the vacuum saturation principle and the results are as follows: total open porosity is 0.87 m^3/ m^3, bulk density 235 kg/m^3 and matrix density 2047 kg/m^3.

Experimental results showed a relatively good agreement between measured data and the empirical formulas of Topp's and Malicki's in the range of lower moisture content up to 0.20 m^3/m^3. For higher moisture content the results of Topp's curve were systematically higher and the results of Malicki's function systematically lower. This is, however, not very surprising result. The empirical and semi-empirical formulas for evaluation of moisture content from measured relative permittivity designed for application in soil science cannot be universal. As most soils exhibit a very low hygroscopicity, the application of soil-science formulas particularly for hygroscopic building materials is not straightforward and should always be done with care. Very good agreement was obtained by application of Lichtenecker's equation and Polder's and van Santen's formula for needle orientation of inclusions. Results of Birchak's equation and Polder's and van Santen's formula for plate orientation of inclusions were also very promising but only in the range of moisture content up to 0.50 m^3/m^3. On the other hand, the formulas proposed by Looyenga and Polder and van Santen for spherical orientation of intrusions completely failed in the whole range of measured moisture content. The most successful results were achieved for the application of Dobson and de Loor formulas which contain the amount of bound water as free parameter. This seems to be a critical factor for building materials which – contrary to most soils – often contain a considerable amount of hygroscopic moisture.

The experiments and calculations performed in this paper can be considered as further step towards regular application of TDR technique for monitoring moisture content in building materials. The main finding was that methods for calculation of moisture content from measured relative permittivity commonly used in soil science are not applicable for building materials in general. However, the application range of some of the methods can be extended to a wider class of materials relatively easily.

References:

[1] Z. PAVLÍK, M. JIŘIČKOVÁ, R. ČERNÝ, H, SOBCZUK, Z. SUCHORAB: *Determination of Moisture Diffusivity Using the Time Domain Reflectometry (TDR) Method,* Journal of Buiding Physics, Vol. 30, No. 1, 2006, pp. 59-70.

[2] M. JIŘIČKOVÁ: *Application of TDR Microprobes, Minitensiometry and Minihygrometry to the Determination of Moisture Transport and Moisture Storage Parameters of Building Materials,* Prague: Czech Technical University, 2004.

This work was funded by the Czech Ministry of Education within the framework of the KONTAKT program, under the Czech-Polish bilateral cooperation project No. CZ - 2.

Properties of Biological Agricultural Materials Measured by Methods Common in Building Physics

Z. Pavlík, M. Pavlíková, R. Černý

pavlikz@fsv.cvut.cz

Department of Building Materials, Faculty of Civil Engineering, Czech Technical University, Thákurova 7, 166 29 Prague 6

Biological agricultural materials consist of highly heterogeneous sets of different substances, mixtures and structural components, including complex organic structures. Their inhomogeneous composition and high variability affect their behavior and cause complicated and variable physical properties. Physical properties of biological agricultural materials are dependent on moisture and temperature of the studied material, and mostly show a considerable hysteresis.

Complete knowledge of physical properties of agricultural materials has a decisive importance for the realization of many technological processes, especially for monitoring their quality and health harmlessness during their production and storage. The quality assessment and guarantee of the safety of foodstuff belong to the main priorities in food industry.

HACCP – Hazard Analysis and Critical Control Point System [1] represents scientifically sophisticated approach to the problems of the protection of foodstuff quality. It is internationally accepted system guarantying the foodstuff safety aimed to the identification, evaluation and risks control in the whole technological procedure of foodstuff production. Its successful application is subject to the complete knowledge of physical properties of foodstuff.

From the point of view of optimization of a technological procedure the temperature and moisture have the crucial importance. They present the most important parameters having clear relation to the character of physical, chemical and physiological processes in biological agricultural materials. Physical processes, above all heat and moisture transport, affect the intensity of physiological processes, nominally of breath, germination, microorganisms progress and many others and in consequence determine the final quality of food sources. The modern trends in storage and subsequent processing of agricultural products are currently based on application of complex mechanization and automation. For their optimization, it is necessary to know physical material parameters and to relate them with the environmental conditions.

In this work, determination of thermal conductivity and specific heat capacity, as main parameters for description of heat transport and storage, of several types of granular agricultural products, namely of spring oat, wheat mixture Axis, barley mixture Expres, corn mixture and soybean Evans, is presented. The measurements were done using commercially developed device ISOMET 104 (Applied Precision, Lt.D.) The apparatus is based on the analysis of the temperature response of the analyzed material to heat flow impulses. The heat flow is induced by electrical heating using a resistor heater having a direct thermal contact with the surface of the sample.

The material samples were provided by Slovak University of Agriculture in Nitra, Faculty of Agricultural Engineering, Department of Physics. The obtained materials were first dried according to instructions given in [2, 3]. The measurement of thermal conductivity in dependence on moisture content was done from the dry state to the fully water saturated state. The samples were stored first in refrigerator at 4°C for ten days in plastic weighing bottles to distribute humidity homogeneously. Then, they were conditioned to 25°C for about six hours, moved to the measuring cylinder and measured using the needle probe. The dependence of specific heat capacity on moisture content was calculated by the simple mixing rule based on the additive character of the specific heat capacity. Since the apparatus ISOMET 104 provides determination of volumetric heat capacity, for the application of the mixing rule it was necessary to measure bulk density of the studied materials.

The experimental results showed that the highest value of thermal conductivity for dry materials exhibited the wheat mixture Axis (0.087 W/mK). The results achieved for other materials were very similar each other. Taking into account the effect of moisture, the highest thermal conductivity was observed for the wheat mixture Axis, barley mixture Expres and corn mixture; for the saturated moisture content the values were typically about 0.25 W/mK. On the other hand, the value of thermal conductivity of the soybean Evans at saturated moisture content was markedly lower. The oat spring has shown only slight dependence of thermal conductivity on moisture content. The values of specific heat capacity were for all studied materials very similar except for the wheat mixture Axis that had the lowest specific heat capacity. The effect of moisture on the specific heat capacity was quite remarkable, which is a consequence of the high specific heat capacity of water.

The results presented in this paper can find utilization in food industry in such processes where heat transport and storage properties of granular agricultural materials are indispensable. They can be applied for instance for the adjustments of drying rate, for the calculations of the economical drying time and for the determination of energetic balances of drying processes.

References:

[1] V. VOZÁROVÁ: *Meranie a modelovanie transportných javov v biologických pol'nohospodárskych materiáloch,* Ph.D. thesis, Department of Physics, Faculty of Civil Engineering, Slovak University of Agriculture in Nitra 2006.

[2] V. VOZÁROVÁ: *Thermophysical Properties of Granular Food Materials,* International Agrophysics, Vol. 19, No. 2, 2005, pp. 187-192.

[3] Z. HLAVÁČOVÁ, V. VOZÁROVÁ: *Tepelné vlastnosti biologických materiálov z hl'adiska odovzdávania vody,* Sborník Mezinárodní slovenský a český kaloriemtrický smeinář, Ostravksá univerzita, Ostrava, 1998, pp. 35-38.

This work was funded by the Czech Ministry of Education within the framework of the KONTAKT program, under the Czech-Slovak bilateral cooperation project No. 3.

Degradation of Structure and Fatigue Properties of Structural CrMo Steels ČSN 15 313 and P91

M.Svobodová, J. Kunz

M.Svobodova@sh.cvut.cz

Department of Materials, Faculty of Nuclear Sciences and Physical Engineering,
Czech Technical University, Trojanova 13, 120 00 Prague 2, Czech Republic

Structural steels ČSN 15 313 a P91 were long-time annealed in laboratory with the aim to simulate the degradation of materials during operation service. Steel 15 313 was studied in following three states: the initial heat treatment, after annealing 650°C/500 h/air and after 650°C/1 000 h/air. Similarly, steel P91 was studied after the initial heat treatment, and after annealing 625°C/5 000 h/air.

Microstructure of the steels was studied by SEM and evaluated by quantitative structure analysis by means of software LUCIA and software for statistic data processing [2]. The microstructure of steel ČSN 15 313 after the initial heat treatment is bainitic, respectively ferritic-bainitic in larger sectional areas. Granular carbides are precipitated on grain boundaries as well as inside of original austenite grains. Carbides in bainite grains are coarser and of larger number. Long-time annealing at temperature more than 650 °C leads to coarsening of carbides particles, only, but the beginning of annealing is followed with significant nucleation of new carbides closed to grain boundaries. Therefore, the quantitative analysis of carbides particles was provided for grains and boundaries separately. The results showed that at the beginning it deals with non-equilibrium process because of the coarsening followed with a new nucleation. In addition, there is probably a change of chemical composition of carbides, perhaps dissolution of thermodynamic non-stable particles. In case of steel P91, the annealing at temperature less than 650°C leads to precipitation of inter-metallic phases changing its behaviour. Therefore, steel P91 was annealed at the temperature 625°C. The microstructure of the steel P91 is ferritic, whereas the ferritic lattice contains homogenously distributed granular carbides, which coarse during the annealing. The changes of carbides dispersion were studied by quantitative structure analysis. The measurement of mean particle size showed a nucleation of new particles in the beginning of isothermal dwell(??) at all temperatures. Only annealing for more than 500 hours results in the coarsening of precipitated carbides. In this case, there is also significant decrease of the volume number of carbides.

Fatigue tests were provided on CT samples of thickness $B = 8$ mm, width $W = 50$ mm (from the middle of the pin hole) and with initial nominal crack length $a_o = 12{,}5$ mm at two levels of stress ratio $R \cong 0{,}05$ a $R \cong 0{,}3$. The fatigue crack length was monitored simultaneously by two independent methods – optical method (direct measuring of crack mouth length on the specimen surface) and electrical potential method (indirect measuring, the result of which is the mean crack length characterising a damage ratio of the whole cross section). The fatigue test programme was planned with the aim to study effects of following factors: the direction of crack propagation (respectively loading direction) with regard to material texture, specimen location in a pipe cross-section, heat treatment, and stress ratio (i.e., mean static preload). The results were expressed in the form the fatigue crack growth rate $v = da/dN$ as a function of stress intensity factor range ΔK. The data analysis has established no significant effect of the first two mentioned factors. Similarly, the annealing of steel ČSN 15 313 has no effect on its fatigue behaviour [1,3]. Thus, the stress ratio R has

become the main observed factor. The experimental results demonstrated the increase in the fatigue crack growth rate and decrease in threshold stress intensity factor range ΔK_p with stress ratio increasing.

Following the fatigue tests, detailed quantitative and qualitative fractographic analysis of fracture surfaces of damaged specimens were carried out. From the results obtained is evident that there is no difference between the fatigue mechanism and static cracking of both studied steels from qualitative point of view [1]. The spontaneous initiation of partial fatigue cracks started in spark-out notch root. After their connection, the major fatigue crack has formed and propagated through the entire cross-section. Considering quantitative point of view, the mechanism of fatigue failure of both steels after initial heat treatment as well as annealing is the same. The cracks propagate previously by striation mechanism. Striation spacing is independent of heat treatment. The different microstructure of the steels under study results in some semi-quantitative differences, e.g., in the initiation area of fatigue crack in steel P91, intergranular fracture facets were found in some isolated cases. Furthermore, in the case of steel ČSN 15 313, the striation patches were longer and wider than in the case of steel P91 at the same value of ΔK. Furthermore, there is a higher number of secondary cracks on fatigue fracture of steel P91 than on the fracture of steel ČSN 15 313. In addition considering long-time annealed samples of steel P91, this higher number occurs especially in case of longer cracks. In the area of final static failure, ductile dimples are characteristic. There are no significant differences between steels P91 and ČSN 15 313 in size and shape of ductile dimples.

Fatigue behaviour of both steels is very similar, i.e., same values of macroscopic fatigue crack growth rate correspond to practically identical quantitative and qualitative fractographic characteristics of fatigue fracture. Concerning the resistance to time-variable loading, both steels have practically the same properties. Experimental results obtained during the laboratory tests simulating service conditions have shown no significant effect of a long-time operation at high temperature on the fatigue resistance.

References:

[1] KUNZ, J. – SIEGL, J. – LAUSCHMANN, H. – KOPŘIVA, P.: *Studium únavových vlastností Cr-Mo ocelí P91 a ČSN 15 313* [Report V-KMAT-596/04] Prague, ČVUT-FJFI-KMAT, 2004, 61 p.

[2] SVOBODOVÁ, M.: *Vlastnosti legovaných konstrukčních CrMo ocelí a jejich změny při dlouhodobém účinku teploty* [Degree thesis] Prague, ČVUT-FJFI-KMAT, 2005, 93 p.

[3] KUNZ,J. – SIEGL, J. – KOPŘIVA,P.: *Vliv provozních podmínek na únavové vlastnosti ocelí pro potrubní systémy v chemickém průmyslu* Materiálové inžinierstvo, 12, No.3, 2005, pp. 52-56.

[4] MADDOX, S.J.: *An Investigation of the Influence of Applied Stress Ratio on Fatigue Crack Propagation in Structural Steels* [Report 72/1987] Welding Institute 1987.

This research has been supported by MPO „Konsorcia“ FD-K3/041 and MSM6840770021.

Computational Design of the Properties of Water Vapor Retarders for Interior Thermal Insulations

M. Jerman, J. Maděra, R. Černý

madera@fsv.cvut.cz

Department of Mechanics, Faculty of Civil Engineering, Czech Technical University, Thákurova 7, 166 29 Praha 6, Czech Republic

The building physical solution of an envelope with interior thermal insulation system is a difficult task. If no water vapor barrier is used, there is an increased risk of water condensation in the insulation layer and on the interface between this layer and the load bearing structure in the winter period. If a non-ideal contact between the insulation layer and the load bearing structure exists, water condensed in the air gap is very difficult to evaporate, and the long-term appearance of liquid water can severely damage the structure. A common solution to this problem consists in placing a vapor barrier just under the internal plaster, on the surface of the insulation layer, so that both the insulation layer and the load bearing structure are protected against water vapor penatration. However, this is a solution, which can perform well on the theoretical level only. In the practice, it is often not possible to avoid mechanical damage of water vapor barrier placed in such an inappropriate way. A sole nail or hook driven into the wall for instance if hanging up a painting can destroy the function of the barrier. In addition, even in the case that the barrier would perform without mechanical damage, the absence of water vapor removal from the interior through the envelope in the winter period, when air ventilation in the interior is usually limited, would lead to undesirable increase of relative humidity in the interior and worsening of the internal microclimate.

In this computational analysis, we have chosen an interior thermal insulation system consisting of internal plaster, insulation material and water vapor retarder. On the interior side there was lime-metakaolin plaster with the thickness of 10 mm. As the thermal insulation material, hydrophilic insulation boards on the mineral wool basis PARGRO developed by Rockwool, SA, were used. The thickness of mineral wool was 100 mm for the brick wall and 150 mm for the concrete wall. The thickness of water vapor retarder was 10 mm. We assumed no air gap between the water vapor retarder and the load-bearing structure. We considered glue or mastic as the water vapor retarder, which was applied directly on the old structure. As old bearing structure we have chosen a brick wall with the thickness of 450 mm and concrete wall with the thickness of 400 mm. On the external side there was the same plaster as inside, with the thickness of 10 mm.

Table 1: Basic material properties of the water vapor retarder

ρ[kg/m^3]	θ_{sat} [m^3/m^3]	λ[W/mK]	C [J/kgK]
1500	0.5	0.25	1000

The main aim of the computational simulations performed was to analyze the hygrothermal performance of the designed insulation system with different values of the water vapor diffusion resistance factor μ, moisture diffusivity κ and hygroscopic moisture content θ_{hyg} of the water vapor retarder. The basic material parameters of the retarder are shown in Table 1, the optional parameters in Table 2.

Table 2: Optional material parameters of the water vapor retarder

	$\kappa=1\cdot10^{-8}$ m^2/s	$\kappa=1\cdot10^{-12}$ m^2/s
μ = 5, θ_{hyg} = 2 % vol.	V1K1	V1K2
μ = 50, θ_{hyg} = 0.5 % vol.	V2K1	V2K2

For the calculations we employed the computer simulation tool TRANSMAT 4.2 [1] which was developed in the Department of Mechanics, Faculty of Civil Engineering, Czech Technical University in Prague. The construction of the code is based on the application of the general finite element computer simulation tool SIFEL (SImple Finite ELements). The moisture and heat balance equations were formulated in the simplified form suggested by Künzel [2].

The proper initial and boundary conditions of the model are crucial factor affecting the reliability of the calculations. Therefore, the boundary conditions for the external side should be as accurate as possible and the initial conditions should be realistic. In our computational analysis, the 1st of July was chosen as the starting point. For the insulation systems, there were taken initial values of field variables corresponding to values inside. The systems with interior thermal insulations were exposed from inside to constant conditions (temperature equal 21 °C and relative humidity equal 55, 70 %) and from outside to climatic conditions corresponding to the reference year for Prague. We have chosen two critical profiles in the evaluation of the hygrothermal performance of the envelope, A-A´, B-B´, where the profile A-A´ was between water vapor retarder and insulation material, profile B-B´ was between load-bearing structure and water vapor retarder. In these profiles we calculated the dependence of the relative humidity and temperature on the time.

For the brick wall we found the optimum value of water vapor diffusion resistance factor equal to 5 and the value of moisture diffusivity equal to 1.10^{-8} m^2/s. The maximum values of relative humidity were then about 85 %, which is still far from the condensation limit. For the concrete wall we found the same optimal value of water vapor diffusion resistance factor equal to 5 and the value of moisture diffusivity equal to 1.10^{-8} m^2/s. The optimum values of the analyzed parameters of the retarder were the same for both values of inside relative humidity.

References:

[1] MADĚRA, J.– ČERNÝ, R.: *TRANSMAT- A Computer Simulation Tool for Modeling Coupled Heat and Moisture Transport in Building Materials.* Proceedings of Workshop 2005, CTU in Prague, 2005, pp. 470 - 471.

[2] KUENZEL, H.M.: *Simultaneous Heat and Moisture Transport in Building Components. PhD Thesis,* IRB Verlag, Stuttgart, 1995.

This research has been supported by the Ministry of Industry and Trade of Czech Republic, under grant No FI – IM3/188.

Methods for Assessment of Utility Properties of Modified Calcium Sulfate Hemihydrates

P. Tesárek, P. Konvalinka*, R. Černý

tesarek@fsv.cvut.cz

Department of Mechanics, Faculty of Civil Engineering, Czech Technical University, Thákurova 7, 166 29 Praha 6, Czech Republic

*Experimental Center, Faculty of Civil Engineering, Czech Technical University, Thákurova 7, 166 29 Praha 6, Czech Republic

The assessment of utility properties of modified calcium sulfate hemihydrates is based on the evaluation of various mechanical, hygric and thermal properties.

Thermal conductivity, thermal diffusivity, and volumetric heat capacity are determined using the commercial device ISOMET 2104 (Applied Precision, Ltd.). ISOMET 2104 is a multifunctional instrument equipped with various types of optional probes. Needle probes are for porous, fibrous or soft materials, surface probes are suitable for hard materials. The measurement is based on the analysis of the temperature response of the analyzed material to heat flow impulses. The heat flow is induced by electrical heating using a resistor heater having a direct thermal contact with the surface of the sample.

The moisture diffusivity is measured using two different methods. First, the apparent value of moisture diffusivity is determined from a water sorption experiment. Then, the dependence of moisture diffusivity on moisture content is calculated using an inverse analysis of moisture profiles.

For the determination of moisture diffusivity from a water sorption experiment, a common experimental setup is chosen. The known water flux into the specimen during the suction process is employed to the determination of the water absorption coefficient. For the calculation of the apparent moisture diffusivity, an approximate relation is employed.

In the determination of moisture dependent moisture diffusivity from moisture profiles, the capacitance method is used for measurement of moisture content. The measuring frequency is 250 – 350 kHz. The parallel electrodes of the capacitance moisture meter have the dimensions of 20 x 40 mm. The moisture profiles are measured using a common capillary suction 1-D experiment in the horizontal position. Lateral sides of specimens are water and vapor-proof insulated. Moisture meter reading along the specimen is done every 5 mm. The calibration curve is determined after the last moisture meter reading, when the moisture penetration front is at about one half of the length of the specimen, using this last reading and the standard gravimetric method after cutting the specimen into 1 cm wide pieces. The final calibration curve for the material is constructed from the data of 6 samples. The moisture profiles are then calculated from the calibration curve. The measurements are done at 25^0C ambient temperature. Moisture diffusivity is determined by the Matano method and double integration method [1].

The water vapor diffusion resistance factor is determined by standard cup methods. In the dry cup method the sealed cup containing silica gel is placed in a controlled climate chamber with 50% relative humidity and weighed periodically. For wet cup method sealed cup containing water is placed in an environment with the temperature of 25^0C and relative humidity of 50%. The measurements are done at 25^0C in a period of two weeks. The steady

state values of mass gain or mass loss determined by linear regression for the last five readings are used for the determination of water vapor transfer properties. Then, the water vapor diffusion coefficient is calculated from the measured data. Using the diffusion coefficient, the water vapor diffusion resistance factor as a parameter more common in building practice is determined.

The measurements of adsorption isotherms are performed in laboratory conditions, at 25^0C. The samples are placed in desiccators with different solutions to simulate different values of relative humidity. The initial state for all the measurements is dry material. The experiment is performed in parallel in all desiccators in the same way. The mass of samples is measured in specified time periods until the steady state value of the mass is achieved. Then, the moisture content by mass is calculated. The measurement of desorption isotherms is carried out in the same way as for the adsorption isotherms, except that the initial state is a specimen with maximum hygroscopic moisture content.

Methods for assessment of mechanical properties are based on the measurement of bending strength and compressive strength. The measurement of bending strength are performed according to the Czech standard ČSN 72 2301 on the 40 x 40 x 160 mm prisms. The specimens are demolded 15 minutes after the final setting time and stored in the testing room. Every specimen is positioned in such a way that the sides that were horizontal during the preparation were in the vertical position during the test. The experiment is performed as a common three-point bending test using the WPM 50 kN device. The distance of the supporting cylinders is 100 mm. The bending strength is calculated according to the standard evaluation procedure. The measurements are done at the times of 2 hours, 1 day, 3 days, 7 days, 14 days and 28 days after mixing.

Compressive strength is determined in accordance with the Czech standard ČSN 72 2301 on the halves of the specimens left over after the bending tests. The specimens are placed between the two plates of the WPM 100 kN device in such a way that their lateral sides adjoining during the preparation to the vertical sides of the molds are in contact with the plates. In this way, the imprecision of the geometry on the upper cut off side is not affecting negatively the experiment. The compressive strength is calculated as the ratio of the ultimate force and the load area.

The methods described above will be used for the development of modified calcium sulfate hemihydrates. The criterion for successful development of a new technology will be the comparison with the recent technology.

References:

[1] J. DRCHALOVÁ, R. ČERNÝ: *Non-Steady-State Methods for Determining the Moisture Diffusivity of Porous Materials,* Int. Comm. in Heat and Mass Transfer, 1998, pp. 109-116.

This research has been supported by the Ministry of Industry and Trade of Czech Republic, under grant No. FT-TA3/005.

X-ray Stress Analysis of Oxide Layers Formed on Zr Alloys Specimens with ZrO2-gel Coating

G.Gosmanová*, I.Kraus*, M.kolega,V.Vrtílková**

gosmanov@troja.fjfi.cvut.cz

*CTU, Faculty of Nuclear and Physical Engineering, Dept.of Solid State Engineering, Trojanova 13, 120 00 Prague 2, Czech Republic
**NTC, West Bohemian University, Univerzitní 8, 306 14 Plzeň, Czech Republic
UJP Praha Inc., Nad Kamínkou 1345, 156 10 Prague – Zbraslav, Czech Republic

Zirconium alloys are currently used as cladding materials of fuel elements of water-cooled reactors. However, their behavior under several corrosion conditions is still the object of extensive research.

The aim of the present study was to find out the effect of ZrO_2-gel coating on the properties of oxide layers formed on zirconium alloys during high temperature oxidation.

The part of tubular specimens based on the Zr1Nb and Zry-4 S alloys was coated with ZrO_2-gel using a special technique. The coated specimens were annealed in the oxygen atmosphere at 400 °C. This procedure was 5x repeated. Then the coated and uncoated specimens of both alloys were oxidized in pure water at 360 °C for various exposures. The kinetics of oxidation of the alloys under investigation were represented by weight gain (or T_{ox}) being measured after each exposure.

The X-ray diffraction method [1] was used to determine the macroscopic residual stresses σ in oxide layers. The method is based on the determination of lattice strains ε^{hkl} from which, subsequently, the stresses were calculated by using appropriate macroscopic Young's moduli. A D-8 Discovery powder diffractometer with CoKα radiation was used to measure diffraction patterns. In oxide layers of the samples investigated the measurements were performed on the {10-4} planes with $2\theta = 85.2°$ for CoKα radiation. The fitting procedure had to be used to obtain the accurate profile characteristics.

The results of experiment are given in tables 1 and 2.

Table 1
Macroscopic stresses σ and the absolute values of their differences Δ for coated (G) and uncoated (NG) specimens of Zr1Nb alloy oxidized in pure water at 360 °C

Exposure (days)	specimen G	Tox G (μm)	σ G (MPa)	specimen NG	Tox NG (μm)	σ NG (MPa)	|Δ| G-NG (MPa)
7	T1936012	1,11	-1025	NT1936112	1,69	-1009	16
14	T1936015	1,51	-1051	NT1936115	1,97	-925	125
21	T1936018	2,43	-1124	NT1936118	3,28	-1005	119
63	1936028	3,63	-1029	1936128	4,92	-966	63
189	1936023	6,15	-926	1936123	5,86	-948	21
294	T47	5,63	-866	NT47	6,52	-825	41
336	T37	5,96	-913	NT37	7,09	-792	121
357	T22	6,68	-919	Nt22	7,28	-840	79

Table 2
Macroscopic stresses σ and the absolute values of their differences Δ for coated (G) and uncoated (NG) specimens of Zry-4 S alloy oxidized in pure water at 360 °C

Exposure (days)	specimen G	Tox G (μm)	σ G (MPa)	specimen NG	Tox NG (μm)	σ NG (MPa)	|Δ| G-NG (MPa)
0,125	T4936011	0,10	-1079	NT4936111	0,47	-965	114
7	T4936012	0,91	-904	NT4936112	1,37	-1088	184
14	T4936015	1,10	-978	NT4936115	1,49	-1044	65
21	T4936018	1,39	-953	NT4936118	2,05	-1000	47
63	4936028	1,61	-901	4936128	2,31	-883	18
189	4936023	4,19	-816	4936123	5,02	-805	11

It follows from the data tabulated that:
- the values of macroscopic residual stresses σ are different for the coated and uncoated specimens of the both alloys,
- the values of their differences in the major part are greater then value of standard deviation of measurement which amounts to 32 MPa.

It can be concluded that the oxide layers formed during high temperature oxidation on the coated with ZrO_2-gel or uncoated specimens of zirconium alloys have the different characteristics probably due to different mechanical properties of the adhesive compact “gel” and ”grown” layers.

The authors would like to thank Doc. Dr. Z. Weishauptová for effectual cooperation.

References:

[1] KRAUS,I. - TROFIMOV,V.: *Rentgenová tenzometrie,* ACADEMIA, Prague, 1988

This research has been supported by 6840770021.

Effect of Alloying on the Microstructure of Aluminium Sheets Prepared by Accumulative Roll Bonding Process

P. Homola*', M. Slámová*, M. Karlík****

Homola@kmat.fjfi.cvut.cz

* Research Institute for Metals, Panenské Břežany 50, 250 70 Odolena Voda

** Czech Technical University, Faculty of Nuclear Sciences and Physical Engineering, Department of Materials, Trojanova 13, 120 00 Praha 2

The accumulative roll bonding (ARB) process is a method for manufacturing ultra-fine grained (UFG) materials by severe plastic deformation [1]. ARB does not require any special equipment and, in addition, it enables the production of large amounts of UFG materials. These are the major advantages making ARB suitable for industrial applications. The ARB process consists in repeated rolling of sheets, cutting, stacking and further rolling (roll-bonding). After several cycles of processing UFG materials with high strength and good ductility are produced. The paper reports the results of a study mainly aimed at an alloying effect on thermal stability of ARB aluminium sheets, which is an important characteristic, for example, with respect to superplastic forming.

Two different materials were used for investigation of alloying effect on microstructure evolution during ARB and subsequent heat treatment. High purity aluminium (Al99.99) and twin-roll cast aluminium alloy AA8006 (Al-1.5Fe-0.4Mn-0.16Si in wt.%) were fully recrystallized by annealing for 30 minutes at 350°C and 450°C, respectively. ARB processing was performed at ambient temperature and consisted in the repetition of 5 steps: i) degreasing in 4-chlorethylene; ii) wire-brushing with stainless steel brush (0.3 mm wire); iii) stacking of pieces of 300×50×2 mm^3; iv) joining by Al wires; v) rolling with 50% reduction without lubricant. Roll diameter of 340 mm and peripheral speed of 30 $m \cdot min^{-1}$ were applied in both cases.

The microstructure and properties of the material during processing and annealing treatment were studied using a variety of experimental methods. The work hardening evolution during ARB processing was evaluated by Vickers hardness measurements performed on sheet surface. Thermal stability of prepared specimens was studied by isochronal annealing at different temperatures. The microstructure in the initial state before ARB was observed by light microscopy (LM). Transmission electron microscopy (TEM) was used for the characterization of subgrain and grain structures of ARB processed samples. TEM foils were prepared by electrolytic twin-jet polishing (15°C, 15V) using 30% solution of HNO_3 in methanol and observed in JEOL JEM 2000FX at 200 kV. Electron back-scattered diffraction (EBSD) system in scanning electron microscope Quanta 200 FEG was used to investigate the grain structure in selected deformed and annealed specimens. All microstructure examinations were performed in the long transverse plane (TD-plane).

In the initial recrystallized state of experimental materials the mean grain size was 15 and 46 μm in the rolling direction (RD), and 12 and 38 μm in the normal direction (ND) for AA8006 alloy and Al99.99, respectively. During ARB processing LM and TEM observations

revealed a lamellar boundary (LB) structure in all specimens that is typical for heavily deformed materials [2].

The hardness increases significantly only during the first ARB cycle. In AA8006, there is a small or no hardening in subsequent cycles, whereas, a noticeable softening occurs in high purity aluminium. Dynamic recovery has occurred in both materials and it is more intensive in Al99.99 that results in coarser subgrains in high purity aluminium. After the 6th ARB cycle, the mean grain size in ND is 330nm and 500nm in AA8006 and Al99.99, respectively. Another results concerning the microstructure and mechanical properties of these two materials during ARB processing are presented elsewhere [3,4].

The annealing investigations have shown that the thermal stability of A8006 alloy structure is better than that of high purity aluminium. Hardness decrease starts at 150°C in the Al99.99 samples, whereas, a significant hardness drop is observed in the AA8006 alloy above 200°C. Very coarse grains form due to recrystallization and grain growth in AA99.99 specimen annealed at 250°C but fine-grained microstructure is observed in AA8006 alloy. The refined grains in the recrystallized alloy are a consequence of intensive grain boundary pinning by closely spaced particles. After recrystallization, grain growth is observed only in the Al99.99 specimens annealed at 300°C whilst the grains coarsen only a little in the AA8006 specimen annealed at 450°C.

Moreover, the number of ARB cycles affects the grain size in annealed materials. The higher strain induced by ARB, the smaller grain size in both annealed materials is developed. The mean grain size for AA8006 annealed at 450°C is 5.1 and 3.5 μm for the 2^{nd} and the 6^{th} ARB cycle, respectively. And, in the case of high purity aluminium Al99.99 the mean grain size is 13.4 and 11.2 μm after the 2^{nd} and the 6^{th} ARB cycle, respectively.

References:

[1] TSUJI, N.: *Production of bulk nanostructured metals by accumulative roll bonding (ARB) process.* In: Severe Plastic Deformation, Toward Bulk Production of Nanostructured Materials, Nova Science Publishers, 2005, pp. 543–564.

[2] HANSEN, N.: *Deformation microstructures with a structural scale from the micrometre to the nanometre dimension.* In: Evolution of Deformation Microstructures in 3D, Proc. 25th Riso International Symposium on Materials Science, 2004, pp. 13–32.

[3] SLÁMOVÁ, M. – HOMOLA, P. – SLÁMA, P. – ČÍŽEK, J. – PROCHÁZKA, I.– CIESLAR, M.: *Microstructure, Texture and Property Changes of High Purity Aluminium during Accumulative Roll Bonding and Conventional Rolling* Materials Science Forum Vols. 503-504, 2006, pp. 711–716.

[4] SLÁMOVÁ, M. – HOMOLA, P. – SLÁMA, P. – ČÍŽEK, J. – PROCHÁZKA, I.– CIESLAR, M.: *Effect of the Temperature of Accumulative Roll Bonding on the Microstructure and Properties of Twin-Roll Cast AA8006 Alloy.* Materials Science Forum Vols. 503-504, 2006, pp. 281–286.

This research has been supported by MŠMT grants No. MSM 2631691901 and MSM 6840770021.

Deformation Induced Martensitic Transformation in Austenitic Stainless Steel

P. Haušild[1], M. Karlík[1], M. Landa[2], K. Kolařík[3], V. Jezequel[4]

Petr.Hausild@ fjfi.cvut.cz

[1] Department of Materials, Faculty of Nuclear Sciences and Physical Engineering, Czech Technical University, Trojanova 13, 120 00 Praha 2

[2] Ústav termomechaniky AVČR, Dolejšova 5, 182 00 Praha 8

[3] Department of Solid State Engineering, Faculty of Nuclear Sciences and Physical Engineering, Czech Technical University, Trojanova 13, 120 00 Praha 2

[4] Laboratoire Génie Mécanique et Matériaux, Université de Bretagne Sud, Rue Saint Maudé, 56321 Lorient, France

Austenitic stainless steels are widely used for deep drawing thanks to their good mechanical properties and excellent corrosion resistance of worked products. A deformation induced transformation of austenite to martensite can occur in these steels during the forming [1]. The internal stresses can be created in each phase (austenite/martensite) as the result of martensitic transformation which can lead to the phenomenon of delayed cracking (appearing of cracks several hours or days after deep drawing process).

In this study, a characterization of the deformation induced martensitic transformation has been carried out in austenitic stainless steel with low nickel content corresponding to the AISI 301L. The microstructure of the material has been studied after different steps of straining (deformation of 0, 5, 10, 15 and 20%), using metallographic observations (optical and scanning electron microscopy). The volume fraction of martensitic phase was measured by X-Ray diffraction by standard-less quantitative method. The initial (as received) state was austenitic with very low initial content of martensite, after 10% of tensile deformation the volume fraction of martensite started significantly to increase and after 20% of deformation the volume fraction of martensite was estimated to about 35%.

Table 1 Chemical composition of studied austenitic steel.

C	Cr	Ni	Si	Mn	Mo	Al	Cu	N
0.0554	16.7634	6.9612	0.4894	1.4576	0.1187	0.0018	0.1	0.0392

Tensile tests with acoustic emission (AE) have been performed at room temperature. AE technique provides a well-suited method to detect rapid micromechanical events, such as avalanche dislocation movement [2], mechanical twinning, martensitic transformation [3] or microcracking [4]. Combining this method with metallographic and fractographic analysis in scanning electron microscope, different micromechanisms of damage can be identified.

Two-threshold level system of detection and evaluation of AE, recently recommended by an ASTM standard has been applied. The AE signals are filtered, amplified and then evaluated at two threshold levels to get two AE counts denoted N_{C1} and N_{C2} (count thresholds c1=556 mV, c2=1200 mV). The total gain was about 100 dB.

Table 2 Tensile properties of studied austenitic steel at different loading rates.

crosshead speed	$R_p0,2$ [MPa]	R_m [MPa]	A [%]
2mm/min	305	933	28
20mm/min	325	918	37.5
200mm/min	345	856	32

The flat tensile specimens were loaded to fracture using crosshead speed 2, 4, 20 and 200 mm/min. In all specimens the martensitic transformation was revealed by distinct increase of AE counts. In specimens loaded using crosshead speed 2 and 4 mm/min, the final fracture was preceded by several high-energy acoustic events. High strain rate generated heating in specimens loaded using crosshead speed 20 and 200 mm/min.

The fractographic analysis showed that the fracture surfaces of specimens fractured using crosshead speed 2 and 4 mm/min exhibit transgranular cleavage facets surrounded by ductile dimpled fracture, whereas on the fracture surfaces of specimens fractured using crosshead speed 20 and 200 mm/min only ductile dimpled fracture was found. The cleavage facets contained distinct slip lines and therefore were formed before final ductile fracture.

Combining the AE and fractographic analysis results, it can be concluded that the high-energy acoustic events preceding the final fracture in specimens loaded using low crosshead speed correspond to the cleavage cracking of transformed martensite. The absence of cleavage facets in specimens loaded using high crosshead speed is due to heating generated by high strain rate.

[1] GALLÉE, S.: *Caractérisation expérimentale et simulation numérique des procédés d'emboutissage profond : application aux aciers inoxydables austénitiques*, PhD thesis Université de Bretagne Sud, 2005.
[2] CHMELÍK, F. - ZIEGENBEIN, A. - NEUHÄUSER, H. - LUKÁČ P.: *Investigating the Portevin–Le Châtelier effect by the acoustic emission and laser extensometry techniques,* Materials Science and Engineering A, 324 (1-2), 2002, 200-207.
[3] LONG, Q. Y. – ZHU, Z. – ZHANG, X. M. – LI, D. F.: *Acoustic emission of martensitic transformation induced by strain during tensile testing in a Fe-Ni-C alloy*, Scripta metall. mater. 26, 1992, 1095-1100.
[4] LAMBERT, A. - GARAT, X. - STUREL, T. - GOURGUES, A.F. - GINGELL A.: *Application of acoustic emission to the study of cleavage fracture mechanism in a HSLA steel*, Scripta mater. 43, 2000, 161–166.

This research has been financially supported by project MSM 6840770021 Diagnostika materiálů.

Usage of Binarized Image in Evaluation of Plastics and Composites

Hana Harcová

h.harcova@email.cz

Department of Mechanics, Klokner Institute, Czech Technical University,
Šolínova 7, 16608 Prague 6

Binarized image is used mainly during evaluation of microscopic images. Every image consists of thousands of different types of shades. To achieve better elaboration of the images, only two colors should be chosen (the most common are black and white). This way we can highlight specific structures, which we would be interested in.

This type of procedure is used to determine the width of the surface layer on plastics.
The surface layer is white, while the other environment is black or is of a size of the spherulite. When dealing with composites, we use binarized approach to find out the fiber volume content or number of fiber in the bundle.

The main goal of binarization is to determine more exact measures through programs, which are used to evaluate microscopic images (Cell – F, Lucia…). Using programs can be easier in determining the area of fibers or their diameter than highlighting the structures by hand or try to approximate the boarder using flat formation.

The process of binarization is as follows:
Before binarize an image, the image should be sharpened (in program Cell – F using "Sharpen" filter) and should be enhanced with contrasts (function "Execute intensity").

Adjusted image should be transferred into black and white (function "Separate Intensity"). As a result, the image is only in shades of grey and it is easier to set up the color spectrum, and pick what shade would be transferred into black and into white.

Next step is to set up binarized profile. Structures on the images are in various colors due to the different kinds of polarization filters. For example, composite fibers have green and brown color and the environment is in yellow and green when looking through the microscope. When the image is transferred into black and white, the fibers have black and grey color and the rest is light grey. Computer program is able to create a colored histogram, in which all shades of grey are in presence. Dark shades of grey representing fibers would be reflected on the histogram as an extreme. This extreme can be stored into the memory and then changed into white color using binarization profile. All else would be assigned as black color. Result is black image with white areas representing the fibers.

Binarized colored image is harder to set up. The image needs to be divided into three colors, so we would have three separated histograms (green, red, and blue). Green – brown color, which is the color of fibers, has to be divided into brown and green. Brown then has to be divided onto green and red. Such color distribution creates histograms with no extremes, thus it makes it difficult to determine what shade or color tone represents fibers and what is matrix.

Such complex binarization set up is done only before the first measuring. Thus it is more efficient when evaluating large number of images. To evaluate one or two images is not time efficient.
Once the image has been binarized, we can perform many different measures. Program packages such as Cell – F or Lucia allows us to find out the middle value of the fibers' diameter (diameter of white areas), or ratio of the fibers (ratio between white and black), or number of fibers in the whole sample.

Binarization of polymer is used to determine the width of the surface layer. This layer also includes spherulites. On the image, we can see white amorphous layer and then white surface layer with black areas, which get bigger in a size as they get closer to the center until the area is completely black. In this case, we perform an intense profile. Y axis represents amount of black color and x axis represent the distance from the edge of the sample. Amorphous white color is reflected on the graph as a minimum, its width would be subtracted on the x axis. Black center is reflected as a maximum. The difference between min and max is the width of the surface layer.

Determination of the size of spherulites is similar to the determination of fibers' diameter. Only spherulite images that are created in the laboratory can be binarized. Otherwise, binarization is very difficult.

Diameter of spherulite evaluated by Cell – F:

Statistical Function	2D Object Diameter Mean	2D Object Diameter Min	2D Object Diameter Max
Base Unit	μm	μm	μm
Count	10	10	10
Mean	**31.82**	**26.81**	**34.89**
Minimum	28.24	22.97	30.54
Maximum	33.85	29.75	37.17
Standard Deviation	1.83	2.26	2.13
Sum	318.18	268.11	348.87
Average Deviation	1.42	1.84	1.66

References:

[1] LEDNICKÝ, F.: *Pohledy do mikrosvěta* Nepublikováno
[2] LOBO, H.: *Handbook of plastics amalysis* Marcel Dekker, New York 2003, pp. 88-95.

This research has been supported by MŠMT grant No. MSM6840770015. .

Moisture Absorption of Carbon/Epoxy Composites

M.Černý, D.Čuprová

cerny@klok.cvut.cz

Department of Mechanics, Klokner Institute, Czech Technical University,
Šolínova 7, 16608 Prague 6

Introduction

Composites are usually subjected to changing environmental conditions during final use and it is important to include the effects of such changes in the analysis. Among the many environmental conditions that may influence composite mechanical behavior, changes in temperature and moisture content may have particularly important effect on polymer matrix. Effects of moisture are often referred as hygroscopic effects. The glass transition temperature indicates a transition from glassy behavior to rubbery behavior. Plasticization of the polymer matrix by absorbed moisture causes a reduction in the glass transition temperature and a corresponding degradation of composite properties. Moisture absorption to G/VE composites has been studied earlier [1-2]. Moisture absorption to C/E composites is described in [3].

Carbon fibre/ Epoxy Sample Sheets

Two types of prepregs have been handled: E8025C-25N and NT81500-525S, Nippon Graphite Fiber Corp. (Japan), Tab.1. According to manufacturer there is no essential difference of mechanical properties for both prepregs. The carbon fibres were of type CN-80, E 780 GPa, resin 25R, T_g 130^0C (NGF Co.). Sample sheets (CFRP) have been prepared by the autoclave technique from both types of prepregs with all fibres parallel, total thickness of sheets was 2.2 mm.

		E 8025C – 25N	NT 81500 – 525S
Fibre Weight	[g/m^2]	250	150
Total Weight	[g/m^2]	359	200
Resin Content	[%]	32	25
Thickness	[mm]	0.21	0.11

Tab.1 Properties of prepreg E 8025C – 25N and NT 81500 – 525S

Testing

The volume content of fibres in composites has been evaluated by microscopy method based on image analysis. It has been found that composite sample sheet made from E8025C-25N prepreg differs from NT81500-525S in volume content of carbon fibres (0.61 vers. 0.68).
Specimens for immersion tests were cut from the sample sheets. Test specimens were of size 15x 100 mm. The thickness was given by the thickness of the sheet (average 2.2 mm). The sheets have been immersed for 1000 h to distilled water with temperature 20ºC. The long-term sorption of corrosive media into composite specimen E8025C-25N and NT 81500 – 525S was evaluated. Results are shown in Table 2.

The hardness of composite before and after exposure has been tested by Barcol method according to ČSN EN 59. Results are shown in Table 3.

i	t [min]	E 8025 C-25 N		NT 81500-525 S	
		w_c [-]	w_m [-]	w_c [-]	w_m [-]
1	0	0.0000	0.0000	0.0000	0.0000
2	1320	0.0120	0.0450	0.0135	0.0504
3	2710	0.0211	0.0787	0.0555	0.2078
4	4205	0.0301	0.1125	0.0538	0.2015
5	5675	0.0316	0.1181	0.0589	0.2204
6	7075	0.0496	0.1855	0.0706	0.2644
7	11062	0.0511	0.1911	0.0958	0.3589
8	12865	0.0647	0.2417	0.1076	0.4029
9	17245	0.0752	0.2810	0.1211	0.4532
10	18635	0.0752	0.2810	0.1211	0.4532
11	21505	0.0767	0.2866	0.1379	0.5162
12	27230	0.0918	0.3427	0.1564	0.5853
13	30145	0.0933	0.3483	0.1446	0.5412
14	32935	0.0948	0.3539	0.1749	0.6545
15	39595	0.1053	0.3932	0.1665	0.6230
16	40970	0.1053	0.3932	0.1715	0.6419
17	42350	0.1113	0.4156	0.1749	0.6544
18	43790	0.1143	0.4269	0.1715	0.6418
19	59455	0.1489	0.5558	0.2136	0.7988
20	60865	0.1489	0.5558	0.2152	0.8051

Tab.2 Moisture absorption of composite from prepreg E 8025C – 25N and NT 81500 – 525S

t [min]	E 8025 C-25 N	NT 81500-525 S
	° Barcol	° Barcol
0	40	35
60865	28	20

Tab.3 Barcol hardness of composites before and after exposure

Conclusions

The absorption to NT81500-525S has been found higher then to E8025C-25N. Effect of different moisture absorption is caused by the destruction of carbon fibre/ matrix interface due to hygrothermal action of distilled water, which is higher for NT81500-525S then for E8025C-25N. Epoxy resins absorb water from corrosive environment and the hardness decreases due to plasticization of the matrix.

References:

[1] ČERNÝ, M. – KOŘÍNEK, Z.: *Effect of Corrosive Environment on Properties of Vinyl-ester /Glass Laminates* CMSE/1 Conference, Proceedings, 2001, pp. č. 101-104.

[2] ČERNÝ, M.: *Micromechanical Modeling of Degradation Processes in Composites* MC/ Conference, 2002, pp.č. 39-42.

[3] SHEN,C.H. – SPRINGER, G.S.: *Moisture Absorption and Desorption of Composite Materials* Journal of Composite Materials 10, 1976, pp. č.2– 20.

This research has been supported by MŠMT grant No. MSM6840770015.

Micro-mechanisms of Fracture in 15Ch2MFA Steel

Š. Válek, P. Haušild, M. Kytka*

Stepan.Valek@fjfi.cvut.cz

Department of Materials, Faculty of Nuclear Sciences and Physical Engineering, Czech Technical University, Trojanova 13, 120 00 Praha 2, Czech Republic

*Nuclear Research Institute Řež, Division of Integrity and Technical Engineering, Husinec-Řež 130, 250 68 Řež, Czech Republic

In this study, micro-mechanisms of brittle fracture and influence of microstructural parameters on fracture behaviour of 15Ch2MFA steel are investigated. The bainitic steel 15Ch2MFA is widely used for manufacturing pressure vessel of nuclear reactors VVER440. Because the safety of this component is of primary concern, the extensive knowledge of the material and its possible mechanisms of failure are essential. The characterization of microstructure (such as bainitic packet size or distribution of second phase particles), mechanical testing and quantitative fractographic analysis was made [1]. The influence of irradiation on ductile fracture was also investigated [2].

Using the light microscopy, the metallographic cuts were investigated and the mean bainitic packet size was determined. It was found that the microstructure is the same for all three directions of forging and the mean bainitic packet size is around 30μm. Using Scanning Electron Microscopy (SEM) the microanalysis of second phase particles (inclusions) was done. X-Ray analysis revealed the MnS inclusions. The distribution of these inclusions was obtained using image analysis. The image analysis was done for magnifications 200x, 1000x using images obtained from both electron and light microscopy. For the electron microscopy the backscattered electron signal (mode COMPO) was used. Total number of found particles was 1882 and the investigated area was 28.8mm^2. Good agreement in distribution of sizes of particles for both electron and light microscopy and for different magnification was found.

Using SEM in secondary electron mode the polished and etched specimens were investigated in order to characterize the distribution of fine carbides in bainitic microstructure. For the image analysis the magnification 10 000x was used. On the area of 1228μm^2 there were found 1342 particles. It can be concluded, that there are two different populations of particles: Mns inclusions and carbides each with its own independent distribution of particle sizes.

On the fracture surfaces of Charpy specimens broken at different temperatures the quantitative fractographic analysis was undertaken. The influence of neutron irradiation was observed. Using the same method as in Ref. [3] the areas of different type of fracture were measured from the images obtained using CCD camera. On the fracture surfaces of specimens broken in the region of ductile to brittle transition both cleavage facets and ductile dimples were observed. The specimens were broken in the transition region by transgranular cleavage fracture, preceded by ductile dimpled fracture. It was confirmed, that the dependence of fraction of ductile fracture on temperature has the same character as transition curve for energy absorbed during fracture process. With increasing irradiation the proportion of ductile fracture decreased.

The distribution of ductile dimple sizes on fracture surfaces of Charpy specimens was determined using the image analysis. For image analysis, the micrographs obtained at different magnifications (10 000x, 3000x, 1000x, 300x and 100x) were used. The distribution of

dimple sizes was obtained for each magnification. Altogether 13 810 dimples were identified. It was found that distributions of dimple sizes obtained at different magnification are superimposed, which prove accuracy of our measurement. It was also found that the dimple size distribution joined from all magnifications is continuous in spite of existence of two different distributions of second phase particles (inclusions and carbides), participating in ductile rupture. This result is in good agreement with [4]. It was found that the distribution of dimple sizes does not change with increasing distance form notch root.

From instrumented Charpy tests the values of energy and displacement of striker, associated with different stages of fracture, were determined. The fracture energy was correlated with displacement at the initiation of unstable crack propagation (initiation of cleavage fracture) and was found linearly dependent. The correlation of values of energy on areas of fracture surfaces, which belong to different type of fracture, was found. The best correlation was found for dependency of crack initiation energy on area of ductile fracture adjacent to the notch. From that it can be concluded, that most of the absorbed energy belongs to the stage preceding the cleavage crack initiation, which is represented by small area of ductile fracture adjacent to the notch. It was also found that both the fracture energy and the proportion of ductile fracture is decreasing with increasing irradiation.

References:

[1] Š. VÁLEK: *Physical mechanism of brittle fracture in low alloy steels,* Master thesis - KMAT 2006, pp. 1-75.

[2] P. HAUŠILD, M. KYTKA, M. KARLÍK, P. PEŠEK: *Influence of irradiation on the ductile fracture of a reactor pressure vessel steel,* Journal of Nuclear Materials 341(2-3), 2005, pp. 184-188.

[3] P. HAUŠILD, I. NEDBAL, C. BERDIN, C. PRIOUL: *The ingluence of ductile tearing on fracture energy in the ductile-to-brittle transition temperature range.* Materials Science and Engineering, 2002, pp 164-174.

[4] S. H. GOODS, L. M. BROWN: *The Nucleation of Cavities by Plastic Deformation,* Acta Metallurgica, 1979, No. 1, pp. 71 – 85.

This research has been supported by the Ministry of Education, Youth and sports of Czech Republic in the frame of the project MSM 6840770020.

Fracture behaviour of Fe_3Al based alloys with Cr and Zr addition

A. Kubošová, M. Karlík, P. Haušild, J. Prahl

Andrea.Kubosova@fjfi.cvut.cz

CTU, Faculty of Nuclear Sciences and Physical Engineering,
Department of Materials, Trojanova 13, 120 00 Praha 2

This paper presents a study of fracture behaviour of two Fe_3Al based intermetallic alloys [1] with different Zr content given in the table 1. The alloys were prepared by vacuum induction melting and casting. The ingots were hot rolled at 1100°C to plates 13 and 7 mm thick and subsequently quenched into mineral oil. After machining by milling, all the test specimens were annealed in air at 700°C for 2 hours to relieve internal stresses and then quenched into mineral oil. The microstructure of specimens machined from both hot rolled plates was recovered, with elongated grains having up to 1 mm in the direction of rolling and up to 300 μm in the transverse direction.

Table 1: Chemical composition of studied materials

Alloy		Al	Cr	Zr	C	Fe
FA02Z	(at.%)	31.46	3.5	0.25	0.19	Balance
	(wt.%)	18.2	3.9	0.49	0.05	Balance
FA06Z	(at.%)	29.5	2.35	0.63	0.2	Balance
	(wt.%)	16.8	2.58	1.21	0.05	Balance

Static tensile tests were carried out at temperatures 20 (RT), 200, 300, 400, 500, and 600 °C respectively on INSTRON 1195 testing machine equipped with a resistance-heated furnace. At each temperature, two cylindrical buttonhead specimens of the alloy FA02Z having 3 mm in diameter and 22 mm gauge length were tested at constant crosshead sped of 2 mm/min (initial strain rate 1.6×10^{-3} s^{-1}). Testing samples from the FA06Z alloy having M12 thread heads were 5 mm in diameter and 26 mm in gauge length. The crosshead speed was also 2 mm/min.

The basic mechanical characteristics, 0.2% proof stress ($R_p0.2$), ultimate tensile strength (R_m) and tensile elongation (A), were measured at temperatures up to 600°C. Considering the range from 20°C to 540°C ($D0_3$ ordered region), $R_p0.2$ and R_m had their minimum at 200°C, while the maximum values were reached at 300°C (R_m) and 500°C ($R_p0.2$), respectively. For both alloys, measured values at 20°C and 400°C were comparable and the values of $R_p0.2$ and R_m at 600°C (B2 ordered region) were practically identical. Tensile elongation at elevated temperatures was 3 to 4 times higher than tensile elongation at room temperature. In the $D0_3$ ordered region the elongation slightly increased with temperature, except for 400°C, where the value dropped down to 10%. At 600°C, in B2 ordered region, the elongation was substantially higher than at 500°C ($D0_3$ ordered region). Described temperature dependencies are in good agreement with the dependencies from Ref. [2] (experiments on Fe-28Al-3.6Cr-0.1Ce-0.16C (at.%) alloy). The only difference consists in the evolution of elongation with temperature. While in Ref. [2] the elongation after reaching its maximum value (11.5%) drops approximately to the same value as at RT (~2.5%) at 300°C, in the present study the elongation was higher (17.2%) at 500°C than of RT and 300°C values. Fracture surfaces of ruptured tensile specimens changed from transgranular cleavage facets at RT to entirely ductile dimpled fracture at 600°C.

Fatigue crack growth experiments were carried out on FA02Z alloy on compact tension (CT) specimens 5 mm thick, 50 mm wide and 48 mm high. The loading frequency was 10 Hz at 20, 150, 300, and 500 °C (in the $D0_3$ ordered region) and 2.5 Hz at 600°C (in the B2 ordered region). A constant maximum load F_{max} = 4.8 kN was used, the stress ratio R was 0.042. The crack length during fatigue test was measured by temperature independent potential method with the frequency of 4 Hz, using TECHLAB SRT-2K device controlled by Fatigue Crack Growth Monitor software. The temperature dependence of fatigue life (including crack initiation and propagation at a constant maximum load F_{max} = 4.8 kN) is summarized in table 2.

Table 2: Results of fatigue experiments

Testing T [°C]	20	150	300	500	600
Fatigue life [cycles]	245 000	480 000	228 000	6 000	4 400

The fatigue crack growth rate is much higher at 20°C than that at elevated temperatures. It means that the slope of $v(\Delta K)$ curves is much steeper and the exponent m in the Paris equation $v = C(\Delta K)^m$ is much higher at 20°C. At elevated temperatures, the value of the m exponent remains nearly the same, and the shape of the $v(\Delta K)$ curves for different T is very similar. An important difference is in the fatigue crack growth rate: at 500°C and 600°C it is about two orders higher than at 150°C and 300°C. The fatigue crack growth resistance of the alloy with Zr is higher than that of the similar alloy with Ce addition [2-4].

The main fracture micromechanism is transgranular cleavage and it does not change significantly with increasing temperature. Fracture surfaces consist of facets varying in the arrangement, size and micromorphology. Most of the facets are classical transgranular cleavage but also other types of facets were found (transgranular quasicleavage, intergranular decohesion, and, exceptionally, transgranular facets with ductile dimples). Some of the cleavage facets are covered by brittle fatigue striations. In addition, the fracture surface at 150°C (or at 500°C in the $D0_3$ ordered region) was very similar to the fracture surface at 20°C (or even at 600°C in the B2 ordered region). That means that the fracture mechanism under dynamic loading practically did not change during the transformation $D0_3 \leftrightarrow$ B2. On the other hand under static loading, after the transformation $D0_3 \leftrightarrow$ B2 transgranular cleavage changes to ductile dimpled fracture.

References:

[1] WESTBROOK, J. H. – FLEISHER, R.L.: Intermetallic Compounds. John Wiley, New York, 1995.

[2] HAUŠILD, P. – KARLÍK, M. – NEDBAL, I. – PRAHL, J.: *Fatigue Crack Propagation in an Fe_3Al-based Alloy Tested at Elevated Temperatures*, Kovové Materiály 42, 2004, pp. 156-164.

[3] KARLÍK, M. – NEDBAL, I. – SIEGL, J. – PRAHL, J.: *Behaviour of an Fe-28Al-3Cr-Ce alloy under cyclic loading*. Journal of Alloys and Compounds, 378, 2004, pp. 263-267.

[4] PRAHL, J. – HAUŠILD, P. – KARLÍK, M. – CRENN, J.-F.: *Fracture behaviour of Fe_3Al alloy with additions of Zr and C at different temperatures*, Kovové materiály – Metallic Materials, 43, 2005, pp. 134-144.

This research has been supported by Ministry of Education, Youth and Sports of the Czech Republic (Project MSM6840770021).

Local Conditions at the Growing Fatigue Crack in CCT Specimens of Different Thicknesses

O. Šimek, V. Oliva, A. Materna

ondrej.simek@fjfi.cvut.cz

Department of Materials, Faculty of Nuclear Sciences and Physical Engineering, Czech Technical University, Trojanova 13, Praha 2, 120 00

The fracture mechanics is able to predict stable fatigue crack growth in a flat specimen, but standard *K*-factor concept is failing for example in geometrically complicated bodies. An alternative approach is being developed at the Department of Materials [1, 2, 3]. Cyclic plastic strain as well as the cyclic stress field around the crack front is studied in detail through modeling of growing fatigue crack using Finite Element Method (FEM). The FEM simulation itself does not represent a greatest problem in spite of the fact, that the plasticity induced crack closing, crack opening and very small crack advances have to be modeled. The cardinal issue is how to predict fatigue crack growth rate from comprehensive knowledge of local cyclic deformation mechanics at the crack front.

An energetic approach based on local low-cycle fatigue conditions immediately at the crack front and on a critical value of plastic strain energy density is investigated. Let's assume a material element in the crack plane and ahead of the crack front in some very small distance (typically several micrometers). Such element is considered as an independent element which undergoes the loading cycles coincident with FEM model. When the accumulated plastic strain energy density reaches the critical value the element is broken down and the corresponding part of the crack front moves into the new position. Since the loading cycle is extensive, the lifetime of the element falls to low-cycle fatigue domain. Unfortunately such energetic prediction of the fatigue crack rate is complicated by the fact that the critical energy density is most likely not a material constant [1, 2]. FEM simulation of the local loading conditions along the real fatigue crack front and generalization of the Sih's energetic criterion [4] is the main goal of the present research.

A growth of modeled fatigue cracks was experimentally observed (by means of an optical microscope) in CCT specimens of different thicknesses (5, 3, 1, and 0.5 mm respectively) under uniform cyclic loading. Real curved crack-fronts were highlighted on fracture surfaces by overloading cycles. Highlighted front shapes were subsequently determined by fractographic analysis using scanning electron microscope. Basic mechanical properties of utilized D16CT1 aluminum alloy were determined from tensile test. Results of elastic-plastic FEM simulations have provided a detailed description of the cyclic stress and strain cycle in front of curved fatigue crack fronts during steady-state growth, a description of the crack closing and opening and information about plastic strain energy dissipation in the cyclic plastic zone in front of the crack [1]. The main conclusions can be formulated as follows:

1) The local loading conditions at the fatigue crack front vary with a depth under the free surface. The tensile stress in very thin surface layer (several tens of micrometers) is not much higher than the yield stress, but the local plastic strain range is very intensive due to lack of out-of-plane constraint. At the vast majority of crack-front length (out of the surface layer), there are nearly plane strain conditions

independent on specimen thickness. Plastic strain range under the high constraint is not so intensive whereas the tensile stress reaches very high value, exceeding three times the yield stress.

2) The material in front of the crack and near the free surface is hardly pre-damaged by intensive cyclic plastic strain and therefore even the small tensile stress is sufficient for the final local fracture. Final rupture of less damaged material in a depth of the specimen occurs under much higher stresses.

3) The stress distribution near the free surface is practically uninfluenced by the specimen thickness. However, the plastic strain amplitude and the plastic strain energy dissipated during the fatigue cycle in the surface layer are noticeably promoted by decreasing thickness of the specimen.

4) The fatigue crack growth rate due to Laird's plastic mechanism of blunting and resharpening of the crack front (without the fracture) is almost by one order of magnitude lower than the experimental crack rate. That means that the "high-cycle" fatigue crack growth might be controlled namely by local low-cycle fatigue of material in front of the crack.

5) For given fatigue crack length, the critical value of the plastic strain energy density (connected with elementary fatigue fracture at the crack front) is dependent on the specimen thickness and on the depth under the free surface. Both these effects can be roughly covered by plastic strain range vs. critical energy dependency.

6) Presented conclusions should be verified through succeeding experiments, during which the same loading will be applied on cracks of different lengths.

References:

[1] ŠIMEK, O.: *Fatigue Crack Growth in CCT Specimens of Different Thickness (Master's degree thesis) [in czech],* KMAT-FNSPE-CTU Prague, 2006, 85 p.

[2] DENK, T., OLIVA, V., MATERNA.: *Critical Strain Energy Density Along the Curved Front of the Growing Fatigue Crack,* Materials Science Forum,Vol. 482, 2005, pp. 307-310.

[3] OLIVA, V., MATERNA, A., DENK, T.: *Stress and strain cycle ahead the curved fatigue crack front in the thick wall,* In: Engineering Mechanics, 2003, 10 p.

[4] SIH, G. C., MOYER JR, E. T..: *Path Dependent Nature of Fatigue Crack Growth,* Engng Fracture Mech., 1983, pp. 269-280.

This research has been supported by MŠMT grant No. MSM 6840770021.

Quantitative Texture Analysis by the Orientation-Distribution Function (ODF) on the KSN-2 Diffractometer

S. Vratislav*, M. Dlouhá*, L. Kalvoda*, A. Grishin*

vratisla@troja.fjfi.cvut.cz

*Department of Solid State Engineering, Faculty of Nuclear Sciences and Physical Engineering, Czech Technical University, Břehová 7, 115 19 Prague 1, Czech Republic

The grain orientation distribution (texture) gives important information about this structure and influences the properties of materials. The term texture is used in connection with the preferred crystallographic orientation of the polycrystalline aggregates in metallurgy, polymer materials and also in geology. The theoretical basis and the formalism of this analytical description were worked out deeply by J. Bunge [1] and J. Roe [2]. Such methods of texture description could help us to explain quantitatively the behaviour of polycrystalline materials during mechanical and thermal treatment, as also the phenomenon of the anisotropy of various physical properties in polycrystalline aggregates.

The neutron diffraction method is used on a large scale in solid-state physics and materials research. The high penetration of neutrons through the majority of materials is the main advantage for examination of the textures of coarse-grained materials like oriented transformer sheets.

Our laboratory developed and tested experimental and calculation techniques for quantitative texture analysis based on the ODF (orientation distribution function) combined with the diffraction of thermal neutrons. The texture experiments were carried out on the KSN-2 diffractometer using the TG-1 texture goniometer [3]. The measured data are corrected and normalized and then they are used to calculate (by means of the TODFN [3] computer package) the coefficients of expansion to express the measured direct pole figures using spherical functions. The determined pole figures are used to calculate the coefficients of expansion Clμν for expanding the ODF function into a number of generalized spherical functions. All texture characteristics can be obtained from these TODFND-codes [3, 4]: pole figures, inverse pole figures, ODF (f(g) values in the 5o steps), parameters of the ideal orientations (HKL)< uvw>, texture index J, volume fraction coefficient f, fibre texture distribution. In this article we have given the results, which were obtained on the oriented coarse-grained steel sheets and on the texture measurements of polymer foils.

We have examined the coarse-grained samples of the Fe-3%Si oriented silicon steel and the relationship between the final texture form and the temperatures of the primary and secondary cold rolling was characterized. The complete texture parameters were determined by the ODF function from neutron diffraction data:

- The texture of the silicon steel sheets after different processing stages was described using a few fibre orientations: <110> axis parallel to ND, <001> parallel to RD.
- The f(g) values of the (110)<001> ideal orientations, texture index J and volume fraction coefficients *f* were determined.
- We can conclude, that the best texture form and f(g) values were obtained at $T_{IV}=T_{IIV}= 20$ °C, i.e. for sample 1 (power losses Z_p are lowest and the value magnetization B is highest). In this technological treatment we have determined very sharp and narrow form of the f(g) values in the neighborhood of the (110)<001> ideal orientation. If the temperatures are going up to

200 °C, the texture values are going down and the texture peak half-width is wider. The complete results of the quantitative texture analysis are given in [4].

The results obtained for the PVC samples are summarized in Table 1 and can be interpreted as follows: Polymer main-chains forming crystalline domains are preferentially oriented parallel with the foil plane [5]. Slight reduction of the neutron scattering intensity related to amorphous phase was observed with ε_A increasing what suggests there is a part of polymer chains originally contributing to amorphous phase transforming itself into a new crystalline phase during the plastic deformation process. This phase identifies itself by a strong diffraction maximum corresponding to an inter-planar distance of 0.520 nm, observed exclusively in diffraction patterns of samples in symmetrical reflection position. The highest intensity of the reflection was obtained for the equally bi-axially drawn foils.

Table 1. Parameters of the investigated PVC foils

Sample	ε_A [cm^2/cm^2]	α_0 [deg]	P^{SD}_{Reg1}	P^{TD}_{Reg1}	P^{ND}_{Reg1}
1.7 x 1.7	2.89	0	0.50	0.73	0.87
2.4 x 1.4	3.36	10	0.56	0.47	0.86
2.2 x 2.2	4.84	25	0.53	0.64	0.76

Remark: α_0 is the observed declination of the optical indicatrix from the direction

At present time our laboratory prepared experimental and computing techniques for quantitative texture analysis based on the ODF combined with the Rietveld refinement of powder diffraction patterns. The utilization of these techniques is directed to the quantitative texture analysis such materials as: rocks, polymers, intermetallic compounds, high-T_C ceramics or composite materials.

References:

[1] H. J. BUNGE: *Textures and Microstructures* Vol 5, 1982, pp. 153-162.

[2] R. J. ROE: *J Appl. Phys.* Vol. 36, 1965, pp. 2024- 2030.

[3] S. VRATISLAV, M. DLOUHÁ, L. KALVODA: *Proc. of The International Conference Mathematical Methods of Texture Analysis,* March 21 - 24, 1995, Dubna, Russia 1995, pp. 48 - 51.

[4] S. VRATISLAV, M. DLOUHÁ, L. KALVODA: *Solid State Phenomena* Vol. 105, 2005 pp. 175-180.

[5] L. KALVODA, M. DLOUHÁ, S. VRATISLAV: *Solid State Phenomena* Vol 105, 2005 pp. 439 - 446.

This work was funded by the Czech Ministry of Education within the framework of the grant No. MSM 6840770021.

Effect of Austenitizing Parameters on Structural Characteristics of Steels Type HSLACS.

J.Cejp, K.Macek

Jiri.Cejp@fs.cvut.cz

CTU,Faculty of Mechanical Engineering,Dept. of Materials Engineering
Karlovo nám.13,121035 Praha 2

Grain size refining and precipitation strengthening are the most significant factors with respect to increasing of yield strength of microalloyed cast steel with low carbon content. The properties of thin-walled castings are also strongly affected by cooling rate both during crystallization and during austenite transformation. Considerations concerning the heat treatment begin with choice of conditions for austenitization which starts solution annealing, normalizing or quenching. Tempering is very often used as the last stage of heat treatment with a view to modify the transition temperature to brittle fracture on required level.

Aside from monitoring of influence of heat treatment on mechanical properties of cast steels microalloyed with vanadium, titanium and niobium the austenitization temperature was theoretically optimised with respect to ferrite grain size strengthening and precipitation strengthening. Influence of microalloying elements individually and in binary combinations on structural characteristics in normalized state was investigated. Relation between grain size of ferrite, conditions of austenitization and rate cooling was discussed.

Starting study was fixated on optimalization of conditions for austenitization before normalising. Austenitizing process works not only austenite grain size but after air cooling secondary grain size as well. It has also expressive influence on solution of carbides, nitrides and carbonitrides in austenite consequently on precipitation potential [1]. After maximization of precipitation potential, increasing temperature and elongation time of austenitization was detected undesirable course austenite grain. Temperature of isochronal austenitization (2 hours) in our experimental was chosen in accordance with thermodynamic equations so that approximately one third or one half of the total content of microalloying elements (vanadium, niobium, titanium) was soluted in austenite.

Microstructure of microalloyed steels consists from fine grained polyhedral ferrite and pearlite if the temperature was fairly low and vanadium is present, niobium supports formation of acicular ferrite.

Mechanical properties of low carbon steels significantly consist in ferrite grain size, which depends on austenite grain size and cooling rate during transformation to ferrite in temperature interval A_{r3} and A_{r1}. Since experimental programme afforded sufficiency of dates relation between grain size of ferrite [2], conditions of austenitization and rate cooling by means of grain size of austenite kinetics was determined:

$$d_\alpha = A.\exp\left(\frac{-B}{T}\right).t^a.\left(\frac{\Delta T}{\Delta t}\right)^b_{8/5}$$

where T = austenitizing temperature, t = time of austenitization , $(\Delta T / \Delta t)_{8/5}$ = average cooling rate between 800 and 500°C.
Constants A, B, a, b were expressed for steel 17Mn6 and 22MnVNb6 between 930 and 1070°C (activation energy was taken by T.Gladman [3]), time 1 and 8 hours and cooling rate from 0,05 to 8 K/s and are given in table 1.

Table 1. Values of constants in equation for ferrite grain size.

Steel	A [μm . K^{-b}. s^{b-a}]	B [K]	a [1]	b [1]	Temperature [K]
17Mn6	$3,5 . 10^{11}$	-33580	0,32	-0,41	1203
	$2,6 . 10^{10}$	-33580	0,32	-0,41	1343
22MnVNb6	$1,5 . 10^{15}$	-42100	0,18	-0,39	1203
	$4,2 . 10^{13}$	-42100	0,18	-0,39	1343

The kinetics of growth of austenite grain is characterized by exponent *a* and detected values good express the influence of dispersed particles of carbonitrides on austenite grain boundary migration. After comparison of calculated and experimental values of ferrite grain size for steel 22MnVNb6 excellent harmony for cooling rate less than 1,04 K/s was discovered. It means that ferrite grain size and austenitizing and cooling parameters are related according to mentioned equation just for real conditions during cooling of thin-walled castings.

References:

[1] H.R.LIN, A.A.HENDRICKSON : *Metallurg.Trans.* Vol.19 A, 1988, pp.1471-1480.
[2] A.G.SPEKTOR,E.E.UNDERWOOD: *Quantitative Stereology.* Addison-Wesley Publ.Comp.,Reading, Mass.1990, p.126.
[3] T.GLADMAN: *The Physical Metalurgy of Microalloyed Steels.* The Institute of Materials, London 1997, p.363.

This research has been supported by MŠMT grant. No.6840770021

Welding of Commercially Pure Titanium

Z.Kinter, J.Prajer, J.Cejp

KinterZdenek@seznam.cz

CTU,Faculty of Mechanical Engineering,Dept. of Materials Engineering
Karlovo nám.13,121035 Praha 2

Titanium and its alloys have been considered as one of the best engineering materials for industrial applications because offer excellent combination of properties. High strength to weight ratio, fatigue life, good toughness, corrosion resistance, good formability make them attractive for a different applications ranging from structural components to aircraft and aerospace applications [1, 2, 3].

Titanium and titanium alloys may be joined by a wide variety of fusion processes including gas tungsten arc welding, gas metal arc welding, plasma arc welding, laser beam welding and electron beam welding. The primary precaution is to avoid contamination of the fusion and heat affected zones and to shield metal from contact with air.

This work is a result of collaboration between CTU, Faculty of Mechanical Engineering and AERO Vodochody in examination of various procedures of welding and selection of the best methods of joining titanium alloys used in aircraft industry. In accordance with requirements, two technologies were evaluated first – gas tungsten arc welding (GTAW) and a special laser welding method (LBW). Other procedures will be supplemented later, such as resistance spot welding or plasma welding. The GTAW method was selected with respect to the fact that supplementary material may be added to the welding arc independently, while the protective inert gas atmosphere facilitates clean and high-quality welds.

The initial study and experimental programme were carried out with commercial GRADE 1 titanium, often marked as Ti99.5. This material, demonstrating exceptional ductility, good formability and excellent weldability, was available as hot rolled sheet in thickness of 1 mm. The chemical composition of the material complied with the standard, demonstrating admixtures of 0.15 % Fe, 0.18 % O, 0.02 % N, 0.05 % C in wt.% to Ti. Strength and plasticity qualities were verified by means of a tensile test, using an INSTRON device, at ambient temperature: yield strength YS= 280 MPa, tensile strength TS= 335 MPa, elongation A= 44%.The material microstructure consisted of grains of α phase, occasionally interspersed with deformation twins, and small particles both within the grains and at grain boundaries.

Welding by the GTAW method included prevention of absorption of nitrogen and oxygen from the atmosphere by replacement of the welding atmosphere with high purity argon and welding itself took place under power drain P = 4 kW. Laser welding LBW was performed by an Nd:YAG laser, wavelength of 1064 nm, frequency = 350 Hz, pulse length and energy = 100 J, power drain = 3.1 kW, laser beam motion velocity = 1,500 mm per minute. In the experimental programme, welds were examined for welding of parts aligned in the direction of rolling as well as perpendicular to the rolling direction, with several welds made in alternating pattern (one piece aligned with and one perpendicular to the rolling direction).

Quality of welds was investigated using non-destructive tests, visual examination as per CSN EN 970, and radiology test as per CSN EN 1435. The visual examination in accordance with CSN EN ISO 13919-1 evaluated the presence of fissures, cold joints, non-welded root gaps, elevation and overreach of welds in terms of size and position of the imperfection. The

radiation test protocol followed the requirements of the standard CSN EN 1435, evaluation and description of imperfections was made in compliance with CSN ISO 5817.

The following findings were resulted from examination of the welded joints prepared:
Laser-welded joints:
- 60 % of welds were of high quality without detectable imperfections;
- unsatisfactory welds demonstrated most frequently imperfections in the form of round gas fissures and imperfections related to non-welded root gaps with notching effect;
- high quality welds were in most cases found on joints made in the direction of rolling, while majority of the failed welds was made perpendicular to the direction of rolling.

Joints by GTAW:
- only one third of all welds were of satisfactory quality, the rest demonstrated imperfections in the form of elongated cavities and non-welded root gaps;
- similar to laser welding, joints made perpendicular to the direction of rolling proved to be thoroughly unsatisfactory.

The non-destructive tests, which clearly upheld the higher quality of laser welds, will be supplemented with mechanical tests, such as transverse tensile test, bend test, and hardness test. Also analysed will be weld structure, and the extent and shape of heat-affected area of welded material.

References:

[1] E. SCHUBERT, M. KLASSEN, I. ZERNER, C. WALZ AND G. SEPOLD: *Light-Weight Structures Produced by Laser Beam Joining for Future Applications in Automobile and Aerospace Industry.* Journal of Materials Processing Technology.Volume 115, Issue 1, 22 August, 2001, pp.2-8.

[2] Z. LI, S. L. GOBBI : *Laser Welding for Lightweight Structures* . Journal of Materials Processing Technology, Volume 70, Issues 1-3 , October 1997, pp.137-144 .

[3] Q.YUNLIAN, D. JU, H. QUAN, Z. LIYING : *Electron Beam Welding, Laser Beam Welding and Gas Tungsten Arc Welding of Titanium Sheet* . Materials Science and Engineering A,Volume 280, Issue 1 , 15 March 2000, pp.177-181.

This research has been supported by MŠMT grant. No.6840770021

Laser Surface Treatment of 2024 - T3 Aluminium Alloy

J.Cejp, I.Pavlásková

Jiri.Cejp@fs.cvut.cz

CTU,Faculty of Mechanical Engineering,Dept. of Materials Engineering
Karlovo nám.13,121035 Praha 2

There are different ways how to improve use value of Al-alloy by laser technology. The most often methods work on the coat melting and microstructure change system (LSM - Laser surface melting) use coat hardening by residual pressure strain (LSP - Laser shot processing) or alloy the surface with the suitable components (LSA- Laser surface alloying). All these methods significantly improve fatigue and corrosion properties and wear resistant [1,2,3].The report deals with the issue of laser beam interaction with the surface Al-alloy used in aircraft industry.

Laser beam was generated by two different laser generators. Firstly was used pulse generator Nd:YAG laser with wavelength 1060 nm, frequency range 1 – 18 kHz and the peak output 50 W. The feed speed of the laser beam was chosen from 5 to the 35 $mm.s^{-1}$. Secondly was used continual laser beam generated by diode laser with the output 3.1 kW. The material, which was used for the experiments, was a commercial EN AW – 2024 - T3 (4,4% Cu, 1,5% Mg, 0,6% Mn, solution treated, cold rolled and naturally aged) in plate form with a thickness 0.8 mm.

The laser beam was applied on the 60x40 mm samples that were on air or in water. When the laser beam has come through the water, the small bubbles were on the metal sheet and have created another boundary-line for the beam. After those experiments the samples were afloat only. The frequency was chosen in range 5000-15000 Hz for the first experiments. As absolutely unsuitably frequency was found out the 5000 Hz frequency. By using this frequency, the material was pull-out from the surface, the laser path was rough and the surface was burned. There was no material treatment nearly the laser path. When the 10000 and 15000 frequency was used, soft almost invisible path was created. This path was hardly observed with a microscope. For the next experiments the frequency 16000 Hz and more was applied, the beam speed was only 5-15 $mm.s^{-1}$. Under this condition, the good observed path was created. The area and the intensity were measured by course of a micro hardness.

Alloy 2024 belongs to the most widespread material used in aircraft industry. A tendency to improve the manufacture qualities leads to the experiments that try to prepare structure composite of the sandwich type. Thereby the laser beam was applied from both sides of the metal sheet in 10x50 mm area with minimum laser path overlapping, tensile stress was used on this way prepared sample. The results of this test didn't endorse estimated hardening effect.

Diode laser was applied for other samples which were put in the focus or max. 10 mm above the focus, during the tests was laser output changed in 475-800 W range and the laser beam speed was 1200 $mm.s^{-1}$. Produced path was linear and well visible. Microscope

observation has showed a heat treatment zone with the depth up to 300 μm. This area was confirmed by the microhardness measurement. The microhardness profile, of the single paths, proved by evidence the structure change and the material properties intensity. With the 850 W laser output and with the sample distance 10 mm above the focus, melted zone on the surface was visible and the column grains arisen in the microstructure, which showed epitaxial growth from the unmelted zone. The significant strength degradation was observed in the middle of the path, while the hardening in the transition area – between base and heat treatment material. Laser beam with the 585 W output applied on the sample far 5 mm above the focus didn't melt the surface but the hardness was increased. The laser output is the most important parameter for the path pattern. Even if the small difference of the output (5 W) leads to the significant material structure change.

In case of optimal laser parameters melted zone on the surface is not observed and the structure change in the laser path increases the hardness to 14% [4].

Experiments, that were made, confirmed the possibility of Al 2024, in T3 condition, surface hardening. The hardening effect depends not only on the base sheet structure but fundamentally on the laser parameters. More suitable laser source for the material heat treatment was appeared the diode laser. Expressive hardening effect can be expected after coatings, which will lead to the higher laser beam absorption or under shielding gas.

References:

[1] T.T.WONG, G.Y.LIANG, C.Y.TAN G: *The Surface Character and Substructure of Aluminium Alloys by Laser Melting Treatment.* Journal of Materials Processing Technology, Volume 66, Issues 1-3, Apriel 1997, pp.172-178.

[2] P.PYERE, R.FABBRO, P.MERRIEN, H.P.LIEURADE: *Laser Shock Processing of Aluminium Alloys. Application to High Cycle Fatique Behaviour.* Materials Science and Engineering A, Volume 210, Issues 1-2, June 1996, pp.102-113.

[3] Z.HONG, Z.SHUYI, Z.XIAORONG, C.LAN, R.NAIFEI: *Investigation of the Surface Qualities of Laser Shock Processed Zones and the Effect on Fatique Life of Aluminium Alloy.* Surface and Coatings Technology, Volume 92, Issues 1-2, June 1997, pp.104-109.

[4] I.PAVLÁSKOVÁ: *Aluminium Alloy Laser Modification* CTU, Faculty of Mechanical Engineering,Dept. of Materials Engineering , Thesis 2006.

This research has been supported by MŠMT grant. No.6840770021

INDEX

Adámek, P., 28
Andrlík, V., 410
Armas Arciniega, J., 246
Aubrecht, J., 280
Aubrecht, L., 86
Bacarreza Nogales, O., 314
Balík, L., 270, 310
Balík, M., 156
Barva, M., 480
Bečvář, Z., 242, 160
Bém, P., 446
Benda, P., 98
Beneš, M., 16
Bensch, J., 278
Beran, L., 702
Beran, P., 532
Beran, V., 612
Beránek, J., 288
Berka, V., 756
Berková, V., 690, 700
Bezděk, P., 616
Bezpalec, P., 162
Bíba, J., 100
Bláha, J., 720
Bodnár, M., 82
Boháč, L., 42
Bolshakova, I., 446
Bouchner, P., 718
Bouška, P., 582
Brabec, T., 124
Bradna, J., 424
Broukalová, I., 608, 596, 606
Bryknar, Z., 88, 330
Buchar, P., 26
Bureš, M., 482
Burian, Z., 300, 304, 246
Cajthaml, J., 692, 698
Cejp, J., 366, 362, 364
Clavel, M., 316
Čadík, M., 186
Čáp, J., 78
Čapek, M., 500
Čápová, D., 750
Černý, M., 350, 352
Černý, R., 336, 334, 274, 276, 298, 322, 308, 340, 282, 284, 342, 286, 294, 320
Čeřovský, Z., 430
Česák, P., 230
Číhal, V., 290
Čížek, J., 390
Čtyroký, J., 708
Čudejko, M., 550
Čulík, J., 516
Čundev, D., 428
Čuprová, D., 352
Dalíková, K., 290
Demo, P., 44
Diels, J., 34
Djimaldé, G., 264
Dlask, P., 612
Dlouhá, M., 62, 80, 360, 204
Dobrev, D., 468
Dohnal, M., 636
Dohnal, P., 188
Doleček, V., 174
Doležal, B., 740
Doležal, F., 636
Doležel, T., 312
Doležílková, H., 528
Dostál, M., 440
Doubrava, M., 52, 38
Dráb, M., 204
Drahorád, M., 534, 626
Drahotušská, Z., 702
Drda, F., 708, 704
Drška, L., 28, 68
Drtinová, B., 462
Dřížďal, T., 476
Ďuran, I., 446
Dušek, J., 636
Eichler, F., 586
Eliaš, M., 648
Eliášová, M., 566, 552
Elmahalawy, A., 144
Faber, J., 722, 720
Fabián, V., 484
Fejtová, M., 154
Ferkl, L., 120
Fiala, C., 662, 638
Fiala, L., 334, 262
Fiala, P., 214
Ficenec, J., 524
Fischer, J., 240
Fitl, P., 498
Foglar, M., 536, 630, 658
Foltýn, L., 102
Forstová, K., 272
Fragner, B., 704, 702
Frantová, M., 620
Freiberg, F., 758, 738
Fresar, D., 726
Fričová, M., 506
Frková, J., 632, 612
Frýbort, J., 448
Funda, T., 492
Galuška, M., 38
Gerla, V., 486
Goldmann, T., 512
Gosmanová, G., 344
Granja Bustamante, C., 68, 84
Grishin, A., 360, 60
Grünwald, A., 668, 670, 672
Gudowski, W., 438
Haghi-Ashtiani, P., 316
Hájek, P., 662, 638, 594, 618
Halounová, L., 700
Hamal, K., 32, 244, 138
Hampl, P., 172
Hána, K., 492, 494, 500, 514, 518
Hanzík, F., 736
Harcová, H., 350
Haušild, P., 354, 306, 326, 278, 356, 348
Havlena, V., 122
Hazdra, P., 252, 254, 248
Heraltová, L., 442
Hermová, H., 682
Herrera Martinez, M., 134
Heřmanová, L., 552
Himmlová, L., 512
Hlaváč, O., 302
Hlaváč, V., 480
Hlinovský, V., 432
Hluší, L., 324
Hoffmann, K., 222
Hofreiter, M., 210

Holčík, J., 496, 514
Holeček, M., 674
Holiš, J., 218
Homola, P., 346
Hošek, J., 406, 408, 418
Hrachová, V., 78
Hrdoušek, V., 656
Hromada, E., 632, 612, 530
Hudec, P., 222
Huml, O., 454
Husáková, V., 526
Hykšová, M., 22
Hyniová, K., 170
Chichev, A., 62, 332
Chlouba, J., 592, 564
Chromiak, P., 554
Chudáček, V., 488
Ibehejová, M., 270
Jakoubek, P., 258
Jakůbek, J., 68, 84
Jakubše, J., 584
Jalová, M., 410
Jalový, M., 410
Janáček, J., 500
Janda, T., 296
Jandák, V., 216
Jandera, M., 556
Jareš, M., 714
Jelínek, I., 164, 156, 206
Jelínek, M., 498
Jelínková, H., 30
Jerie, J., 74
Jerman, M., 340
Jeřábek, M., 140
Jeřábek, V., 302, 246
Ježek, A., 558
Ježek, J., 92
Jilemnická, L., 754
Jiříček, O., 216
Jiřikovský, T., 694
Jisl, P., 104
Jun, R., 206
Juříčková, M., 452
Kajnar, P., 408
Kálal, M., 66
Kalvoda, L., 280, 360, 268, 60, 204
Kaňka, A., 78
Karásek, J., 590
Karlický, P., 734
Karlík, M., 346, 306, 326, 316, 356, 348
Karola, R., 474
Kašpar, M., 644
Katovský, K., 458, 454, 456
Kavan, M., 730
Kelnar, J., 294
Kinter, Z., 364
Klenko, J., 70
Klepáček, R., 268
Klíma, M., 184
Klír, D., 72, 58, 56
Kobylka, D., 444
Kocourek, T., 498
Kodet, J., 244
Kohout, K., 106, 144
Kohoutková, A., 318, 538, 608, 596, 546, 606
Kohut, M., 514
Koláček, K., 66
Kolář, J., 292
Kolář, K., 292
Kolařík, K., 348
Kolařík, L., 420
Kolísko, J., 270
Kolman, P., 108
Kolros, A., 438, 442, 458, 454
Komárek, M., 126
Koňařík, D., 498
Konopka, L., 172
Konvalinka, P., 298, 342, 286, 312, 292, 324
Konvičková, S., 508, 512
Kopecký, M., 210
Kopecký, P., 662
Kopřiva, P., 538
Koranda, P., 30
Kordík, P., 196
Kořínek, T., 220
Kos, J., 570
Koska, B., 634, 256, 18
Košetická, B., 738
Kovář, P., 226
Kozelek, P., 496, 514
Krajník, T., 112
Král, L., 32
Krása, J., 722, 720
Kratochvíl, J., 588
Kraus, I., 344
Kravárik, J., 72, 58, 56
Krčál, J., 140
Krčálová, L., 140
Krejčí, J., 698
Kremlová, L., 750
Kropík, M., 452, 450
Kryštůfek, J., 472
Křeček, J., 574
Křemen, P., 110
Křemen, T., 644, 256
Křístek, V., 610, 658, 640
Kuba, J., 68
Kubeček, V., 34
Kubeš, P., 72, 58, 56
Kubínová, L., 500
Kubošová, A., 306, 356
Kučerová, A., 182
Kudláček, I., 414
Kudláček, J., 420
Kukaň, V., 534, 626
Kuklík, P., 614
Kuklíková, A., 614, 568
Kuna, A., 232
Kunz, J., 290, 338
Kupcová, K., 616
Kusý, P., 746
Kvochová, S., 570
Kybic, J., 480
Kytka, M., 354, 326
Laciok, A., 462
Landa, M., 94
Lánská, M., 716
Laube, P., 684
Lehovec, F., 734, 736
Lepš, M., 182
Leys, C., 64, 54
Lhotská, L., 488, 490, 486
Linhart, V., 68
Lórencz, R., 124
Lucki, M., 42
Lupíšek, A., 662, 618
Máca, J., 532
Macaš, M., 490
Macek, D., 728
Macek, K., 362
Maděra, J., 308, 340, 294
Mach, K., 522
Machyl, J., 404
Maier, K., 708, 704
Majlingová, O., 36
Malkovská, N., 680

Malý, I., 192
Malý, K., 108
Marek, P., 540
Martínková, M., 66
Matas, J., 116
Matějka, K., 456
Materna, A., 358
Menšík, A., 542
Mikeš, K., 562
Mikisek, M., 448
Mikš, A., 408, 46, 48, 50
Mikšovský, M., 698
Mindl, P., 430, 428
Mňahončáková, E., 298, 284, 286
Moravec, J., 398
Mukařovský, J., 662
Musil, D., 616
Musílek, J., 560
Musilová, Z., 562
Mušálek, R., 278
Mužík, J., 494
Myslík, M., 302
Nágl, J., 688
Nahodil, P., 144, 150
Nehéz, M., 190
Němcová, Š., 78
Němec, M., 138
Němeček, J., 272
Nenadálová, L., 578
Neškudla, J., 234
Neumanová, J., 646
Niewald, J., 640
Novák, J., 662, 46, 48, 50
Novák, L., 576
Novák, O., 130
Novák, P., 154, 502, 46, 48, 50
Novák, R., 518
Nováková, L., 180, 502
Novotný, S., 718
Novotný, T., 582
Nožička, J., 390
Obr, V., 18
Oliva, V., 358
Oppl, L., 478
Paclt, Z., 426
Pačes, P., 236
Pačesová, H., 724
Pánek, P., 586
Pavelka, K., 208
Pavlásková, I., 366
Pavlík, Z., 336, 334, 322
Pavlíková, M., 336, 322, 284, 320, 328
Pekárek, S., 64, 54, 76
Pernicová, R., 322
Persson, C., 438
Pešková, Z., 686
Pešťák, J., 698
Peterka, T., 742
Petrík, M., 20
Piekník, R., 718
Píchal, J., 40
Píše, M., 128
Plachý, M., 744
Plachý, T., 642
Pleninger, S., 722
Pohořelský, L., 400
Pokorná, N., 318
Polák, M., 642
Popelová, L., 702
Pospíšil, J., 706, 634, 644, 256
Pospíšil, M., 54
Pospíšil, S., 68, 84
Potůček, Z., 88, 330
Pourová, M., 416
Prahl, J., 306, 316, 356
Prajer, J., 364
Prajer, M., 732
Prajzler, V., 300, 302, 304, 246
Procházka, I., 32, 244, 138
Procházka, J., 676
Prostějovská, Z., 612
Přeučil, L., 112
Půbal, Z., 598
Punčochář, P., 574
Puričer, P., 224
Rataj, J., 450
Rey, C., 316
Rezek, A., 642
Rieger, F., 398
Rogalewicz, A., 666
Rohrböcková, S., 604
Rozinek, O., 504
Roztočil, J., 232
Růžička, J., 662, 594
Rybár, P., 312
Řeřábek, M., 250
Řezáč, K., 72, 58, 56
Římal, J., 600, 602, 658, 604
Samec, Z., 464
Samek, L., 600
Saska, M., 112
Semerák, P., 44
Sentkerestiová, J., 446
Schneiderová, R., 750
Schusterová, M., 704
Siegl, J., 278
Silber, R., 466, 468
Skala, J., 676
Sklenička, R., 96
Sklenka, L., 456, 450
Slavíček, M., 668, 670, 672
Slavíčková, K., 668, 670, 672
Slepička, P., 176, 160
Smrčka, P., 500
Sochor, M., 510
Sojka, J., 720
Sopko, V., 600, 36
Soukup, P., 148
Staněk, K., 662, 660
Starý, V., 266
Strnadel, B., 326
Studenovský, K., 418
Studnička, J., 554
Suchá, J., 706
Suchánek, P., 238
Suchý, J., 114
Svatoš, V., 150
Svatušková, J., 208
Svoboda, J., 214
Svoboda, T., 116
Svobodová, M., 338
Szabó, Z., 504
Šanda, M., 576
Šebera, J., 464
Šedlbauer, M., 450
Šenberger, T., 704, 702
Šimák, B., 166
Šimeček, I., 196, 198, 200, 202
Šimek, M., 146
Šimek, O., 358
Šindler, D., 602, 656
Šiňor, M., 68
Šmídová, M., 738
Špaček, J., 226
Šrytr, P., 578

Štamberg, K., 462
Šťastný, B., 666, 668, 670, 672
Šťáva, M., 130
Šťava, O., 200
Štemberk, P., 536, 318, 630, 628
Štěpánková, O., 180
Štrausová, K., 580
Štroner, M., 696, 706, 634
Šulc, J., 30
Šupol, J., 132
Švihlík, J., 228
Tatíček, F., 420
Tesárek, P., 298, 342, 286
Těšínský, M., 438
Tichá, P., 44
Tichý, D., 192
Tichý, T., 722, 720
Tolde, Z., 266
Toman, J., 282
Tománková, J., 750
Tožičková, L., 544, 624
Tran, N., 628
Trnka, P., 210, 258, 122
Třeštík, J., 240
Tywoniak, J., 662, 660
Uher, J., 68
Uhlíř, A., 592, 564
Urlich, P., 702
Vacek, V., 392, 52, 38
Vála, L., 74
Válek, Š., 354
Valchářová, V., 702
Valoušek, P., 136
Válová, M., 402, 420
Vaněk, T., 178
Vašková, J., 624, 620
Vébr, L., 650, 652, 654, 664
Vedral, J., 234
Vejpustková, J., 510
Velický, M., 466
Vencl, R., 566
Veselý, R., 668, 670, 672
Veverka, B., 698
Vídenský, J., 568
Vilímek, M., 508
Vinš, M., 458
Vinš, V., 392
Vistr, T., 546
Vítek, T., 168
Vlček, M., 142
Vobecký, J., 254
Vočka, R., 448
Vodička, J., 264, 622
Vogel, T., 636
Vokál, A., 466, 468
Volf, J., 152
Volf, M., 752
Vonka, M., 662
Vopálka, D., 462
Voráček, M., 158
Vorel, J., 708, 704
Vorel, V., 646, 648
Vorlík, P., 704, 702
Vráblík, L., 610, 548, 640
Vraný, T., 558, 560
Vratislav, S., 62, 80, 360, 204
Vrba, J., 478, 416, 476
Vrba, T., 436
Vrchota, P., 712
Vykydal, Z., 68, 84
Vyskočil, Z., 688
Vytlačil, D., 760
Vytvar, D., 622
Wald, F., 544, 592, 564
Weinzettel, J., 414
Zahradník, P., 176
Zajíček, R., 478
Záleský, J., 572
Záleský, M., 572
Záliš, S., 464
Zavadilová, A., 34
Zděnek, J., 194
Zela, J., 222
Zeman, J., 182, 394
Zicha, J., 78
Zimmermann, K., 116
Zimová, R., 698
Zlámaný, M., 704, 702
Zralý, M., 748
Zuda, L., 274, 276
Žáková, M., 118
Žďára, V., 662
Ženka, M., 660
Žilka, M., 746
Žofka, P., 148